IAEA-TECDOC-1288

Verification of analysis methods for predicting the behaviour of seismically isolated nuclear structures

Final report of a co-ordinated research project
1996–1999

INTERNATIONAL ATOMIC ENERGY AGENCY IAEA

June 2002

The originating Section of this publication in the IAEA was:

Nuclear Power Technology Development Section
International Atomic Energy Agency
Wagramer Strasse 5
P. O. Box 100
A-1400 Vienna, Austria

VERIFICATION OF ANALYSIS METHODS FOR PREDICTING THE BEHAVIOUR OF SEISMICALLY ISOLATED NUCLEAR STRUCTURES

IAEA, VIENNA, 2002
IAEA-TECDOC-1288
ISSN 1011–4289

Printed by the IAEA in Austria
June 2002

FOREWORD

This report is a summary of the work performed under a co-ordinated research project (CRP) entitled Verification of Analysis Methods for Predicting the Behaviour of Seismically Isolated Nuclear Structures. The project was organized by the IAEA on the recommendation of the IAEA's Technical Working Group on Fast Reactors (TWGFR) and carried out from 1996 to 1999.

One of the primary requirements for nuclear power plants and facilities is to ensure safety and the absence of damage under strong external dynamic loading from, for example, earthquakes. The designs of liquid metal cooled fast reactors (LMFRs) include systems which operate at low pressure and include components which are thin-walled and flexible. These systems and components could be considerably affected by earthquakes in seismic zones. Therefore, the IAEA through its advanced reactor technology development programme supports the activities of Member States to apply seismic isolation technology to LMFRs. The application of this technology to LMFRs and other nuclear plants and related facilities would offer the advantage that standard designs may be safely used in areas with a seismic risk. The technology may also provide a means of seismically upgrading nuclear facilities. Design analyses applied to such critical structures need to be firmly established, and the CRP provided a valuable tool in assessing their reliability.

Ten organizations from India, Italy, Japan, the Republic of Korea, the Russian Federation, the United Kingdom, the United States of America and the European Commission co-operated in this CRP.

This report documents the CRP activities, provides the main results and recommendations and includes the work carried out by the research groups at the participating institutes within the CRP on verification of their analysis methods for predicting the behaviour of seismically isolated nuclear structures.

The IAEA would like to express its appreciation to all who took part in the project and in the preparation of this report. Special thanks go to A. Martelli of the National Agency for New Technology (ENEA), Italy who acted as Chairman throughout the Research Co-ordination Meetings. The IAEA officer responsible for this publication was A. Stanculescu of the Division of Nuclear Power.

EDITORIAL NOTE

This publication has been prepared from the original material as submitted by the authors. The views expressed do not necessarily reflect those of the IAEA, the governments of the nominating Member States or the nominating organizations.

The use of particular designations of countries or territories does not imply any judgement by the publisher, the IAEA, as to the legal status of such countries or territories, of their authorities and institutions or of the delimitation of their boundaries.

The mention of names of specific companies or products (whether or not indicated as registered) does not imply any intention to infringe proprietary rights, nor should it be construed as an endorsement or recommendation on the part of the IAEA.

The authors are responsible for having obtained the necessary permission for the IAEA to reproduce, translate or use material from sources already protected by copyrights.

CONTENTS

SUMMARY

1. BACKGROUND FOR THE CO-ORDINATED RESEARCH PROJECT (CRP)

1.1. INTRODUCTION

The use of seismic isolation for structures has been gaining worldwide acceptance as an approach to a seismic design. Seismic isolation to important building such as nuclear power plants would result in reduction of the seismically induced load and hence more economical structural design

Liquid metal cooled fast reactors operate at high temperature, which induces high thermal stresses during transients. Hence the thickness of the structures have to be minimised to limit the thermal stresses, which approach contradicts the requirements of conventional aseismic design to make the structures more rigid. It is possible to meet these contradictory requirements by adopting seismic isolation.

Seismic isolation is included in the GE (United States of America) advanced liquid metal cooled fast reactor (ALMR) to decouple the reactor and its safety equipment from potentially damaging ground motions. Flexible isolation elements with high vertical and low horizontal stiffness are used between the building basement and the superstructure to transform high energy seismic input motions into harmonic response cycles with significantly reduced accelerations. This approach is well suited for the low pressure liquid metal reactor system, which has thin-walled components and structures. Some of these components are flexible in the horizontal direction, and reduced accelerations lead to reduced stresses and displacements or enhanced safety margins. The technology programme objective is to demonstrate that the seismic isolation elements perform during earthquakes as designed, with a high reliability throughout their 60-year design life. A testing programme of variously sized seismic isolation bearings indicated that a consistently high horizontal displacement capability can be achieved, and that the bearings have substantial margins for accommodating earthquakes beyond the safety shutdown earthquake.

Horizontal seismic isolation has been adopted for the ALMR design to simplify the reactor and nuclear island design and the in-service inspection programme, and to enhance design margins for beyond-design basis earthquakes. An added economic and licensing benefit of seismic isolation is the ability to achieve reactor design standardization for site locations with different seismic conditions and soil properties. The seismic isolation system decouples the reactor, its safety equipment, and the intermediate heat transport system (including the steam generator) from potentially damaging ground motion by transforming high energy, high frequency seismic inputs into lower frequency response cycles with significantly reduced acceleration. The isolated system responds to horizontal ground motion essentially as a rigid body, with little amplification of the ground acceleration. This limits the inertial loads and increases the structural margins for critical components and structures. Also reduced are relative displacements between components. This is helpful for limiting the potential for seismic interference between the control drives and their guide elements, and for minimizing the forcing function for seismic core compaction.

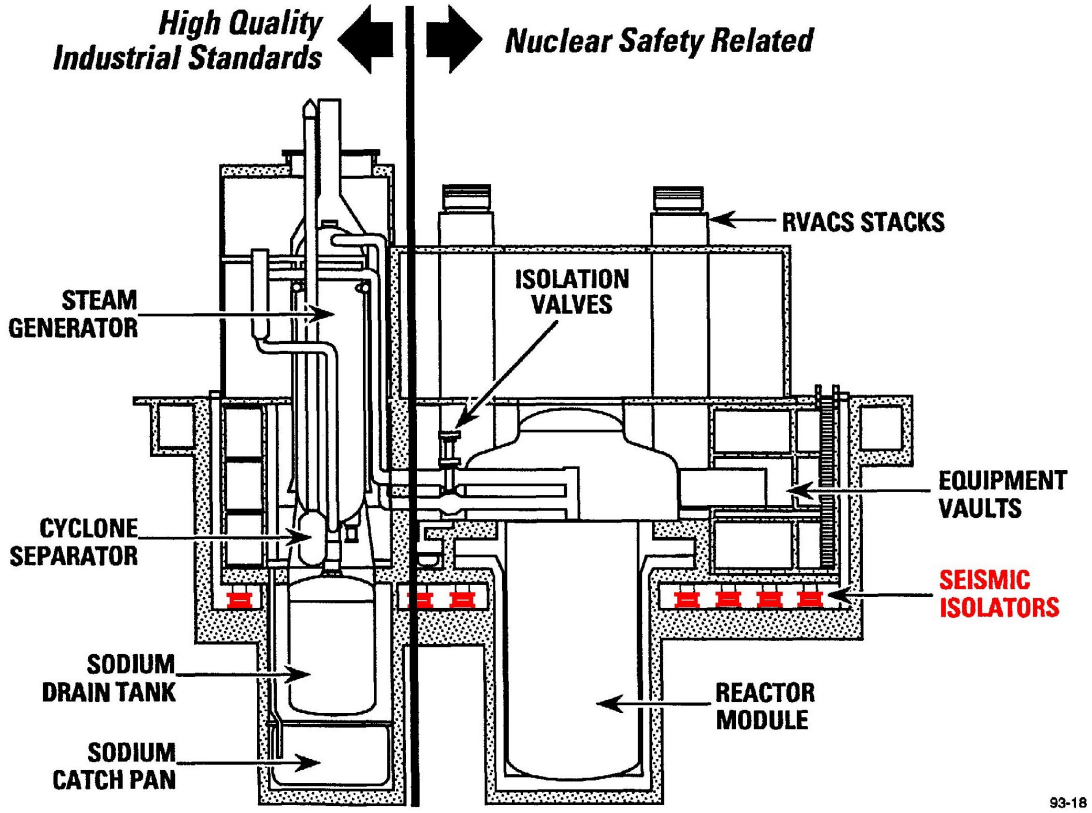

Figure1: ALMR (USA): Reactor Supply System — Mod B.

The ALMR nuclear island (Fig. 1) is supported from a common, seismically isolated platform, with a horizontal isolation frequency of 0.7 Hz and a maximum displacement of 19 cm during a safe shutdown earthquake (SSE) with 0.3g zero period acceleration (ZPA) ground acceleration. The design earthquake was specified to envelop the Nuclear Regulatory Commission's (NRC) Regulatory Guide 1.60 spectra. The selected criteria are expected to apply to over 80% of potential nuclear sites in the USA. Options for siting in seismic zones with higher ground accelerations were investigated and found acceptable. The seismically isolated ALMR system has the capability of accommodating at 0.5g ZPA earthquake. Sixty-six seismic isolators with access and space for in-service inspection and replacement, if necessary, are included. Each isolator is a composite of laminated steel plates and high damping rubber layers encased in rubber. There is a substantial experience base for this isolator design. Performance testing of the isolator bearings has been underway at the University of California (Berkeley) Seismic Engineering Laboratory. A powerful testing machine with a horizontal dynamic load capability of 150t and a vertical capability of 750t was built at the Energy Technology Engineering Center. Tests performed with half-size bearings demonstrated a significant margin to failure (three to seven times the expected SSE displacement). The experimental data have been provided to the CRP participants.

A seismic bearing qualification programme has been implemented. This includes: (1) static and dynamic performance tests of bearings; (2) the evaluation of aging and environmental effects, such as temperature, gamma radiation; and (3) seismic isolation system shake table tests to evaluate performance characteristics and margins. The vertically stiff reactor assembly places the vertical natural frequencies of critical structures well above the dominant ground

motion frequencies, thereby providing sufficient vertical seismic margins without isolation. In co-operation with Italy's Agency for New Technologies, Energy, and Environment, a proposal for seismic isolation design guidelines for seismically isolated nuclear power plants was developed. Extension of this work is intended to establish a framework of design rules accepted by the American Society of Civil Engineers (ASCE) and the NRC.

Seismic isolation is included in the European advanced liquid metal cooled fast reactor (EFR). The reactor building together with the adjacent steam generator buildings, switchgear building and auxiliary building are all on a common basement with bearing pads for effective isolation of horizontal earthquake-induced loads (Fig. 2). The reactor vault is additionally separated from the basement by spring to reduce the vertical seismic loads (Fig. 3). This last feature is optimal and required only in sites of very high earthquake activity. The isolation assures an essentially common seismic resistant design for a range of site conditions.

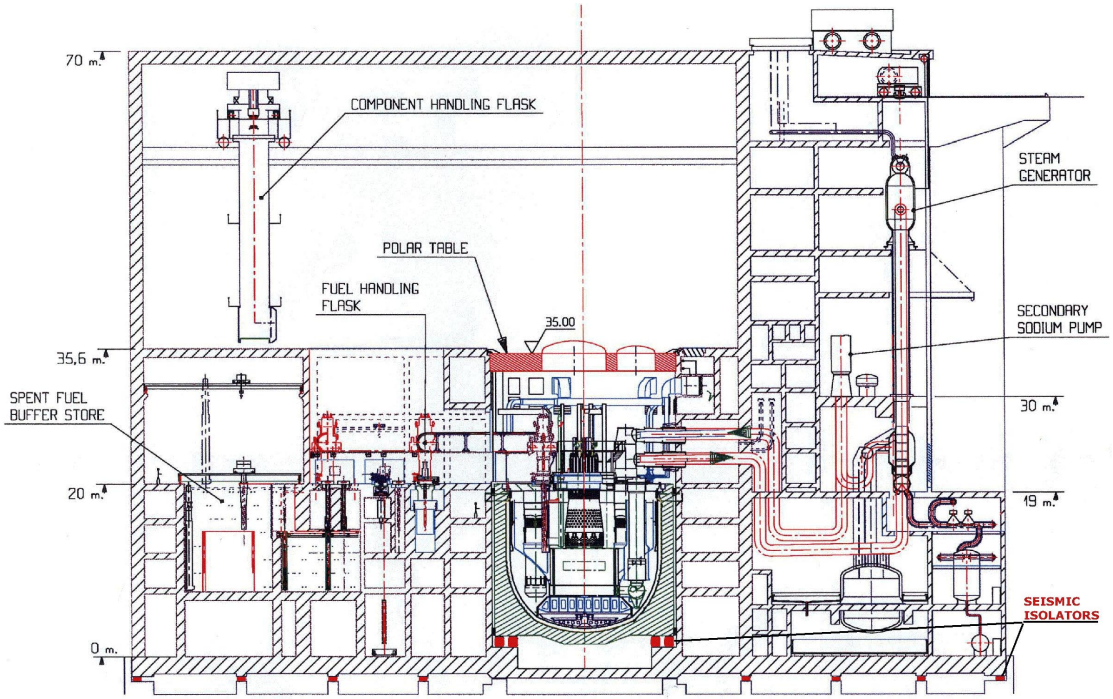

Figure 2: EFR: Nuclear island layout-elevation.

Seismic isolation technology is relatively new to nuclear power plants and has been investigated only in special, limited applications. Many experimental and numerical studies are required on isolation pads to substantiate the adequacy of design conditions so that they can be used for LMFR applications. The major studies include deformation characteristics and damping of isolation pads. Due to the complexity of the dynamic behaviour of seismic isolation devices, the high cost of their tests and the significant number of devices having excellent potential for NPPs applications, several Member States judged it to be of great interest to extend verification of their numerical models of such devices by the analysis of experimental data obtained by others.

It is with this focus that the IAEA sponsored the Co-ordinated Research Project on the implementation of base isolation for nuclear structures under the auspices of the TWGFR.

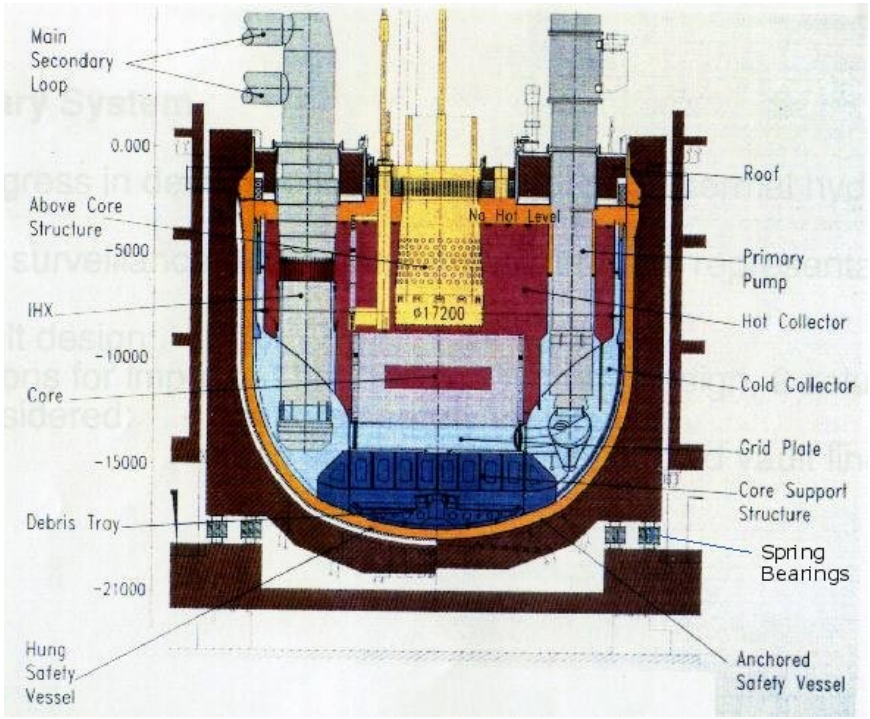

Figure 3: European Fast Reactor: longitudinal cut of the reactor.

1.2. OBJECTIVES

The objectives of the co-ordinated research project are to verify the numerical analysis methods and computer codes by comparing predictions with the benchmark test data provided by participant organizations, for the force-deformation characteristics of seismic isolation bearings and the response of isolated nuclear structures and to improve the analysis methods on seismic isolation technology

Experimental data for use in the project were provided by EERC, KAERI and ENEL on high damping rubber bearings (HDRB), by CRIEPI on natural rubber bearings (NRB) and lead rubber bearings (LRB) with both small and large lead core. Shaking — table test results were provided by CRIEPI, for a rigid structure, by ENEL for a flexible model structure and by KAERI for a test on a seismically isolated spent fuel storage pool. The seismic isolation bearings which generally use rubber as the elastomer are constructed from layers of elastomer bonded to steel reinforcing plates, with or without a central hole filled with a lead core.

The technical challenge in predicting the seismic response of an isolated structure is the need to develop a simple but accurate dynamic model of the isolators that can be combined with the dynamic analysis program that will simulate the rigid and flexible isolated structures. The technical challenge in the analysis of seismic isolation bearing is the large number of mesh elements needed and the fact that a fully 3-D analysis is required to cover all aspects of the bearing behaviour.

1.3. PARTICIPANTS

The participating institutes and chief scientific investigators are:

Indira Gandhi Centre for Atomic Research (IGCAR), India (P. Chellapandi)

National Agency for New Technology (ENEA), Italy (A. Martelli)
ENEL-HYDRO Hydraulic and Structure Centre (ENEL),Italy (F. Bettinaly)
ENEL-HYDRO-ISMES Engineering and Testing Centre (ISMES, Italy (G. Bonacina)
Central Research Institute of Electric Power Industry (CRIEPI), Japan (K. Hirata)
Korea Atomic Energy Research Institute (KAERI), Republic of Korea (B. Yoo)
Research Centre of Fundamental Engineering (RCFE), Russian Federation (V. S. Beliaev)
Tun Abdul Razak Research Centre (TARRC), UK (K. N. G. Fuller)
Earthquake Engineering Research Centre (EERC), USA (J. M. Kelly)
Centre (JRC) of the European Commission, Ispra (V. Rendo)
The programme has been co-ordinated through annual meetings of the chief scientific investigators from the participating institutes.

2. SCOPE OF THE CRP

High damping rubber bearings (HDRB) or lead rubber bearings (LRB) provide a simple and economical isolation system They possess the low horizontal stiffness needed and are capable of safely withstanding the large horizontal displacements imposed on them during an earthquake. The need for additional dampers is avoided. In the HDRBs damping is incorporated into the rubber compound. For the LRBs, the damping is provided by a cylinder of lead within the rubber bearing. A diagrammatic section of an HDRB is seen in Figs 4 and 5.

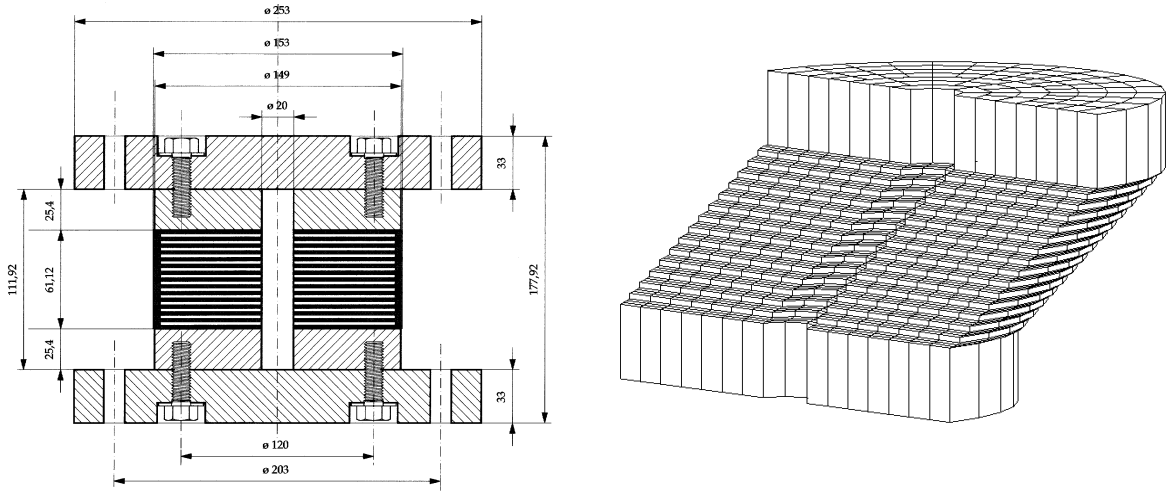

Figures 4, 5: Sketch of the 1:8 scale prototype of the ALMR high damping isolation bearing; HDRB deformed under a compression and shear strain.

2.1. ISOLATOR BEHAVIOUR

Isolation of structures from horizontal ground motions is gradually becoming a more common method of providing protection from earthquake damage. In contrast to conventional technology, seismic isolation not only upgrades the earthquake resistance of a structure, but also offers the possibility of protecting the contents and secondary structural features of a building or plant because seismic forces transmitted to the structure are reduced. The operability and safety of plant can thus be enhanced. The isolation system functions principally not by absorbing the energy of the ground motion but by providing an interface able to reflect the earthquake energy back into the ground. The natural frequency of the

structure mounted on the isolators is made to be below the frequencies of strong ground shaking. Damping is needed to limit the displacement of the isolators and — to control any response at the isolation frequency.

The proper functioning of isolation systems requires bearings with certain characteristics. The principal ones are:

- horizontal stiffness, K_H
- vertical load capacity
- horizontal displacement capacity, d_{max}
- damping.

The isolation frequency is determined by the horizontal stiffness and the gravity load supported. The ability to predict K_H and d_{max} reliably by FEA (finite element analysis) would mean that the isolator design could be verified with a reasonable degree of confidence before the isolators are submitted to a prototype test programme.

Several isolators were analysed within the Project by FE methods to see how well the FEA predicted their force-deformation behaviour. The predictions of individual Partners were compared with the test data from prototype isolators. Those analysed included:

LRB	manufactured and tested in Japan
HDRB	manufactured and tested in Italy
HDRB	manufactured and tested in The Republic of Korea
HDRB	manufactured in Italy and tested in the USA.

In addition to bearing test results, characterisation data for the rubber used in the manufacture was provided; the latter is required by the FE programmes. Again each partner chose the model to fit the data, and carried out the associated analysis to determine the value of the model's parameters.

Within the Project, two other types of isolator:

- low-damping rubber bearing
- pneumatic, 3D isolation device

were also analysed. As an adjunct to the FEA of isolators, a benchmark problem — the torsion of a rubber cylinder — was chosen by TARRC to assess how well the results obtained by the FE solvers compared with those based on an exact analytical solution.

2.2. RESPONSE OF STRUCTURES

The design of isolation systems for critical structures obviously requires confidence in the methods used to predict the responses of the structure and isolation system to earthquake inputs. Factors involved include the adequacy of:

- the model describing the dynamic behaviour of the isolators;
- the model of the structure.

By effectively reducing the seismic input to the structure, and, indeed, allowing the possibility that the response can be kept within the elastic range, the use of isolation may be expected to lead to more reliable analyses.

Within the Project the response of the following seismically isolated structures was investigated:

- rigid mass
- steel-frame structure (MISS)
- spent fuel pool
- full-scale section of WWER-640 reactor building.

Partners used their own method for analysing the structural response, and also developed the representation of the dynamic behaviour of the isolator necessary for the computations. The results of individual partner's computer predictions were compared with the test observations.

3. SUMMARY OF ACTIVITIES WITHIN THE CRP

TARRC's [Tun Abdul Razak Research Centre (United Kingdom)] participation over the course of the programme was directed towards verifying a simplified model for the isolators to facilitate prediction of the response of isolated structures to earthquakes, and verifying finite element methods for the prediction of isolator force-deformation behaviour.

Verification of the design of base isolation systems requires predicting their response to earthquake inputs. This needs a model of the isolators sufficiently simple to be tractable but able to take the main features of their horizontal force-deformation characteristics into account. A curvilinear hysteretic model (A) able to accommodate stiffening at large shear deflections was developed for high damping rubber isolators. Predictions using the curvilinear hysteretic model were compared with those using a simple linear spring and a dashpot model (B). Structural accelerations and isolator displacement produced by design earthquakes and those above the design level were calculated. Generally, model (A) predicted higher peak displacements and accelerations (typically up to 20% for 2 times design level inputs) than those from model (B). The discrepancies were only slightly less for design level earthquakes

In the case of an above design level earthquake input based on El Centro, the non-linearity was clearly important, and resulted in differences in the peak structural acceleration response of up to 40%. Analysis of the isolators based on simple linear viscous damping models should therefore be treated with caution, certainly for above design level earthquakes.

The finite element analysis (FEA) concerned three key areas:
(a) benchmark problems,
(b) material models as input to FEA, and
(c) calculation of force-deformation behaviour for high damping rubber isolator and lead-rubber isolators.

The analytical solution to the torsion of an elastomeric cylinder is suggested as a "benchmark" for the FEA of elastomeric components. The problem is used to establish the magnitude of the error associated with the numerical integration process involved in FEA of components. It is not a test of the material models, though the type of function used to describe the material behaviour may influence the accuracy of the numerical process. Two computer codes, namely MARC and ABAQUS, and two material models are used for the comparison between the

analytical and FE results. The FE 3-dimensional analysis for a coarse-mesh model with 500 elements gave results generally within 5% of the analytical solutions for the couple required to deform the cylinder. For the axial load required to keep the height of the cylinder unchanged the errors were up to 10%. Better levels of accuracy are obtained if the density of the mesh is increased, but this is at the cost of much longer computing time.

Evaluation of elastomer strain energy functions available on commercial FE codes has been carried out. It was shown that even a five-term series Rivlin function [(W (I_1, I_2)], where I_1 and I_2 are the strain invariants is incapable of catering for the rapid changes of modulus at small strains. The two-term Ogden strain energy function also gave a fairly poor fit at small strains. Increasing the number of terms to three did not apparently produce significant improvement, though the use of sophisticated non-linear curve fitting algorithms, rather than visual inspection, may enable better fits to be obtained. A strain energy function based on the assumption that the energy of deformation depends on I_1 only has been found to fit most uniaxial test data. The function, which involves two adjustable powers of (I_1–3), is able to cater for material non-linearity both at small and large strains. If a material could be adequately characterised with this form of strain energy function only a simple uniaxial tension test is required to find its coefficients. Components, such as laminated rubber steel isolators, for which multiaxial stresses or deformations are important may, however, require the I_2 invariant term in the strain energy function to be considered.

FE analysis of a single layer of rubber bonded on both sides, and subjected to an initial compressive load followed by a shear deformation has been performed. When using some types of strain energy functions, the results show that the initial decrease in the thickness of the layer may be at least partially reversed after the imposition of the shear deformation. Rivlin has shown analytically that for the stresses required to maintain an incompressible block in simple shear there are, as well as the shear stress, normal stresses on at least two pairs of faces of the block.

One normal stress is dependent on $-\gamma^2 \frac{\partial W}{\partial I_2}$ (where γ is the shear strain). If $\partial W/\partial I_2$ is positive, the height increases under shear, consistent with the FE analysis. An isolator under combined compression and shear exhibits a further height drop as the shear is applied. Thus the FE analysis of a single layer of rubber cannot predict the vertical deformation of a complete isolator.

The force-deformation behaviour of high damping rubber isolators were predicted using FEA. The calculation for shear agreed well with the experimental data up to large shear strains (200%); agreement could be ensured by strongly weighting the material characterisation data towards the range of strains of interest. The predicted behaviour under combined shear and compression was poor. Behaviour similar to that from the analysis of single rubber layers is obtained, whereas complete isolators show a continuous height drop when tested in shear.

The force-deformation behaviour of lead rubber bearings (LRB) was also calculated using FEA for the case of increasing shear load only. Characterising lead for use in FE still requires research effort. Material data obtained for lead from shear tests were converted into stress-strain curves for the tensile mode of deformation; the FE code used (MARC) was only capable of using tensile data for modelling the behaviour of the lead core of the isolator. The predicted force-deformation of the LRB in shear was reasonable up to shear strains of 50%, but at higher strains the force was increasingly overestimated.

KAERI's [Korea Atomic Energy Research Institute (Republic of Korea)] activities within the frame of the CRP were as follows:

— the provision of spent fuel storage pool and KAERI High Damping Rubber Bearing test data,
— benchmark comparisons between analysis and test results of seismic isolation bearings for Italian soft and hard ENEA HDRB, CRIEPI Natural Rubber Bearing and Lead Rubber Bearing, and KAERI HDRB,
— benchmark comparisons between analysis and test results of seismically isolated nuclear structures for CRIEPI rigid mass mock-up and for Italian MISS.

The benchmark exercise was fulfilled in four stages which covered the following items:

In the first stage, FEM analyses using ABAQUS in combined compression and shear, and only in compression, for ENEA HDRB with high shear modulus and for CRIEPI NRB, have been performed and compared with test results to verify the validity of the used analysis procedures. The purpose of the analyses was to predict the quasi-static force-deflection behavior of laminated rubber bearing from rubber test data. Several kinds of strain energy density function representing the hyperelastic characteristics of rubber were tested. For the ENEA HDRB benchmarks, three different rubber models, Mooney-Rivlin, Ogden and polynomial methods were evaluated. The Ogden and polynomial models can be recommended. For the CRIEPI NRB benchmarks, analysis results using coefficients of the derivatives of the strain energy function show good agreement with the test results. In the compression analysis with no shear strain offset, analysis results agree well with test results up to 400% design vertical load, however in the compression with offsets the displacements obtained by the combined compression and shear analyses are smaller than those by tests.

In the second stage, the combined shear and compression behaviours of the ENEA HDRB with low shear modulus and the CRIEPI LRB were analyzed using the hyperelasticity material option of the ABAQUS computer program. For ENEA HDRB using the 2D model, the solution accuracy is investigated by changing the number of the elements for a rubber layer in the rubber thickness direction. The Ogden model is used in this analysis. The horizontal force and displacement relations show no differences with respect to the number of the elements for a rubber layer. According to the material models of rubber, however, there are some different results. The Mooney-Rivlin model, with a linearity of material properties, gives a large discrepancy from the test results, but the polynomial (N=2) and the Ogden (N=3) methods give results which compare very well with the test results, up to a shear displacement of 60 mm. For the 3D solid model, the results using the polynomial, and the Ogden models are close to the test data in the lower shear strain region up to 200% which equals the shear displacement of 60 mm. The Seki model predict a higher shear force than the test data, and the results obtained from the Mooney-Rivlin model also show important deviations from the test data. With respect to computing efficiency, the 3D model takes over 10 times longer than the 2D model. In vertical deformation analyses, a minimum of two elements in the thickness direction for a rubber layer is required to get accurate results. The polynomial and Ogden models are much better than the Mooney-Rivlin model, and the Seki model is the worst because the volumetric tests data are not considered in the formulation. The finite element analyses using the 2D model were performed for the CRIEPI LRB. Two stress-strain curves for the lead plug are used in these analyses, where the initial yield stresses are assumed by the static and the dynamic yield stresses representing the soft and hard properties, respectively. For combined compression and shear analyses, the results modeled by the hard lead properties

agree well with the test data until 200% shear strain, at which point convergence problem occurs. The shear force calculated using the soft lead properties is somewhat smaller than that of the test results. The calculated horizontal forces according to the rubber material models such as Ogden and polynomial agree well with experimental results up to a 200% strain. There is a small discrepancy between the solutions of the 2D and 3D models, but the computation time using the 3D model is over 10 times longer than for the 2D model.

In the third stage, the combined shear and compression behaviour of the KAERI HDRB made of MRPRA rubber and the shaking responses of the CRIEPI isolated rigid mass mock-up were analyzed. For FEM analyses of KAERI HDRB, three kinds of strain energy density functions of the ABAQUS program were used as constitutive laws for the rubber with hyperelastic characteristics. The results were compared with test results, for each of the constitutive models.

The calculated horizontal forces using the Ogden rubber material models (N=3) agree well with the experimental data up to 300% strain. There is a small discrepancy between the 2D and 3D analyses. The simulation results for the shaking table tests of the CRIEPI rigid mass mock-up supported by scaled lead rubber bearings are obtained by ABAQUS time history analysis. In the analysis, the linear and bilinear hysteresis models simulating the behaviours of the rubber bearing are used. The calculated accelerations and displacements for the isolated structure under design earthquake motion(1.5S1) agree well with the test results. The calculated accelerations for isolated structure under beyond design earthquake motion (4.6S1) are larger than those in the tests, but the calculated displacements agree well with those in the tests. When some of the bearings are in tension due to the rotational motion of the mock-up, the vertical stiffness of the bearings is changed, which greatly influences the structural responses in the high frequency range.

In the fourth stage, the seismic responses for the shaking — table tests of the Italian MISS structure, both fixed and isolated, were calculated using the ABAQUS time history analysis. For the analysis of the isolated MISS structure, the modified bilinear model for isolation bearings was used. The analysis results for both the fixed and isolated MISS structures agree well with the test results.

ENEL-HYDRO Hydraulic/ENEL-HYDRO-ISMES Engineering (Italy) as a co-ordinator of an EC funded project concerning the optimization of high damping rubber bearings (HDRBs), supplied test results concerning both HDRBs and an isolated steel frame structure mockup (MISS, Model of Isolated Steel Structure), which had been subjected to a wide-ranging experimental campaign in the framework of the aforementioned project. Test data provided by the other countries were also re-analyzed by ENEL to improve its mathematical models and to validate the new models developed within the framework of the CRP activities.

Extensive numerical work was performed by ENEL. Finite Element (FE) analyses were carried out on USA scaled HDRBs that had been manufactured in Italy and tested by the University of California at Berkeley; and on Natural Rubber Bearings (NRBs) and Lead Rubber Bearings (LRBs) manufactured in Japan for CRIEPI. The compression, and combined compression and shear behaviour of the bearings were analysed with the help of the ABAQUS code, using different FE models and different hyperelastic strain energy functions. Elastomer constitutive models, available in ABAQUS for representing the non-linear and hysteretic behaviour of bearings, were used to solve the problem. Mooney-Rivlin and Ogden strain energy functions and some user-defined strain energy functions were used in modelling the

rubber. Results from different meshes with different discretizations and types of element (axisymmetric, axisymmetric with non axisymmetric deformation, shell and solid) were compared with the experimental data. The appropriate strain energy function, the type of the element and FE mesh were examined, and their ability to model the behaviour of elastomeric bearings were studied.

For the Japanese NRBs and LRBs both three-dimensional (3D) and axisymmetric finite-element models were developed and implemented in the ABAQUS computer program by ENEL, while similar models were developed and implemented in the same code by ENEA for the USA HDRBs. Hyperelastic models of the rubber, defined according to the results of suitable tests on both scragged and unscragged rubber specimens, were also implemented in ABAQUS. Extensive numerical work was performed by considering meshes with different refinements and different element types. The numerical analyses aimed at investigating the effects of the different variables on the solution for predicting, up to large strains, the response of the isolators, thereby optimizing the type of material model, the discretization and elements to be adopted.

For the Japanese NRBs, good agreement between numerical and experimental results was found by ENEL for horizontal stiffness (similar to the results of ENEA for the US HDRBs); however, the agreement for compression tests was satisfactory only when compressibility was taken into account. This confirmed the importance of volumetric tests on rubber specimens to correctly evaluate bearing vertical stiffness correctly, especially in the case of large shape factors.

The ENEL analysis also confirmed that planar tests on specimens should be performed up to very large deformations, in order to allow for the definition of adequate hyperelastic models of the rubber. Moreover, it was found again that the unscragged rubber model should be used for reproducing the bearing behaviour to 50%–100% shear strain, while the scragged model should be used for larger deformations. Only slight differences were found between the results of 3D and axisymmetric models to 200%–300% shear strain. 3D models should be used for larger deformations. Similar to HDRBs and NRBs, the numerical analysis of LRBs showed adequate results for the horizontal stiffness up to 300% shear strain; however, at larger strains some analytical results showed hardening, contrary to test data, because of inadequacies in the material model used. In addition, large discrepancy was found between the numerical results and the test data for LRBs under compression; this may be attributed again to modeling rubber as incompressible.

Similar to the NRBs, the need was stressed for an improvement of the analyses for the LRBs. These analyses should be based on more precise data concerning the characterization of the materials (natural rubber and lead), including effects of rubber compressibility. In addition, an attempt should be made to consider temperature effects on lead behaviour. In any case, the achieved results confirmed again the conclusions of previous studies that FEMs are useful tools for both the detailed design of elastomeric bearings and their qualification. For the latter, they allow for a considerable reduction of the number of tests to be performed (e.g. those concerning effects of parameters like temperature, aging, vertical load on horizontal stiffness, initial or arisen defects, etc.).

In order to asses the accuracy of both the FE model meshing and FE solver, a torsional benchmark problem was presented jointly by TARRC and ENEL. Prediction of the couple and axial load acting on the cylinder was obtained by ENEL from FE calculations using

ABAQUS, and was compared to the analytical solutions for two types of material models, Mooney-Rivlin and Ogden. Extensive numerical work was performed by considering meshes with different refinements and different element types. The results showed an excellent agreement. In addition to the numerical activities, ENEL carried out in 1997 a complete material characterization of KAERI HDRBs by testing rubber specimens, and distributed the results to other participants.

Finally, ENEL, partly in the framework of the CRP, developed a new non-linear simplified isolator model, with exponential constitutive law describing the rubber behaviour. The model was implemented as a "User Subroutine" in the ABAQUS FE code. The new model, based on three rubber parameters, allows for a very accurate evaluation of the response of seismically isolated structures. Although it was developed for elastomeric bearings, the proposed model can be applied to other types of isolation devices having a continuously decreasing stiffness with increasing displacement (e.g. rubber or helical springs coupled with metallic yielding elements, wire rope friction isolators, etc.)

ENEA's [National Agency for New Technology (Italy)] activities within the frame of the CRP were as follows. The first data, among those provided by other countries, which were jointly analysed by ENEL and ENEA concerned USA scaled HDRBs manufactured in Italy and tested by University of California at Berkeley; then, Natural Rubber Bearings (NRBs) and Lead Rubber Bearings (LRBs) manufactured in Japan for CRIEPI were analysed. For the USA HDRBs both three-dimensional (3D) and axisymmetric finite-element models (FEMs) were developed and implemented in the ABAQUS computer program by ENEA, while similar models were developed and implemented in the same code by ENEL for the Japanese NRBs and LRBs. Hyperelastic models of the rubber, defined according to the results of suitable tests on both scragged and unscragged rubber specimens, were also implemented in ABAQUS. The numerical analyses, aimed at investigating the effects of the numerous variables of the problem, allowed for optimizing the type of material model, discretization and elements to be adopted, up to large strains.

For the USA HDRBs, good agreement between numerical and experimental results was found for horizontal stiffness (similar to the results of ENEL for the Japanese NRBs); however, the agreement for compression tests was satisfactory only when compressibility was taken into account. This confirmed the importance of volumetric tests on rubber specimens to evaluate bearing vertical stiffness correctly, especially in the case of large shape factors. Analysis of ENEA also stressed that planar tests on specimens shall be performed to very large deformation, in order to allow for the definition of adequate hyperelastic models of the rubber. Moreover, it was found that the unscragged rubber model should be used for reproducing bearing behaviour 50%–100% shear strain, while the scragged model should be used for larger deformations. Only slight differences were found between the results of 3D and axisymmetric models from 200% to 300% shear strain, while 3D models must be used for larger deformations.

In any case, the achieved results confirmed the conclusions that FEMs are useful tools for both the detailed design of elastomeric bearings and their qualification; for the latter, they allow for a considerable reduction of the number of tests to be performed (e.g. those concerning effects of parameters like temperature, aging, vertical load on horizontal stiffness, initial or arisen defects, etc.).

The CRIEPI [Central Research Institute of Electric Power Industry (Japan)] has conducted various isolator tests, shaking table tests, and proposed design guidelines for LMFR based isolation systems.

The test data prepared by CRIEPI consist of rubber bearing test data and shaking — table test data. Rubber bearing test data apply to both NRB and LRB of different scales. For LRB, test data for two types of specimen were provided by the participating organizations: one with a thin lead plug, the other with a thick lead plug. As for horizontal loading tests, both cyclic loading test data and breaking test data under monotonically loading were provided. For vertical loading tests, cyclic loading test data without initial shear deformation were provided. Strain energy functions were determined from biaxial tensile tests and from volumetric strain tests of rubber specimen. The determined strain energy functions were given to the participants of the CRP. Shaking — table tests of a base isolated rigid mass, supported by eight LRBs, were conducted by CRIEPI. Acceleration time histories measured on the model and the shaking table, displacement time histories of the isolators during the shaking, and also cyclic loading test data of the LRB used were provided to the participants of the CRP.

Numerical simulations of the rubber bearing tests for NRB, LRB (data provided by CRIEPI) and HDRB (data provided by ENEA/ENEL and by KAERI) were conducted using the computer code ABAQUS. As for the material properties of HDRBs, test results of rubber material were provided by ENEA/ENEL and by KAERI and strain energy functions were determined from these test results. For NRB, it was shown that the numerical simulations agree fairly well with the test results of both horizontal and vertical loading. As for LRBs, numerical simulations show good agreement with test results, except for the case of the LRB with thick lead plug, implying problems concerning the modeling of the lead plug. The HDRB simulation results showed good agreement with the test results; however, the accuracy of the simulation proved to be lower compared with the case of NRB or LRB. This is because material nonlinearity of the high damping rubber is not taken into account by the strain energy function.

Numerical simulation of the shaking table tests were conducted for the case of the rigid mass (conducted by CRIEPI) and the steel frame model (conducted by ENEL/ENEA). In the simulation of the rigid mass model tests, where LRBs were used, isolators are modeled either by bilinear or poly-linear models. In both cases, the simulation results showed good agreement with the test results. For the steel frame model, test data for both the base isolated and fixed-base cases were provided. At first, simulation for the fixed base model was conducted to obtain an accurate model of the superstructure before the simulation of the base-isolated frame. In the case where HDRBs were used as isolators, the test results of the bearing were provided by ENEL/ENEA. Combined nonlinear elastic springs and elasto-plastic springs were used to model the isolators. For the improvement of the simulation results, it was pointed out that modeling of the isolators taking account of the hardening effect at high strain is desirable.

The IGCAR [Indira Gandhi Centre for Atomic Research (India)] as a first step, initiated a feasibility study for the 500 MW(e) prototype fast breeder reactor (PFBR) to evaluate the potential benefits of the design incorporating seismic isolation compared to conventional fixed base design. It was found that seismic isolation devices reduce the floor response acceleration thereby decreasing the loads on the components. However, for further studies, detailed analysis incorporating the actual behaviour of the seismic isolator needed to be carried out. The general purpose finite element program ABAQUS was studied for the numerical predictions of the behaviour of the rubber bearings. Five sets of experimental data on laminated rubber bearings were supplied by Italy, Japan (two sets), The Republic of Korea

and USA. The validation is carried out as explained below. The analysis was done using three types of finite element models viz.:

1) Single layer model,
2) Axisymmetric model, and
3) 3-D model.

Rubber is modelled as a hyperelastic material. The required material properties were computed from the experimental data of the rubber specimen. Two forms of strain energy density functions were used, viz.:

1) Polynomial form (with N=2) and
2) Ogden form (with N=2 and 3).

Analysis for the Italian HDRB was performed for three different loading cases viz:

1) Combined compression with vertical load of 50 kN and shear up to 400%,
2) Combined compression with vertical load of 100 kN and shear up to 250%, and
3) Compression up to 1200% of design vertical load.

For the Japanese NRB, analyses were carried out for:

1) Combined compression and shear up to 300%, and
2) Compression with different offset shear strain.

The major conclusions of these analyses were:

1) the polynomial form of strain energy density function predicts deformation behaviour better than the Ogden form,
2) the predictions of all the three models (single layer model, axisymmetric model and 3-D model) are similar,
3) the single layer model can be effective for the purpose of validating the constitutive model of rubber, and
4) the deviation of the numerical predictions from the experimental results for the case of the combined compression with different offset shear strain is found to be large.

The model with polynomial form N=2 gave results which matched closer with the experimental results than the other two models. Thus, from the above analyses it is seen that the force deformation behaviour of HDRBs and LRB is well predicted by finite element analysis. Hence the finite element method can be used for analysing seismically isolated nuclear structures.

In the second stage of the CRP, the dynamic response of model of isolated steel structures (MISS) and CRIEPI isolated rigid mass mockup was carried out.

MISS is a five storied framed steel structure. The base isolation of MISS is provided by six HDRB. Detailed modeling of the HDRB as done in the first stage of the CRP, while performing the dynamic analysis of the base isolated structure is highly computationally intensive. For obviating this problem, a simplified model of the rubber bearing is resorted to.

The HDRBs are modelled by an equivalent multiple elasto-plastic (MEP) model. The hysteretic damping is simulated by the plastic deformation of the elasto-plastic member of the MEP model.

The computer code CASTEM 2000 has been used in the present analysis. The analysis was carried out in two stages. In the first stage, the equivalent MEP model is derived, reproducing the actual hysterisis loop of the HDRB. In the second stage the HDRBs are replaced by the equivalent MEP model and the structure is analysed for the given base excitation.

Results obtained through CASTEM 2000 show good agreement with the experimental data. In the case of the CRIEPI Rigid Mass Mockup, the isolation system is provided through scaled lead rubber bearings. The dynamic response is obtained, first by arriving at an equivalent MEP model simulating the lead rubber bearings and using this MEP model for obtaining the Rigid Mass dynamic response. The analysis indicated good agreement between computed and experimental results.

EERC's [Earthquake Engineering Research Center (EERC) of the University of California at Berkeley (USA)] contributions are as follows. As part of the design validation of the seismic isolation scheme for the ALMR, a procurement specification was developed, reduced-scale isolation bearings were purchased from two different manufacturers, and an extensive series of tests were performed on these bearings. The objective of this reduced-scale bearing test program was to establish bearing mechanical properties and failure characteristics that can be used for later experimental and analytical evaluation of seismic isolation concepts using these bearings. In particular, emphasis was placed on determining the variation in observed bearing shear properties as a function of shear-strain amplitude, loading frequency, applied axial stress, and load history. Shear failure tests were performed to establish margins for use in analyses of beyond-design level earthquakes. Two different bearing designs, with scale factors of one-quarter and one- eighth, were tested to investigate the influence of size on isolator properties. This aspect is of particular interest, because reduced-scale bearings will be required for earthquake simulator tests of a system model. This work includes a development of the bearing designs and the specification that was developed for the procurement of bearings for the ALMR project. The specification was developed so that it could be used for the procurement of both reduced-scale and full-size bearings. The bearings provided by KAERI for this testing project were intended to be in general accordance with the ALMR bearing specification. The test data on bearings were provided to participating organizations in the CRP to validate the computer codes.

At the RCFE [Research Centre of Fundamental Engineering (Russian Federation)], innovative pneumatic multicomponent low-frequency seismic isolation bearings for input acceleration up to 0,5g have been developed. This anti-seismic protection device incorporates both supporting spherical elements, which provide displacements in the horizontal direction, and pneumatic dampers with rubber diaphragms for displacement in the vertical direction. Damping devices had been specially elaborated for the reactor building seismic isolation system as a result of substantial advances in the design and operation of the high damping type of hydrodampers. The anti-seismic protection system of the reactor plant is based on supporting pneumatic and pneumatic hydraulic isolators of 2 to 8 MN load-carrying capacity, applicable to low-frequency seismic isolation systems of buildings. The proposed pneumatic isolators are installed in the foundation of the structure between the lower and the upper base slabs. Arrangement of seismic isolators in the design corresponds to the construction features and stiffness characteristics of the structure, as well as to the condition of uniform loading.

Usually, a block of seismic isolators consists of a common steel part and a set of seismic isolators. This common steel part allows horizontal displacement and the seismic isolators allow vertical displacement. Depending on the number of seismic isolators in the block, its load-carrying capacity varies from tens of tons to thousands of tons.

Each seismic isolation device consists of a skittle-shaped central rack and pneumatic isolators fixed thereto with the help of bracings. Load-carrying capacity of one isolation unit is 300 to 1000 tons. The upper and lower ends of the central rack of the seismic isolators are semi-spherical, having a flat face at their contacting areas. This provides not only for the relative horizontal displacement of the superstructure with respect to the ground, but also acts as a restoring force mechanism. The pneumatic isolators have passed static and dynamic tests. The tests did not show any external damage or degradation. Nowadays, the norms and standards for the design, calculation and operation of seismic isolation systems are under development.

For the new-generation nuclear power reactors in the Russian Federation (WWER-640, WWER-1000) an effective base isolation multi-component system with low horizontal stiffness between the superstructure and the foundation to decouple the structure from the ground has been developed, and analytically and experimentally investigated.

Partly in the framework of this CRP, a 300-ton (dimensions 22 × 6 × 7m) sector of the seismically isolated reactor WWER-640 was tested on a shake platform with dimensions of 30 × 15m using explosive techniques. The experimental studies were certainly very advanced as clearly pointed out by the CRP participants. Furthemore, studies allowed methods to be assessed that are not only applicable to the WWER-640 specific case, but to nuclear power concepts in general. The experimental data were used for verification of analysis methods and codes.

An accurate analysis of the 3D seismic isolation system (SIS) with pneumatic seismic isolators (PSI) and high viscous dampers (HVD) for the reactor building (RB) was carried out. Benchmark exercises have been used for the methods and codes verification, as well as for investigating the efficiency of the seismic isolation system (SIS). For seismic analysis of the SIS the CKTI-Vibroseism computer code “SEISM 2000” was used that allowed to take into consideration the real experimental non-linear characteristics of different seismic devices, isolators and dampers. The analytical models of anti-seismic protection devices in the “SEISM 2000” software practically fully reflect a real design. The natural frequencies of the system in cases of soft/hard soil and big/light pull-back motions can vary by several times.

The 3D seismic excitation to the RB was applied as time histories generated from US NRC spectra. Two levels of seismic impact were used in this analysis: 0.2g and 0.5g peak ground acceleration (PGA). It was observed that the use of the SIS dramatically decreases the amplification of the RB floor response spectra at the elevation of the reactor support. The influence of soil condition on horizontal and vertical floor response spectra was observed. The influence of PGA input level on spectra view was shown. In the case of 0.2 g PGA level the SIS decreases floor peak acceleration for soft soil conditions approximately three times. Installation of dampers in SIS slightly influences the acceleration level. The positive features of dampers’ installation were demonstrated. Use of HVD leads to considerable decrease of relative displacements and rocking angles in the SIS and gives a possibility to achieve the specified deflection capacity.

A method to determine the damper parameters of isolated structures was developed at the Center of Earthquake Engineering and Natural Disaster Reduction (CEENDR). In solving this problem two kinds of friction ratios f_{opt} and f_{st} of damping devices were found to be very important. The first ratio f_{opt} was named as the optimal friction ratio. When the friction ratio is equal to its optimal value the maximum acceleration of the system at its lowest value. The second ratio f_{st} was termed as stabilizing friction ratio. When the friction ratio is equal to its stabilizing value the maximum of the system mutual displacement becomes small. For $f = f_{opt}$ the system can experience too large a displacement and for $f = f_{st}$ — too large an acceleration. Therefore the range between the optimal and stabilizing friction ratios is used to determine the design value of the friction ratio. This range was named as the working range of friction ratios. The value of the design friction ratio depends on the set of calculating accelerograms. The method of evaluating the design acceleration level for structures with different functions was developed based on the analysis of more than 300 recordings of earthquake accelerations.
The activities in the framework of this CRP have also been concentrated on the verification and improvement of advanced mathematical models of isolators and isolated nuclear structures. Owing to the test data on isolators provided by ENEA, KAERI and CRIEPI, and a rigid and flexible model structures, provided by CRIEPI and ENEL respectively, a special non-linear elastic theory method, using a continuum transformation approach has been verified.

The Joint Research Centre (JRC) of the European Commission is in charge of the European Laboratory for Structural Assessment (ELSA) that is a unique facility in Europe to test full/large scale models of structures against earthquakes. ELSA has been engaged in the validation of the pseudo-dynamic method to test base-isolated structures. The experimental campaign includes both the comparison between dynamic and pseudo-dynamic snap-back tests performed at ELSA and the comparison between tests performed at ELSA and shaking-table tests performed at ISMES-Bergamo. In particular, the pseudo-dynamic method needs to be validated for base isolation when the system is composed of materials with a strain-rate dependend behaviour. This is the case, for instance, for rubber bearings or rubber-lead bearings, commonly used for NPP isolation purposes.

The pseudo-dynamic method has been validated by the folowing steps:

- the first step of the comparison performed at ELSA consisted in testing a four storey steel frame isolated at the base with HDRB provided by ALGA and made with special rubber material produced by TARRC. To adjust the method, the parameters of the software governing the method have been calculated in such a way as to reproduce with tests a dynamic snap-back of the structure also performed at ELSA.

- the second step was to verify the methodology using actual earthquake statistics. To this end, a series of characterization tests have been performed on the isolators for strain rates. This allowed to find a correction factor for the tests. At this stage, tests were performed on a base isolated structure provided by ENEL and previously tested on the shaking table of ISMES. The comparison between the dynamic shaking table tests and the pseudo-dynamic tests showed a very good agreement.

- based on this verification it was possible to validate the pseudo-dynamic method to test base isolated structures following a standard procedure. This is based on a preliminary characterization of the isolators for a range of frequencies of the order of the expansion factor applied to for the tests.

- the last step was to perform tests for structures protected with base isolation and/or energy dissipation devices with the substructuring technique that allows to test very big structures when one part remains linearly elastic.

The results obtained show that the pseudo-dinamic method can be used for that scope and that ELSA can be considered validated for this type of test. The contribution of ELSA, through its capability of testing large scale models of protected systems and the performance of its control systems, will be important for the validation of designs that include these innovative technologies.

4. MAIN RESULTS OF THE CRP, CONCLUSIONS AND RECOMMENDATIONS

4.1. COMPUTER CODES AND ANALYSIS METHODS VERIFIED IN THE CRP: RESULTS FROM INDIVIDUAL PROJECTS

(i) Computer codes for isolation analysis

The computer code verified at IGCAR was ABAQUS with Ogden using polynomial models for the rubber, and applied these to the identical types of isolator.

The investigation at KAERI included ABAQUS with Mooney-Rivlin, Ogden, polynomial and Seki models for the rubber and applied these to compression and combined shear and compression of both the ENEA HDRB and CRIEPI LRB isolators.

The code verified at ENEL, ENEA and ISMES was ABAQUS with the rubber modelled by the polynomial, Ogden or Seki method. Different meshes and different types of elements were investigated by ENEA and ENEL.

The ABAQUS code with the rubber modelled by Seki was applied by CRIEPI to NRB and LRB; Ogden and polynomial models were applied to HDRB isolators.

The computer code verified at TARRC was MARC. Various types of material modelling, including Mooney-Rivlin and Ogden, were appraised in detail. TARRC used a benchmark problem to assess the accuracy of finite element analysis.

The Russian team verified a special non-linear elastic theory method using continuum transformation, and applied this to HRDB and LRB isolators.

The USA team conducted an experiment on ALMR high damping rubber bearings with a shape suitable for verification of computer codes and analysis methods.

(ii) Analysis methods for dynamic simulation

The computer codes verified for the isolator analysis cannot be combined with a dynamic analysis program, and a simpler isolator model is needed. All teams developed a bilinear model for all isolator types, with the exception of CRIEPI and IGCAR, who combined that model with the programs TDAPIII and CASTEM-2000, respectively.

CRIEPI verified a poly-linear model for the isolator with a superposition of elasto-plastic springs with a non-linear elastic spring.

ENEL investigated a large strain non-linear constitutive model to represent the hardening of the elastomer, which has been implemented as an user material in ABAQUS.

KAERI developed a user-defined sub-routine implemented in ABAQUS for non-linear behavior of isolation systems.

IGCAR also investigated the use of a Wen model, but so far has not used it in the analyses.

The Russian team carried out experimental tests of a low frequency 3D seismic-isolation system using an explosively driven seismic simulation test facility.

4.2. FINITE ELEMENT ANALYSIS (FEA) OF ISOLATOR BEHAVIOUR: COMPARISON THE PREDICTIONS WITH TEST DATA

The FEA concentrated on prediction of:

- vertical force-deflection behaviour
- horizontal force-deflection behaviour combined with gravity load.

Aspects investigated included:

- accuracy of axisymmetric model versus fully 3-D analysis
- accuracy of analysis based on single rubber layer
- influence of mesh density
- effect of different types of material model for rubber
- influence of finite compressibility of rubber.

4.2.1. High damping rubber bearings

The FEA predictions were concerned with the quasi-static force-deflection behaviour and did not attempt to predict the dynamic characteristics. The material models used to characterise the rubber stress-strain behaviour were:

- Rivlin polynomial series based on strain invariants
- Ogden model
- Seki model.

As an example, results of analysis of the HDRB bearing shown in Figure 4 are considered. The predicted horizontal force-deflection behaviour whilst the bearing is also subjected to vertical load is given in Figure 6 along with the force-deflection hysteresis loop for the maximum shear strain analysed (150%). As stated before the FEA is aimed only at predicting the quasi-static stiffness. The close agreement between the maximum load in the hysteresis loop and the load calculated for the maximum strain within the loop establishes the capability of the FEA. Overall the behaviour predicted by the partners agreed reasonably well with the test results.

For analysis up to moderate shear strains, it was found that the results from an axisymmetric model or a single rubber layer give reasonable results with consequent substantial savings in computing time. For prediction of the vertical stiffness, it is necessary to include the finite compressibility of rubber in the material characterization. Modelling each rubber lamination with a single layer of elements was acceptable in predicting the horizontal stiffness. At least two or three layers (the required number differed between Partners) were needed for the vertical stiffness. Provided the rubber material properties data covered a sufficient range of strains and accounted for compressibility, none of the material models chosen to fit the data gave better results overall. The agreement at large rubber shear strains (>200%) even with 3D models was less satisfactory. Moreover, the vertical force-deflection behaviour under imposed shear strains was not well predicted. TARRC found it to be sensitive to terms in the material model that are not fitted robustly by the normal characterisation data.

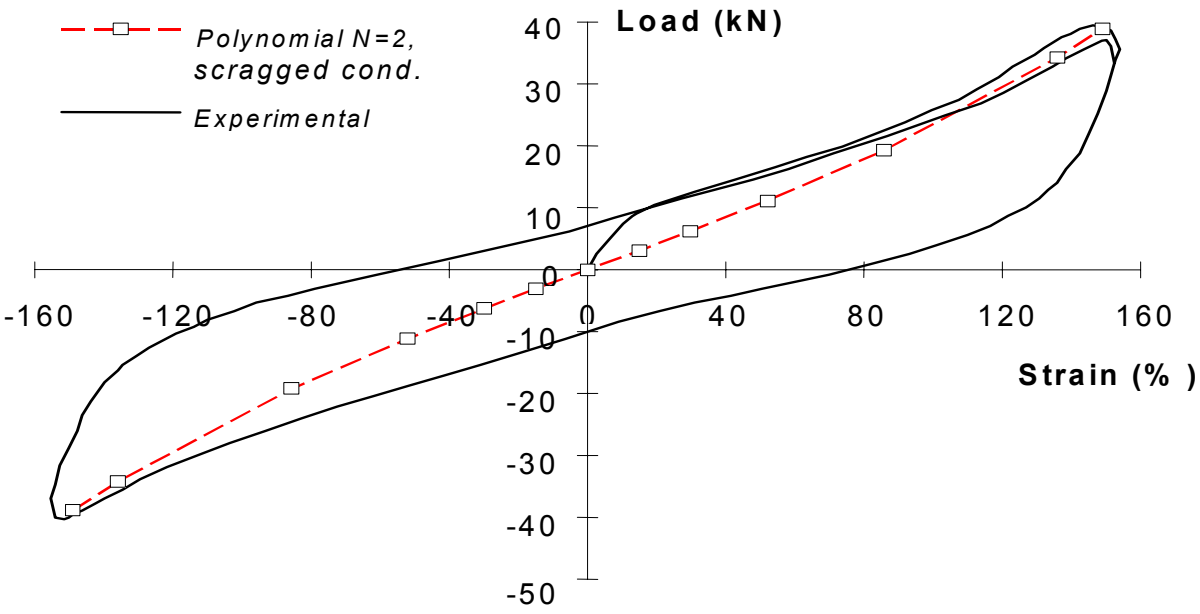

Figure 6: Comparison between measured and calculated horizontal stiffness of an ALMR HDR bearing (1:8 scale, diameter=146 mm, total height=61 mm, rubber shear modulus, G =1.4MPa, bolts attachment system) during a combined compression (44kN) and 150% shear strain test performed at EERC.(3-D analysis; the deformed mesh is illustrated in Fig. 5).

FE modelling of elastomeric isolators requires an appropriate choice of strain energy function able to describe the non-linear behaviour of elastomers over a wide range of strains and different types of deformation. The TARRC studies included detailed assessment of how well the two functions commonly used — Ogden and Rivlin polynomial series — fit experimental stress-strain data; in addition a more recently proposed function was assessed. The work confirmed that the Ogden and Rivlin functions are unable to model well the stiffening of filled elastomers (as used in the fabrication of isolators) at low strains. This deficiency is not a major problem if the FE analysis is mainly concerned with deformations causing high strains, provided the function coefficients are selected to fit the rubber behaviour in the strain range of principal interest. The Odgen function suffered from the additional disadvantage that calculation of the optimum coefficients was difficult. The investigation showed that uniaxial test data (and this includes equibiaxial tension which is equivalent to unaxial compression)

can be modelled well by a function of the strain invariant I_1, alone. In order to fit the stiffening at low strains the function has to involve fractional powers. A function of I_1 alone, however, may only be adequate for predicting the forces in the principal deformation direction.

4.1.2. Lead rubber bearings

In addition to the factors that need to be taken into account for HDRB, the LRB also require consideration of the behaviour of the lead and how to treat the lead-rubber interface. The horizontal force-deflection behaviour was predicted quite well by the Partners up to large (400%) rubber shear strains. The vertical force-deflection analysis (for zero shear) also agreed well with test data. One comparison between FEA calculations and observations for the horizontal behaviour is shown for an LRB in Figure 7. Because the hysteresis derives from the yield of the lead, the quasi-static force-deflection curve should be close to the hysteresis loop except at very small strain; this is seen to be the case.

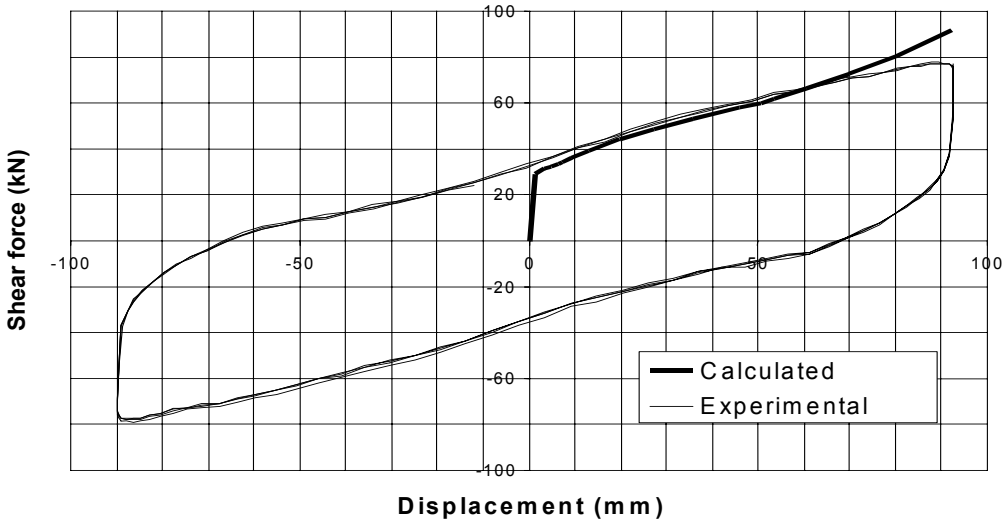

Figure 7: Comparison between the measured and FEA calculated shear force-displacement behaviour for LRB. Diameter 280mm. Lead Plug diameter 70mm. Total Rubber thickness 46mm(complete FEM, 3D, mesh density:11,904 solid elements and 19774 nodes).

With the analyses of the LRB, it was concluded from the Partners' results that:

- the lead may be modelled as elastic — perfectly plastic
- friction between lead plug and rubber may be ignored
- axisymmetric FE models work well
- single rubber layer models predict horizontal stiffness reliably.

The FE analysis of the whole of the rubber bearing carried out at ENEL,ENEA,TARRC and IGCAR (Table 1) showed that the analysis of a single layer of the bearing can be used to predict the horizontal deformation of the bearing by scaling up the results. This is significant in the sense that it reduces the computational time greatly. Further, this model can be used effectively to validate the material behaviour.

TABLE 1. COMPARISON OF THREE MODELS UNDER COMBINED COMPRESSION (50 KN) AND SHEAR UP TO 40% SHEAR STRAIN

Horizontal Displacement	Shear Force [kN]						
	3-D model		Axysimmetric model		Single Layer model		Experiment
[mm]	Poly.	Ogden	Poly.	Ogden	Poly.	Ogden	
15.0	2.0	2.05	1.882	2.042	2.0	2.0	3.61
30.0	4.2	4.25	4.007	4.237	4.2	4.2	4.68
60.0	10.1	10.1	10.17	9.742	10.4	10.2	9.86
90.0	19.9	18.1	20.02	18.69	20.4	19.6	22.2
120.0	34.0	32.0	34.92	32.92	36.0	34.0	41.2

4.2.3. Benchmark problem

Before the analysis of critical components it is desirable that the FE solvers are validated by benchmark problems. Within the Project one has been identified and the results from two FE programmes — MARC and ABAQUS — compared respectively by TARRC and ENEL with analytical solutions. The problem is the torsion of a cylinder for which Rivlin has given a solution. The FEA determined the couple to deform the cylinder and the axial load required to keep the length constant during torsion. Results for the couple within 5% of the analytical solution, and for the axial load within 10% could be obtained without resort to a very fine mesh provided certain types of element were avoided. The reduced integration solid element in MARC gave relatively poor results.

4.3. RESPONSE OF ISOLATED STRUCTURES

4.3.1. Simplified model of HDRB and LRB

The determination of the response of isolated structures requires a simplified model of the dynamic horizontal force-deformation characteristics of the isolators. The aim here is not to predict the isolator behaviour as with the FEA, but simply to fit the test data. The model has to take account of the damping provided by the isolator, and ideally its non-linear deformation behaviour. One type consists of an elastic spring (linear or multi-linear) in combination with a dashpot element. A more realistic model is provided by an elastic spring, in parallel with one or more elasto-plastic elements to model the damping. The ability of such a multi-linear elasto-plastic model (MEP) with a single elasto-plastic element to fit large shear strain hysteresis loops for an HDRB is shown in Figure 8. It is apparent that the hysteresis at large strain is underestimated. More elasto-plastic elements would improve the fit; such a model has been developed and implemented within the ABAQUS code by ENEL.

It has been further refined to take account of the stiffening of HDRBs seen at large shear strains. The good fit obtained, even into the region of stiffening behaviour, to observed shear deformation hysteresis loops for an HDRB (rubber shear modulus, G = 0.8MPa) is seen in Figure 9. The model is equally well applied to LRBs.

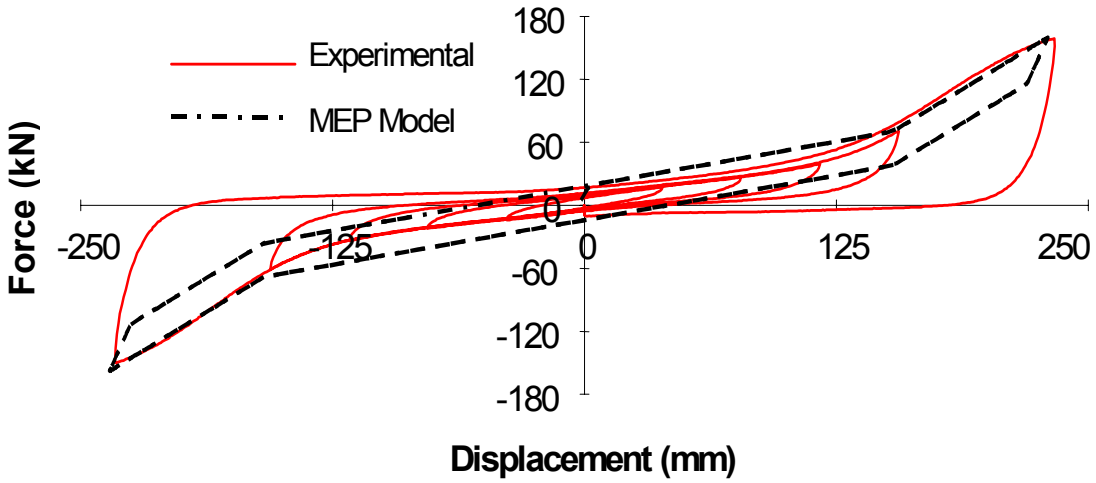

Figure 8: The hysteresis loop of HDRB fitted by MEP simplified model with a single elasto-plastic element.

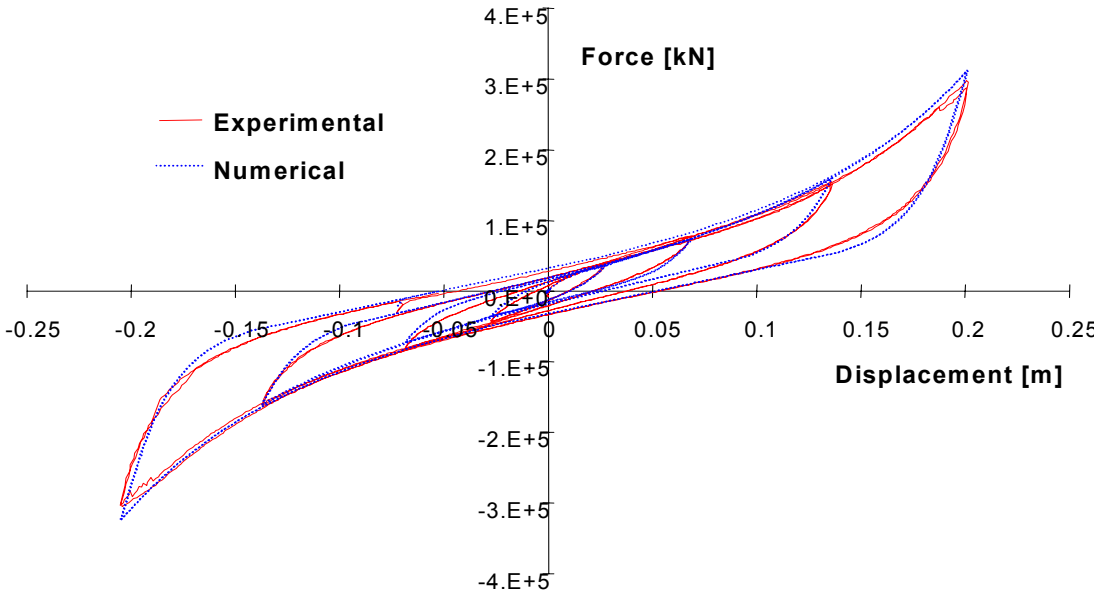

Figure 9: Experimental and numerical hysteresis loops for a HDRB. (G = 0.8 MPa).

4.3.2. Rigid mass

This was tested at CRIEPI in 1989. The structure consisted of a concrete frame of 178kN weight and size 3 × 2.1 × 2.8 (height)m. It was isolated by 8 LRBs. Prediction of an acceleration time-history using the refined multi-element elasto-plastic model is compared in Figure 10 with the observed history. The fit is seen to be very good.

The predictions of the Partners generally agreed well with observed parameters. An exception reported by KAERI was the response to beyond design level earthquakes for which the large rotational motion of the mock-up places isolators in tension; the predictions became sensitive to the vertical stiffness chosen for the isolators.

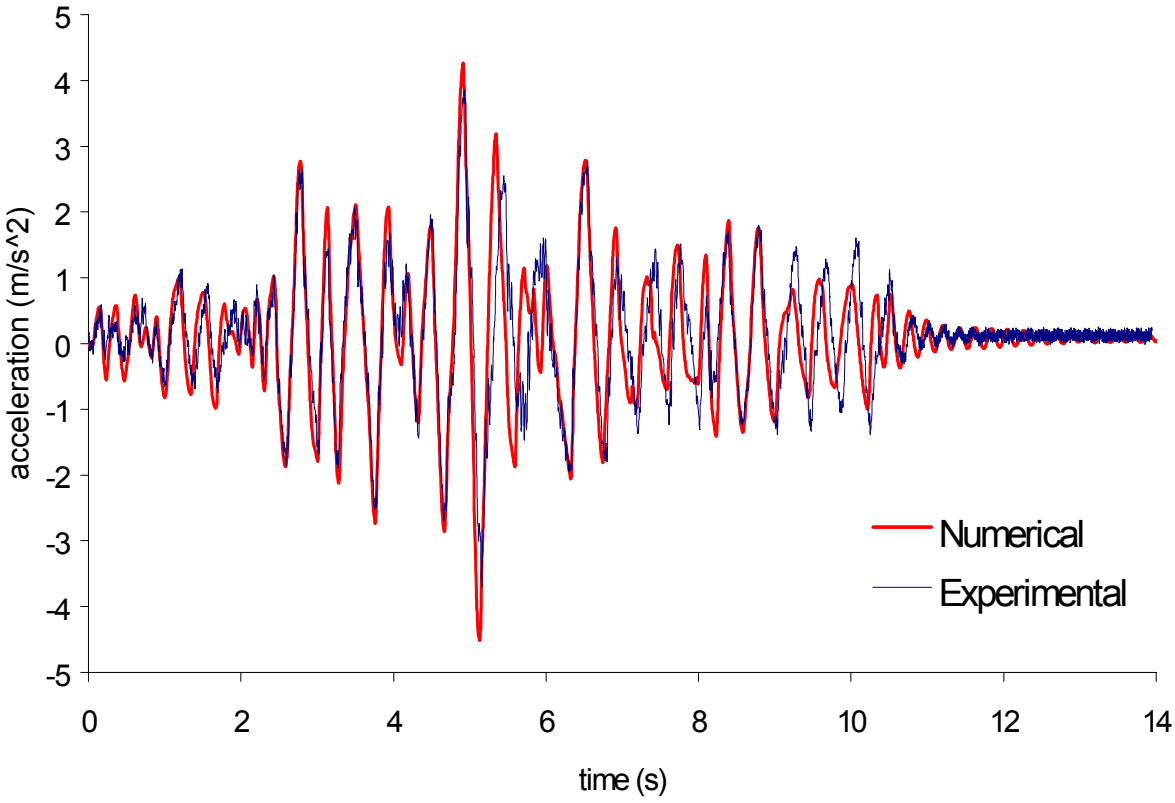

Figure 10: Experimental and calculated (ENEA/ENEL) acceleration-time histories for rigid mass isolated by LRBs subjected to the design earthquake record.

4.3.3. Steel frame structure (MISS)

The fit is seen to be very good. The predictions of the Partners generally agreed well with observed parameters. An exception reported by KAERI was the response to beyond design level earthquakes for which the large rotational motion of the mock-up places isolators in tension; the predictions became sensitive to the vertical stiffness chosen for the isolators.

MISS is a steel frame structure mock-up with a rectangular base of 2.1 m × 3.3 m, and four storeys, with an interstorey distance either of 0.9 m or of 1.1 m. It can support up to 20 concrete masses, each weighting 13 kN. The frequency of the structure can be chosen over quite a large range, depending on the interstorey distance and the number of masses used and their disposition. It has been tested at ENEA on the shaking-table both fixed-base and isolated. For the latter, it was mounted on 6 HDRBs (125 mm diameter, 30 mm total rubber height) fabricated with a soft rubber compound (G = 0.4 MPa) and each attached by bolts and dowel.

The observations of bearing displacement whilst MISS was subjected to the 1981 Calitri ground-motion record are compared (Figure 11) with predictions using the refined ENEL model mentioned above. The agreement is seen to be good.

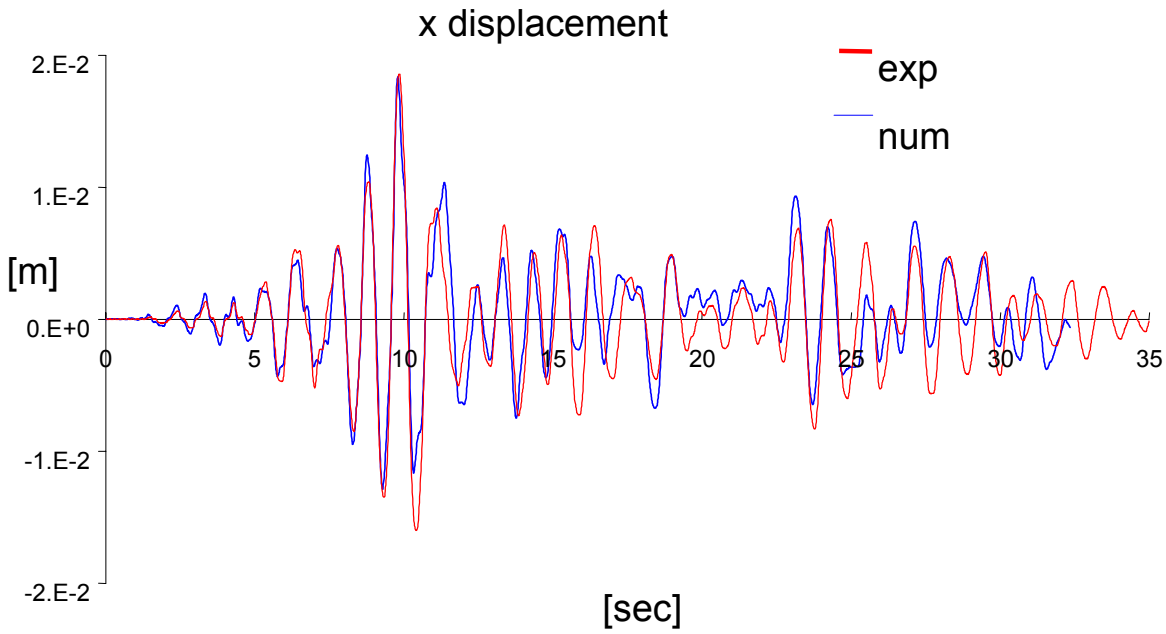

Figure 11: Bearing displacement (x component)-time history for MISS steel frame mock-up isolated on HDRBs and subjected to the 1981, Calitri record. (ENEA/ENEL).

Generally, the Partners' predictions of the response of the isolated structure agreed well with the shaking-table observations except for the high frequency content. The calculated response of the fixed-base structure, as reported by KAERI for example, showed more significant discrepancies.

4.3. CONCLUSIONS

Numerical simulation of rubber bearings by FE code packages such as ABAQUS gives satisfactory results as long as material properties are evaluated properly and a suitable strain energy density function and mesh density is selected.
Rubber material can be characterized for FE analysis by forms of the strain energy density: such as the Rivlin strain invariant polynomial or Ogden function. Generally, either provides a fit to the rubber stress-strain data adequate for modeling the horizontal force-deflection behaviour of bearings.

Except for very coarse meshes, the density did not significantly influence the vertical force-deflection behaviour in the absence of shear. At shear deflections large enough to produce severe distortions of the rubber near the free surface, a fine mesh, at least in the highly distorted regions, is needed accurately to predict the shear stiffness and the height drop under combined shear and compression.

The analysis of a single layer of the bearing can be used to predict the horizontal deformation of the bearing by scaling up the results. This is significant in the sense that it reduces the computational time greatly. Further, this model can be used effectively to validate the material behaviour. However, more detailed three-dimensional FEM is necessary to analyse the stress distribution within the isolator or to evaluate the behaviour of the bearing at very large deformation.

The achieved results confirmed that overall FE methods are useful tools for both the detailed analysis of elastomeric bearings and improving their. They permit a considerable reduction of the number of validation tests to be performed.

When the same input data was used all codes provided predictions of the horizontal force-deformation characteristics of all isolators consistent with the test data except at very small deformation.

All predictions of vertical behaviour in the absence of horizontal displacement were consistent with the test data provided the compressibility of the rubber is accounted for. Some deviation of the numerical prediction of vertical displacement when compression loading is combined with shear was found even after allowing for compressibility of the rubber

The modelling of lead proved to be a problem for all teams as the material is deformed in shear within the isolators, whereas the codes require as input data in tension. Continuing research is needed on the accurate prediction of isolator hysteresis. The benchmark torsion problem proved to be an useful tool for the assessment of the accuracy of the two main computer codes MARC and ABAQUS.

Simplified model of HDRB and LRB have been used successfully to predict the response of two base isolated test structures subjected to earthquake inputs in shaking-table tests. The use of the bilinear model was very accurate in predicting the dynamic response of the rigid mass shake-table model up to the level of design and can be considered reliable for use in design. For beyond design basis predictions multi-linear, exponential modelling were successfully used, with vertical motion due to rocking incorporated through vertical springs. For the flexible structure the response was accurately predicted if the modelling of the superstructure is accurate. To predict floor responses, an improved model of the isolation system is needed.

The CRP has shown that predicting the force-deflection characteristics of isolators, and calculating the response of isolated structures can often be done with good results. Areas requiring further work have been identified.

4.4. RECOMMENDATIONS FOR FUTURE RESEARCH AND DEVELOPMENT WORK

(i) General

The main recommendation derived from the results of the CRP is that the study of isolated nuclear structures should be continued and extended to non-seismic extreme load conditions.

(ii) Isolator modelling

The refinement of the characterization of hyper-elastic behavior of the elastomer is needed to predict multi-directional response under combined loading. The modelling of the flexibility of the reinforced plates and connecting plates should be improved. Investigation of the impact on material characteristics of the special environmental conditions of nuclear facilities is needed. Investigation of the finite element prediction of isolator failure mechanisms is needed.

(iii) Dynamic simulation

Simple, accurate, reliable models for the isolator response over a wide range of multi-directional deformation is essential for accurately predicting floor response spectra and other dynamic design quantities. Future research work should also look at the development of alternative seismic protective technologies such as passive, semi-active and active control for the seismic protection of nuclear facilities and components.

(iv) Pseudodynamic method using

The pseudodynamic method to test large scale structures has been validated for base-isolated civil structures and should be extended to isolated nuclear facilities. The influence of vertical ground input on the response of all internal components of an isolated nuclear structure should be investigated.

BACKGROUND PAPER

ANALYSIS METHODS FOR PREDICTING THE BEHAVIOUR OF ISOLATORS AND FORMULATION OF SIMPLIFIED MODELS FOR USE IN PREDICTING RESPONSE OF STRUCTURES TO EARTHQUAKE TYPE INPUT

Tun Abdul Razak Research Centre, United Kingdom

Abstract

This report describes the simplified models for predicting the response of high-damping natural rubber bearings (HDNRB) to earthquake ground motions and benchmark problems for assessing the accuracy of finite element analyses in designing base-isolators.

1. INTRODUCTION

The first part is directed towards accounting for non-linear stress-strain behaviour of the base-isolators when predicting the response of the isolated structures to earthquake type inputs. A simplified model for the isolators capable of representing the major features of their behaviour is therefore discussed. The remaining part is aimed at the use of finite element analysis (FEA) in designing base-isolators. In this area the behaviour of the isolators when subjected to vertical and horizontal deformations is of interest. Currently two main commercial codes capable of solving large deformation non-linear problems are available. Both codes allow the use of either Rivlin or Ogden strain energy functions in modelling the rubber. Alternatively, a user defined strain energy function can be used. The choice of the appropriate strain energy function and mesh elements density is an important area of research. There is also an interest in establishing the degree of agreement between the predictions of different finite element codes.

This chapter therefore discusses the following:

(i) Simplified models for predicting the response of high-damping natural rubbers to earthquake ground motions.
(ii) Appropriate choices of strain energy function and mesh elements density for modelling the behaviour of non-linear rubbers using finite element analysis.
(iii) Benchmark problems for assessing the accuracy of finite element solvers. The particular example of the torsion of an elastomeric cylinder is considered.
(iv) Finite element analysis of test bearings.
(v) Predicting the stiffness of an isolator under compression and shear.
(vi) Compression stiffness of a rubber pad bonded between extensible layers.

2. SIMPLIFIED MODELS

2.1. Introduction

Prediction of the response of an isolated structure to earthquake ground motions requires a simplified model for the isolators that enables the efficient use of computer processing time. The majority of the commercially available software currently used by designers for predicting the response of conventional structures to seismic inputs has the

facility to model the isolators either as a combination of springs and dashpots or as a combination of elasto-plastic elements. he studies presented here discuss the source of the non-linearity in the force-deformation behaviour of the isolators. It uses a curvilinear hysteretic model to predict the response of a typical High Damping Rubber Bearing (HDRB) to earthquakes at levels corresponding to the design level and much higher. These predictions are used as a basis to identify the degree of reliability of the simpler models currently available.

2.2. Non-linearity of High Damping Natural Rubbers (HDNR)

The use of reinforcing fillers, such as carbon black of small particle size, leads to non-linear stress-strain behaviour in high damping natural rubber compounds. Figure 1 shows the hysteresis loops for a typical HDNR compound when subjected to sinusoidal excitation in simple shear. The non-elliptical form of these loops is a manifestation of the non-linear stress-strain behaviour of the compound. The use of reinforcing fillers also leads to strain history effects, as is seen by the difference between the two sets of loops. Departure from a linear force response during a sinusoidal displacement at fixed amplitude may be quantified by measuring the harmonic components of the response (Fig. 2). For amplitudes up to 100-150% shear strain, the level of the third and fifth harmonics are relatively modest and only when the strain amplitude is increased beyond this level do the higher harmonics become stronger.

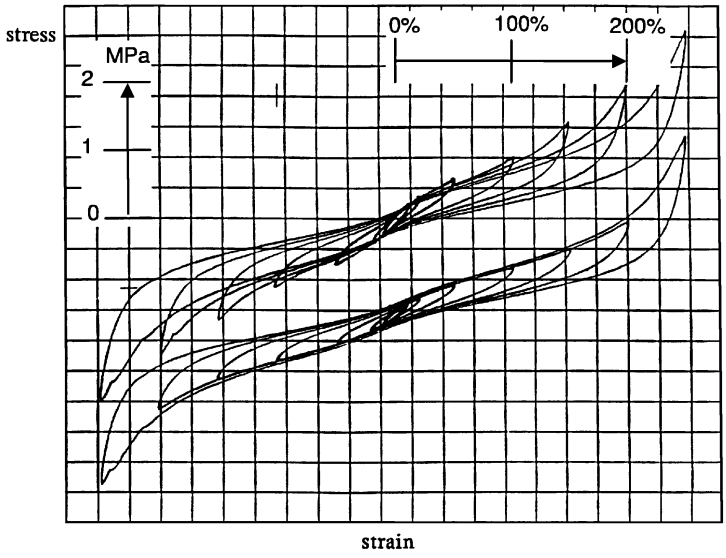

FIG. 1. Shear stress-strain loops of a typical HDNR compound tested sinusoidally at 0.5Hz. Top set – Sample tested at successively larger amplitudes. Bottom set – The same sample tested at successively larger amplitudes with a 250% scragging strain interposed between each test.

Experimental results have shown that when a carbon-black filled vulcanizate is subjected to a certain complex waveform, it can present a linear dynamic behaviour (Harris, 1987). Two sinusoidal waveforms were superimposed, one with high amplitude and low frequency and the other with high frequency and low amplitude. Using Fourier analysis to decompose the force signal into its components, it was observed that whenever the frequencies or amplitudes of the two sinusoidal inputs were such that there were no strain retractions due to the low amplitude waveform, the stiffnesses associated with the inputs were equal. The non-linearity in the dynamic behaviour of a carbon-black filled rubber thus appears to be a consequence of strain retraction.

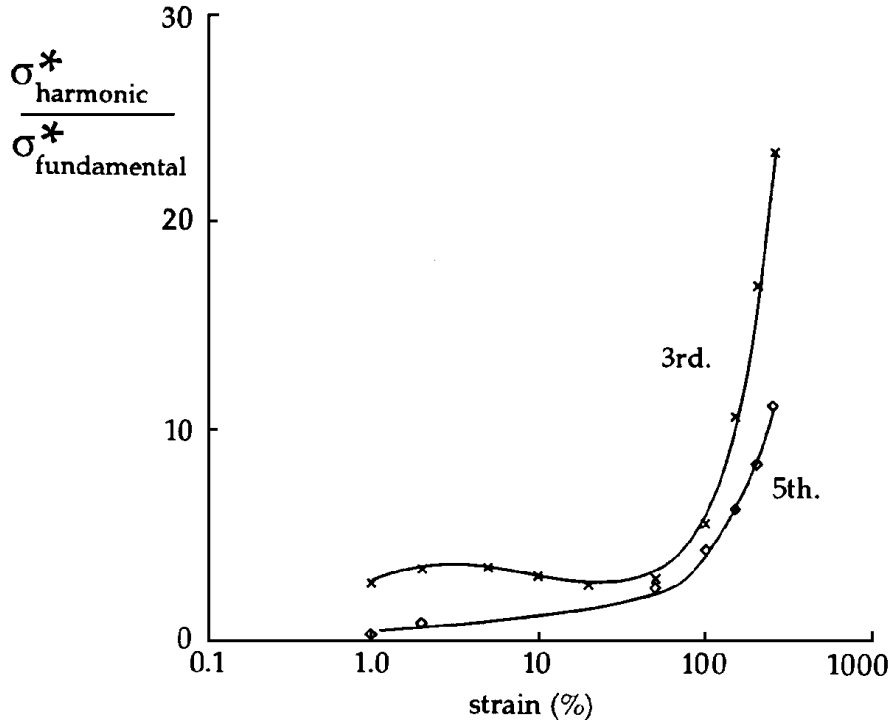

FIG. 2. Amplitude of third and fifth harmonics of stress response as a percentage of first harmonic for the same tests as used to generate the top set of loops in FIG. 1.

Experiments have been performed to study more closely the extent to which HDNR can be modelled linearly (Ahmadi et al., 1991). A test piece of HDNR was subjected to a shear-displacement history representative of that experienced by an isolator during an earthquake, and the resulting shear-force history was monitored. The chosen displacement history was calculated by applying El Centro 1940 earthquake to a single degree-of-freedom mass on a Kelvin model system with a natural frequency of 0.5Hz and damping 0.1 of critical, and taking the difference between the ground and the mass displacements. The displacement history obtained had a very strong component at the isolation frequency and approximated to a modulated, 0.5Hz sinusoidal signal as anticipated theoretically (Housner, 1959) and observed in shaking-table experiments (Derham and Thomas, 1980). The observed force signal corresponding to the displacement history was first analysed by dividing the force level at peaks (and troughs) by the corresponding peak displacements. The resulting stiffness values were compared with 6th cycle stiffnesses obtained from standard sinusoidal tests. The two sets of data were remarkably similar showing that the degree of non-linearity in the dynamic behaviour of the material is retained during an earthquake. Nevertheless, the force response history in this case is predicted quite well using a simple linear Kelvin model provided that the parameters in the model are set appropriately.

Generally, for seismic isolation only the maximum forces, acceleration and displacements are of interest to the designer. Therefore, if the modulus appropriate to the maximum strain amplitude occurring during an earthquake is chosen, the linear Kelvin model may be expected to give a reasonable prediction of the level of the peak force experienced by the structure. Setting the modulus values involves an iterative procedure. For earthquakes comparable to the design level earthquake, the response is usually obtained after one integration run due to the relative insensitivity of the stiffness of the isolators to strain amplitude at around the design level (i.e. 100%).

For larger earthquakes (of the order of the maximum probable earthquake) linear analysis becomes less reliable; moreover, the harmonics generated during the response by the material non-linearity may have to be considered. A non-linear hysteretic model capable of catering for the large strain non-linearity of HDNR may therefore be required.

2.3. Curvilinear hysteretic model

The model, a refinement of the multi-linear model described by Ahmadi et al. (1996) describes the shear stress-strain behaviour of HDNR. In using the model to predict the response of an isolation system to earthquakes, the assumption is made that the horizontal force-deflection behaviour of the isolators is well described by the same model. It is based on the observed stress-strain loop of the compound tested in simple shear at a frequency of 0.5Hz and at the largest strain amplitude of interest; the loop after several cycles is the one taken. The upper half of the model hysteresis loop (Fig. 3) partly follows the curve τ_1 and the lower half the curve τ_2. The two curves are assumed to possess a centre of symmetry about the origin, and are constructed from the observed hysteresis loops. The method of calculating the retraction parts of the loop (the dashed lines in Fig. 3) and the stress response to an arbitrary strain history is described below.

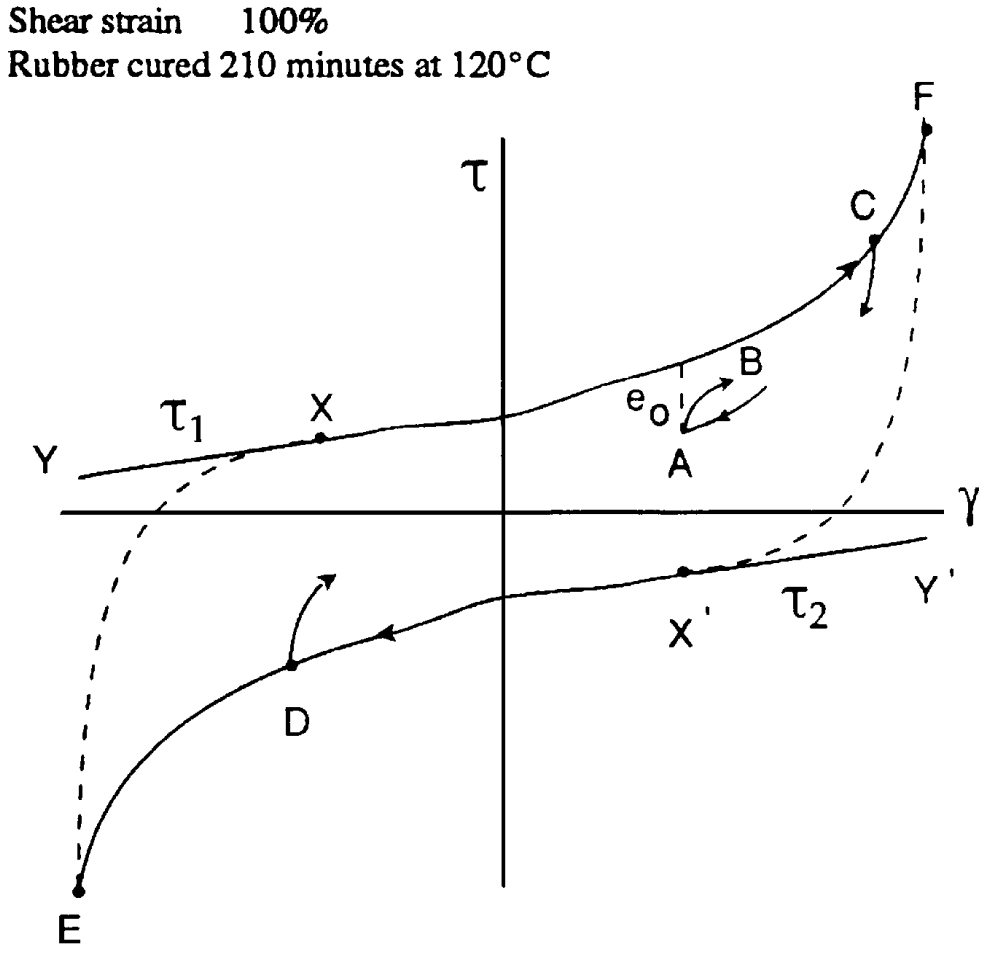

FIG. 3. Schematic diagram of stress (τ) - shear strain (γ) loop envelope used in curvilinear hysteretic model.

During a general deflection-time history, a strain reversal may occur at any point such as A within the model loop. For the case in which the strain changes from decreasing to increasing (here the sign attached to the strain has to be taken into account) i.e. for loading, the amount e_o by which the stress at A falls below τ_1 (extrapolated to lower strains if necessary) is considered. The loading path B is defined by the relation:

$$\frac{d\tau}{d\gamma} = \frac{d\tau_1}{d\gamma}\left(1 + G_1\frac{e}{e_o}\right) + L\frac{e}{e_o} \qquad (1)$$

$$\text{where } L = G_2\left|\frac{d\tau_1}{d\gamma} - \frac{d\tau_2}{d\gamma}\right|$$

and e is the amount by which the stress at strain γ differs from that given by the curve τ_1; G_1 and G_2 are constants. If after reversing the direction of deformation the strain is decreasing, the subscripts 1 and 2 are reversed in equation (1), and e_o and e are measured from the curve τ_2.

Each strain reversal defines a new starting position. Both the retraction path from any point such as C or D on the loop envelope, and the retraction parts of the loop envelope beginning at the points E and F (the dashed lines in the figure) are assumed to be described by equation (1). The model loop for an intermediate strain amplitude is determined from the curves τ_1 and τ_2 and the retraction curves calculated from the appropriate strain reversal points. The curve τ_1 between the points X and F is constructed from the corresponding section of the observed hysteresis loop. The waisting of the observed loop is followed in determining τ_1 to avoid overestimation of the damping. The points X and X' are chosen so that they are outside the waisted part of the loop. The XY section of τ_1 and the corresponding section X'Y' of τ_2 are straight lines of identical slope. Varying the magnitude of the slope provides fine adjustment enabling the model loops to give the best representation of the strain amplitude dependence of the loss factor. The parameters with the major influence on the magnitude of the loss factor are G_1 and G_2. These are adjusted to give an area for the model loops as close as possible to that of the observed loops. The lower strain amplitude loops (γ_{max} typically less than 150%), for which there is no significant upturn, are influenced primarily by G_1 and the higher strain ones by G_2. For the observed loops shown in Fig. 4, the fitted values for G_1 and G_2 are 0.9 and 4.5 respectively. Figures 5 and 6 show the variation of dynamic properties and the ratio of the third and fifth harmonic to the fundamental in the sinusoidal stress response with shear strain amplitude for both experimental data and predictions using the model. The experimental loops and those predicted by the model are shown for 100 and 300% strain amplitudes in Fig. 7.

The double shear test piece used to generate the observed loops in Fig. 4 was later subjected to a history involving reversals within the main loop. The waveform was scaled for each test so that the peak strain in the rubber was varied from 50% to 300%. The experimental and predicted hysteresis loops are shown in Fig. 8 for peak strains in the rubber of 100 and 300%. The predicted behaviour agrees reasonably well with the observations, except that the observed damping within the subsidiary loops is underestimated by the model. The discrepancy suggests that some rate-dependent damping should be added to the model.

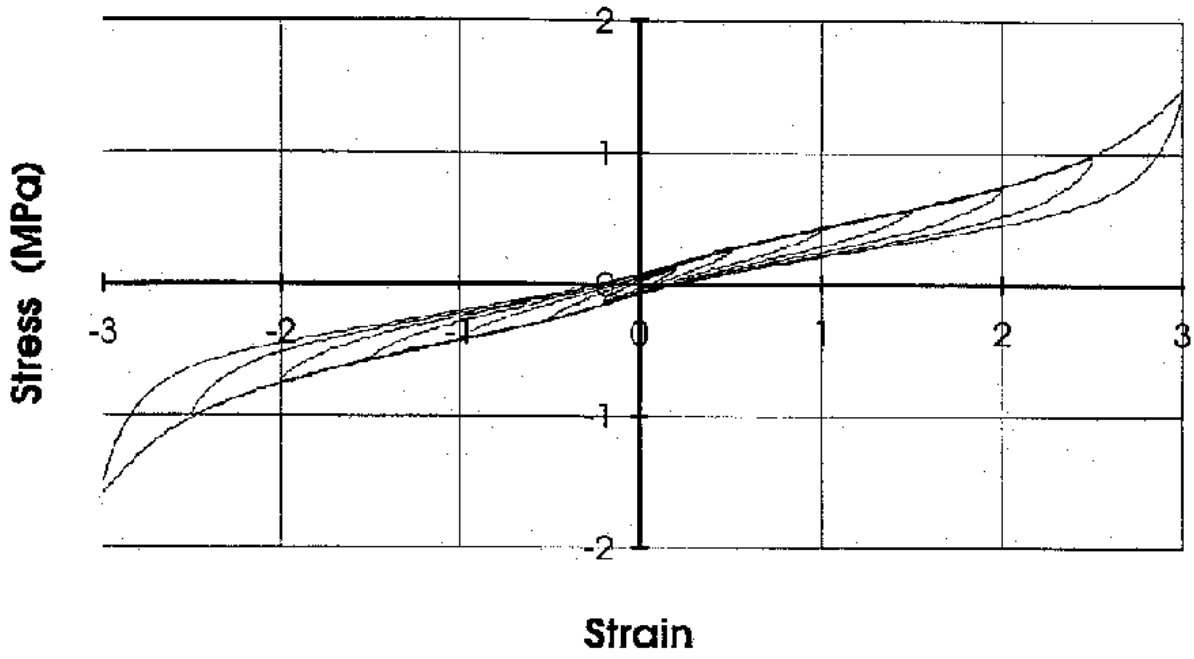

FIG. 4. Observed shear stress-strain loops for a low stiffness HDNR compound tested sinusoidally at 0.5Hz at successively larger strain amplitudes from 20 to 300%. Six 300% strain amplitude cycles followed by 1 minute pause were interposed between each strain test. $|G^*|$ at 100% = 0.46Mpa.

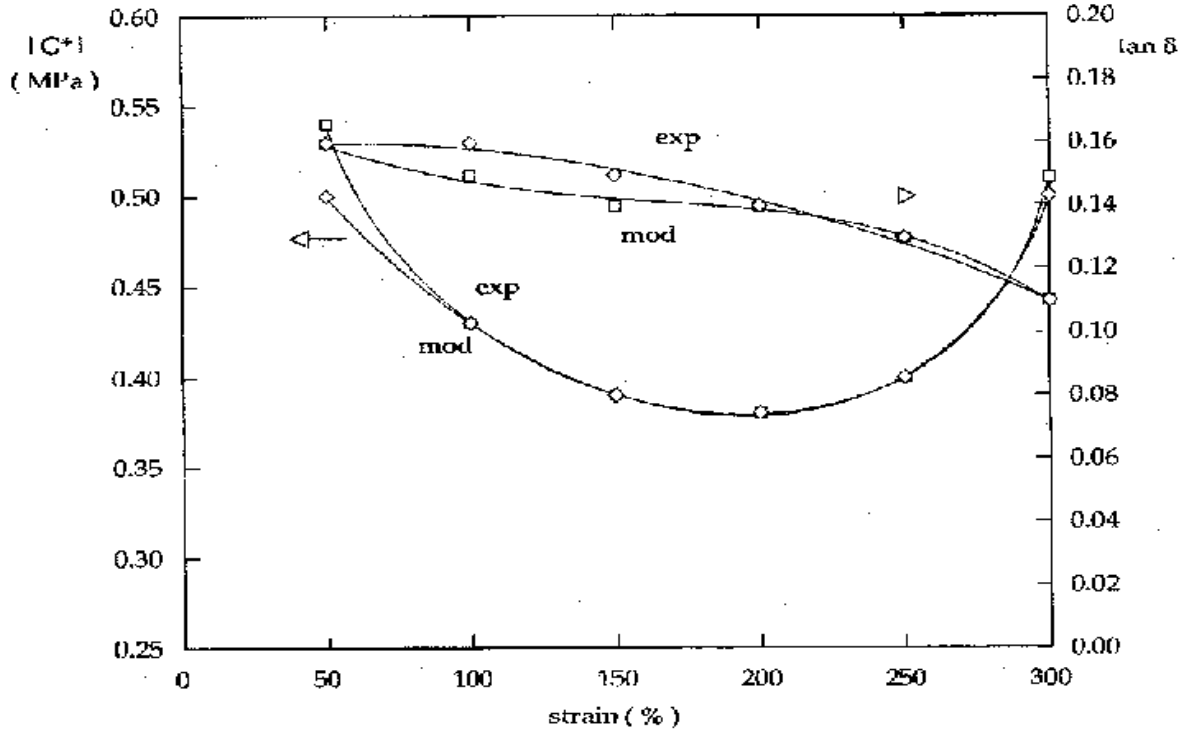

FIG. 5. Variation of secant shear modulus $|G^*|$ and $\tan\delta$ with shear strain measured experimentally (exp) and predicted using the curvilinear hysteretic model (mod) for the HDNR shown in FIG. 4.

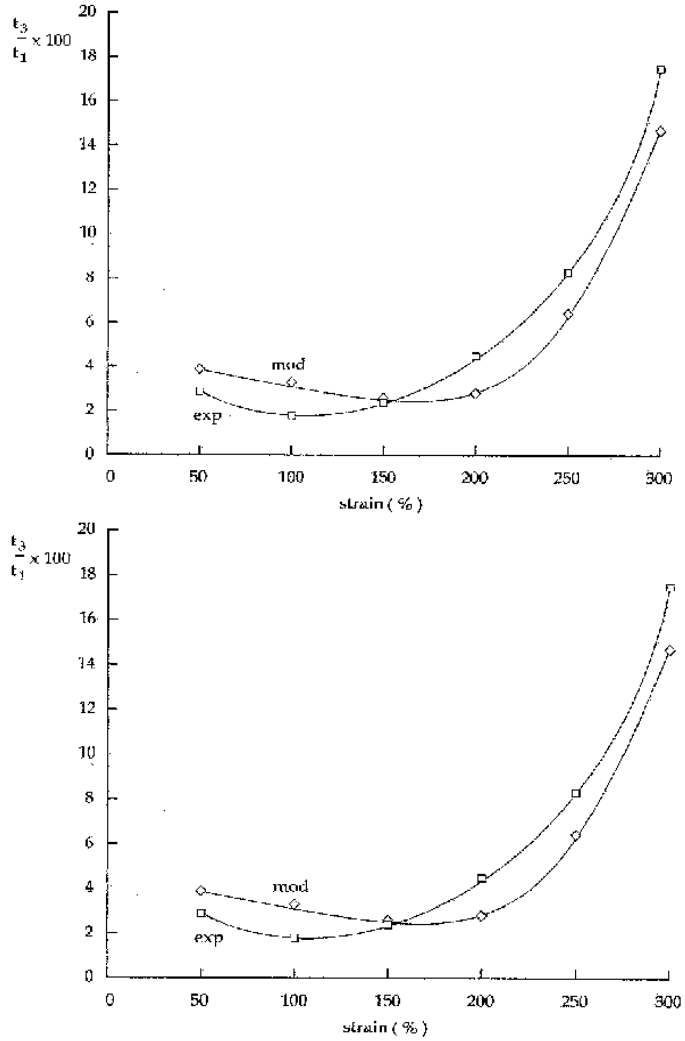

FIG. 6. (top) Variation of the relative strength of third harmonic stress response to a sinusoidal deformation with shear strain calculated using experimental loops (exp) and loops generated from the curvilinear model (mod). (bottom) Similar to (a) but for the fifth harmonic.

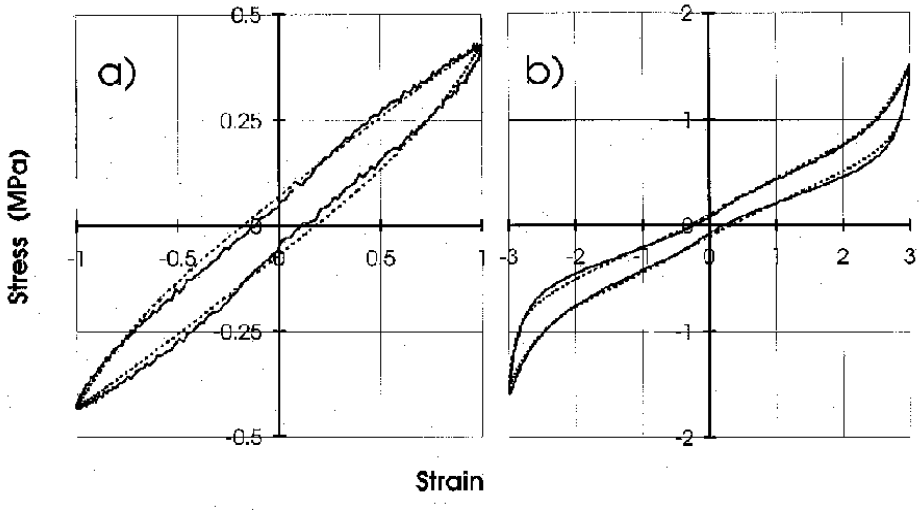

FIG. 7. The experimental hysteresis loops (–) for (a) 100% and (b) 300% shear strain amplitude shown in FIG. 4 compared with those predicted by the curvilinear hysteretic model (- - -) with $G_1 = 0.9$ and $G_2 = 4.5$.

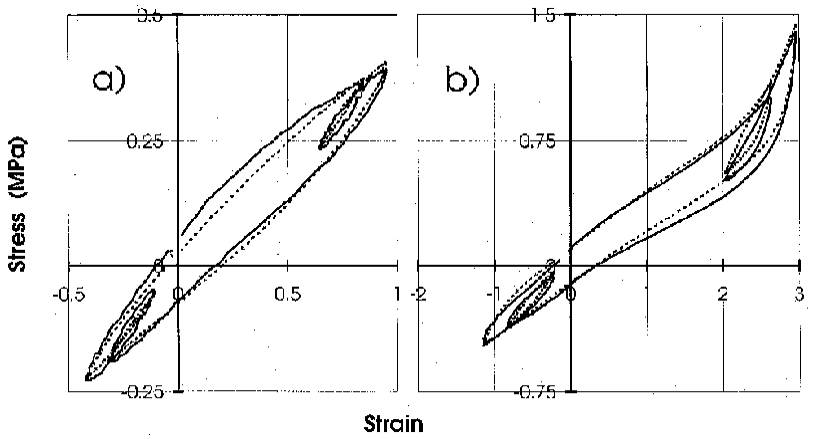

FIG. 8. Experimental loops (-----) and loops calculated using the curvilinear hysteretic model for the HDNR (- - - -). The testpiece was subjected to superimposed sinusoidal deformations. The peak shear strains in the HDNR were (a) 100% and (b) 300%.

2.4. Results: Predicted response to earthquakes

2.4.1. Model parameters

The curvilinear model fitted to an intermediate modulus HDNR ($|G^*|$ = 0.64MPa at 100% shear strain 0.5Hz) whose stress-strain loops are similar to those shown in Fig. 4 is used to predict the response of a rigid structure to large earthquakes. The horizontal force-deformation behaviour of the isolators is assumed to be proportional to the HDNR stress-strain behaviour as given by the model. The equation of motion is integrated numerically using the instantaneous value of the restoring force from the model. The predictions of the curvilinear hysteretic model are compared with those calculated using a linear spring and dashpot (Kelvin viscoelastic) model for the HDNR and isolators. The linear parameters are calculated based on the secant linearization method (Ahmadi et al., 1996).

The isolation systems analysed are such that they give a natural frequency of 0.5Hz at a rubber shear strain of 100%; thus the secant stiffness at that rubber strain is π^2M where M is the mass of the isolated structure. The horizontal component earthquake records investigated are El Centro (SOOE) and records derived from the Pacoima and Parkfield strong motions. Those three records unscaled are each taken as design level earthquakes. For each, the peak isolator displacement is calculated using the linear spring and dashpot model with the parameters set for 100% rubber shear strain. By making the rubber thickness in the isolators equal to that displacement, the latter corresponds to the 100% strain assumed in setting the linear parameters.

2.4.2. Design level earthquakes

The response of the three isolators to the corresponding design level earthquake records as calculated by the curvilinear hysteretic model is given in Tab. 1; included in the table are the calculations using the linear model with the 100% strain parameters. It is apparent that at the design level the linear (viscous damping) and curvilinear (hysteretic damping) calculations differ by up to 15%; only in the case of El Centro are the linear values larger and thus conservative (it is assumed in the discussion that the curvilinear (hysteretic damping) model gives values closer to what would be observed).

TABLE 1. PEAK RESPONSES TO DESIGN LEVEL EARTHQUAKES

	Peak responses to design level earthquakes		
Responses	Strong motion record		
	El Centro	Parkfield	Pacoima
Curvilinear/hysteretic model			
Acceleration ms^{-2}	1.34	0.99	0.77
Displacement mm	131	105	82
Linear/viscous model			
Acceleration ms^{-2}	1.54	0.93	0.72
Displacement mm	151	90	69
Bilinear model			
Acceleration ms^{-2}	1.20	1.00	0.79
Displacement mm	112	104	83

2.4.3. Large earthquakes

The response of the three isolators to the corresponding earthquake records listed in Tab. 1 but scaled by factors of 2 and 2.5 are given in Tab. 2. Calculations for the curvilinear hysteretic and linear viscous models are presented. For the latter the secant parameters are determined at the rubber shear strain corresponding to the maximum bearing displacement; an iterative procedure is used to obtain a self-consistent result. For the intermediate stiffness compound investigated here, the responses (both structural acceleration and bearing displacement) to large earthquakes predicted by the linear model are smaller than the predictions of the curvilinear model for all the records in Tab. 2. The linear model predictions for the 2.5 × scaled El Centro record are very low the acceleration response being under-predicted by nearly 40%. The response acceleration time-history calculated with the curviliner model shows the stiffening of the isolator force-deflection characteristic to come strongly into play for this record. Overall the results show that though linear calculations for large earthquake inputs may generally be within 20% of non-linear ones, exceptions certainly exist, and so linear analysis results need to be used with caution. The discrepancies are generally only slightly higher than those found for a soft (less non-linear) HDNR compound (Ahmadi et al., 1996), again suggesting that the difference in the way the damping is modelled as well as the introduction of non-linearity in the force-deflection behaviour is important.

3. CHOICE OF A STRAIN ENERGY FUNCTION

3.1. Introduction

The stress-strain behaviour of high damping rubbers, commonly employed in seismic isolation, is highly non-linear. Finite element modelling of an isolator requires an appropriate choice of strain energy function which correctly described the non-linear behaviour over a broad range of strains and types of deformation. Two types of function based on a Mooney-Rivlin series and the Ogden strain energy function, are both commonly incorporated into finite element codes. Also considered was an equation proposed by Gregory et al. (1997) which could be utilised by Finite Element Analysis with the aid of a user subroutine. The performance of these functions was assessed by examining the quality of fits to experimental data for various types of deformation.

TABLE 2. PEAK RESPONSES TO EARTHQUAKES AT ABOVE DESIGN LEVEL

	Peak responses to earthquakes at above design level		
Responses	Strong motion		
	El Centro	Parkfield	Pacoima
Curvilinear model		Scaling factor × 2	
Acceleration ms^{-2}	3.25	2.15	1.37
Displacement mm	349	219	154
Linear model			
Acceleration ms^{-2}	3.22	1.70	1.23
Displacement mm	336	185	135
Curvilinear model		Scaling factor × 2.5	
Acceleration ms^{-2}	6.52	3.66	2.00
Displacement mm	453	265	183
Linear model			
Acceleration ms^{-2}	4.02	2.90	-
Displacement mm	382	242	-

3.2. Fit to 5-term Mooney Rivlin function (Rivlin & Saunders, 1951; Treloar, 1975)

The general form of the Mooney-Rivlin strain energy function is:

$$W = \sum_{i+j=1}^{N} C_{ij}(I_1 - 3)^i (I_2 - 3)^j \tag{2}$$

The MARC finite element package provides a 5-term truncation of equation (2):

$$\mathbf{W} = C_{10}(I_1 - 3) + C_{01}(I_2 - 3) + C_{11}(I_1 - 3)(I_2 - 3) + C_{20}(I_1 - 3)^2 + C_{30}(I_1 - 3)^3 \tag{3}$$

where I_1 and I_2 are the first and second strain invariants:

$$I_1 = \lambda_1^2 + \lambda_2^2 + \lambda_3^2$$

$$I_2 = \lambda_1^2\lambda_2^2 + \lambda_2^2\lambda_3^2 + \lambda_3^2\lambda_1^2 \tag{4}$$

where λ_i are the principal stretches or extension ratios. Rivlin (1948) showed that the nominal stress in tension or compression is given by:

$$\sigma_T = 2(\lambda - \lambda^{-2})\left[\frac{\partial W}{\partial I_1} + \frac{1}{\lambda}\frac{\partial W}{\partial I_2}\right] \tag{5}$$

in simple shear, the shear stresses:

$$\tau = 2\gamma\left[\frac{\partial W}{\partial I_1} + \frac{\partial W}{\partial I_2}\right] \tag{6}$$

and in pure shear, the nominal stress in the direction of extension is:

$$\sigma_p = 2\left(\lambda - \frac{1}{\lambda^3}\right)\left[\frac{\partial W}{\partial I_1} + \frac{\partial W}{\partial I_2}\right] \tag{7}$$

Figures 9a-c show the stress-strain data for the vulcanizate "BE64-750" tested in tension and compression, simple shear and pure shear. On each plot two fitted curves using a five term Mooney-Rivlin series (C_{10}, C_{01},C_{11}, C_{20}, C_{30}) are shown. One curve is produced by only using the experimental data shown in the plot and the other is produced by fitting the function to the experimental data for all three modes of deformations. The curve fitting program is supplied by MARC. This figures show that generally the agreement with the experimental data is much better when the fit is to the one set of data rather than all three simultaneously. It has to be remembered that the quality of fit may be weighted more towards one mode of deformation, if, for instance, the number of data points in that mode is more than in the others. The fit for pure shear (Fig. 9c) is perhaps the worst. It is very poor for both sets of curves. That fitted to only the experimental data for pure shear (solid curve in the figure) oscillates about the experimental curve and there is no region in which the quality of the fit is good.

By differentiating equation (3) and substituting, equations (5) (6) and (7) may be expressed respectively as tension:

$$\frac{\sigma_T}{2(\lambda - \lambda)^{-2}} = C_{10} + C_{11}(I_1 - 3) + 2C_{20}(I_1 - 3) + 3C_{30}(I_1 - 3)^2 + \frac{1}{\lambda}\left(C_{01} + C_{11}(I_1 - 3)\right) \tag{8}$$

simple shear:

$$\frac{\tau}{2\gamma} = C_{10} + C_{01} + 2(C_{11} + C_{20})(I_1 - 3) + 3C_{30}(I_1 - 3)^2 \tag{9}$$

pure shear:

$$\frac{\sigma_p}{2\left(\lambda - \frac{1}{\lambda^3}\right)} = C_{10} + C_{01} + 2(C_{11} + C_{20})(I_1 - 3) + 3C_{30}(I_1 - 3)^2 \tag{10}$$

Figure 10 shows plots of the left-hand sides of equations (8) to (10) against $I_1 - 3$, obtained both by fitting to a 5-term Mooney-Rivlin series and calculated from the experimental data.

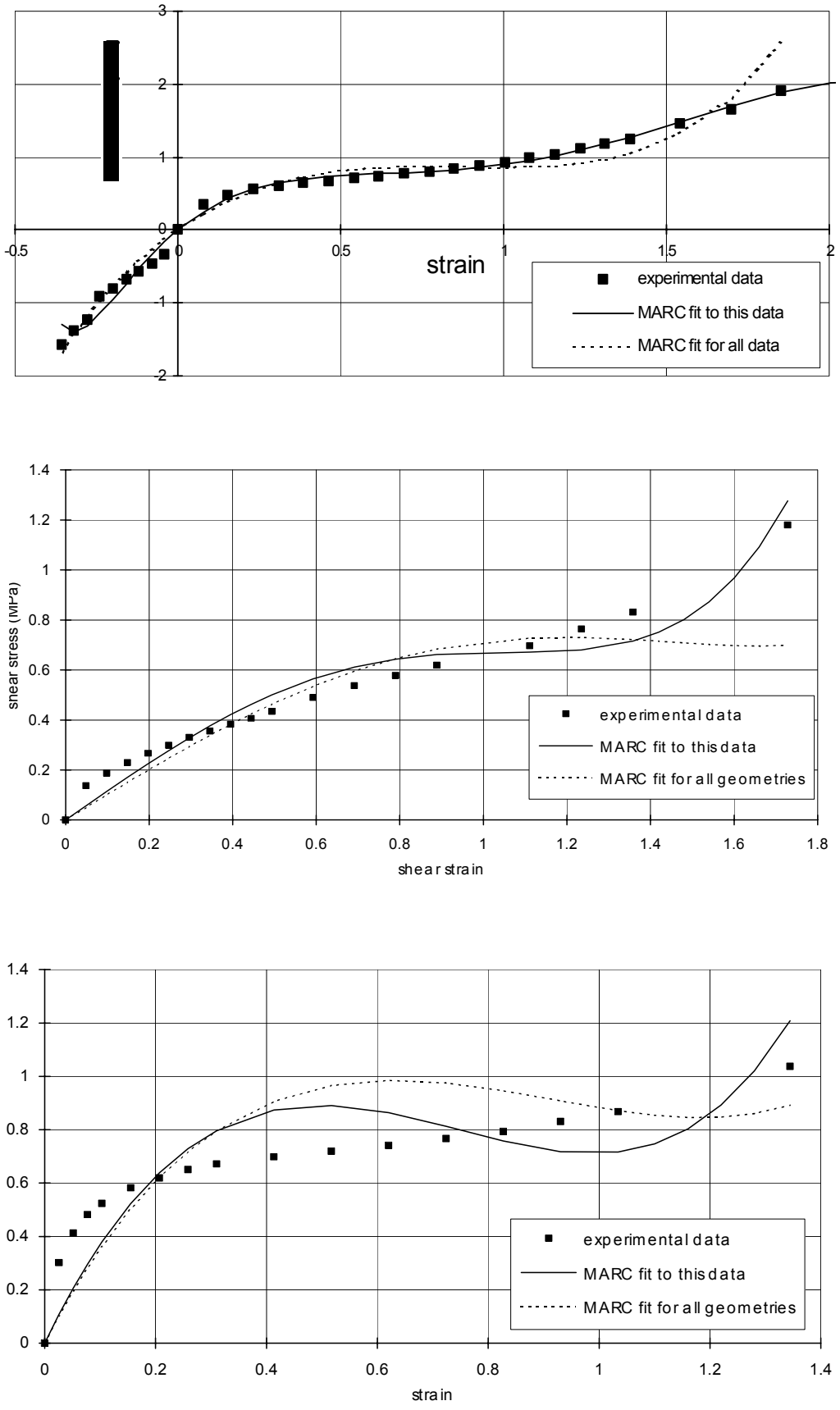

FIG. 9. Variation of nominal stress with strain for three data modes of deformation. Top: Compression and tension, Middle: Simple shear and Bottom: Pure shear. Material model used for fit to experimental data: Mooney-Rivlin with C_{10}, C_{01},C_{11}, C_{20} and C_{30}.

(a)

$$\frac{\sigma}{2(\lambda - \frac{1}{\lambda^2})}\ \text{MPa}$$

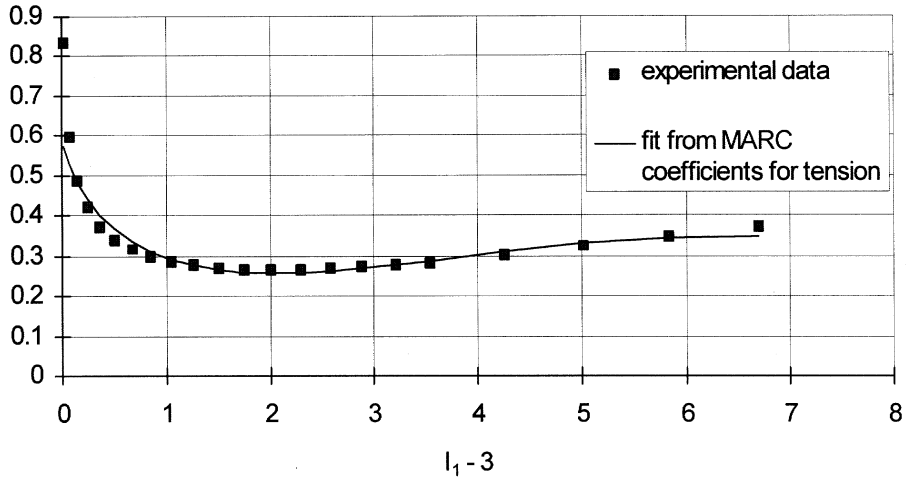

(b)

$$\frac{\tau}{2\gamma}\ (\text{MPa})$$

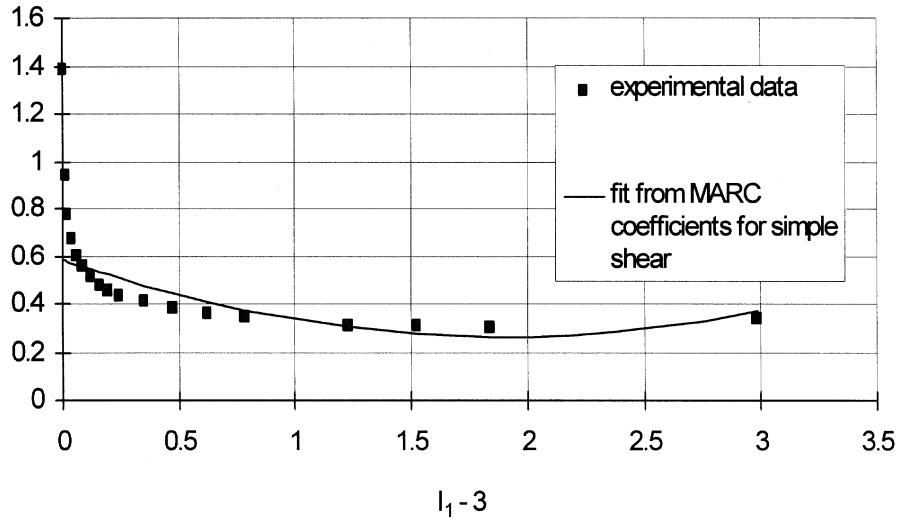

(c)

$$\frac{\sigma}{2\left(\lambda - \frac{1}{\lambda^3}\right)}\ (\text{MPa})$$

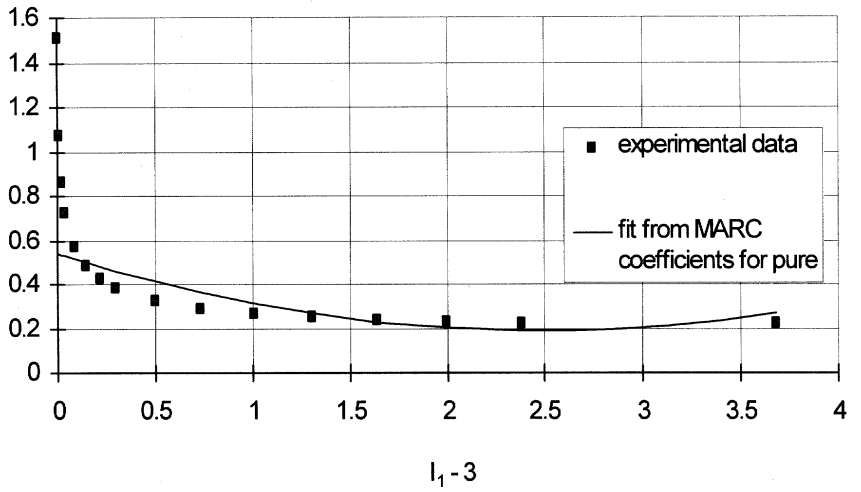

FIG. 10. Experimental and fitted data using Mooney-Rivlin formulation with coefficients as in FIG. 9. (a) Variation of $\sigma/2(\lambda - 1/\lambda^2)$ with $(I_1 - 3)$ for tension mode of deformation, (b) Variation $\tau/2\gamma$ with $(I_1 - 3)$ for simple shear mode of deformation, and (c) Variation of $\sigma/2(\lambda - 1/\lambda^3)$ with $I_1 - 3$ for pure shear mode of deformation.

It is clear from Fig. 10b and c that, for shear, the fit of the Mooney-Rivlin series is poor. The reason is that equations (9) and (10) are quadratic in (I_1 – 3) and cannot follow the rapid stiffening at low strains. The fit in tension (Fig. 10a) is better due to the higher degree of freedom in equation (8) relative to equations (9) and (10).

The comparisons show that the Mooney-Rivlin function may not be flexible enough to model material properties over a large range of deformations. Hence, the use of other forms of the strain energy function may be more appropriate, particularly for cases where strains in the rubber are small to intermediate.

3.3.3. Function of I_1 only

Gregory (1979) has proposed the simplifying assumption that for filled rubbers W is a function of I_1 only. A 'modulus' (in simple shear, G and the other geometries referred to as H) equal to twice the expression in square brackets in equations (5) to (7) can be calculated for all the above types of deformation. On a plot of G or H against I_1-3 the points should collapse onto a single curve if the assumption of Gregory applies. It can be seen from Fig. 11 that this is indeed the case, and G or H can be approximately equated to 2 $\partial W/\partial I_2$. If this simplifying assumption is made, experimental characterization of the material becomes straightforward as the dependence of W on strain can be obtained from a single test in, say, uniaxial tension, thus removing the need for a comprehensive range of deformations to be investigated.

Assuming W is a function of I_1 only, Davis, De and Thomas (1994) proposed a strain energy function of the form:

$$W = \frac{A}{2(1-n/2)}\left(I_1 - 3 + C^2\right)^{(1-n/2)} + k\left(I_1 - 3\right)^2 \qquad (11)$$

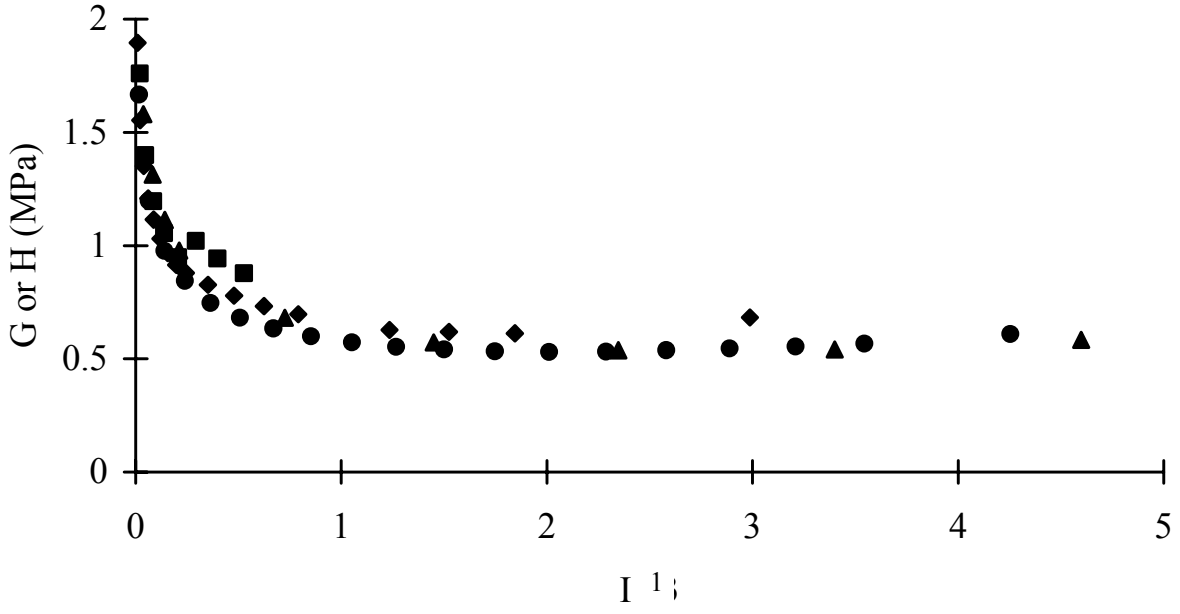

FIG. 11. Comparison of modulus (G or H) calculated from data for various geometries: ● tension; ■ compression; ▲ pure sure; ♦ simple shear.

The first term is able to model the marked softening with increasing strain seen at low strains. The second term provides for stiffening at high strains. The constant, C, is incorporated to ensure a finite value of the modulus at zero strain.

Gregory et al. (1997) modified the Davies et al function by allowing a variable power for the second term to improve the flexibility of the fit at moderate strains:

$$W = \frac{A}{(2-n)}\left(I_1 - 3\right)^{(1-n/2)} + \frac{B}{(2+m)}\left(I_1 - 3\right)^{(1+m/2)} \tag{12}$$

It is possible to incorporate a constant, C, as for the Davies et al function if a finite modulus at zero strain is required, for example when using FEA. This function was fitted to all deformation modes simultaneously by expressing the data in the form shown in Fig. 11. By differentiating equation (12), the relation:

$$2\frac{\partial W}{\partial I_1} = A\left(I_1 - 3\right)^{-n/2} + B\left(I_1 - 3\right)^{m/2} \tag{13}$$

is obtained. A best fit of the right-hand side of equation (13) to the experimental points was found with the aid of a commercial curve-fitting package. Weighting was applied to data points to ensure all strains and types of deformation were of equal significance. The fit is given in Fig. 12. A much better modelling of the strain softening at small strains is achieved than was obtained with the Mooney-Rivlin function.

3.4. Fit to Ogden function

The Ogden strain energy function is given by (Ogden, 1972):

$$W = \sum_{i=1}^{N} \frac{\mu_i}{\alpha_i}\left(\lambda_1^{\alpha_i} + \lambda_2^{\alpha_i} + \lambda_3^{\alpha_i} - 3\right) \tag{14}$$

where μ_I and α_I are not restricted to integral values.

Two or more terms are required to provide an adequate fit to the experimental data. The effect of the choice of values for the coefficients has been discussed by Ogden (1972). Figure 13 shows a two-term fit to experimental data obtained in four modes of deformation and selected to cover only moderate strains. Expressions were derived through differentiation of equation (14) for the stress in each mode of deformation as a function of λ. The fit was obtained by considering one deformation mode initially (tension was chosen) and, following the procedure outlined by Ogden, adjusting the values of the coefficients until a visual best fit was found. These coefficients were then applied to the other deformation modes and further small adjustments made, if necessary, to achieve a satisfactory fit to all deformations. A value of $\alpha_1<1$ is required to accommodate the strain softening effect at low strains, while a large α_2 value models the upturn at high strains. μ_1 and μ_2 control the magnitude and relative weight of the two terms. It can be seen from Fig. 13 that the two-term Ogden function is unable to provide enough curvature to enable a good fit to be obtained at small strains in any of the geometries tested. Ogden recommended the introduction of a third term to accommodate the

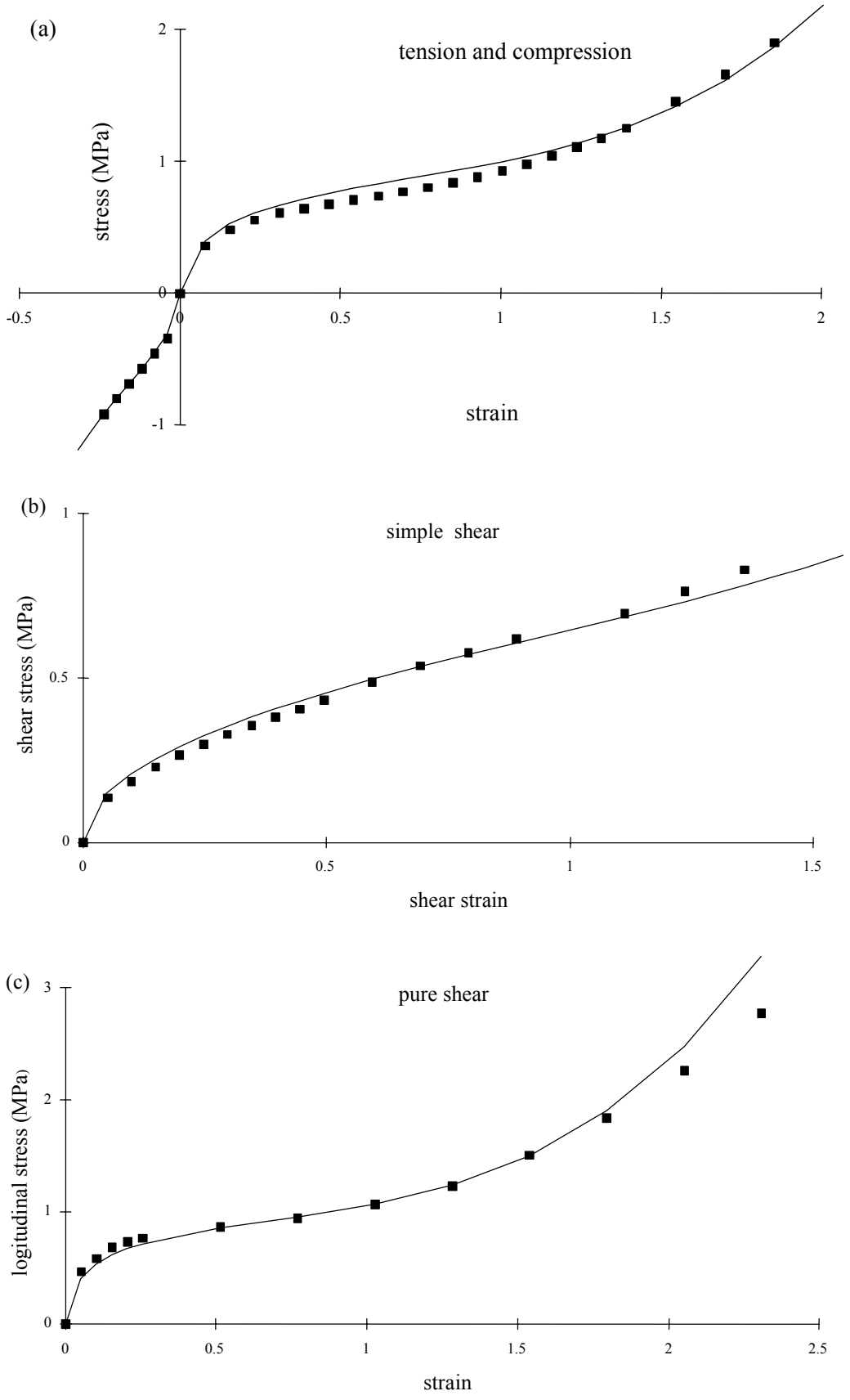

FIG. 12. Fit of equation (12) to experimental data obtained in (a) uniaxial tension/compression; (b) simple shear; (c) pure shear; ■ experimental points; fit for A = 0.637MPa; n = 0.517MPa; B = 0.0098MPa; m = 3.8Mpa.

behaviour at large biaxial strains. Introducing a third term was not found to improve the poor fit at low strains in the present work.

As stated, the fits presented in Fig. 13 were obtained by a simple method of inspection. It was hoped that a quicker and more accurate best-fit could be determined with the aid of a computerized curve fitting package. Difficulties were experienced; sometimes the algorithms failed to converge, whereas on other occasions more than one solution, depending on the initial values selected for the coefficients, was obtained. The curve-fitting package available on MARC yielded unrealistic values for the coefficients. It appears that more sophisticated non-linear curve fitting procedures such as the one proposed by Twizell and Ogden (1983) are needed if this function is to be used to represent the hyperelastic behaviour of high damping natural rubbers reliably over a large range of strains and be successfully implemented in finite element packages.

3.5. Conclusions

Both the 5-term Mooney-Rivlin function and the two-term Ogden function give rather poor fits to the experimental data, especially at small strains. A better fit is achieved with the equation of Gregory, Muhr and Stephens which is a function of I_1 only. However, this equation is not currently available in commercial finite element codes and requires the use of an appropriate subroutine.

4. TORSION OF A RUBBER CYLINDER – A BENCHMARK PROBLEM FOR FEA

4.1. Introduction

Predicting the force-deformation behaviour of elastomeric components by finite element analysis (FEA) requires several steps, namely:

(a) Defining the FE model;
(b) Modelling the behaviour of the material;
(c) Solving the problem using a finite element code.

The first part of this section assesses the accuracy of steps (a) and (c) by comparing the FE analysis with the analytical solution to a particular problem. The one chosen is the torsion of a cylinder; though reasonably complex it is capable of analytical solution whether the strain-energy function of the elastomer is expressed in terms of the strain invariants or expressed in terms of the principal stretch ratios (Ogden & Chadwick, 1972). The comparison is not concerned with the best choice of material model, and because the benchmark is an analytical solution rather than experimental data the comparison is not influenced by the effectiveness of the material model, the reliability of the material characterisation data, nor by the reliability of force-deformation measurements on the cylinder. The form of the material model may influence the accuracy of the finite element solver, and such an influence will be apparent in the comparisons presented. Comparatively little work has been published to illustrate the level of errors associated with the numerical analysis of elastomeric components. This is true for not only the way in which the FE model is defined, but also the numerical integration results.

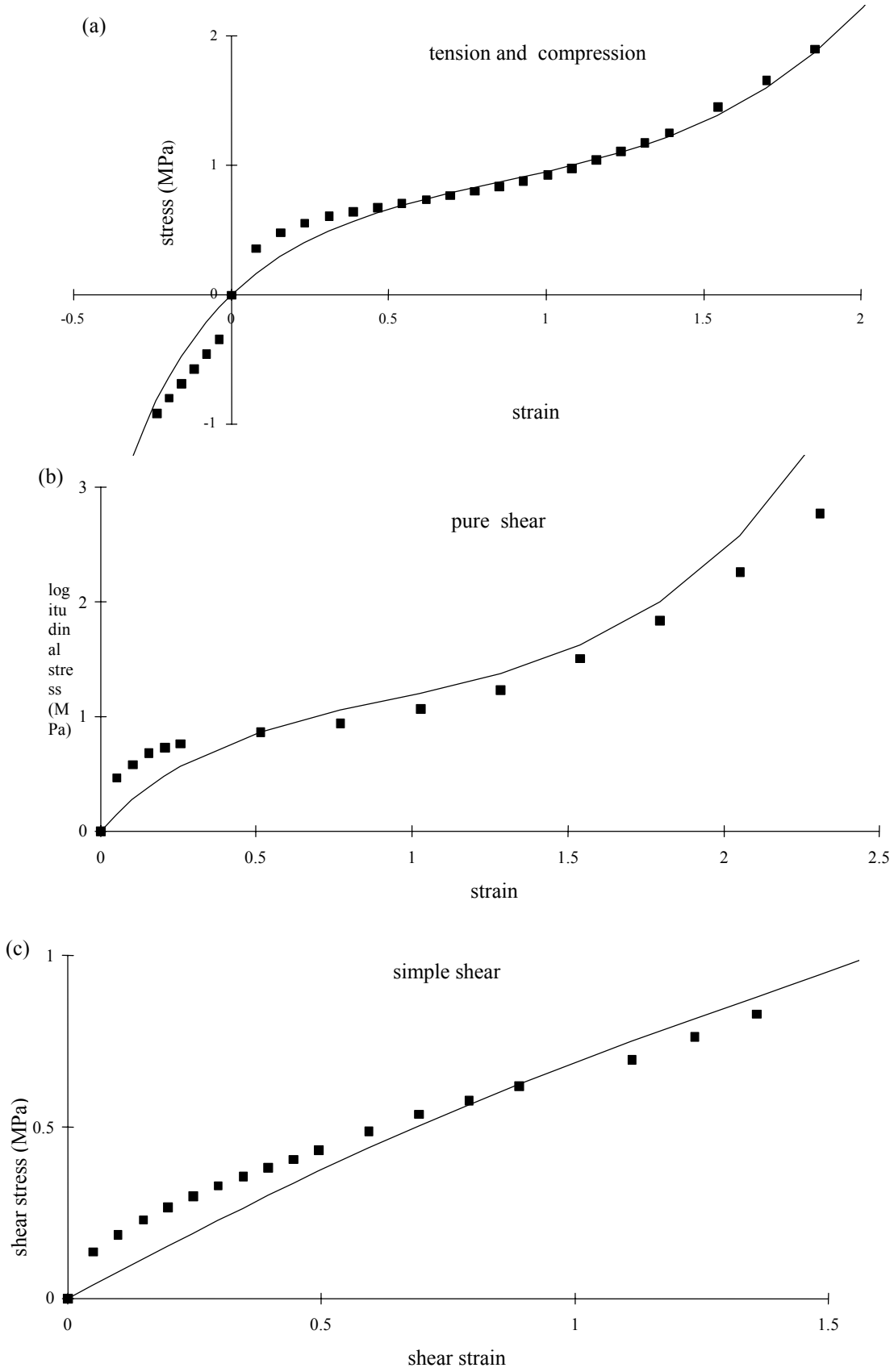

FIG. 13. Fit of two-term Ogden equation to experimental data. ■ *experimental points; fit for* $\mu_1 = 7MPa$, $\alpha_1 = 0.22MPa$, $\mu_2 = 0.002Mpa$, $\alpha_2 = 6.9Mpa$. *(a) uniaxial tension/compression; (b) pure shear; (c) simple shear.*

4.2. Theoretical background

Consider a circular solid cylinder of radius a and height l. When the top of the cylinder is rotated through an angle θ (= ψ) with respect to the bottom surface, the cylinder height being held fixed, the resulting state of strain in the cylinder is not homogeneous and varies with radial position r. The shear strain (γ) in an element at the position r is given by:

$$\gamma = \psi r \tag{15}$$

For a material deformed in simple shear:

$$\lambda_2 = \frac{1}{\lambda_1} \text{ and } \lambda_3 = 1 \qquad \text{and } \gamma = \lambda_1 - \frac{1}{\lambda_1} \tag{16}$$

where λ_i are the principal extension ratios at radius r. Therefore:

$$r = \frac{1}{\psi}\left(\lambda_1 - \frac{1}{\lambda_1}\right) \tag{17}$$

Rivlin (see Treloar (1975)) showed that the axial component of stress (t_{zz}), the component of the stress along the θ_z direction ($t_{\theta z}$), the total couple (M) needed to produce the angular rotation θ and the axial load (N) required to maintain the height unchanged are given by:

$$t_{zz} = 2\psi^2\left(\int_a^r r\frac{\partial W}{\partial I_1}dr - r^2\frac{\partial W}{\partial I_2}\right)$$

$$t_{\theta z} = 2\psi r\left[\frac{\partial W}{\partial I_1} + \frac{\partial W}{\partial I_2}\right] \tag{18}$$

$$N = -2\pi\psi^2\int_o^a r^3\left(\frac{\partial W}{\partial I_1} + 2\frac{\partial W}{\partial I_2}\right)dr$$

$$M = 4\pi\psi\int_o^a r^3\left(\frac{\partial W}{\partial I_1} + \frac{\partial W}{\partial I_2}\right)dr \tag{19}$$

W is the strain energy function and I_1 and I_2 are strain invariants given by equations (4).

4.3. Strain energy functions

4.3.1. Mooney-Rivlin strain energy function

The general form of Mooney-Rivlin strain energy function is given by equation (2). In simple shear $\lambda_2 = \frac{1}{\lambda_1}$, hence equations (4) with equations (15) and (16) gives:

$$I_1 - 3 = I_2 - 3 = \lambda_1^2 + \frac{1}{\lambda_1^2} - 2 = \gamma^2 = \psi^2 r^2 \tag{20}$$

ABAQUS in its default state allows a five-terms form of equation (2):

$$W = C_{10}(I_1 - 3) + C_{01}(I_2 - 3) + C_{11}(I_1 - 3)(I_2 - 3) + C_{20}(I_1 - 3)^2 + C_{02}(I_2 - 3)^2 \tag{21}$$

leading to:

$$\frac{\partial W}{\partial I_1} = C_{10} + (C_{11} + 2C_{20})\,\psi^2 r^2$$

$$\frac{\partial W}{\partial I_2} = C_{01} + (C_{11} + 2C_{02})\,\psi^2 r^2 \tag{22}$$

Substituting equations (22) into equation (18) and (19) and integrating gives:

$$t_{zz} = 2\psi^2\left[C_{10}\left(\frac{r^2 - a^2}{2}\right) + (C_{11} + 2C_{20})\left(\frac{r^4 - a^4}{4}\right)\psi^2 - r^2 C_{01} - (C_{11} + 2C_{02})r^4\psi^2\right]$$

$$t_{\theta z} = (C_{10} + C_{01})2\psi r + 4\psi^3 r^3 (C_{11} + C_{20} + C_{02}) \tag{23}$$

$$M = \pi\psi a^4 (C_{10} + C_{01}) + \frac{4\pi}{3}\psi^3 (C_{11} + C_{02} + C_{20})a^6$$

$$N = -\frac{1}{2}\pi\psi^2 a^4 (C_{10} + 2C_{01}) - \frac{\pi}{3}\psi^4 (3C_{11} + 2C_{20} + 4C_{02})a^6 \tag{24}$$

4.3.2. Ogden strain energy function

The Ogden strain energy function is given by equation (14). Substituting $\lambda_3 = \frac{1}{\lambda_1\lambda_2}$ (for an incompressible material, differentiating, and substituting $\lambda_2 = \frac{1}{\lambda_1}$, gives:

$$\frac{\partial W}{\partial \lambda_1} = \sum_{i-1}^{N} \frac{\mu_i}{\lambda_1}\left(\lambda_1^{\alpha_i} - 1\right)$$

and

$$\frac{\partial W}{\partial \lambda_2} = \sum_{i-1}^{N} \mu_i \lambda_1 \left(\lambda_1^{-\alpha_i} - 1\right) \tag{25}$$

Equation (25) is written in terms of $\partial W/\partial\lambda_I$ and use of equations (18) and (19) require expressions in terms of $\partial W/\partial\lambda_I$. This is achieved by using the relationships:

$$\frac{\partial W}{\partial \lambda_1} = \frac{\partial W}{\partial I_1}\frac{\partial I_1}{\partial \lambda_1} + \frac{\partial W}{\partial I_2}\frac{\partial I_2}{\partial \lambda_1}$$

$$\frac{\partial W}{\partial \lambda_2} = \frac{\partial W}{\partial I_1}\frac{\partial I_1}{\partial \lambda_2} + \frac{\partial W}{\partial I_2}\frac{\partial I_2}{\partial \lambda_2} \tag{26}$$

to provide expressions for $\partial W/\partial I_i$ in terms of $\partial W/\partial \lambda_i$ where expressions for $\partial I_i/\partial \lambda_j$ may be obtained by differentiating equations (3). The calculations are given in more detail in Fuller et al., 1997.

4.4. Finite element analysis

A joint effort has been conducted between TARRC and Ricerca Polo Idraulico e Strutturale, ENEL to compare the predictions of MARC and ABAQUS with each other and the results of analytical calculations. MARC is used by the former and ABAQUS by the latter institution.

4.4.1. Description of the problem

The FE problem is the torsional behaviour of a cylinder of rubber as analysed in Section 4.2. The variables of interest are the couple required to deform one end of the cylinder with respect to the other through an angle θ, the axial force required to keep the height of the cylinder constant, and the distributions of stresses t_{zz} and $t_{\theta z}$ along the radius at one end of the cylinder.

geometry of the cylinder	diameter	1 unit of length
	height	1 unit of length

3-D models were analysed; Fig. 14 shows two with differing mesh densities. The finer-mesh model consists of dividing each element of the coarser model by 2 along the three orthogonal axes, thereby increasing the number of elements 8-fold. Table 3 details the models used.

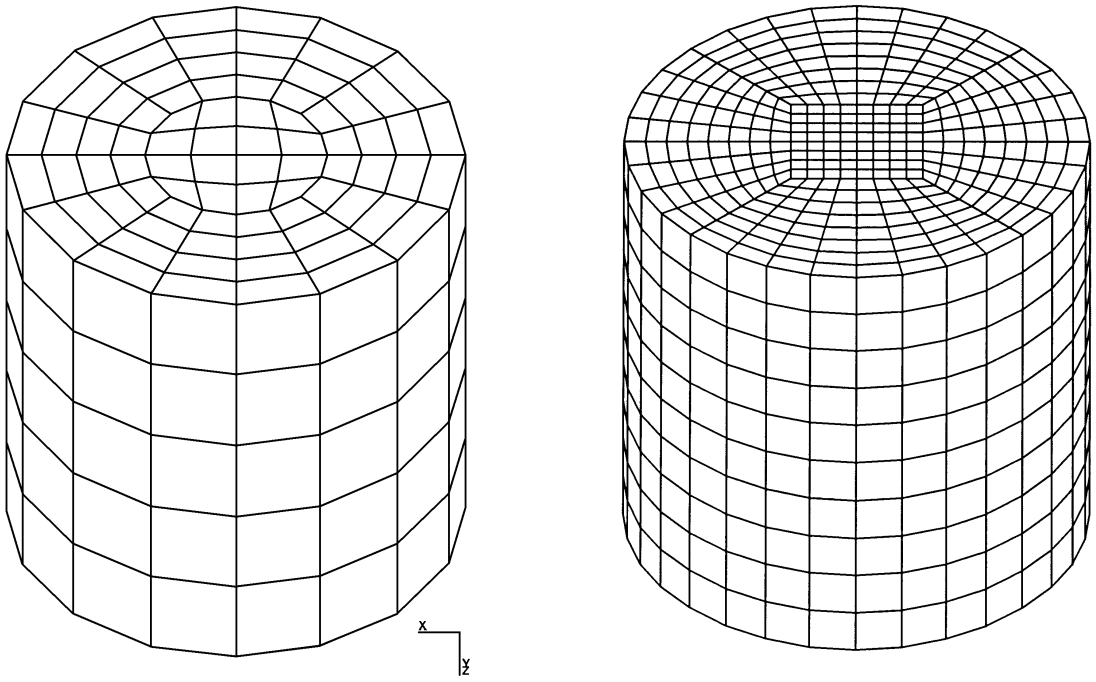

FIG. 14. FEA models showing coarse-mesh (Models 1,2,5) and refined-mesh (Model 3). (see TAB. 3).

TABLE 3. DETAILS OF FEA MODELS

Details of FEA models								
Model No.	MARC				ABAQUS			
	Element type	No. of Elements			Element type	No. of Elements		
		R	C	A		R	C	A
1	84*	6	16	5	C3D8H*	6	16	5
2	120**	6	16	5	C3D8H	6	16	15
3	84	12	32	10	C3D8H	12	32	10
4	-	-			C3D8H	8	32	15
5	-	-			C3D20H	6	16	5

R: radial
C: circumferential
A: axial full integration – Herman formulation
** reduced integration - Hermann formulation.

The nodes on the lower base of the cylinder were fully constrained. All the nodes on the upper face of the cylinder were rigidly connected to an external node outside of the model. A rotational deformation was applied to this external node while all the nodes on the upper face were constrained in the axial (z) direction. The maximum angular deformation applied was 180°.

4.5. Material models

The rubber was modelled using two strain energy functions as detailed below. In both cases the behaviour predicted from the analytical solution was also obtained by substituting the coefficients of the strain energy function into the equations presented in Section 4.3. Thus comparison of the FE and analytical solutions does not depend on the choice of material model.

4.5.1. Mooney-Rivlin

ABAQUS coefficients used were C_{10}, C_{01}, C_{11}, C_{20} and C_{02}. MARC's standard function, however, provides the user with C_{10}, C_{01}, C_{11}, C_{20} and C_{30}. A subroutine UENERG allowing user-defined strain energy functions was employed to define a function identical to that in ABAQUS. The material modelled was a high damping natural rubber. The values of the coefficients (in N/m^2) were:

$$C_{10} = 0.3344 \times 10^6$$
$$C_{01} = -0.008198 \times 10^6$$
$$C_{11} = -0.006334 \times 10^6$$
$$C_{20} = 0.02373 \times 10^6$$
$$C_{02} = 0.001235 \times 10^6$$

4.5.2. Ogden

A three-term Ogden strain energy function with the following coefficients was used:

$\mu_1 = 618030$	$\mu_2 = 1177.2$	$\mu_3 = -9810$
$\alpha_1 = 1.3$	$\alpha_2 = 5.0$	$\alpha_3 = -2.0$

the μ_n being in units of N/m^2. The shear modulus G in the limit of small deformations is related to the parameters μ_n and α_n by $2G = \Sigma\mu_n\alpha_n$, giving a value of G = 0.414MPa.

Ogden and Chadwick (1972) reported a good agreement between this three-term strain energy function and the data of Treloar (1944) from experiments on vulcanized natural rubber in simple tension, pure shear and equi-biaxial tension. This material model was therefore chosen not only because of the availability of material characterization data in the literature but also because Ogden and Chadwick's analytical solution to the problem of the torsion of an elastomeric cylinder can be compared with that calculated from Rivlin's general solution.

4.6. Results & discussion

4.6.1. Mooney-Rivlin

Figures 15 and 16 show the FE predicted results (using ABAQUS and MARC respectively) for the variation of the applied couple with the angle of twist and the axial load required to keep the height of the cylinder constant as a function of angle of twist squared. The analytical results predicted using equations (24) are also shown, together with vertical lines representing 5% deviations from the predictions.

For both codes all models give results for the applied couple that are within 5% of the analytical solution except where reduced integration solid elements were used (see Fig. 16). The following remarks can be made from the analyses using ABAQUS. The predicted FE results for Model 1 (the coarse-mesh model shown in Fig. 14) gives the largest deviation from the analytical solution (~10-12%). However, changing the element model from C3D8H to C3D20H, ie from 8-noded to 20-noded solid elements (Model 5), improves the degree of accuracy substantially. Model 3 improves the accuracy of the results further. This is perhaps expected since the number of elements is 8-fold larger. The results for Models 2 and 4 suggest that the accuracy improves if the number of elements along either the axial or radial direction is increased with respect to the coarse-mesh model. The best results for the axial load were obtained for Model 3. The results predicted using MARC were within the 5% error margin for the coarse-mesh model (Model 1 – Tab. 3) for both the applied couple and the axial load.

Figures 17 show the MARC predictions for the distribution of the axial stress (t_{zz}) and azimuthal stress ($t_{\theta z}$) at the end face of the cylinder when $\theta = 130°$. The analytical solutions were obtained using equation (23). The accuracy of the refined-mesh model prediction of the axial stress distribution is less than that for the coarse-mesh model. This is puzzling and may be related to the fact that the coarse model used the direct iterative solver whereas a sparse iterative solver was used in the refined-mesh case.

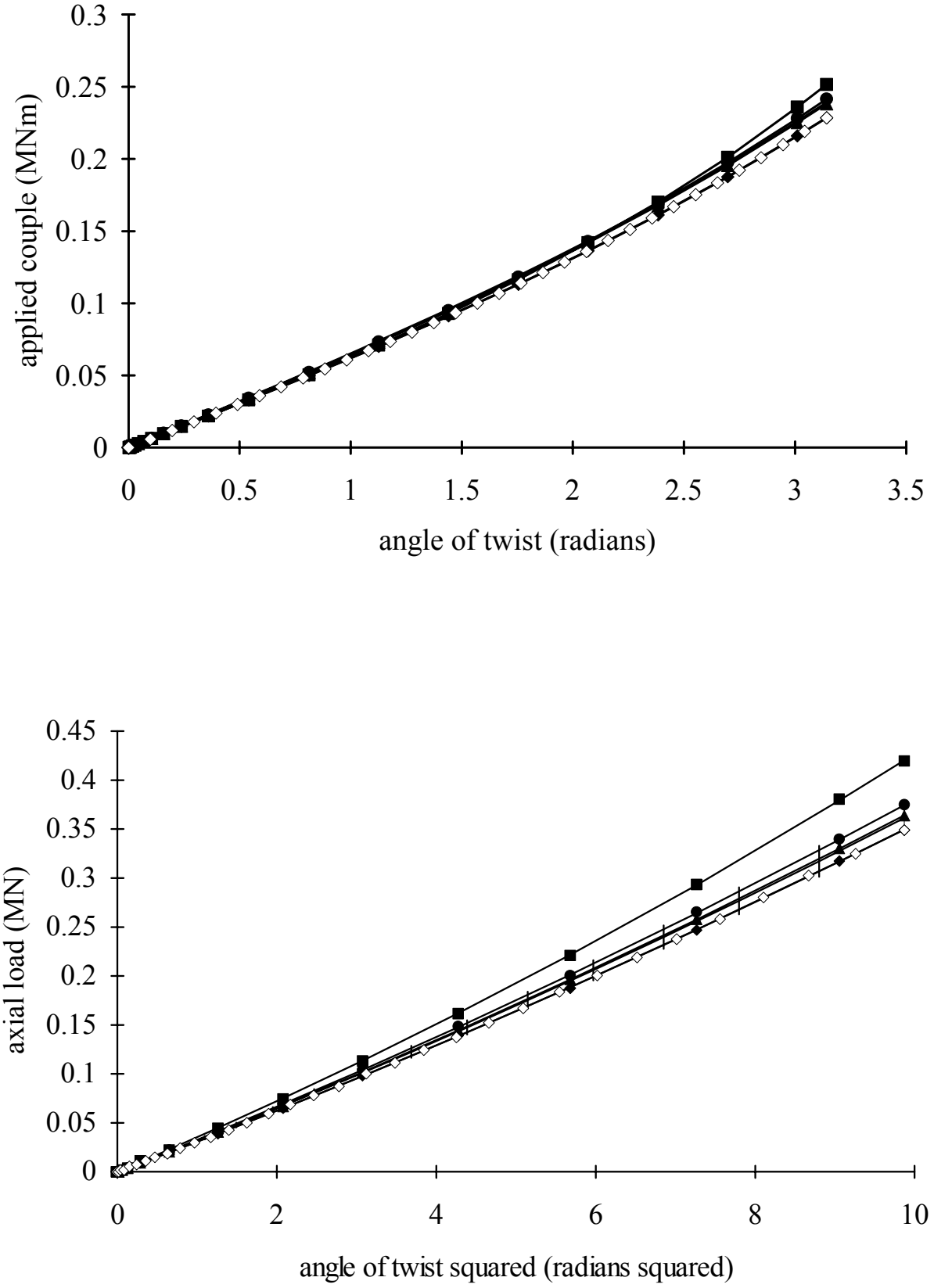

FIG. 15. Comparison of ABAQUS and analytical results for dependence of couple upon angle of twist (upper plot) and axial load upon (angle of twist)^2 (lower plot. Material characterization using truncated Rivlin series. Thick line is analytical results; ±5% deviation indicated. FEA results:
■ Model 1; ♦ Model 2; ▲ Model 3; ● Model 4; ◊ Model 5; (see TAB. 3 for details).

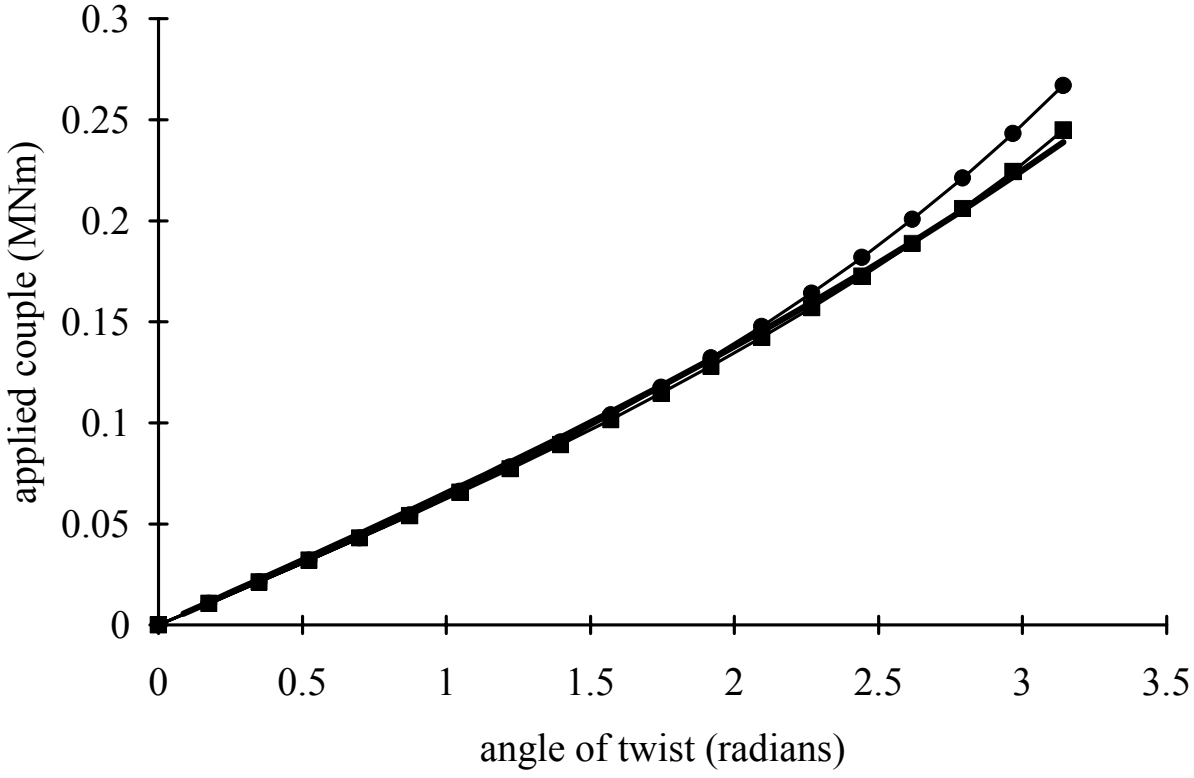

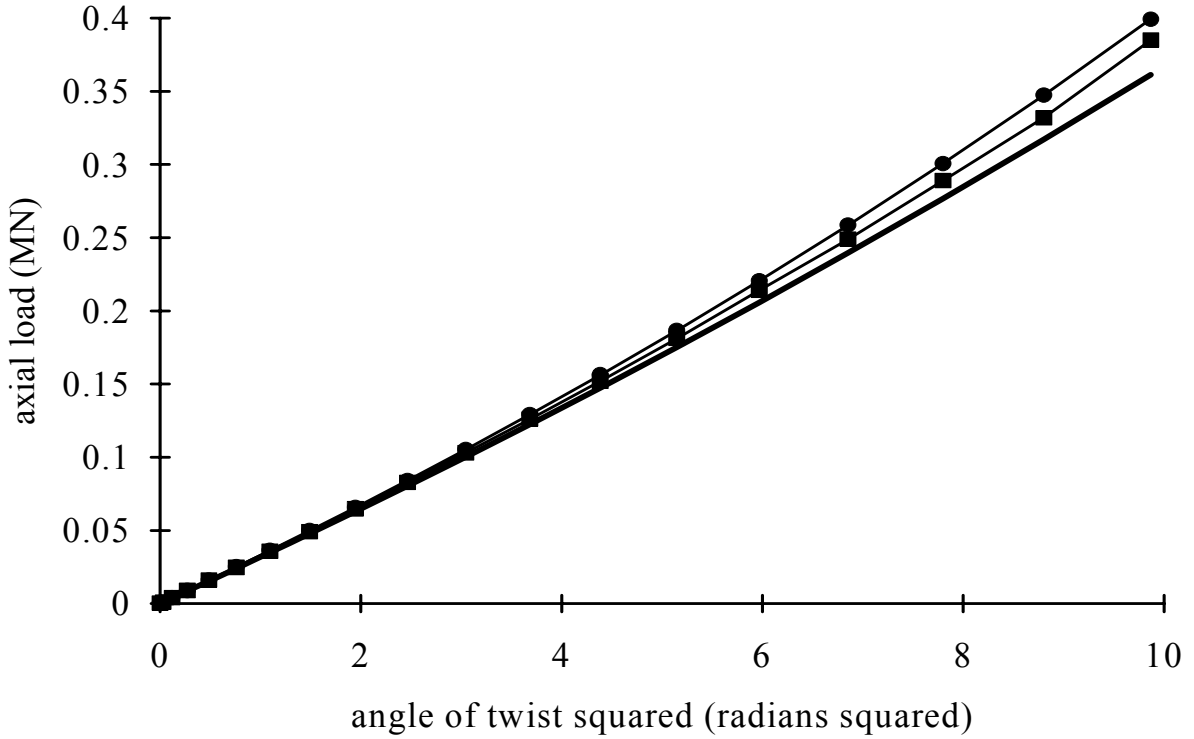

FIG. 16. Comparison of MARC and analytical results for dependence of couple upon angle of twist (upper plot) and axial load upon (angle of twist)^2 (lower plot). Material characterization using truncated using truncated Rivlin series. Thick line is analytical results; ±5% deviation indicated. FEA results: ■ Model 1; ● Model 2; (see TAB. 3 for details).

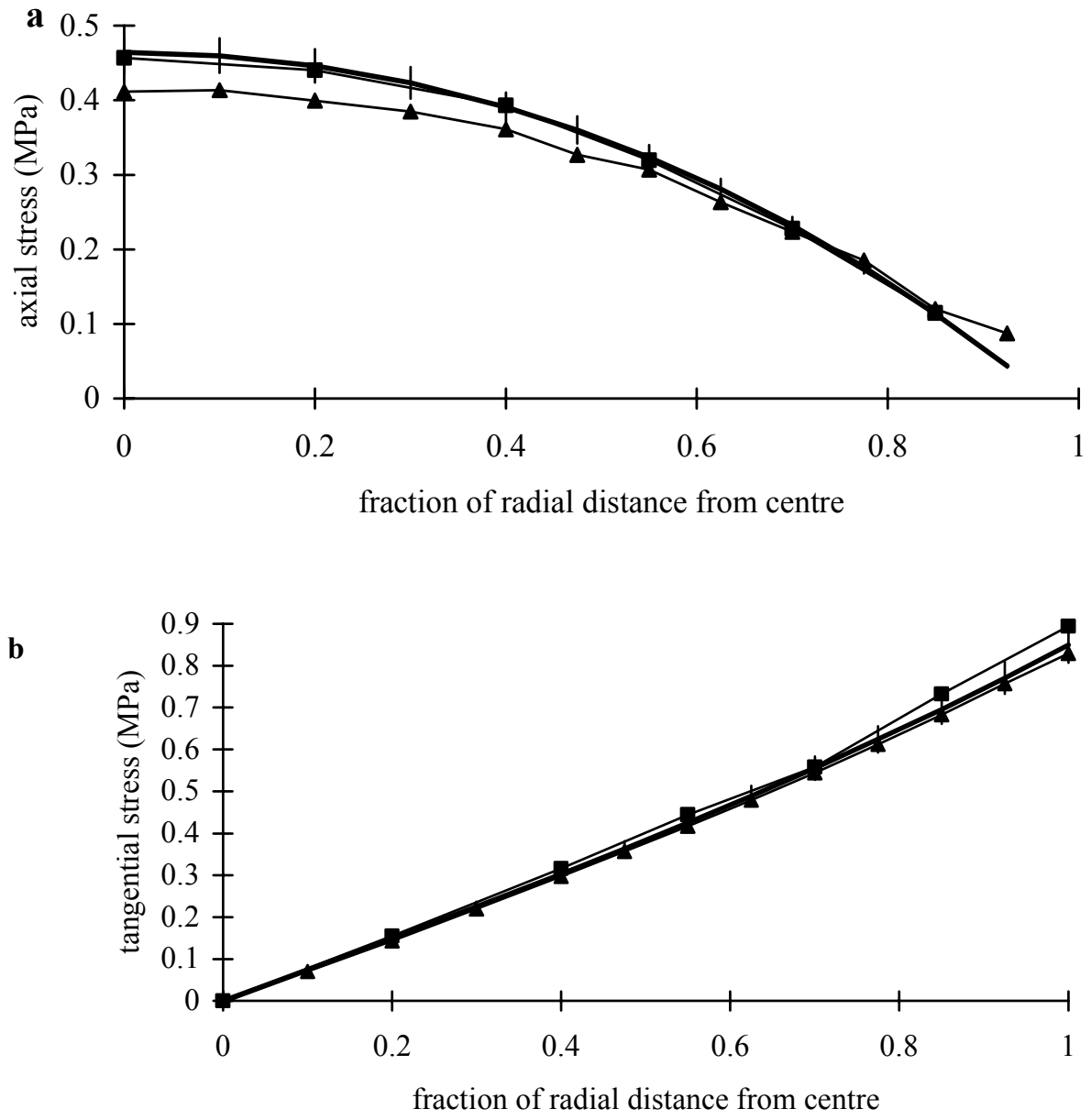

FIG. 17. MARC predictions of stress distributions at the fixed end of a cylinder subjected to torsion through an angle of twist of 130 and kept at constant height. Material characterization using truncated Rivlin series. (a) axial stress; (b) tangential stress. Thick line, analytical results. ±5% deviation indicated; ■ *coarse-mesh;* ▲ *refined-mesh; (see TAB. 3 for details*).

4.6.2. Ogden

Figures 18 and 19 show the FE results together with the analytical results. The analytical results agree with those predicted by Ogden and Chadwick (1972). For both FE Codes the applied couple results generally fall within 5% of the analytical solution.

The axial load results for Model 1 (coarse-mesh model) using ABAQUS give the largest percentage error - as in the case for the comparisons based on the Mooney-Rivlin material model. Interestingly, the MARC results for the coarse-mesh model are reasonable. The refined-mesh model (Model 3) using MARC predicts the axial load very well; the results for the couple are less accurate, but still easily within the 5% error band.

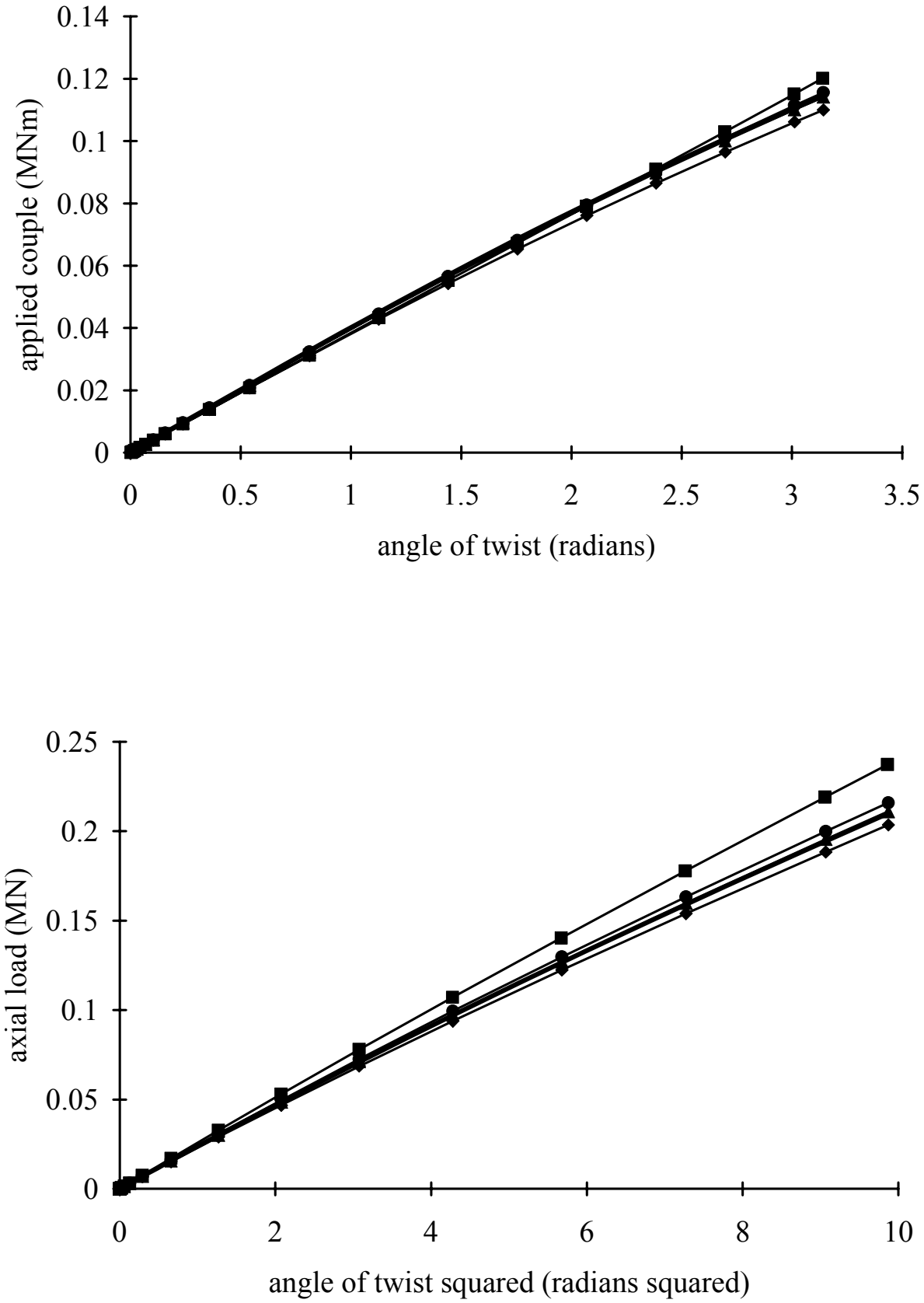

FIG. 18. Comparison of ABAQUS and analytical results for the dependence of couple on angle of twist (upper plot) and axial load on (angle of twist)^2 (lower plot). Material characterization using an Ogden function. Thick line, analytical results: ■ Model 1; ♦ Model 2; ▲ Model 3; ● Model 4;(see TAB. 3 for details).

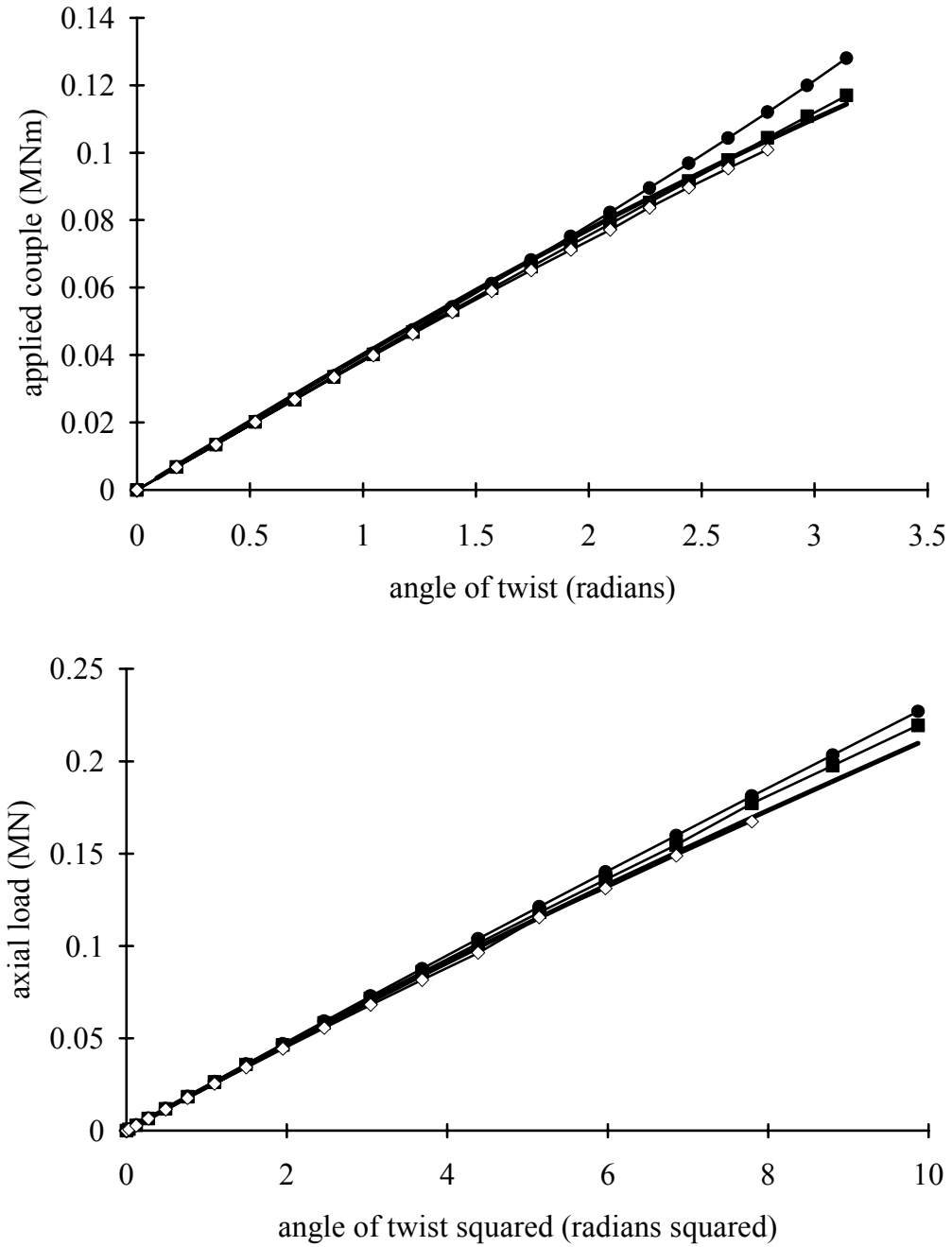

FIG. 19. Comparison of MARC and analytical results. ■ *Model 1;* ● *Model 2;* ◊ *Model 3; Other details as for FIG. 18.*

5. FE ANALYSIS OF SEISMIC ISOLATORS: COMPARISON WITH EXPERIMENTAL RESULTS

5.1. Introduction

This paper deals with the Finite Element Analysis of the test bearings and the comparison of the predicted results with the experimental data. The bearings analysed were:

(a) ENEA High Damping Rubber Bearing (HDRB)
(b) CRIEPI Natural Rubber Bearing (NRB)

(c) Korean High Damping Rubber Bearing (HDRB)
(d) CRIEPI Lead Rubber Bearing (LRB).

The FE analysis was carried out on a Silicon Graphic Indigo2-RISC4000 processor with 128MByte of RAM. The code used was MARC non-linear FE software supplied by MSC Software Ltd. The isolators were mainly modelled in 3D. Due to the symmetry of the problem only half of the bearings were modelled. The rubber layers were mainly modelled by three layers of solid elements – element 84 which has eight nodes with Herrmann formulation and full integration capability. The metal layers were modelled using shell elements with five layers.

5.2. ENEA high damping rubber bearing

Figure 20 shows the geometrical data for the ENEA bearing. The material model for the rubber was a five-term truncated Rivlin formulation provided by ENEL and ENEA. The coefficients for the model were fitted to the test data for shear deformation up to 200%. This corresponds to the maximum shear strain bearings tested. A bulk modulus of 2500MPa was used. Figure 21a shows the predicted shear response of the bearing under 50kN compressive load and subjected subsequently to a 200% shear deformation. There is a close agreement between the predicted results and the experimental data. Figure 21b shows the compressive response of the bearing to a load 11 times the working load for the bearing. The agreement between the FE results and the experimental data is much better at lower loads.

Diameter of HDRB (mm)	125
Rubber Thickness (mm)	2.5
No. of Rubber Layers	12
Total Rubber Height (mm)	30
Shim Plate Thickness (mm)	1.0
No. of Shim Plates	11
Shape Factor	12

FIG. 20. Geometrical data for ENEA HDRB.

Further numerical investigations were carried out on three bearings. These all had the same total height as those for ENEA HDRB but the number of rubber layers were different: namely 6 layers of 5mm or 12 layers of 2.5mm or 24 layers of 1.25mm giving a total thickness of 30mm. The material model used was that described above. Figure 22a shows the predicted shear response of the bearings to the same conditions as for Fig. 20. It is apparent that the FE results indicates that the shear stiffness of the lowest shape factor bearing (that with 6 rubber layers) is stiffer than the other two bearings. The reason for this unexpected result is not clear and further investigation is required. Figures 22b and c show the vertical deflection of the bearings subjected first to a 50kN load and then to a 200% shear strain. The lowest shape factor bearing shows the highest vertical deflection under the 50kN load (Fig. 22b) as expected. However, the vertical deflection due to a subsequent shear deformation shows that the height of the bearing will increase after the imposition of the shear load (Fig. 22c). This is not the case for the 12 and 24 layer bearings. The reason for this unphysical behaviour has been investigated and is discussed in Section 6.

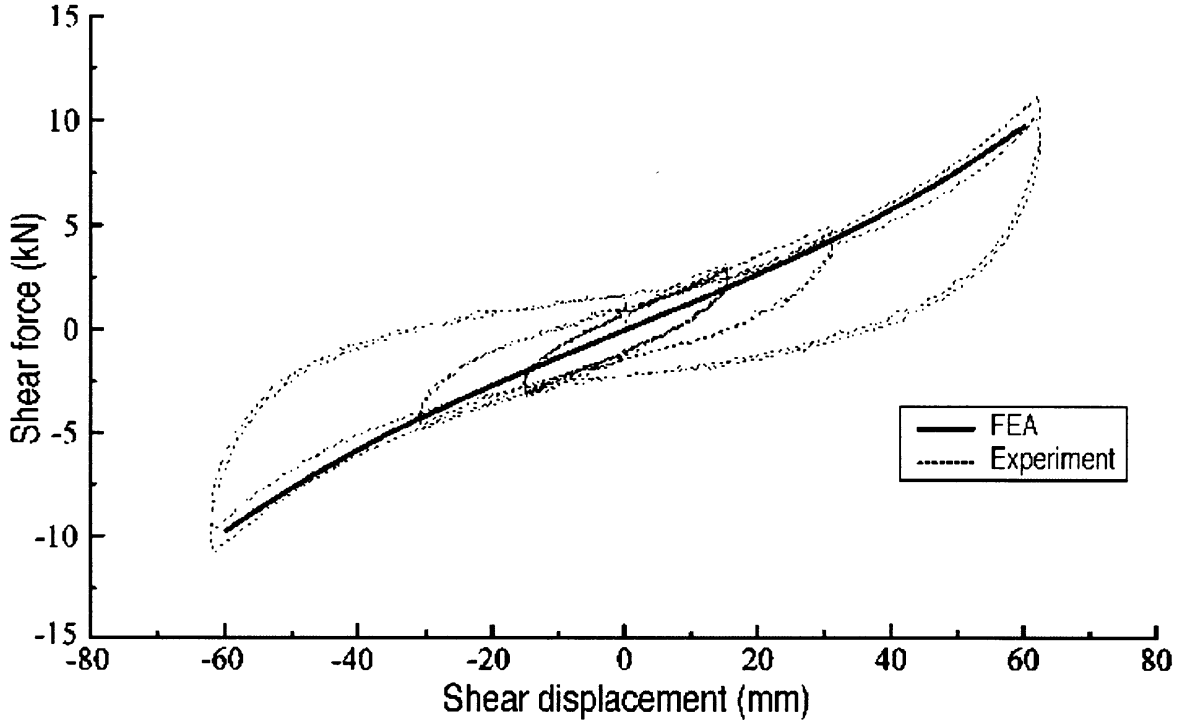

FIG. 21a. Shear deformation behaviour of the ENEA bearing.

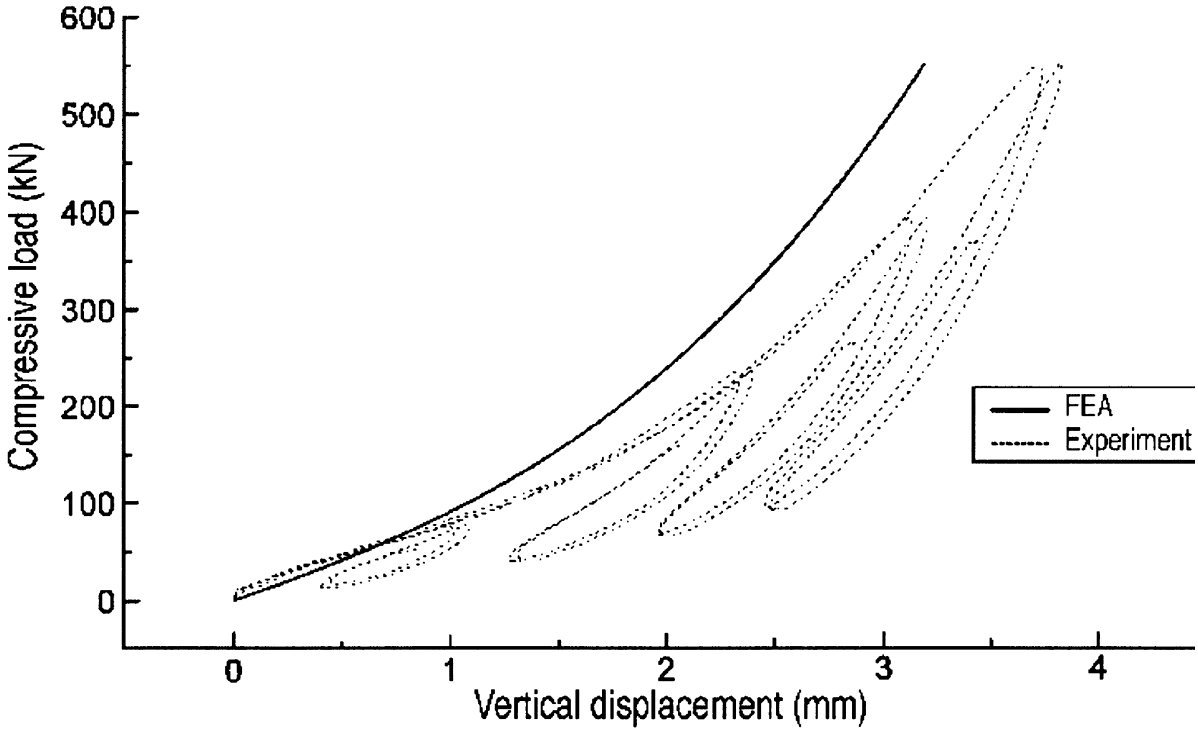

FIG. 21b. Vertical compressive load vs displacement of ENEA bearing.

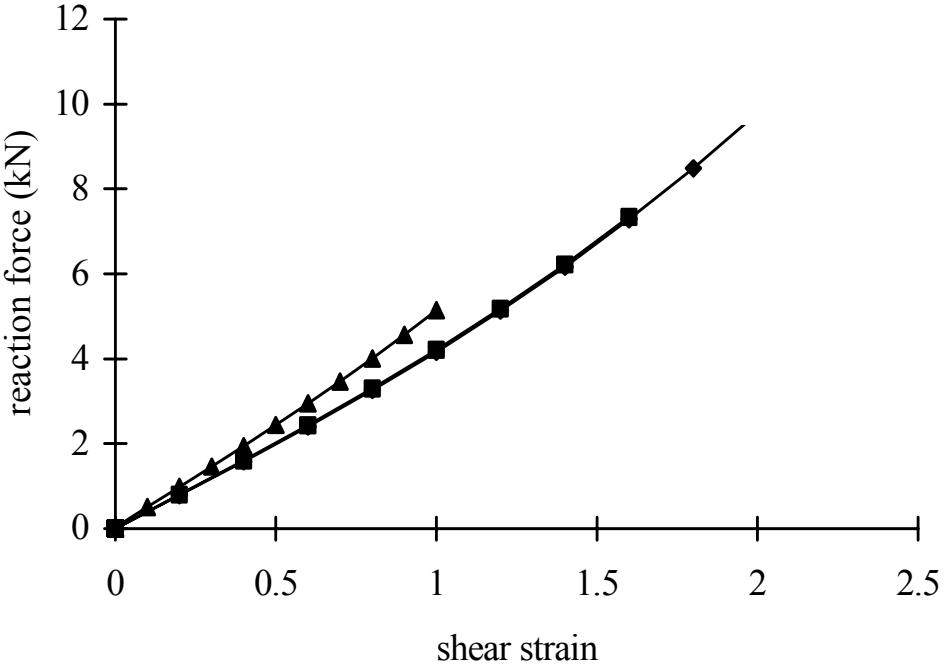

FIG. 22a. Force-deformation behaviour in shear for ENEA bearing. ■ high shape factor (24 layers); ♦ medium shape factor (12 layers); ▲ low shape factor (6 layers).

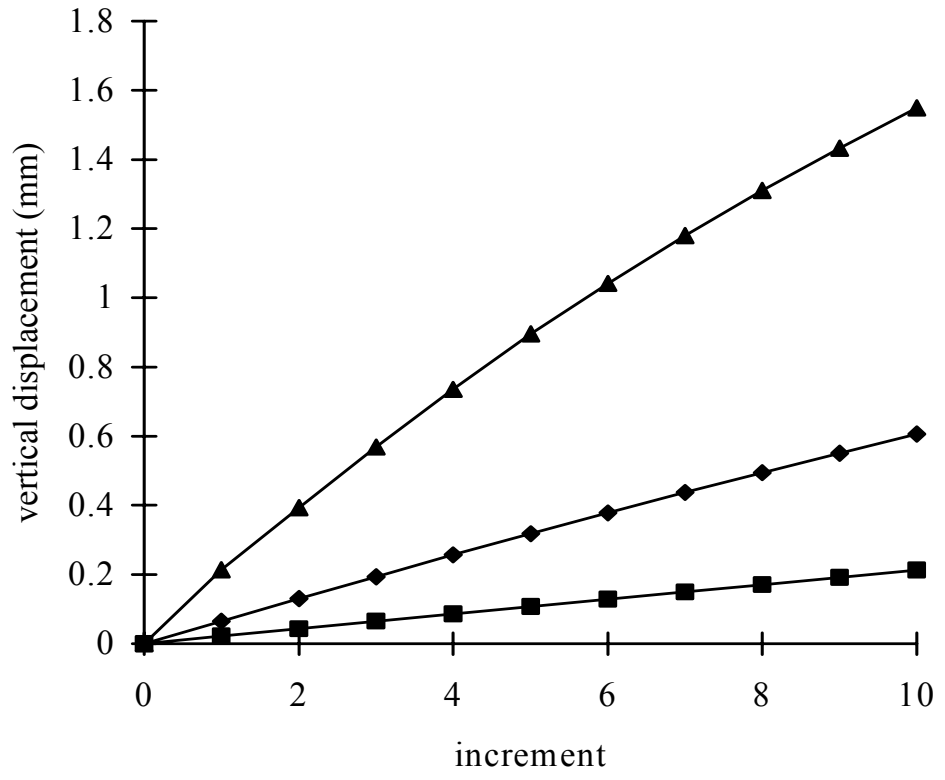

FIG. 22b. Vertical displacement of the ENEA bearing subjected to 50kN vertical load. ■ high shape factor (24 layers); ♦ medium shape factor (12 layers); ▲ low shape factor (6 layers).

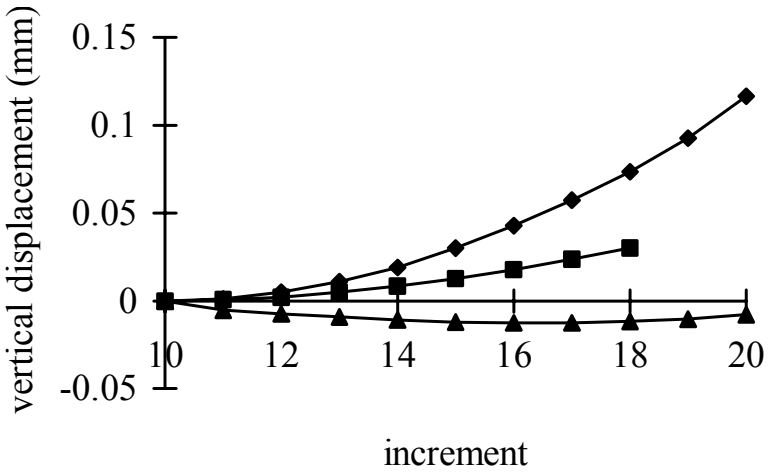

FIG. 22c. Vertical displacement of the ENEA bearing subjected to 50kN vertical load and 200% shear strain (following 50kN vertical load). ■ high shape factor (24 layers); ♦ medium shape factor (12 layers); ▲ low shape factor (6 layers).

Geometric data:	
	5.7
Thickness of rubber sheet (mm)	25
Number of rubber layers	142.5 (5.7 × 25)
Total thickness of rubber layers (mm)	3.1
Thickness of steel plate (mm)	24
Number of steel plates	1012
Diameter of rubber (mm)	126
Diameter of inner hole (mm)	38.9
Primary shape factor	7.1
Secondary shape factor	
Specification:	
	200tonf
Design vertical load (1/1.58 scale model of prototype 500tonf bearing)	25kgf/cm/cm
Design vertical stress	0.5Hz (Th = 2sec)
Horizontal frequency fh	>20Hz
Vertical frequency fv	6kgf/cm/cm
Shear modulus G of rubber	

FIG. 23a. Data on natural rubber bearing.

5.3. CRIEPI Natural rubber bearing

Figures 23a and b shows the geometrical data and the FE mesh for this bearing. The Material model was suggested by Seki 1987, and was supplied by CRIEPI. This model was implemented on MARC using UENERG user-defined subroutine. Figure 24 shows the shear force-shear displacement for the bearing subjected to a pre-compressive load of 150tonf and subjected to a shear deformation corresponding to 200% shear strain in the rubber. The material was modelled as incompressible. The effect of changing the bulk modulus of the rubber on the vertical and shear response of the bearing was also investigated. The values of the bulk moduli used were 120, 250 and 2.5×10^6 tonf/cm^2. The predicted shear response is

independent of the value of the bulk modulus used. However there is a large discrepancy between the vertical deflection as predicted using FEA under the 150tonf and those received experimentally (see Fig. 25a). The reasons for this is not clear. Figure 25b shows the vertical height of the bearing from when the shear deformation is applied. Again these results show that when the bulk modulus for the rubber is set to low values the height of the bearing increases following the application of the shear load. This is marginally improved when bulk modulus (K) was equal to 250tonf/cm^2.

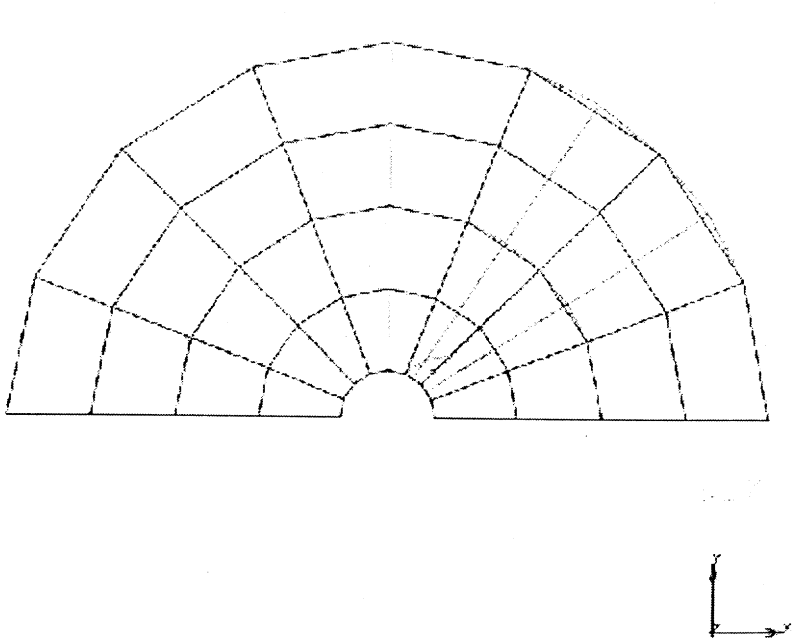

FIG. 23b. FE Mesh.

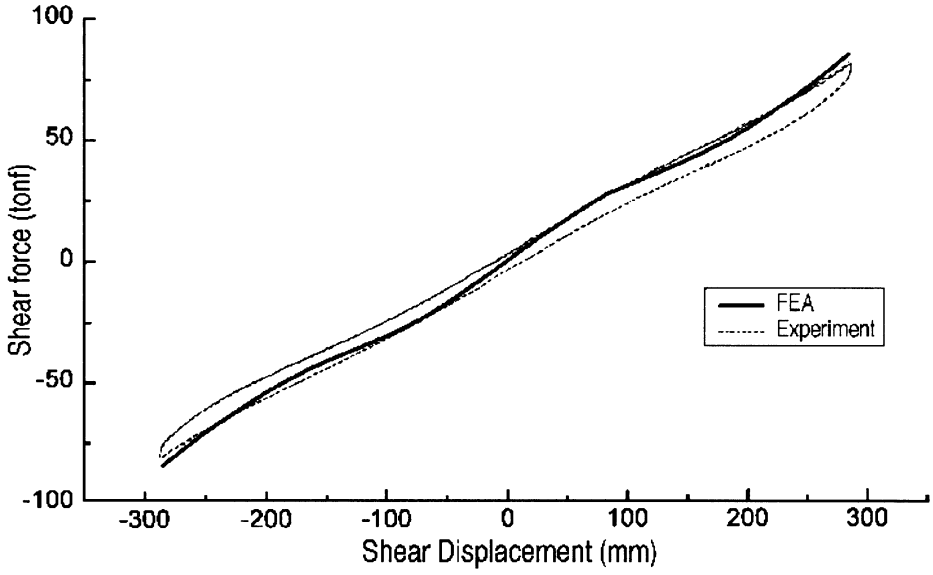

FIG. 24. Shear deformation behaviour of CRIEPI-NRB.

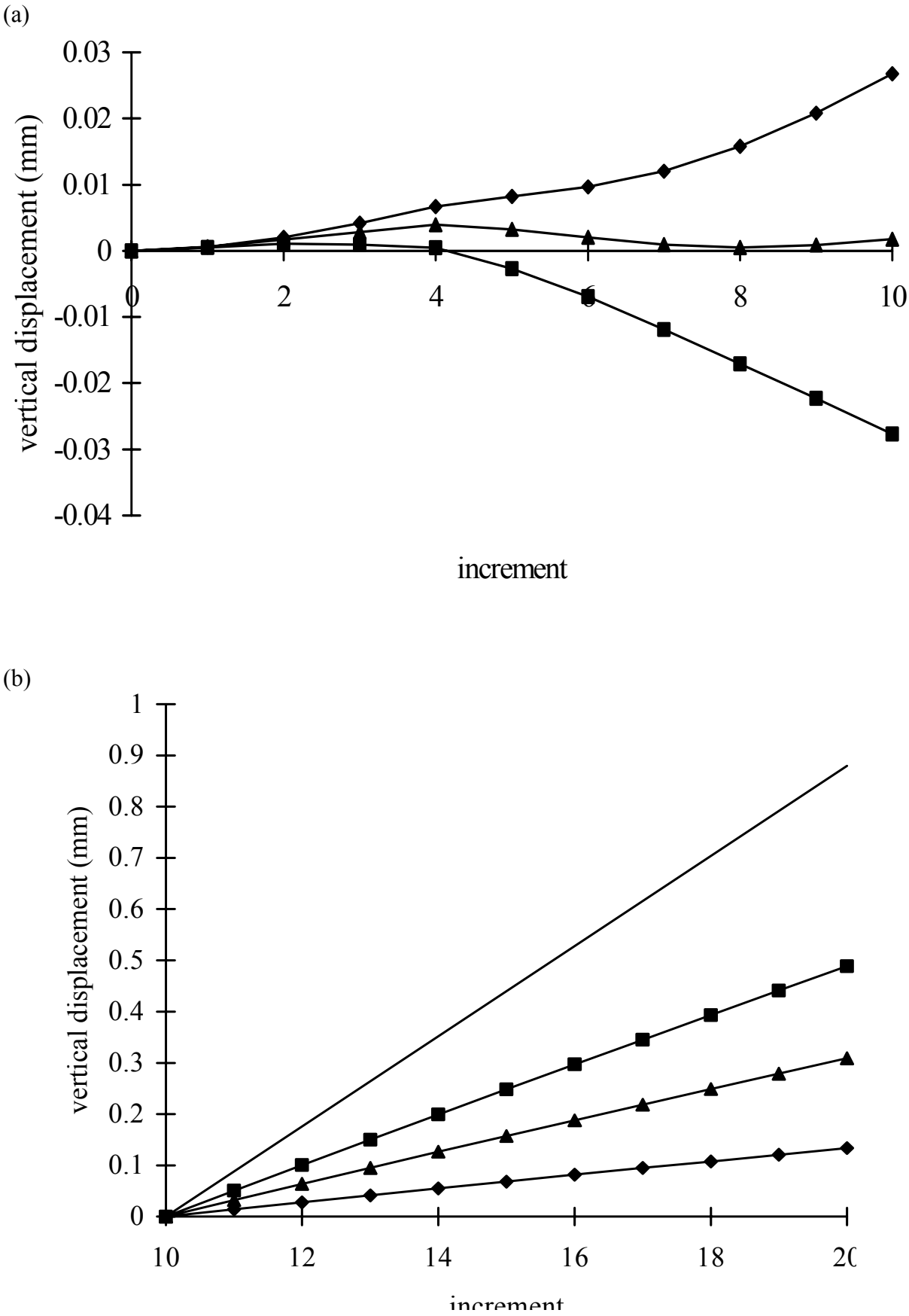

FIG. 25. Vertical displacement of the CRIEPI-NRB subjected to (a) shear strain followed by (b) vertical load. The bulk moduli were ■ 1.2x 10^5 kgf/cm^2; ▲ 2.5 × 10^5 kgf/cm^2; ♦ 2.5 × 10^9 kgf/cm^2 ; — experimental results.

5.4. Korean high damping rubber bearing

Figure 26a and b show the geometrical and FE mesh for this bearing. Three forms of strain energy functions were used to model the high damping natural rubber used to manufacture his bearing. These were a five-term truncated Rivlin series (see equation 3), a neo-Hookean and the strain energy function proposed by Gregory et al. (1997) (see Section 3.3). A series of tests were carried out to characterize the material for the FEA. These were uni-axial tension, pure shear, uni-axial compression and bi-axial extension. Figures 27a-d show the three strain energy functions fitted to the experimental data. The quality of the fit is very good for all modes of deformations except that for the uni-axial tension tests. Figure 28 shows all the experimental data plotted in terms of modulus versus I_1-3 (see Section 3.3). All of the data collapse on the same curve except that for the uni-axial tension data, suggesting the presence of an artefact in the tension experiment. The values of the coefficients used for each function are as follows:

(a) truncated Rivlin $C_{10} = 0.814$, $C_{01} = -0.168$, $C_{11} = 0.0226$, $C_{20} = -0.02559$, and, $C_{30} = 0.0005$;
(b) neo-Hookean $G = 1.174$;
(c) Gregory et al. $A = 1.031$, $B = 0.028$, $n = 0.344$, $m = 3.322$.

Total height	200
Rubber layer thickness (mm)	1.2
Steel plate thickness (mm)	1.6
No. of rubber layers	29
External diameter	156
Cover layer thickness (mm)	3
Internal diameter (mm)	19

FIG. 26a. Geometrical data for the Korean HDR.

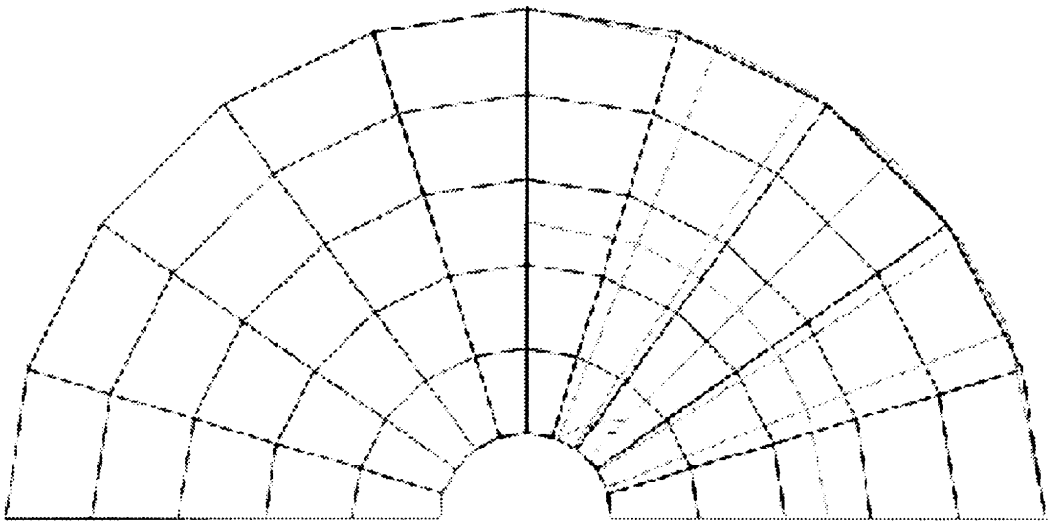

FIG. 26b. Plan view of mesh used to model Korean HDRB.

(a)

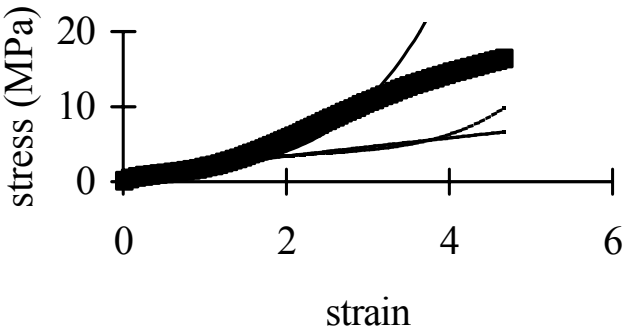

(b)

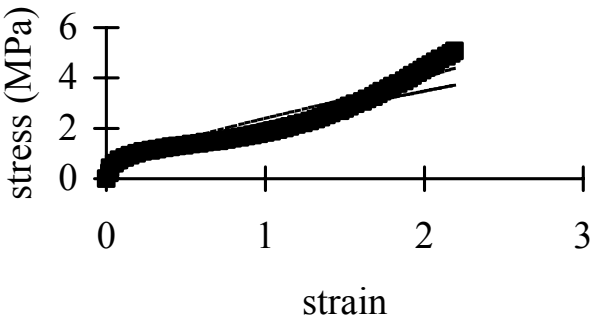

(c)

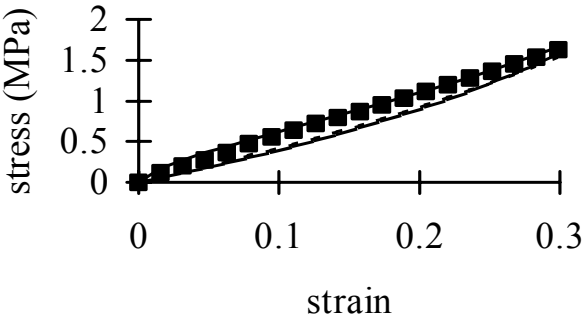

(d)

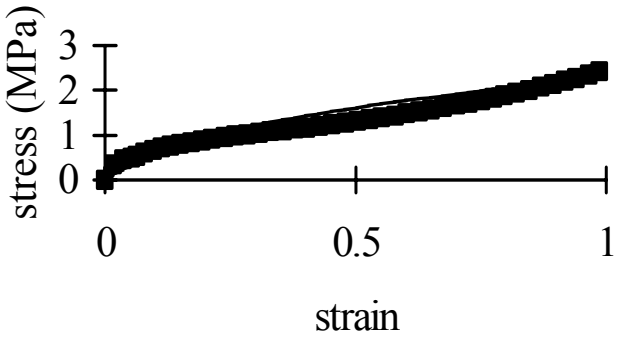

FIG. 27. Stress-strain behaviour of rubber used for Korean high damping bearing. (a) uni-axial tension, (b) pure shear, (c) uni-axial compression, (d) ■ experimental points; — fit to Gregory et al. (1997); – – – – fit to neo-Hookean; - - - - - fit to truncated Rivlin series.

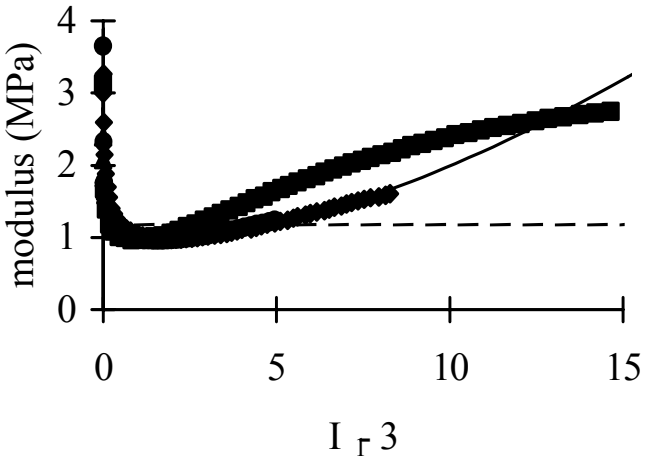

FIG. 28. Comparison of experimental data, presented in FIG. 27, assuming strain energy is a function of I_1 only.

(a)

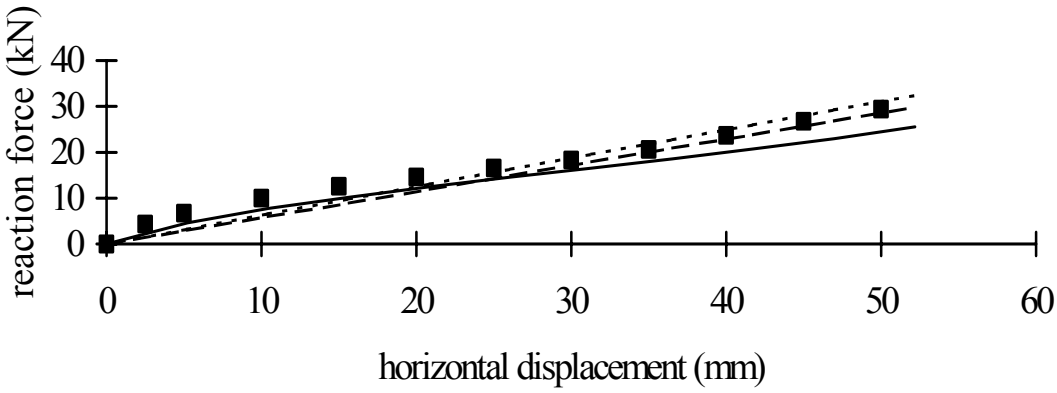

(b)

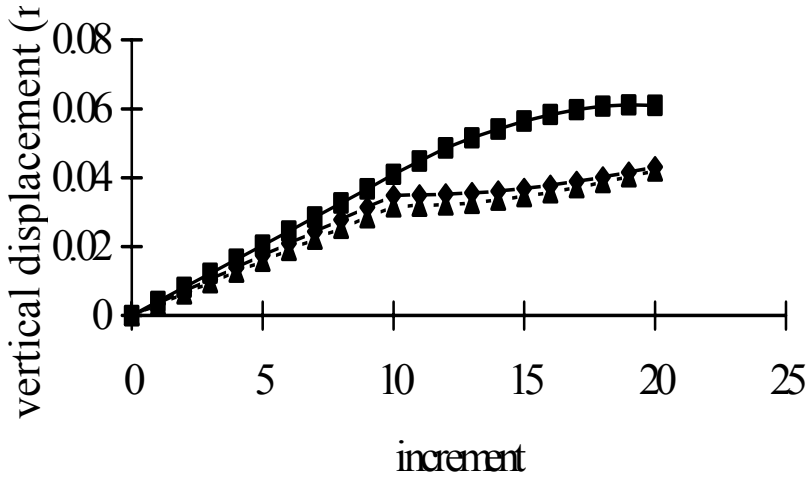

FIG. 29. Force-deflection behaviour of Korean bearing under a compressive load of 50kN, followed by a shear to 150% compared to predictions. (a) behaviour in shear, (b) vertical displacement.
■ *experiment;* — *Gregory et al. (1997);* – – – *neo-Hookean;* - - - - - *truncated Rivlin series.*
Note: *in FIG. 29b experimental data is not included.* —■— *represents truncated Rivlin series.*

Figures 29a and b show the FE predicted behaviour of the bearing when subjected to an initial vertical load of 50kN followed by a shear deformation of 150%. The experimental data is also shown in Fig. 29a. The prediction using the Gregory et al. (1997) strain energy function is much closer to the experimental data allow shear deflections than the other two functions. However, the ranking is reversed at the higher end of the deflection axes. Figure 29b shows the vertical displacement of the bearing for the initial compression load and the subsequent shear deformation. There is generally good agreement between the predictions of the vertical displacement for the first phase of the loading using all three material models. However for the second phase, the vertical displacement predicted using the Gregory et al. (1997) strain energy function was very different to the predictions using the other two models. There is no change in the form of the curve around the point where the shear load is applied to the bearing. This result is interesting and is now being investigated.

5. CRIEPI LEAD RUBBER BEARING

The Lead Rubber Bearing analysed was chosen so that the size of the lead core was significant compared with the overall dimensions of the baring. This ensures that the contribution of the lead core to the overall resisting force of the bearing is not masked by that coming from the rubber layers. The dimensions of the bearing are as follows:

	cm
Outer diameter	28
Inner diameter	7
Thickness of rubber layer	0.20
Number of rubber layers	23
Thickness of steel plates	0.16
Number of steel plates	22
Diameter of lead plug	70
Design vertical load	56.84tonf

The analysis of the LRB using a 3-D mesh proved to be very time consuming on the RISC 4000 machine currently in use at TARRC. It was particularly slow due to the small loading steps required in order to achieve convergence. The number of integration steps used is an order of magnitude higher than those used in the analysis of rubber bearings without the lead core.

The FE analysis of the whole of the bearing carried out at ENEL and ENEA showed that the analysis of a single layer of the bearing can be used to predict the response of the bearing by scaling up the results. It was therefore decided to analyse a single layer of the bearing. Figure 5.30 shows the plan view of the mesh used to model the layer. The rubber layer is modelled by 4 solid elements along the radial direction, 16 elements along the circumference and 3 elements through its thickness. The lead core was modelled using 8 elements in its plan and 3 through the thickness. The rubber layers were modelled using the Seki (1987) strain energy function. After discussion with ENEL and ENEA, it was decided to assume an elastic-perfectly plastic behaviour for the lead. The yield stress of the lead in shear was estimated to be about 75kg/cm^2, giving a yield stress in tension of 130kg/cm^2 based on Von Mises criterion. The Young's modulus and Poisson's ratio used were 175000kg/cm^2 and 0.44 respectively. The criteria chosen for the yield surfaces was Von Mises together with an isotropic strain hardening rule. MARC does not allow the Tresca yield surface criteria.

Figure 31 shows the FE predicted behaviour of the LRB in shear up to 200% strain. The experimental loops for the 200% cyclic deformations under the design vertical load are also shown. The FE solver did not converge on the initial retraction cycle beyond the 150% shear strain, hence the presence of the discontinuous curves. The FE predicted behaviour appears to agree reasonably well up to 150% shear strain. However, the predicted peak of the shear force at 200% is about 15% higher than the experimental data.

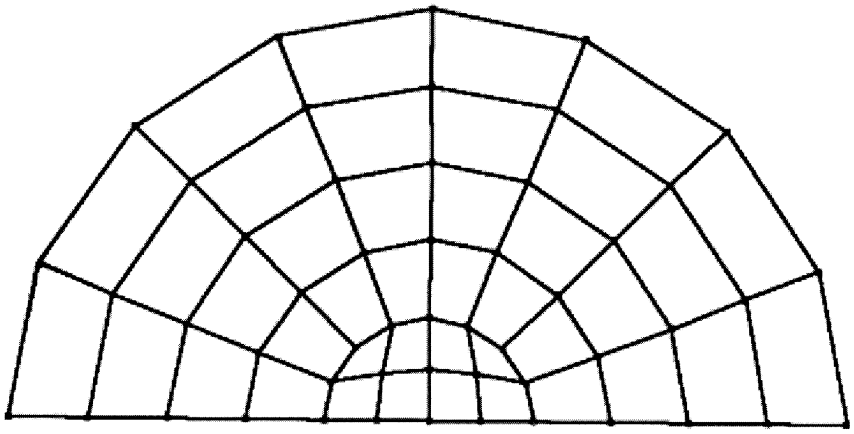

FIG. 30. FE 3-D mesh for a single layer of LRB (plan view).

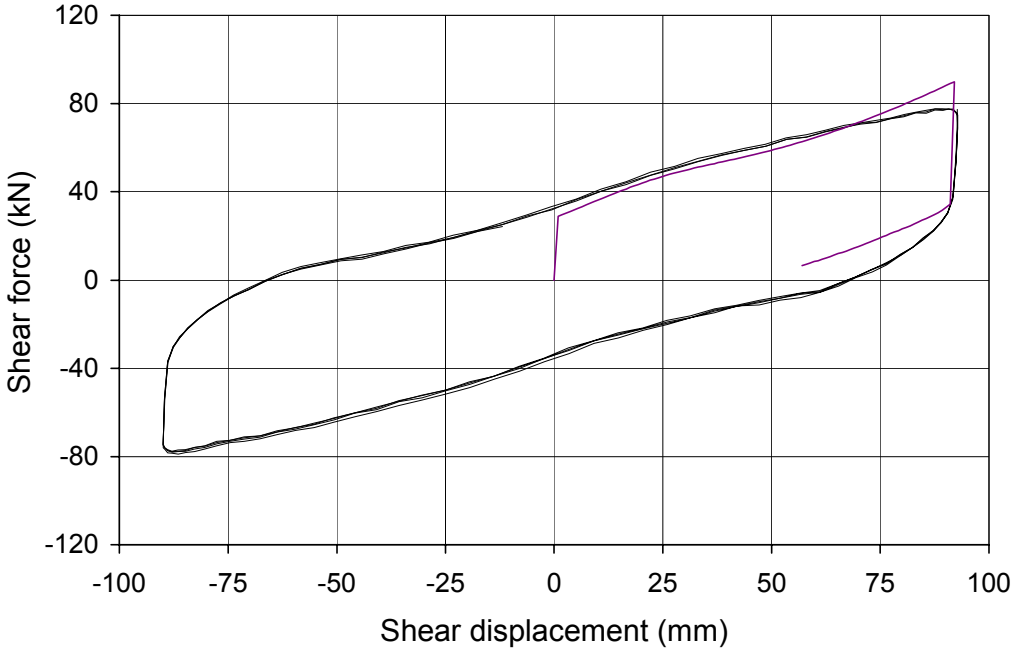

FIG. 31. FE predicted behaviour of LRB in shear up to 200% strain.

6. PREDICTING THE STIFFNESS OF AN ISOLATOR UNDER COMPRESSION AND SHEAR

6.1. Introduction

Finite element analysis provides a useful tool for predicting the behaviour of isolators under service conditions. Initially, a three-dimensional finite element model of a thin disc, bonded on both sides, was used. A small compression was applied, followed by a shear to

200% using a Mooney-Rivlin or Ogden strain energy function for the material. An unexpected result of the analysis was that the height of the disc increased under large shear strains. The details of the behaviour depended on both the strain energy function and finite element code. The height increase was not observed experimentally. Prompted by these interesting results, a more detailed analysis of the behaviour of rubber blocks under compressive and shear loads was carried out using two-and three-dimensional models.

6.2. The role of the mesh density

A unit square block of rubber was modelled using a mesh with different numbers of quadrilateral elements along each of its directions. The material model was neo-Hookean with C_{10}=0.25. The block was subjected to an initial compressive load of 0.1 followed by a shear deformation of 100% strain in the horizontal direction. Two other models, one a rectangular block with one unit of length high and eight units wide, and the other of a unit cube were also analysed in a similar manner. A typical deformed mesh for a 32 × 32 element model in plane strain is shown in Fig. 32.

Figure 33 shows the change in the height of the square block after the imposition of the compressive and shear deformation for different mesh densities. The compressive displacement in the vertical direction is not strongly affected by the mesh density, except for the very coarse meshes. However, the height drop during the shear phase is very sensitive to the density of the mesh. An increase in the number of the elements in either direction affects the predictions of the height drop. The prediction of the shear stiffness of the block, shown in Figure 34, also indicates that the mesh density influences the shear response. The sensitivity of the height drop and shear stiffness to the mesh density is due to the large distortions of the mesh along and close to the free sides of the block. A finer mesh predicts more accurately the deformation of these regions and hence their contribution to the overall stiffness of the block (see Fig. 32).

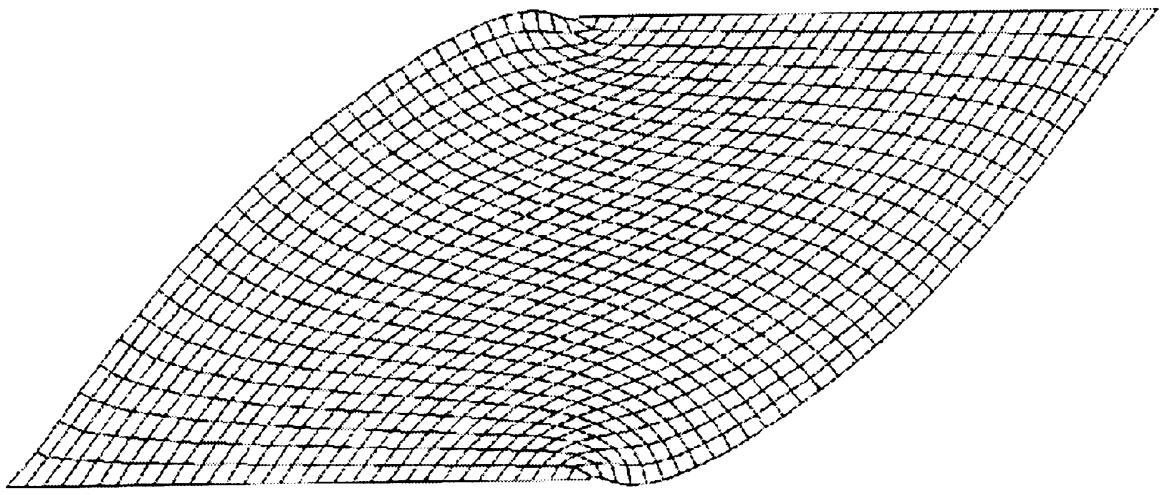

FIG. 32. Deformed FE mesh showing distortion and bending of edge elements.

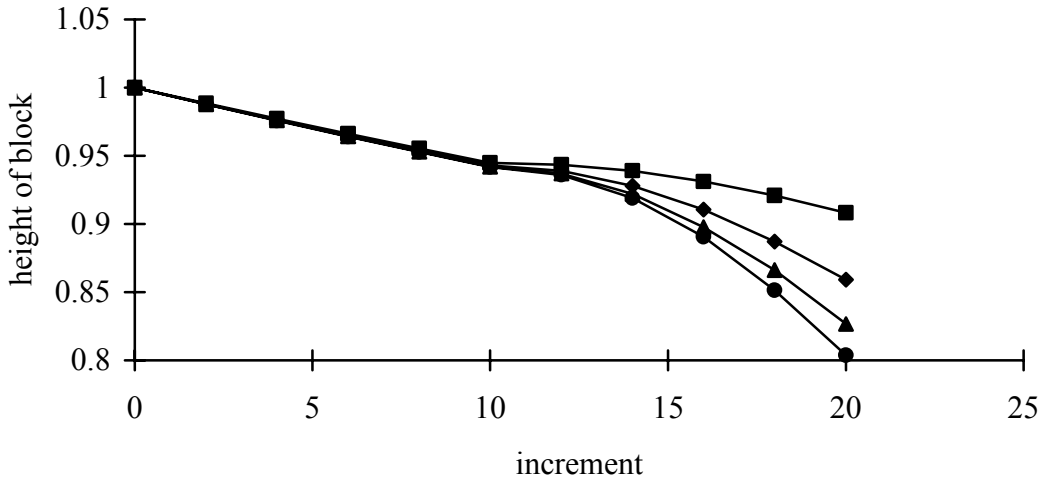

FIG. 33. Effect of mesh density on the height change of a unit block in plane stress. A load of 0.1, followed by a shear of 1 was applied to a neo-Hookean material with C_{10}=0.25. Number of mesh subdivisions across the width and the height respectively were: ■ 2,2; ♦ 4,4; ▲ 8,8; ● *16,16.*

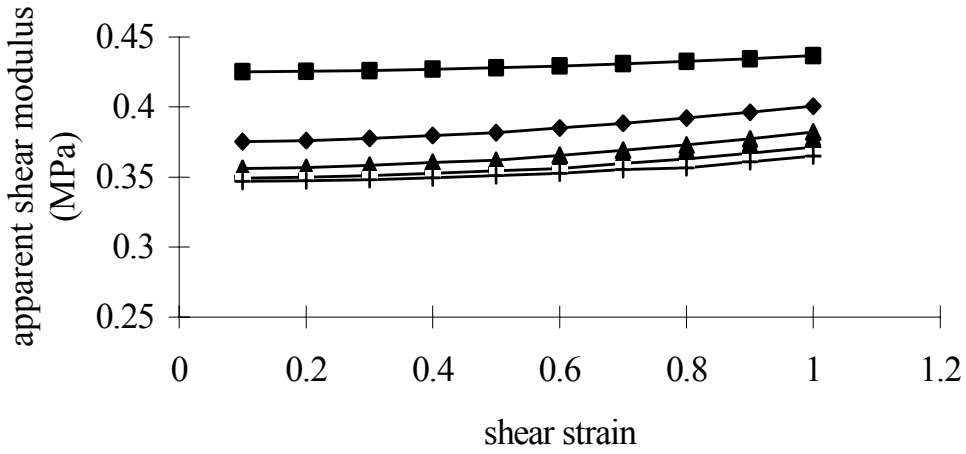

FIG. 34. Effect of mesh density on the apparent shear modulus of a unit block in plane stress load of 0.1, followed by a shear of 1 was applied to a neo-Hookean material with C_{10}=0.25. Number of mesh subdivisions across the width and the height respectively were: ■ *2,2;* ♦ 4,4; ▲ *8,8;* ● *16,16; + 32, 32.*

For higher shape factor blocks of rubber under compression and shear loads, it has been found that providing the portion of the rubber outside the overlapping region between the top and bottom surfaces of the pad are meshed reasonably finely the prediction of the change in the height of the pad will be reasonably accurate.

6.3. The choice of the strain energy function

Rivlin (1948) derived a set of equations relating the stresses required to maintain a block of rubber in simple shear. The differences between pairs of Cauchy stress for a simple shear in the x-direction of a x-y plane are given by:

$$t_{xx} - t_{zz} = 2\gamma^2 \frac{\partial W}{\partial I_1} \tag{27}$$

$$t_{yy} - t_{zz} = -2\gamma^2 \frac{\partial W}{\partial I_2} \tag{28}$$

Equations (27) and (28) indicate that in order to maintain the state of simple shear, as well as the shear stress, two normal stresses on at least two pairs of the faces of the block must be present. For the case of plane stress boundary condition (i.e. $t_{zz} = 0$), the normal stress t_{yy} and the shear stress t_{xx} are given by:

$$\begin{aligned} t_{xx} &= 2\gamma^2 \frac{\partial W}{\partial I_1} \\ t_{yy} &= -2\gamma^2 \frac{\partial W}{\partial I_2} \end{aligned} \tag{29}$$

Hence, the normal stress t_{yy} in the direction orthogonal to the direction of shear is proportional to the square of the shear strain and the first partial derivative of strain energy function with respect to I_2. Equations (27) to (29) indicate that the choice of the strain energy function is important in predicting the magnitude of the normal stresses. Clearly, the response of a pad of rubber to a compressive and shear load will depend on the boundary conditions and the extent of its departure from a simple shear deformation. The results of an FE investigation on the effect of the choice of the strain energy function on the prediction of shear and normal response of a pad of rubber under combined compression and shear loadings is reported in the remaining part of this section.

In order to avoid the use of meshes with large number of elements, it is advantageous to solve the problem in two dimensions and assume that the behaviour in the third dimension approximates sufficiently accurately to either plane strain or plane stress. Therefore, solutions for cases in plane strain, plane stress and some 3-D cases were considered.

The main material models considered were neo-Hookean with C_{10}=0.25MPa and Mooney with C_{10}=0.225 and C_{01}=0.025MPa. An Ogden strain energy function was also used. The parameters for this function were taken from Ogden (1972) fit to the stress-strain data of Treloar. All three models give a shear modulus for the rubber of G=0.5MPa at around zero strain.

Figures 35 and 36 show the mesh for the pad modelled as a 2-D and 3-D problem respectively. The shape factor for the 2-D case was 1.83 and for the 3-D was 2. In order to maximise the accuracy of the solution whilst avoiding excessively long computing times the mesh density near the free edges was increased as much as possible while leaving a rather coarse mesh in the central region of the pad. Figures 37 and 38 show the differences in the predicted change in the height of the pad under an initial compressive load followed by a shear deformation of 200% for both the plane strain and plane stress case. For the plane strain case, the choice of the strain energy function has little effect on the predicted behaviour, whereas for plane stress a much smaller height drop is predicted for the Mooney function (for which $\partial W/\partial I_2$ is positive) than for the neo-Hookean function for which $\partial W/\partial I_2$=0. For the

Ogden strain energy function the derivatives of the strain energy function with respect to I_1 and I_2 were calculated from $W(\lambda_1, \lambda_2)$. Using equations given in Section 4.2, Fig. 39 shows the variation of $\partial W/\partial I_1$ and $\partial W/\partial I_2$ with strain for the Ogden function used in the analysis. The height drop of the pad, modelled in 3-D, under a compression followed by a shear of 200% is shown in Figure 40. It is apparent that, as for the plane stress case examined earlier (see Fig. 38), there is a considerable difference between the different strain energy functions with a smaller height drop for material models with a positive rather than zero $\partial W/\partial I_2$ term.

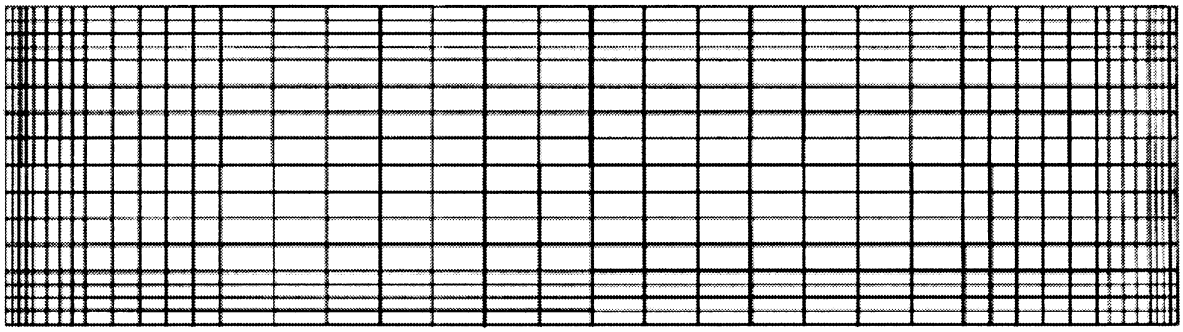

FIG. 35. 2-dimensional finite element mesh for measurement of the height drop of a block.

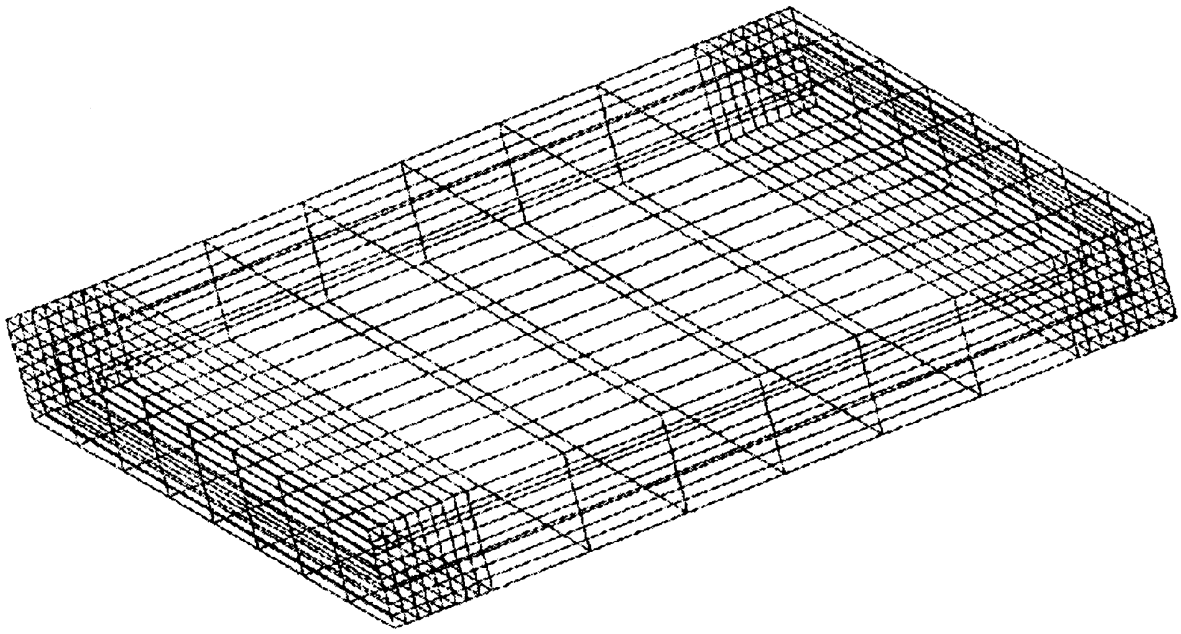

FIG. 36. 3-dimensional finite element mesh for measurement of the height drop of a block.

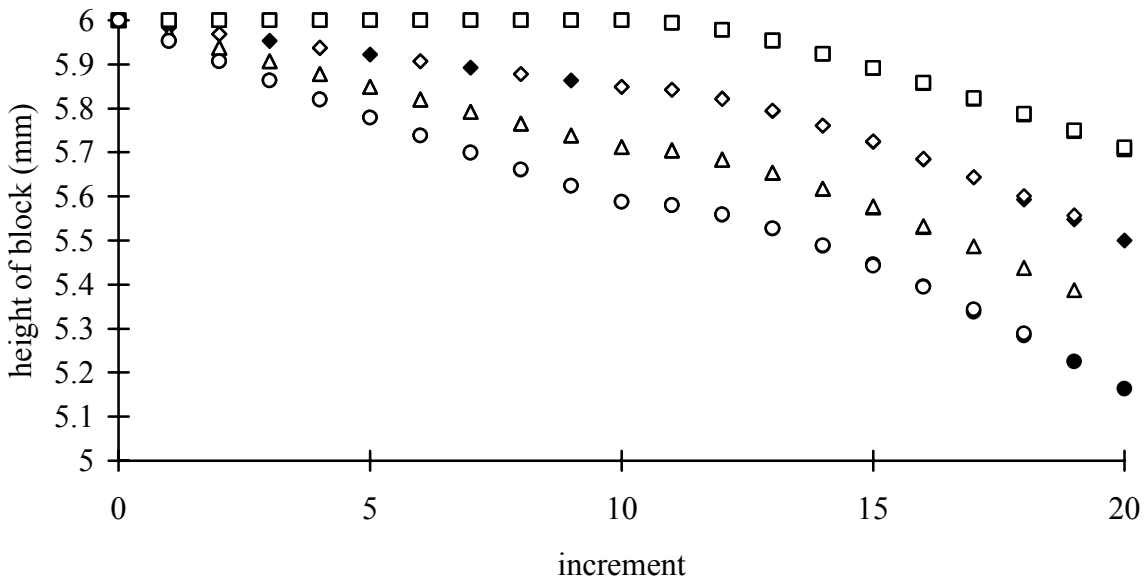

FIG. 37. Comparison of neo-Hookean (C_{10}=0.25MPa) and Mooney (C_{10}=0.225; C_{01}=0.025MPa) models of the height of a bonded block in plane strain of initial height 6mm and length 22mm subjected to a compressive load applied in 10 increments followed by a shear of 2 applied in a further 10 increments. ■ neo-Hookean, no compressive load; ♦ neo-Hookean, 5kN compressive load; ▲neo Hookean, 10kN compressive load; ● neo-Hookean, 15kN compressive load □ Mooney, no compressive load; ◊ Mooney, 5kN compressive load; Δ Mooney, 10kN compressive load; ○ Mooney, 15kN compressive load.

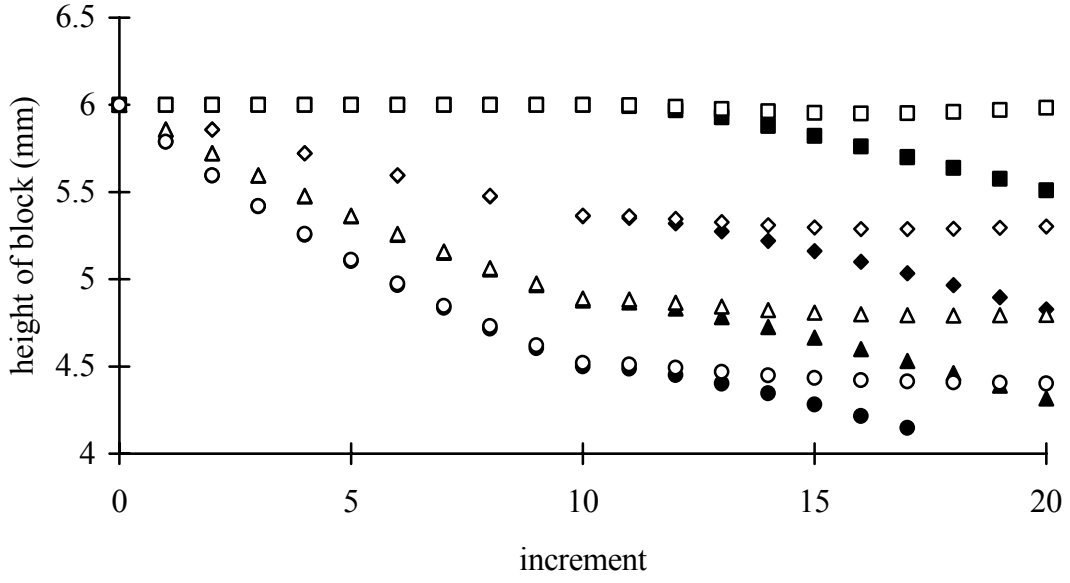

FIG. 38. Comparison of neo-Hookean and Mooney models of the height of a bonded block in plane stress. ■ neo-Hookean, no compressive load; ♦ neo-Hookean, 5kN compressive load; ▲ neo-Hookean, 10kN compressive load; ● neo-Hookean, 15kN compressive load; □ Mooney, no compressive load; ◊ Mooney, 5kN compressive load; Δ Mooney, 10kN compressive load; ○ Mooney, 15kN compressive load.

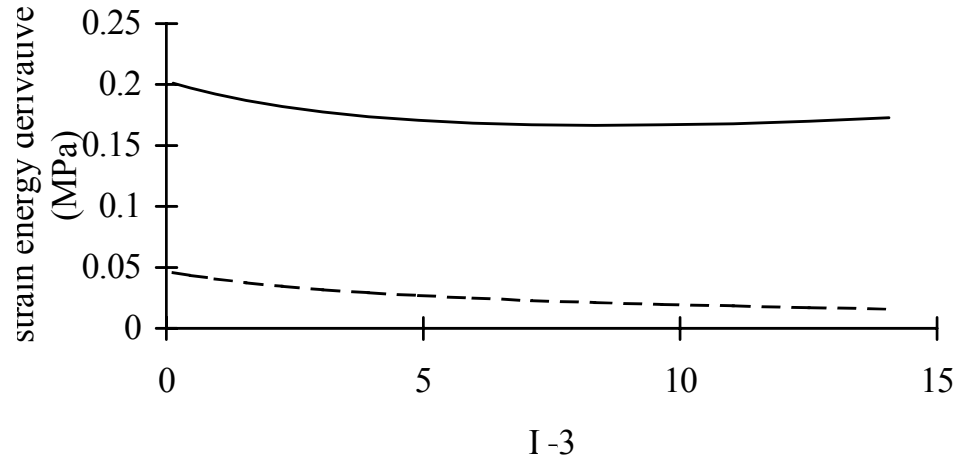

FIG. 39. Variation of $\partial W/\partial I_1$ and $\partial W/\partial I_2$ with I_1-3 for an Ogden type strain energy function with $\mu_1 = 0.7455$, $\alpha_1 = 1.3$, $\mu_2 = 0.00142$, $\alpha_2 = 5$, $\mu_3 = -0.01183$, $\alpha_3 = -2.0$; — $\partial W/\partial I_1$; - - - - - - $\partial W/\partial I_2$.

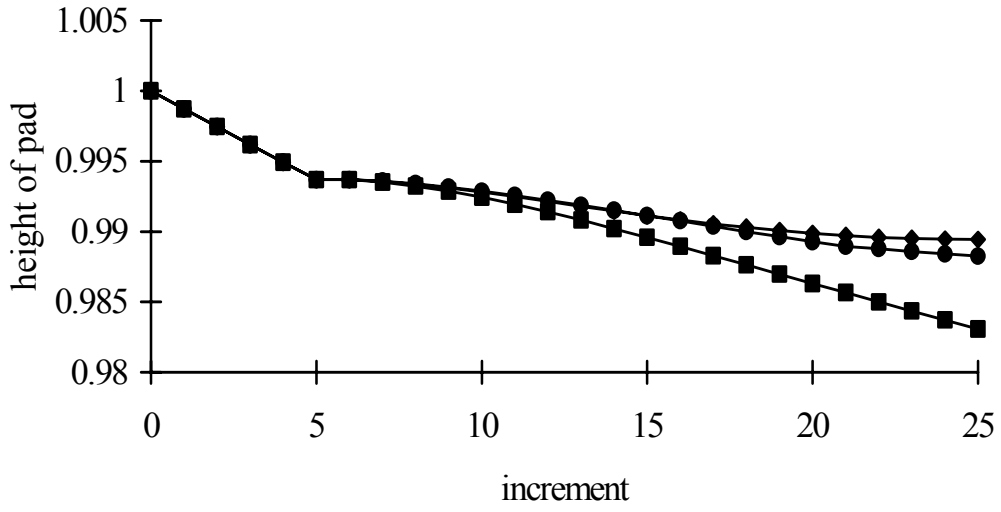

FIG. 40. Comparison of neo-Hookean and Mooney models of the height of a square block of height 1 and width 8, subjected to a compressive load of 6.4 followed by a shear strain of 2. ■ neo-Hookena, $C_{10} = 0.25$; ♦ Mooney, $C_{10} = 0.225$, $C_{01} = 0.025$; ● Ogden, $\mu_1 = 0.7455$, $\alpha_1 = 1.3$, $\mu_2 = 0.00142$, $\alpha_2 = 5$, $\mu_3 = -0.01183$, $\alpha_3 = -2.0$.

Owing to the qualitative similarity between the 3-D and plane stress models, further work was carried out in plane stress to avoid extensive computing times. Figure 41 shows the prediction of a plane stress model. In addition to the three material models examined, an additional Mooney model with negative $\partial W/\partial I_2$ was also included. This model has the same shear modulus as the other Mooney material but the sign of its C_{01} term is negative.

Again, the predicted height drop is determined by the magnitude of $\partial W/\partial I_2$. For the two materials where $\partial W/\partial I_2$ was positive, an increase (rather than a decrease) in the height of the block was predicted. For the material with a negative $\partial W/\partial I_2$ an especially large drop in the height was seen. It is also interesting that changing the sign of the C_{01} has not changed the

predicted deflection during the first phase of the loading where only a compressive load is being applied. Therefore the sign and the magnitude of the $\partial W/\partial I_2$ term plays a significant role in the prediction of the height change only during the shear phase. The effect of the strain energy function is more pronounced in plane stress than for the 3-D model. This is expected due to the lower constraint on lateral dimensional changes in plane stress.

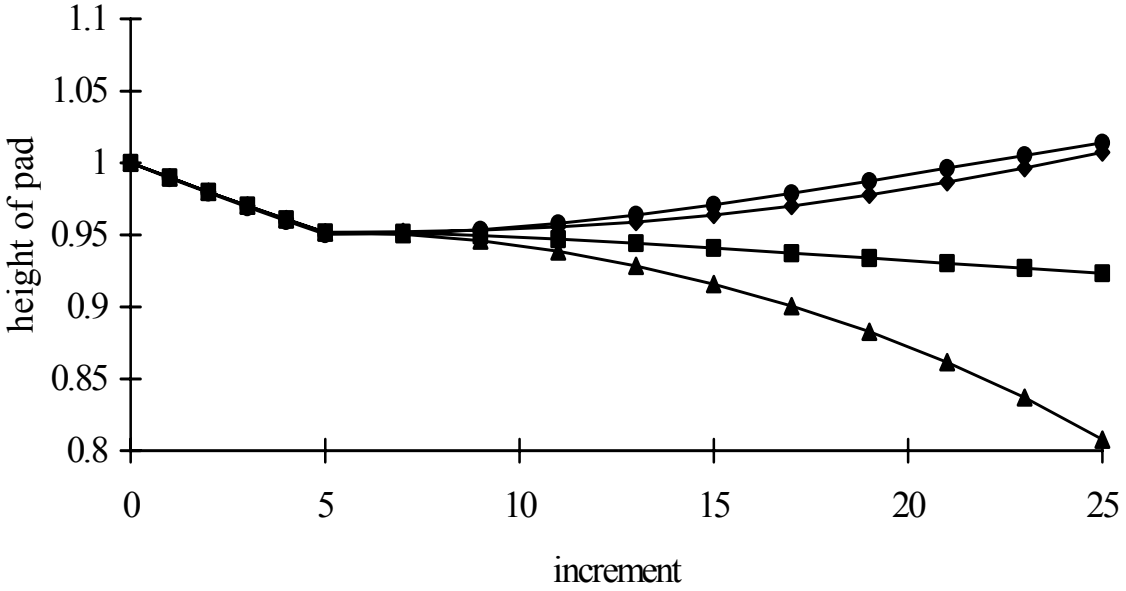

FIG. 41. Effect of strain energy function on the height drop of a pad of length 8 and initial height 1 in plane stress subjected to a compressive load of 0.8 followed by a shear strain of 2. ■ *neo-Hookean,* $C_{10} = 0.25$; ♦ *Mooney,* $C_{10} = 0.225$, $C_{01} = 0.025$; ▲ *Mooney,* $C_{10} = 0.275$, $C_{01} = -0.025$; ● *Ogden strain energy function with* $\mu_1 = 0.7455$; $\alpha_1 = 1.3$, $\mu_2 = 0.00142$, $\alpha_2 = 5$, $\mu_3 = -0.01183$, $\alpha_3 = -2.0$.

5.6.4. Conclusions

The FEA revealed the following features for a layer of rubber under compression and shear.

(i) The height drop is very sensitive to mesh density, especially near the free edges of the block. This effect is more pronounced for lower shape factor pads.

(ii) For an infinitely wide pad, the application of a compressive stress in the direction orthogonal to the shear deformation is required to achieve a state of simple shear. Otherwise there will be a gain in the height of the pad. The magnitude of this rise in the height is approximately proportional to $-\gamma^2\, \partial W/\partial I_2$.

However for a pad with finite width there will be a height drop under the action of the combined compressive and shear loads due to the edge effect. Therefore the prediction of the change in the height of the pad is a balance between the edge effects and the normal stress required to keep the simple shear mode of deformation. The larger the $\partial W/\partial I_2$ or the shear strain the higher the contribution of the latter.

This suggests that in choosing the form of the strain energy function, and also when fitting the model to experimental data the magnitude of the $\partial W/\partial I_2$ term plays an important role in predicting the behaviour of the pad in the direction orthogonal to the direction of the shear.

(iii) This study shows that a given material model may predict the behaviour of an elastomeric component reasonably well along one loading direction yet be unreliable in predicting the behaviour in another.

5.7. Compression stiffness of a rubber pad bonded between extensible layers

5.7.1. Theory

Kelly (1998) has derived an expression for the compression stiffness of an infinitely long block of rubber sandwiched between two layers of an extensible material as shown in Figure 11. The extensible reinforcement has a thickness of t_f and Young's modulus of E_f.

The compressive modulus (E_c) of the pad is given by the following:

$$E_c = \frac{Pt}{A\Delta} = \frac{E_f t_f}{t}\left(1 - \frac{\tanh \alpha b}{\alpha b}\right) \tag{30}$$

where P is the applied load, t is the thickness of the rubber layer, A is the cross-sectional area, is the compressive deflection, b is the half width of the block and α is defined by:

$$\alpha^2 = 12G / E_f t_f t \tag{31}$$

where G is the shear modulus of the rubber.

5.7.2. Finite element analysis of the pad

The block was modelled as a rectangle in plane strain. The symmetry of the problem was exploited by modelling only half of the pad. The thickness of the rubber was 0.05 units of length, modelled by 10 quadrilateral elements. The thickness of each layer of reinforcement was 0.005, modelled using one element through its thickness. Blocks of shape factors of 1, 5, 10 and 20 were considered by using different numbers of elements across the width. The central part of the block was modelled using elements of width 0.025. Elements near the edge of the block were further subdivided. An example of the mesh for a block with the shape factor of 10 is shown in Fig. 12. The rubber was modelled as a neo-Hookean material with a shear modulus of 0.5MPa and a bulk modulus of 2500MPa. The reinforcement was modelled as an isotropic material with a Poisson's ratio of 0.4 and a Young's modulus which was varied to test the effects of different stiffnesses of reinforcement.

A compressive deflection of 0.001 was applied to the top reinforcing layer in 10 increments. $E_c/4GS$ was obtained from the reaction force using equation (30) and plotted as a function of $12\alpha^2b^2$ for comparison with the theory.

The results are shown in Fig. 42. The finite element results for the pad with shape factor 1 predicted a much higher normalized stiffness than the theoretical results and have been omitted from the graph for clarity.

The finite element analysis generally predicts higher normalized compression moduli than Kelly's theory. This is to be expected for low shape factors, such as S=1, where the difference between Kelly's (1998) approximation to the compression modulus for the incompressible case; $E_c=4GS^2$, differs significantly from the more accurate $E_c=4G(1+S^2)$ (Gent & Lindley, 1959). At higher shape factors, where this correction is unlikely to be significant, the reasons for the difference are less clear.

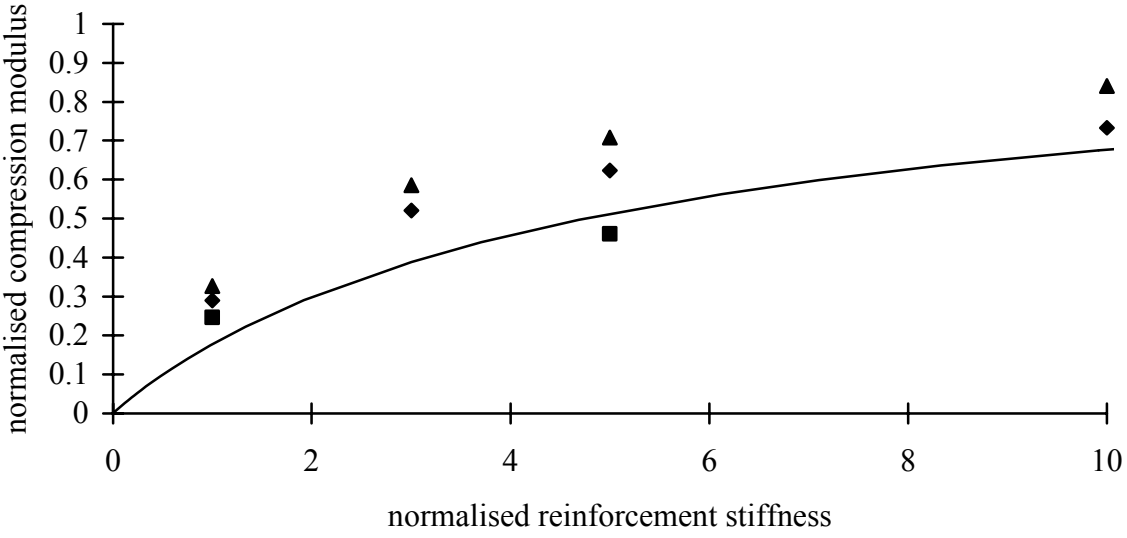

FIG. 42. Comparison of theory (Kelly, 1998) and finite element analysis for the compression stiffness of a pad with extensible reinforcement. ■ *FEA, shape factor = 20;* ♦ *FEA, shape factor = 10;* ▲ *FEA, shape factor = 5; ------theory.*

REFERENCES

Ahmadi, H.R., Coveney, V.A., Fuller, K.N.G., (1991), "High damping natural rubber for seismic isolation bearings", Transactions of 11th conference on Structural Mechanics in Reactor Technology, (Tokyo, August 1991) volume K2, p.151

Ahmadi, H.R., Fuller, K.N.G., Muhr, A.H., (1996), "Predicting Response of non-linear damping rubber isolation systems". Proceedings of 11th World Conference in Earthquake Engineering, Acapulco

Davies, C.K.L., De, D.K., Thomas, A.G., (1994), "Characterisation of the behaviour of rubber for engineering design purposes (1) Stress and strain relations", Rubber Chem. Tech., **67**, 716

Derham, C.J., Thomas, A.G., (1980), "The design and use of rubber bearings for vibration isolation and seismic protection of structure", Eng. Struct. 2, 171

Dusi, A., Forni, M., Martelli, A., (1998), "Contribution of Italy to the activities on intercomparison of analysis methods for seismically isolated nuclear structures: Finite element analysis of lead rubber bearings. Proc. third IAEA Research Co-ordination Meeting, Hertford, UK

Fuller, K.N.G., Gough, J., Ahmadi, H.R., (1998), "FE analysis of seismic isolators: comparison with experimental results". Proc. third IAEA Research Co-ordination Meeting, Hertford, UK

Fuller, K.N.G., Gough, J., Ahmadi, H.R., Dusi, A., (1997), "Contribution of the United Kingdom to the activities on intercomparison of analysis methods for seismically isolated nuclear structures". International Post-SMiRT Conference Seminar on Seismic Isolation, Passive Energy Dissipation & Active Control of Seismic Vibrations of Structures Taormina, Italy

Gent, A.N., Lindley, P.B., (1959), "The compression of bonded rubber blocks". Proc. Instn. Mech. Engineers, **173**, 111

Gregory, I.H., Muhr, A.H., Stephens, I.J., (1997), "Engineering applications of rubber in simple extension", Plastics, Rubber and Composites: Processing and Applications, **26**, 118

Gregory, M.J., (1979), "The stress-strain behaviour of filled rubber at moderate strain", Plastics & Rubber: Materials and Applications, **4**, 184

Harris, J.A., (1987), "Dynamic testing under non-sinusoidal conditions", Rubber Chem. & Tech., 60, 870

Housner, G.W., (1959), "Behaviour of structures during earthquakes", J. Eng. Mechs. Divison (Proc. ASCE), EM4, 109

Kelly, J.M., (1998), "A predictive model for the stiffness and damping properties of fiber-reinforced bearings". Proc. third IAEA Research Co-ordination Meeting, Hertford, UK

Ogden, R.W., (1972), "Large deformation isotropic elasticity - on the correlation of theory and experiment for incompressible rubberlike solids", Proc. Roy. Soc. Lond., **A326**, 565

Ogden, R.W., Chadwick, P., (1972), "On the deformation of solid and tubular cylinders of incompressible isotropic elastic material", J. Mech. Phys. Solids, **20**, 77

Rivlin, R.S., (1948), "Large elastic deformations of isotropic materials IV. Further developments of the general theory". Phil. Trans. R. Soc. A**241**, 379

Rivlin, R.S., Saunders, D.W., (1951), Phil. Trans. R. Soc. A**243**, 251

Seki, W., Fukahori, Y., et al., (1987), "A large-deformation finite-element analysis for multi-layer elastomeric bearings". 133rd American Chemical Society, Rubber Division, Montreal, Canada

Treloar, L.R.G., (1975), "The physics of rubber elasticity", 3rd edition, Clarendon Press, Oxford

Treloar, L.R.G., (1944), "Strain-stress data for vulcanized rubber under various types of deformation", Trans. Faraday Soc., **40**, 59

Twizell, E.H., Ogden, R.W., (1983), "Non-linear optimization of the material constants in Ogden's stress-deformation function for incompressible isotropic elastic materials", J. Austral. Math. Soc., **B24**, 424

COMPARISON OF COMPUTER SIMULATED AND OBSERVED FORCE DEFORMATION CHARACTERISTICS OF ANTI-SEISMIC DEVICES AND ISOLATED STRUCTURES

S.B. BHOJE, P. CHELLAPANDI, S. CHETAL,
R. MURALIKRISHNA, T. SALVARAJ
Indira Gandhi Centre for Atomic Research, India

Abstract

The paper discusses the finite element analysis of the force deformation characteristics of high damping rubber bearings, lead rubber bearings and natural rubber bearings. The dynamic response of structures isolated using bearings is also presented. The general purpose finite element program ABAQUS has been used for the numerical predictions under monotonic loads. For computing the dynamic response, a simplified model of the rubber bearing in the form of elasto-plastic system is used. This equivalent model is implemented using the computer code CASTEM-2000 and the dynamic response is obtained. The numerical results are found to match well with the experimental results.

1. INTRODUCTION

The use of seismic isolation for structures has been gaining worldwide acceptance as an approach to aseismic design. Seismic isolation is achieved by providing suitable devices called base isolation devices between the superstructure and the foundation. The principle of base isolation is to reduce the structures natural frequency by using devices with low horizontal stiffness at the base to decouple the structure from the ground, Me Entee [1]. The basic feature of a base isolation system is that the superstructure vibrates almost like a rigid body due to the combination of the flexibility and energy dissipation mechanisms of the components of the base isolation system. The flexibility of the base isolation system is usually achieved by providing elastomeric bearings made of laminated rubber bearings reinforced with steel. The energy absorption devices make use of the phenomena of hysteretic damping for the energy absorption. These hysteretic dampers utilise the yielding properties of the steel present in the bearings. In some isolation devices like the lead/rubber bearing, the yielding of lead is made use of for realising hysteretic damping.

Seismic isolation of Nuclear Power Plants (NPP) has been addressed by Plichon and Jolivet [2] who concluded that base isolation would result in reduction in seismic induced load and hence economical structural design. Two French built Pressurised Water Reactors employ base isolation systems. The plants are at Koeburg in South Africa and Cruas in France. Seismic base isolation of LMFBRs has been addressed by Me Entee [1]. Fast Breeder Reactors (FBR) operate at high temperature which induces high thermal stresses during transients. Hence the thickness has to be minimised to limit the thermal stresses which is contradicting the requirements of conventional aseismic design of making the structures more rigid. It is possible to meet this contradictory requirement by adopting seismic isolation. Seismic base isolation has been adopted for the ALMR project, Me Entee [1].

A variety of base isolation devices including Laminated Rubber Bearing (LRB), frictional bearing etc. have been developed. Among the isolation systems that have gained acceptance for practical implementation, LRB isolation pads are most widely used. Full scale and reduced scale isolation devices have been developed and tested in countries like Italy, Japan, and USA. Many experimental and numerical studies are required on isolation pads to substantiate

the adequacy of design and service conditions so that they can be used for FBR applications. The major studies include deformation characteristics, aging behaviour and damping of isolation pads. In this context IAEA is sponsoring Coordinated Research Programme (CRP) on "Intercomparison of Analysis Methods for Seismically Isolated Nuclear Structures" under the auspices of International Working Group of Fast Reactors (IWGFR). India, having a long term R&D interest in the development of seismic isolation bearings, is participating in this CRP along with the countries, Italy, USA, Japan, South Korea, Russia and European Commission. In this CRP, the participants were provided with experimental data on the base isolation devices and the dynamic response of structures isolated with these base isolation devices. The participants were asked to work on these benchmark problems. The analysis methods and results were periodically discussed in the Research Coordination Meetings (RCM). The results worked out by us for the benchmark problems are presented in the following sections.

2. EXPERIMENTAL INPUT DATA

2.1 Italian data

Italy has supplied experimental results on HDRB such as deformation characteristics under combined compression & shear and vertical loads obtained on single bearing (Fig. 1). The main geometrical details of isolation bearing are given below

Along with this, the experimental results on rubber specimen have also been supplied so as to define material properties for rubber. These include results of (nominal stress and nominal strain) uniaxial, biaxial and planar test data on simple rubber specimen (Fig. 2a-2c).

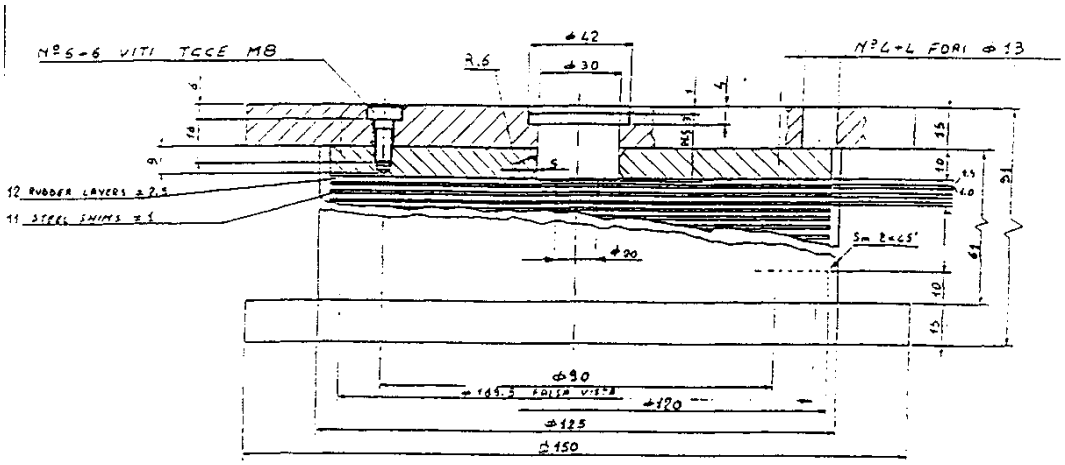

Thickness of rubber sheets	= 2.5 mm
Number of rubber layers	= 12
Total thickness of rubber layers	= 30 mm
Thickness of steel plate	= 1 mm
Number of steel plates	= 11
Thickness of steel end plates	= 10 mm
Diameter of rubber sheet	= 125 mm
Diameter of inner hole	= 20 mm
Design vertical load	= 50kN
Design horizontal deformation	= 30 mm (100% shear strain)

FIG. 1. High damping rubber bearing (Italy).

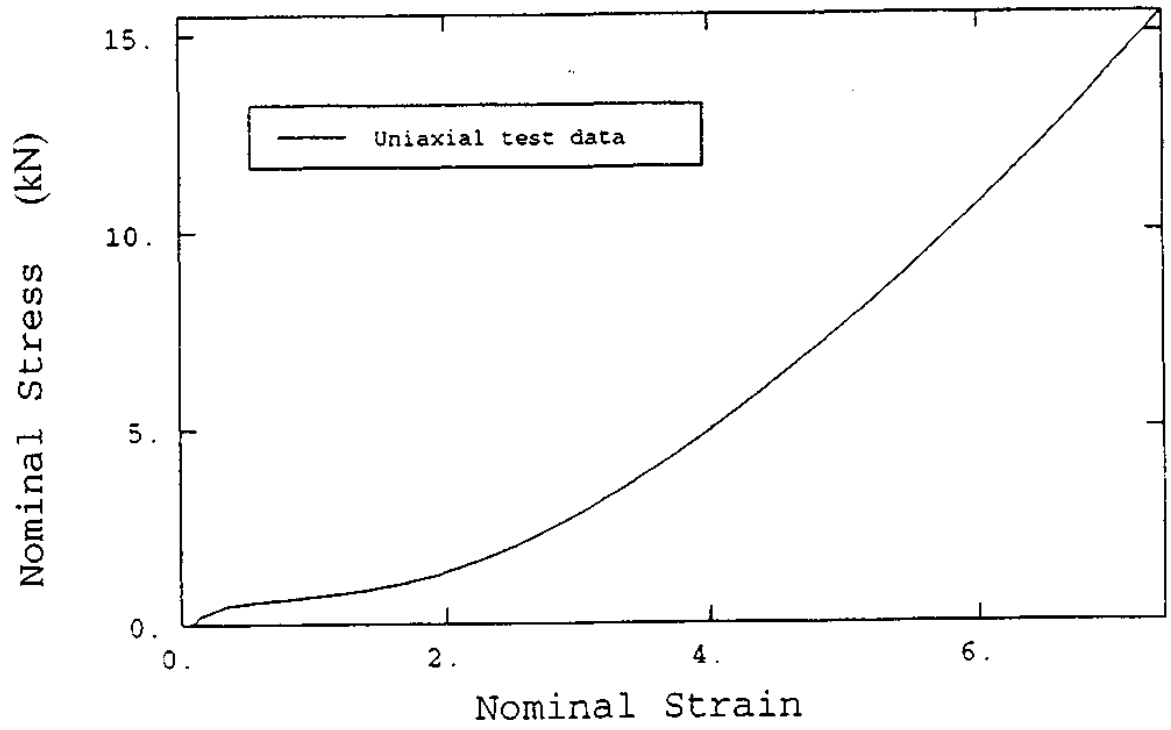

FIG. 2a. Uniaxial test date (Italy).

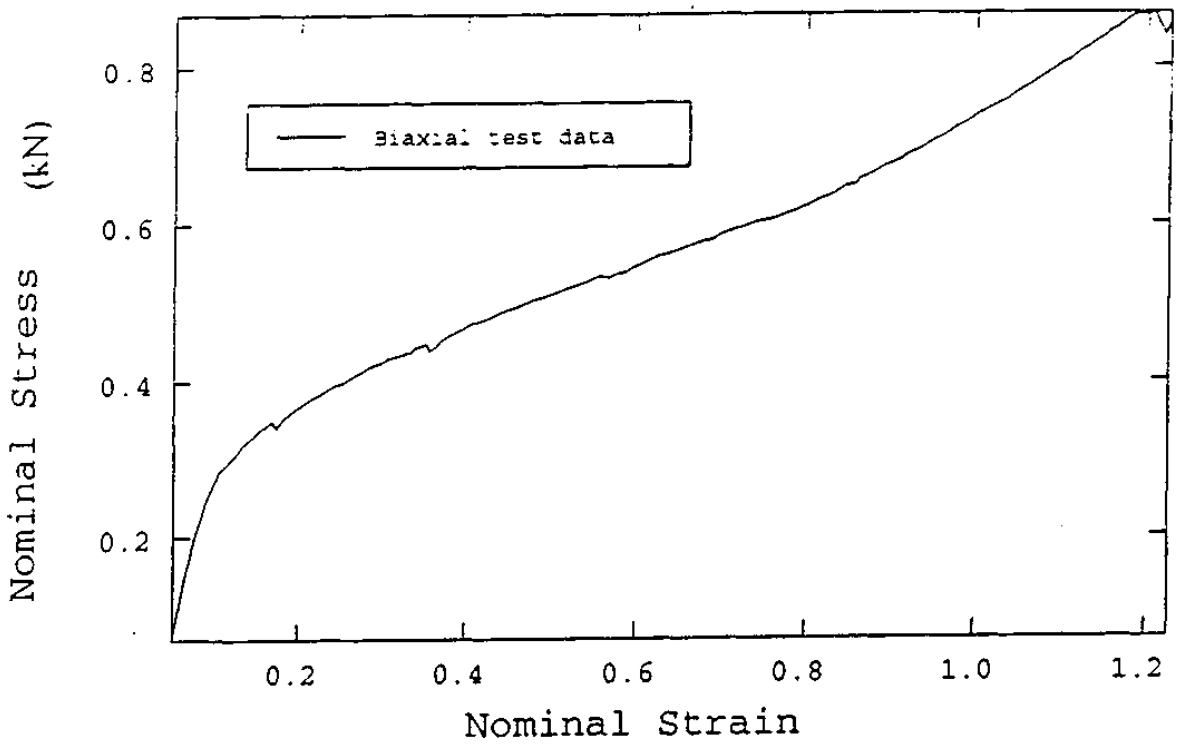

FIG. 2b. Biaxial test date (Italy).

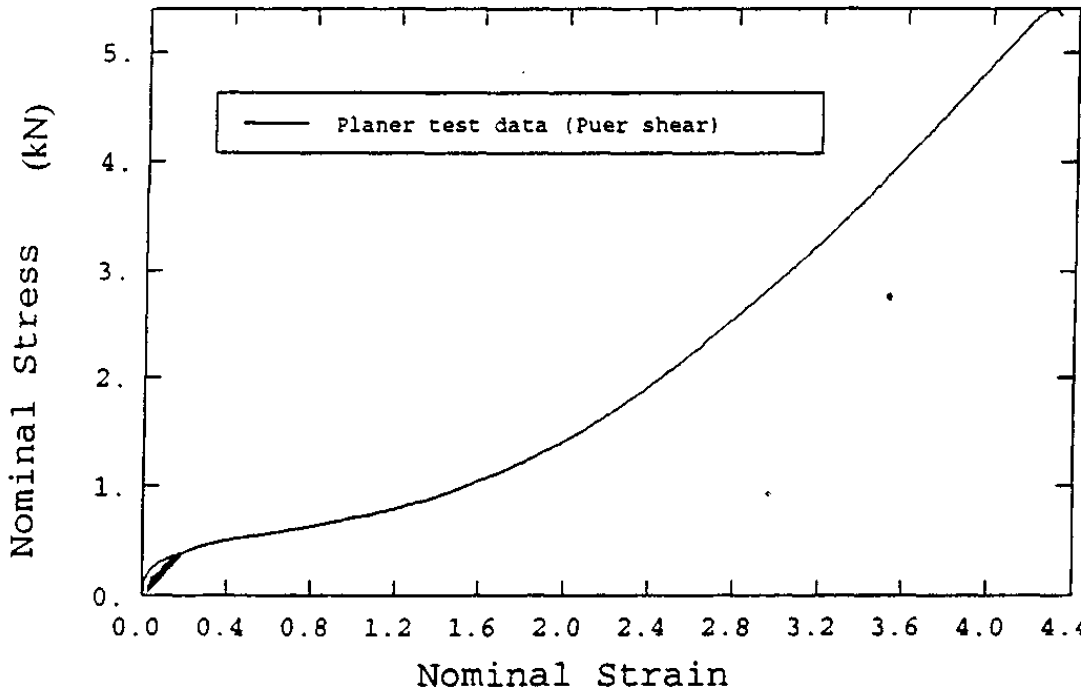

FIG. 2c. Planar test data (Italy).

2.2 Japanese data on Natural Rubber Bearing

Japan has supplied geometrical (Fig. 3) and test data on Natural Rubber Bearing (NRB) & Lead Rubber Bearing. Also the derivative of strain energy as the function of strain invariants (I, & I_2) has been supplied to characterise the rubber material (Fig. 4). The details of geometric data of the NRB is given below:

Thickness of rubber sheet = 5.7 mm
Number of rubber layers = *25*

Total thickness of rubber layers - 142.5 mm =

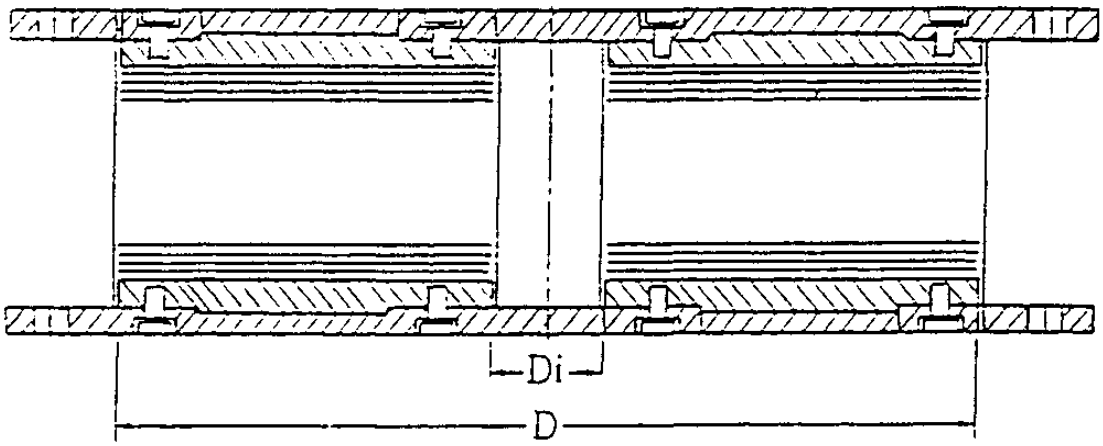

FIG. 3. Natural rubber bearing (Japan).

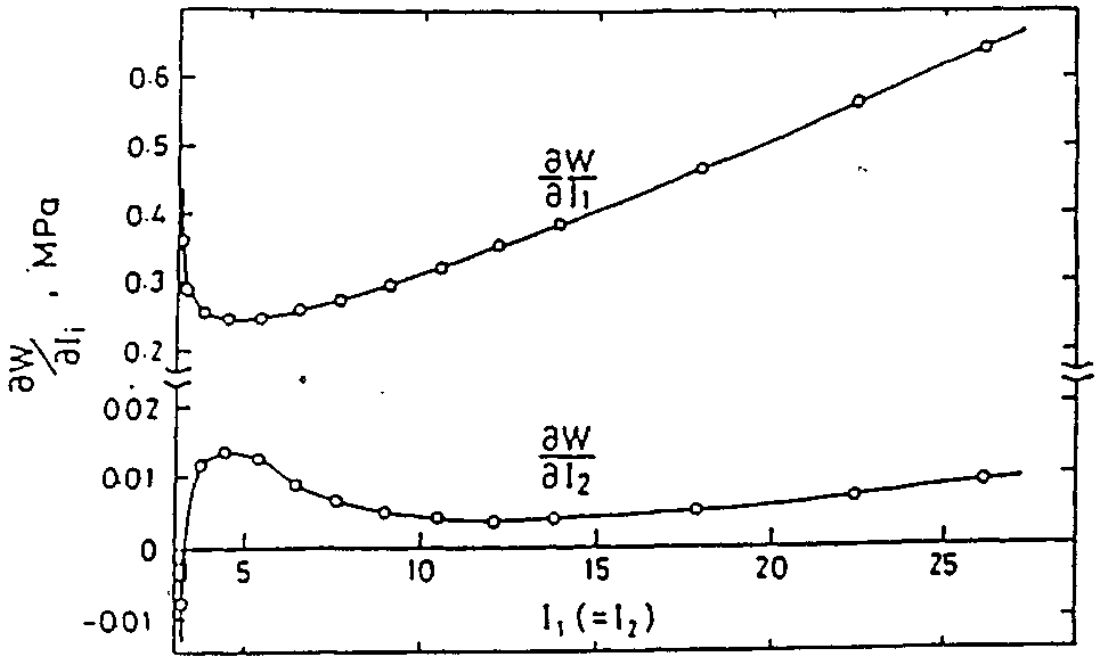

FIG. 4. Strain energy density function (Japan).

The experimental results include combined compression & shear and compression with different offset shear strain.

2.3 CRIEPI Lead Rubber Bearing Data Supplied By Japan

The main geometrical and other details of the CRIEPI Lead Rubber Bearing are given below:

Thickness of rubber sheets	= 4.9 mm
Number of rubber layers	= 25
Total thickness of rubber layers	- 122.5 mm
Thickness of steel plate	= 3.1 mm
Number of steel plates	*= 24*
Diameter of rubber sheet	= 876 mm
Diameter of inner hole	= 98.0 mm
Design vertical load	= 1500kN
Shear modulus of rubber	= 6.0 MPa
p	= 200 GPa
V_{steel}	= 0.271
E_{lead}	= 17500 MPa
V_{lead}	= 0.44

The experimental results on rubber specimen have also been supplied to define material properties for rubber. These include results of strip biaxial test data where the derivative of strain energy as the function of strain invariants (I, & I_2) are given. The other data include test results on combined compression & shear and compression with different offset shear strain.

2.4 Korean data on High Damping Rubber Bearing

Korea has supplied experimental results on HDRB such as deformation characteristics under combined compression & shear on single bearing. The main geometrical and other details of the KAERI HDRB are given below:

Thickness of rubber sheets	= 1.2 mm
Number of rubber layers	= 29
Total thickness of rubber layers	= 34.8 mm
Thickness of steel plate	= 1.6 mm
Number of steel plates	= 28
Thickness of steel end plates	= 30 mm
Diameter of rubber sheet	= 156 mm
Diameter of inner hole	= 10.5 mm
Design axial stress	= 2.55 MPa
Design horizontal deformation	= 34.8 mm (100% shear strain)

The experimental results on rubber specimen have also been supplied so as to define material properties for rubber. These include results of (nominal stress and nominal strain) uniaxial, biaxial, planar and confined volumetric test data on simple rubber specimen.

2.5 ALMR High Damping Rubber Bearing Data Supplied By USA

The main geometrical and other details of the ALMR HDRB (1:8 scale) are given below:

Thickness of rubber sheets	= 2.3 mm
Number of rubber layers	= *15*
Total thickness of rubber layers	= 34.5 mm
Thickness of steel plate	= 1.9 mm
Number of steel plates	= 14
Thickness of steel end plates	= 33 mm
Diameter of rubber sheet	= 153 mm
Diameter of inner hole	= 20 mm
Design axial stress	= 44kN
Shear modulus of rubber	= 1.4MPa

3. ANALYSIS PROCEDURE

In the first stage of the CRP, a single isolation bearing is analysed to predict the deformation characteristics under monotonic loadings. The loading combination for Italian HDRB are combined compression & shear and pure compression. For Japanese case , they are combined compression & shear and compression with different offset shear strain. For the KAERI HDRB, ALMR HDRB and CRIEPI Lead Rubber Bearing, the loading combinations are combined compression and shear with 100% design vertical load. In the second stage of the CRP, the dynamic response of structures isolated with the above bearings is computed.

3.1 Material Characterisation Of Rubber

The Laminated Rubber Bearing (LRB) is formed by alternated vulcanised rubber layers and steel shims. This rubber bearing has the features necessary for seismic isolation viz., high stiffness in vertical direction to take care of vertical load and low horizontal stiffness to reduce the acceleration load to the superstructure under seismic conditions. The LRB undergo large finite deformation before they fail. Rubber materials do not follow linear stress strain law and exhibit hyperelastic behaviour.

The isolation pads which undergo large deformation under seismic excitations thus exhibit strong nonlinear behaviour. Further the behaviour is complicated by the interaction of time dependence and sources of nonlinearities, Christensen, [3]. Thus the numerical modelling need to take care of high material and geometrical nonlinearities The hyperelastic material is characterised by the existence of strain energy function U, measured per unit volume of reference state, which is a function of deformation gradient.

For the present analysis, the Finite Element code, ABAQUS 5.6-1, [4] has been used. Rubber material can be characterised by using ABAQUS by two important forms of strain energy density functions viz polynomial and Ogden form. They are described briefly here. The polynomial form is given by

$$U = \sum_{i+j=1}^{N} C_{ij} (I_1 - 3)^i (I_2 - 3)^j + \sum_{i=1}^{N} \frac{1}{D_i} (J_{el} - 1)^{2i} \qquad (1)$$

Where I, and I_2 are independent invariants of strain and are given by

$$I_1 = \lambda_1^2 + \lambda_2^2 + \lambda_3^2 \qquad (2)$$

$$I_2 = \lambda_1^2 \lambda_2^2 + \lambda_2^2 \lambda_3^2 + \lambda_1^2 \lambda_3^2 \qquad (3)$$

A-J - principal extension ratio, Cy, Dj - material constants, N - order of the polynomial J_{el} - elastic volume ratio.

The second term D_{ℓ} becomes zero for fully incompressible material which is approximately true for rubber like materials. Rubber material undergoes little change in volume at stress levels that cause deformation and thus they can be treated as incompressible and subject to the constraint, $I_3 = 1$, where $I_3 = {}^{t}k_j^2$ A,$_2^2$ A,$_3^2$. Considering N=l, the strain energy density function reduces to the form suggested by Mooney i.e.

U = C,a,-3) + C_2(I_2-3) (4)

which is first two terms in the expansion of U as a double power series about the values I ,=3 and I_2=3 for the undeformed state. For moderate strain Mooney form is used. For high strain region, higher order terms in the strain energy function are required. The Ogden strain energy density function is given by

$$U = \sum_{i=1}^{N} \frac{2\mu_i}{\alpha_i^2} (\lambda_1^{\alpha_i} + \lambda_2^{\alpha_i} + \lambda_3^{\alpha_i} - 3) + \sum_{i=1}^{N} \frac{1}{D_i} (J_{el} - 1)^{2i} \qquad (5)$$

|j<, a, Di are material constants.

The fundamental difference of Ogden from polynomial form is that the strain components can have fractional powers and also the coupling between the principal extension ratios is absent in case of Ogden form.

3.2 Analysis Methodology

There are three major steps in the analysis methodology which are given below.

- The material constants of the strain energy density function for rubber material have to be found from experimental results from simple rubber specimen. Generally, three or more test results are required to determine the material constants. They are uniaxial tension, biaxial tension, planar tension (Pure shear) and volumetric test. From these experimental data of nominal stress vs. nominal strain, the material constants are fit by least square method. Alternatively the material constants can be found if derivative of the strain energy density function with respect to strain invariants ($I_,$, I_2) are given. In this report two forms of strain energy functions (Polynomial and Ogden) have been employed and their behaviour is compared.
- Normally 3-D finite element modelling is adopted to analyse the laminated rubber bearing. In addition to 3-D modelling of 180 deg sector of the isolator, two more models viz. axisymmetric model and single layer model are used because of the following reasons viz. i)the isolator is axisymmetric in geometry and the loading is asymmetric which can be applied through fourier component (n=l) ii) the behaviour of every rubber layer along with the steel plate is similar. The axisymmetric and single layer models are employed here to study the effectiveness in predicting the deformation behaviour of the isolator
- Calculation of displacements using the above FE models for various load cases and comparison with experimental results.

The above procedure is adopted for the analysis of all beaings.

4. NUMERICAL ANALYSIS OF RUBBER BEARING

4.1 Determination of Material Parameters for Rubber of Italian HDRB

The experimental data provided by Italy to evaluate material constants viz. uniaxial tension, biaxial tension and planar tension (Fig 2a-2c) are used to determine the material constants appearing in the strain energy density function (eqn. 1 & 5). ABAQUS has been used to determine the material parameters for the present analysis for polynomial and Ogden forms with N=2.

4.1.1 Finite Element Model

The hybrid C3D8H element and reduced integration element, C3D8R of ABAQUS have been used to model rubber and steel shims respectively. The finite element model consists of 2880 nodes and 1248 elements. Fig 5 shows the finite element mesh used for the analysis. For axisymmetric model, the elements, CAXA8H1 and CAXAR1 of ABAQUS have been used to model rubber and steel plates respectively. The model consists of 370 elements and 1380 nodes. For single layer model, the area resisting the combined compression and shear load is same for both single layer and full isolator. Hence a single layer of rubber is modelled and the deformation behaviour for combined compression (50 kN) & shear upto 400% shear strain has been obtained. For this single layer model, 3-D element of C3D8H is used. The deformation obtained by single layer model has been scaled up by the number of rubber layers (12) for the purpose of comparison with full model.

4.1.2 Finite Element Analysis

The isolator is first compressed with vertical load and then sheared to the required level by keeping the vertical load constant. The following three types of analyses have been completed by using both polynomial and Ogden forms of strain energy density function.

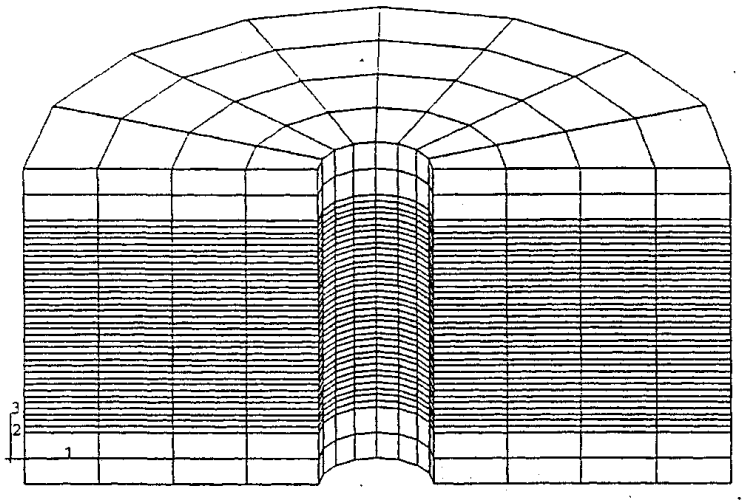

FIG. 5. Finite element mesh of HDRB.

The HDRB is applied with a vertical load of 50 kN (design vertical load) through the dummy node. Subsequently, the bearing is sheared by applying shear force through the same dummy node keeping the vertical force constant at 50 kN. The displacement of the top end plate is extracted with respect to applied shear force. The applied shear force has been increased till the required level of deformation (upto 400%) is reached. A typical deformed shape of isolator under this loading condition is given in Fig 6. The load displacement curve and its comparison with experimental results is shown in Fig 7 for 3-D model, axisymmetric model and single layer model for polynomial form of strain energy density function. Fig 8 gives the same results for Ogden form of strain energy density function.

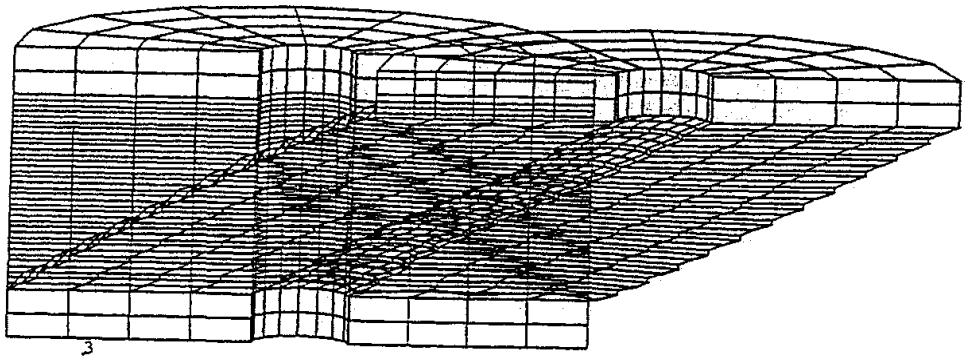

FIG. 6. Deformed shape of HDRB mesh.

The HDRB is next compressed with a vertical load of 100 kN (200% of design vertical load and then sheared, keeping the vertical load constant as explained above. The load displacement curve is shown in Fig 9. The figure also shows the load displacement curve for both polynomial and Ogden forms of strain energy density functions. The effect of compressive force on combined compression and shear is shown in Fig. 10.

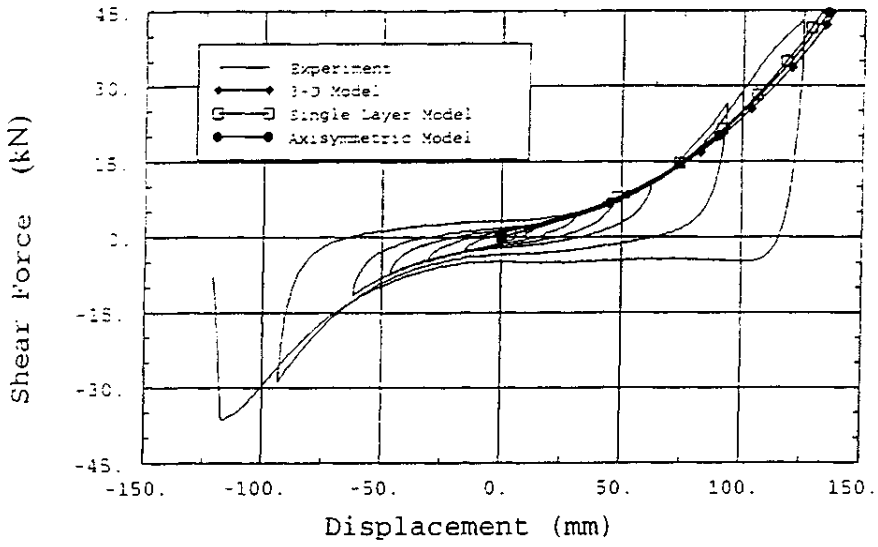

FIG. 7. Combined compression and shear (Poly. N = 2).

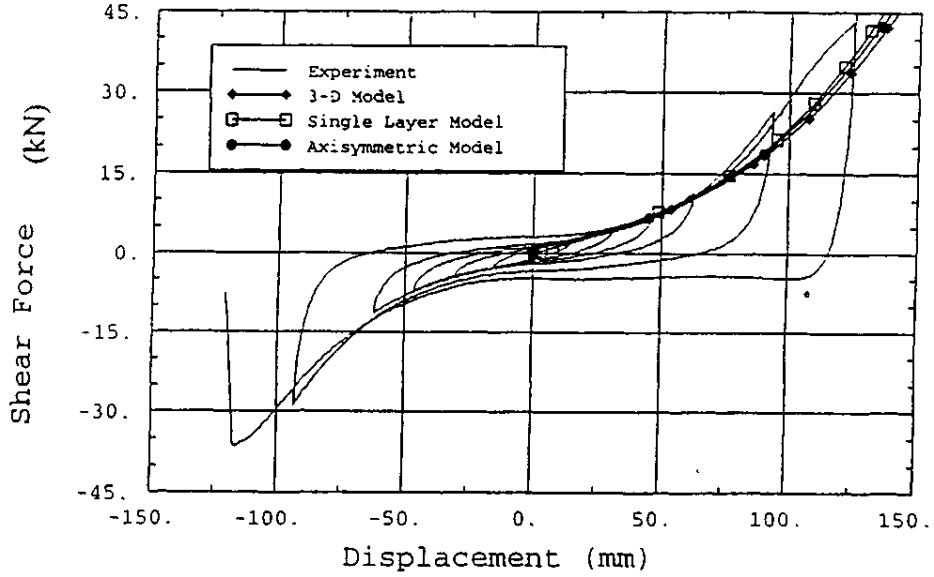

FIG. 8. Combined compression and shear (Ogden N= 2).

A vertical load upto 1200% of design load (600 kN) is applied next. For this case, analysis with only 3-D model is done. The vertical load displacement curve is shown in Fig 11.

4.2 Determination of Material Parameters for Rubber of KAERI HDRB

From the test data provided the material constants were found by the automatic curve fitting capability available with ABAQUS, as explained above. The material parameters are obtained for both polynomial and Ogden strain energy density function forms using ABAQUS.

4.2.1 Finite Element Model

As indicated in 3.2, considering the symmetry in geometry and loading conditions a 180° sector of the isolator only was modeled. The hybrid C3D8H element and reduced integration element C3D8R of ABAQUS have been used to model the rubber and steel shims respectively. The finite element model consisted of 12367 nodes and 6152 elements.

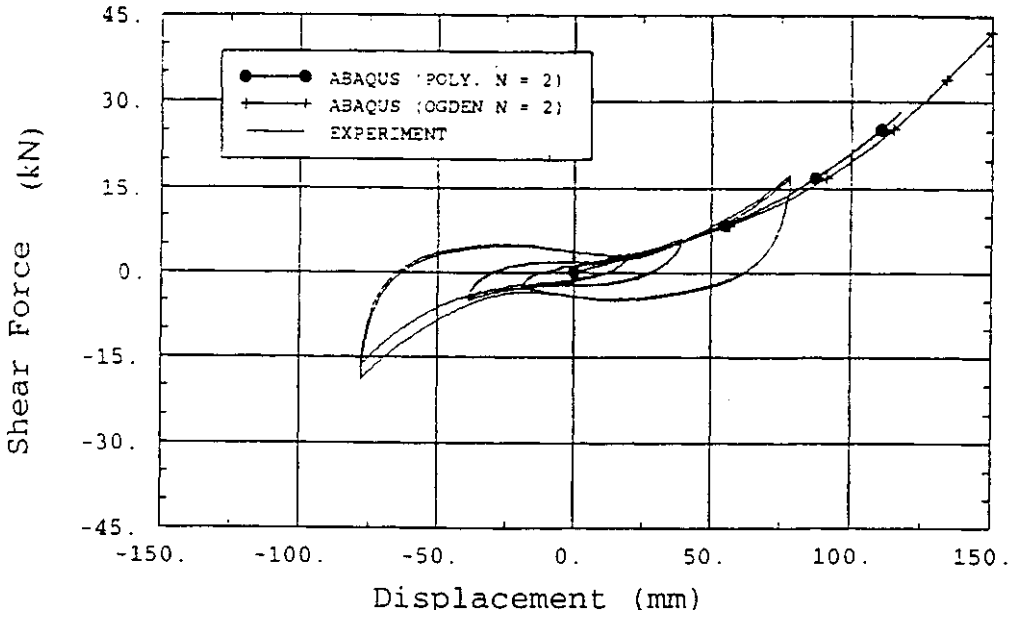

FIG. 9. Combined compression (100 kN and shear.

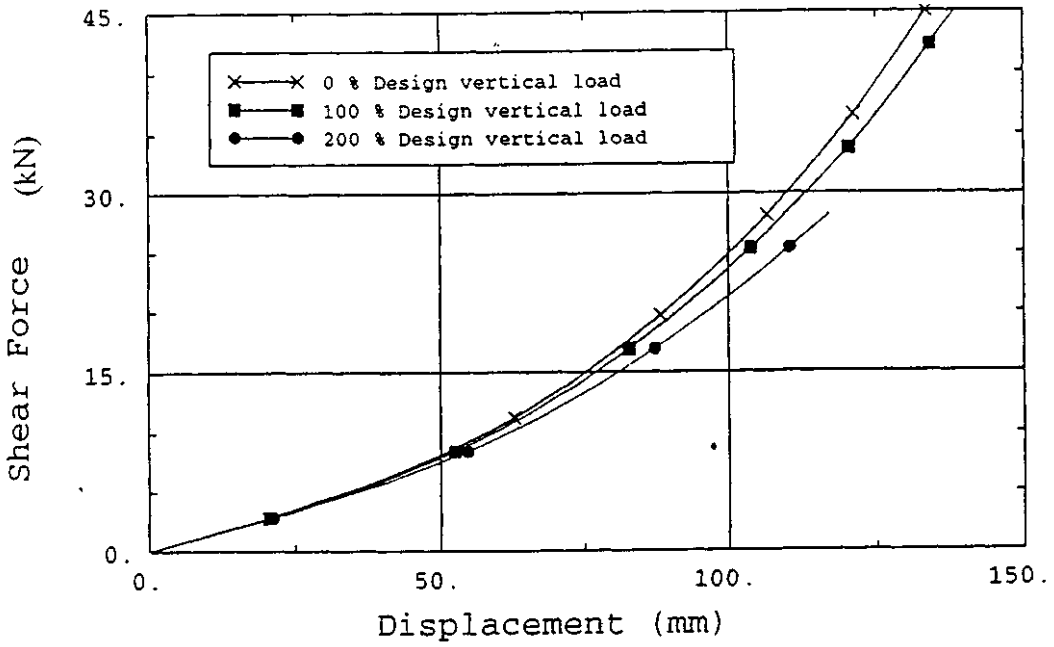

FIG. 10. Effect of compressive force on combined compression and shear.

4.3 Determination of Material Parameters for Rubber of ALMR HDRB

The analysis methodology followed are similar to the one followed for the KAERI HDRB. The Polynomial N=2 option was used. The results show, as with KAERI, the comparison of the calculated results with that of the experiment is good. Details of calculations are given in reference [6].

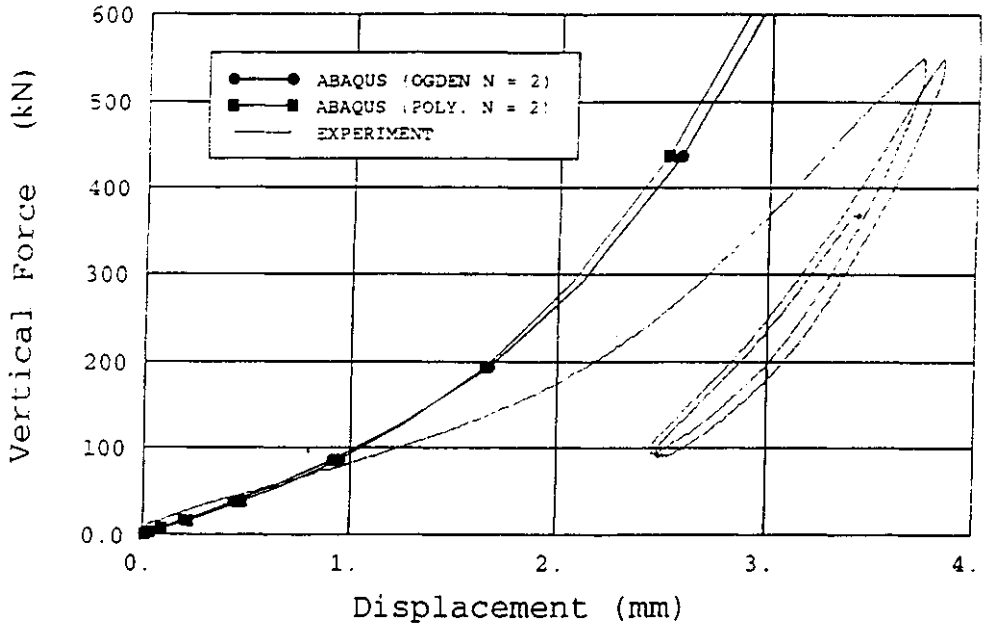

FIG. 11. Pure compression up to 1200% (600 kN) of design vertical load.

4.4 Determination of Material Parameters for Rubber of CRIEPI HDRB

As in the case of KAERI HDRB model, considering the symmetricity of geometry and loading, modelling of half of the isolator is sufficient. The C3D8H and C3D8R elements of ABAQUS have been used to model rubber sheets and steel plates respectively.
For modeling the lead core, the post yield stress strain relationship for lead is given by Hirata [7].

$$\sigma_t = 4.0(1.0+0.096 \log_{10}(\varepsilon'_t))\varepsilon_t^{0.31}$$

where a_t and s_t are the tensile true stress and true strain of the lead respectively and $s\backslash$ is the true strain rate of the lead. Since the data on the strain rate was not available, two models for lead as given in Yoo [8] were adopted where the initial yield stresses were assumed as static and dynamic yield stresses respectively representing the soft and hard lead properties. Also C3D8H elements were used for modelling the lead and interface between the rubber and steel is taken to be continuous without any sliding. The derivative of the strain energy density functions as the function of I, and I_2 is used to model the constitutive behaviour of rubber. The material behaviour is modelled by this derivatives through the user subroutine, UHYPER available with ABAQUS.

4.4.1 Finite Element Analysis & Results

The finite element model of the LRB is applied with 1500kN of compressive force. Subsequently it is sheared to the required level by keeping the compressive force constant. The numerical results are compared with the results of cyclic loading test with 200% shear strain and cyclic loading test with 300% shear strain. The comparison shows that the model with hard lead option compares more closely than the soft lead option when the cyclic shear strain is 200% whereas the model with soft lead compares well with experiment when the cyclic shear strain is 300%. This indicates that at larger strain the bearing softens more than

the present numerical model's predictions. For the calculation with compression with different offset strain, the isolator is first sheared to the required level of offset shear strain. Subsequently the isolator is subjected to compression keeping shear forces constant. The analysis has been repeated for different offset shear strains of 0%, 50%, 100% and 200% as in the case of NRB reported in Selvaraj [9].

In order to see the effect of the vertical load on the displacement due to horizontal shearing loads, a parametric study was done by changing the vertical stress from 0% to 200% of design vertical stress. The results indicate that the effect of increasing the vertical load on the horizontal displacement due to shear loading is not substantial.

4. 5 Numerical Analysis Of Japanese Data Of Natural Rubber Bearing (NRB)

4.5.1 Finite Element Model

For Japanese NRB, only 3-D model and single layer model are studied. The C3D8H and C3D8R elements of ABAQUS have been used to model rubber sheets and steel plates respectively. Fig 12 shows the finite element mesh used for the analysis.

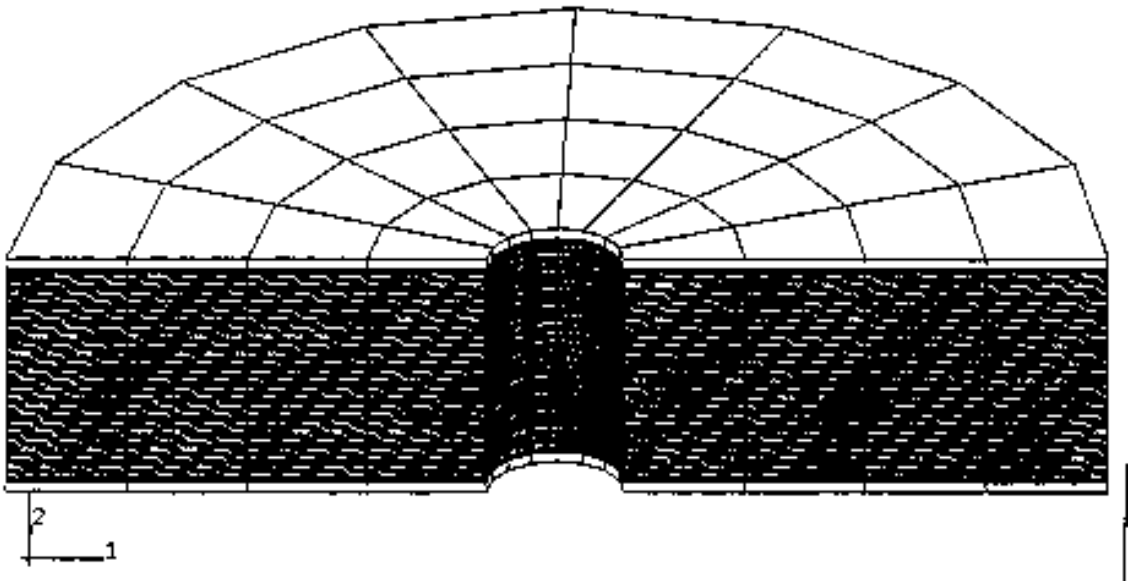

FIG. 12. Finite element mesh of NRB.

4.5.2 Finite Element Analysis & Results

The finite element model of the NRB is applied with 200 tons of compressive force, through the dummy node. Subsequently it is sheared to the required level by keeping the compressive force constant. The load displacement behaviour of the isolator is extracted and shown in Fig. 13a. For the case of offset shear strain, the isolator is first sheared to the required level of offset shear strain. Subsequently the isolator is subjected to compression keeping shear forces constant. The analysis has been repeated for different offset shear strains of 0%, 50%, 100% and 200%. The deformation behaviour under all conditions have been extracted and shown in the Fig.l3b. The results of analyses of Japanese data are similar to that of the numerical results of Italian data. Details of the analyses results are given in reference [6].

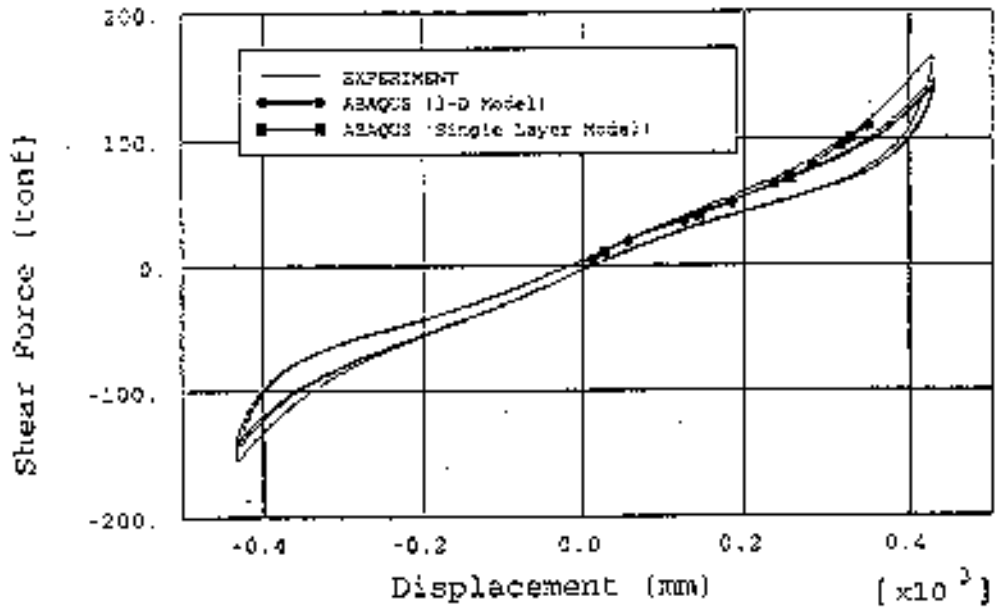

FIG. 13a. Combined compression and shear (NRB).

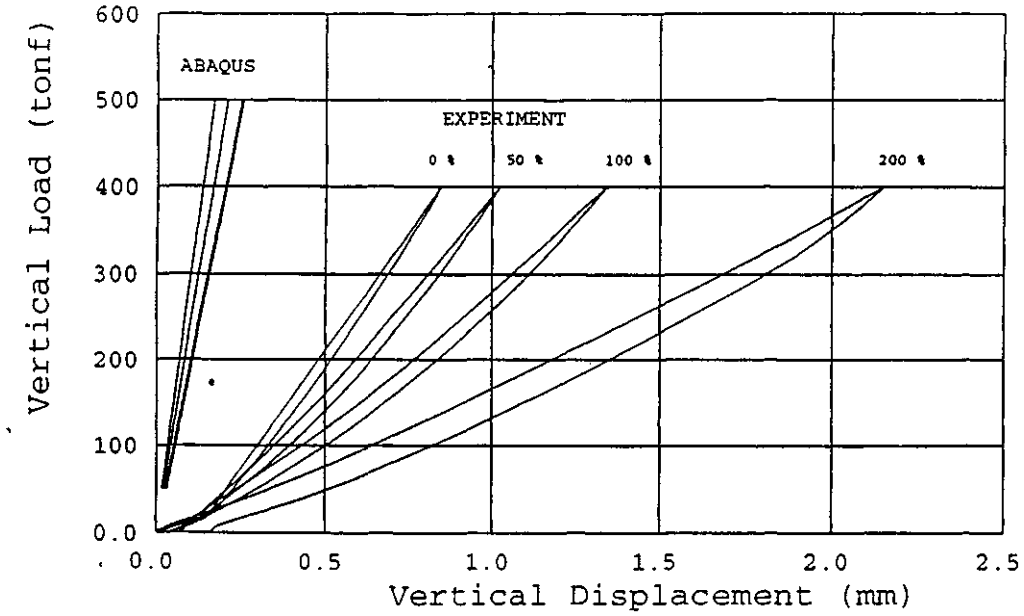

FIG. 13b. Compression with different offset shear strain (NRB).

5. DYNAMIC RESPONSE OF SEISMICALLYISOALTED STRUCTURES

For obtaining the dynamic response of the base isolated structure, using finite element analysis, it becomes computationally prohibitive to model the rubber bearing in full detail as done for studying the quasi-static behaviour of the bearing. The nonlinear behaviour of the rubber and the hysteretic damping make the modeling computationally demanding. Alternate methods for modeling the hysteretic damping are available in the literature, reference [10,11]. In these methods, the restoring force of the hysteretic damper is expressed numerically in terms of nonlinear first order differential equation. The dimensionless parameters of the

nonlinear differential equation are obtained from the experimental data of the bearing. A recent publication, reference [12] gives different methods of modeling hysteretic damping. In this analysis, an equivalent model simulating the hysteresis of the actual bearing is employed in place of the rubber bearings.

5.1 Description of the MISS Structure

MISS (Model of Isolated Steel Structure) is a five storied steel built up framed structure with a rectangular base of 2.1 × 3.3 m. The structure is made of steel sections HEB 100 and HEM 140. Six vertical columns (HEB 100) are bolted on a base frame made of HEM140. Four horizontal frames (HEB 100) can be bolted to the columns to achieve an interstory distance of either 0.9m or 1.1 m. Fig. 14 shows the framed structure of MISS. The schematic of MISS is shown in Fig. MISS can support up to 20 concrete masses each weighing 12.8 kN. The isolation system for MISS is formed by 6 High Damping Rubber Bearings (HDRBs) fabricated with a soft compound (G=0.4 Mpa). The isolators have an overall diameter of 125 mm and are made of 12 rubber layers with a thickness of 2.5mm (30 mm total height), and 11 steel shims 1mm thick bonded to the rubber layers. Experiments were carried out on MISS for the following configurations, viz.l) Cl - no masses and fixed base, 2) C2- 16 masses (4 for each floor) and fixed base, and 3) C3- 16 masses (4 for each floor) and isolated base.

5.2 Natural Frequency of MISS

Computer code CASTEM-2000 has been used for determining the natural frequencies of MISS. The fundamental frequencies for configurations Cl and C2 are found to be 8.8 Hz and 2.78 Hz. The mode shape is shown in Fig. 15 . The connection between the column and the beam of MISS is actually a bolted connection. For modeling this bolted connection, the stiffness properties of the members adjacent to the bolted connection are modified so that the resulting natural frequencies match with the experimentally measured frequencies. The other way of modelling the bolted connection are to introduce springs with appropriate rotational stiffness in either direction at the connection and do the analysis.

5.3 Dynamic Response of MISS

The input excitation to MISS is shown in Fig. 18 and Fig.21. The analysis for configuration C2 does not involve consideration of any nonlinear nature. The displacement response of MISS at the measurement point 13 is shown in Fig. 19.

5.3.1 MEP Model for Bearing of MISS

For obtaining the equivalent model, the method proposed by Forni et.al [13] (called the Multilinear ELasto-plastic model - MEP model) is used. In this model, the hysteretic nature of the rubber bearing is modeled by a simple elasto-plastic system. An elastic spring is coupled with an elasto-plastic member , Fig. 16 . While the elastic spring simulates the stiffness of the rubber bearing, the elasto-plastic member through its plastic deformation simulates the hysteretic damping of the rubber bearing. For arriving at the properties of the elastic spring and the elasto-plastic member, the experimental data of the rubber bearing is made use of. This analysis methodology is incorporated using the computer code CASTEM-2000. The results of CASTEM-2000 for the case of the isolator used in MISS for 100% shear strain, are shown in Fig. 17. Similarly, the MEP model for other cases (for varying shear strains) are obtained.

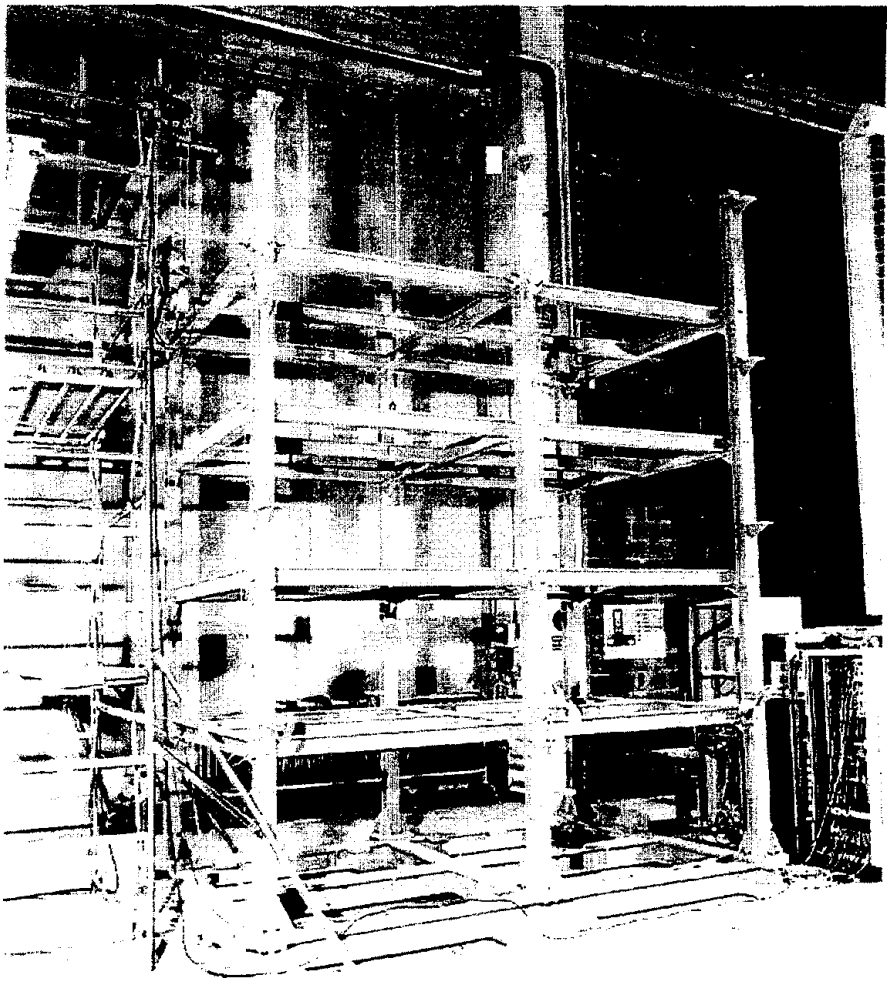

FIG. 14. MISS steel frame.

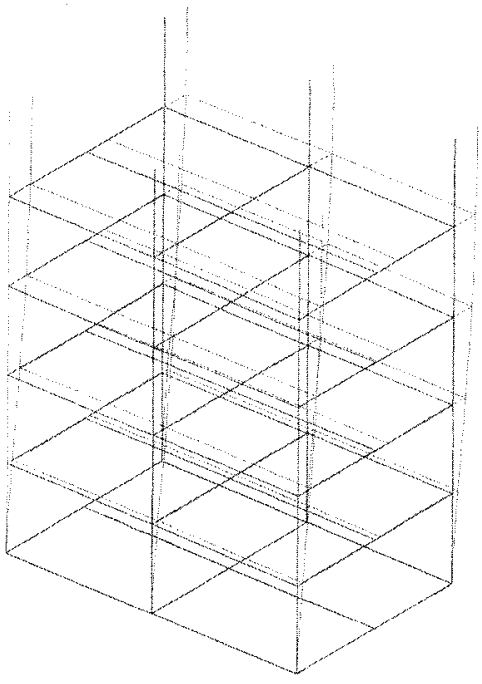

FIG. 15. Deformed shape of MISS in C2 configuration.

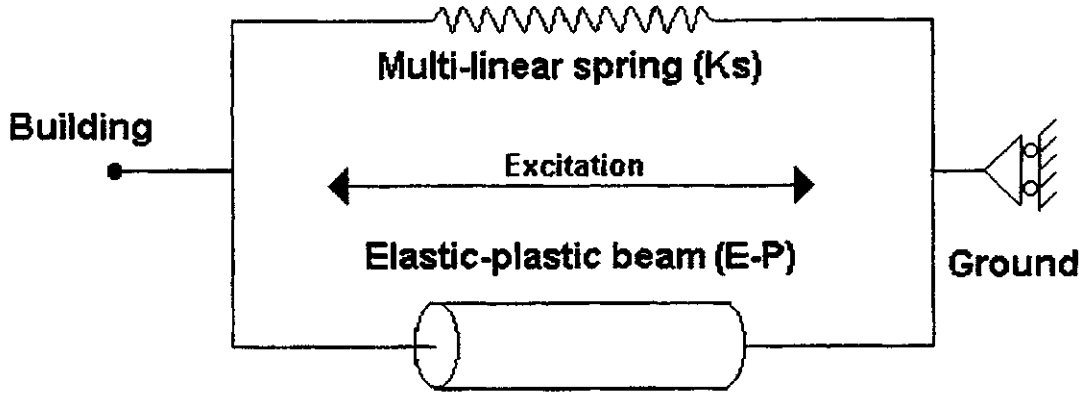

FIG. 16. MEP model for HDRB.

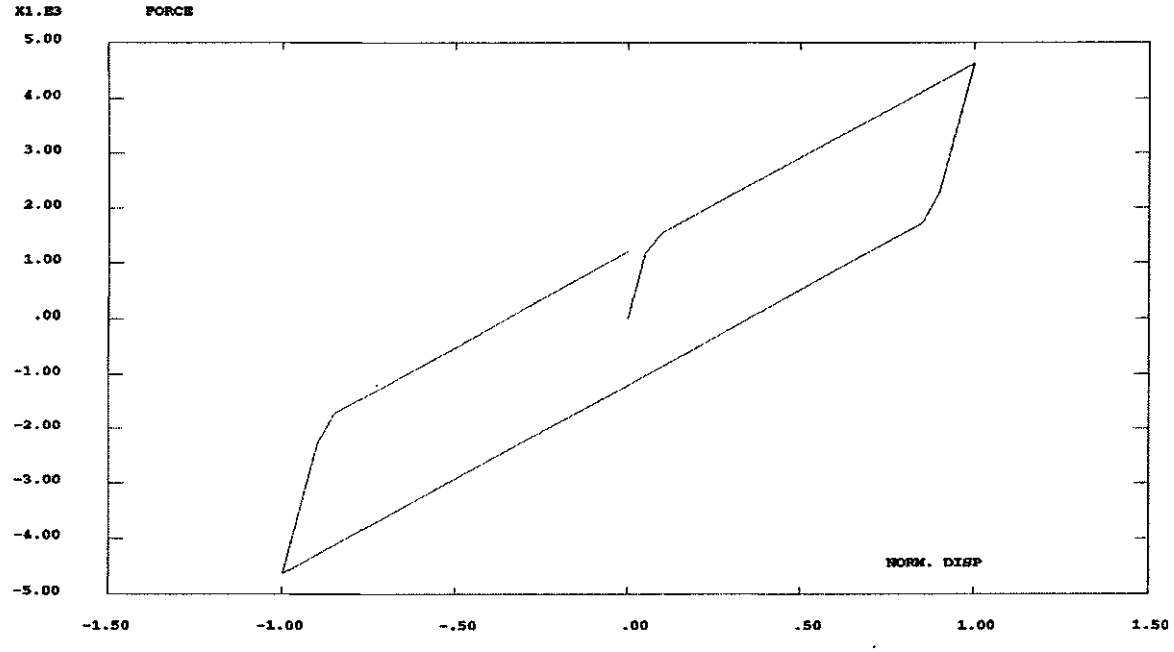

FIG. 17. Force displacement curve for MEP model.

5.3.2 Dynamic Response of MISS in C3 Configuration

For the input excitation shown in Fig. 18 , configurations C3 of MISS is analysed incorporating the above MEP model and the results are shown in Fig. 20. It is worth observing that the deformed shape of the frame at any time instant is more of a rigid body movement of the entire frame. Fig.22 shows the response of MISS for the input excitation of Fig. 21.

5.4 Dynamic Response Of CRIEPI Rigid Mass Mockup

A rigid mass of 17.9 tonnes is isolated through 8 bearings. The schematic of the rigid mass is shown in Fig.23 The natural frequencies of the rigid mass system are obtained as 4.3 Hz and 42.0 Hz for the horizontal and vertical directions respectively. The input base excitation is shown in Fig. 24.

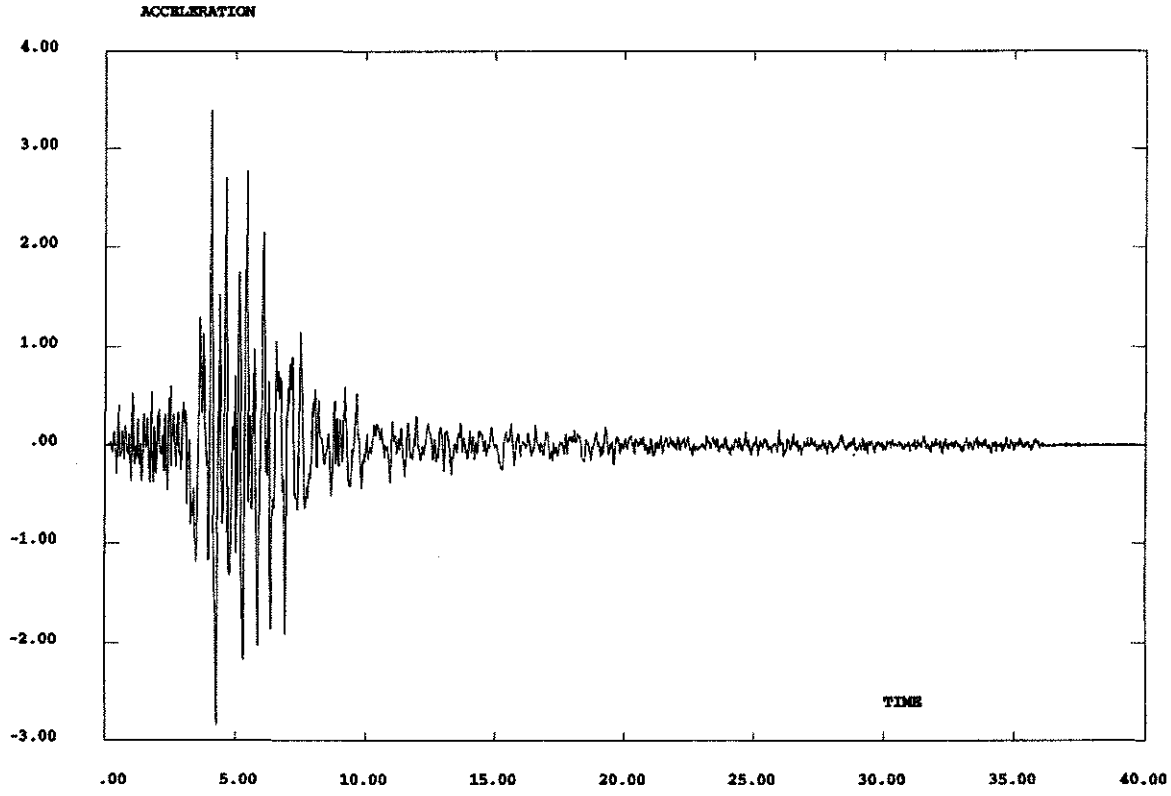

FIG. 18. Input excitation for MISS.

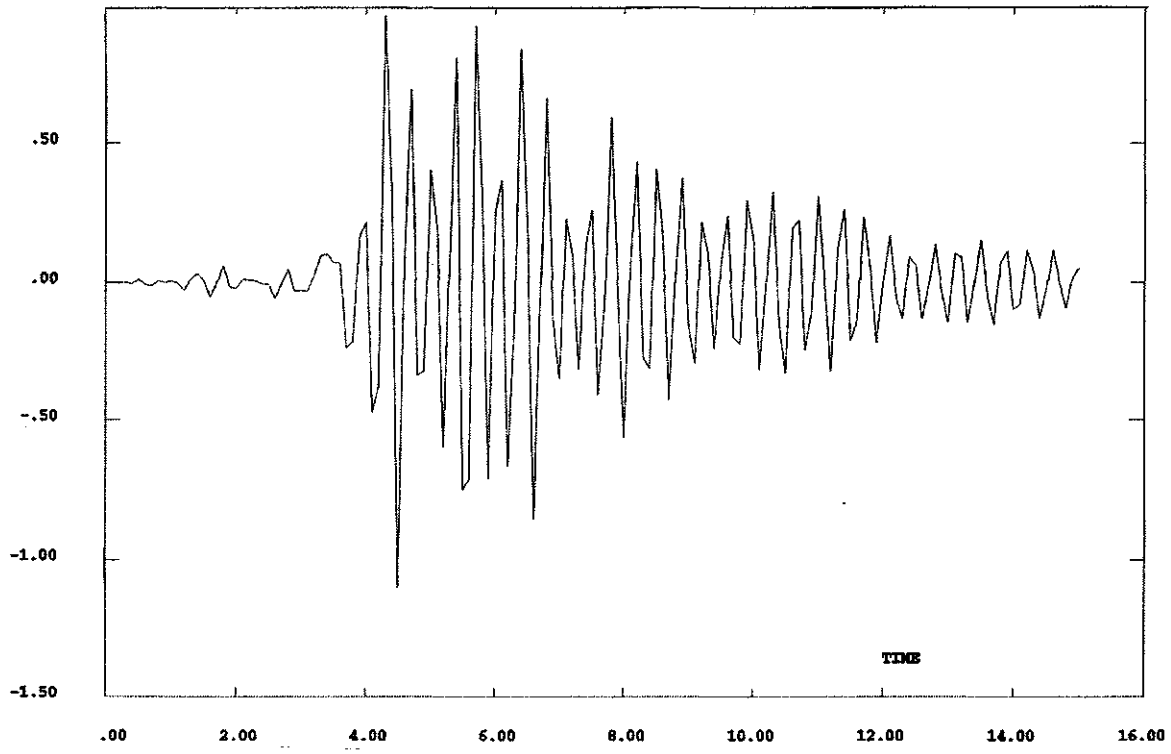

FIG. 19. Response of MISS in configuration C2.

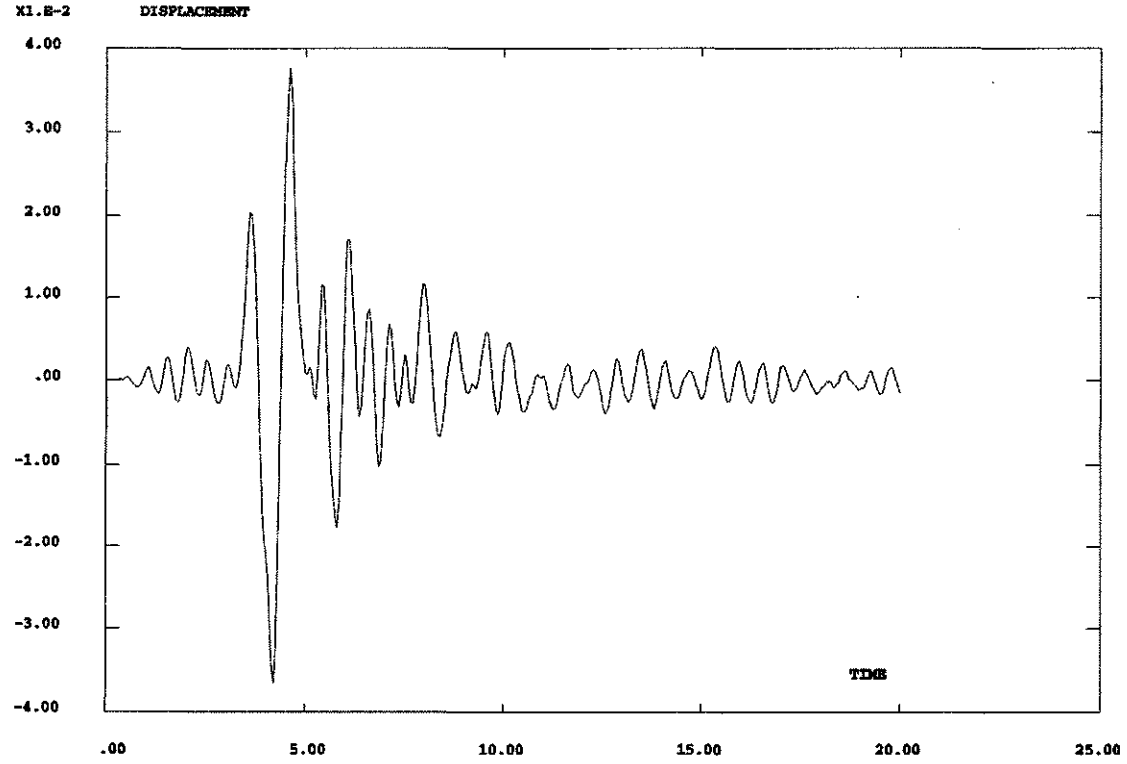

FIG. 20. Response of MISS in configuration C3.

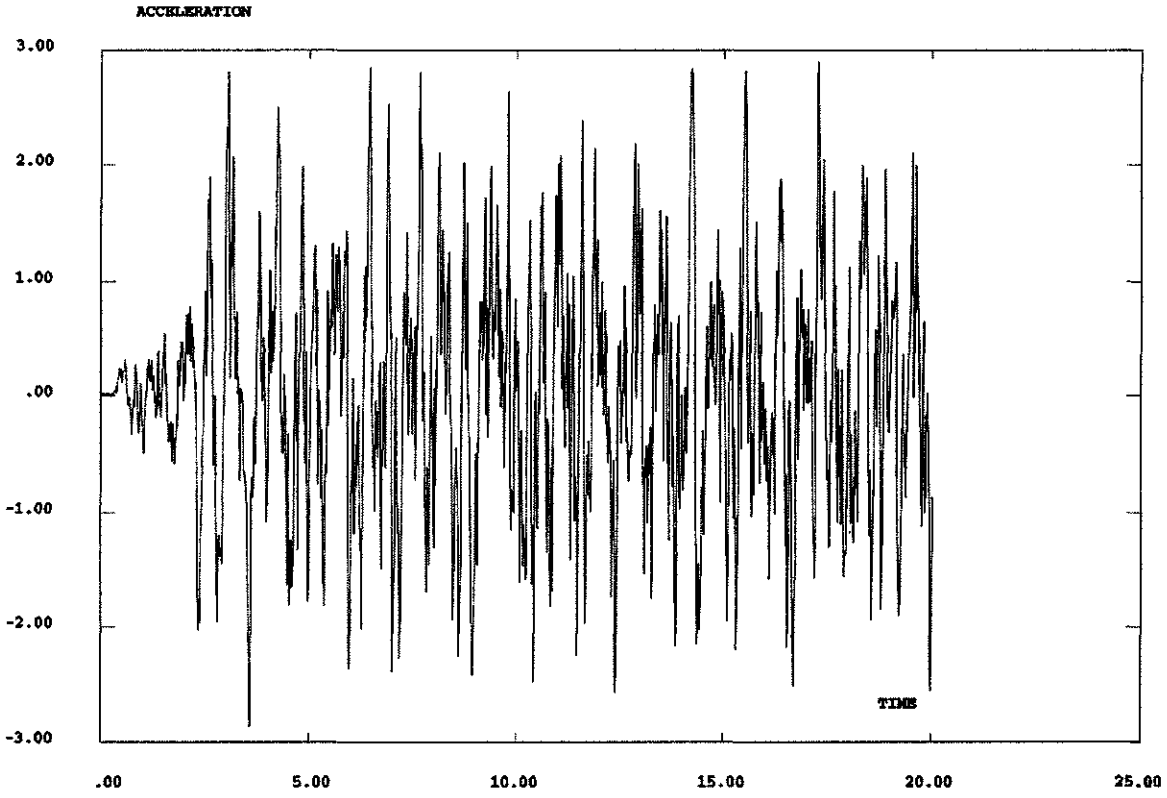

FIG. 21. Artificial input excitation to MISS.

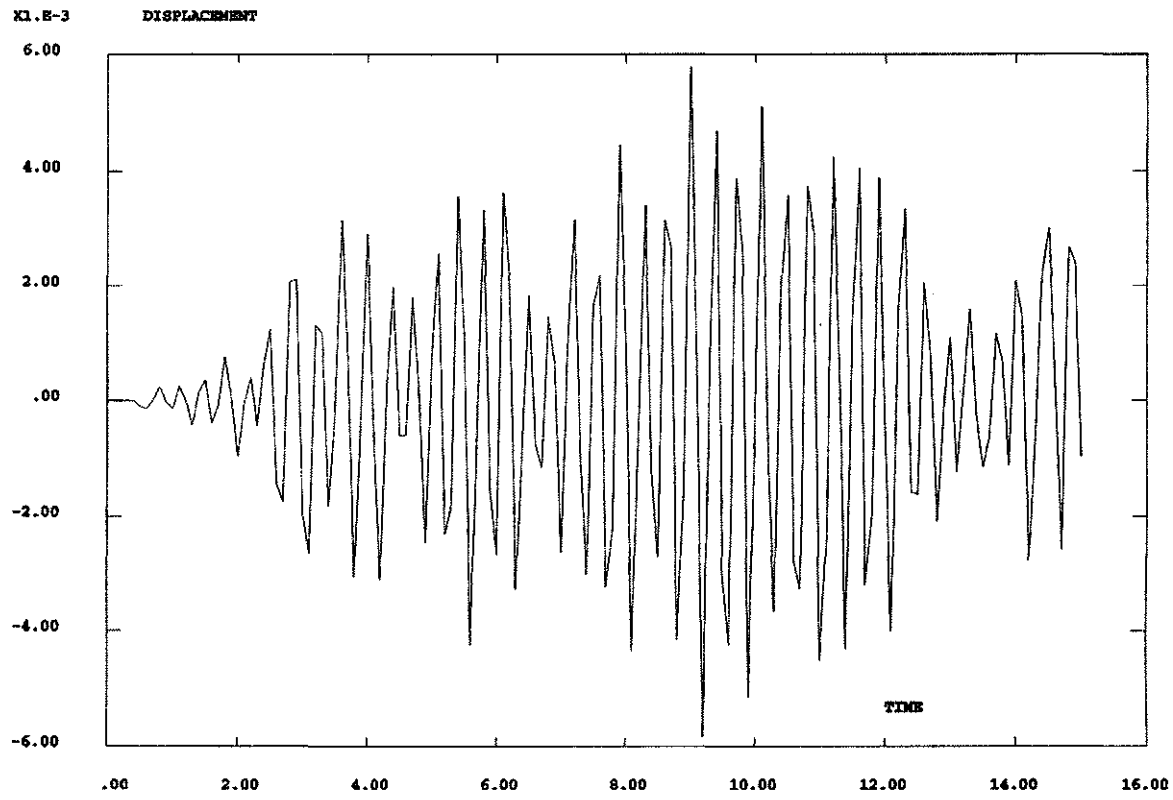

FIG. 22. Response of MISS to excitation shown in Fig. 11.

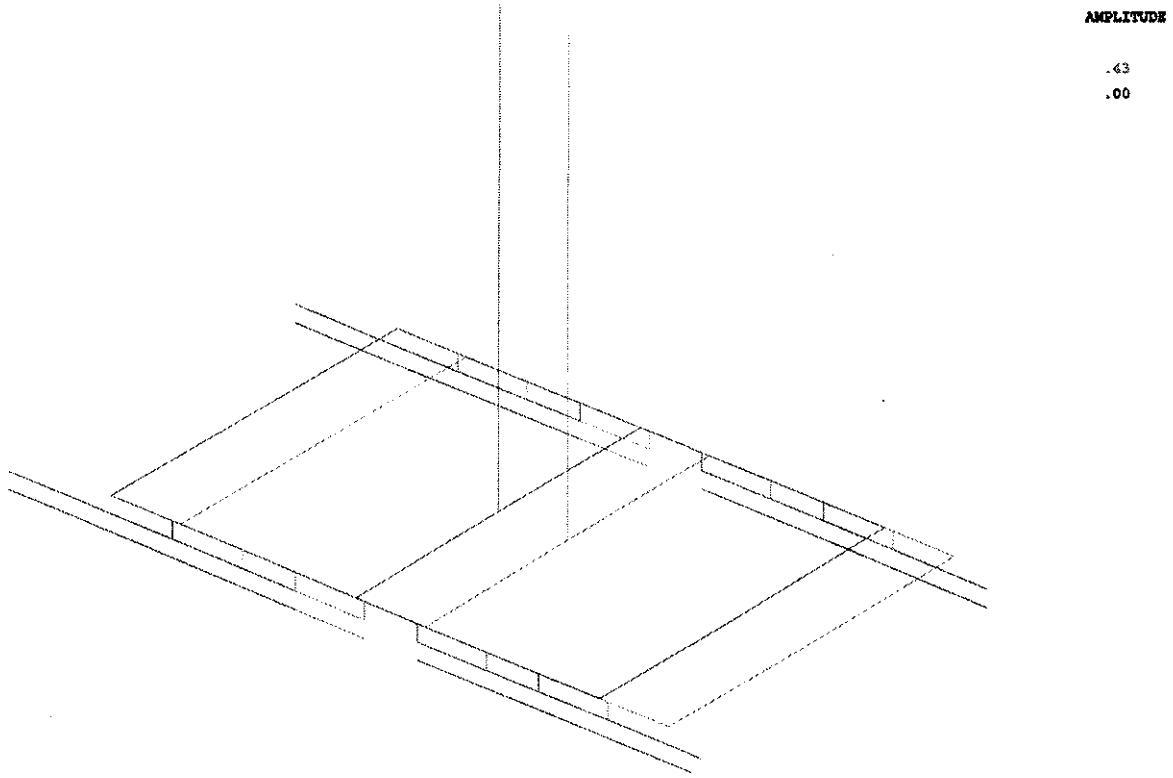

FIG. 23. Model of CRIEPI rigid mass mockup.

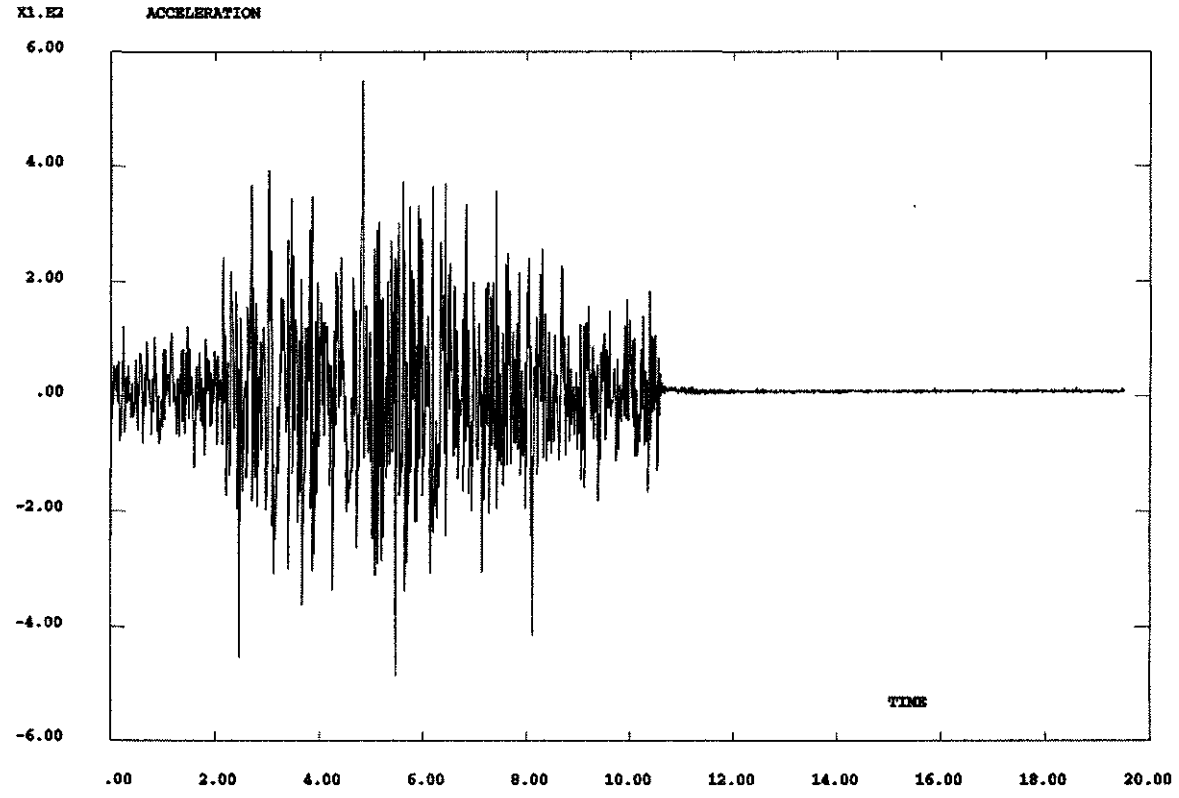

FIG. 24. Input excitation to CRIEPI rigid mass mockup.

The vertical stiffness of the bearings are modeled by a simple elastic spring. The response of the rigid mass for this base excitation is shown in Fig.26 For modeling the horizontal response of the bearing, an equivalent MEP model is first arrived at , as explained in the previous section. The response of the rigid mass when subjected to base excitation in the horizontal direction, is shown in Fig. 25.

6 INTERCOM?ARISON OF RESULTS

6.1. Discussion of Analysis Results for Italian data

The numerical predictions are quite good under combined compression and shear in the region of normal working range (100% vertical load and 100% shear strain) of an isolator for both forms of strain energy density functions. The numerical predictions under pure compression is also good upto 100 kN (200% of design vertical load). The numerical predictions by polynomial form of strain energy density function is more closer to experiments than Ogden form under combined compression & shear and vice versa for pure compression case. The prediction by single layer model is also good and more closer than 3-D and axisymmetric models.

The experimental results of HDRB show more hardening at high strain region than the numerical predictions under combined compression and shear. It has been reported Ishida, [5] that the hardening of isolator with high damping rubber increases with increase in strain rate at high strain region. In this context, the effect of strain rate on the load deformation characteristic of HDRB has to be seen as a factor to explain the deviation of numerical results from the experimental results at high strain region.

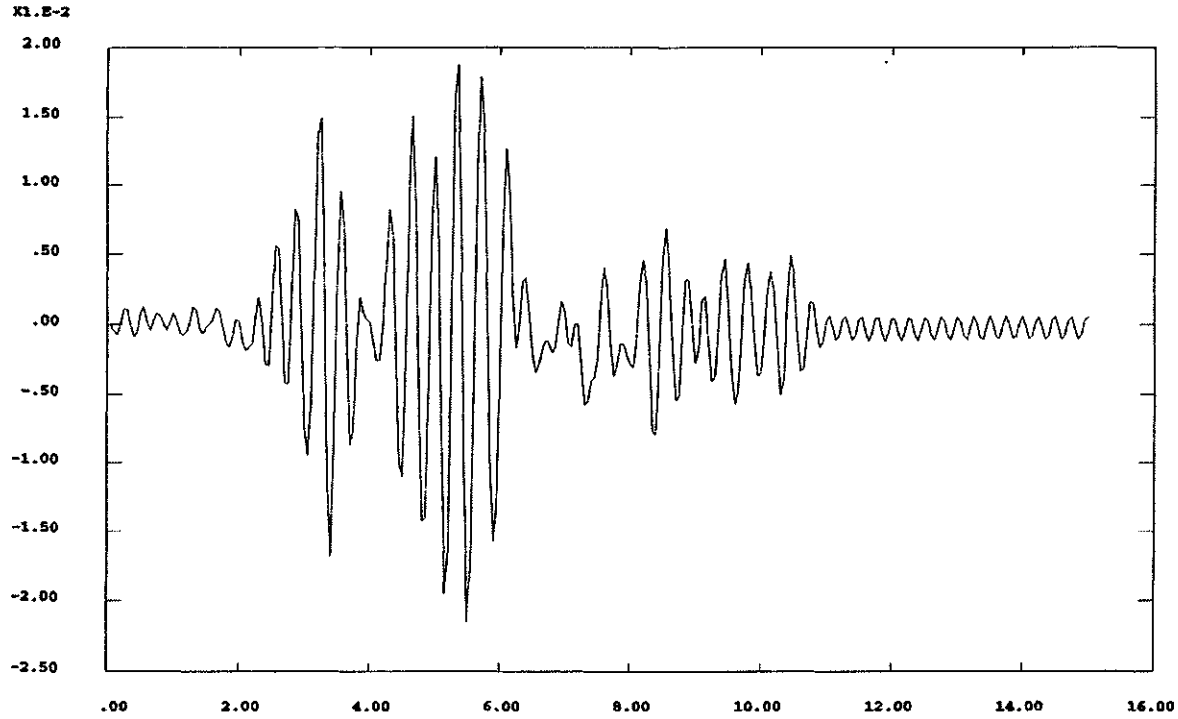

FIG. 25. Horizontal displacement response of rigid mass.

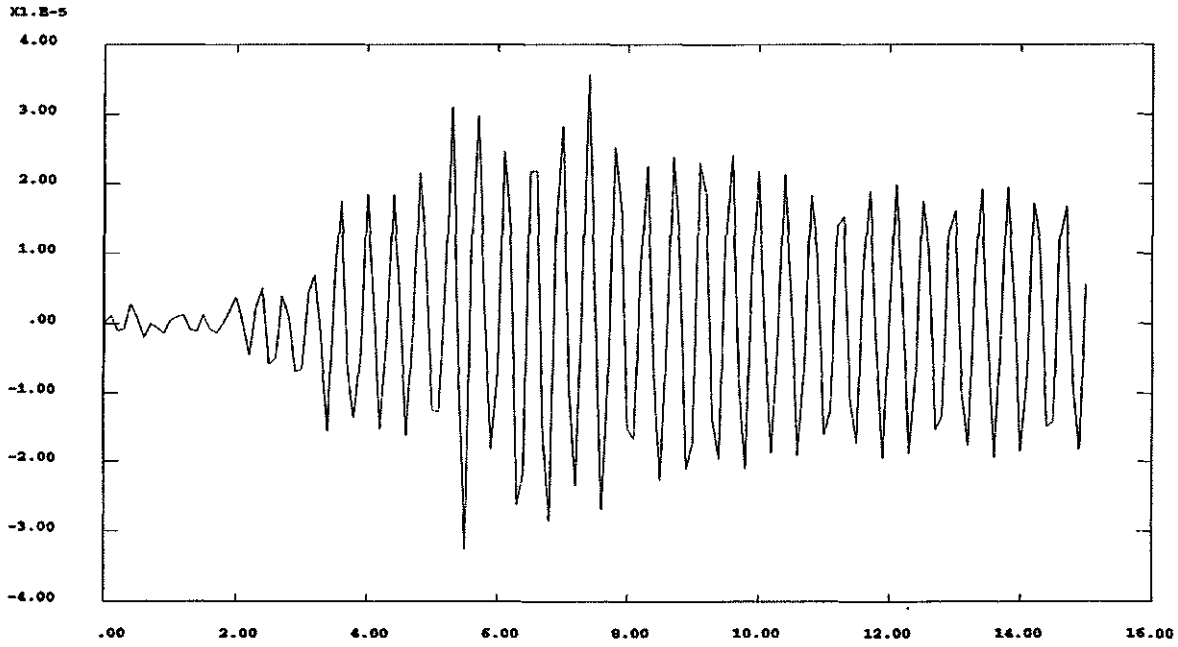

FIG. 26. Vertical displacement response of rigid mass.

6.2. Numerical Results & Discussion for KAERI data

Calculations were performed for combined compression and shear with 100% design vertical load. Three sets of calculations with rubber modeled using Polynomial N=2, Ogden N=2 and Ogden N=3 forms of strain energy density functions were performed. In the above calculations the vertical stress was held constant equal to 2.55 MPa (design vertical stress). In

order to see the effect of increasing the vertical load on the displacement due to horizontal shearing loads, a parametric study was done by changing the vertical stress from 0% to 200% of design vertical stress. Details of above calculations are given in reference [6].

From the results, it can be seen that Ogden N=3 gives more closer results than the polynomial N=2 and Ogden N=2. Similarly for the large strain case also, the comparison of the calculation results with shear failure test results show that Ogden N=3 was able to give better results than the other two models. The results of Polynomial N=2 and Ogden N=2 are almost similar. The effect of increasing the vertical load on the horizontal displacement due to shear loading is not substantial which indicates that the compressibility effect is not very high.

6.3 Finite Element Analysis *&* Results for CRIEPI data

The finite element model of the LRB is applied with 1500kN of compressive force. Subsequently it is sheared to the required level by keeping the compressive force constant. The numerical results are compared with the results of cyclic loading test with 200% shear strain and cyclic loading test with 300% shear strain. The comparison shows that the model with hard lead option compares more closely than the soft lead option when the cyclic shear strain is 200% whereas the model with soft lead compares well with experiment when the cyclic shear strain is 300%. This indicates that at larger strain the bearing softens more than the present numerical model's predictions. For the calculation with compression with different offset strain, the isolator is first sheared to the required level of offset shear strain. Subsequently the isolator is subjected to compression keeping shear forces constant. The analysis has been repeated for different offset shear strains of 0%, 50%, 100% and 200% as in the case of NRB reported in Selvaraj [9].

In order to see the effect of the vertical load on the displacement due to horizontal shearing loads, a parametric study was done by changing the vertical stress from 0% to 200% of design vertical stress. The results indicate that the effect of increasing the vertical load on the horizontal displacement due to shear loading is not substantial.

6.4. Finite Element Analysis & Results of Natural Rubber Bearing

The finite element model of the NRB is applied with 200 tons of compressive force, through the dummy node. Subsequently it is sheared to the required level by keeping the compressive force constant. The load displacement behaviour of the isolator is extracted and shown in Fig.l3a. For the case of offset shear strain, the isolator is first sheared to the required level of offset shear strain. Subsequently the isolator is subjected to compression keeping shear forces constant. The analysis has been repeated for different offset shear strains of 0%, 50%, 100% and 200%. The deformation behaviour under all conditions have been extracted and shown in the Fig.l3b. The results of analyses of Japanese data are similar to that of the numerical results of Italian data. Details of the analyses results are given in reference [6].

6.5 Results of dynamic response of MISS

For the dynamic response of MISS, the results of the present analysis match well with the experimental results as shown by the comparison in Fig. It is significant observing that the response of MISS is more like the rigid body response. The maximum displacement obtained is around 40 mm in the direction of excitation which is slightly higher than the experimentally observed displacement. The relative displacement between the top of the frame and the base is around 6 mm.

7. CONCLUSIONS

The force-deformation behaviour of the Italian HDRB, Japanese Lead Rubber Bearing and NRB, KAERI HDRB, ALMR HDRB have been predicted using finite element analysis. The results indicate good comparison with experimental results. For the static analysis of the rubber bearings, the single layer model has been found to be computationally effective. The results of the single layer model are found to be match well with the experimental results. The dynamic response of structures isolated with bearings has been carried out in two stages. In the first stage a simple multiple elasto-plastic model for simulating the hysteresis of the bearing has been obtained. This MEP model is used in the second stage for getting the dynamic response of the isolated structure. The results thus obtained are found to match closely with the experimental results.

REFERENCES

[1] McENTEE,C.C., "Seismic Base Isolation of LMFBRs", in Seismic & Environment Qualification of Equipment, Papers presented at IMech E Seminar, 7th October 1992.

[2] PLICHON,C and JOLIVET,F., "Aseismic Foudnation System for Nuclear Foundation System for Nuclear Power Stations", in Engineering Design for Earthquake Environment, IMechE, 1978.

[3] CHRISTENSEN, R.M., "A Nonlinear Theory of Viscoelasticity for Application to Elastomers", Journal of Applied Mechanics", Vol. 47 (1980), pp 762-768.

[4] ABAQUS Manuals, 1996, Version 5.6, Hibbit, Karlsson & Sorensen Inc., Providence, Rhode Island, USA.

[5] ISfflDA, K., SHIOJIRI, H., IIZUKA, M., MIZUKOSHI, K., TAKABAYASHI, K., 1991 "Failure tests of Laminated Rubber Bearings", Transactions of SMiRT 11, vol. K, Tokyo, Japan, pp 241-246.

[6] RAVI,R., SELVARAJ, T., CHELLAPANDIJP., CHETAL,S.C., BHOJE,S.B., " Finite Element Analysis of Laminated Rubber Bearings - Verification with KAERI HDRB, ALMR HDRB and CRIEPI LRB Data", in the Third Research Coordination Meeting of the International Atomic Energy Agency's Coordinated Research Program on "Intercomparison of Analysis Methods for Seismically Isolated Nuclear Structures", Hertford, UK, May25-29, 1998.

[7] HIRATA,K., MATSUDA,A. and YABANA,S,, " Contribution of Japan to the activities of Intercomparison of analysis methods for seismically isolated nuclear structures", in Seismic Isolation, Passive Energy Dissipation and Active Control of Seismic Vibrations of Structures, Proc. of the International Post-SMiRT Conference Seminar, Taormina, Sicily, Italy, August 25-27, 1997.

[8] YOO,B., and LEE,J., "Intercomparison of analysis for seismically isolated nuclear structures (ENEA HDRB and CRIEPI LRB)", in Seismic Isolation, Passive Energy Dissipation and Active Control of Seismic Vibrations of Structures, Proc. of the International Post-SMiRT Conference Seminar, Taormina, Sicily, Italy, August 25-27, 1997.

[9] SELVARAJ, T., RAVI,R., CHELLAPANDI,P., CHETAL,S.C., BHOJE,S.B., " Contribution of India to the activities of intercomparison of analysis methods for seismically isolated nuclear structures", in Seismic Isolation, Passive Energy Dissipation and Active Control of Seismic Vibrations of Structures, Proc. of the International Post-SMiRT Conference Seminar, Taormina, Sicily, Italy, August 25-27, 1997.

[10] SATISH NAGARAJAIAH, REINHORN, A.M., CONSTANTINOU, M.C., "Nonlinear Dynamic Analysis of 3-D Base Isolated structures", Journal of Structural Engineering, Vo.l 17, No.7, (1990), 2035-2054.

[H] CONSTANTINOU, M.C. AND TADJBAKHSH, I.G., "Hysteretic Dampers in Base Isolation: Random Approach", Journal of Structural Engineering, Vo.l 11, No.4 (1985), 705-721.

[12] AMDE, A.M. AND MIRMIRAN, A., " A New Hysteresis Model for Steel Members". International Journal for Numerical Methods in Engineering, 45, (1999), 1007-1-23.

[13] FORNI, M., MARTELLI, A., DUSI, A., AND BETTINALI, F.,1996, "Status of Italian Test Data on Seismic Isolators and Comparison with Computer Predictions", IAEA Research Co-ordination Meeting (RCM) on "Intercomparison of Analysis Methods for Seismically Isolated Nuclear Structures", St. Petersburg, Russian Federation.

VERIFICATION AND IMPROVEMENT OF ANALYTICAL MODELING OF SEISMIC ISOLATION BEARINGS AND ISOLATED STRUCTURES

M. FORNI, M. LA GROTTERIA, A. MARTELLI
National Agency for New Technology

S. BERTOLA, F. BETTINALI, A. DUSI
ENEL-HYDRO Hydraulic and Structure Centre

G. BERGAMO, G. BONACINA
ENEL-HYDRO-ISMES Engineering and Testing Centre

Italy

Abstract

Due to the complexity of dynamic behaviour of seismic isolation (SI) devices, high cost of their tests and non-negligible number of devices having excellent potential for nuclear applications, several countries judged of great interest to extend validation of their numerical models of such devices to the analysis of experimental data obtained by others. Thus, a four-years Coordinated Research Program (CRP) on Intercomparison of Analysis Methods for Isolated Nuclear Structures, proposed by ENEA (1995), was endorsed by the IAEA in 1995. There, Italy was jointly represented by ENEA, ENEL and ISMES, and supplied test results concerning both High Damping Rubber Bearings (HDRBs) and the MISS (Model of Isolated Steel Structure) mock-up, which had been isolated using such bearings. Test data provided by Italy to the other countries were also re-analysed to improve mathematical models. Aim of this final report is to summarise, after a brief description of the devices and structures considered, the most important results and conclusions of the numerical analyses carried out by Italy. For more detailed information, especially as far as the execution of the tests and the implementation of the numerical models are concerned, please refer to the technical reports presented by Italy to the Research Coordination Meetings (RCMs).

INTRODUCTION

At the first RCM held at St. Petersburg (IAEA, 1997) Italy provided test data and results of numerical analyses concerning two HDRBs which were developed within an European Research Programme coordinated by ENEL (1993). In addition to the numerical activities, ENEL carried out in 1997 a complete material characterization of KAERI HDRBs, by testing in its laboratories rubber specimens, and distributed the results to the other participants.

The first data, among those provided by other countries, which were jointly analysed by ENEL and ENEA, concerned U.S. scaled HDRBs that had been manufactured in Italy and tested by University of California at Berkeley; then, Natural Rubber Bearings (NRBs) and Lead Rubber Bearings (LRBs) manufactured in Japan for CRIEPI were analysed. The results concerning U.S HDRBs and Japanese NRBs were presented at the RCM of Taormina (IAEA, 1998a and GLIS, 1998), while information concerning Japanese LRBs was given at the Hertford RCM (IAEA, 1998b). Finally, the results concerning modified Japanese LRBs (with larger lead plug diameter) were presented at the Cheju RCM (IAEA, 1999).

With regard to the analysis of isolated structures, a detailed description of MISS was provided to the other partners (jointly by ENEA, ENEL and ISMES) at the St. Petersburg RCM in 1996. Moreover, at the same RCM, numerical analyses on the behaviour of MISS and other isolated civil buildings were presented. Finally, the results of analyses of an isolated

Korean spent fuel pool and a Japanese isolated rigid mass were presented at the Cheju RCM in 1999.

1. ANALYSIS OF RUBBER BEARINGS

ENEL and ENEA jointly analysed the test data of HDRBs provided by Italy (Martelli et al., 1996; ENEL et al., 1993) and US (Clark et al., 1996) and those concerning Natural Rubber Bearings (NRBs) provided by Japan (Hirata, 1996).

1.1 Description of the Devices

1.1.1 Italian optimised HDRBs

In the framework of the above mentioned research activities involving ENEL, ENEA and other partners (ENEL et al., 1993) a considerable number of optimised HDRBs were designed, manufactured and tested in Italy. These isolators are characterised by:

a) two different rubber compounds: harder (shear modulus G=0.8 MPa) and softer (G=0.4 MPa);
b) two values of the primary shape factor (S = 12 and S = 24);
c) three different geometric scales (diameter D = 125, 250 and 500 mm);
d) two different attachment systems (recess and bolts & dowel).

The devices were produced by ALGA and experimentally tested at ISMES laboratory (Figure 1.1). The optimised bearings analysed using the finite element technique and reported herein, had an overall diameter of 250 mm and both shape factors of 24 and 12. In the case of the higher shape factor, there were 30 elastomeric layers (G = 0.8 MPa), each being of 2.5 mm thick, alternated with 29 steel shims of 2 mm thickness. The steel end plates were 15 mm thick and had a 240 mm diameter. The total height was 114.5 mm. The bearing having S = 12 was formed by 15 layers of rubber (G = 0.8 MPa), each being of 5 mm thick, sandwiching 14 steel shims of 2 mm thickness. The steel end plates were again 15 mm thick, with a diameter of 240 mm. Both the bolts & dowel and the recess attachment systems were considered.

1.1.2 Italian further optimised HDRBs

Tests and FE calculations performed on the so called optimised HDRBs (ENEL et al., 1993) showed the possibility of further improving their stability at large deformations by decreasing their height. Therefore, some 'further optimised' HDRBs were designed by ENEA and produced by ALGA. Several kinds of these devices were manufactured by combining two different shape factors (S = 12 and S = 24), two rubber compounds (G=0.8 and 0.4 MPa), two attachment systems (recess and bolts & dowel) and two geometric scales (D=250 and 125 mm). The 'further optimised' bearing analysed in this study had an overall diameter of 125 mm and a shape factor of 12. There were 12 layers of elastomer (G = 0.4 MPa), each 2.5 mm thick, alternated with 11 steel shims of 1 mm thickness. The steel end plates were 10 mm thick and had a 120 mm diameter. The total height was 61 mm. These devices were used to seismically isolate MISS (§ 3). The Italian HDRBs were also analysed within this CRP by Yoo et al. (1998b) and Selvaraj et al. (1998).

1.1.3 US HDRBs

The test data provided by US concern 1:8 scale prototypes (manufactured by ALGA) of the HDRBs of the ALMR plant (Clark et al., 1996). The bearings are cylindrical supports with a diameter of 146 mm consisting of 15 rubber layers 2.3 mm thick and 14 Fe 430 (Figure 1.4) steel plates 1.9 mm thick. The bearings have a central hole (20 mm diameter) for an easier and

more correct assembly during manufacturing phase and for a better heat exchange during vulcanisation process. Each bearing supports a vertical load of 44 kN.

1.1.4 Japanese NRBs

The bearings proposed by the Japanese CRIEPI (Hirata, 1996) have an overall diameter of 1012 mm, a total rubber height of 142.5 mm and a shape factor S equal to 38.9. There are 25 layers of elastomer, each 5.7 mm thick, alternated with 24 steel plates of 3.1 mm thickness. The bearing were fabricated using a compound with a shear modulus G=0.6 MPa. Each isolator supports a design vertical load of 2000 kN.

1.2 Finite Element Analyses

For the Italian and US HDRBs both three-dimensional (Figures 1.2, 1.5) and axisymmetric finite-element models (FEMs) were developed and implemented in ABAQUS computer program by ENEA (Forni et al., 1996 and Dusi et al., 1998c), while similar models were developed and implemented in the same code by ENEL for the Japanese NRBs (Dusi et al., 1998c). Hyperelastic models of the rubber, defined according to the results of suitable tests on both scragged and unscragged rubber specimens, were also implemented in ABAQUS. Extensive numerical work was performed by considering meshes with different refinements and different element types. The numerical analyses, aimed at investigating the effects of the numerous variables of the problem, allowed for optimising the type of material model, discretisation and elements to be adopted, up to large strains.

For HDRBs, good agreement between numerical and experimental results was found by ENEA for horizontal stiffness (Figures 1.3, 1.6), similar to the results of ENEL for the Japanese NRBs (Dusi et al., 1998c); however, the agreement for compression tests was satisfactory only when compressibility was taken into account. This confirmed the importance of volumetric tests on rubber specimens to correctly evaluate bearing vertical stiffness, especially in the case of large shape factors. Analysis of ENEA also stressed that planar tests on specimens shall be performed to very large deformation, in order to allow for the definition of adequate hyperelastic models of the rubber. Moreover, it was found that the unscragged rubber model should be used for reproducing bearing behaviour to 50%–100% shear strain, while the scragged model should be used for larger deformations. Only slight differences were found between the results of 3D and axisymmetric models to 200%–300% shear strain, while 3D models shall be used for larger deformations.

1.3 Conclusions

The achieved results confirmed the conclusions of previous studies (Forni et al., 1995) that FEMs are useful tools for both the detailed design of elastomeric bearings and their qualification; for the latter, they allow for a considerable reduction of the number of tests to be performed (e.g. those concerning effects of parameters like temperature, ageing, vertical load on horizontal stiffness, initial or arisen defects, etc.). In particular, it is worth noting that:

- volumetric tests on rubber specimens are necessary to better reproduce the vertical behaviour of the berings, but can be neglected for reproducing shear tests;
- planar tests must be performed up to very large deformations (300%–400% minimum);
- axisymmetric elements can be used in the bearing modelisation up to deformations of 150% shear strain; for larger deformations, three-dimensional models (for steel plates also) must be used;

- the unscragged rubber model must be used for reproducing the behaviour of bearing up to 50%–100% shear strain; for larger deformations the scragged model must be used;
- the polynomial form of the Energy Function of the elastomer seems to better reproduce the experimental results for both specimen and bearing tests; moreover, the results provided by this solution are more stable (and independing of the length of the curves given as input data) than those obtained using the Ogden form.

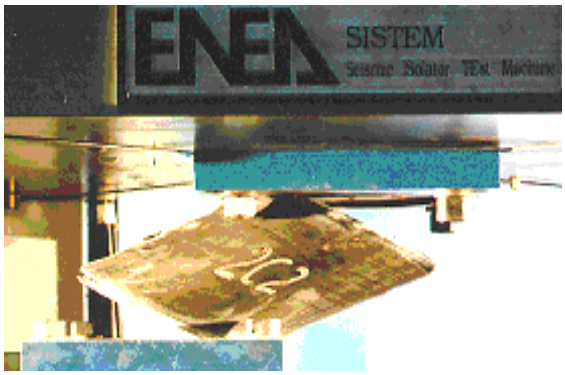

Figure 1.1: Compression and shear test at 300% shear strain on optimised HDRB with recess attachment system.

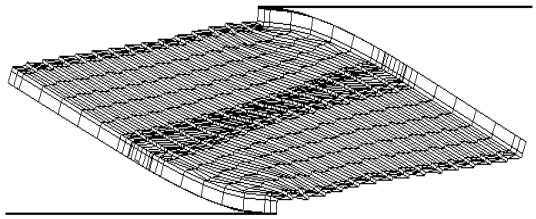

Figure 1.2: FEM of an optimised HDRB at 300% shear strain with recess attachment system.

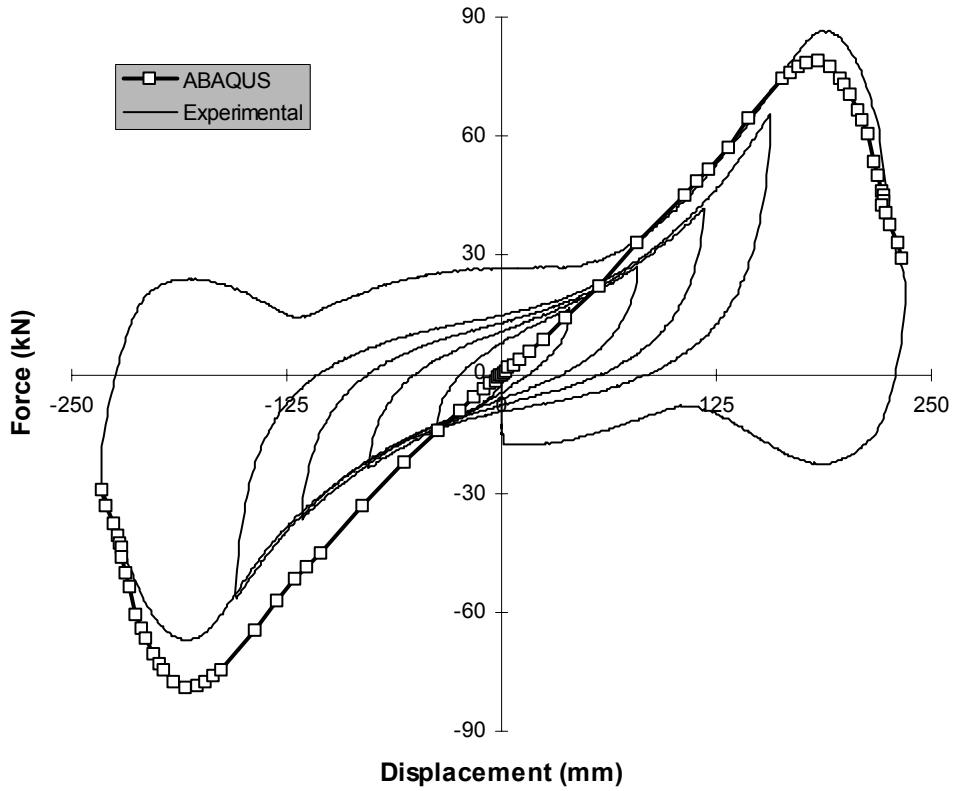

Figure 1.3: Experimental and numerical force-displacement values for a combined compression & 300% shear strain test on optimised HDRB (1:2 scale, diameter=250 mm, H=75 mm, S=12, G=0.8 MPa, recess attachment system).

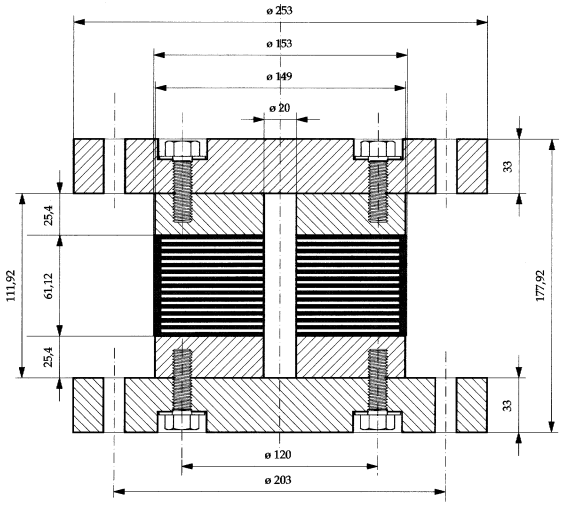

Figure 1.4: Sketch of the 1:8 scale prototype of the ALMR isolation bearing manufactured by ALGA and tested by EERC.

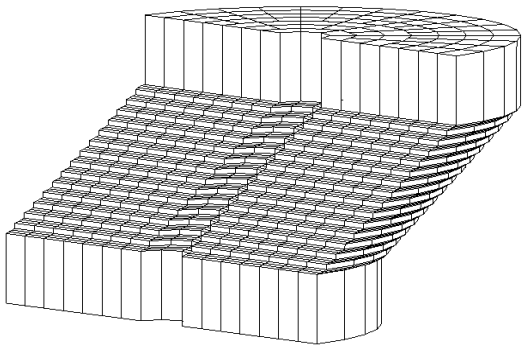

Figure 1.5: Deformed FEM of a bolted ALMR HDRB during a compression (44 kN) and 150% shear strain test.

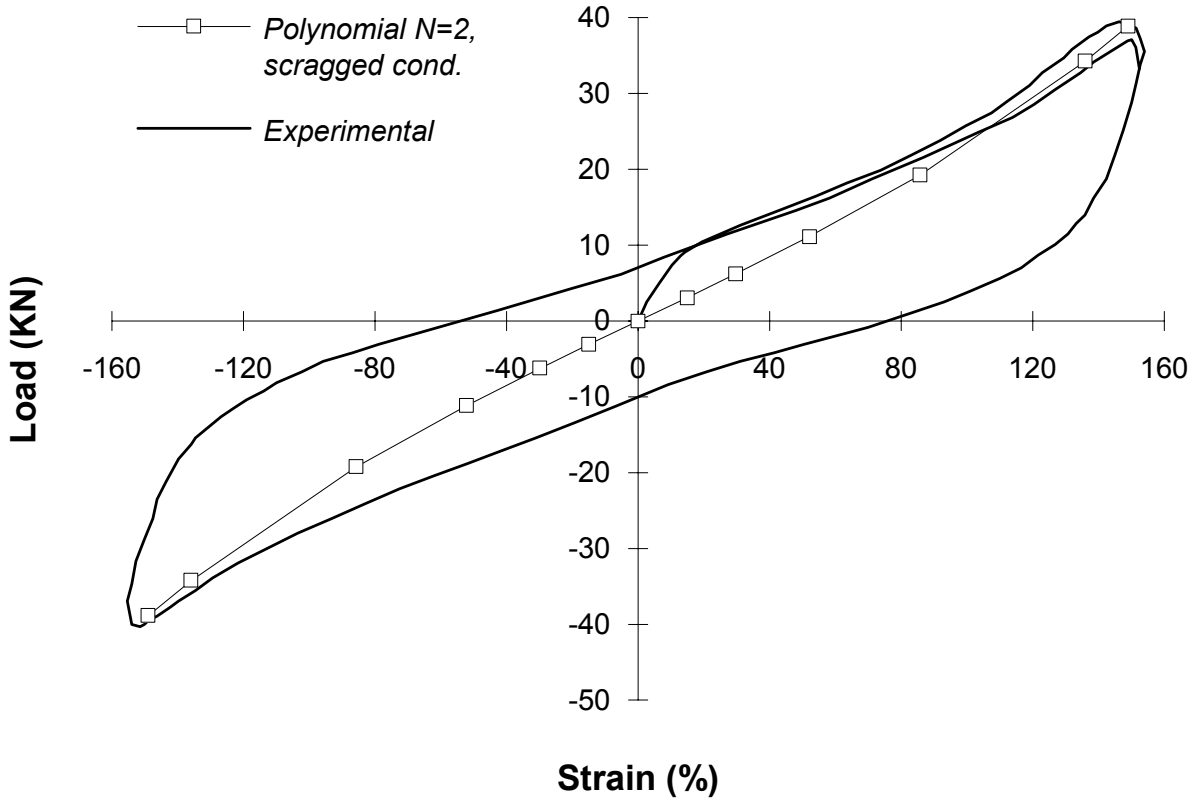

Figure 1.6: Comparison between measured and calculated horizontal stiffness of an ALMR bearing (1:8 scale, diameter=146 mm, H=61 mm, G=1.4 MPa, bolts attachment system) during a combined compression (44 kN) and 150% shear strain test performed at EERC.

2. ANALYSIS OF LEAD RUBBER BEARINGS

ENEL analysed the test data of a first LRBs provided by Japan (Hirata et al., 1998). A second LRB was jointly analysed by ENEL and ENEA (Dusi et al., 1998a).

2.1 Description of the Devices

2.1.1 First LRBs

The first LRB proposed by CRIEPI for intercomparison activities is a 1/1.83 scale prototype of LRBs to be used for the seismic isolation of the Japanese Fast Breeder Reactor. The analysed bearing consists of 25 layers of elastomer (G = 0.6 MPa), 4.9 mm thick, alternated with 24 steel plates having a thickness of 3.1 mm. It has an overall diameter of 876 mm (excluding the coating rubber), a total rubber height of 122.5 mm and a primary shape factor S_1 equal to 44.4. A lead plug of 98 mm diameter is inserted in the centre of the bearing. Each isolator supports a design vertical load of 1500 kN.

2.1.2 Second LRBs

Also the second LRB analysed in the CRP was designed, manufactured and tested by CRIEPI. It consists of 23 layers of elastomer, 2.0 mm thick, alternated with 22 steel plates having a thickness of 1.6 mm. It has an overall diameter of 280 mm and a total rubber height of 46 mm. A lead plug of 70 mm diameter is inserted in the centre of the bearing. The isolator supports a design vertical load of 568.4 kN.

2.2 Finite Element Analyses

2.2.1 First LRBs

Compression test was first analysed using both 3D and axisymmetric finite element models (Dusi et al., 1998a). No sliding effects between lead and rubber were taken into account for these numerical simulations. The comparison between the experimental and numerical results shows that displacements predicted by ABAQUS are smaller than actual ones. No relevant differences were found between 3D and axisymmetric models. Discrepancy between experimental and numerical results is caused by the assumption of incompressible behaviour of rubber in the constitutive equations: as demonstrated by Forni et al., 1995, compressibility should be taken into account in the definition of the strain energy function when analysing compressive loading tests.

The same FE models adopted for the vertical stiffness evaluation were also used for calculating the horizontal stiffness at 25%, 50%, 100%, 200%, 300% and 400% shear strain, under the design vertical compression load. The agreement between tests and calculations is good for horizontal displacements less than about 200 mm. It has however to be observed that, at high shear deformations (more than 200 mm), the simulated response exhibits a higher shear stiffness than the experimental one (at least when considering the second measured cycle).

A comparison between the experimental data and the results obtained from ABAQUS using two different meshes, both with the same materials characterisation and different geometrical discretisation, shows that, for the analysed bearing, mesh density has negligible effects in reproducing the shear behaviour of the isolator.

Results obtained using the simple model, consisting of a single rubber layer, well match those obtained from a 3D FEM, thus demonstrating that the single rubber layer model can be successfully used to calibrate the FEM of the entire isolator and to provide an estimate of its overall horizontal stiffness.

Finally, a comparison between experimental data and numerical simulations obtained considering the effect of sliding at the rubber-lead interface was carried out. An axisymmetric model was used up to 150% shear strain, at which convergence problems occurred. To reach the maximum shear strain (400%) it was then necessary to resort to a detailed 3D model. In spite of the difficulties encountered in setting up the contact problem and the effort in terms of CPU time, results don't differ significantly from those previously obtained.

2.2.2 Second LRBs

The analyses performed on the second LRBs (Dusi et al., 1999a) confirmed the results obtained for the first bearings (see § 2.3). In particular, it was demonstrated that the discrepancies founded by Dusi et al. (1998a) at large deformations between tests and calculations (Figures 21, 2.2) were due to the poor input data for the characterisation of the rubber and not to the lead, which can be assumed elastic — perfectly plastic.

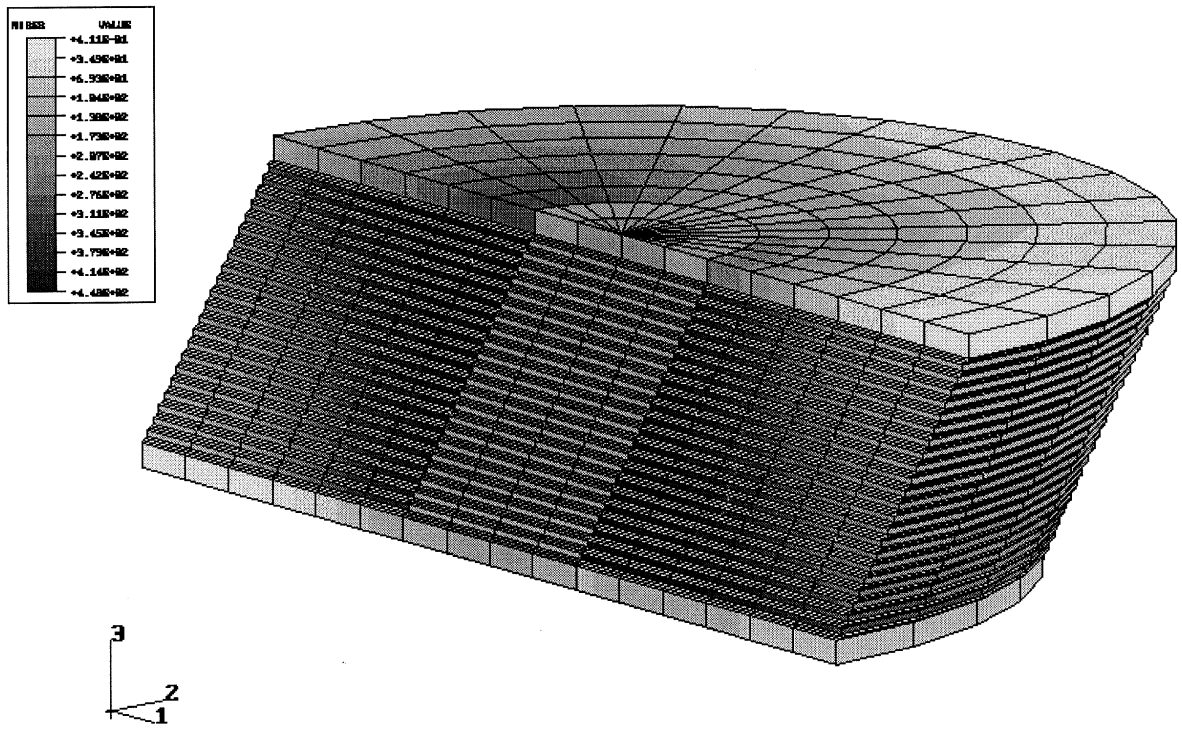

Figure 2.1: Calculated Von Mises stress distribution in the LRB at 150% shear strain.

2.3 Conclusions

From the results obtained in the numerical simulations performed by Dusi et al. (1998a and 1999a) the following considerations may be drawn:

- compressibility must be considered in the strain energy function definition when the behaviour of the bearing under compressive loading has to be analysed;
- mesh density has little effect in reproducing the shear behaviour of the bearing, providing that a sufficient number of elements is used and that the element shape is such to avoid excessive distortions at high deformation;
- axisymmetric elements (with asymmetric deformation) can successfully be used instead of solid element, thus saving computational time;

- the results of a simple model, consisting of a single rubber layer, can be successfully used to calibrate the FEM of the entire isolator and to provide an estimate of its overall horizontal stiffness, greatly reducing computational time;
- when analysing vertical stiffness, at least 3 elements are required in the thickness to get accurate results; on the contrary, in shear deformation the number of elements seems to have little effects on the prediction of the horizontal stiffness
- the behaviour of the lead can be considered elastic — perfectly plastic and the friction effect between lead and rubber can be neglected.

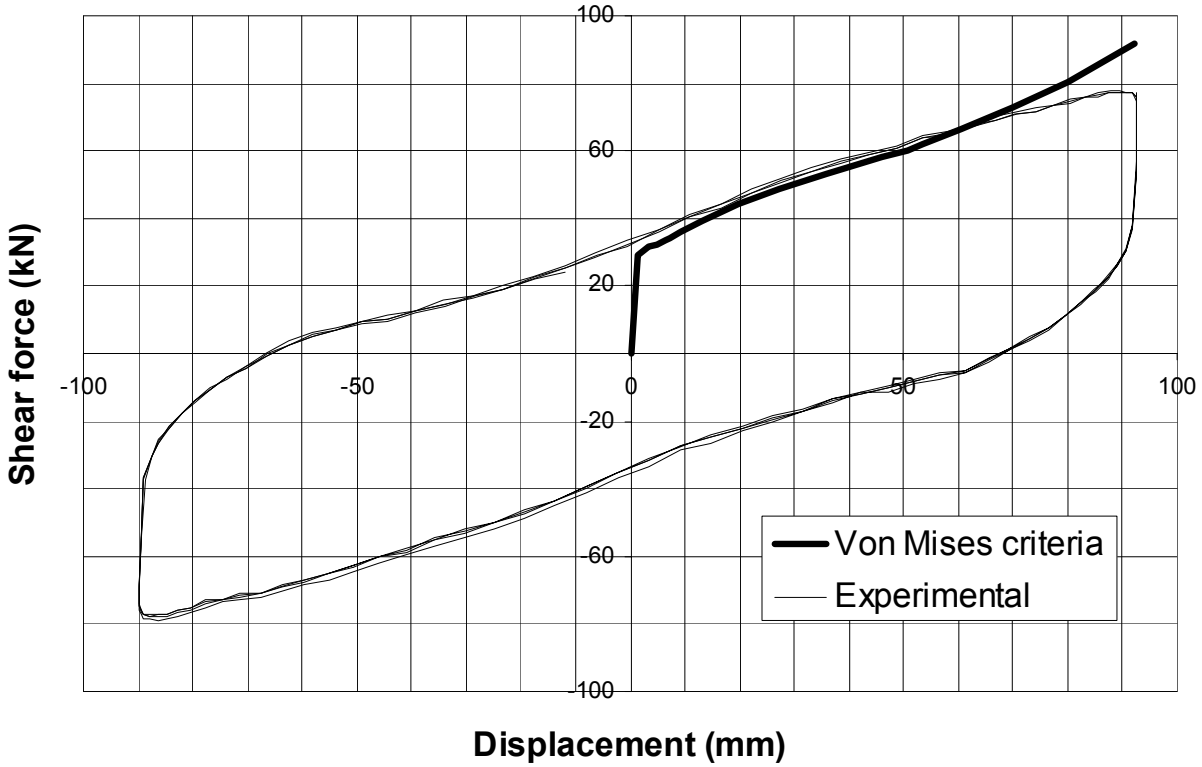

Figure 2.2: Comparison between the measured and calculated hysteresis loops for the LRB (complete FEM, Von Mises criteria).

3. ANALYSIS OF ISOLATED MOCK-UPS WITH SIMPLIFIED FEM OF HDRBS

Two seismically isolated structure mock-ups tested on shaking table were jointly analysed by ENEL and ENEA. The first mock-up was a flexible steel frame (MISS) tested at ISMES in the framework of the above mentioned research programme coordinated by ENEL (1993). The second one was the rigid mass tested by CRIEPI (Hirata et al., 1998). Aim of these analyses was the implementation and validation of a simplified FEM of HDRBs. As a matter of facts, the detailed FEM of isolators described in the previous sections cannot be used in the dynamic analyses of isolated structures and simplified models must be implemented.

3.1 The Multilinear Elastic-Perfectly Plastic (MEP) Simplified Model

The most important problem in the implementation of a simplified model is given by the highly non-linear behaviour of the rubber bearings, especially in terms of damping. The model proposed herein is based on the coupling of a spring, which provides the non-linear stiffness,

and a truss element (that is a beam working in the axial direction only), which provides the hysteretic damping with its plastic deformation.

A sketch of the MEP model is shown by Figure 3.1. The spring K_S can be multilinear and even asymmetric with respect to the origin. Usually, only one K_S variation is sufficient to describe the isolator hardening, which usually begins at 75%–125% shear strain and perfect symmetry between the two deformation ways in the horizontal direction is assumed. The hysteretic damping is provided by the beam, which is subjected to pure compressive load: it is initially elastic, then it strains plastically. The beam stiffness is given by the ratio EA/L, where E is the Young's modulus (the material, of course, is completely free), A is the cross-section area and L is the length. The geometry of the beam is free too; however, to avoid convergence problems in the calculations, it is useful to have a non-excessively large Young's modulus, a length/diameter ratio typical of a beam (say, 10 or 20) and a length that is well larger than the expected deformation.

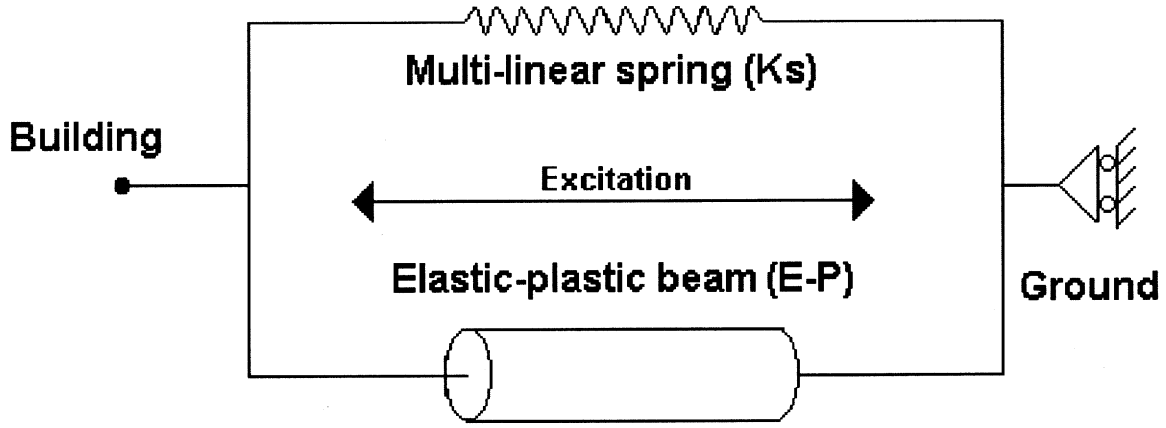

Figure 3.1: Multi-linear elastic-plastic simplified model (MEP) of a rubber bearing (Ks = non-linear spring; E-P = elastic-perfectely plastic beam).

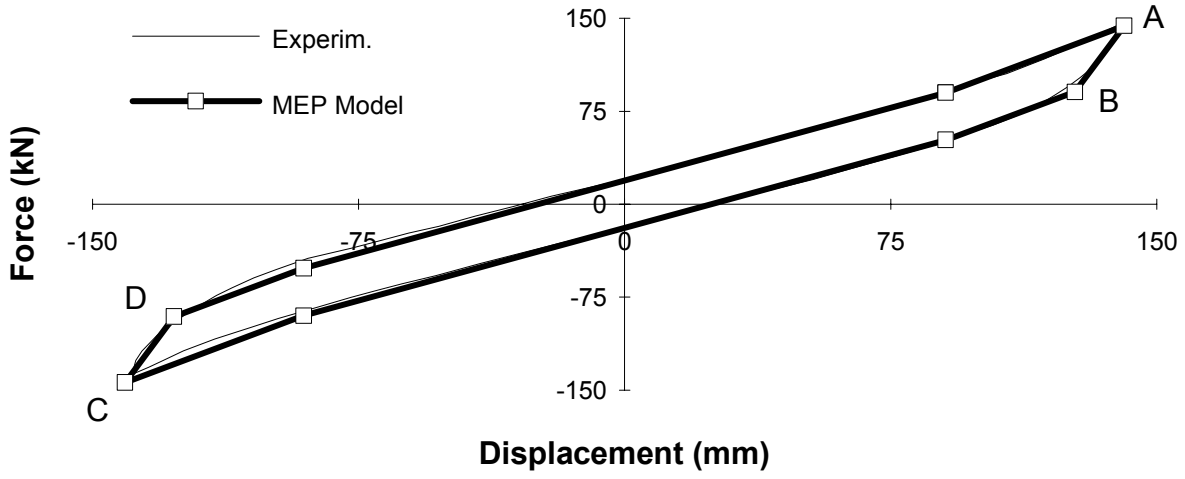

Figure 3.2: Comparison between the experimental and 'MEP' hysteresis loop for the smaller HDRB of the TELECOM Italia building at 100% shear strain (see § 4).

In spite of its simplicity, the MEP model can easily reproduce any given or wanted hysteresis loop (Figure 3.2). Its only limit is given by the constant 'width' of the hysteresis loop, that implies an energy dissipation ratio constant with respect to the deformation rate. Thus, the MEP model shall be calibrated on the maximum expected deformation and used to calculated the response of the structure in this range of deformations. For lower deformations the MEP model will overestimate the damping while, for higher deformations, it will underestimate the energy dissipated (Figure 3.3).

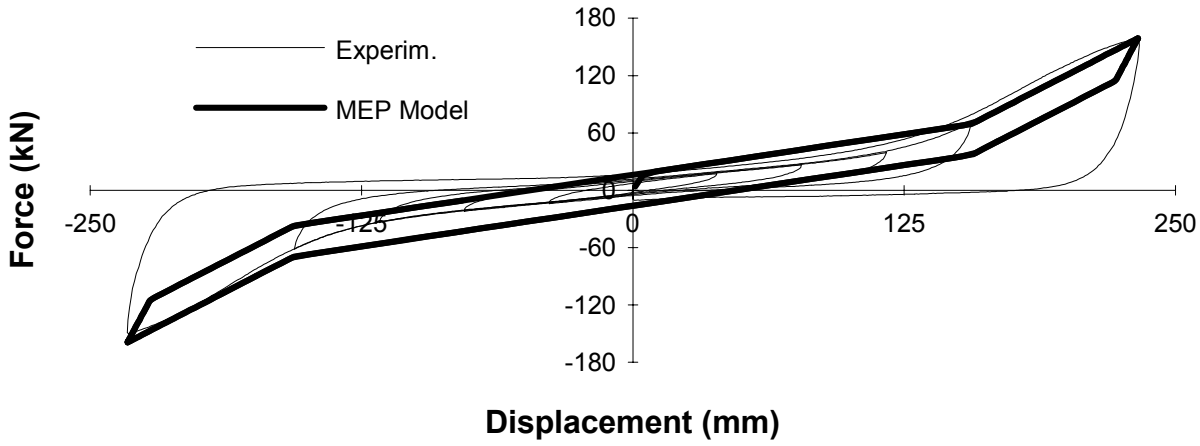

Figure 3.3: The MEP simplified model provides a constant 'width' of the hysteresis loop which underestimates the damping at large shear strain.

3.2 Description of the Structures

3.2.1 MISS

MISS is a steel frame structure mock-up with a rectangular base of 2.1 m × 3.3 m, and four storeys, with an interstorey distance either of 0.9 m or of 1.1 m (Figure 3.4). It can support up to 20 concrete masses, each weighting 13 kN. The frequency of the structure can be chosen in quite a large range, depending on the interstorey distance and the number of masses used and their disposition (which can also be asymmetric). The actual isolation system is formed by 6 isolators fabricated with a soft compound (G = 0.4 MPa, bolts and dowel attachment system, 125 mm diameter, 30 mm rubber height) and provides an isolation frequency in the range of interest for seismic isolation (below 1 Hz). MISS was subjected to a wide ranging experimental campaign of forced vibrations at the top (sinusoidal and random) and shaking table tests consisting in the application of sinusoidal excitations and natural and artificial earthquakes (1D, 2D and 3D) for both the isolated and fixed-base configurations.

3.2.2 CRIEPI Rigid Mass

This rigid mass mock-up was tested by CRIEPI in 1989 and was jointly analysed by ENEA and ENEL (Dusi et al., 1999a). The mock-up consists of a concrete frame of 178 kN weight, 3 × 2.1 × 2.8 m overall sizes, which is supported by 8 LRBs very similar to those described in § 2. The results of the shaking table tests were also analysed by Hirata et al. (1998) and by Yoo et al. (1998a) in the framework of this CRP.

3.3 Finite Element Analyses

The structure mock-ups described in the previous section were modelled by Dusi et al. (1996b and 1999a) and by Forni et al. (1998) using detailed finite element models of the structures (Figure 3.5) and simplified MEP models for the isolation systems. The MEP models were calibrated based on experimental hysteresis loops provided by ISMES and CRIEPI corresponding to maximum deformation obtained during the shaking table tests. Then, the mock-ups FEM were subjected to the excitations really applied on the shaking table and more severe accelerograms, in order to calculate the response of the structures within acceleration range which are impossible to be applied in laboratory. Different types of rubber bearings and wide ranges of deformation and acceleration levels were successfully analysed with the MEP simplified model (Figures 3.6, 3.7 and 3.8).

3.4 Conclusions

The results of shaking table tests performed on a steel frame structure mock-up and an isolated rigid mass have been used for the characterisation and the validation of a simplified finite element model based on the coupling of a spring and a truss element. It was demonstrated that the MEP simplified model can correctly reproduce any given hysteresis loop and the behaviour of an isolated structure, at least in the range of deformations in which the MEP is calibrated.

In section 5, is described a simplified finite element models of HDRBs, implemented by Dusi et al. (1998b) in the ABAQUS code, which can correctly reproduce the behaviour of the bearing independently of the deformation value.

Figure 3.4: MISS on the ISMES shaking table in the fixed-base configuration with 16 masses (250 kN total weight).

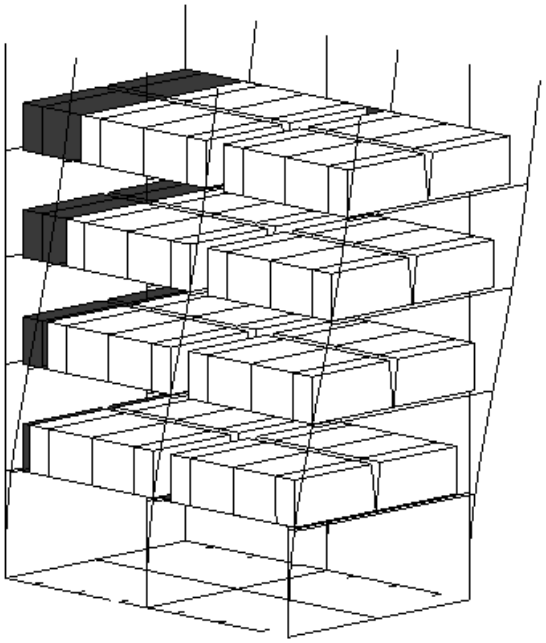

Figure 3.5: 1st modal shape of MISS in the fixed-base conditions with 16 masses (F1=1.49 Hz; exp.=1.5 Hz; α=1.75).

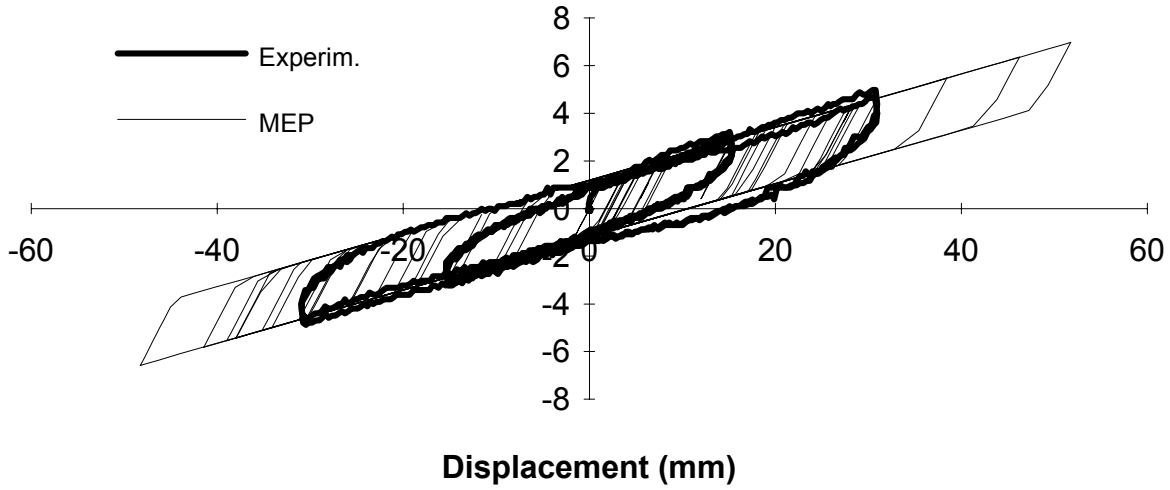

Figure 3.6: Comparison between the hysteresis loops as calculated by the MEP model during the application of a synthetic earthquake and those obtained during the execution of static tests on single device.

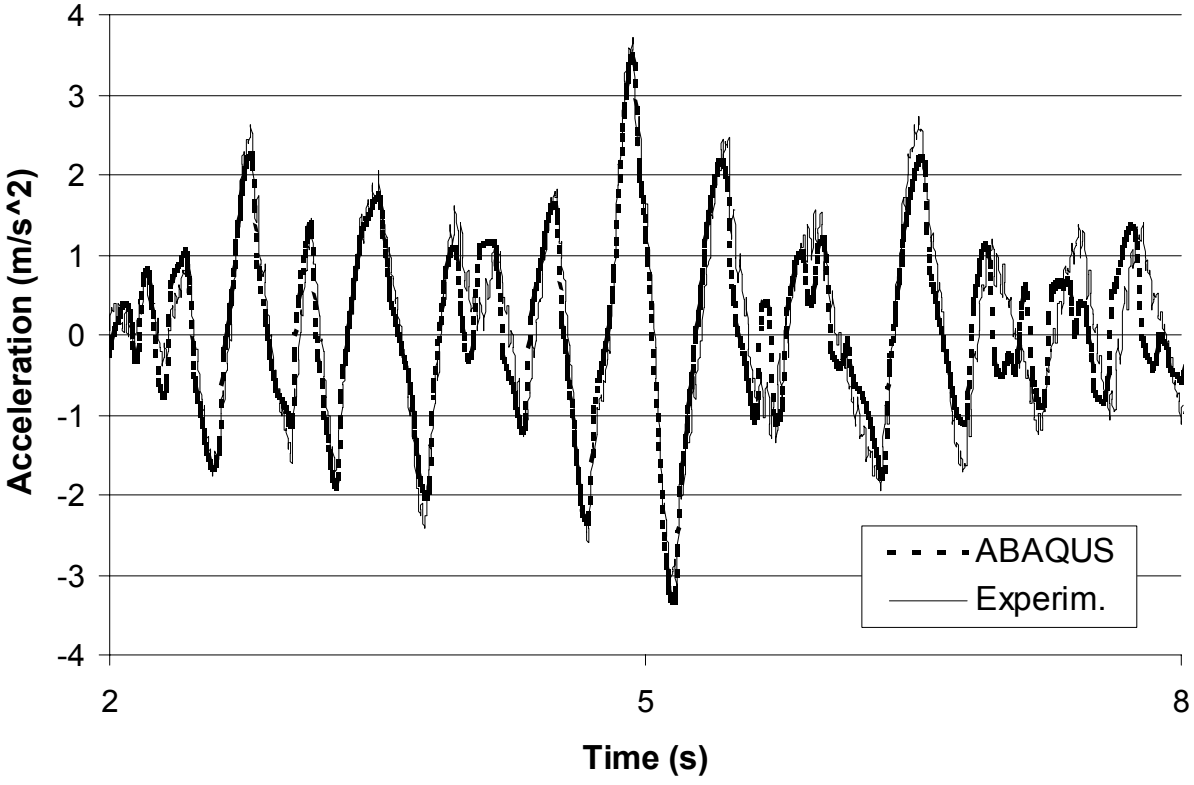

Figure 3.7: Comparison between measured and calculated accelerations at the base of the rigid mass under the A1 acceleration time-history (detail on the strong-motion part).

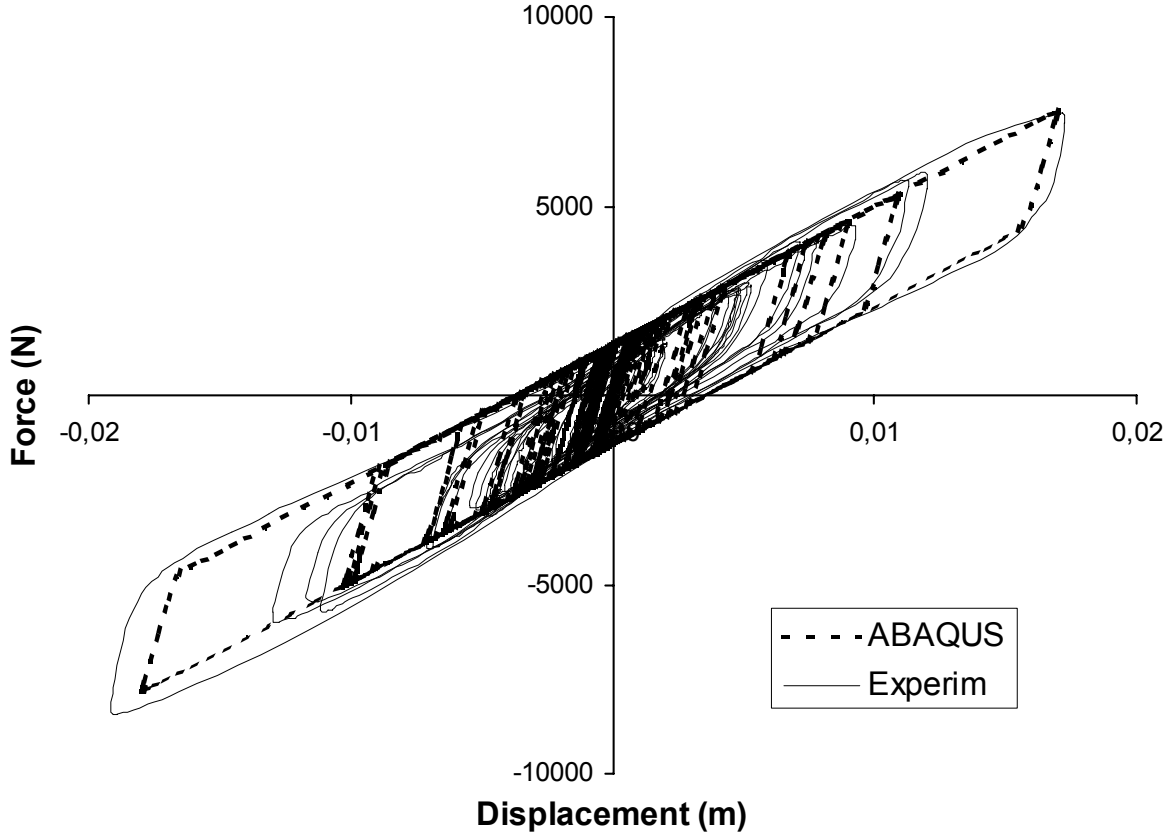

Figure 3.8: Comparison between measured and calculated hysteresis loops under the A1 acceleration time-history.

4. ANALYSIS OF ISOLATED BUILDINGS WITH SIMPLIFIED FEM OF HDRBS

Two Italian seismically isolated civil buildings subjected to on site experimental campaigns were jointly analysed by ENEA and ENEL. Aim of such analyses was the validation of the simplified finite element models of HDRBs described in section 3 in the case of real structures.

4.1 Description of the Buildings

4.1.1 TELECOM Italia building

The TELECOM Italia Center of the Marche Province was built at Ancona in 1991 and is the most important application of base isolation in Italy (Giuliani, 1989). It is formed by five large eight-storey buildings, connected among themselves. The resistant structures are reinforced concrete frames that are highly irregular (Figure 4.1). The buildings contain computers and other sophisticated hardware for which the protection from seismic actions is essential. The isolation system consists of HDRBs with hard rubber compound (shear modulus G = 0.8 MPa) and 'recess' attachment system (Bettinali et al., 1991); the devices, similar to those described in § 1.1.1, have a total rubber height of 144 mm and two different diameters (500 mm and 600 mm) corresponding, respectively, to 1,600 kN and 2,600 kN design vertical load (combination of the dead load of the structure with vertical seismic actions). The buildings have a first response frequency close to 0.6 Hz, with quite a high isolation ratio α, close to 7 (α being the ratio of the fixed-base structure frequency over the

isolated one). During the design earthquake, the expected displacement is equal to 144 mm, corresponding to a bearing deformation of 100% shear strain. Somewhat beyond this displacement, a fail-safe system, formed by rubber bumpers, gradually stops the building motion.

The building analysed in the CRP was subjected to a wide-ranging experimental campaign including forced vibration and pull-back tests (Bettinali et al., 1991). Aim of the forced vibration tests, carried out by use of a mechanical vibrator placed on the roof, was to measure the fundamental response frequencies of the building superstructure. The pull-back tests, which consisted in providing an initial displacement to the isolation system by means of hydraulic actuators acting on the base of the building superstructure, aimed at observing the free-vibrations following the istantaneous release of the building itself. They were performed using collapsible devices provided with explosive bolts. These tests allowed for the measurement of the frequencies of the isolated structure (and the isolation ratio) and were suitable to characterise the mechanical properties of the isolation system.

4.1.2 The twin apartment houses at Squillace

The two buildings, one conventional and the other base-isolated, have identical geometrical and mechanical characteristics, apart the foundations and the isolation system (Forni et al., 1993). The buildings have four storeys, three above and one below ground. The resistant structure is a reinforced concrete frame, symmetrical with respect to the central transversal axis, while on the longitudinal axis the mass and stiffness centres are nearly coincident. The first interstorey is stiffer than the others, due to the presence of a shear reinforced concrete wall. The isolation devices are underneath the first floor, below them there is a rigid box structure acting as foundation, while a framed structure rests on them. They consist of 27 HDRBs with recess attachment system, 132 mm rubber height and two different diameters (400 mm and 500 mm), the largest for the internal columns, which carry a higher vertical load (1,190 kN), and the smallest for the exterior columns (770 kN). The bearings were fabricated using hard rubber compound (G = 0.8 MPa) and were designed to obtain an isolation frequency close to 0.8 Hz, with an isolation ratio of 8.3.

At the time of in-situ tests the frames of the two structures had been completed but the buildings were not complete; neither the roof nor the flooring were in place. In the conventional structure the external masonry walls and internal partitions were present, while the isolated structure had only the external walls. With the aim of characterising the dynamic properties of the buildings, forced vibration tests were carried out by use of a mechanical exciter placed on the roof of the two buildings, in an eccentric position. Excitations were provided in two normal directions (Forni et al., 1993).

4.2 Finite Element Analyses

Detailed FEM of the buildings described in the previous sections were implemented in the ABAQUS code (Figure 4.2). The numerical models of the buildings were calibrated based on the results of the on-site forced vibration tests (Figure 4.3), while the simplified MEP models were calibrated based on the results of laboratory tests on single HDRBs and the pull-back test on the TELECOM building (Figure 4.4).

After the validation of the superstructure and isolation system models, many artificial and natural earthquakes were applied to both the TELECOM and Squillace buildings with the aim of analysing the structure behaviour for different soil conditions, acceleration levels and isolation ratios, even in the case of absence of seismic isolation (Bettinali et al., 1996). Modal analysis (taking into account the first 9 modes) was used for the calculations at fixed-base, while direct integration (implicit method) was adopted for the runs concerning the base-

isolated building. The analysis showed that the isolation system provides a reduction of a factor 4 to the accelerations (therefore to the inertial loads) acting at the top of the building during an earthquake which provides the maximum design displacement. Thus, not only the frame but also the contents are better protected from seismic actions.

4.3 Conclusions

The analyses on isolated buildings performed by Bettinali et al. (1996) confirmed the results obtained for the isolated mock-ups (§ 3): in spite of its simplicity, the simplified model of rubber bearing based on the coupling of a multilinear spring and an elastic-plastic beam can be successfully used in the non-linear dynamic analyses of isolated structures.

Figure 4.1: Base-isolated building of the TELECOM Italia Center.

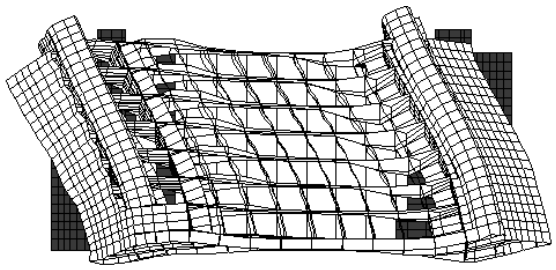

Figure 4.2: 4th modal shape of the TELECOM Italia building.

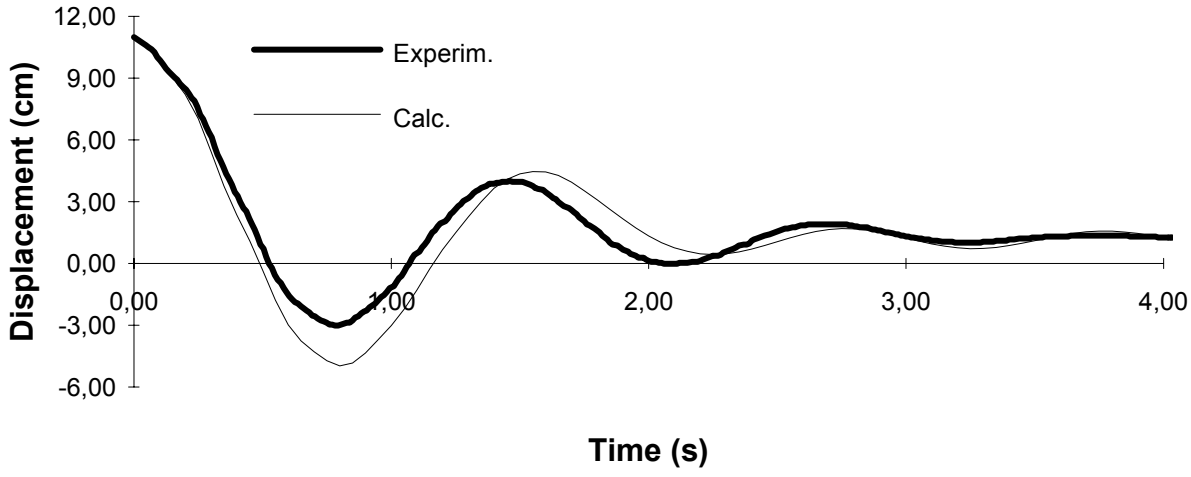

Figure 4.3: Experimental and calculated displacements during the pull-back test at 11 cm on the TELECOM Italia building.

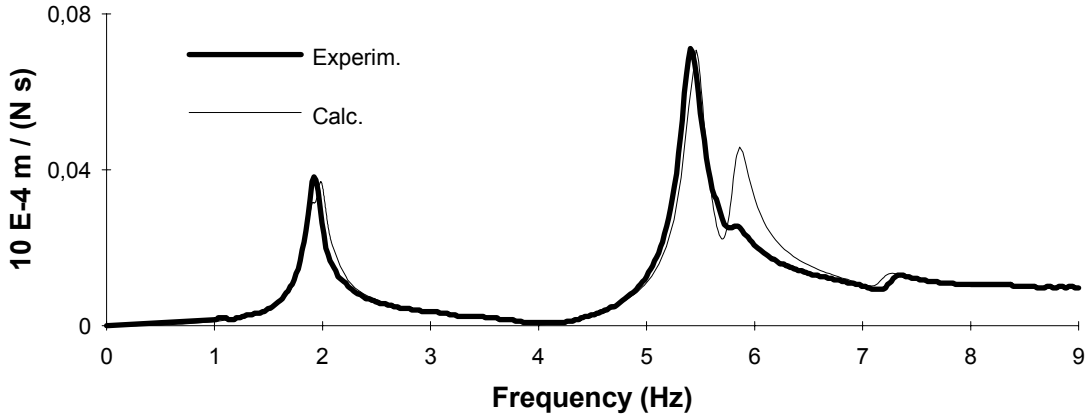

Figure 4.4: Measured and calculated transfer functions between velocity and excitation force in the longitudinal direction at the roof of the TELECOM Italia building.

5. PARALLEL ELASTOPLASTIC MODEL OF HDRBS

5.1 Model description

A parallel elasto-plastic model with exponential constitutive law for seismic isolator, able to represent the nonlinear behaviour has been developed by ENEL and ISMES (Dusi et al., 1999b). The model has been developed considering HDRBs, but it can be adequately applied to other types of isolation devices having a continuously decreasing stiffness with increasing displacement. An example of application of the model to LRBs is reported. The proposed model, implemented in an existing nonlinear finite element computer code, is particularly suited to compute the time history dynamic response of base isolated structures. Its reliability is checked by comparing the numerically computed and experimentally recorder motions of both single devices and different base isolated mock-ups subjected to different earthquake motions on shaking table.

The model proposed in this CRP, assumes a decreasing exponential constitutive law G(γ) for the rubber compound; this behaviour has been implemented in the finite element ABAQUS code through a parallel scheme of elastoplastic elements. A peculiar feature of developed model is the capability to reproduce the complex behaviour of HDRBs using only very simple information concerning the rubber compound, without any need of experimental data relevant to tests on actual devices.

The nonlinear model is hysteretic with the following assumptions:

i) tangent modulus with decreasing exponential law, defined through 3 parameters related to the compound, i.e.:

G_∞ G value at design shear strain

G_O G value at $\gamma=0$

b exponent multiplier;

ii) overall bearing behaviour defined through 2 geometric data: normal area of bearing and total rubber thickness;

iii) no viscous effects, i.e. velocity does not affect the force-displacement relationship.

The assumed G(γ) relationship can be expressed by the following two mathematical expressions, valid for a loading and unloading curve, respectively:

$$G_t(\gamma) = \frac{d\tau}{d\gamma} = G_\infty + ae^{-b(\gamma-\gamma_{\min})} \qquad (5.1)$$

$$G_t(\gamma) = \frac{d\tau}{d\gamma} = G_\infty + ae^{-b(\gamma_{max} - \gamma)} \qquad (5.2)$$

where:

$a = G_\infty - G_O$,

γ_{min} = starting strain value for increasing load phase

γ_{max} = starting strain value for decreasing load phase.

Hysteretic curves with continuously decreasing stiffness can be easily discretised using the parallel modelling concept. The above $G(\gamma)$ relationship has been reproduced by means of a set of elasto-plastic elements working in parallel; the parameters of each element in parallel must be calibrated to correctly reproduce the experimental bearing behaviour.

The parallel model previously described is able to reproduce the observed experimental behaviour of HDLRB as far as the maximum shear strain does not exceed a limit value around 100%. A more refined constitutive model was therefore set up to allow for the reproduction of the high shear strain behaviour. This was obtained by putting in parallel to the original model, a second one, whose $G_h(\gamma)$ function has the following expression:

$$G_h(\gamma) = c(e^{d|\gamma|} - 1) \qquad (5.3)$$

where parameters *c* and *d* define slope and curvature of exponential law.

5.2 Example of application

Figures 5.1 shows the comparisons between HDLRBs experimental hysteresis loops (obtained from quasi-static monoaxial tests) and numerical results.

In Figure 5.2 is reported the comparison between experimental and numerical hysteresis loops for a LRB having a diameter of 107 mm, a total rubber height of 15 mm and a lead plug of 12 mm diameter.

The numerical model of elastomeric bearings has been used to reproduce the dynamic behaviour of real base isolated structures subjected to seismic excitation. Different tests carried out using a shaking table have been considered for the validation of the model.

Among other tests, shaking table experiments have been conducted on the above mentioned (§3) Japanese isolated rigid mass. Comparison between recorded and numerical mass accelerations is reported in Figure 5.3. Finally, an example of application to a flexible mock-up, namely MISS (§3) is reported in Figure 5.4.

5.3 Conclusions

Comparisons between experimental tests and numerical analyses show that the numerical model with an exponential constitutive law, implemented through the parallel elastoplastic scheme, is able to reproduce the seismic behaviour of bearings with a high degree of accuracy. Hysteresis loops, multiaxial excitations and hardening effects are accurately reproduced.

The availability of a routine implementing the bearings behaviour inside a commercial available finite element code (ABAQUS) allows the user to perform time histories analyses of isolated structures, simply by defining an element having the same bearing dimension and whose material characteristics (related to the compound parameters) are given in a user subroutine.

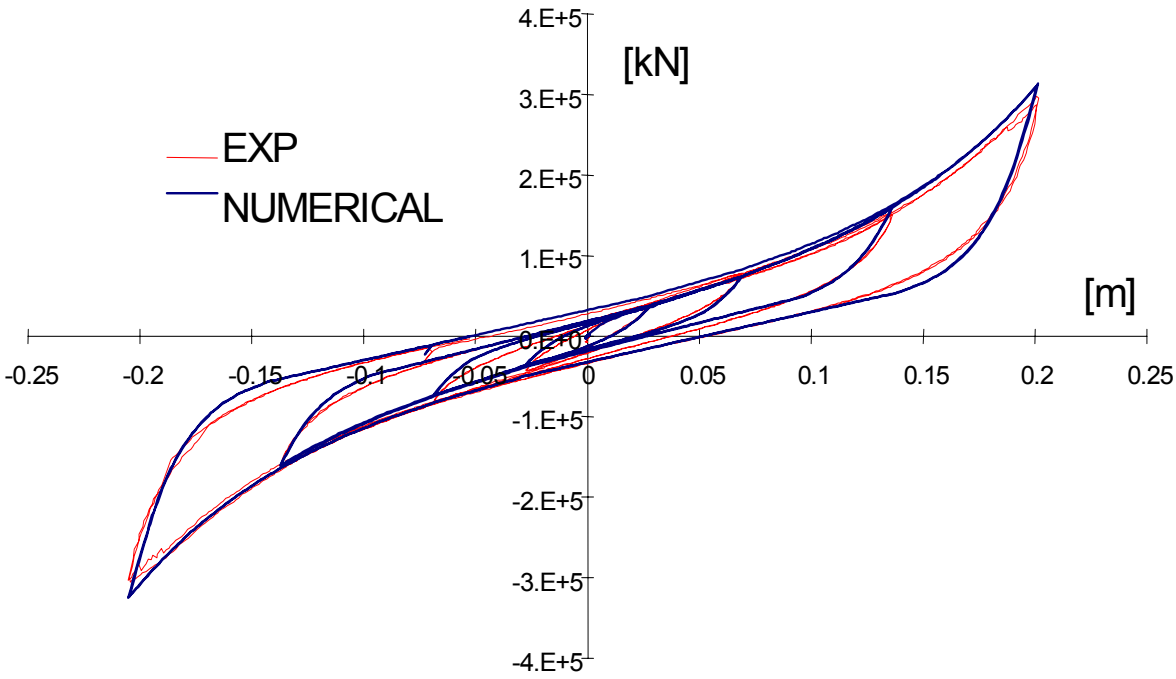

Figure 5.1: Experimental and numerical hysteresis loops for a rigid HDLRB (G = 0.8 MPa).

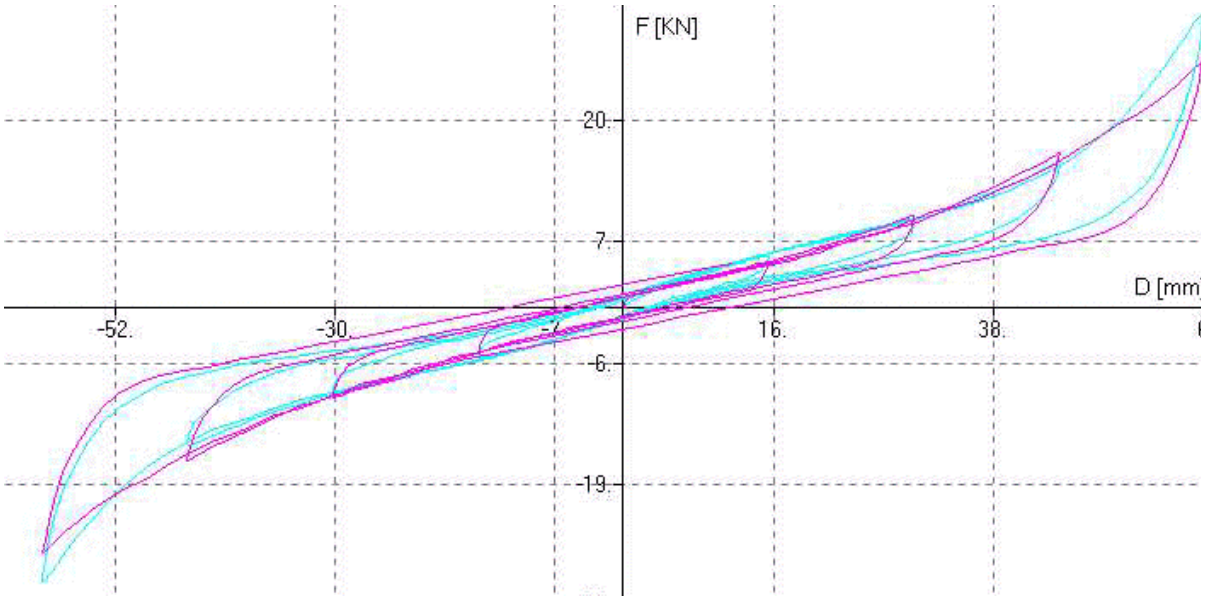

Figure 5.2: Experimental and numerical hysteresis loops for a LRB.

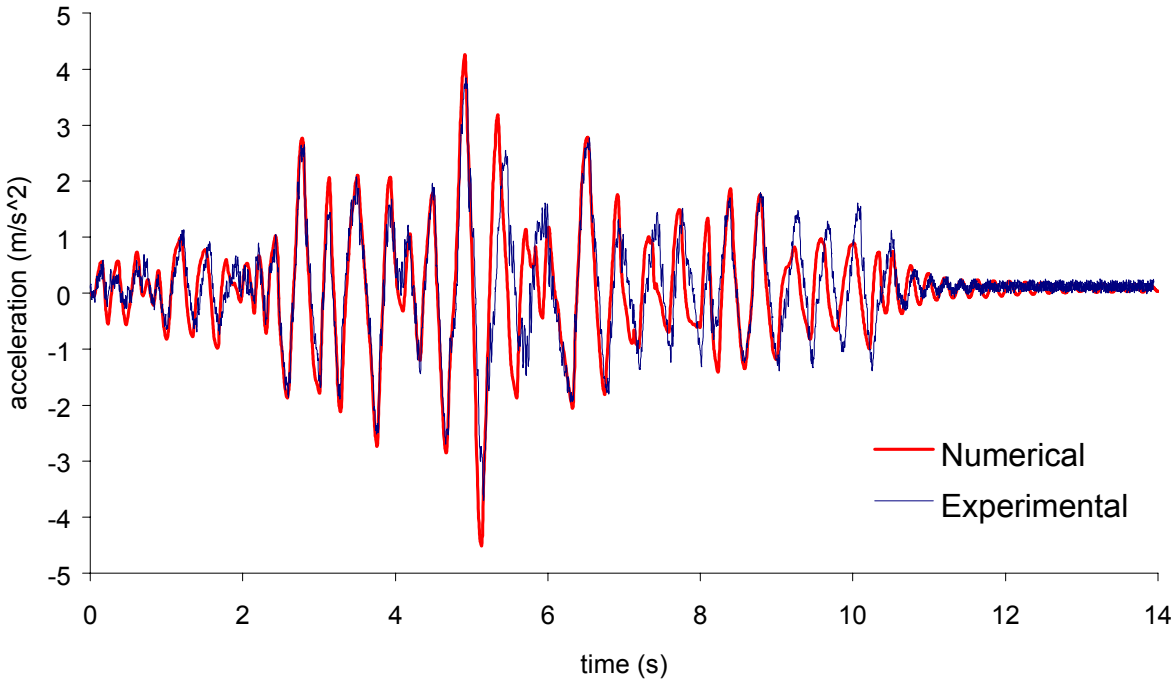

Figure 5.3: Experimental and numerical acceleration of a 179 kN isolated mock-up under the design earthquake record.

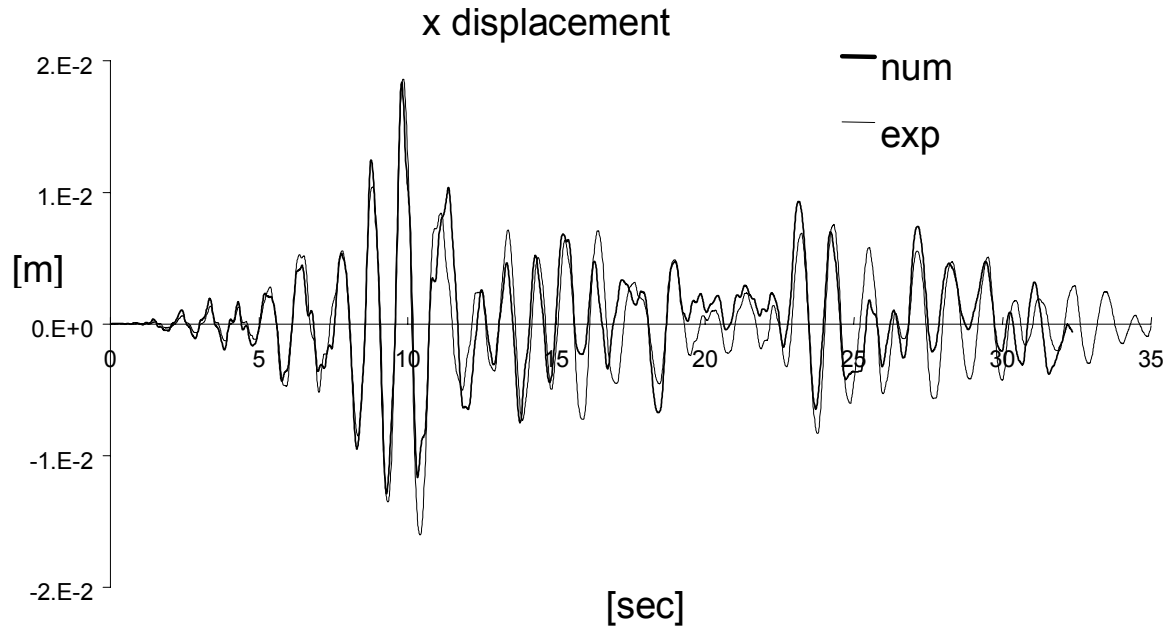

Figure 5.4: Experimental and numerical relative displacement (x component) of a steel frame isolated mock-up under the 1981 Calitri record.

6. BENCHMARK ON THE TORSION OF A ELASTOMERIC CYLINDER

6.1 Introduction

In order to asses the accuracy of both the FE model meshing and FE solver, a torsional benchmark problem was presented jointly by TARRC and ENEL. Prediction of the couple and axial load acting on the cylinder was obtained by ENEL from FE calculations using ABAQUS, and was compared to the analytical solutions for two types of material models, Mooney-Rivlin and Ogden. An extensive numerical work was performed by considering meshes with different refinements and different element types. The results, presented during the RCM Taormina by Fuller et al. (1998), showed an excellent agreement.

6.2 Description of the Activity

The analytical solution to the torsion of an elastomeric cylinder is suggested as a "benchmark" for the finite element analysis of elastomeric components. A general solution due to Rivlin is presented. It can be expressed for the two forms of the strain energy function commonly used to describe the stress-strain behaviour of elastomers — a function of either strain invariants or principal stretch ratio. Hence the accuracy of the FEA predictions, for either form of material model, can be assessed for two commercial FE Codes, namely MARC and ABAQUS. The response of a cylinder to torsional deformation is predicted. The comparison of the FE analysis with an analytical solution rather than experimental data means that the assessment of the FEA is not influenced by the effectiveness of the material model or the reliability of experimental data. Two material models that are available as default in the codes — a five term Mooney-Rivlin function and a three-term Ogden function — are used. The latter is included because of the availability in the literature of both material model data and an analytical solution to the torsion problem for that strain energy function due to Ogden and Chadwick. The FE 3-dimensional analysis for a coarse-mesh model with 500 elements (Figure 6.1) gives results generally within 5% of the analytical solutions for the couple required to deform the cylinder. For the axial load required to keep the height of the cylinder unchanged the errors are up to 10%. However, better levels of accuracy are obtained if the density of the mesh is increased. This is at the cost of much longer computing times.

The second part of the work evaluates two forms of strain energy function for describing the behaviour of high damping natural rubber compounds. The Ogden strain energy function is used to fit experimental data for a range of homogeneous deformations and it was observed that the quality of fit is not very good at small strains. Increasing the number of terms from 2 to 3 does not produce significant improvement. The use of sophisticated non-linear curve fitting algorithms may improve this. A second material model based on the assumption that the strain energy is a function of only one of the strain invariants (I_1) is proposed. It was found not only that a better quality of fit may be obtained but also that such a model can lead to much simpler material characterisation tests.

6.3 Conclusion

Rivlin's general solution to the torsional deformation of an elastomeric cylinder has been used as a "benchmark" problem to assess the accuracy of commercially available FE packages such as MARC and ABAQUS. The generality of the solution allows the prediction of the behaviour of the cylinder whether the stress-strain behaviour of the material is modelled as a function of strain invariants or modelled as a function of principal stretch ratios. The analytical solution thus provides a useful tool to assess the accuracy of the FE solvers.

The FE results using MARC and ABAQUS gave to an accuracy within 5% the couple that is required to twist one end of the cylinder with respect to the other through an angle of θ.

The degree of accuracy was reduced to 10% for the axial load required to keep the height of the cylinder constant. Refining the mesh density improved the accuracy at the cost of much increased computing time.

The use of the Ogden strain energy function to model the behaviour of high damping natural rubber compounds was found to suffer from the disadvantages that fitting the parameters to the experimental data using standard curve-fitting software is difficult, and that this form of function is not flexible enough to allow for the material non-linearity at small strains.

A strain energy function based on the assumption that the energy of deformation depends on I_1 only is proposed. The function is able to cater for material non-linearity both at small and large strains. If a material can be adequately characterised with this form of strain energy function only a simple uniaxial tension test is required to find its coefficients.

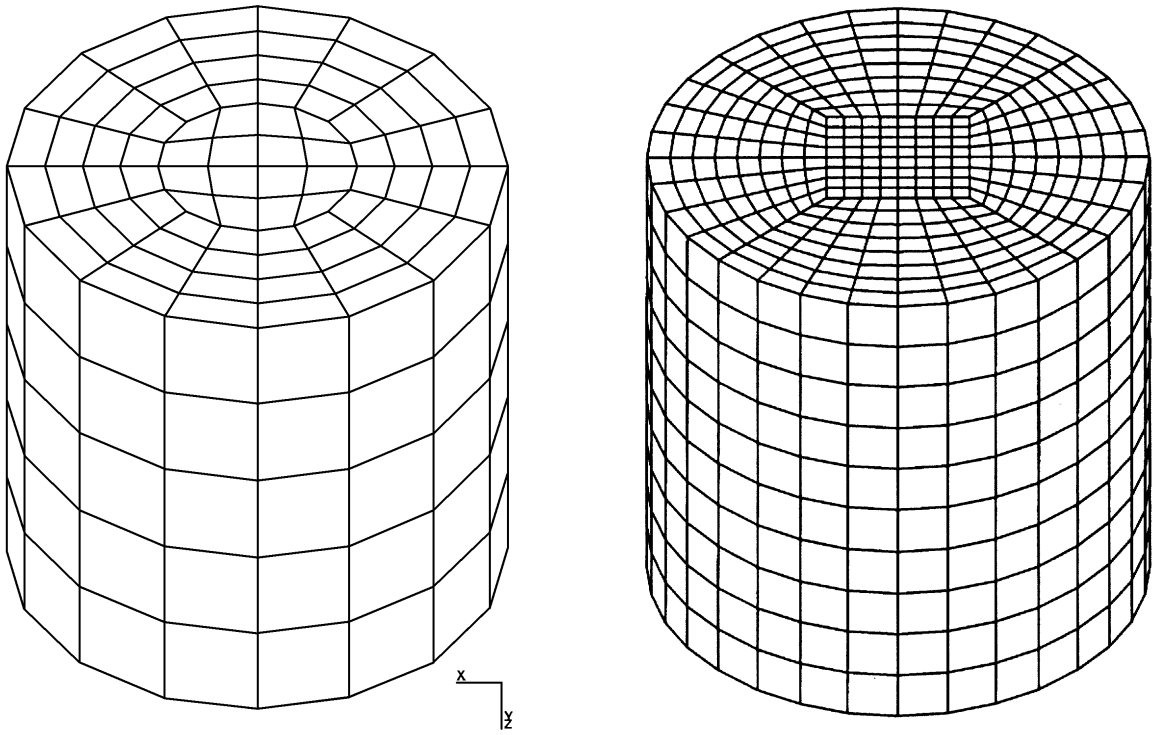

Figure 6.1: FEA models showing coarse-mesh (Models 1,2,5) and refined-mesh (Model 3).

GENERAL CONCLUSIONS

Italy, represented by ENEA, ENEL and ISMES, participated actively in this CRP by providing and analysing experimental test data on both isolation devices and isolated structures. Moreover, test data provided by the others countries were analysed jointly by ENEL and ENEA in order to improve the existing mathematical models and to validate the new models developed within this CRP. In particular, Finite Element (FE) analyses were carried out on U.S. scaled HDRBs that had been manufactured in Italy and tested by University of California at Berkeley; and on Natural Rubber Bearings (NRBs) and Lead Rubber Bearings (LRBs) manufactured in Japan for CRIEPI. The results concerning U.S HDRBs and Japanese NRBs

were presented at the Research Coordination Meetings (RCMs) of St. Petersburg and Taormina, while information concerning Japanese LRBs was given at the Hertford RCM. Finally, the results concerning modified Japanese LRBs (with larger lead plug diameter) were presented at the Cheju RCM.

The compression and combined compression and shear behaviour of the bearings were analysed, using different FE models and different hyperelastic strain energy functions, by means of the ABAQUS code. Elastomers' constitutive models, available in the ABAQUS package to represent the non-linear and hysteretic behaviour of bearings, were used to solve the problem. Mooney-Rivlin and Ogden forms with different order of the strain energy function, and, alternatively, user-defined strain energy function, were used in modelling the rubber. Results from different meshes, with different discretisations and different types of elements (axisymmetric, axisymmetric with non axisymmetric deformation, shell and solid) were compared to the experimental data. The choices of the appropriate strain energy function, element selection and FE modelling were examined and their ability to model the behaviour of elastomeric bearings presented and discussed in the report provided to the Agency.

For the Japanese NRBs and LRBs both three-dimensional and axisymmetric finite-element models were developed and implemented in ABAQUS computer program by ENEL, while similar models were developed and implemented in the same code by ENEA for the U.S. HDRBs. Hyperelastic models of the rubber, defined according to the results of suitable tests on both scragged and unscragged rubber specimens, were also implemented in ABAQUS. Extensive numerical work was performed by considering meshes with different refinements and different element types. The numerical analyses, aimed at investigating the effects of the numerous variables of the problem, allowed for optimizing the type of material model, discretization and elements to be adopted, up to large strains.

For the Japanese NRBs, good agreement between numerical and experimental results was found by ENEL for horizontal stiffness (similar to the results of ENEA for the U.S. HDRBs); however, the agreement for compression tests was again satisfactory only when compressibility was taken into account. This confirmed the importance of volumetric tests on rubber specimens to correctly evaluate bearing vertical stiffness, especially in the case of large shape factors. Analysis of ENEL also confirmed that planar tests on specimens shall be performed to very large deformation, in order to allow for the definition of adequate hyperelastic models of the rubber. Moreover, it was found again that the unscragged rubber model should be used for reproducing bearing behavior to 50%–100% shear strain, while the scragged model should be used for larger deformations. Only slight differences were found between the results of 3D and axisymmetric models to 200%–300% shear strain, while 3D models shall be used for larger deformations.

Similar to the analysis performed for HDRBs and NRBs, also for LRBs, numerical analysis of ENEL was found adequate for horizontal stiffness, to 300% shear strain; however, at larger strains the numerical results showed hardening, contrary to test data. In addition, large discrepancy was found between the numerical results and test data for LRBs under compression with different offset strains: this must be attributed again to modeling rubber as incompressible in constitutive equations. Similar to the NRBs, for LRBs, the need was stressed for an improvement of the analyses, based on more precise data concerning the characterization of materials (natural rubber and lead), including effects of rubber compressibility. In addition, an attempt should be made to consider temperature effects on lead behavior.

In any case, the achieved results confirmed again the conclusions of previous studies that FEMs are useful tools for both the detailed design of elastomeric bearings and their qualification; for the latter, they allow for a considerable reduction of the number of tests to be

performed (e.g. those concerning effects of parameters like temperature, aging, vertical load on horizontal stiffness, initial or arisen defects, etc.).

In order to asses the accuracy of both the FE model meshing and FE solver, a torsional benchmark problem was presented jointly by TARRC and ENEL. Prediction of the couple and axial load acting on the cylinder was obtained by ENEL from FE calculations using ABAQUS, and was compared to the analytical solutions for two types of material models, Mooney-Rivlin and Ogden. An extensive numerical work was performed by considering meshes with different refinements and different element types. The results, presented during the RCM Taormina, showed an excellent agreement.

Finally, ENEL developed a new non-linear simplified isolator model, with exponential constitutive law describing the rubber behavior. The main features of the model were presented at the Hertford RCM in 1998. The model was implemented as a "User Subroutine" in the ABAQUS FE code. The new model, based on three rubber parameters allows for a very accurate evaluation of the response of seismically isolated structures. Although it was developed for elastomeric bearings, the proposed model can be adequately applied to other types of isolation devices having a continuously decreasing stiffness with increasing displacement (e.g. rubber or helical springs coupled with metallic yielding elements, wire rope friction isolators, etc.). Results of the numerical analyses of isolated structures carried out with the new model were presented by ENEL at the Cheju RCM in 1999.

The activities performed within this CRP allowed a better understanding of the analysis methods for seismically isolated structures, by highlighting the most important items to be taken into account and by evaluating limitations and advantages of different approaches. A better knowledge of numerical methods to predict the response of both isolation devices and isolated structures has been achieved.

REFERENCES

Bettinali, F., Forni, M., Indirli, M., Martelli, A., Masoni, P., Pucci, G., Bonacina, G., Serino, G. and G.C. Giuliani, 1991, In-situ dynamic tests of a large seismically isolated building, Proc. 1991 ASME-PVP Conference, San Diego, California, USA, PVP-Vol. 222, H.H. Chung Ed., ASME, New York, pp. 77–89.

Bettinali, F., Dusi, A., Martelli, A. and M. Forni, 1996, "Status of Italian Test Data on Isolated Structures and Comparison with Computer Predictions: Analysis of Isolated Structures", Proceedings, The First Research Coordination Meeting Held in San Petersburg, Russian Federation, 27–31 May 1996," Report IAEA-RC-624 (IWGFR/94), Vienna, Austria.

Clark, P.W., Aiken, I.D., Kelly, J.M., 1996, "Experimental testing of reduced-scale seismic isolation bearing for the Advanced Liquid Metal Reactor", Proceedings, The First Research Coordination Meeting Held in San Petersburg, Russian Federation, 27–31 May 1996," Report IAEA-RC-624 (IWGFR/94), Vienna, Austria.

Dusi, A., Forni, M., and A. Martelli, 1998a, "Contribution of Italy to the Activities on Intercomparison of Analysis Methods for Seismically Isolated Nuclear Structures: Finite Element Analysis of Lead Rubber Bearings," Proceedings, Third Research Co-ordination Meeting of IAEA CRP on "Intercomparison of Analysis Methods for Seismically Isolated Nuclear Structures", Hertford, UK, Report IAEA-RC-624.3 (IWGFR/95), Vienna, Austria, pp. 50–63.

Dusi, A., and V. Rebecchi, 1998b, "Contribution of Italy to the Activities on Intercomparison of Analysis Methods for Seismically Isolated Nuclear Structures: a Parallel Elastic-Plastic

Model for Non-Linear Analysis of Base Isolated Structures," Proceedings, Third Research Co-ordination Meeting of IAEA CRP on "Intercomparison of Analysis Methods for Seismically Isolated Nuclear Structures", Hertford, UK, Report IAEA-RC-624.3 (IWGFR/95), Vienna, Austria, pp. 42–49.

Dusi, A., Bertola, S., Forni, M., La Grotteria M., and Martelli, A., 1998c, "Status of Italian Activities on Intercomparison of Analysis Methods for Seismically Isolated Nuclear Structures," Seismic Isolation, Passive Energy Dissipation and Active Control of Seismic Vibrations of Structures — Proceedings of the International Post-SMiRT Conference Seminar, Taormina, Italy August 25 to 27, 1997, A. Martelli and M. Forni eds., GLIS, Bologna, Italy, pp. 515–534.

Dusi, A. and M. Forni, 1999a, "Status of Italian Activities on Intercomparison of Analysis Methods for Seismically Isolated Nuclear Structures: Lead Rubber Bearings with Larger Plug, Isolated Rigid Mass and Isolated Spent Fuel Pool", Seismic Isolation, Passive Energy Dissipation and Active Control of Seismic Vibrations of Structures — Proceedings of the International Post-SMiRT Conference Seminar, Cheju, Korea, August 23–27, 1999, (to be published).

Dusi, A. and V. Rebecchi, 1999b, "A Simplified Model for Nonlinear Analysis of Base Isolated Structures: Model Description and Validation", Seismic Isolation, Passive Energy Dissipation and Active Control of Seismic Vibrations of Structures — Proceedings of the International Post-SMiRT Conference Seminar, Cheju, Korea, August 23–27, 1999, (to be published).

ENEA, 1995, "Proposed CRP of IAEA on Intercomparison of Analysis Methods for Seismically Isolated Nuclear Structures," A. Rinejski ed., IAEA, Vienna, Austria.

ENEL, ALGA, DYWIDAG, ENEA, MRPRA, SHW, and STIN, 1993, "Optimisation of Design and Performance of High Damping Rubber Bearings for Seismic and Vibration Isolation," EC Contract BR2-CT93-0524, Project BE7010, Bruxelles, Belgium.

Forni, M., Martelli, A., Grassi, L., Sobrero, E., Vestroni, F., Bettinali, F., Bonacina, G., and E. Pizzigalli, 1993, Analysis of in-situ forced vibration tests of twin isolated and non-isolated buildings, Proc. of the 1993 ASME-PVP Conference, Denver, Colorado, USA, PVP-Vol. 256–2, Y.K. Tang Ed., ASME, New York, pp. 217–229.

Forni, M., A. Martelli, Bettinali, F., and Dusi, A., 1995, "Finite element models of rubber bearings and guidelines development for isolated nuclear facilities in Italy," Seismic Isolation, Passive Energy Dissipation and Active Control of Seismic Vibrations of Structures — Proceedings of the International Post-SMiRT Conference Seminar, Santiago, Chile, August 21 to 23, 1995, Universitad de Chile ed., pp. 310–336.

Forni, M., Martelli, A., Dusi, A. and F. Bettinali, 1996, "Status of Italian Test Data on Seismic Isolators and Comparison with Computer Predictions: Analysis of HDRBs", Proceedings, The First Research Coordination Meeting Held in San Petersburg, Russian Federation, 27–31 May 1996," Report IAEA-RC-624 (IWGFR/94), Vienna, Austria.

Forni, M., Martelli, A. and A. Dusi, 1998, "Contribution of Italy to the Activities on Intercomparison of Analysis Methods for Seismically Isolated Nuclear Structures: Shake Table Tests on a Steel Frame Structure Mock-up", Proceedings, Third Research Co-ordination Meeting of IAEA CRP on "Intercomparison of Analysis Methods for Seismically Isolated Nuclear Structures", Hertford, UK, Report IAEA-RC-624.3 (IWGFR/95), Vienna, Austria, pp. 64–100.

Fuller, K.N.G., Gough, J., Ahmadi, H. R., and A. Dusi, 1998, "Contribution to United Kingdom to the Activities on Intercomparison of Analysis Methods for Seismically Isolated Nuclear Structures," Seismic Isolation, Passive Energy Dissipation and Active Control of Seismic Vibrations of Structures — Proceedings of the International Post-SMiRT Conference Seminar, Taormina, Italy August 25 to 27, 1997, A. Martelli and M. Forni eds., GLIS, Bologna, Italy, pp. 559–579.

Giuliani, G. C., 1989, Design experience on seismically isolated building, Proc. First Int. Seminar on Seismic Base Isolation for Nuclear Power Facilities, San Francisco, California, USA.

GLIS, 1998, “Seismic Isolation, Passive Energy Dissipation and Active Control of Seismic Vibrations of Structures — Proceedings of the International Post-SMiRT Conference Seminar, Taormina, Italy, August 25 to 27, 1997,” A. Martelli and M. Forni eds., Bologna, Italy.

Hirata, K., 1996, "Test Data on Natural Rubber Bearings", Proceedings, The First Research Coordination Meeting Held in San Petersburg, Russian Federation, 27–31 May 1996," Report IAEA-RC-624 (IWGFR/94), Vienna, Austria.

Hirata, K., Matsuda, A., and Yabana, S., 1998, "Contribution of Japan to the Activities on Intercomparison of Analysis Methods for Seismically Isolated Nuclear Structures," Seismic Isolation, Passive Energy Dissipation and Active Control of Seismic Vibrations of Structures — Proceedings of the International Post-SMiRT Conference Seminar, Taormina, Italy August 25 to 27, 1997, A. Martelli and M. Forni eds., GLIS, Bologna, Italy, pp. 461–483.

IAEA, 1997, "Intercomparison of Analysis Methods for Seismically Isolated Nuclear Structures — Part 1: Advanced Test Data and Numerical Methods — The First Research Coordination Meeting Held in San Petersburg, Russian Federation, 27–31 May 1996," Report IAEA-RC-624 / IWGFR/94, Vienna, Austria.

IAEA, 1998a, "Second Research Co-ordination Meeting of the IAEA Research Co-ordination Programme on Intercomparison of Analysis Methods for Seismically Isolated Nuclear Structures held in Taormina, Italy, 25–29 August, 1997," IAEA Summary Report, Vienna, Austria.

IAEA, 1998b, "Intercomparison of Analysis Methods for Seismically Isolated Nuclear Structures — Papers and Working Material Presented at The Third Research Coordination Meeting Held in Hertford, 25–29 May 1998," IAEA-RC-624.3 / IWGFR/95 Rep., Vienna, Austria.

IAEA, 1999, "Fourth Research Co-ordination Meeting of the IAEA Research Co-ordination Programme on Intercomparison of Analysis Methods for Seismically Isolated Nuclear Structures held in Cheju, Korea, 22–27 August, 1999," IAEA Summary Report, Vienna, Austria.

Martelli, A. and M. Forni, 1996, "Scope and Status of Contribution of Italy"**,** Proceedings, The First Research Coordination Meeting Held in San Petersburg, Russian Federation, 27–31 May 1996," Report IAEA-RC-624 (IWGFR/94), Vienna, Austria.

Selvaraj, T., Ravi, R., Chellapandi, P., Chetal, S.C. and Bhoje, S.B., 1998, "Contribution of India to the Intercomparison of Analysis Methods for Seismically Isolated Nuclear Structures)", Seismic Isolation, Passive Energy Dissipation and Active Control of Seismic Vibrations of Structures — Proceedings of the International Post-SMiRT Conference

Seminar, Taormina, Italy August 25 to 27, 1997, A. Martelli and M. Forni eds., GLIS, Bologna, Italy, pp. 597-613.

Yoo, B., Lee, J.H., Koo, G.H., 1998a, "Intercomparison of Analysis Methods for Seismically Isolated Nuclear Structures: Kaeri HDRB and CRIEPI Isolated Rigid Mass Mock-up)", Proceedings, Third Research Co-ordination Meeting of IAEA CRP on “Intercomparison of Analysis Methods for Seismically Isolated Nuclear Structures", Hertford, UK, Report IAEA-RC-624.3 (IWGFR/95), Vienna, Austria.

Yoo, B., Lee, J.H., 1998b, "Intercomparison of Analysis Methods for Seismically Isolated Nuclear Structures: ENEA HDRBs and CRIEPI LRBs)", Seismic Isolation, Passive Energy Dissipation and Active Control of Seismic Vibrations of Structures — Proceedings of the International Post-SMiRT Conference Seminar, Taormina, Italy August 25 to 27, 1997, A. Martelli and M. Forni eds., GLIS, Bologna, Italy, pp. 549–558.

NUMERICAL SIMULATIONS OF RUBBER BEARING TESTS AND SHAKING TABLE TESTS

K. HIRATA, A. MATSUDA, S. YABANA
Central Research Institute of Electric Power Industry, Japan

Abstract

Test data concerning rubber bearing tests and shaking table tests of base-isolated model conducted by CRIEPI are provided to the participants of Coordinated Research Program (CRP) on "Intercomparison of Analysis Methods for predicting the behaviour of Seismically Isolated Nuclear Structure", which is organized by International Atomic Energy Agency (IAEA), for the comparison study of numerical simulation of base-isolated structure. In this paper outlines of the test data provided and the numerical simulations of bearing tests and shaking table tests are described. Using computer code ABAQUS, numerical simulations of rubber bearing tests are conducted for NRBs, LRBs (data provided by CRIEPI) and for HDRs (data provided by ENEA/ENEL and KAERI). Several strain energy functions are specified according to the rubber material test corresponding to each rubber bearing. As for lead plug material in LRB, mechanical characteristics are reevaluated and are made use of. Simulation results for these rubber bearings show satisfactory agreement with the test results. Shaking table test conducted by CRIEPI is of a base isolated rigid mass supported by LRB. Acceleration time histories, displacement time histories of the isolators as well as cyclic loading test data of the LRB used for the shaking table test are provided to the participants of the CRP. Simulations of shaking table tests are conducted for this rigid mass, and also for the steel frame model which is conducted by ENEL/ENEA. In the simulation of the rigid mass model test, where LRBs are used, isolators are modeled either by bilinear model or polylinear model. In both cases of modeling of isolators, simulation results show good agreement with the test results. In the case of the steel frame model, where HDRs are used as isolators, bilinear model and polylinear model are also used for modeling isolators. The response of the model is simulated comparatively well in the low frequency range of the floor response, however, in the high frequency range discrepancies from the test result becomes larger, implying the requirement of more detailed or proper modeling of the rubber bearing and the steel frame.

1. INTRODUCTION

In Japan, the demonstration test for FBR base isolation system has been carried out in the past decade by several organizations In particular, CRIEPI (Central Research Institute of Electric Power Industry) has played a leading role in this project and conducted various isolator tests, shaking table tests, and the design guidelines for FBR base isolation system are prepared by CRIEPI. CRIEPI, as a participant of Coordinated Research Program (CRP) on Intercomparison of Analysis Methods for Seismically Isolated Nuclear Structure organized by International Atomic Energy Agency (IAEA), provided rubber bearing test data and shaking table test data to the participants of the CRP. The CRP started in 1996 and continued until 1999. In this CRP the test data have been used for the intercomparison of the simulation, and the results of the numerical simulations that CRP participants have conducted are reported and the related information have been exchanged at the RCM (Research Coordination Meeting) of this CRP.

2. RUBBER BEARING TESTS CONDUCTED IN CRIEPI

2.1. Testing facilities

Static two-dimensional loading test machine designed and manufactured especially for testing isolation element was used (Fig. 1). The machine is composed of two actuators giving axial and shear force to test specimens, and the actuators are controlled under load control mode and/or displacement control mode. Maximum available load of each actuator is 600 tons. Maximum shear displacement available is ± 600 mm (bi-directional mode) or 1200 mm (unidirectional mode), and maximum axial displacement available is ± 350 mm (bi-directional mode) or 700 mm (unidirectional mode). By using this machine full-scale rubber bearing tests and scale model tests have been conducted. Even using this test machine it is impossible to give rubber bearings large deformation to cause rupture, and scale-models of rubber bearing are used for the break test.

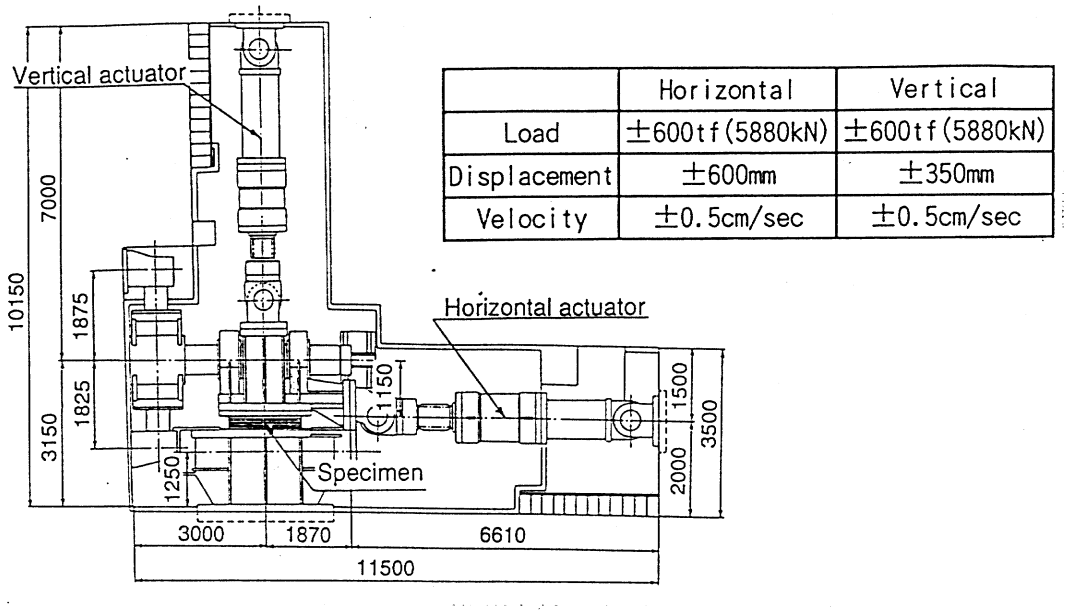

	Horizontal	Vertical
Load	±600tf(5880kN)	±600tf(5880kN)
Displacement	±600mm	±350mm
Velocity	±0.5cm/sec	±0.5cm/sec

Fig. 1 Schematic view of static test machine

2.2. Specifications and geometrical data of NRB

Full-scale NRB presumed to be used for the FBR building is 1600 mm in diameter and its design vertical load is 500–1000 tons. Test data for the scale models of NRB (Scale: 1/1.58 and 1/3.168) [8][12][13] are used for the comparative study between the experiment and the numerical simulation.

Specifications and geometrical data of the scale models of the NRB are as follows.

(1) 200 ton NRB
[Specifications]
- Design vertical load: 200 tons (1/1.58 scale model of prototype 500 tons bearing)

- Design vertical stress: 25 kgf/cm^2
- Horizontal frequency fh of Prototype: 0.5 Hz (Th = 2 sec)
- Vertical frequency fv of Prototype: > 20 Hz
- Shear modulus G 6 kgf/cm^2

[Geometrical data]
- Thickness of rubber sheet: 5.7 mm
- Number of rubber layers: 25
- Thickness of rubber layers: 142.5 mm (5.7 mm × 25)
- Thickness of steel plate: 3.1 mm
- Number of steel plates: 24
- Diameter of rubber D: 1012 mm
- Inner diameter of rubber D_i: 126 mm
- Primary shape factor Sc1: 38.9

(2) 50 ton NRB
[Specifications]
- Design vertical load: 50 tons (1/3.168 scale model of prototype 500 tons bearing)
- Design vertical stress: 25 kgf/cm^2
- Horizontal frequency fh of Prototype: 0.5 Hz (Th = 2sec)
- Vertical frequency fv of Prototype: > 20 Hz
- Shear modulus G 6 kgf/cm^2

[Geometrical data]
- Thickness of rubber sheet: 2.8 mm
- Number of rubber layers: 25
- Total thickness of rubber layers: 70 mm (2.8 mm × 25)
- Thickness of steel plate: 1.6 mm
- Number of steel plates: 24
- Diameter of rubber D: 506 mm
- Inner diameter of rubber D_i 63 mm
- Primary shape factor Sc1: 38.9

2.3. Specifications and geometrical data of LRB with thin lead plug

Full-scale LRB presumed to be used for the FBR building is 1600 mm in diameter and its design vertical load is 500–1000 tons. Test data on the scale model of LRB (Scale: 1/1.83 and 1/3.16) [8][12][13] are used for the comparative study between the experiment and the numerical simulation.

Specifications and geometrical data of the scale models of the LRB are as follows.

(1) 150 ton LRB
[Specifications]

- Design vertical load: 150 tons (1/1.83 scale model of prototype 500 tons bearing)
- Design vertical stress: 25 kgf/cm^2
- Horizontal frequency fh of Prototype: 0.5 Hz (Th = 2 sec)
- Vertical frequency fv of Prototype: > 20 Hz
- Shear modulus G 6 kgf/cm^2

[Geometrical data]
- Thickness of rubber sheet: 4.9 mm
- Number of rubber layers: 25
- Total thickness of rubber layers: 122.5 mm (4.9 mm × 25)
- Thickness of steel plate: 3.1 mm
- Number of steel plates: 24
- Diameter of rubber D: 876 mm
- Inner diameter of rubber D_i: 98 mm
- Diameter of lead plug 98 mm
- Height of lead plug > 196.9 mm
- Primary shape factor Sc1: 39.4

(2) 50 ton LRB
[Specifications]
- Design vertical load: 50 tons (1/3.16 scale model of prototype 500 tons bearing)
- Design vertical stress: 25 kgf/cm^2
- Horizontal frequency fh of Prototype: 0.5 Hz (Th = 2sec)
- Vertical frequency fv of Prototype: > 20 Hz
- Shear modulus G 6 kgf/cm^2

[Geometrical data]
- Thickness of rubber sheet: 2.8 mm
- Number of rubber layers: 25
- Total thickness of rubber layers: 70 mm (2.8 mm × 25)
- Thickness of steel plate: 1.6 mm
- Number of steel plates: 24
- Diameter of rubber D: 506 mm
- Inner diameter of rubber D_i: 57 mm
- Diameter of lead plug 57 mm
- Height of lead plug > 108.4 mm
- Primary shape factor Sc1: 39.4

2.4. Specifications and geometrical data of LRB with thick lead plug

LRB described in the subsection 2.3 has comparatively thin lead plug. Diameter ratio of the lead plug to the rubber is 1:8.9 (= 98 mm: 876 mm) and there arises a question that the accuracy of the simulation on lead plug part may not influence the simulated

force-displacement relationship of LRB as a whole. For this reason test data of LRB with thick lead plug was provided by JAERI/CRIEPI, in which the diameter ratio of lead plug to rubber is 1:4, for additional case of numerical simulation.

Specifications and geometrical data of the scale models of these LRB are as follows.

(1) ϕ500-LRB

[Specifications]

- Design vertical load:	181.25 tons (500/1200 scale model of prototype 1044 tons bearing)
- Design vertical stress:	100 kgf/cm^2
- Horizontal frequency fh of Prototype:	0.25 Hz (Th = 4 sec)
- Vertical frequency fv of Prototype:	10 Hz

[Geometrical data]

- Thickness of rubber sheet:	3.6 mm
- Number of rubber layers:	23
- Total thickness of rubber layers:	82.8 mm (3.6 mm $\times$ 23)
- Thickness of steel plate:	2.5 mm
- Number of steel plates:	22
- Diameter of rubber D:	500 mm
- Inner diameter of rubber D_i:	125 mm
- Diameter of lead plug	125 mm
- Height of lead plug	152.8mm
- Primary shape factor Sc1:	32.6

(2) ϕ280-LRB

[Specifications]

- Design vertical load:	56.84 tons (280/1200 scale model of prototype 1044 tons bearing)
- Design vertical stress:	100 kgf/cm^2
- Horizontal frequency fh of Prototype:	0.25 Hz (Th = 4 sec)
- Vertical frequency fv of Prototype:	10 Hz

[Geometrical data]

- Thickness of rubber sheet:	2.0 mm
- Number of rubber layers:	23
- Total thickness of rubber layers:	46 mm (2.0 mm $\times$ 23)
- Thickness of steel plate:	2.5 mm
- Number of steel plates:	22
- Diameter of rubber D:	280 mm
- Inner diameter of rubber D_i:	70 mm
- Diameter of lead plug	70 mm
- Height of lead plug	93.6 mm
- Primary shape factor Sc1:	32.6

In this case, NRB with the same rubber material and geometrical shape of laminated rubber part as the above-described LRB was tested to investigate the effect of the lead plug. As is shown in the subsequent section this result was used to "extract" mechanical characteristics of lead plug from the test result of LRB.

2.5. Test methods and results

Three kinds of rubber bearing tests, i.e. horizontal cyclic loading test, vertical cyclic loading test and failure test were conducted [12][13].

Horizontal cyclic loading tests were conducted to evaluate horizontal stiffness and damping of the rubber bearing. These tests are performed giving shear loading of low frequency (under 0.01 Hz) with axial loading. Four cycles of sinusoidal shear deformation are applied to rubber bearings under constant vertical load. For the evaluation of the stiffness and the damping of the rubber bearing, loading test data of the third cycle is usually used. Amplitude of shear deformation is varied from ± 25 to ± 400% of shear strain of the rubber.

Vertical cyclic loading tests were conducted to evaluate vertical stiffness and damping of the rubber bearing. These tests are conducted giving vertical loading of low frequency in the same way as the horizontal cyclic loading test. In this test also four cycles of sinusoidal vertical loading is applied after giving initial static vertical load and constant shear strain (offset shear strain). Amplitude of the applied sinusoidal vertical loading is up to 200% of the design vertical load.

Failure tests are conducted to evaluate ultimate capacity of the rubber bearings and their mechanical characteristics in the ultimate state. Test data provided to the participants of the CRP are concerning shear failure tests in which under constant vertical load shear deformation is given to the rubber bearing until failure occurs. In the shear failure tests, four cycles of static sinusoidal shear load is first applied up to 400% of shear strain under design vertical loading, then horizontal deformation is given monotonically until the failure of rubber bearing occurs.

3. SIMILATION OF THE BEARING TESTS

3.1. Material properties

3.1.1. Properties of natural rubber material

In the simulation of shear loading tests of NRB and LRB which were conducted in CRIEPI, following strain energy functions for deviatoric components proposed by Seki [16] are used.

$$W = \sum_{i=1}^{2}[a_i(I_i - 3) + \frac{b_i}{2}(I_i - 3)^2 + \frac{c_i}{3}(I_i - 3)^3 + \frac{d_i}{e_i}\exp(e_i(I_i - 3))] \quad (1)$$

where W is the strain energy function, I_1 and I_2 are invariants expressed by stretches principal λ_1, λ_2, λ_3 as,

$$I_1 = \lambda_1^2 + \lambda_2^2 + \lambda_3^2 \quad I_2 = \lambda_1^2\lambda_2^2 + \lambda_2^2\lambda_3^2 + \lambda_3^2\lambda_1^2 \qquad (2)$$

and coefficients a_i, b_i, d_i, c_i and e_i are obtained from biaxial tensile test of the rubber sheet as [16],

$a_1 = 2.09$, $b_1 = 1.35\times 10^{-1}$, $c_1 = 2.4\times 10^{-3}$, $d_1 = 1.75$, $e_1 = -2.12$, $a_2 = 0.138$, $b_2 = -1.64\times 10^{-2}$, $c_2 = 6.44\times 10^{-4}$, $d_2 = -0.7$, $e_2 = -6.44$ (unit: kgf/cm^2)

For volumetric component, following strain energy function is used.

$$U = \sum_{i=1}^{4} \frac{1}{D_i}(J^{el} - 1)^{2i} \quad (3)$$

where J^{el} is the elastic volume ratio and the coefficients D_i are obtained from the volumetric compression test as [11],

$D_1 = 3.366\times 10^{-4}$, $D_2 = 3.297\times 10^{-8}$, $D_3 = -8.709\times 10^{-12}$, $D_4 = 7.295\times 10^{-15}$ (unit: kgf/cm^2)

3.1.2. Properties of high damping rubber material (1)

In the simulation of shear loading test of HDR conducted in Italy following strain energy function of polynomial form [6] is used, and the coefficients were determined from the material test data provided from Italy. The function is given as,

$$U = \sum_{i+j=1}^{2} C_{ij}(\bar{I}_1 - 1)^i(\bar{I}_2 - 1)^j + \sum_{i=1}^{2} \frac{1}{D_i}(J^{el} - 1)^{2i} \quad (4)$$

where $\bar{I}_1$ *and* $\bar{I}_2$ are the first and the second deviatoric strain invariants. Coefficients C_{ij} and D_i are determined from the tensile test data of the rubber sheet and the volumetric test data of the rubber, which were provided from Italy.

3.1.3. Properties of high damping rubber material (2)

In the simulation of the shear loading test of HDR conducted in Korea strain energy function of polynomial form expressed by Eq. (4) and Ogden's formulation given below are used. In both formulations, coefficients were determined from the material test data provided from Korea.

$$U = \sum_{i=1}^{6} C_{ij} \frac{2\mu_i}{\alpha_i^2}(\bar{\lambda}_1^{\alpha i} + \bar{\lambda}_2^{\alpha i} + \bar{\lambda}_3^{\alpha i} - 3) + \sum_{i=1}^{6} \frac{1}{D_i}(J^{el} - 1)^{2i} \quad (5)$$

3.1.4. Properties of lead

Mechanical properties of the lead used in LRB were determined by two ways. In the first way, material properties was determined from the test results of uniaxial tensile test of the lead specimen as [7],

- Young's modulus E = 1750 kgf/mm^2
- Poisson's ratio $\nu = 0.44$
- Yield stress = 0.2 kgf /mm^2

After yielding, stress-strain relationship of the lead used is expressed as [7]

$$\sigma_t = 4.0(1 + 0.096 \log_{10} \varepsilon_t)\varepsilon_t^{0.31} \quad (6)$$

where c_t and ε_t are the tensile true stress and true strain of lead respectively, and ε_t is the true strain rate of the lead. And isotropic hardening rule is applied.

In the second way, the test results of LRB with thick lead plug and NRB are used, where force-displacement relationship of the NRB is subtracted from that of the LRB and the stress-strain relationship of the lead plug is evaluated considering that the lead plug is subjected to pure shear deformation [5] (Fig. 2). In this case, the lead is modeled as an elasto-plastic material with the following characteristics;

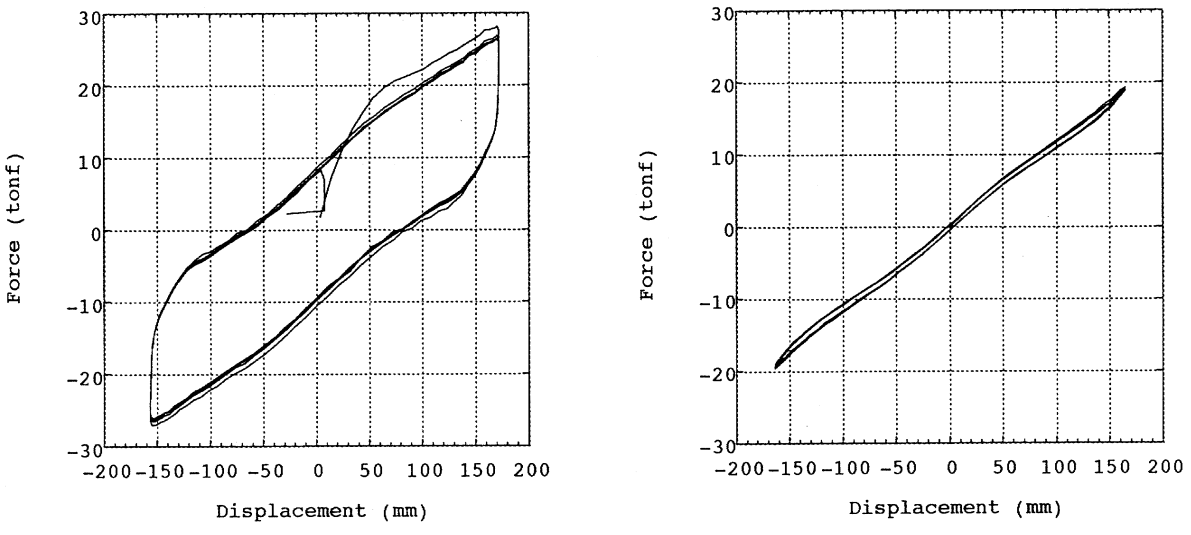

(a) Hysteresis loop of LRB

(b) Hysteresis loop of NRB

Fig. 2 Hysteresis loop of lead plug extracted from LRB and NRB tests

- Young's modulus E_0 = 1166.6 kgf/cm^2
- Poisson's ratio $\nu = 0.44$

and the stress-strain (logarithmic strain) relationship is given as multi-linear expression (Fig. 3).

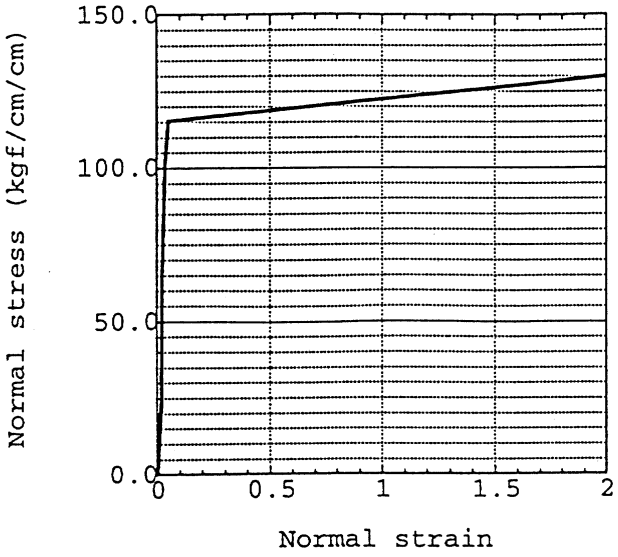

Fig. 3 Stress-strain relationship of lead

3.1.5. Properties of steel

Material properties of the steel for the steel shim plate are as follows.

- Young's modulus E = 1.97 × 10^4 kgf/mm^2
- Poisson's ratio = 0.271
- Yield stress c_y = 25.5 kgf/mm^2

As for hardening rule, isotropic hardening is assumed. However, in the simulation of the rubber bearings yielding of the steel shim plate did not to occur.

3.2. Computer code and computational conditions

Bearing test data on NRB and LRB provided by CRIEPI and test data on HDR provided by ENEA were used for the comparison between the experiment and the numerical simulation. Numerical simulation was conducted using computer code ABAQUS [6]. For the rubber and the lead plug 8-node linear brick, hybrid, constant pressure element C3D8H (ABAQUS/Standard User's Manual, 1996)is used, and C3D8I element is used for the steel shim plate. In the simulation of LRB continuity between the lead plug and other part of the

bearing is assumed (i.e. no sliding is allowed). Half section model of the rubber bearings was used and divided into 6 elements in radial direction and 8 elements in circumferential direction. Lead plug of LRB is divided into 2 elements in radial direction and 8 elements in circumferential direction. Each rubber layer and steel shim plate is divided respectively into 3 and 2 layers (Fig. 4).

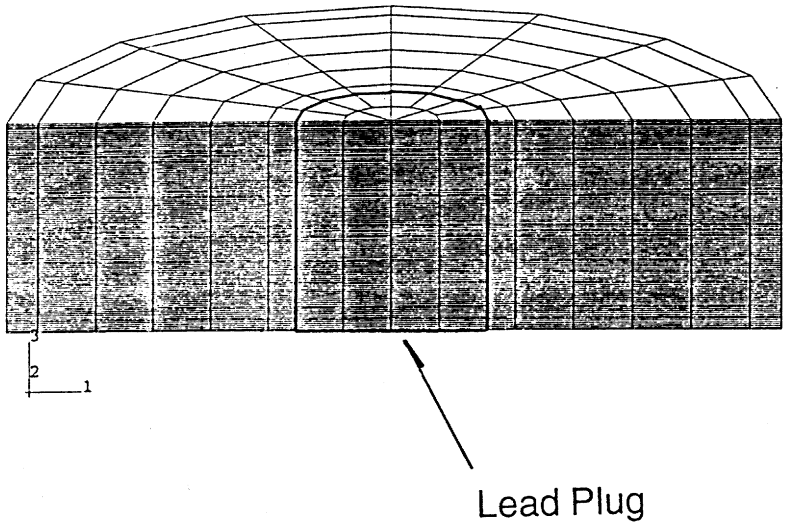

Fig. 4 Finite element mesh of HDR with thick lead plug

3.3. Results of numerical simulation

3.3.1. Simulation of NRB test

Numerical simulations were conducted for the bearings of different scale with similar geometrical shape, i.e. “200 ton NRB” and “50 ton NRB”. The bearing tests are; shear loading test under design compressive load and compressive loading test with 0% shear strain of rubber bearing. Comparisons of numerical simulations and the test results are shown in Figs. 5 through 8. In the case of the shear deformation tests simulated results show good agreement with the initial loading curve of the test results up to the shear deformation of about 600 mm for 200 ton NRB and 260 mm for 50 ton NRB (or 400% of shear strain).

As for the compressive loading test, simulated results show good agreement with the experimental results.

3.3.2. Simulation of LRB test

Numerical simulations were conducted for the tests of two types of LRB conducted in CRIEPI. One type is the LRB with slender lead plug, “150 ton LRB” and “50 ton LRB” with similar geometrical shape. Another type is the LRB with thick lead plug. The bearing tests are; shear loading test under design compressive load and compressive loading test with 0% shear strain of rubber bearing (for LRB with slender lead plug).

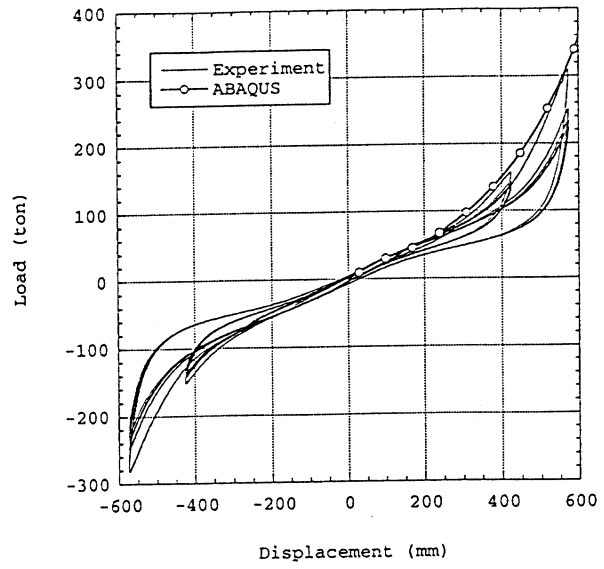

Fig. 5 Experiment and simulation of horizontal loading ('200 ton NRB' under vertical load of 200tons)

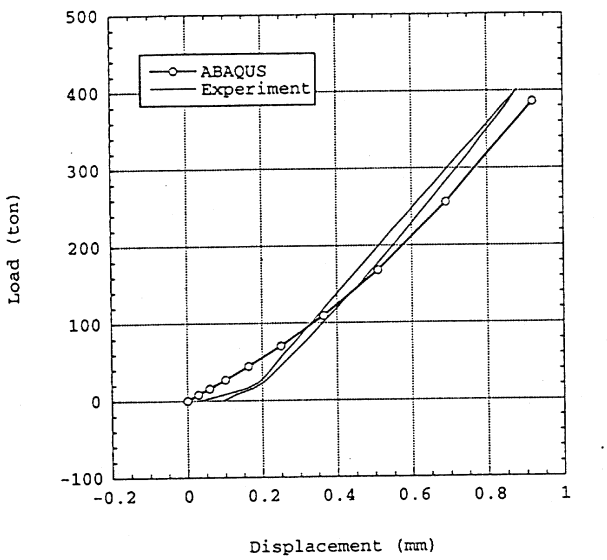

Fig. 6 Experiment and simulation of vertical loading ('200 ton NRB' with 0% offset shear strain)

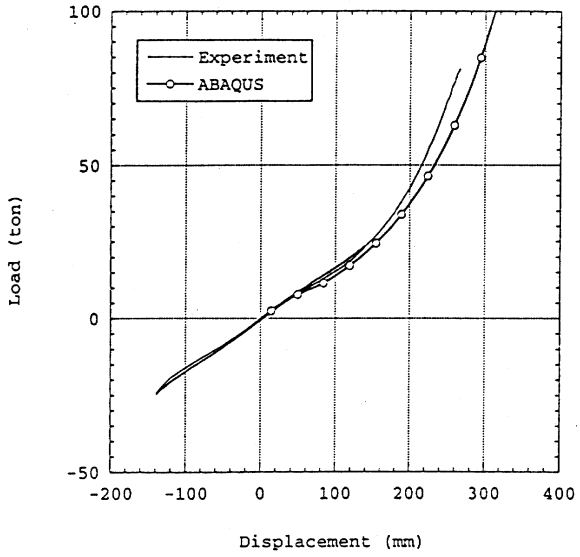

Fig. 7 Experiment and simulation of horizontal loading ('50 ton NRB' under vertical load of 50 tons)

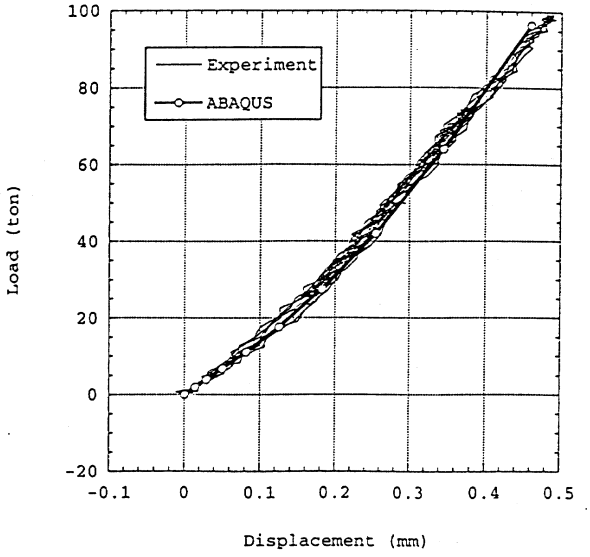

Fig. 8 Experiment and simulation of vertical loading ('50 ton NRB' with 0% offset shear strain)

At first, numerical simulation was conducted using mechanical characteristics of lead given by Eq. (6). For the LRB with thin lead plug (diameter ratio of lead to rubber = 1:8.9), numerical simulations show good agreement with test results for both shear loading and vertical loading tests (Figs. 9 through 12). However, for the LRB with thick lead plug numerical simulation did not agree well with the test result. Using mechanical characteristics of the lead shown in Fig. 3, numerical simulation was conducted, proving that the numerical simulation showed good agreement with the test results (Fig. 13). In Fig. 13 “old” and “new”

mean simulation with lead properties given by Eq. (6) and Fig. 3 respectively. Using this lead characteristic, simulation of LRB with slender lead plug was also conducted. The result shows that this mechanical characteristic is also valid for the LRB of different geometrical shape (Fig. 14; "old" and "new" are used in the same sense as in Fig. 13) and can be regarded as a general one for the lead plug under pure shear deformation.

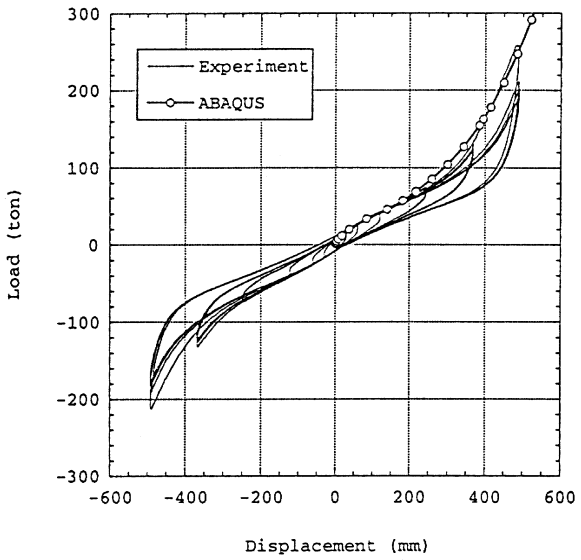

Fig. 9 Experiment and simulation of horizontal loading ('150 ton LRB' under vertical load of 150 tons)

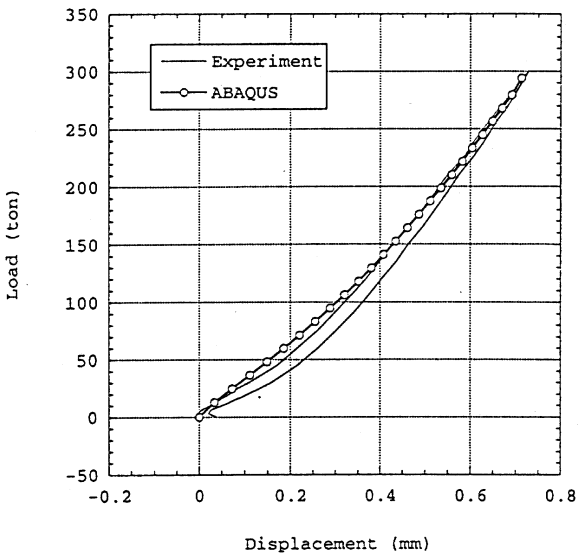

Fig. 10 Experiment and simulation of vertical loading ('150 ton LRB' with 0% offset shear strain)

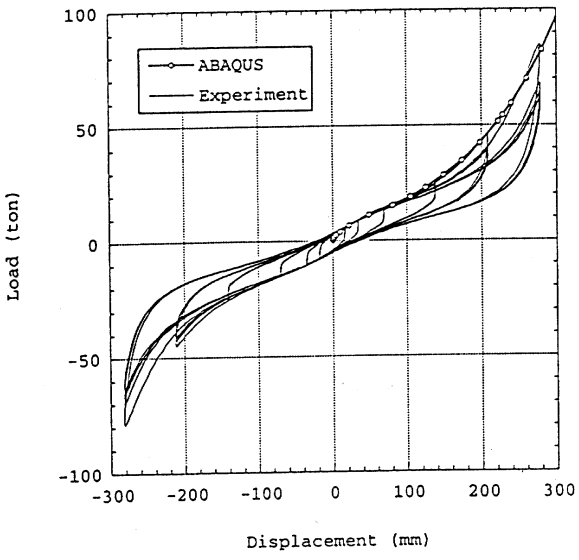

Fig. 11 Experiment and simulation of horizontal loading ('50 ton LRB' under vertical load of 50tons)

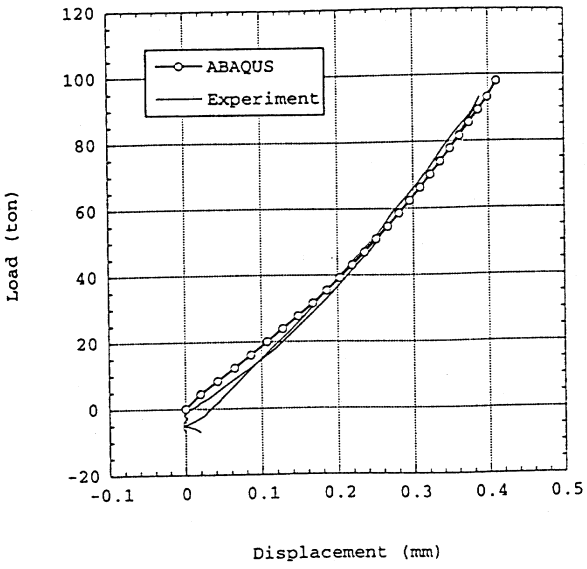

Fig. 12 Experiment and simulation of vertical loading ('50 ton LRB' with 0% offset shear strain)

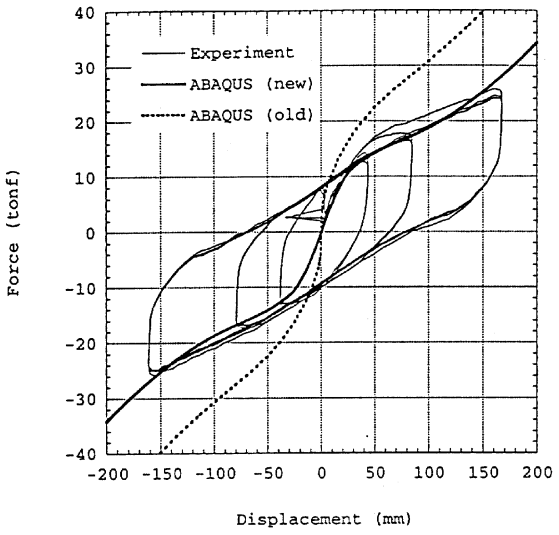

Fig. 13 Force - displacement relationship of LRB with thick lead plug (Test and Simulation)

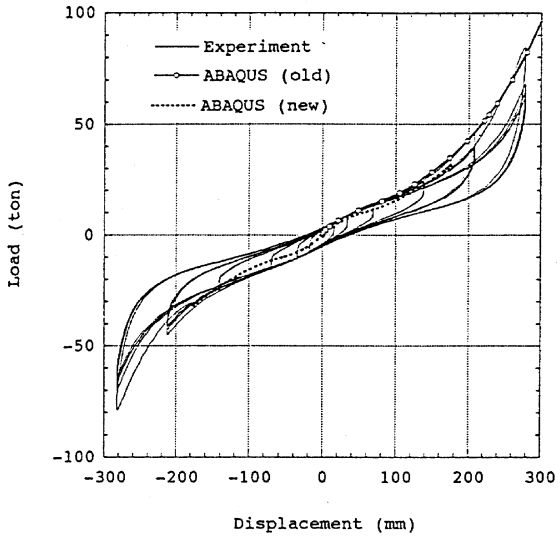

Fig. 14 Experiment and simulation of horizontal loading ('50 ton LRB' under vertical load of 50tons)

3.3.3. Simulation of HDR test

Numerical simulations were conducted for the bearing test conducted in Italy and Korea. Figs. 15 and 16 show the results of the simulation for the shear loading test of HDR conducted by ENEL/ENEA [1][2]. In these cases simulated results agree well with the test results up to about 50 mm of shear deformation (or about 160% of shear strain of rubber or higher). Fig. 17 shows the result of the simulation for the compressive loading test of HDR. In this case both simulated and test results show good agreement, particularly, nonlinear relationship between force and displacement is simulated satisfactorily.

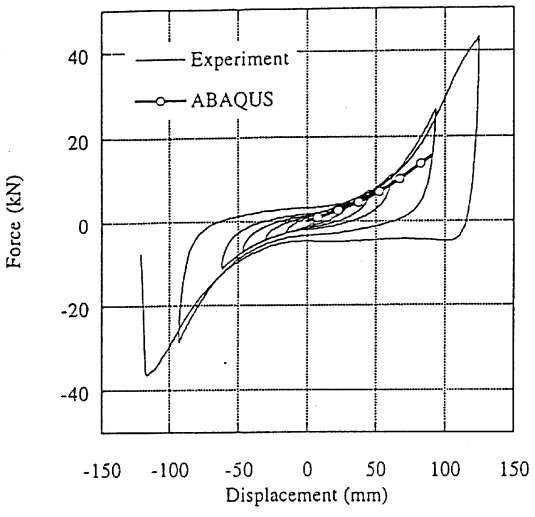

Fig. 15 Experiment and simulation of shear loading (HDR data from Italy, Compressive load: 50kN)

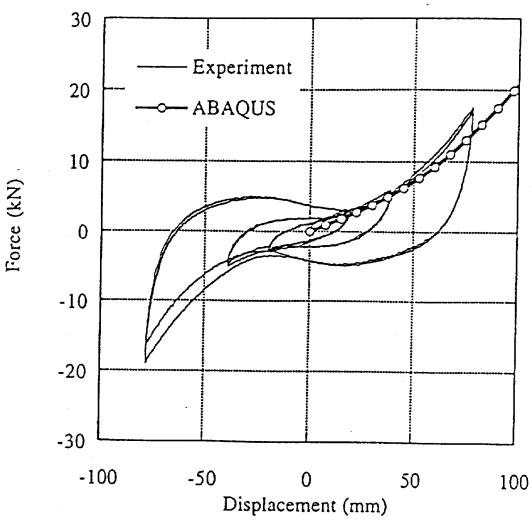

Fig. 16 Experiment and simulation of shear loading (HDR data from Italy, Compressive load: 100kN)

Figs. 18 and 19 show results of shear loading test of HDR provided by KAERI, results of cyclic loading test and failure test under monotonical loading [18]. Numerical simulations were conducted using two types of strain energy function; polynomial formulation given by Eq. (4) and Ogden's formulation given by Eq. (5). For the cyclic loading tests, numerical simulation using strain energy function of polynomial formulation seems to give better agreement with the test. However, for the failure test, where displacement is larger than the cyclic loading test, simulation using Ogden's formulation gives better results.

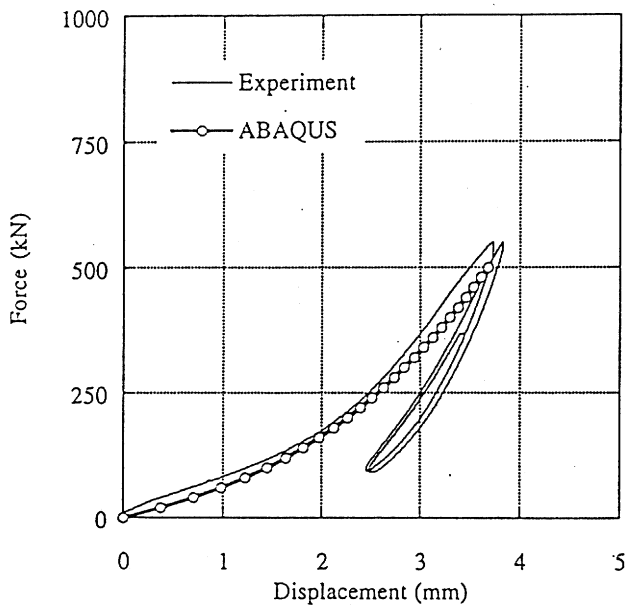

Fig. 17 Experiment and simulation of vertical loading
(HDR data from Italy, Offset shear strain 0%)

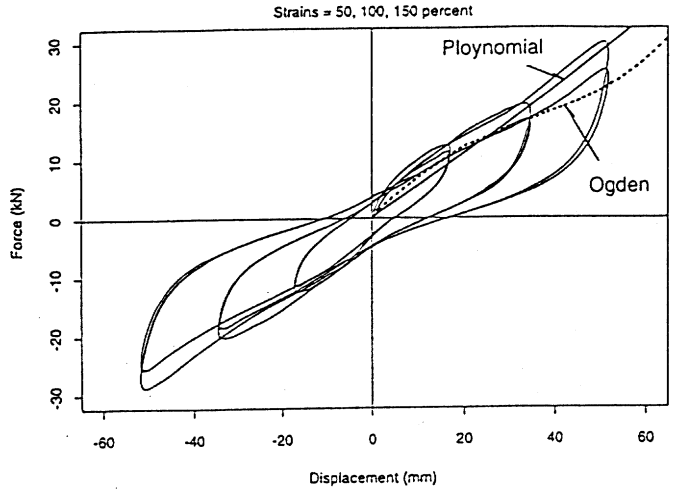

Fig. 18 Experiment and simulation of shear loading
(HDR data from Korea)

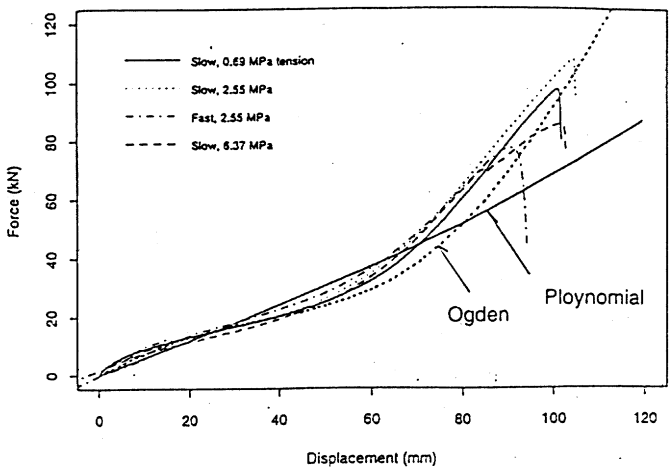

Fig. 19 Experiment and simulation of failure test
(HDR data from Korea)

4. SHAKING TABLE TESTS CONDUCTED BY CRIEPI

4.1. Outline of the test

Shaking table test of a scale model of rigid isolated structure was conducted by CRIEPI [9][14]. The main purpose of the test is to investigate dynamic behavior of isolated structure and the rubber bearings under extremely strong earthquake. Increasing the input acceleration level, response characteristics of the base-isolated model up to the vicinity of the ultimate state of the rubber bearings was investigated. The model is a rigid mass of 17.8 ton weight supported by 8 LRBs (Fig. 20). Similitude applied to the shaking table test is determined considering following points.

- Stress of the model bearings be equal to that of the prototype
- Amplitude of input acceleration to the model structure be equal to that of the prototype
- Geometrical shape of the model bearing be similar to that of the prototype with the scale of 1/15.

LRBs used in the test are geometrically 1/15 reduced scale of prototype bearing supporting vertical load of 2.25 tons each. Rubber bearing tests of the bearings were performed before the shaking table test and the test results are shown in Fig. 21.

In Japan two levels of design earthquake motion S1 and S2 are used in the seismic design of nuclear power plant. In the shaking table test, input earthquake motion S1 consistent with the tentative design spectrum proposed for the base-isolated nuclear power plant was used basically. In this case amplitude of the input earthquake motion S2 is 1.5 times as large as that of S1 (i.e. S2 = 1.5× S1). For the purpose of the comparison between the test and the simulation, test results for the input motion of design earthquake motion S2 (=1.5×S1) and the those for the input motion three times as large as the design earthquake motion (3×S2) are provided to the participants of the CRP.

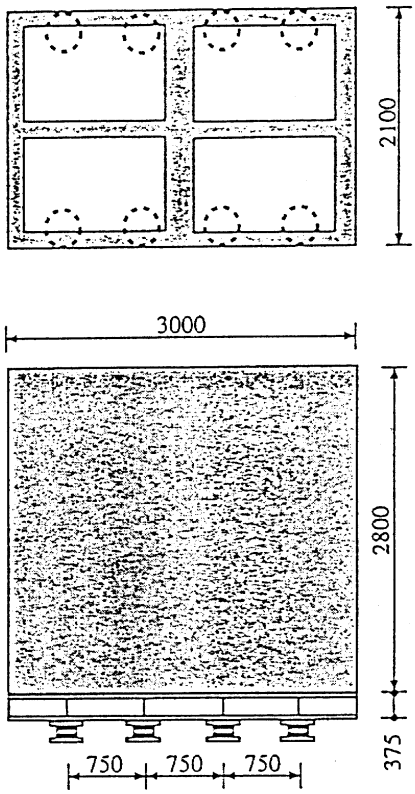

Fig. 20 Schematic view of base-isolated rigid mass

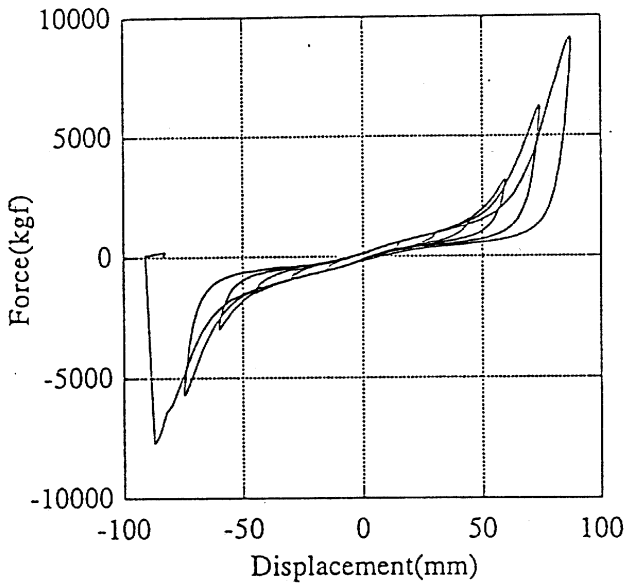

Fig. 21 Shear loading test of LRB used for base-isolated rigid mass

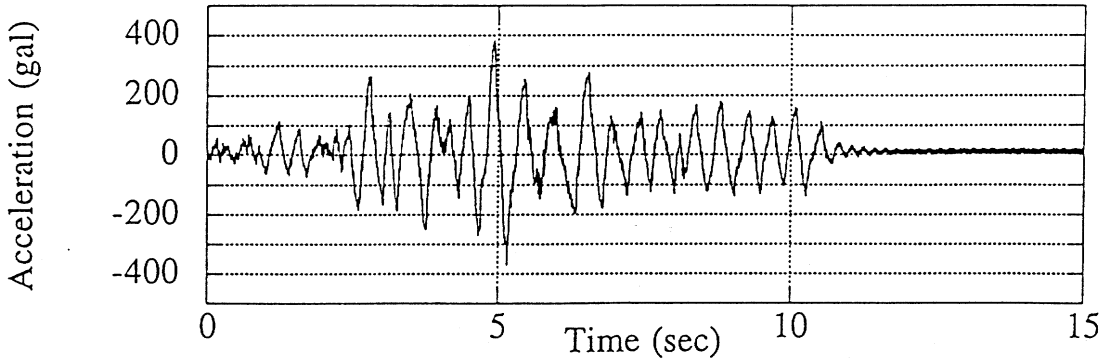

Fig. 22 Response acceleration of rigid mass (top)

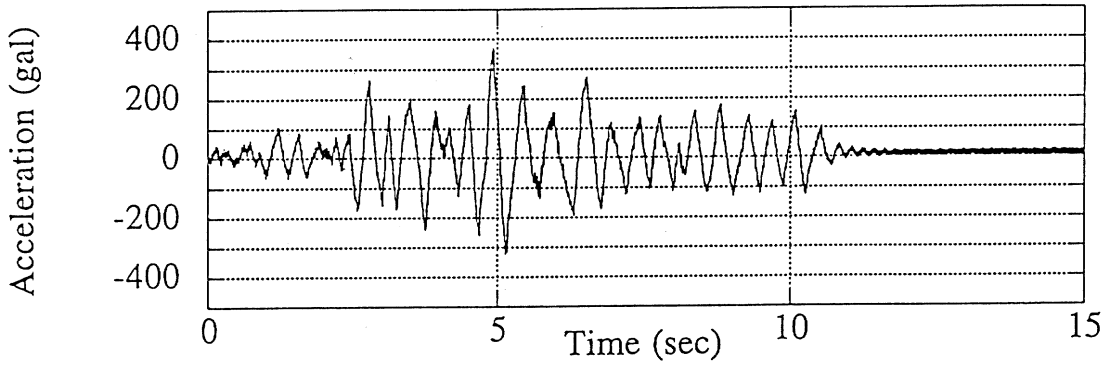

Fig. 23 Response acceleration of rigid mass (base)

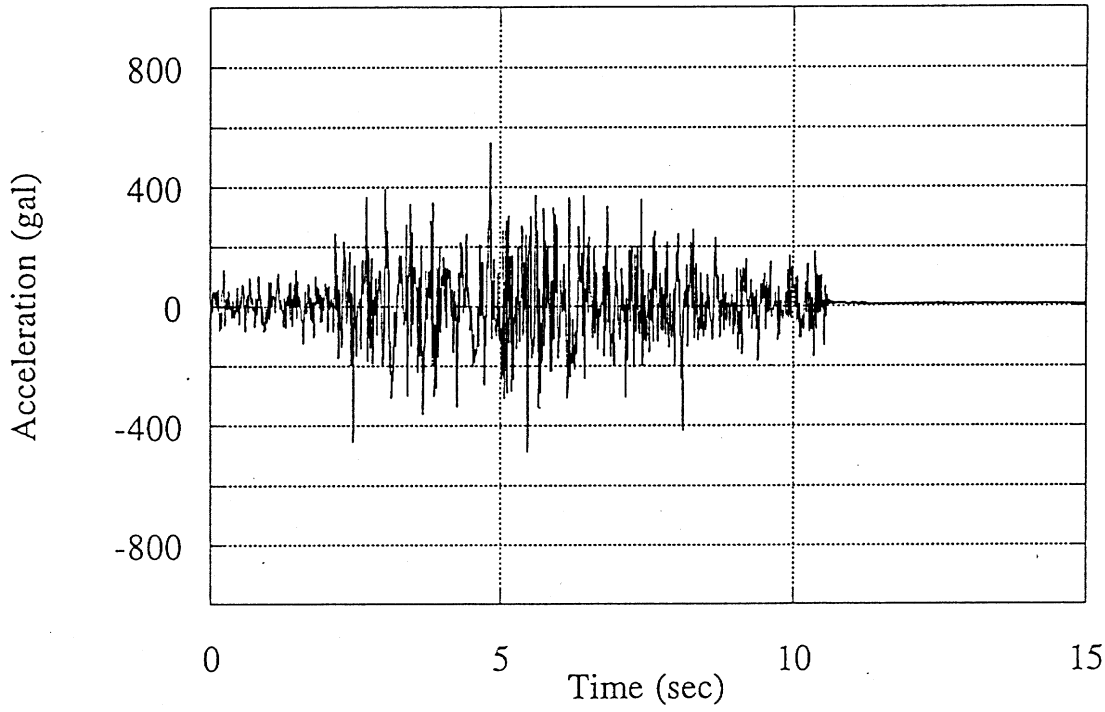

Fig. 24 Input acceleration (1.5S1)

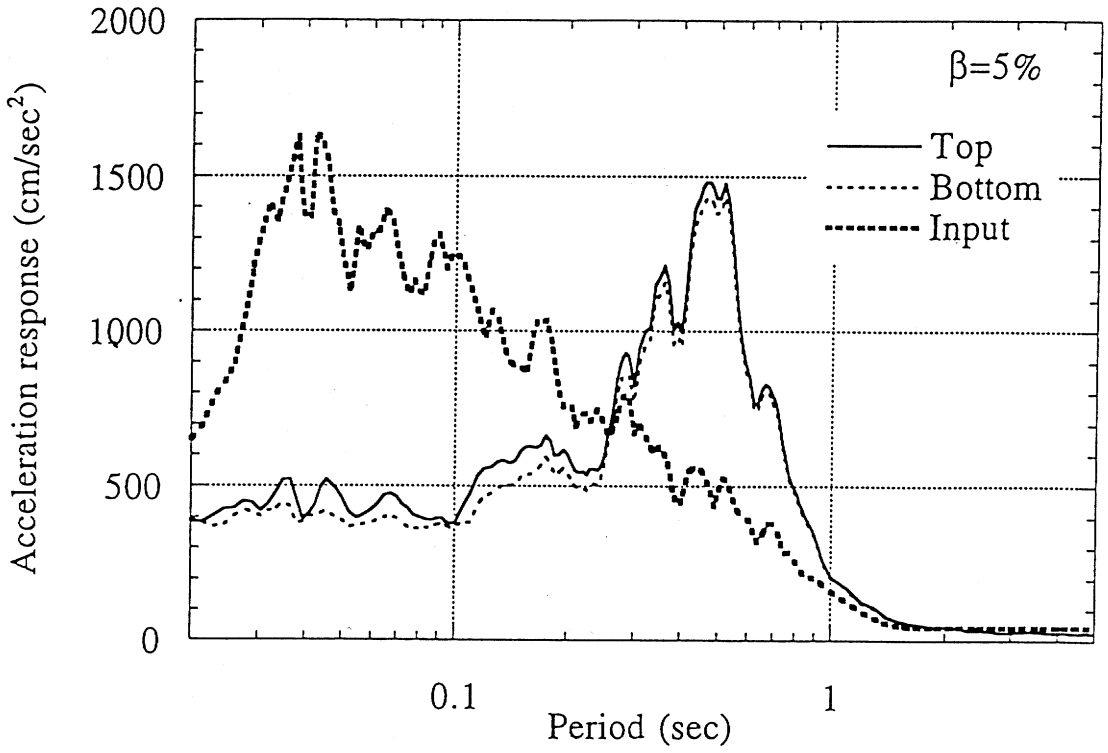

Fig. 25 Acceleration response spectra (test results, input: 1.5S1)

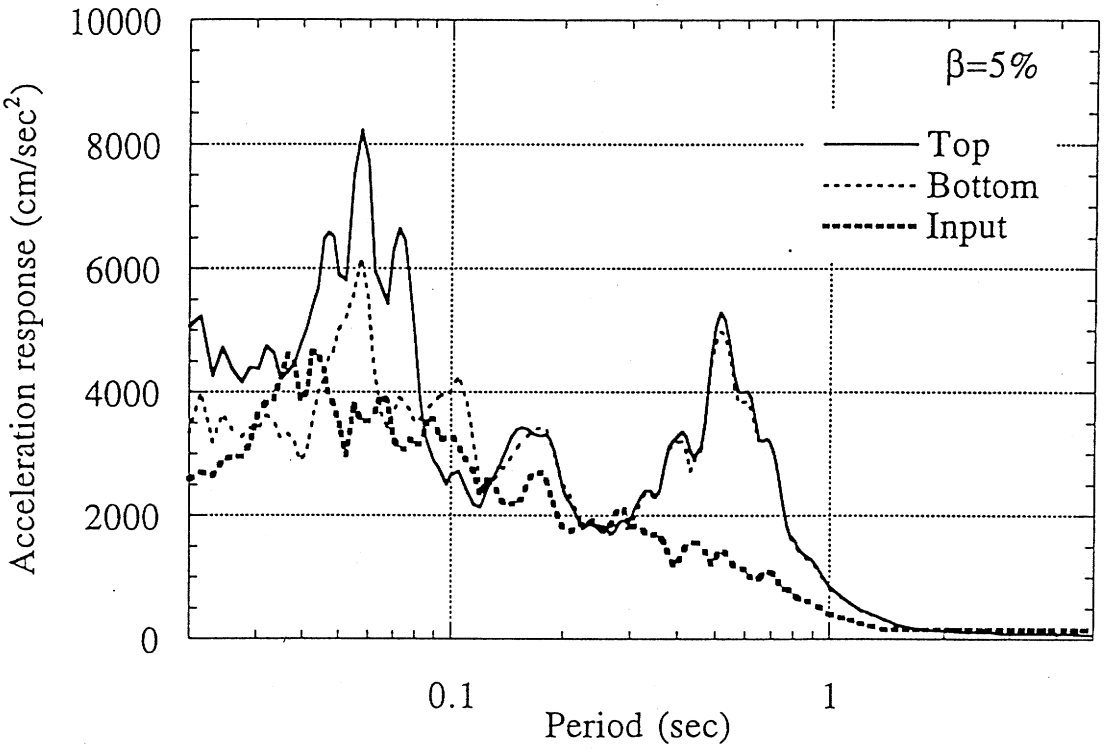

Fig. 26 Acceleration response spectra (test results, input: 4.6S1)

4.2. Test results

Figs. 22 through 24 show acceleration time histories of the shaking table, response accelerations at the top and the bottom of the rigid mass. Figs. 25 and 26 show acceleration response spectra with the damping 5% of critical at the top and the bottom of the rigid mass for the input earthquake motion of 1.5×S1 and 4.6×S1 (Measured acceleration amplitude of the shaking table in the test was 4.6 times as large as that of S1). In the case of the input earthquake motion of 1.5×S1, response spectra at the bottom and the top are similar and it is perceived that the rocking motion is small and the swaying motion is dominant. However, in the case of the input earthquake motion of 4.6×S1 difference of the spectra is perceived at the top and the bottom.

Figs. 27 and 28 show the force-displacement relationship of the rubber bearing during the shaking. In the case of the input earthquake motion of 1.5×S1 response shear deformation remains under the linear limit of the rubber bearing and hardening of the rubber bearing does not occur, whereas in the case of the input earthquake motion of 4.6×S1 the rubber bearing exceeds the linear limit and enters the hardening region causing the loss of isolation effect as shown in Fig. 26.

5. SIMULATION OF SHAKING TABLE TESTS

5.1. Simulation of CRIEPI shaking table test

5.1.1. Modeling of isolators

In the simulation, isolator was modeled in two ways. The first way is modeling isolator as a parallel combination of an elasto-plastic spring and an elastic spring (herein called bilinear model) as shown Fig. 29. In this case parameters of bilinear spring were determined from the static test result of HDR.

The second way is to model isolator as a parallel combination of several elasto-plastic springs and a non-linear elastic spring (herein called polylinear model) as shown in Fig. 29. Parameters specifying each elasto-plastic spring are determined so that the energy dissipated per one cycle becomes equal to that evaluated from the bearing test. Suppose stiffness and yield displacement of each elasto-plastic component are given as K_i and δ_i, and δ_i is corresponding to displacement amplitude of cyclic loading test of rubber bearing. Then energy dissipated per one cycle denoted by W_{i+1} at an amplitude of δ_{i+1} is given as

$$W_{i+1} = \sum_{l=0}^{i} 4(\delta_{i+1} - \delta_l)K_l\delta_l \quad (i = 0,1\cdots\cdots\cdots) \quad (7)$$

Subtracting W_i from W_{i+1} one can obtain

$$W_{i+1} - W_i = 4(\delta_{i+1} - \delta_i)\sum_{l=0}^{i-1} K_l\delta_l + 4(\delta_{i+1} - \delta_i)K_i\delta_i$$

$$= 4(\delta_{i+1} - \delta_i)\sum_{l=0}^{i-1}(Q_y)_l + 4(\delta_{i+1} - \delta_i)(Q_y)_i \quad (8)$$

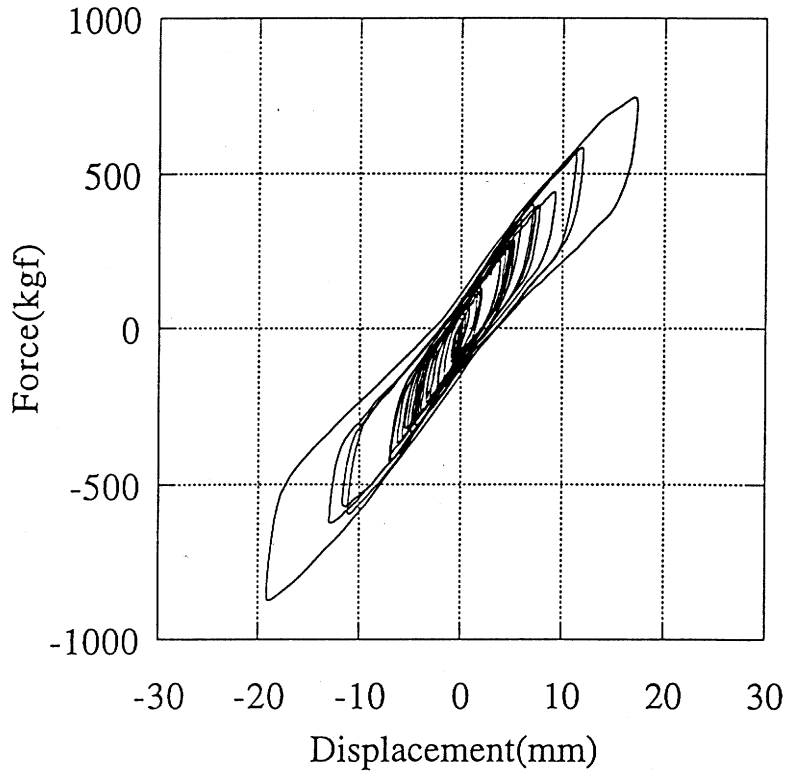

Fig. 27 Force -displacement relationship (test result, input: 1.5S1)

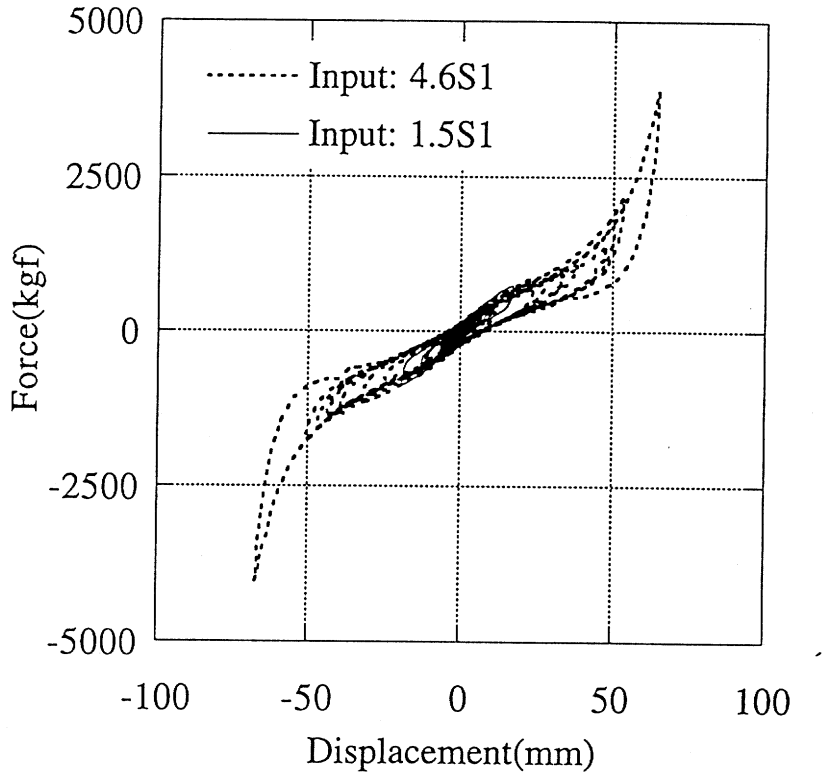

Fig. 28 Force -displacement relationship (test result, input: 4.6S1)

where $(Q_y)_i$ is the yielding force for i-th elasto-plastic spring, then each spring constant K_i of elasto-plastic spring is given as

$$K_i = \frac{(Q_y)_i}{\delta_i} = \frac{(W_{i+1} - W_i)}{4(\delta_{i+1} - \delta_i)} - \sum_{l=0}^{i-1} (Q_y)_l \times \frac{1}{\delta_i} \quad (9)$$

Eq. (9) is a recurrent formula, and $(Q_y)_i$, δ_i and W_i are given and evaluated from the experiment.

5.1.2. Simulation of base-isolated rigid mass

In the numerical simulation of the shaking table test, isolated structure is modeled as shown in Fig. 30. For the simulation of the test case where the response of the rubber bearing remains under the linear limit as shown in Fig. 27, simple bilinear spring is used to model the rubber bearing. Fig. 31 shows the comparison between the test result and the simulated result using bilinear model in terms of response spectrum for 1.5×S1 input motion. Both results agree fairly well. For this level of input motion bilinear modeling of the LRB gives enough accurate results. In these figures simulated results using polylinear model are shown as well. For the simulation where the response of the rubber bearing exceeds linear limit, several models are proposed which can take hardening effect, slip effect in the hysteresis of the rubber into account [10][17]. The polylinear model is one of those models. For the level of input motion 1.5×S1 simulated results using polylinear model show only slight difference compared with those using bilinear model.

5.2. Simulation of MISS shaking table test

The mock-up MISS is a Model of Isolated Steel Structure designed and manufactured in the research project conducted by ENEL/ENEA and the shaking table test was conducted at ISMES laboratory [3]. The model is a five-story steel frame and tested in different configurations, i.e. with/without additional masses and with/without base isolation. Base-isolated MISS is supported by 6 HDRs. In this CRP, the test data were provided by ENEL, and CRIEPI conducted numerical simulations of the tests for configuration C2 (16 masses base-fixed) and C3 (16 masses base-isolated) subjected to Tolmezzo NS earthquake component to short side direction (Y-direction) of the frame (test No. 135).

5.2.1. Eigen value analysis of base-fixed steel frame

At first, eigen value analysis for the base-fixed MISS (C2) was conducted. Eigen frequencies and modal participation factors are shown in Table 1. Mode shapes for principle modes are shown in Fig. 29. It is reported that the main frequencies in Y-direction evaluated from sine sweep test are 2.37Hz, 9.2Hz, 18.92Hz [3]. The result of the eigen value analysis shows good agreement with the experimental result.

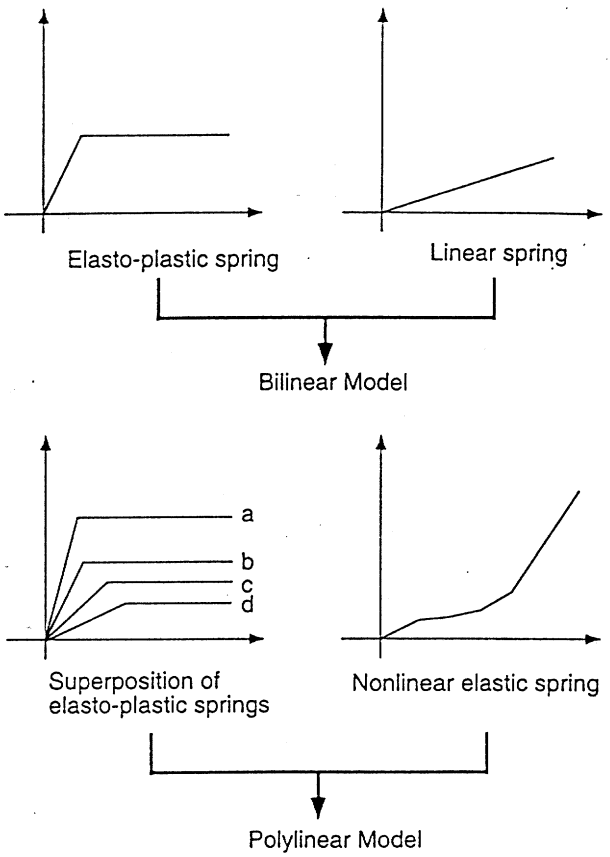

Fig. 29 Bilinear and polylinear model

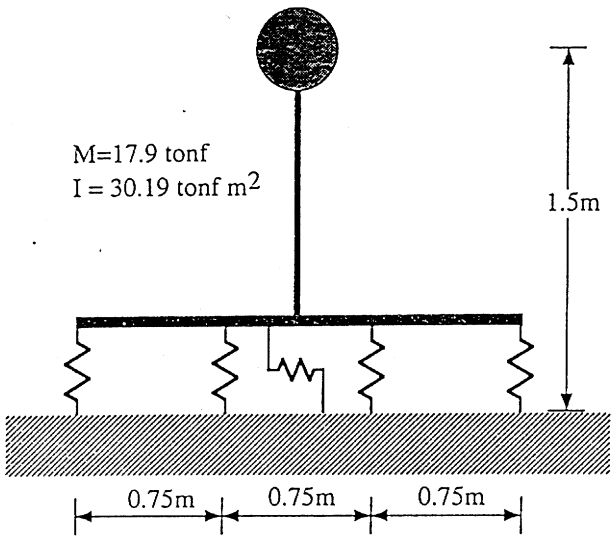

Fig. 30 Modeling of base-isolated rigid mass

Table 1 Eigen frequencies of base-fixed MISS

Order	Freq.(Hz)	Period(sec)	Modal participation factor (X)	Modal participation factor (Y)
1	2.60	0.39	1.04E-11	4.56E+00
2	3.77	0.27	-4.53E+00	7.25E-12
3	4.75	0.21	1.61E-11	1.86E-11
4	8.21	0.12	4.08E-13	1.48E+00
5	12.18	0.08	-1.54E+00	2.35E-13
6	14.69	0.07	-1.98E-12	7.63E-01
7	14.98	0.07	1.03E-12	5.09E-12
8	20.97	0.05	-2.30E-14	3.49E-01
9	22.52	0.04	-8.30E-01	-1.71E-15
10	26.88	0.04	-4.89E-13	2.22E-13

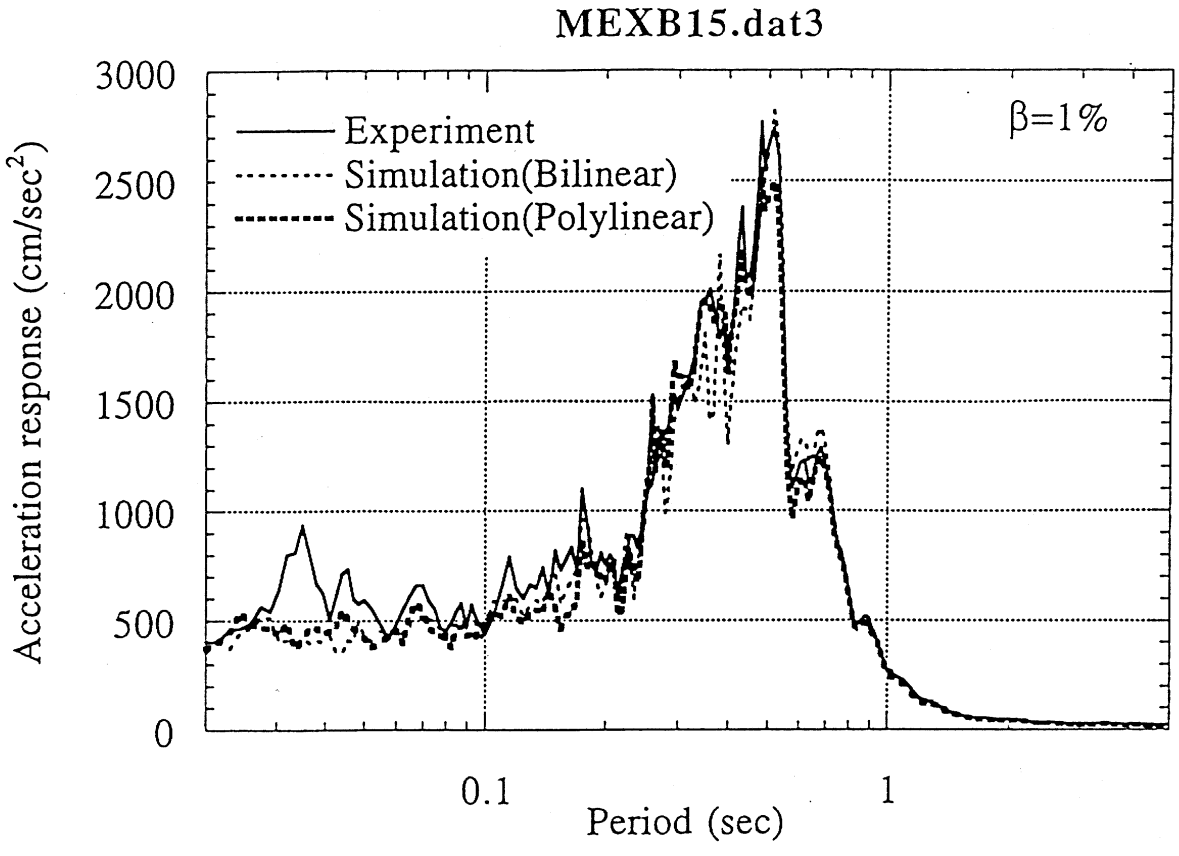

Fig. 31 Comparison of test and simulation for base-isolated rigid mass model (1.5S1 input)

5.2.2. Simulation of base-fixed steel frame

Using superstructure model used for eigen value analysis, response analysis was performed. Modal damping factor of 1.7% is given for the first mode, which was evaluated from the test, and for the rest of the modes modal damping factor of 0.85%(=1.7%/2) is given. Figs. 30 and 31 show acceleration time histories from the test and the simulation. Figs. 35 and 36 show FRS (Floor Response Spectra) obtained from the test and the simulation with damping of 1%. Agreement between both results can be perceived.

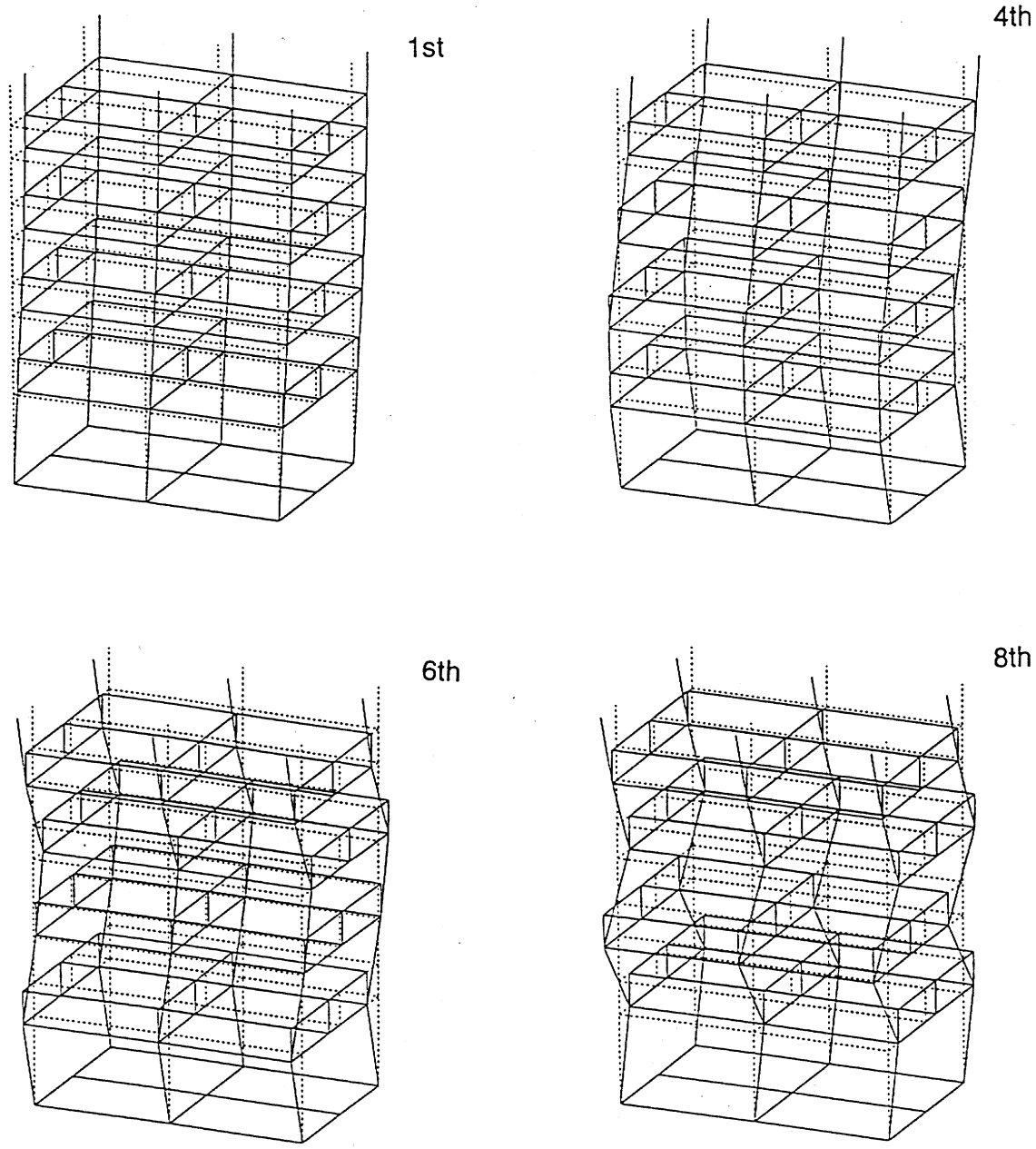

Fig. 32 Mode shape of base-fixed MISS

5.2.3. Simulation of base isolated steel frame

At first, exigent value analysis was conducted for base-isolated MISS, where HDR is modeled using bilinear model. Eigen frequencies and modal participation factors are shown in Table 2. Mode shapes for the principle modes are shown in Fig. 37. Modeling isolators in the way mentioned in *5.1.1*, response analyses of base-isolated MISS were performed. From the damping of the superstructure and the rubber bearing, weighted modal damping [15], which is proportional to the maximum strain energy, is evaluated. Weighted modal damping ratio is given by following equation.

$$\beta_{ieq} = \frac{\sum_j D_j k_j \Delta_{ij}^2 + D_{iso} k_{iso} \Delta I_{i-iso}^2}{\sum_j k_j \Delta_{ij}^2 + k_{iso} \Delta_{i-iso}^2} \quad (10)$$

where β_{ieq} is the modal damping ratio for i-th mode, D_j and D_{iso} are respectively damping ratio of the superstructure and the rubber bearing, k_j is stiffness of j-th member of the superstructure and k_{iso} is the total stiffness of the rubber bearings, Δ_{ij} is the i-th modal strain of j-th member of the superstructure and Δ_{i-iso} is the i-th modal displacement of rubber bearing. 1.7% of damping for the superstructure and 2% of additional damping for the rubber bearings are used.

HDRs used for the MISS are modeled by two models. One is bilinear model and the other is polylinear model. Parameters specifying these models are determined from the experimental results as described in *5.1.1*. Figs 38 and 39 show hysteresis loop of isolators in the numerical simulation compared with static rubber bearing test result. Comparisons of displacement response time history of rubber bearing are shown in Figs. 40 and 41, where bilinear model and polylinear model are used. Both simulation results show agreement with the test results to some extent, and in this case polylinear modeling did not necessarily give improvement. Fig. 42 shows comparison of the FRS obtained from the test and the simulation using bi-linear model for HDR. Around the fundamental period both results show agreement, however in shorter period range, discrepancy becomes larger. Fig. 43 shows the results of the simulation using polylinear model, and the improvement of the simulation is not perceived.

Text cont. on page 164.

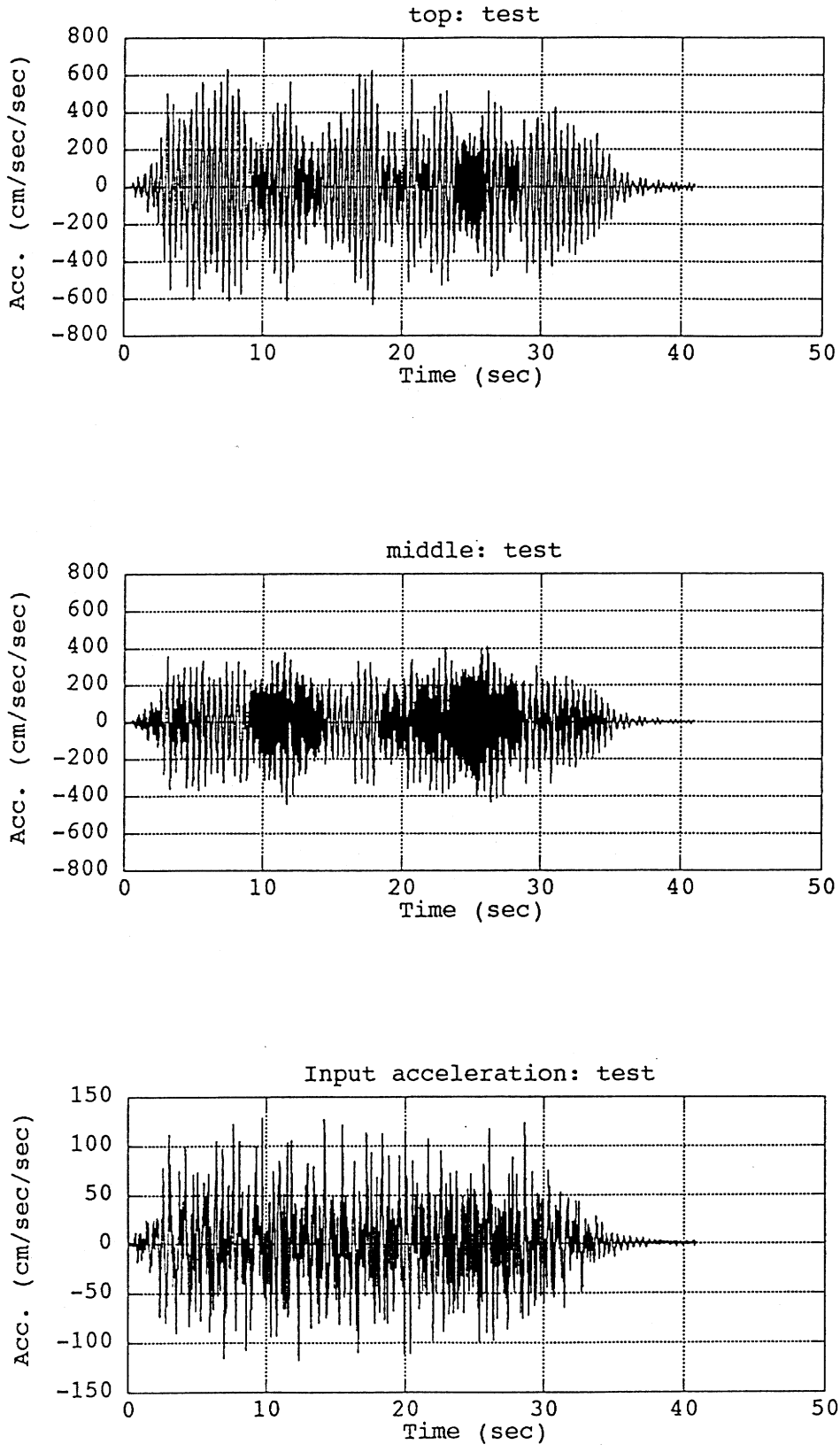

Fig. 33 Test results of acceleration response of base-fixed MISS (Tolmezzo NS)

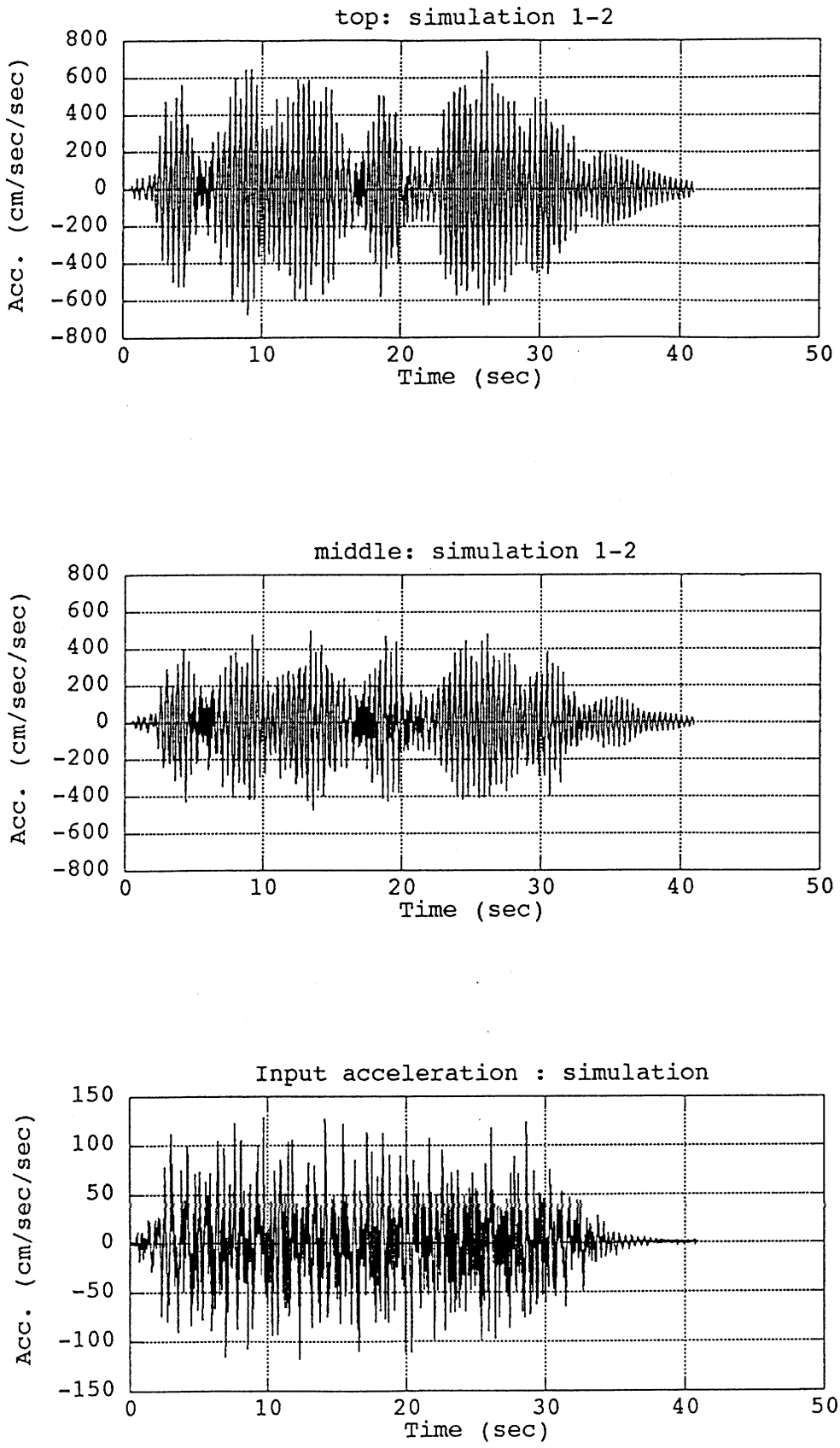

Fig. 34 Simulation results of acceleration response of base-fixed MISS (Tolmezzo NS)

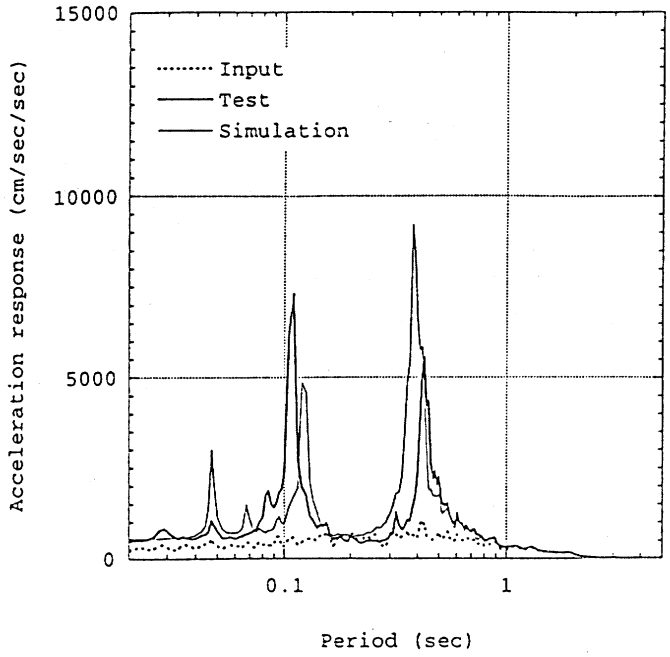

Fig. 35 Acceleration response spectra of base-fixed MISS (1% damping) test and simulation (at the middle level, model 3BH)

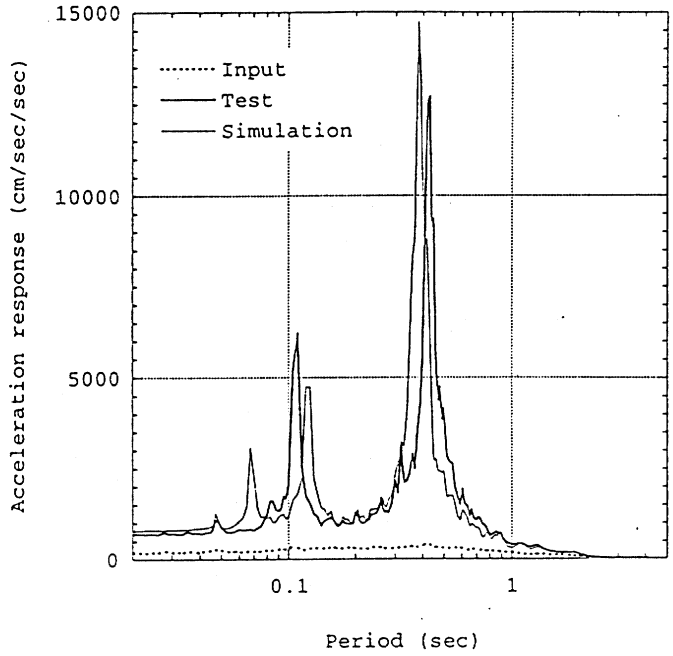

Fig. 36 Acceleration response spectra of base-fixed MISS (1% damping) test and simulation (at the top, model 3BH)

Table 2 Eigen frequencies of base-isolated MISS

Order	Freq.(Hz)	Period(sec)	Modal participation factor (X)	Modal participation factor (Y)
1	1.06	0.94	3.77E-10	5.01E+00
2	1.11	0.90	-5.01E+00	3.76E-10
3	4.55	0.22	5.31E-12	2.24E-11
4	5.69	0.18	-1.52E-12	-2.96E-01
5	7.93	0.13	1.56E-01	5.33E-13
6	11.87	0.08	5.11E-14	8.04E-02
7	14.28	0.07	1.36E-12	-1.73E-12
8	17.41	0.06	-3.79E-02	8.35E-14
9	18.63	0.05	-2.68E-13	3.90E-02
10	23.72	0.04	-2.70E-14	-3.23E-02
11	25.60	0.04	4.33E-14	8.65E-14
12	28.49	0.04	1.67E-02	2.08E-14

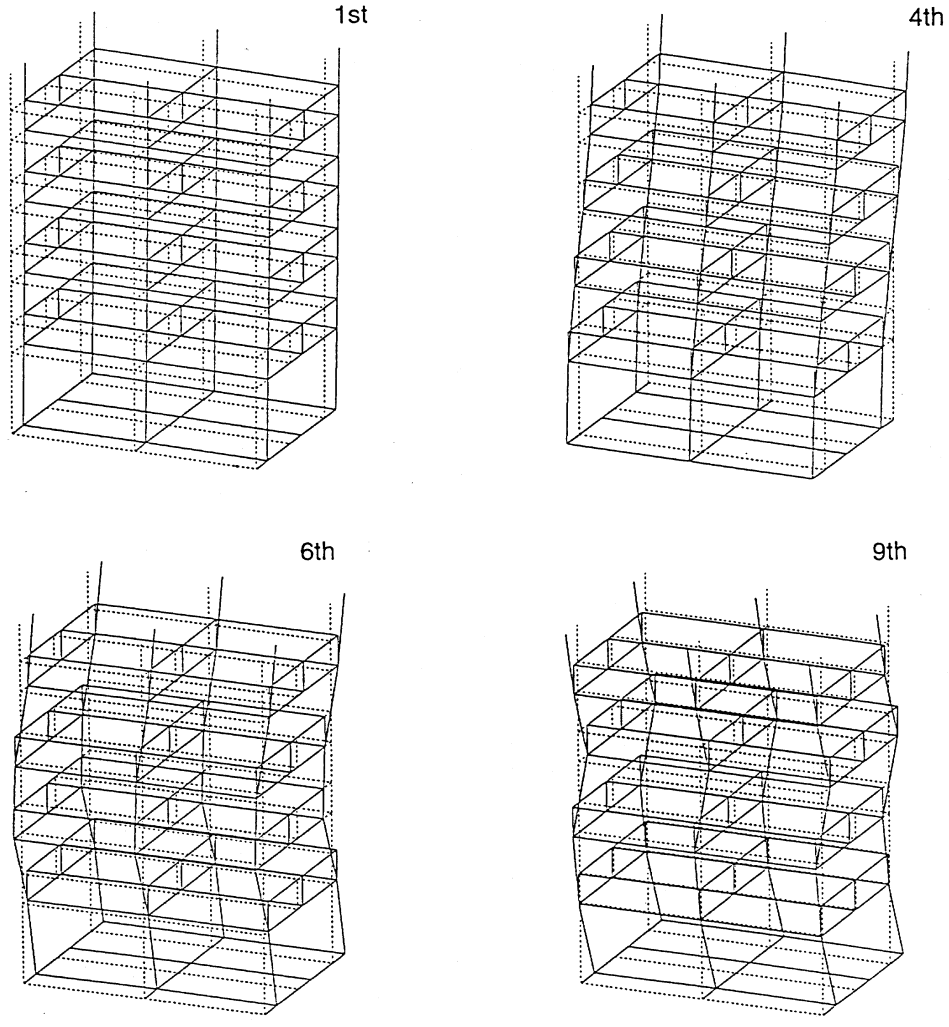

Fig. 37 Mode shape of base-isolated MISS

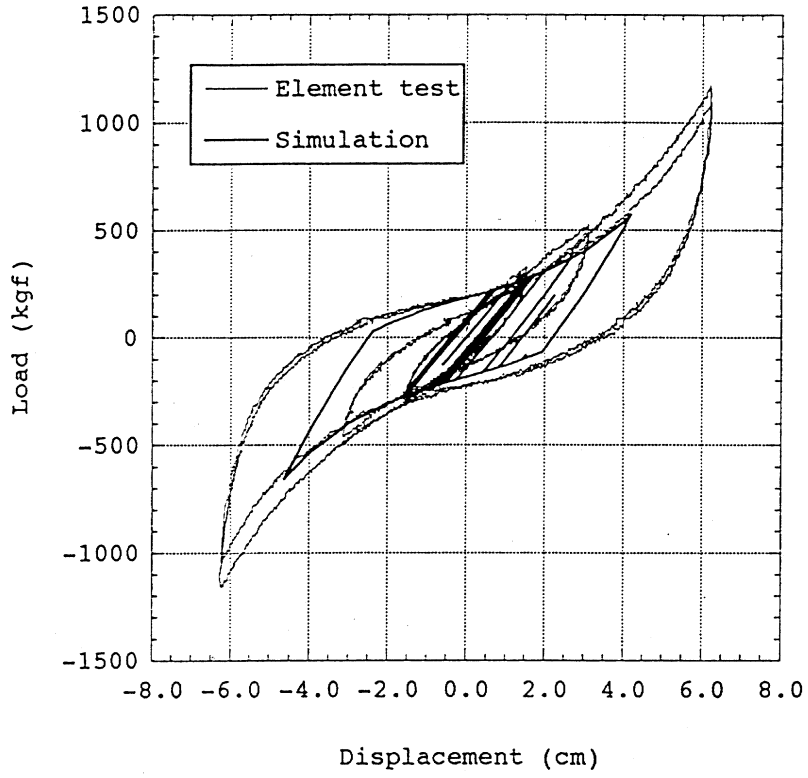

Fig. 38 Force -displacement relationship of HDR
(Simulation with bilinear model)

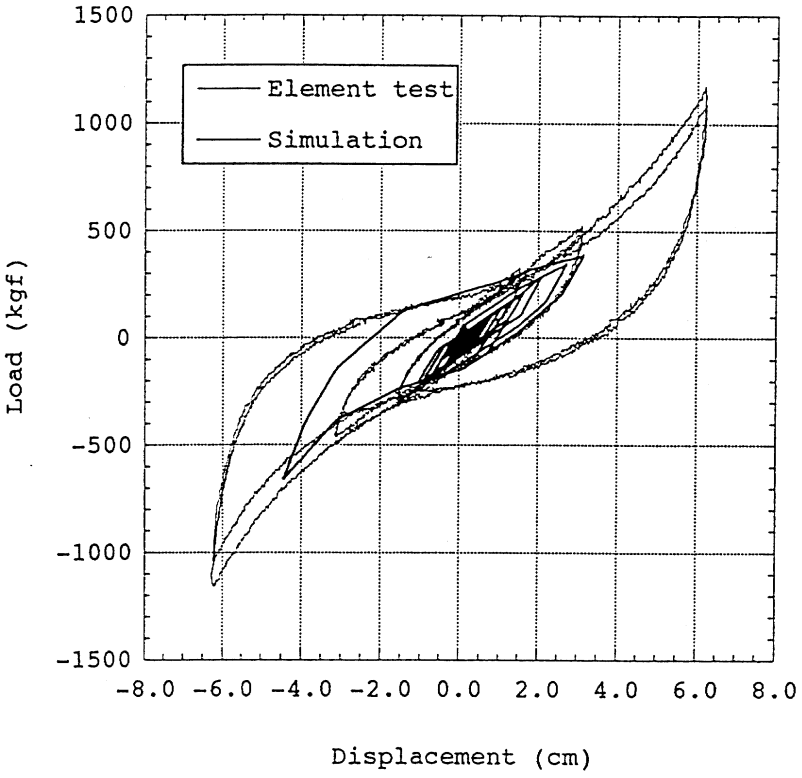

Fig. 39 Force -displacement relationship of HDR
(Simulation with polylinear model)

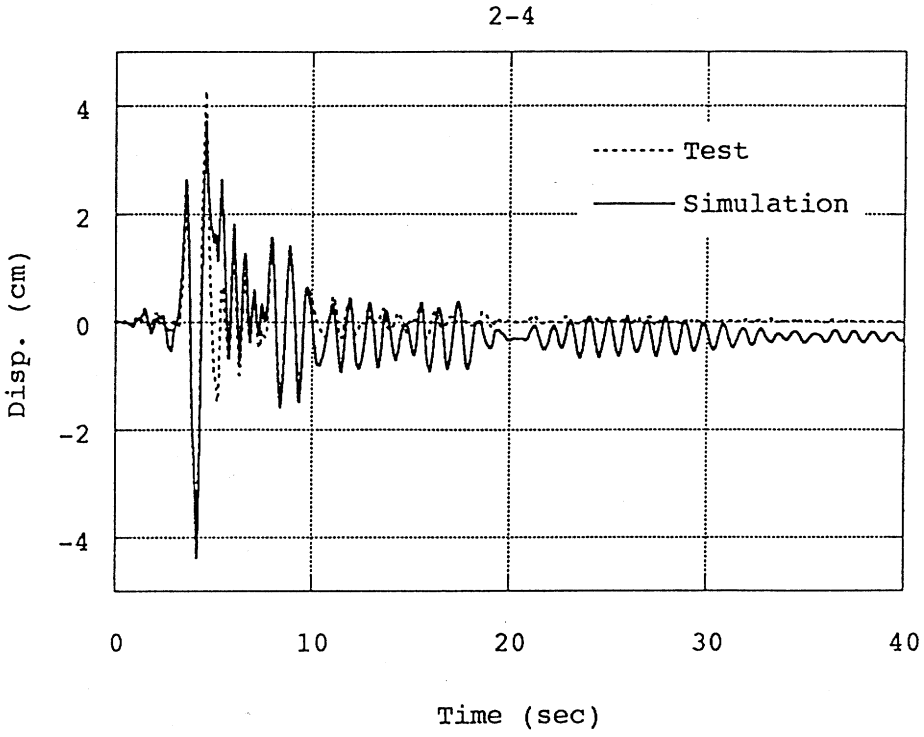

Fig. 40 Comparison of time displacement response of HDR (Simulation with bilinear model)

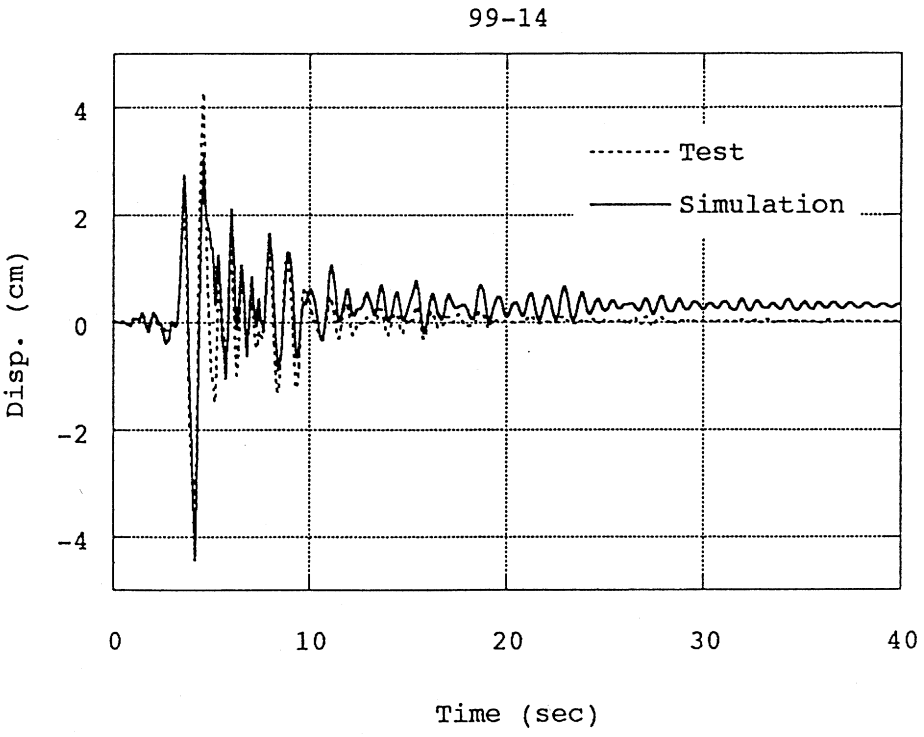

Fig. 41 Comparison of time displacement response of HDR (Simulation with polylinear model)

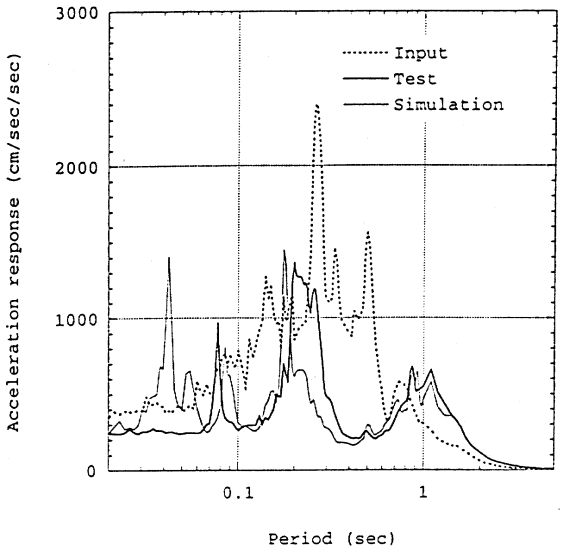

Acceleration response spectra (1% damping)
test and simulation (at the base)
(Base-isolated model, Tolmezzo NS)
sim. 2-4

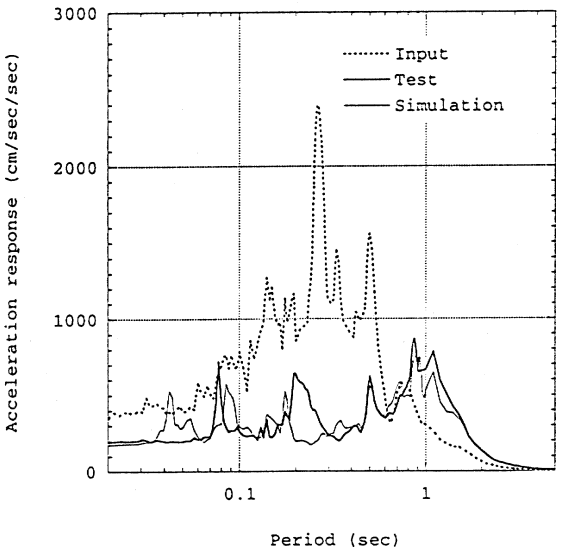

Acceleration response spectra (1% damping)
test and simulation (at the middle)
(Base-isolated model, Tolmezzo NS)
sim. 2-4

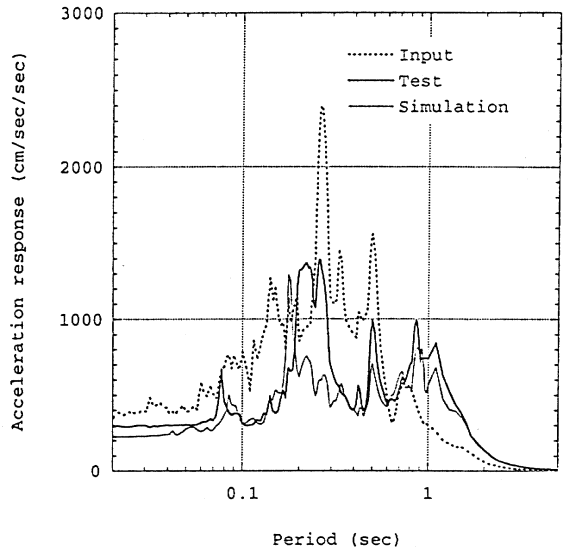

Acceleration response spectra (1% damping)
test and simulation (at the top)
(Base-isolated model, Tolmezzo NS)
sim. 2-4

Fig. 42 Comparison of FRS from test and simulation
(Simulation with bilinear model)

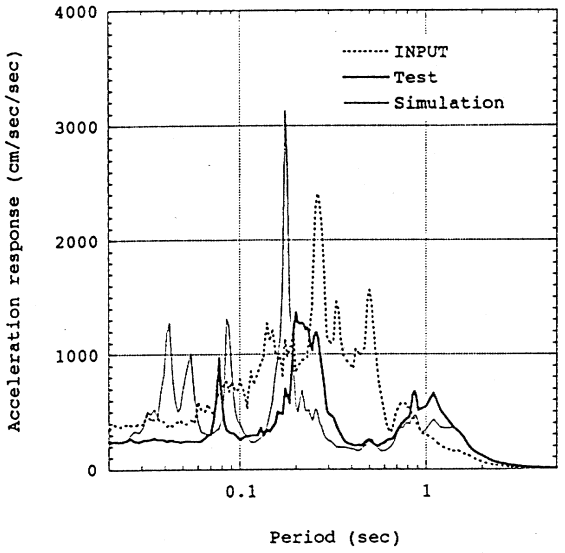

Acceleration response spectra (1% damping)
test and simulation (at the base)
(Base-isolated model, Tolmezzo NS)
sim. 99-14

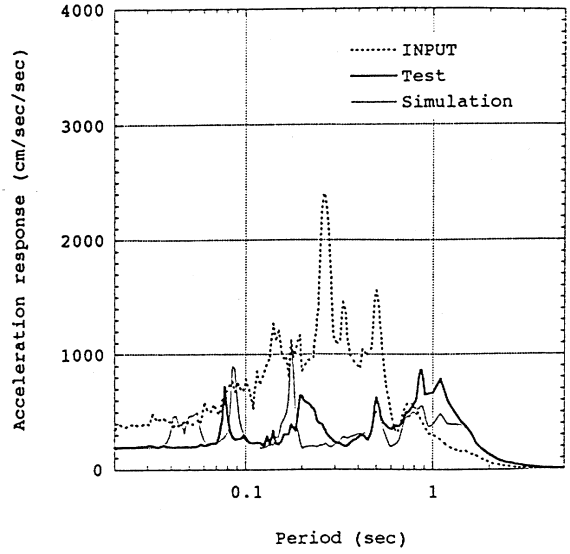

Acceleration response spectra (1% damping)
test and simulation (at the middle)
(Base-isolated model, Tolmezzo NS)
sim. 99-14

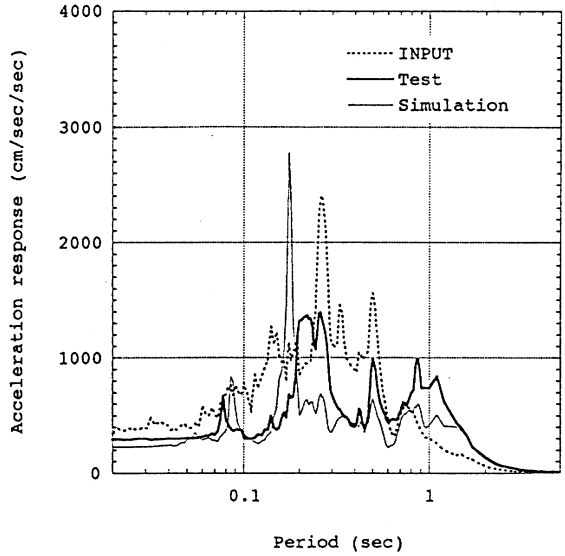

Acceleration response spectra (1% damping)
test and simulation (at the top)
(Base-isolated model, Tolmezzo NS)
sim. 99-14

Fig. 43 Comparison of FRS from test and simulation
(Simulation with polylinear model)

6. CONCLUSIONS

Using computer code ABAQUS, numerical simulations of rubber bearing tests are conducted for NRBs, LRBs (data provided by CRIEPI) and for HDRs (data provided by ENEA/ENEL and KAERI). Several strain energy functions are specified according to the rubber material test corresponding to each rubber bearing. As for lead plug material in LRB, mechanical characteristics are reevaluated and are made use of. Simulation results for these rubber bearings show satisfactory agreement with the test results.

Simulations of shaking table tests are conducted for this rigid mass model supported by LRBs and for the steel frame model supported by HDRs. In the simulation of the rigid mass model test, where LRBs are used, isolators are modeled either by bilinear model or polylinear model. In both cases of modeling of isolators, simulation results show good agreement with the test results. In the case of the steel frame model, where HDRs are used as isolators, bilinear model and polylinear model are also used for modeling isolators. The response of the model is simulated comparatively well in the low frequency range of the floor response; however, in the high frequency range discrepancies from the test result becomes larger, implying the requirement of more detailed or proper modeling of the rubber bearing and the steel frame.

ACKNOWLEDGEMENTS

Rubbers bearing tests and shaking table test carried out in CRIEPI were conducted in the research project “Verification Test of Seismic Isolation System for Fast Breeder Reactor” sponsored by Ministry of International Trade and Industry, Japan. LRB with thick lead plug was tested in the research project sponsored by Japan Atomic Energy Research Institute (JAERI) and Dr. Tada of JAERI is appreciated for providing the data. Authors would like to express their appreciation to Mr. S. Nomura of D.C.C. Ltd. for his contribution to the computational work.

REFERENCES

[1] Dusi, A and Bertola, S., et al., 1997, “Status of Italian activities on intercomparison of analysis methods for seismically isolated nuclear structures”, International Post-SMiRT Conference Seminar on Seismic Isolation, Passive Energy Dissipation and Active Control of Seismic Vibration of Structures, Taormina, Italy

[2] Dusi, A., Forni, M. and Martelli, A., 1998, “Contribution of Italy to the activities on intercomparison of analysis methods for seismically isolated nuclear structures: Finite Element Analysis of lead rubber bearings”, IAEA RCM material, Hertford, UK

[3] Forni, M., Martelli, A. and Dusi, A., 1998, “Contribution of Italy to the activities on intercomparison of analysis methods for seismically isolated nuclear structures: Shake table tests on a steel frame structure mock-up”, IAEA RCM material, Hertford, UK

[4] Hirata, K., Matsuda, A. and Yabana, S., 1997, “Contribution of Japan to the activities on intercomparison of analysis methods for seismically isolated nuclear structures”, Proc. International Post-SMiRT Conference Seminar on Seismic Isolation, Passive Energy Dissipation and Active Control of Seismic Vibrations of Structures, Taormina, Italy

[5] Hirata, K and Matsuda, A., 1999, “Contribution of Japan to the activities on intercomparison of analysis methods for seismically isolated nuclear structures”, Proc. International Post-SMiRT Conference Seminar on Seismic Isolation, Passive Energy Dissipation and Active Control of Seismic Vibrations of Structures, Cheju, Korea

[6] Hibbitt, Karlson &Sorensen, Inc., 1996, “ABAQUS/Standard User’s Manual”

[7] JSME, 1982, “Investigation report on the development of computer code for the structural analysis of spent fuel transport packaging (in Japanese)”

[8] Ishida, K., et al., 1991, “Failure tests of laminated rubber bearings”, Trans. 11th SMiRT, vol. K2

[9] Ishida, K., Shiojiri, H, et al., 1992, “Shaking table test on ultimate behavior of seismic isolation system Part 2: Response behavior of rubber bearings”, Proc. 10th WCEE, Barcelona, Spain

[10] Ishida, K., Yabana, S., et al., 1993, “Analytical study on ultimate response characteristics of base isolated structures”, Trans. of 12th SMiRT, vol. K, Stuttgart, Germany

[11] Matsuda, A., Y. Otori, et al., 1999, “Simulation on the laminated rubber bearing tests using large deformation finite element method (in Japanese)”, Trans. of JSME, vol. 65, No. 635 A

[12] Mazda, T., Moteki, M., et al., 1989, “Test on large-scale seismic isolation elements”, Trans. 10th SMiRT, vol. K2

[13] Mazda, T., Shiojiri, H., et al., 1991, “Test on large-scale seismic isolation elements Part 2”, Trans. 11th SMiRT, vol. K2

[14] Moteki, M, Kawai, N., et al., 1992, “Shaking table test on ultimate behavior of seismic isolation system Part 1: Outline of the test and response of superstructure”, Proc. 10th WCEE, Barcelona, Spain

[15] Roesset, J.M, Whitman, et al., 1973, “Modal analysis for structures with foundation interaction”, J. of St. Div., Proc. ASCE, ST3

[16] Seki, W., Fukahori, Y., et al., 1987, “A large-deformation finite-element analysis for multilayer elastomeric bearings”, 133rd American Chemical Society, Rubber Division, Montreal, Canada

[17] Suhara, M., Takeda, M., et al, 1992, “Dynamic ultimate test of base-isolated system”, Proc. 10th WCEE, Barcelona, Spain

[18] Yoo, B and Lee, J-H, 1997, “Intercomparison of analysis methods for seismically isolated nuclear structures (ENEA HDRB and CRIEPI LRB)”, International Post-SMiRT Conference Seminar on Seismic Isolation, Passive Energy Dissipation and Active Control of Seismic Vibration of Structures, Taormina, Italy

DEVELOPMENT OF ANALYSIS METHODS FOR SEISMICALLY ISOLATED NUCLEAR STRUCTURES

BONG YOO, JAE-HAN LEE, GYENG-HOI KOO
Korea Atomic Energy Research Institute, Republic of Korea

Abstract

KAERI's contributions to the project entitled Development of Analysis Methods for Seismically Isolated Nuclear Structures under IAEA CRP of the intercomparison of analysis methods for predicting the behaviour of seismically isolated nuclear structures during 1996-1999 in effort to develop the numerical analysis methods and to compare the analysis results with the benchmark test results of seismic isolation bearings and isolated nuclear structures provided by participating countries are briefly described. Certain progress in the analysis procedures for isolation bearings and isolated nuclear structures has been made throughout the IAEA CRPs and the analysis methods developed can be improved for future nuclear facility applications.

1. INTRODUCTION

The contributions to CRP by KAERI are (1) the provision of test data for a spent fuel storage pool and KAERI HLRB(High Damping Rubber Bearing), (2) benchmark comparisons between analysis and test results of seismic isolation bearings for Italian soft and hard ENEA HDRB(High Damping Rubber Bearing), CRIEPI NRB(Natural Rubber Bearing) and LRB(Lead Rubber Bearing), and KAERI HLRB, and (3) of seismically isolated nuclear structures for CRIEPI rigid mass mock-up and for Italian MISS. A summary of work done during 1996 - 1999 is as follows.

In the first RCM held in St. Petersburg, Russian Federation, May 27-31,1996, FEM analyses using ABAQUS in combined compression and shear tests for ENEA HDRB with high shear modulus and for CRIEPI NRB have been performed and compared with test results to verify the analysis procedures. The purpose of the analyses is to predict the quasi-static force-deflection behavior of laminated rubber bearings from rubber test data. Several kinds of strain energy density functions representing the hyperelastic characteristics of rubber were tried [l].

In the second RCM held in Taormina, Italy in conjunction with POST-SMIRT 14, August 25-27, 1997,the combined shear and compression behaviors of the ENEA HDRB with low shear modulus and the CRIEPI LRB are analyzed using the hyperelasticity material option of the ABAQUS computer program [2]. For ENEA HDRB, using the 2D model the solution accuracy is investigated by changing the number of elements for a rubber layer in the rubber thickness direction. The Ogden model is used in this analysis [3].

In the third RCM held in Hertford, UK in May 1998, the combined shear and compression behaviors of the KAERI HLRB made of MRPRA rubber and the shaking responses of the CRIEPI isolated rigid mass mock-up are analyzed. For FEM analyses of KAERI HLRB, three kinds of strain energy density functions of the ABAQUS program are used as constitutive law for rubber with hyperelastic characteristics. The analysis results are compared with test results, depending on the constitutive models [4].

In the fourth RCM held at Cheju Island, Korea, in conjunction with POST-SMIRT 15, August 22-27, 1999, the seismic responses for the shaking table tests of the Italian MISS with the fixed and the isolated conditions are calculated using ABAQUS time history analyses to compare with test results [5].

Based upon the information test data given for the benchmark analysis, computer codes and analytical methods developed are applied to obtain simulation results, which have been compared to the test results of isolation bearings and seismically isolated nuclear structures, hi this paper, test data, computer codes and analytical methods, code improvements and result comparisons are briefly described.

2. TEST DATA FOR BENCHMARK OF SEISMICALLY ISOLATED STRUCTURES

2.1 ENEA HDRB with low shear modulus

Test data of HDRB are given with bearing geometry. The isolators have a diameter of 125 mm, a rubber height of 30mm with a rubber thickness of 2.5mm, and a primary shape factor is 12. The four kinds of test data of the rubber compound are represented in Fig. 1. The vertical load of the bearing is 5000kN. Test data of HDRB are the combined compression and shear tests (shear strain; 50, 100, 200, 400%, break) and the compression tests.

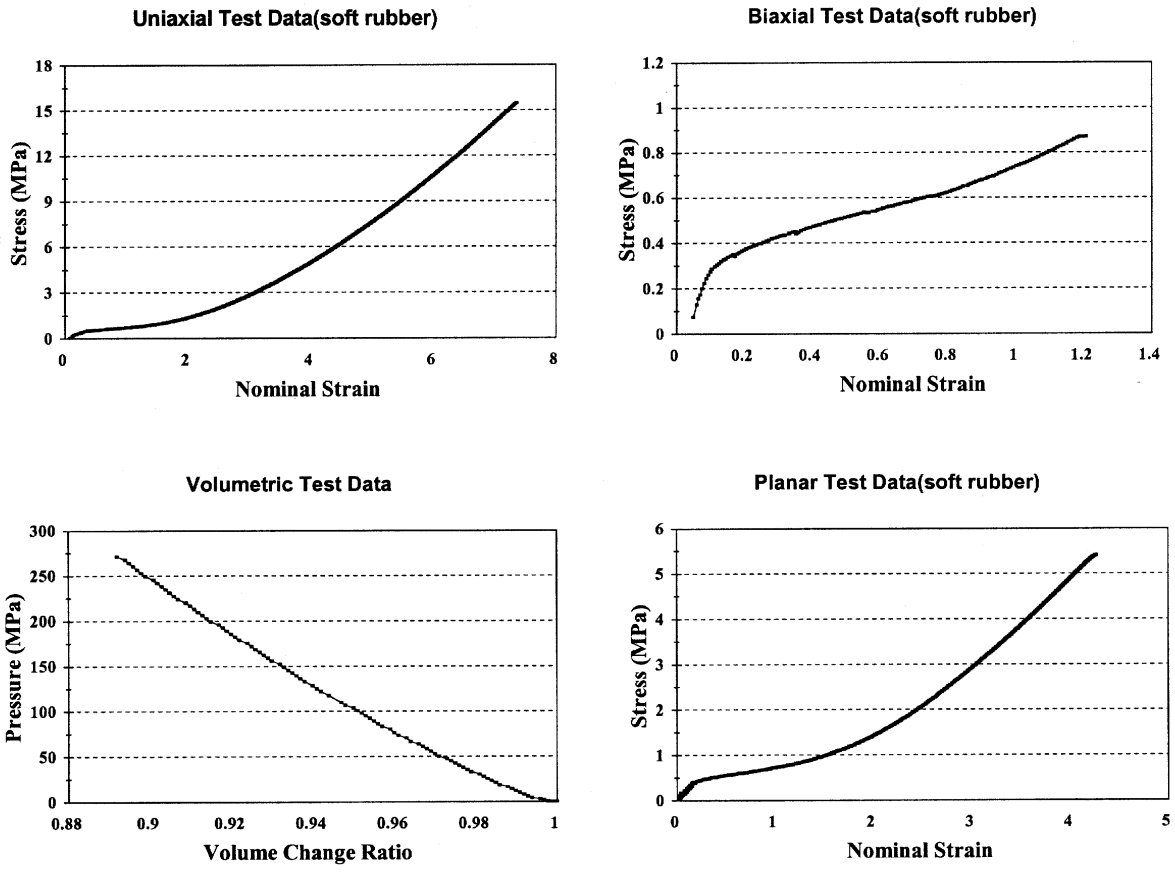

FIG 1. Soft Rubber Compounds Material Properties (ENEA HDRB).

2.2 **CRIEPI NRB**

For CRIEPI NRB benchmarks, the rubber compound test data of strip-biaxial test and the coefficients of derivatives of strain energy function are given. Test data of NRB are the combined compression and shear tests (shear strain; 20,50, 100, 200, 300, 400%, break) and the compression tests of design vertical load of 200tons and loading tests with different shear strain offsets (0, 50, 100, 200%). The geometry of CRIEPI NRB is given in Table 1, The primary and secondary shape factors are 38.9 and 7.1, respectively. The applied loading frequency is 0.01 Hz.

TABLE 1. GEOMETRY FEATURES OF THE CRIEPINRB

Diameter of isolator	1012mm
Diameter of internal hole	126mm
Thickness of rubber layer	5.7mm
Thickness of internal steel plates	3.1 mm
Number of rubber layers	25
Design vertical load	200 tons

2.3 CRIEPI LRB

Test data of the LRB (Lead Rubber Bearing) and its rubber specimens are given with the bearing geometry. From the rubber compound test data the coefficients of strain energy density function (U) are calculated as following, under incompressible conditions:

i	a_t	*bt*	*Ci*	*dt*	*et*
1	0.209	0.0135	0.00024	0.175	-2.12
2	0.0138	-0.00164	0.000064	-0.070	-6.44

Tests of the LRB are the combined compression and shear tests (shear strain; 25, 50, 100, 200, 300, 400%, break) and the compression tests. The outer diameter of the rubber bearing is 876 mm (excluding the coated rubber), the inner diameter of the lead plug is 98 mm, which was changed to 200mm after this analysis, the thicknesses of the rubber and steel shim plates are 4.9 mm and 3.1 mm respectively. The number of rubber layers is 25.

2.4 KAERI HLRB

The four kinds of test data for the rubber compound are given like as ENEA rubber. The geometry of HLRB and the test data for the combined compression and shear tests (shear strains; 50, 100, 150%) are shown Fig. 2 [6]. The horizontal displacements are applied to 300% strain of the total rubber height under the vertical pressure of 2.55 MPa.

2.5 CRIEPI isolated rigid mass mock-up

Test data of the rigid mock-up isolated with 8 reduced scale lead rubber bearings are given with the bearing geometry. The shear deformation test results of rubber bearing are represented in Fig. 3. Tests of the LRB are the combined compression and shear tests (shear strains; 25, 50, 100, 200, 300, 400, 500%) and the axial cyclic compression tests. The test mockup and model are represented in Fig. 4.

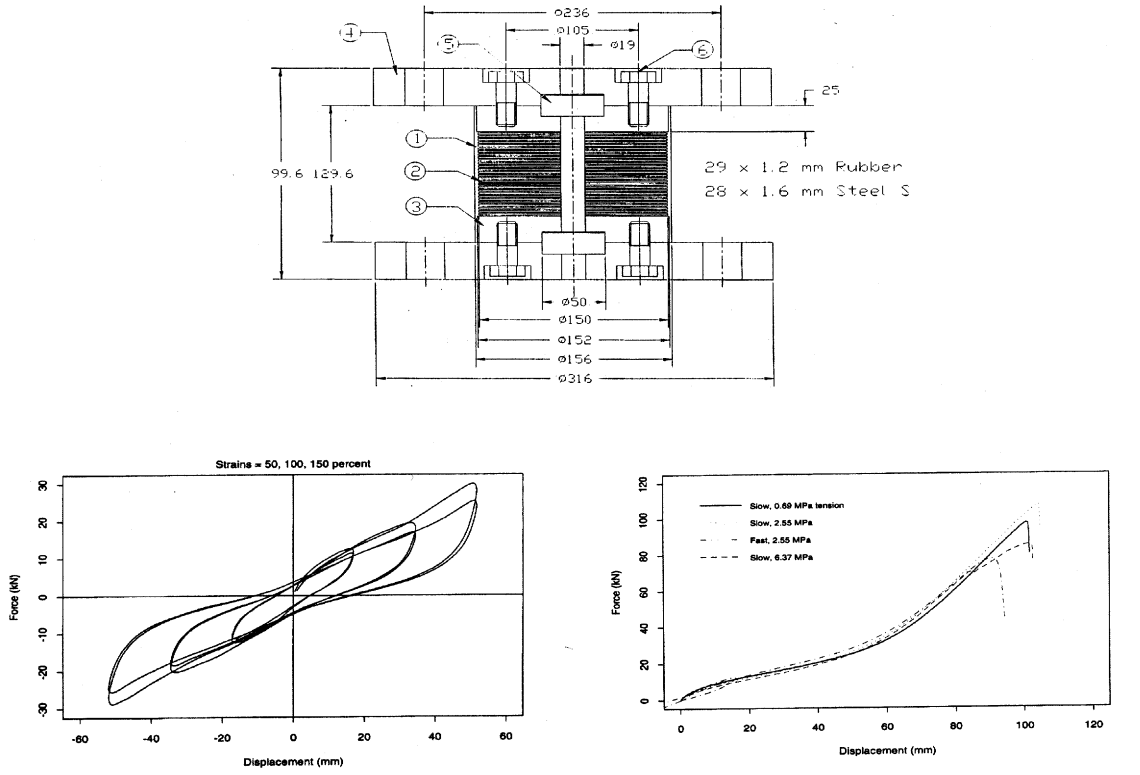

FIG. 2. Geometry Data and Shear Deformation Tests of KAERI.

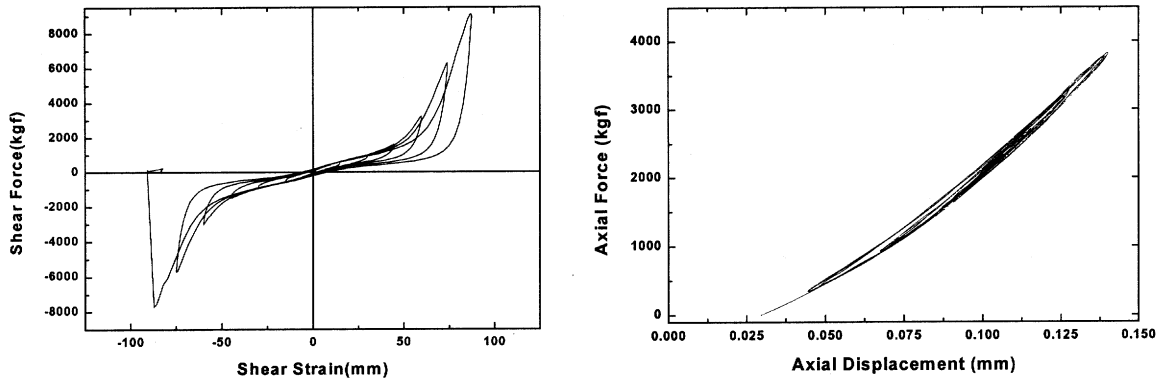

FIG. 3. Hysteresis of Horizontal and Vertical Force-displacements of LRB.

2.6 MISS structure

MISS is a five story steel frame structure mock-up, 27.6 kN weight, with a rectangular base of 2.1 × 3.3m. The structure is composed of 6 vertical columns (HEB 100) 4.5 m high, bolted on a base frame manufactured using HEM 140 beams. Four horizontal frames (HEB 100) are bolted at the columns, with a distance of 0.9m between stories [7]. Feature drawings of the MISS are shown in Fig. 5.

The geometry and performance features of the HDRBs used for the seismic isolation are given and listed in Table 2.

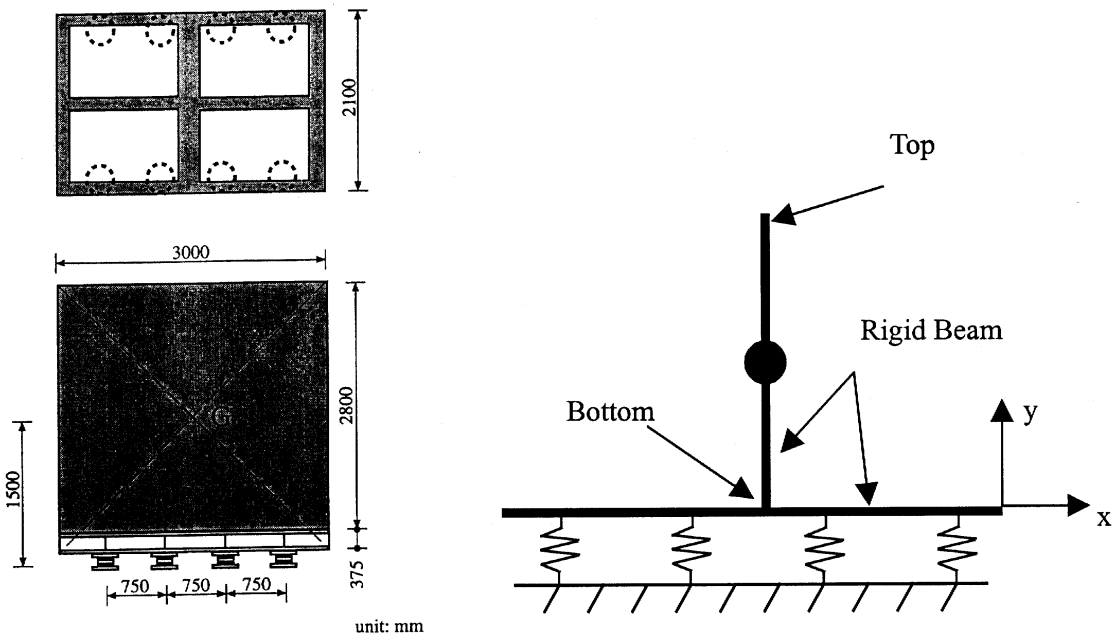

FIG. 4. Lumved Mass-Beam Model of Rigid Mock-Uv.

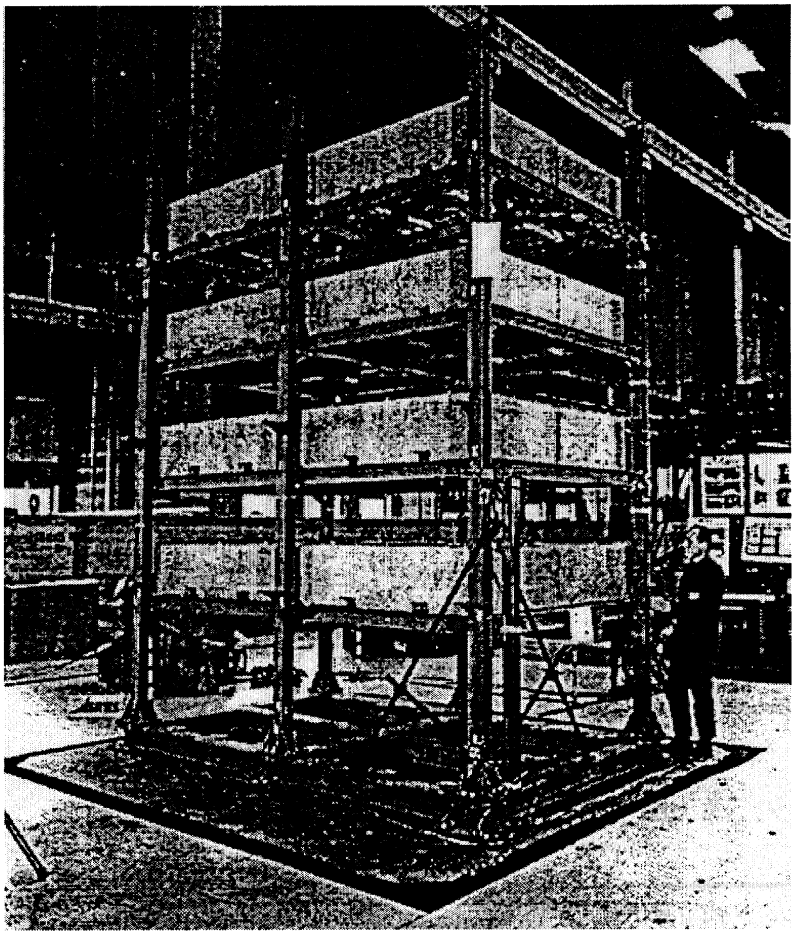

FIG. 5. MISS in the C2 Configuration.

TABLE 2. FEATURES OF THE HDRBS USED FOR THE SEISMIC ISOLATION OF MISS

Diameter of isolator (rubber layers)	125 mm
Diameter of steel plates	120mm
Diameter of internal hole	20mm
Thickness of rubber layer	2.5 mm
Thickness of internal steel plates	1.0mm
Thickness of external steel plates	10mm
Number of rubber layers	12
Number of internal steel plates	11
Rubber Young's modulus	0.4 MPa
Design vertical load	50 kN
Vertical stiffness	lOOkN/mm
Horizontal stiffness at 100% shear strain	160N/mm
Damping at 100% shear strain	14%
Attachment system	Bolts and central dowel

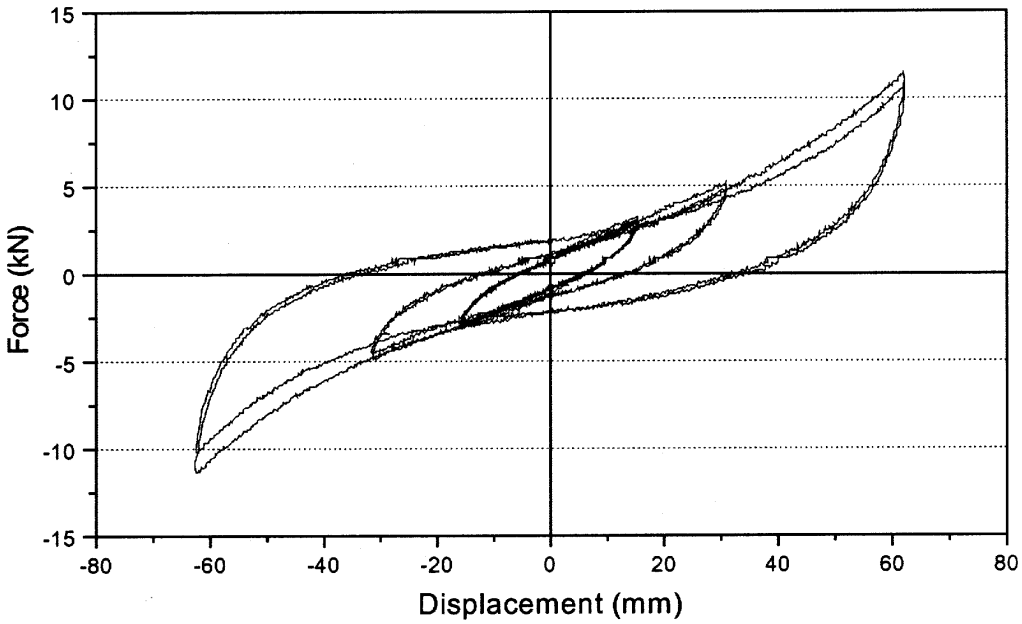

FIG. 6. Hysteresis of Horizontal Force-Displacements of HLRB.

The shear force and deformation test results of rubber bearings are represented in Fig. 6. The tests of the HDRB are the combined compression and shear tests (shear strains; 50, 100, 200%).

3. COMPUTER CODES, ANALYTICAL METHODS, AND IMPROVEMENT OF CODES

For the analysis of isolators and isolated structures, ABAQUS computer code is used. The numerical evaluation models are listed in Table 3 and explained in detail as follows.

TABLE 3. NUMERICAL MODELS FOR RUBBER BEARINGS AND ISOLATED STRUCTURES

Items		Numerical Models	Computer Code
LRB& LLRB	Rubber	• Strain Energy Functions - Mooney Rivlin/ -Polynomial - Ogden/ -Seki	ABAQUS
	Steel Shim	• Linear Elastic	
	Lead	• Elastic-Plasticity Constitutive Law	
LRB Structure behaviors for Isolated Structures		• Linear Model • Bilinear/Modified Bilinear Model • Rate Model	ABAQUS User Subroutine

3.1 Material modeling of rubber layer

In modeling the rubber layer, strain energy density functions are used in ABAQUS. In ABAQUS there are two options of simulating rubber behavior. One needs the input data of the rubber specimen test results in numeric form, and the other needs the strain energy density functions calculated from the rubber specimen test data. In the first option, at least two of the three rubber test data of the uniaxial, equibiaxial, and planar tests are required for horizontal displacement analysis, and the volumetric test data are required to calculate the vertical deformation.

An accurate modeling to represent the behavior of the rubber bearing is important because the rubber endures a very large displacement. There are several types of material models for the isotropic rubber materials with the strain energy density function (U) consisting of deviator invariants, and the following models are used in this paper for the simulation of the behavior of rubber bearings.

3.1.1 Polynomial strain energy density function

To derive the governing equation of rubber behavior, the strain energy density function (U) is defined as [2]:

$$U = \sum_{i+j=1}^{N} C_{ij} (\bar{I}_1 - 3)^i (\bar{I}_2 - 3)^j + \sum_{i=1}^{N} \frac{1}{D_i} (\bar{J}_{el} - 1)^{2i},$$

where $I\backslash$ and 72 are the first and the second invariants of deviatoric deformation that are represented by the following principal stretches (A i, A 2, A $_3$).

$$\bar{I}_1 = \bar{\lambda}_1^2 + \bar{\lambda}_2^2 + \bar{\lambda}_3^2,$$
$$\bar{I}_2 = \bar{\lambda}_1^2 \bar{\lambda}_2^2 + \bar{\lambda}_2^2 \bar{\lambda}_3^2 + \bar{\lambda}_1^2 \bar{\lambda}_3^2,$$

where $J_e i$ is elastic volume ratio, C_{tj} and D_i are constants of strain energy density function, TV is the order of function, and D_f is the compressibility of the rubber. $C_{\&}$ is calculated from the

relations between the_ rubber test data and the derivatives of the strain energy density function with respect to /1, /2 and J_{el} at the simple boundaries [2].

- Uniaxial
- Equibiaxial mode
- Planar (pure shear) mode
- Volumetric mode

$$
\begin{aligned}
&: \ \bar{\lambda}_1 = \bar{\lambda}_U, \bar{\lambda}_2 = \bar{\lambda}_3 = \bar{\lambda}_U^{-1/2}, \bar{\lambda}_U = 1 + \varepsilon_U \\
&: \ \bar{\lambda}_1 = \bar{\lambda}_2 = \bar{\lambda}_B, \bar{\lambda}_3 = \bar{\lambda}_B^{2}, \bar{\lambda}_B = 1 + \varepsilon_B \\
&: \ \bar{\lambda}_1 = \bar{\lambda}_S, \bar{\lambda}_2 = 1, \bar{\lambda}_3 = \bar{\lambda}_S^{-1}, \bar{\lambda}_S = 1 + \varepsilon_S \\
&: \ \bar{\lambda}_1 = \bar{\lambda}_2 = \bar{\lambda}_3 = \bar{\lambda}_V, J = \bar{\lambda}_V^{3}
\end{aligned}
$$

When N=l, the function becomes a Mooney-Rivlin model.

3.1.2 Ogden strain energy density function

The strain energy density function (U) is represented by the following principal stretches.

$$U = \sum_{i=1}^{N} \frac{2\mu_i}{\alpha_i^2} (\bar{\lambda}_1^{\alpha_i} + \bar{\lambda}_2^{\alpha_i} + \bar{\lambda}_3^{\alpha_i} - 3)^i + \sum_{i=1}^{N} \frac{1}{D_i} (\bar{J}_{el} - 1)^{2i},$$

where /j/5a,.,£),. are constants of the function, N is the order of energy function, D_i and represents the compressibility of rubber. The ju^a, are determined from the relations between the stress and strain of rubber specimen tests with simple boundaries.

3.1.3 Seki model

To predict the rubber behavior more accurately in small strain regions Seki introduced the following strain energy density function which includes exponential terms [8]:

$$\frac{\partial W}{\partial I_i} = a_i + b_i(I_1 - 3) + c_i(I_2 - 3)^2 + d_i \exp(e_i(I_i - 3), i = 1,2,3,$$

where 7j and /$_2$ are the first and second invariants of deviatoric deformation. To calculate the constants of this function, the previous rubber specimen tests or strip-biaxial test are required. When 7$_3$ =1 means the incompressible condition.

3.2 FEM model of isolator

For the finite element analysis of the rubber bearing with a cylindrical shape, the 3D half-model and non-axisymmetric load conditions are adopted for a combined compression and shear analysis.

For a 2D model, the element types for steel shims and rubber layers are the CAXA41 and CAXA8H1 respectively, which have an axisymmetric geometry with a non-axisymmetric load. In 2D model, the solution accuracy is investigated by changing the number of the elements for a rubber layer from one to four in the rubber thickness direction.

For a 3D model to get more accurate results, the 3D solid element of C3D8H of ABAQUS is used. The number of elements is 5 in a radial direction and 19 in a circumferential direction as shown in Fig.7. The 2 or 3 elements for a rubber layer are used.

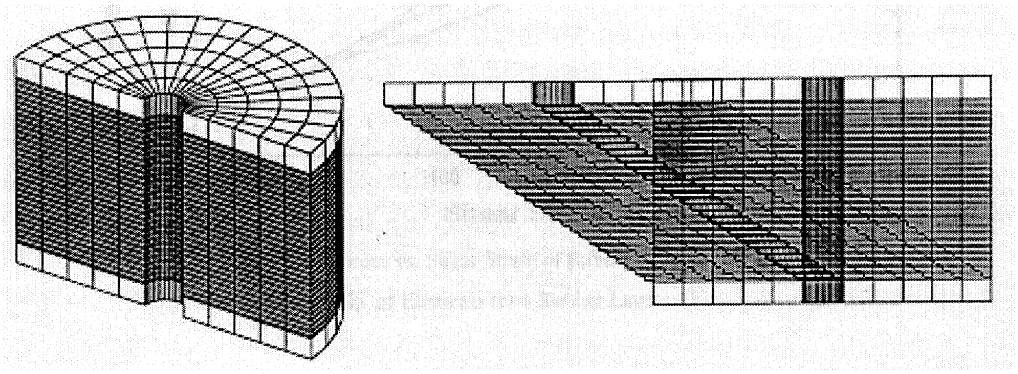

FIG. 7. Finite Element Mesh (3D and 2D).

The stress- strain relations of the lead plug used in the analysis of lead rubber bearings are modeled as a nonlinear curves, and the stress- strain relations above the initial yield used for the two models are obtained by using the G = 16/^, where G is shear modulus and ^is shear strain [9].

The lead plug is modeled with an axisymmetric element type with the nonaxisymmetric loads, CAXA41 for the combined compression and shear analysis. The boundaries are fixed at the bottom of the bearing, and vertically coupled and horizontally freed at the top of the bearing.

3.3 Structural model of isolator

Based on the shear deformation and vertical deformation test results of rubber bearings, several kinds of hysteresis models of rubber bearings such as linear, bilinear and modified bilinear models are developed [10] and applied to time history response analyses for seismic inputs.

3.3.1 Linear model

In the equivalent model, the rubber bearing is modeled by a joint element (JOINTC) for equivalent stiffness and by a dashpot element (DASHPOT) for viscous damping. The stiffness values for three types of equivalent models are shown in Fig. 8.

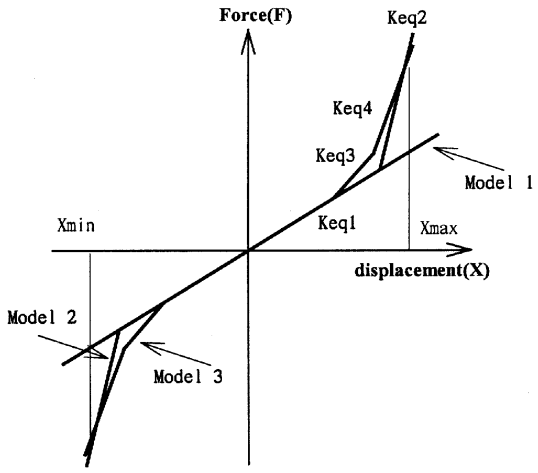

FIG. 8. Horizontal Equivalent Stiffness Models.

In model 2 of the equivalent model, the horizontal stiffness has severe hardening characteristics in the high strain region as Keql, Keq2. The Keql is determined by an equivalent stiffness in the range of the displacement response up to the linear strain limit. The Keq2 acts on the strain hardening. The viscous damping coefficient is usually used for equivalent damping at the maximum shear strain to be experienced (for example, 12% damping).

3.3.2 Bilinear model

In the bilinear model, the hysteretic characteristics of rubber bearing is represented by the material properties of a two-dimensional truss element (type=CID2), for simplicity that has a unit cross-section area with zero density and the element length by the 100% shear displacement of a rubber bearing. Young's modulus (E) of this truss element is represented by the KL/A. Here K is the horizontal stiffness obtained from the hysteretic curve of rubber bearing tests, L element length, and A cross section area of the truss element. The bilinear model requires only three parameters, which are initial stiffness (Kl), the second softened stiffness (K2), and yield load value (Qd) as shown in Fig. 9. These are determined from the isolator hysteretic curves of the shear strain test results. The bilinear model can have many shapes depending on the parameters, Kl, K2 and Qd to be determined. In the model, the yield load values (Qd) of hysteresis curves can be changed according to the maximum shear strain to take into account of the hysteresis characteristics. The relations between the equivalent model and bilinear model are represented as follows:

Heq = 2Qd(Xmax-Xy)/[3.14(Qd+K2 Xmax)Xmax], Xy=Qd/(Kl-K2) Keq = [Kl Xy+K2(Xmax-Xy)]/Xmax.

The equivalent damping value of the bilinear model is largely varied according to the shear displacement. In general the high damping rubber bearing has a relatively constant equivalent stiffness and damping according to shear deformation of the rubber bearing [11]. For example, K2 and Kl are decided as 40 and 160 respectively, and Qd is determined as 6.0 at the 100% strain. In this case, the equivalent damping values of the bilinear model at 50% and 100% strains are calculated by about 14.2% and 8.5% respectively. The equivalent stiffness of the bilinear model is rapidly reduced to 50% shear strain but is relatively constant above 100% shear strain region as shown in Fig.ll. In the modified bilinear model, the second strain hardening stiffness (K3) is considered in the high strain region as shown in Fig. 10. The damping at the high strain region would be increased a little from that in the bilinear model without the hardening effect. The UMAT subroutine of ABAQUS is utilized to implement the biliner models of the hysteresis curves of a rubber bearing.

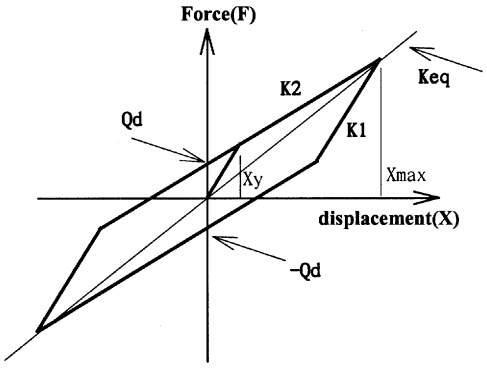

FIG. 9. Simple Bilinear Model

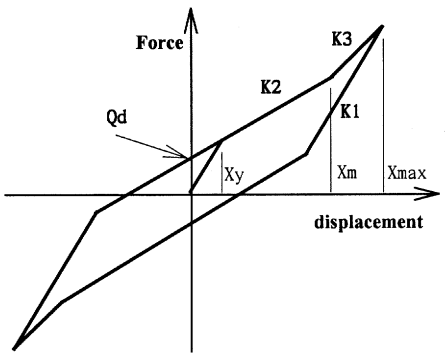

FIG. 10. Modified Bilinear Model

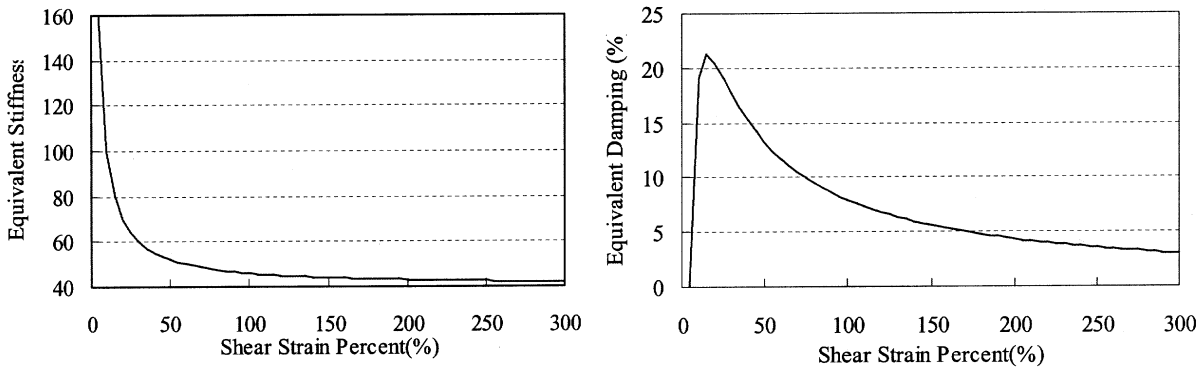

FIG. 11. Equivalent Stiffness and Damping vs. Shear Strain (%) of Bilinear.

4. COMPARISON OF ANALYSIS RESULTS AND BENCHMARK TESTS

4.1 ENEA HDRB with low shear modulus

The horizontal force and displacement relations show no differences with respect to the number of elements for a rubber layer as shown in Fig. 12. According to the material models of rubber, however, there are some different results. The Mooney-Rivlin model, with a linearity of material properties, gives a large discrepancy from the test results, but the Polynomial (N=2) and the Ogden (N=3) methods give results which compare accurately with the test results, up to a shear displacement of 60 mm.

The analysis results for the 3D solid model are represented in Fig. 13, the results using the Polynomial and the Ogden models are close to the test data in the lower shear strain region up to 200%, which equals the shear displacement of 60 mm. The Seki model calculates a higher shear force than the test data, and the Mooney-Rivlin model shows much difference from the test data. In vertical deformation analyses, a minimum of two elements in thickness direction for a rubber layer is required to get accurate results. The Polynomial and Ogden models are much better than the Mooney-Rivlin model, and the Seki model is the worst because the volumetric tests data are not considered in the formulation. In computing efficiency, the 3D model is taken to be above 10 times longer than the 2D model.

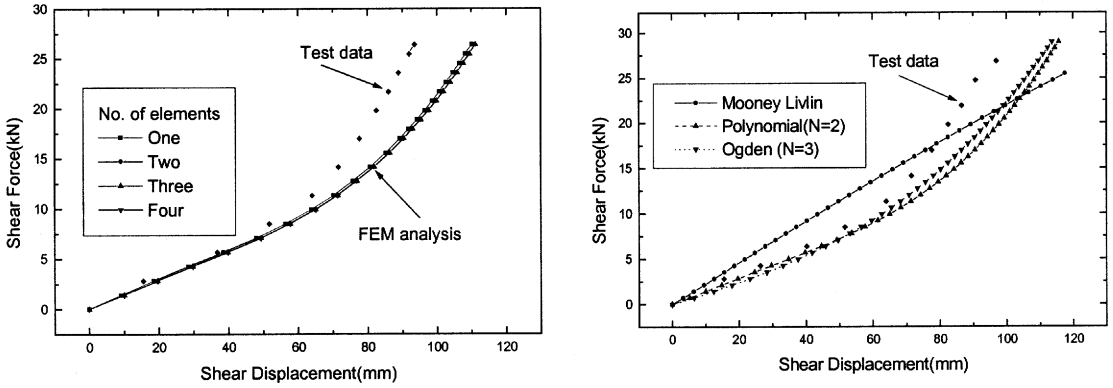

(Rubber Material Model: Ogden(N=3)) (No. of Elements of a Rubber Layers)

FIG. 12. Deformations of Isolators with 2D Model for ENEA HDRB.

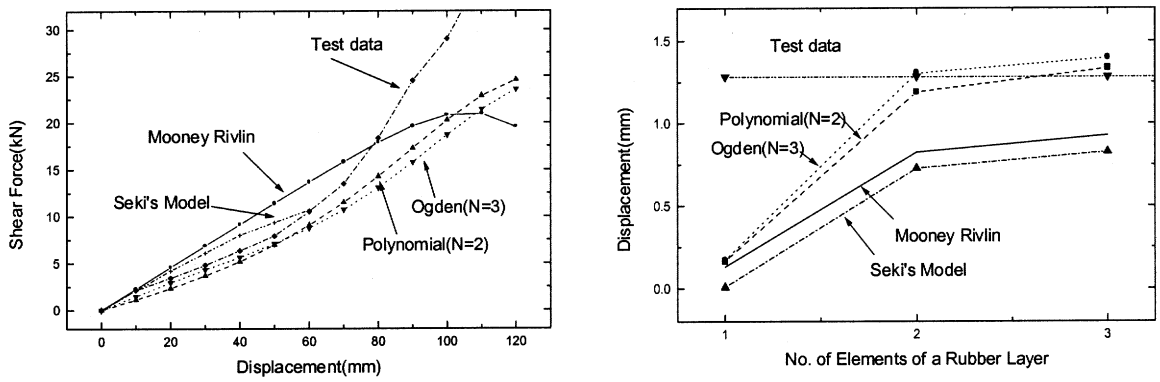

FIG. 13. Deformations of Isolators with 3D Model for ENEA HDRB.

4.2 CRIEPINRB

For CRIEPI NRB benchmarks, analysis results using coefficients of the derivatives of strain energy function show good agreements with the test results. In the compression analysis with no shear strain offset, analysis results agree well with test results up to 400% design vertical load, however in the compression with offsets the displacements obtained by the combined compression and shear analyses are smaller than those by tests.

4.3 CRIEPI LRB

The finite element analyses using the 3D element are performed for the CRIEPI LRB. The two kinds of stress- strain curves of the lead plug are used in these analyses as shown in Fig. 14, where the initial yield stresses are assumed by the static and the dynamic yield stresses representing the soft and hard properties respectively [12]. The results for combined compression and shear analyses are represented in Fig. 15. The results modeled by the hard lead properties agree well with the test ones until a 200% shear strain, at which the convergence problem occurs. The shear force using the soft lead in this analysis is little lower than that of the test results. The calculated horizontal forces according to the rubber material models such as Ogden and Polynomial agree well with experimental ones up to a 200% strain. There is little discrepancy of the solution accuracy between the 2D and 3D models but the computation time using the 3D model is taken to be over 10 times longer than that using the 2D model.

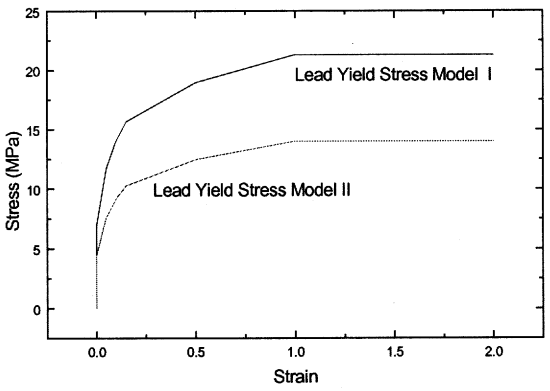

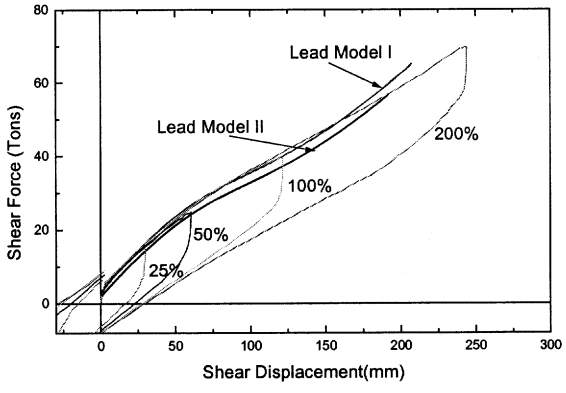

FIG. 14. Stress-Strain Curves of Lead Plug. *FIG 15. Analysis and Test Results for LRB.*

4.4 KAERI HLRB

The results for KAERI HLRB are represented in Fig. 16. In the 2D model, the analysis with the Ogden (N=3) method results in a relatively good agreement with the test results up to a shear displacement of 63 mm (equivalent to 180% shear strain). In the 3D solid model, the results using the Ogden model are closer to the test data, as in case of the 2D model. The calculated horizontal forces using the rubber material models of Ogden (N=3) agree well with experimental ones up to 300% strain. There is little discrepancy of the solutions between the 2D and 3D analyses.

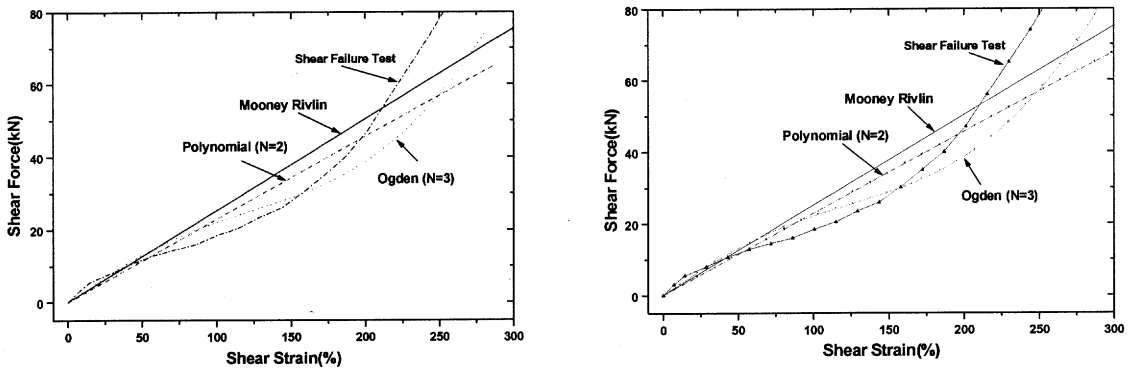

No. of Elements for a Rubber Layer :3(2D) No. of Elements for a Rubber Layer : 1(3D)

FIG. 16. Shear Forces vs. Shear Strain of Rubber Bearing.

4.5 CRIEPI isolated rigid mass mock-up

The simulation results for the shaking table tests as shown in Fig. 17 to Fig 19 of the CRIEPI rigid mass mock-up supported by scaled lead rubber bearings are obtained as shown in Fig. 20 to Fig 23 by ABAQUS time history analyses. In the analysis, the linear and bilinear hysteresis models simulating the behaviors of the rubber bearing are used. The calculated accelerations and displacements for an isolated structure under design earthquake motion (1.5S1) agree well with the test results.

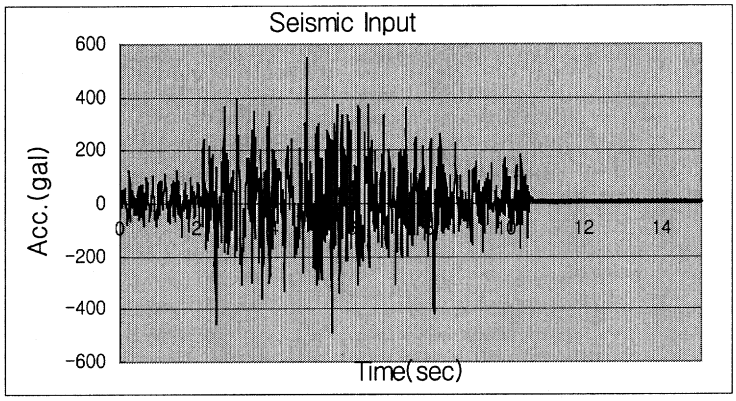

FIG. 17. Time History of Input Acceleration in Shaking Table Tests (1.5 S_1).

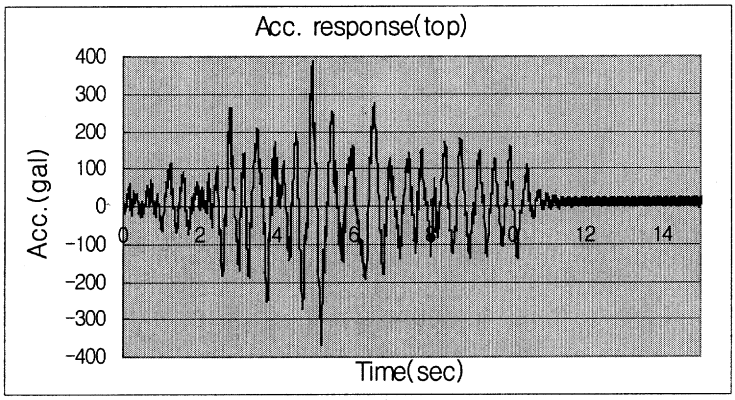

FIG. 18. Time History of Acceleration Response in Shaking Table Tests (1.5 S_1).

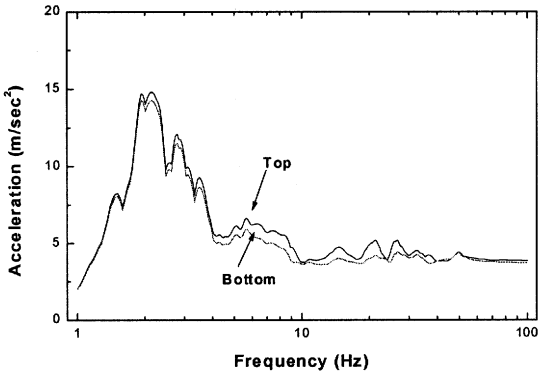

FIG. 19. Response Spectrum of Acceleration in Shaking Table Tests (1.5 S_1).

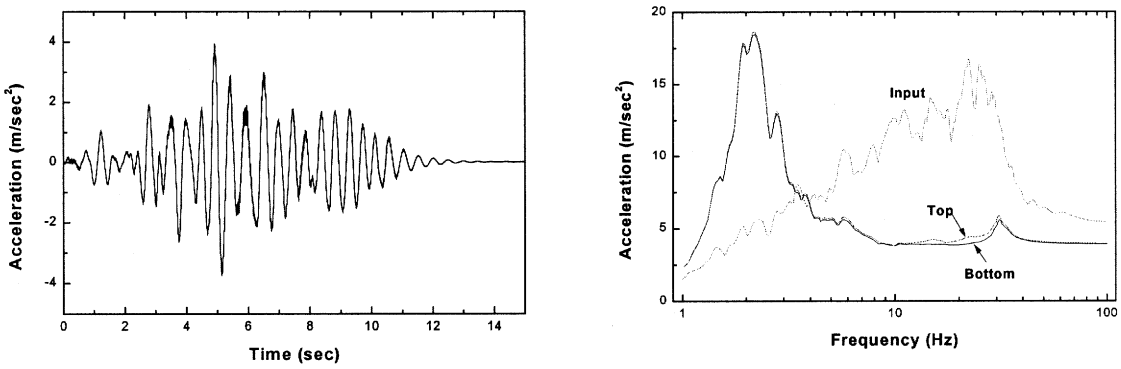

FIG. 20. Acceleration Response of Simulations for 1.5 S_1 (linear model).

For computer simulations for the shaking table tests under beyond design earthquake motion, the vertical tension stiffness and the viscous damping of rubber bearing are implemented in the model. The stiffness is 600 kgf/mm, which is roughly calculated from the vertical tension loading tests of a rubber bearing [13]. In this analysis, the vertical viscous damping of a rubber bearing is assumed to be 5%. The calculated accelerations for isolated structures under beyond design earthquake motion (4.6S1) are larger than the ones in the tests, but the calculated displacements agree well with those in tests. In this case, since the rubber bearings are in tension when a large rotational motion of mock-up occurs, the vertical stiffness of a rubber bearing greatly affects the structural responses in a high frequency region.

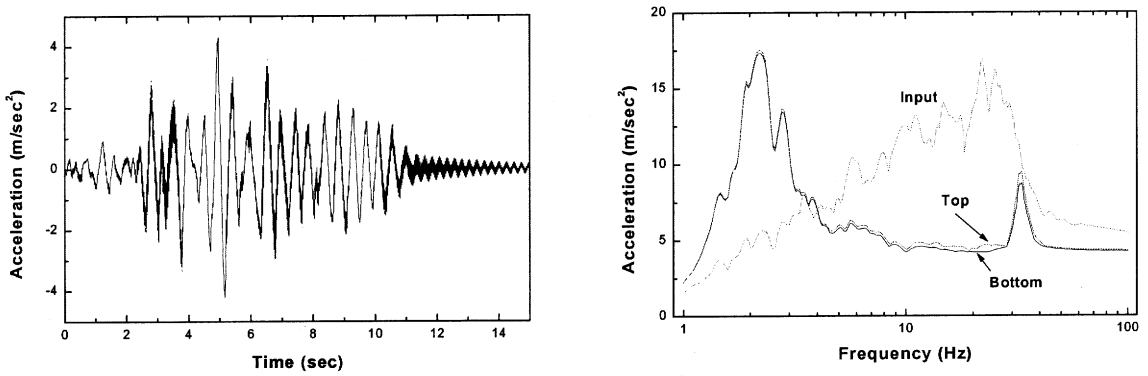

FIG. 21. Acceleration Response of Simulations for 1.5 S_1 (bilinear model).

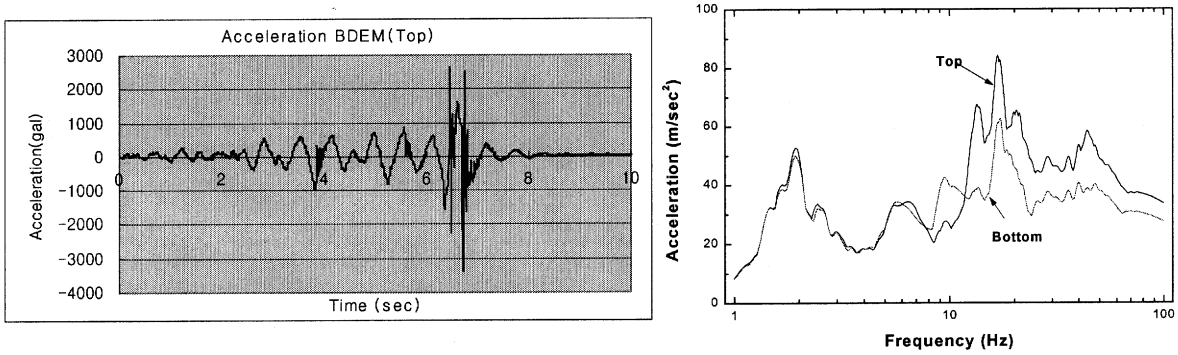

FIG. 22. Acceleration Responses in Shaking Table Tests (4.6 S_1).

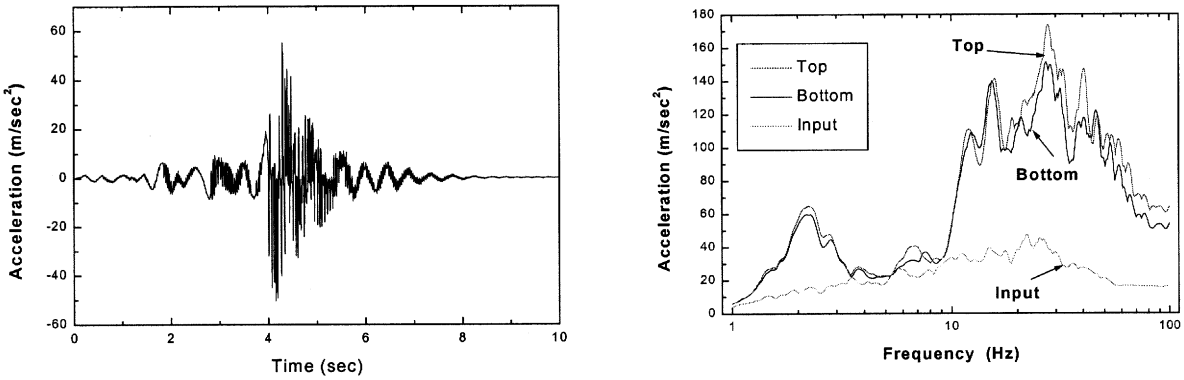

FIG. 23. Acceleration Responses of Simulations for 4.6 S_1 (modified bilinear model).

4.6 MISS structure

The calculated frequencies of the MISS structure, assuming built-in connection in the beam-column joints, do not match with the test frequencies as shown in Table 4. Specially, there are notable differences in x-direction. So, rotational spring elements in beam-column connections of 30 locations are introduced in analysis model for × and y rotations. The rotational spring constants used are $3.8 \times lO^6$ N/radian in x-rotation, and 7.5×10^5 N/radian in y-rotation. The elements of 154 and nodes of 163 are used in the analysis model.

The first and the second frequencies of the fixed structure are 1.46 Hz in x-direction, *2.37 Hz in* y-direction. The higher modes are lower than the test ones as shown in Table 5. The number of effective frequencies of the isolated model is three in each horizontal direction. The first frequency is a horizontal translation and bending mode, the second and the third is 1st and 2nd bending modes of MISS structure. The fundamental frequency for the bilinear model is 1.23 Hz, which is the combined mode of the model's initial stiffness (Kl) of rubber bearings and the 1st bending frequency of the isolated steel structure. When the rubber bearing takes a shear strain of 100%; the equivalent stiffness is 164 N/mm, the fundamental frequency becomes about 0.89Hz. So, the isolation frequency of the isolated structure varies with the bearing stiffness, which is changed as shear deformation and characterized by hysteresis curve.

The time history analysis results for Tolmezzo NS and 3BH earthquakes of y-direction are represented in Table 5. For Tolmezzo earthquake, the analysis results agree well with the test ones, but for the 3BH earthquake, the analysis results are slightly larger than the test ones. The structural displacements at node 16 are obtained by 13mm and 18 mm, respectively. These displacements are larger than the test ones by about 30%.

TABLE 4. COMPARISON THE ANALYSIS FREQUENCIES WITH TEST RESULTS

		Tests (Hz)			Analysis Results (Hz)	
	Direction	Fixed Base	Isolated	Fixed Base*	Fixed Base	Isolated
1	x	1.46	1.09	2.31	1.47	0.84-1.23
2	y	2.37	1.27	2.75	2.39	0.95-1.61
3	X	5.67		7.16	5.12	4.25
4	y	9.20		9.12	8.26	5.86
5	X	12.87		12.4	10.46	8.84
6	y	18.92		17.3	16.70	13.0
Vertical	z	-		-	12.9	12.17
Rotation	Rot-z	-		-	2.65	1.92

* Built-in connection in beam-column joints **4.6.1 Responses to Fixed Base Structure**The Rayleigh damping of 1.7% to 3.4% is implemented in the analysis model of beam and mass block because only the 1.7% damping gives divergent responses compared with the test ones. The direct time history analyses are performed for 15 seconds for the Tolmezzo earthquake, and 40 seconds for the 3BH synthetic earthquake. The time step in the direct integration is 0.005 second.

TABLE 5. ACC. & DISPL. UNDER TOLMEZZO AND 3BH EARTHQUAKES IN Y-DIR. FOR FIXED CASE

	Tolmezzo NS (T29)		3BH Synthetic (T39)	
	Analysis	Tests	Analysis	Tests
rnput-y (m/sec^2)	1.840	1.845	1.281	1.286
A01y(m/sec^2)	5.357	5.335	7.066	6.323
A13y (m/sec^2)	2.917	3.027	4.525	4.426
S16y (mm)	12.86	9.8	18.17	12.5

4.6.2 Responses to Base Isolated Structure

4.6.2.1 Response analyses for Tolmezzo and 3BH Earthquakes of Y-direction

The time history analyses for isolated MISS are performed for the same structural model as the fixed structure except the isolators. The acceleration time histories of the shaking table are

used as inputs for finite element analysis because the Tolmezzo and 3BH earthquakes show some differences with the actual shaking table accelerations.

The analysis results are shown in Fig. 24 and Fig. 25. The time histories of acceleration and displacement agree well with the tests except the high frequency contents. The zero period accelerations for Tolmezzo NS and 3BH synthetic earthquakes are shown in Table 6. The analysis results are a little lower than those of the tests, except at the location of A25y.

The respective maximum values are 33.7 mm and 51.7 mm. These values are much lower than the test ones of 42.5mm and 70mm.

TABLE 6. ACC. & DISPL. UNDER TOLMEZZO AND 3BH EARTHQUAKES IN Y-DIR. FOR AN ISOLATED CASE

	Tolmezzo NS (T135)		3BH Synthetic (T147)	
	Analysis	Tests	Analysis	Tests
Input-y (m/sec^2)	3.398	3.396	2.896	2.896
AOly (m/sec^2)	2.05	2.898	4.265	6.496
A13y (m/sec^2)	1.90	1.903	2.997	4.203
A25y (m/sec^2)	3.22	2.330	4.863	4.613
A25x (m/sec^2)	0.126	0.116	0.171	0.204
S16y(mm)	33.75	42.5	51.73	70.0

4.6.2.2 Response Analyses for Tolmezzo and 3BH Earthquakes of 3-Directions

The analysis results for 3 directional earthquake inputs are shown in Fig.26 and Fig.27, which give similar trends with those of the Y-direction analysis. The zero period accelerations for Tolmezzo and 3BH earthquakes are shown in Table 7. The acceleration responses of the analyses are a little lower than those of the test results, except at the location of A25y.

The maximum shear displacements are about 44.6mm and 25.0mm respectively. The comparison in the displacement between analysis and test shows that the analysis result is in good agreement with the test one for Tolmezzo earthquake, but much lower than the test one for 3BH synthetic earthquake.

The hysteresis curves of the shear displacements of the rubber bearings for various inputs are represented in Fig. 28 to Fig.31.

TABLE 7. ACC. & DISPL. UNDER TOLMEZZO AND 3BH EARTHQUAKES IN 3-DIRS. FOR ISOLATED CASE

	Tolmezzo (T167)		3BH Synthetic (T178)	
	Analysis	Tests	Analysis	Tests
Input-y (m/sec^2)	3.246	3.253	1.679	1.695
AOly (m/sec^2)	3.692	4.649	1.993	2.054
A13y(m/sec^2)	2.541	3.609	1.557	1.693
A25y (m/sec^2)	4.150	4.810	3.120	1.466
A25x (m/sec^2)	5.325	4.437	2.905	1.962
S16y (mm)	44.59	49.5	25.04	37.0

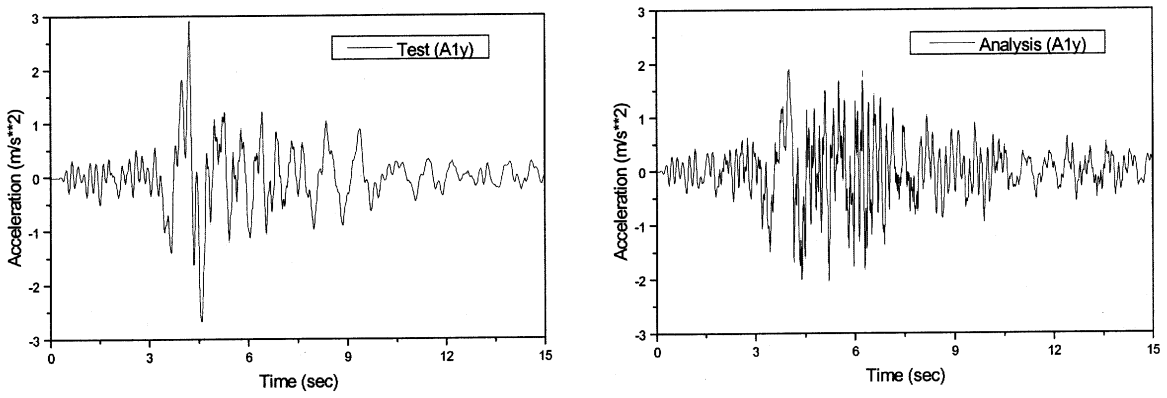

Acceleration of Top Position (A1)

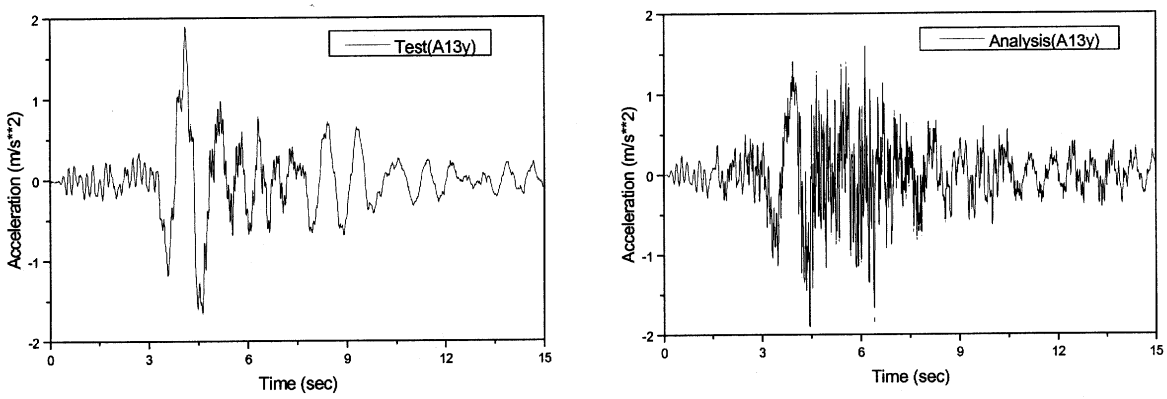

Acceleration of Middle Position (A13)

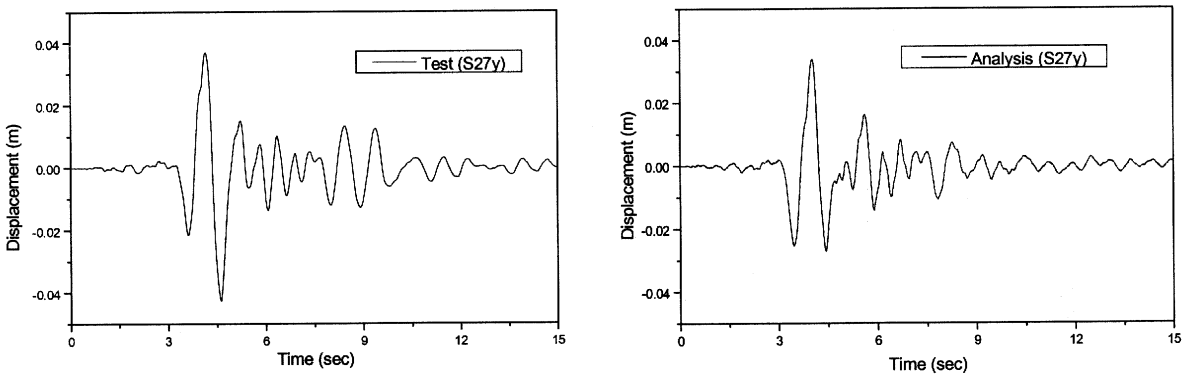

Displacement of Isolator Position (A27)

FIG. 24. Test and Analysis Results for T135 Loads.

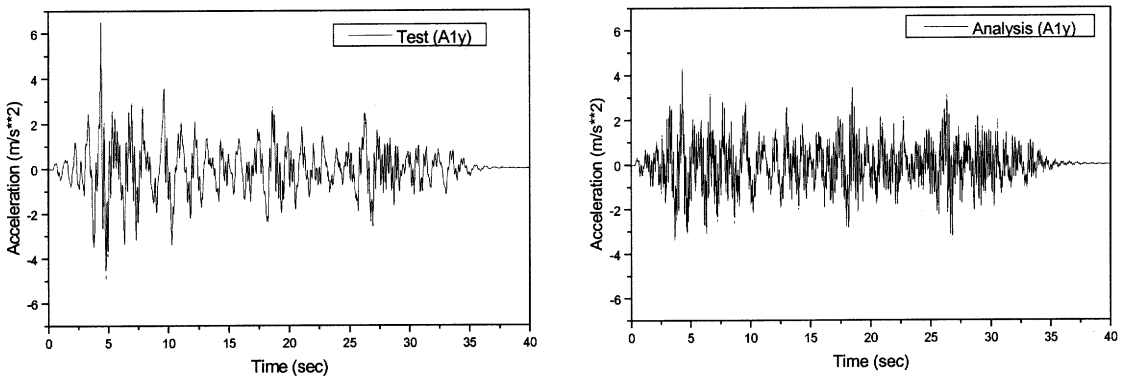

Acceleration of Top Position (A1)

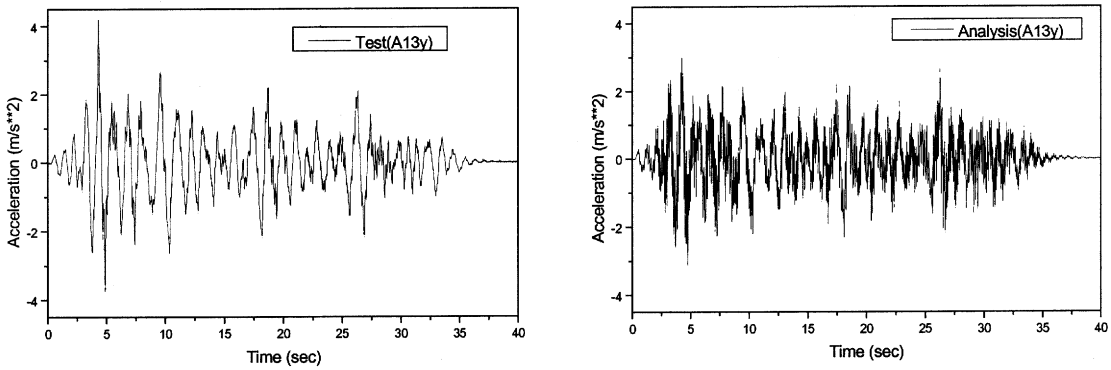

Acceleration of Middle Position (A13)

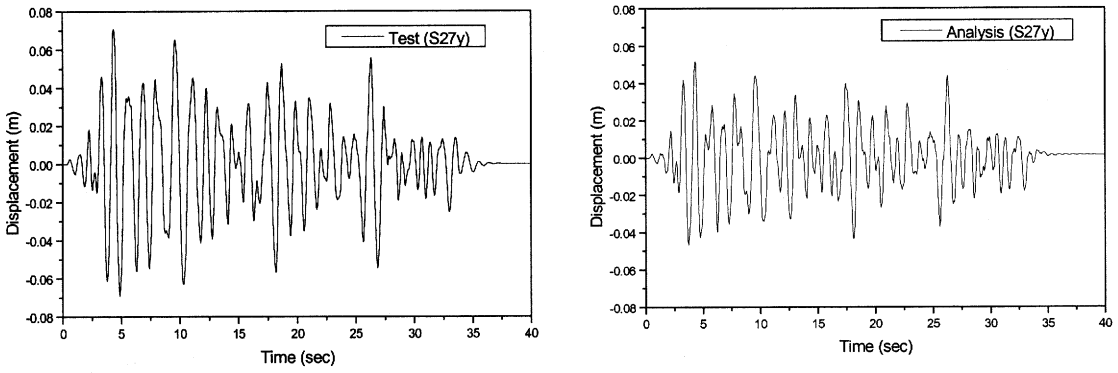

Displacement of Isolator Position (A27)

FIG 25. Test and Analysis Results for T147 Loads.

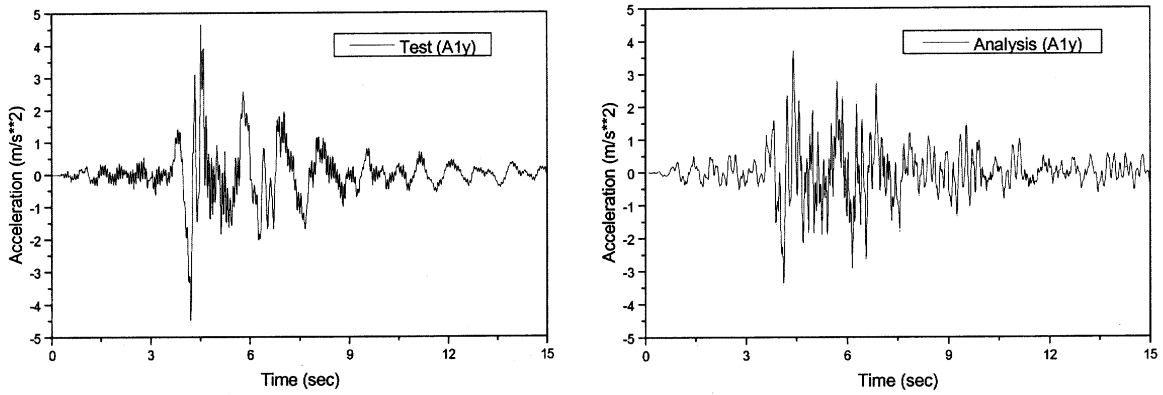

Acceleration of Top Position (A1)

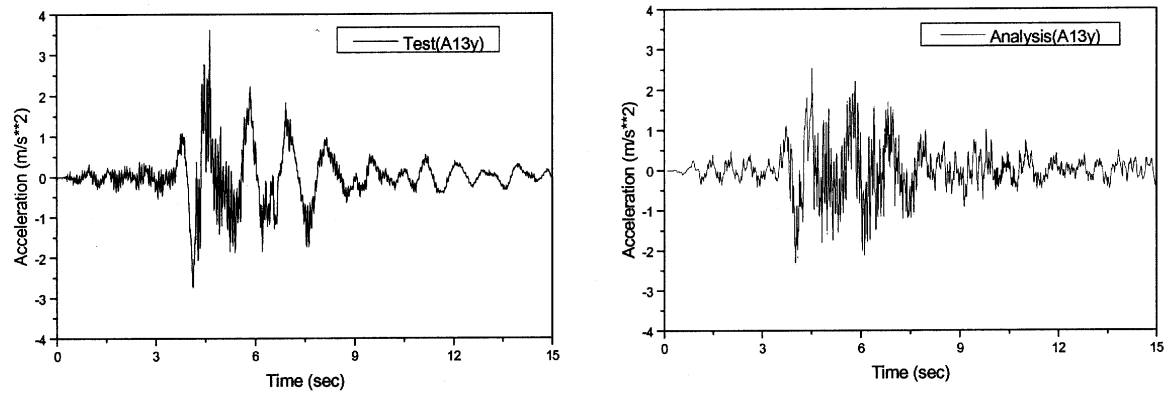

Acceleration of Middle Position (A13)

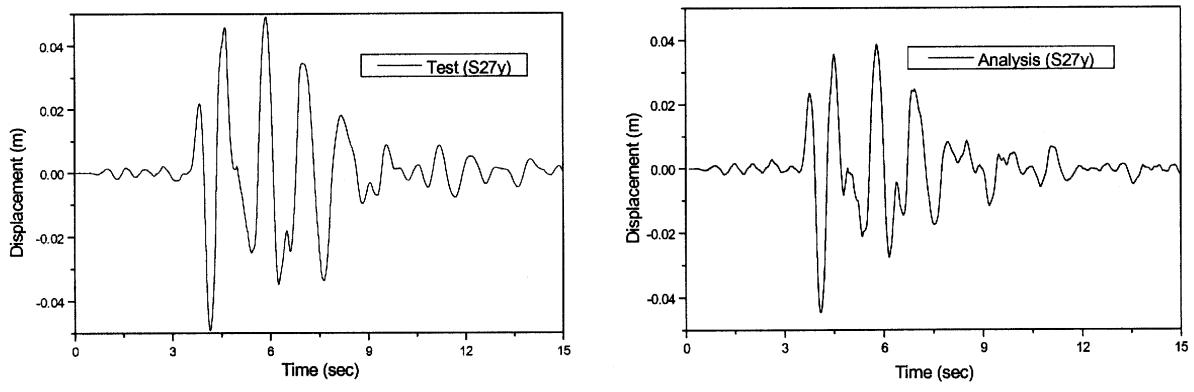

Displacement of Isolator Position (A27)

FIG. 26. Test and Analysis Results for T167 Loads.

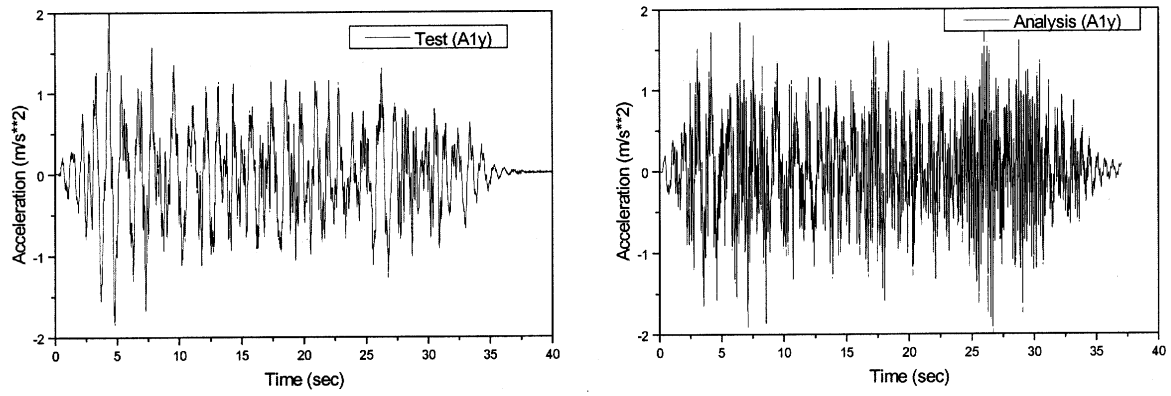

Acceleration of Top Position (A1)

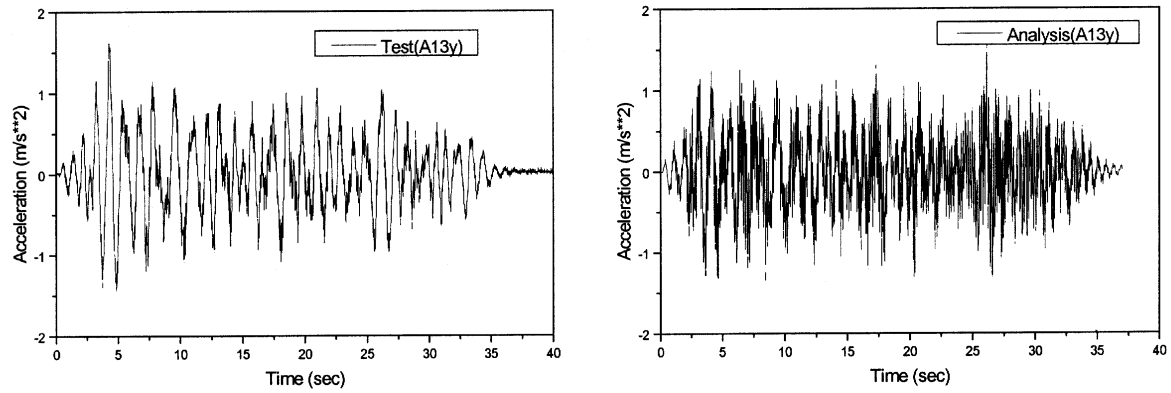

Acceleration of Middle Position (A13)

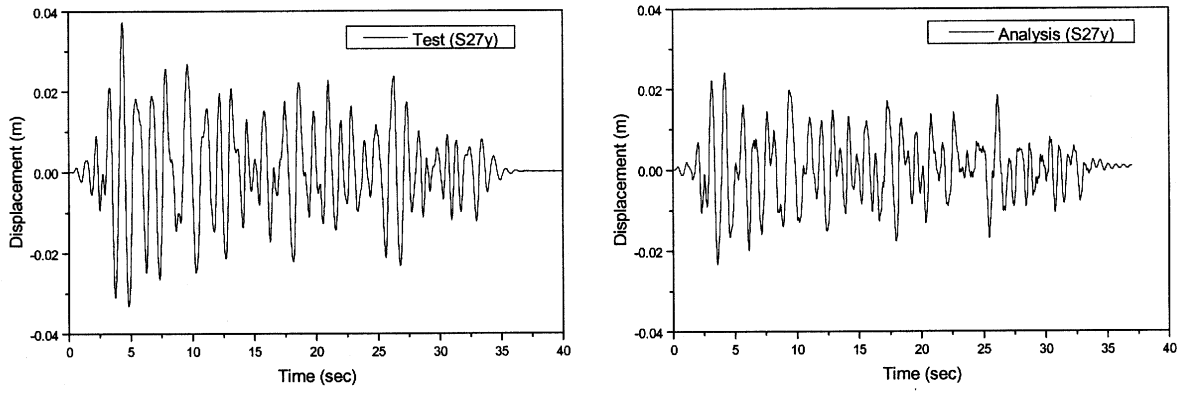

Displacement of Isolator Position (A27)

FIG 27. Test and Analysis Results for Tl 78 Loads.

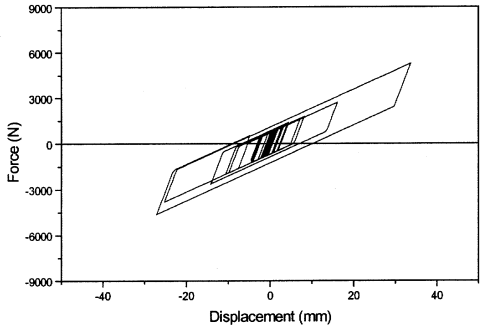

FIG. 28 Hysteresis of Shear Displacements of HLRB1 for Tolmezzo Earthquake (T135)

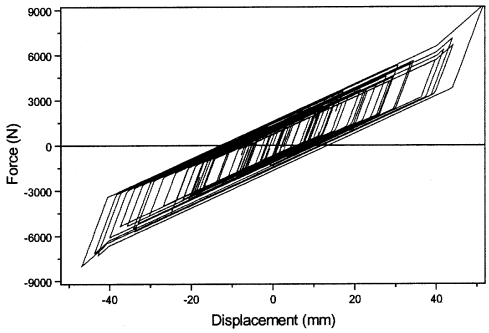

FIG. 29 Hysteresis of Shear Displacements of HLRB1 for 3BH Earthquake (T147)

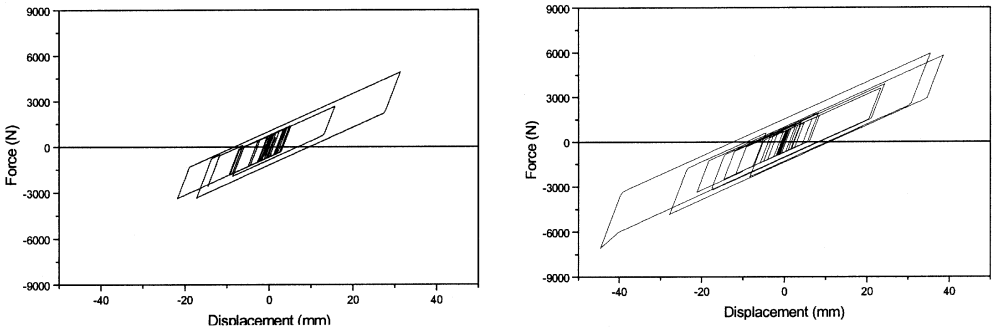

FIG. 30 Hysteresis of Shear Displacements of HLRB1 for Tolmezzo Earthquakes (T167)

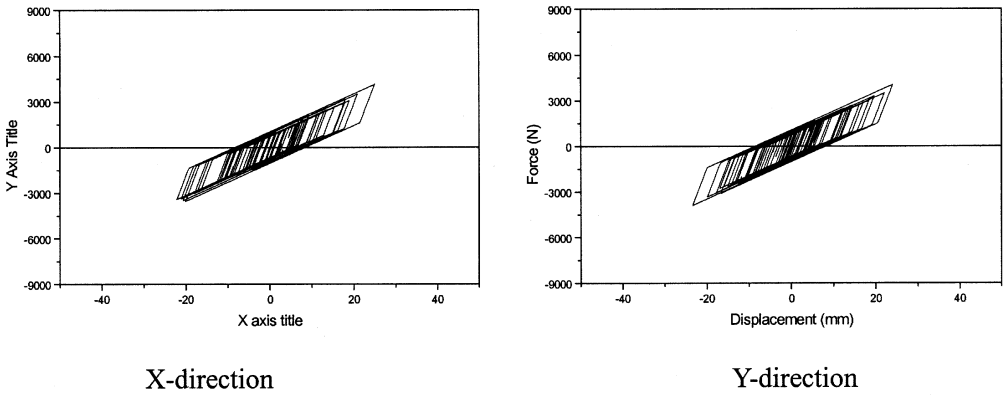

FIG. 31 Hysteresis of Shear Displacements of HLRB1 for 3BH Earthquake (T178)

5. CONCLUSIONS

For the comparison of analysis methods for isolation rubber bearings with test results, the ENEAHDRB and the CRIEPILRB are modeled and analyzed using various strain energy density functions for rubber properties and stress-strain relations for lead property. The calculated horizontal forces according to the rubber material models such as Ogden and Polynomial agree well with the experimental ones up to a 200% strain. There is little

discrepancy of the solution accuracy between the 2D and 3D models but the computation time using the 3D model is taken to be over 10 times longer than that using the 2D model. In vertical deformation analyses, at least 2 elements are required in thickness direction to get accurate results. But in the horizontal deformation analysis, the number of elements has little effect on the results. Up to the 200% shear strain, at which the convergence problem occurs, the shear force results modeled by the hard lead properties follow the test results better than those by the soft lead ones.

For the comparison of analysis methods for isolation rubber bearings with test results, the KAERI HLRB are modeled and analyzed using various strain energy density functions with respect to rubber properties. The calculated shear forces using the rubber material models of Ogden (N=3) agree well with test ones up to 180% strain. There is small discrepancy of the solutions between the 2D and 3D analyses.

In general the results of the analyses for the isolation bearings demonstrate that rubber test data obtained from the various coupon tests can be used to predict nonlinear behavior of an isolator up to some strain range when appropriate energy density functions are selected. But for the extremely large strain range, current coupon tests should be improved more.

For dynamic simulations for shaking table tests of a rigid mass mock-up, the linear and bilinear models are implemented in the modeling of shear-deformation hysteresis curves of scaled lead plugged rubber bearings. The calculated accelerations and displacements for isolated structure under design earthquake motion (1.5SO agree well with test results. The calculated accelerations for isolated structures under beyond design earthquake motion (4.6Si) are larger than those in tests, but the calculated displacements agree well with those in tests. In this case the vertical stiffness of rubber bearing greatly affects the structural responses in a high frequency region.

For the dynamic simulations of shaking table tests of MISS mock-up, the modified bilinear models are implemented in the modeling of shear-deformation hysteresis curves of the HDRBs used for the tests. The calculated accelerations and displacements for fixed structures for Tolmezzo and 3BH earthquakes somehow agree well with test results. The calculated accelerations for an isolated structure under Tolmezzo and 3BH earthquakes are smaller than the tests in the upper structure, and also the calculated displacements are also smaller than those in the tests.

The analyses give smaller acceleration and displacement responses, but much higher frequency contents compared with the tests. So, it is supposed that the structural stiffness of the isolator, modeled by a modified bilinear model based on shear strain test data of rubber bearings, is larger than the actual stiffness existing in rubber bearings during seismic excitation tests.

Two dynamic simulations for shaking table tests verified that analysis methods can be used for the applications of seismic base isolation to nuclear structures to have great benefits by reducing the seismic responses in the isolated structures.

RECOMMENDATIONS

Further researches are recommended in the way how to handle the energy function where the information of strain energy function is insufficient because of limited test results, in dealing the proper damping models for calculating the structural responses. And a three dimensional passive isolation system should be considered more deeply to reduce vertical responses of an

isolated structure, which would be amplified when a horizontal isolation system be used.

Therefore another 3-years CRP is strongly recommended to improve the methodologies and to focus on the three dimensional isolation systems.

Shared and improved knowledge through IAEA CRM international cooperation in this field surely provides confidence in the application of seismic isolation technology in nuclear facilities, an enhancement of the seismic safety of nuclear structures, and economic benefits through the standardization of seismically isolated nuclear plants.

ACKNOWLEDGEMENT

This work was performed under the financial support of the Ministry of Science and Technology of Korea and IAEA.

REFERENCES

[I] YOO, B., LEE, J.-H., KOO, J-H.,IAEA Research Co-ordination Meeting (RCM) on "Intercomparison of Analysis Methods for Seismically Isolated Nuclear Structures," St. Petersburg, Russian Federation (1996).

[2] ABAQUS User's Manual for Revision 5.8, Hibbit, Karlson & Sorenson Inc.(1998).

[3] YOO, B. and LEE, J-H., "Intercomparison of Analysis Methods for Seismically Isolated Nuclear Structures (ENEA HDRB and CRIEPI LRB), The 13th International Post-SMiRT Conference Seminar on Seismic Isolation, Passive Energy Sissipation and Active Control of Seismic Vibration of Structures, Taormina, Italy, August 25-27,(1997).

[4] YOO, B., LEE, J.-H., KOO, G-H., IAEA Research Co-ordination Meeting (RCM) on "Intercomparison of Analysis Methods for Seismically Isolated Nuclear Structures (KAERI HLRB and CRIEPI Isolated Rigid Mock-up)," 3rd IAEA RCM, UK, May 26-27, (1998).

[5] YOO, B., LEE, J.-H., KOO, G-H., IAEA Research Co-ordination Meeting (RCM) on "Intercomparison of Analysis Methods for Seismically Isolated Nuclear Structures (Model of Isolated Steel Structures, MISS)," 4rd IAEA RCM, Cheju,Korea, Auguest 23-27, (1999).

[6] YOO, B., LEE, J.-H., KOO, G-H., Study of Reduced Scale Model Test Results of High Damping Laminataed Rubber Bearing for Liquid Metal Reactor, KAERI/TR-539/95, (1995).

[7] Geometrical, Mechanical and Experimental Data on MISS (Model of Isolated Steel Structure).

[8] SEKI,W., et al., "A Large-Deformation Finite Element Analysis for Multi-layer Elastomeric Bearings," 133th American Chemical Society, Montreal, Canada (1987).

[9] Private Communication in CRIEPI (1997).

[10] YOO, B. et al, Seismic Isolation for Nuclear Reactors in Korea, 13th International POST-SMIRT, Santiage, Chile (1995).

[11] ISHIDA, K., 1991, "Recent research and development activity in Japan," llth SMiRT post conference seminar on seismic isolation of nuclear and non-nuclear structures(pp.l83-240), Nara, Japan, August 26-27.

[12] HOFFMAN,W., Lead and Lead Alloys, Springer-Verlay, Berlin (1970).

[13] HIRATA, K., Experimental Results and Simulation on Isolation Rubber bearing Tests and Shake Table Tests, 14th International POST-SMIRT, Sicily, Italy (1997).

3-D PNEUMATIC SEISMIC ISOLATION OF NUCLEAR POWER PLANTS

V.S. BELIAEV, V.V. VINOGRADOV, V.V. KOSTAREV,
V.P. KUZMITCHEV, S.A. PRIVALOV, V.A. SIRO, I.N. KRYLOVA,
A.A. DOLGAYA, A.M. UZDIN, A.V. VASILIEV
Research Center of Fundamental Engineering,
CKTI-Vibroseism, St. Petersburg, Russian Federation

Abstract

This paper describes the work carried at the Russian Federation Research Center of Fundamental Engineering (RCFE), in development of innovative pneumatic multicomponent low-frequency seismic isolation bearings for advanced nuclear power plants.This device incorporates both supporting spherical elements, which provide displacements in the horizontal direction, and pneumatic dampers with rubber diaphragms for displacement in the vertical direction. To decrease the relative displacements of the isolated object the system uses viscoelastic dampers. Damping devices had been specially elaborated for the reactor building seismic isolation system as a result of substantial advances in the design and operation of the HD-type hydrodampers, created at the CKTI VIBROSEISM. The procedures developed have been used for comparison of the test and computer data on model isolated steel structure (MISS) and isolated rigid mass (IRM) isolators produced by ENEA and KAERI. Most recent work has concentrated on the development of mathematical models of isolators and isolated nuclear structures. Force-deformation characteristics of the HDRB model had been calculated on the basis of a special method of non-linear elastic theory using the continual transformations method.

1. INTRODUCTION

For the last few years specialists from different countries have been developing a concept, which should balance conflicting tendencies in seismic designing of nuclear facilities: safety, which is to be guaranteed, ambiguity of earthquake prediction, standardization of components as well as technical and economic indices. Application of seismic isolation systems can be considered as such a concept. Among the seismic isolation systems three main types can be identified: horizontal isolation of a nuclear structure as a whole; hybrid system, in which the structure is isolated in horizontal direction and the reactor pit is isolated in vertical direction, and global three-dimensional (3D) isolation in both horizontal and vertical directions. Under this conditions the earthquake loading decrease is ensured due to reducing the resonance effects in both equipment and building constructions under the earthquake condition. Choice of a certain type of seismic isolation system and seismic isolation devices essentially depends on the peculiarities of seismic input on a NPP site. Taking into account these peculiarities when predicting the earthquake is a rather complicated problem. Analysis of data of the latest destructive earthquakes had shown that earthquake prediction for a given site in many cases involves large errors in determination both the ground motion amplitude and frequency content, as well as the correlation of its vertical and horizontal component rates. 3D seismic isolation systems are less sensitive to earthquake prediction accuracy. This condition has defined the expediency of such systems development, in spite of the fact that their structure is more complicated as compared with horizontal seismic isolation systems.

The amount of recently well-known designs of three-dimensional seismic isolation systems to be applied in nuclear structures includes the developments of Swiss, German, US,

Japanese and Russian specialists. In the Swiss system [1] slab supports made of natural rubber are installed between the lower and the upper base. Stability of the isolated facility position under normal operation is ensured with the aid of elements made of glass reinforced plastic, which would collapse under earthquake loading. In the seismic isolation system of GERB Company, Germany [2], spring isolators with piston viscous dampers are used. While developing a perspective modular NPP of SAFR-type in USA the possibility to create a global seismic isolation with the help of low-module high-damping laminated elastomeric supports has been under consideration [3]. The supports are flexible in both horizontal and vertical directions. In the 3D isolation system of FBR reactor building foundation, which is under development in Japan [4], the horizontal isolation is ensured by laminated rubber supports which are located on the intermediate plate. Vertical isolation is provided with high pressure pneumatic dampers installed under the intermediate plate. This way seismic isolation system responses along the directions of seismic input are separated.

In Russian multicomponent seismic isolation system for the WWER-640 NPP reactor building [5] pneumatic cinematic supports are used together with viscous dampers. Natural frequency of the system in horizontal direction is 0.1–0.2 Hz, in vertical direction 0.3–0.4 Hz. The use of additional dampers permits to provide for design limitations on the amplitude of isolated building relative displacements while preserving the essential decrease of earthquake loading. The system as a whole extends the feasibility of standard NPP design to the regions with increased seismicity.

Up to now development of seismic isolation system is finalized for type design of NPP with WWER-640, a start had been made on the design and construction of the object-representative of this seismic isolation system on the construction site of a pilot NPP unit in vicinity of St.Petersburg. As a demonstration object provision is made for construction of a seismic isolated cylindrical tank, designed for technological water release from the reactor. Mass-dimension characteristics of the tank are as follows: diameter–23.0 m, height — 13.0 m, weight ~ 6000t. These conditions have defined the necessity of further development of analysis methods of seismic isolated nuclear structures. Analysis methods make up the basis for detailed optimization of the procedure of choosing the optimal structional design of seismic isolated object with the use of a complex of dynamic, technical and economic criteria for the specific conditions of the construction site. Development of analysis methods assumes abandoning the earlier accepted simplifying assumptions, among the other things, on the absolute stiffness of the base slabs. It is especially important for the case of soft soils of the foundation structure of the object-representative. It is to be noted, that accounting for the base slab deformability eventually permits to formulate the requirements to the structure of seismic isolators and to receive the value of extreme tolerance when installing their support elements. A property of seismic isolators to adapt to possible non-collinearity of support elements takes on great importance for provision of dynamic efficiency and stability of static position of the seismic isolated structure.

2. THE STATE OF THE ART OF EXPERIMENTAL AND ANALYTICAL WORK IN THE FIELD OF NUCLEAR SEISMIC TECHNOLOGY

2.1. General systems of seismic isolation

Depending on their designation: seismic isolation of an object as a whole (for example, a reactor building), separate rooms, responsible equipment and engineering communications, the means of seismic isolation can be considered as general, group and local ones.

Taking into account the distinctions in inertial and dimensional characteristics of the objects to be protected, and the level of their seismic stability in seismic isolation systems several types of seismic isolators could be applied.

At present in Russia we have stock-produced supporting pneumatic and pneumatic hydraulic isolators of different load-carrying capacity, used in low-frequency systems of seismic isolation. Usually, it is a block of seismic isolators which consists of a common steel part and a set of seismic isolators. This common steel part ensures horizontal displacement, and the seismic isolators ensure vertical displacement. Depending on the number of the seismic isolators in the block its load-carrying capacity varies from tens of tons to thousand tons. Application of seismic isolation for protection of the most responsible equipment, including the equipment of localization systems, has several special features, related to the opportunity of selective damping of seismic reaction components of bearings in the required frequency area. Under such conditions it is possible to use devices with lower load-carrying capacity on the basis of stock-produced pneumatic and elastic-plastic isolators.

General systems of seismic isolation of nuclear power plant facilities ("nuclear island" as a whole, reactor building, reactors of different types), are based on using, mainly, rubber or steel rubber isolators and are intended for decreasing the horizontal component of seismic effect. To make the universality of such a structure more full in Russia for the new-generation enhanced-safety mean-power NPP (WWER-640) we use effective multicomponent low-frequency system of seismic isolation designed for seismic response with an acceleration up to 0.5 g. This system is to be placed below the reactor building slab (Fig. 1).

This seismic isolation system which we discuss here is based upon the use of pneumatic dampers of original design. The pneumatic dampers in question are combined into seismic isolating devices, which are installed on the foundation of the structure between the lower and the upper base slabs. Arrangement of seismic isolation facilities on the foundation mat is subject to the structural features and stiffness characteristics of the structure, as well as to condition of uniform loading of the facilities. In this case between the building base slabs an interlayer is formed which is vertically and horizontally compliant and isolates the reactor building against seismic wave propagation. Technical characteristics of the seismic isolation system for the NPP WWER-640 reactor building are as follows:

Seismic input	- up to 0.5 g
Mass of the superstructure	- 75000 tons
Number of seismic isolation facilities	- 90–100
Load capacity of each facility	- up to 900 tons
Design structural motions (displacements) of the facilities	
in vertical direction	- 200 mm
horizontally in any direction	- 300 mm
Natural mode frequencies	- 0.2–0.3 Hz
Load attenuation factor	- 20–30

As is well known, under the conditions of long-period seismic effect of deep-focal earthquakes the structure with low-frequency seismic isolation system commits large relative displacements. To decrease them the NPP in question is provided with additional viscous-liquid dampers whenever necessary.

The calculations which were completed using state-of-the art technique have shown that application of the proposed low-frequency multicomponent seismic isolation system leads to sharp decrease of loads on each story of a building (10–30 times) in comparison with the values realized in the damper-free modification.

Thus in highly seismic regions it is possible to use either non-seismic or low-reinforced equipment. This possibility reduces common costs of NPP construction considerably keeping valid the strict requirements imposed on its reliability.Relative displacements for the reactor building with WWER-640 under earthquake with acceleration 0.5 g were in the worth case 400 mm and 120 mm in vertical and horizontal directions respectively. Angular rotation of the block in vertical plane did not exceed 0.0015.The important feature of the system in question is its weak dependence on frequency characteristics of the design seismic load within a range from 0.6 Hz and higher. It is the most saturated part of the spectrum of seismic ground motions. This situation defines a weak effect of accuracy of seismic prognosis on the efficiency of seismic load decrease.

Nowadays, when designing liquid-metal reactors, the blocks of approximately 140 MW are used. Because of this, as a rule, their placement in mine-type shallow deposition is under consideration. Modular construction of BN-type reactors, which are placed in underground mines, facilitates solving the problem of building seismic isolation. Compactness of reactors and relatively small mass create favorable conditions for development of universal structure, non-critical to seismic effect.

Considering the embedded location of reactor a relatively high-frequency area (2–10 Hz) prevails in input spectrum. In this case the most effective is application of low-frequency seismic-isolation devices, ensuring free running frequency of isolated building in the range of 0.3–0.4 Hz. As such devices we can apply supporting pneumatic-cord or pneumatic-hydraulic isolators with load-carrying capacity of 200–400 tons. Placement of supporting isolators on the level of the reactor center of mass permits to ensure its high stability during vibrations of the system and, respectively, small angular vibrations.

It is quite evident, that selection of particular type of general seismic isolation system depends on many factors, the main of which is consideration of the seismic and geological state of a construction site, as well as cost considerations. In some cases, for example, if there is a deep layer of soft soil it is more expedient to apply a single-component seismic isolation system to decrease the prevailing horizontal component of the earthquake effect.

In Russia we have developed a series of similar systems with sliding supports, dynamic columns, steel rubber bearings, dry friction damping devices. Along them it is to be noted a new hydraulic and frictional system of general seismic isolation, in which the gaps between the upper and the lower base slabs are filled with thin layer of fluid. Fluid is under adjustable hydrostatic pressure, and the initial state of layer is ensured with the aid of flexible membrane, installed at the foundation edge. Such a system appears to be effective if the NPP construction site has weak soils and permits to diminish the soil pressure by increase of dimensions of the base slab at uniform load distribution.

2.2. Group and local systems of seismic isolation

For protection of NPP facilities and equipment nowadays in Russia we apply systems of group and local seismic isolation. Thus the domain of primary use of various seismic isolation systems is determined by their designation, namely:

- systems of group seismic isolation are intended for protection of the equipment which is located, as a rule, in one building or in its part;
- systems of local isolation are used for protection of one or several units of equipment, predominantly process-related blocks.

For nuclear facilities there is developed a series of damping devices, which can be used for creation of systems, ensuring the required degree of equipment protection. The systems which are most extensively developed from the structural point of view and had been put through experimental tests are the systems of group seismic isolation with spring devices, power parameter of which is formed due to compression and shear elastic strains of the spring.

When solving the problem of group isolation we can use suspended and supporting bracings of isolated and protected structures. In suspension systems the structure (platform) is attached to building construction elements: floors, walls, columns with the aid of flexible (cables) or rigid (links) connections. Attachment of these connections to seismic isolators is performed with the aid of hinges, blocks and other mechanical units. The suspension is made with the help of links, in which the units, that sustain the loads perpendicular to their deformation axis are used. Otherwise a cable suspension is applied. In the schemes a preliminary tension is realized and additional damping of horizontal vibrations of the structure due to energy dissipation in cable suspension elements is ensured. In supporting systems the installation of platforms is carried out with use of various rolling bearings, which create resetting force acting on the structure. Arrangement of support units on the structure depends on the location of load-carrying elements, building configuration, as well as isolated building geometry. Selection of support units layout is determined by total weight of protected equipment and platform, load-carrying capacity of units, as well as maximum conceivable height of main platform beams. Attachment of the suspension members to the structure is carried out as follows:

- rigid fixing of seismic isolator casing. Attachment unit is high-reliable: load from the structure is transferred directly to isolator, there are no transitional members in tension, compression or bending;
- seismic isolator or suspension members are attached by umbilical doweled connections (threaded connections or with the aid of axis) to construction-welded jacking adapters.

Attachment of suspension to building constructions is carried out with the aid of brackets, installed on pins of embedded pieces. Embedded pieces are predominantly of the following type:

- anchor pins, projecting from floor or covering;
- beyond-anchor steel-iron plate, to which the adapter plate with tapped pin holes is welded.

When the platform center of gravity doesn't coincide with the center of stiffness of seismic isolation systems balancing of the structure is to be carried out. The purpose of this balancing is horizontal installation (suspension) of the structure in horizontal position. As isolation devices for local seismic isolation systems we mainly use all-metal units with elastic plastic operating elements. These units are 3D (six-axis) isolators, operating elements of which are performed as space-located curvilinear rods. During the load input this curvilinear rods experience elastic plastic deformations, ensuring substantial decrease of transmitted dynamic loads due to active energy dissipation on sections of plastic deformation.

When designing local seismic isolation systems there are allowed various layouts of protected equipment. Thus "symmetrical" layouts, in which it is possible to align the center of gravity and the center of system stiffness are preferable. Selection of one of these schemes is determined by mass-dimension characteristics of protected equipment and peculiarities of building structural layouts, where this equipment is located. Depending on the aspect ratio we distinguish low, average and high equipment. For the low and average equipment damping the most widely used are suspended and (or) supporting schemes. For protection of high equipment supporting and stopping, supporting-spacer and console suspension schemes are used. When selecting the suspension scheme it is required to take into account the possibilities of isolators attachment to equipment, which, in main, are determined by:

- design of equipment and utility systems;
- operational requirements;
- requirements on installation;
- aspect ratio of equipment and seismic isolators.

Modes of attachment of the isolator to bearing elements are conditioned by:

- requirements on arrangement of equipment in rooms of buildings;
- characteristics of layout of the building, in which the equipment should be installed;
- limitations on building utilities layout and their supply to equipment;
- availability of embedded pieces and opportunity of their installation.

Selection of structural approaches to seismic isolation which can ensure protection of the equipment is carried out in accordance with requirements of industrial Norms and Standards.

Procedure of seismic isolation selection and design as a rule is multistage. It incorporates the stages of preliminary selection of facility parameters, design assessment of dynamic efficiency of system, selection of structural layout and refined calculation. Thus, taking into consideration the results, received on various stages, necessary correction and verification of parameters of system are carried out: stiffness and inertial characteristics of isolated building, power specifications of units, conditions of equipment placement and fixing.As initial data for realization of selection procedure the following information is required:

1. Data on possible effects:

- parameters of building motions, presented as time dependencies on acceleration, speed and displacement of equipment installation positions;
- ratio of effects, possible temporary intervals between them.

Parameters of motion can be specified in analytical or table form with a step not more than 0.1–0.2 of the minimum duration of separate input half-waves or in the form, suitable for direct computer input from data carriers (magnetic tapes, drums, floppies, hard disks etc).

2. Data on the protected facility:

- geometrical and inertial parameters of protected facilities;
- preliminary layouts (equipment arrangement scheme) with indication of possible gaps for seismic isolation placing and functioning;
- coordinates of attachment of engineering utilities (cable links) and information on their elastic-dissipate characteristics;
- values of building seismic stability when fixed according to specifications, as well as the data on resonance frequency of equipment;
- information on disturbing forces and moments, created by operating vibration-active equipment (if it is available).

As a criteria for dynamic seismic isolation efficiency we use the relation between the required and the actual seismic stability. Data on the actual seismic stability are given in corresponding literature or are determined experimentally. Values of required seismic stability are determined at seismic isolation dynamics design under the conditions of seismic input.

2.3. Characteristics of seismic isolation system

2.3.1. Seismic isolation device

When performing this work two versions of layout and arrangementsof a seismic isolation device were under consideration:

- Version 1 — Supporting spherical seismic isolation device with pneumatic dampers.
- Version 2 — Supporting spherical seismic isolation device

Seismic isolation device (Version-1) ensures the isolated structure displacements in any vertical and horizontal direction. The load capacity of the device is determined by the load capacity of vertical pneumatic dampers with rubber-cord diaphragm.

Seismic isolation device (Version-2) ensures the decrease of isolated structure displacement in vertical direction. The load capacity of the device is determined by the level of specific contact loads on the supporting spherical surfaces of the plates. General view of the seismic isolation device (Version-1) is presented in Figs 2 and 3. Seismic isolation device is a unit which contains a central guiding strut with a supporting element of a telescopic-cylinder shape and five rubber-cord pneumatic dampers located around the strut. The pneumatic damper casings are fixed on the outer cylinder flange of the guiding strut, and the plungers are fixed on the internal cylinder flange of the guiding strut. In the internal cylinder chamber of the central telescopic strut the sixth pneumatic damper with step force characteristic is located. The main parts of the pneumatic damper are casing, plunger and rubber-cord diaphragm. Displacement of the pneumatic damper plunger relative to the casing is followed by roll-over of the rubber-cord diaphragm in the gap between the casing and the plunger. When the load to the damper changes its design provides for plunger movement relative to the casing due to a change of pressure inside the casing and the elastic properties of the rubber-cord diaphragm. When the plunger moves in compression of the damper the pressure inside the casing increases, when the plunger moves in tension — it decreases.

Normal force of the pneumatic damper (load capacity) is determined by the diaphragm rated pressure and effective area. When the damper works in compression as a part of seismic isolation device the plunges of all six pneumatic dampers move thereby ensuring the change of pneumatic damper inner space and pressure. When working in tension the central pneumatic damper plunger in the initial position is butted up against the rigid stop inside the damper and does not participate in the further motion in tension. Thus, five dampers located around the central strut work in tension/compression of the seismic isolation device and ensure monotonous force characteristic. The central damper remaining in the framework of the basic approach, which is common for all pneumatic dampers, has some structural peculiarities, which ensure the step force characteristic of the seismic isolation device.

Seismic isolation device design incorporates five dampers with monotonous characteristics and one damper with step force characteristic and permits to create a seismic isolation system, in which all seismic isolation units display step force characteristic. Thus, this design of isolators ensures free motion of the superstructure under the action of seismic forces in all directions (vertical and horizontal) with return to the initial position when the action is over.

Supporting elements of the central guiding strut are performed as spherical plates and base plates. The centers of sphere radiuses are biased relative to the guiding strut axis. Overall dimensions of the plates are chosen under the condition that ultimate displacements in horizontal direction are equal to 800 mm. Due to rotation of the strut along the spherical surfaces of the base plates the seismic isolated structure moves in horizontal direction. Spherical supports of the strut are fixed on the base plates by means of a hinged bar, preventing the spherical plates from sliding along the base plates. For the isolated structure to be fixed in the initial position (in the horizontal plane) a central part of the spherical plate is flat. Rubber-cord diaphragm of each pneumatic damper is performed on the basis of stock-produced rubber-cord diaphragms, which had undergone a whole cycle of manufacturing, tests and operation on the production-type objects.

Pneumatic damper is filled with gas (compressed nitrogen) with the aid of a special device which is to be installed on the damper filler. This design of a seismic isolation device allows to use central struts as an erection support. Technical data on seismic isolation device (Version-1) are listed in Table 1. General view of the supporting spherical seismic isolation device (Version-2) is presented in Fig. 4. Supporting spherical device incorporates a rocking-type strut, supporting spherical plates, welded casing flanges and stiffening elements: ribs and shells. Supporting spherical plates are fixed on the casing with flanges and bolt joints. Overall

dimensions of the plate are chosen under the condition that ultimate displacements of the superstructure in horizontal direction are ~800 mm. The proposed design of pneumatic dampers allows the superstructure to move vertically within the limit of 10 mm and gives the dampers elastic characteristics of "air spring".

The base plates are fixed on the rocking-type strut casing with hinged bars, thus preventing the spherical plates from sliding along the base plates. Rotation of the telescopic strut allows the superstructure to perform horizontal movement. Horizontal force trying to bring the isolated unit back to its initial position arises due to the vertical response displacement on the opposite ends of the rocking-type strut when it tilts. Spherical plate has a flat area, which permits to receive the step force characteristic of seismic isolation device in horizontal direction. All vendor units, which are used in this seismic isolation device, are designed and produced on industrial enterprises of Russian Federation. Technical data on seismic isolation device (Version-2) are listed in Table 2.

2.3.2. Damping device

In the superstructure seismic isolation system the HD-type damping devices designed in CKTI VIBROSEISM are used. Fig. 5 presents a damping device of this seismic isolation system which consists of a casing, filled with viscous service fluid, a piston and a core, which are immersed in this fluid. To provide for the required characteristics between the casing and the piston additional elements are installed, which in this version are made as thin-walled cylinders. In order to prevent foreign matters and media (water, decontamination solutions, etc.) ingress into the fluid an elastic protective jacket is provided, which is attached to the piston and casing with the help of clamps. The casing is attached to the base, and the piston — to the isolated structure, which is to be protected against dynamic loads under vibration, seismic or other effects. The damper works as follows. Horizontal, vertical and angular impacts are transferred to the piston and cause viscoelastic deformation of the service fluid in the space between core, piston, thin-walled cylinders and the casing. As a result a damping force arises which counteracts the piston displacement. Number of additional elements (thin-walled cylinders) can be changed to achieve the necessary damping value. When the height of piston immersion into the service fluid changes, the core, remaining on the casing bottom, practically does not change the piston operational height. The damper preserves its efficiency in all directions both at small and large amplitudes of impacts, which are comparable with the values of the gaps between the piston and the casing. The dampers ensure the resistance force up to 250 t in all directions.

2.4. Experimental investigations of devices

Pneumatic damper with a rubber-cord diaphragm (Fig. 6), which is similar in design to the damper recommended for SIS, had been developed by the Special Engineering Design Office (St. Petersburg) together with Research and Industrial Enterprise "Progress" (Omsk-city) and is serially produced by Russian industry. The main technical property of the pneumatic damper is stability of its elastic force characteristics (Fig. 7) under long-term operation. Stability of the characteristic is ensured by constant pressure of the service medium (gas) in the preset limits. Nitrogen is used as the service gas in this pneumatic damper. Pneumatic damper is designed to:

- keep the isolated structure in the initial position during the service life;
- decrease the isolated structure overloads under the action of seismic forces to allowable values;
- return the isolated structure to the initial position when the action is over.

Pneumatic damper has the following technical characteristics:

- operating pressure (under static condition) at temperature 20^0 C to $62 \cdot 10^5$ Pa;

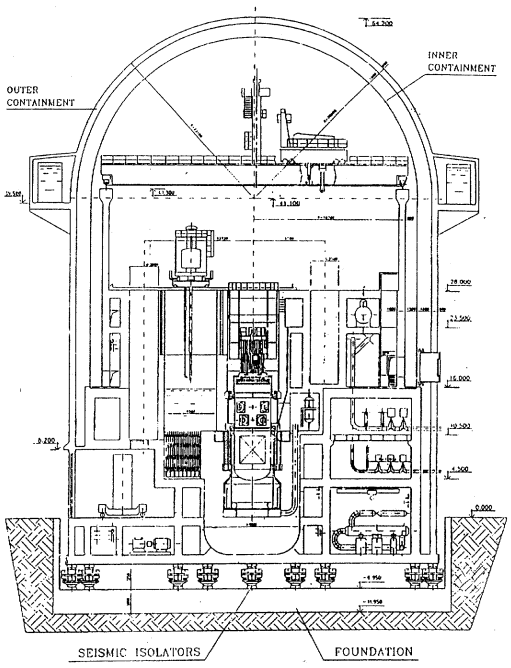

Fig. 1 Seismic isolated building of NPP VVR 640

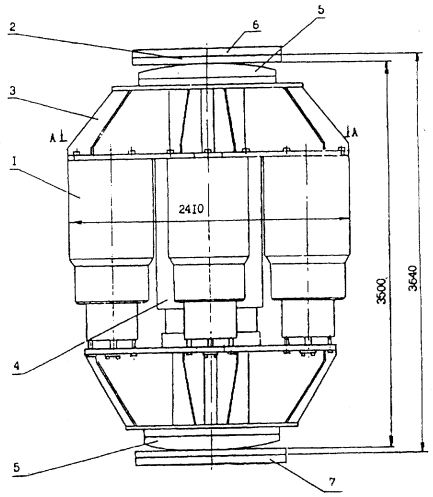

1 - side pneumatic damper with a diaphragm;
2 - base plate;
3 - bracket;
4 - central pneumatic damper with a guiding device;
5 - supporting spherical plate;
6 - embedded piece on the isolated structure;
7 - embedded piece on the superstructure.

Fig. 2 Supporting spherical seismic isolation device with pneumatic dampers (version 1)

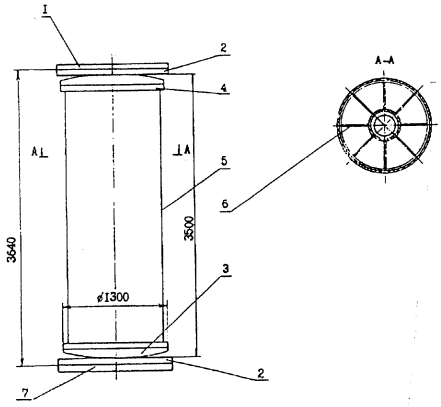

1 - embedded piece on the isolated structure;
2 - base plate;
3 - supporting spherical plate;
4 - rocking-type strut casing flange;
5 - rocking-type strut casing;
6 - stiffening elements of the casing;
7 - embedded piece on the superstructure.

Fig. 4 Supporting spherical seismic isolation device (version 2)

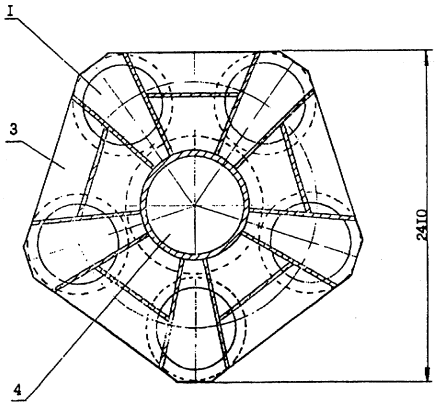

Fig. 3 Supporting spherical seismic isolation device with pneumatic dampers (version 1

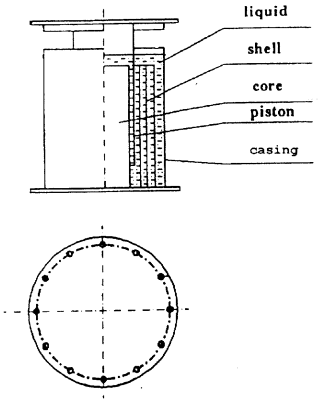

Fig. 5 General view of viscous elastic damper

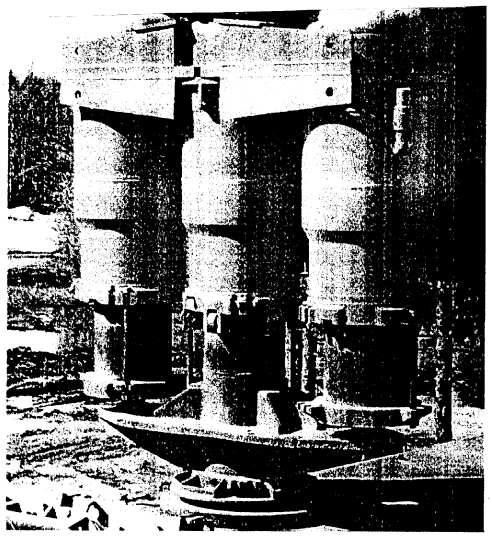

Fig. 6 General view of pneumatic damper

TABLE 1. TECHNICAL DATA ON SEISMIC ISOLATION DEVICE (VERSION-1)

N	Characteristics	Dimensions	Value
1	Mass	t	21
2	Load capacity	KN	8800
3	Overall dimensions	m	3.5 x 2.5 x 2.4
4	Working stroke: in vertical direction in any horizontal direction	m	 to ± 0.2 to 0.8
5	Step force characteristic value: in vertical direction in any horizontal direction	%	 to ± 10
6	Quantity of pneumatic dampers	pc.	6
7	Damper dimensions: height diameter	m	 1.7 0.78
8	Working gas	-	nitrogen
9	Initial volume of gas in a pneumatic damper	Pa	0.43
10	Static pressure in a pneumatic damper	Pa	$62 \cdot 10^5$
11	Dynamic pressure in a pneumatic damper	Pa	$80 \cdot 10^5$
12	Test pressure in a pneumatic damper	Pa	$100 \cdot 10^5$

TABLE 2. TECHNICAL DATA ON SEISMIC ISOLATION DEVICE (VERSION-2)

N	Characteristics	Dimensions	Value
1	Mass	t	5
2	Load capacity	KN	10000
3	Overall dimensions	m	3.5 x ø1.3
4	Working stroke: in vertical direction in any horizontal direction	m	 to ± 0.1 to 0.8

- load capacity under this pressure is ~ 160 tons;
- vertical stroke of the damper:
    - in compression to 340 mm;
    - in tension to 370 mm.

Allowable pressure drop in a pneumatic damper, which is allowed for in the step in elastic characteristic, is ~ 5% of the initial pressure throughout the whole operation period. Each isolator after being properly tested during manufacturing and gas-charging is encapsulated and therefore requires no maintenance during operation. The step in elastic characteristic can be ensured both by cinematic properties of the devices, connecting pneumatic damper and isolated structure, and the construction of the pneumatic damper itself.

Pneumatic damper leak-tightness and guaranteed operability without additional filling with nitrogen throughout the whole operation period are ensured by its structure and control and testing operations during manufacturing of rubber-cord diaphragm and pneumatic damper as a whole. Pneumatic damper structure has only one unit of possible decompression it is the filling branch pipe. The branch pipe is designed for filling the pneumatic damper with compressed gas and controlling the pressure in it. Filling the pneumatic damper with nitrogen is produced with the help of return-type charging valve. Operating position of the charging valve is a closed one. After filling and controlling the pressure in situ the filling branch pipe chamber is filled by oil, which gives rise to a hydraulic seal.

Control and testing procedure set includes:

- production quality control of rubber-cord diaphragm and pneumatic damper;
- testing of each diaphragm and stand testing of each pneumatic damper under static loading condition and for leak-tightness;
- dynamic testing of a batch of pneumatic dampers;
- periodic monitoring of pneumatic dampers state under operation.

Production quality control of rubber-cord diaphragm provides for:

- check of each rubber-cord diaphragm for strength and gas permeability;
- check of physical-mechanical properties of rubber;
- check of stability of the cord thread spacings;
- check of rubber-cord diaphragm exterior view and dimensions.

From any batch of 20 pieces one damper to be chosen at random is tested. Thickness of rubber-cord diaphragm walls and strength reserve factor (up to rupture) of the rubber-cord diaphragm and its boundary zones are to be checked.

Pneumatic damper workmanship as a whole is ensured by:

- technological process which provides for step-by-step leak-check of each welded joint and check of each intermediate assembly strength, leak-check is carried out by helium leak detecting method;
- hydraulic pressure tests of each pneumatic damper for strength;
- leak-check of each pneumatic damper by mass spectrometry method with determination of its actual loss of leak-tightness in sm 53 0/hour (g/hour);
- testing of each pneumatic damper on a static stand with provision of its compression and tension in full working strokes (displacements) (Fig. 8);
- testing of several pneumatic dampers from the amount produced within a year period on a dynamic stand (Fig. 9).

Monitoring of pneumatic dampers state in situ is carried out on the basis of studying isolated structure placements, as well as by visual inspections under the scheduled maintenance procedure.

A number of special investigations and tests preceded the elaboration of technological process of production-type manufacturing of pneumatic dampers. These investigations were carried out in order to forecast damper operability under long-term operation. They include periodic monitoring of the state of a rubber-cord diaphragm installed in experimental demountable pneumatic damper. A comprehensive qualification of manufacturing and testing technology made reliability and operability of pneumatic dampers very high. It has been confirmed by operational experience of production-type pneumatic dampers within approximately 20 years. More than 1000 pneumatic dampers had been manufactured on the production-type basis with no operational failures or unsatisfactory equipment reports.

Acceptance characteristics of each produced pneumatic damper are:

- smooth plunger displacement in working stroke under static loading of a pneumatic damper (Fig. 10);

- leak-tightness, determined by mass-spectrometer control method, which is not to be lower than that prescribed for the pneumatic damper.

The permissible loss of leak-tightness is determined on the basis of allowable gas leakage throughout the service life of the device. Under this control technique conditions it is possible to test encapsulated pneumatic dampers for leakage by means of quantitative estimation of nitrogen mass, which leaks due to faults in the protective pneumatic damper coating into leak-proof chamber. Acceptance characteristics of the pneumatic dampers, subjected to dynamic testing, are as follows:

- absolute vibration damping of the isolated structure in a time that doesn't exceed 8 sec. under dynamic loading of a pneumatic damper;
- required total leak-tightness after dynamic tests.

During factory dynamic testing a pneumatic damper is subjected to dynamic loading at the rate 3 m/sec on impact testing machine (Fig. 11) at least 7 times with subsequent leak-check.

Statistic data on the leak-tightness control of pneumatic dampers testifies that actual loss of leak-tightness for all the pneumatic dampers produced does not exceed 50% of the prescribed value regardless of the year of production. This testifies the reliability of technological process of pneumatic dampers manufacturing and quality control.Forms of vibration oscillograms received at dynamic loading of pneumatic dampers with step and monotonous force characteristics are shown in Fig. 11. During their service life the pneumatic dampers are under compressed nitrogen pressure. The value of rated (static) pressure is 53–62 kgf/sm . Allowable pressure drop in a pneumatic damper throughout its service life makes up 50% of the static pressure. Under operation conditions provision is made for repeated pneumatic dampers dynamic loading in compression and tension at full working strokes (displacements). Under this condition each loading is characterized by absolute vibration damping. In-service monitoring of the pneumatic dampers state is performed remotely with the help of sensors, which fix changes in the setting position of the isolated structure. Pressure control in the operating chamber of pneumatic dampers is carried out:

- during the filling procedure before the acceptance tests on the manufacturing plant;
- after installation at the site;
- after the expire of warranty period of pneumatic damper operation. At present the warranty period of pneumatic damper operation is more than 20 years and can be prolonged on the basis of special investigation results.

These investigations include:

- dynamic and static loading of the demounted pneumatic dampers with expired warranty period on the manufacturing plant stands;
- control of their leak-tightness by mass-spectrometer method;
- removal (Fig. 12) and investigation of rubber-cord diaphragm, including:
    - fault detection of the diaphragm;
    - X ray inspection of the diaphragm;
    - gas permeability testing;
    - testing for determination of the diaphragm reserve strength factor;
    - determination of physical-mechanical indices for the diaphragm.

Investigations of leak-tightness of a series of pneumatic dampers after 20-year operation under static dynamic tests have shown that their actual loss of leak-tightness practically had not changed and did not exceed 50% of the prescribed value.Results of the investigation of physical-mechanical indices of rubber and strength of rubber-cord diaphragm bonds after 20 years of operation and production tests are listed in Table 3. Ultimate values of

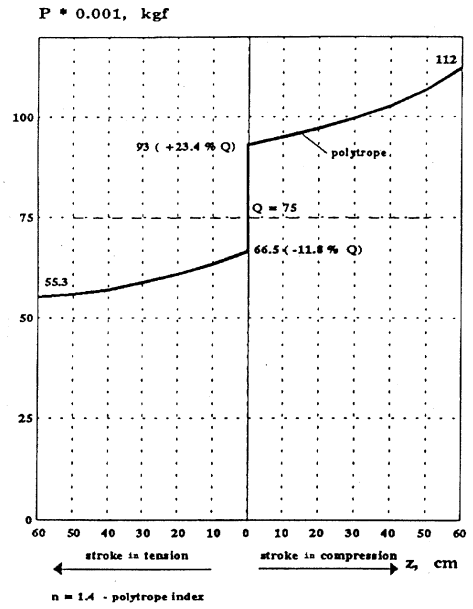

Fig. 7 Design step dynamic characteristic of a pneumatic damper

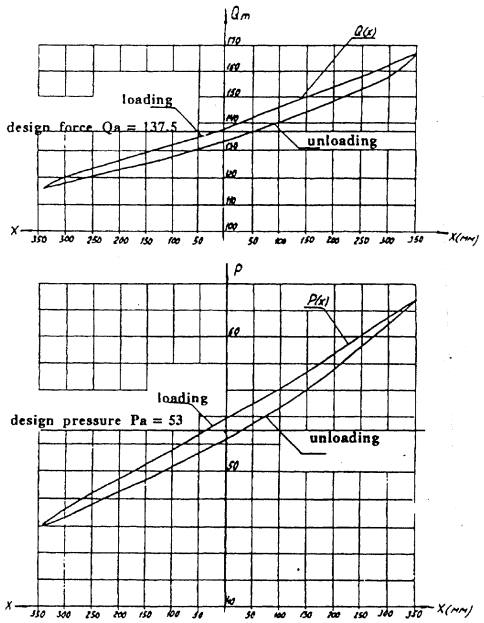

Fig. 8 Plots of force Q(x) and pressure P(x) under static pneumatic damper testings

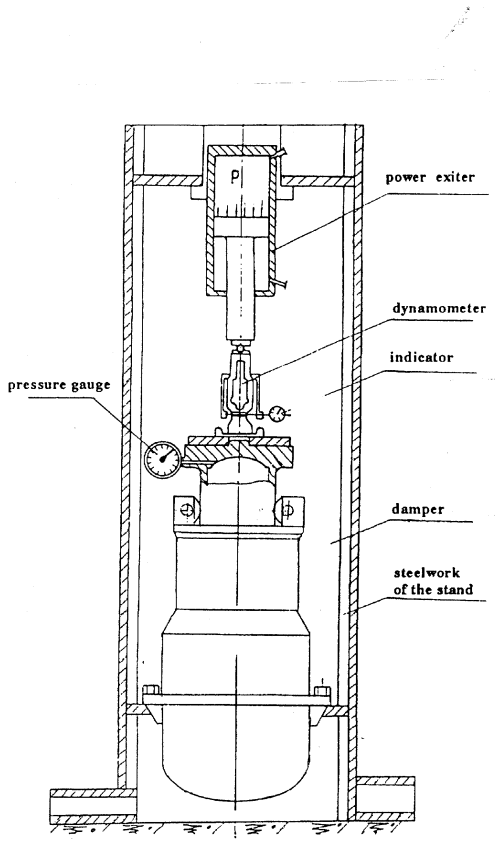

Fig. 10 Pneumatic damper static loading pattern

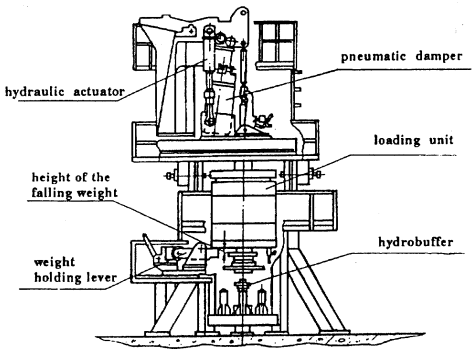

Fig. 9 Pneumatic damper dynamic loading pattern

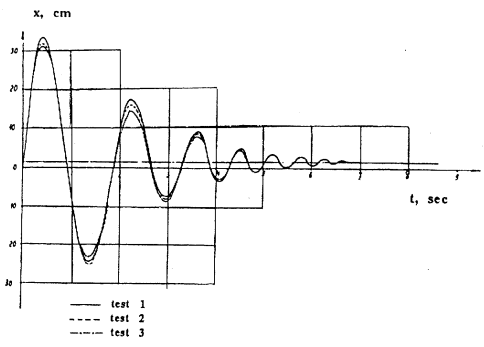

Fig. 11 Vibration damping of the isolated structure simulator under dynamic loading of pneumatic dampers with step force characteristic

TABLE 3. PHYSICAL-MECHANICAL INDICES OF DIAPHRAGM

N	Names of indices	Standard value	Actual value
1	Conventional strength at tension. mPa, no less than	11.8	16.21 - 16.75
2	Relative elongation at rupture. %, no less than	400	480 – 490
3	Relative permanent deformation After rupture. %, no less than	40	11.5 – 12
4	Resistance to lamination, KN/m. no less than	39.2	52 – 53
5	Strength of bonds between diaphragm members under lamination, KN/m. no less than -between coating rubber and frame: -between frame layers.	 4.9 6.9	 10.05 - 13.65 11.80 - 13.80

TABLE 4. DESTRUCTION OF DIAPHRAGM AFTER DIFFERENT TERMS OF SERVICE LIFE

N	Service life			
	After manu-facturing	9 years	15 years	20 years
	Collapsing pressure, mPa			
1		26.8		
2		23.6		
3			22.6	
4			25.6	
5			22.0	
6			25.2	
7				23.0
8				22.4
Mean value	28.0 - 30.0	25.2	23.85	22.7

TABLE 5. PRESSURE CONTROL DATA

N	Pressure in pneumatic damper after installation, adjusted to t=20°C. mPa	Pressure in pneumatic damper after the expiry of warranty, adjusted to t=20°C, mPa	Pressure drop %
1	2	3	4
1	5.38	5.34	0.74
2		5.31	1.3
3		5.33	0.93
4		5.35	0.56
5	5.35	5.32	0.56
6		5.31	0.75
7		5.33	0.37
8		5.34	0.18
9	5.36	5.33	0.56
10		5.35	0.86
11		5.34	0.37
12		5.34	0.37
13	5.36	5.266	1.75
14		5.256	1.94
15		5.256	1.94
16		5.27	1.68
17	5.37	5.32	0.93
18		5.32	0.93
19		5.32	0.93
20		5.36	0.186
21	5.36	5.27	1.68
22		5.27	1.68
23		5.28	1.49
24		5.29	1.3
25	5.36	5.28	1.49
26		5.28	1.49
27		5.28	1.49
28		5.28	1.49
29	5.36	5.30	1.12
30		5.33	0.56
31		5.33	0.56
32		5.32	0.75

1	2	3	4
33	5.36	5.34	0.37
34		5.35	0.186
35		5.34	0.37
36		5.35	0.186
37	5.36	5.307	0.99
38		5.32	0.75
39		5.297	1.17
40		5.297	1.17
41	5.36	5.33	0.56
42		5.30	1.12
43		5.31	0.93
44		5.32	0.75
45	5.36	5.26	1.87
46		5.255	1.96
47		5.255	1.96
48		5.255	1.96
49	5.36	5.28	1.49
50		5.26	1.87
51		5.30	1.12
52		5.27	1.68
53	5.36	5.27	1.68
54		5.25	2.05
55		5.24	2.24
56		5.26	1.87
57	5.36	5.28	1.49
58		5.30	1.12
59		5.29	1.31
60		5.30	1.12
61	5.36	5.25	2.05
62		5.26	1.87
63		5.25	2.05
64		5.257	1.92
65	5.36	5.32	0.75
66		5.31	0.93
67		5.32	0.75
68		5.34	0.37
69	5.36	5.35	0.186
70		5.25	2.05
71		5.36	0.0
72		5.35	0.186

1	2	3	4
73	5,36	5.308	0.97
74		5.32	0.75
75		5.33	0.56
76		5.33	0.56
77	5.36	5.28	1.49
78		5.25	2.05
79		5.27	1.68
80		5.28	1.47

diaphragm destruction characteristic are presented in Table 4. Rubber-cord diaphragms which were demounted from the pneumatic dampers after being under operation within 20 years meet the Norms and Standards by all the parameters checked. Visual inspection of rubber-cord diaphragms, measurement of their working dimensions, analysis of X ray patterns, shears and lamination had not indicated any deviations, which can result in serviceability losses of a diaphragm as a part of pneumatic damper.Results of pressure control in the pneumatic dampers after warranty period expiration are listed in Table 5.The data, listed in Table 5, testify that pressure drop in pneumatic dampers per 20 years of operation (without additional pressurizing) remained within the range 0–2.24%. This value is considerably lower than the prescribed one, accepted as the criterion of no-failure pneumatic damper operation, which is 5% of the filling pressure after installation.HD-type dampers had undergone the whole cycle of qualification tests on the stands of CKTI and Ishikavadzima Harima Heavy Industries Company (Japan) and are recommended for application on nuclear power plants by Atomnadzor of Russian Federation.Recently sufficient experience of successful industrial use of dampers has been accumulated on thermal and nuclear plants, where more than 100 dampers are in service. They are used not only to provide for seismic stability, but also to decrease the vibration of various equipment in vibration isolation systems.

2.5. Analytical determination of force characteristics of seismic isolation system components

The main technical complexity when implementing a multicomponent seismic isolation lies in the necessity to combine the observance of two contradictory requirements:

- seismic isolation system shall constantly remain in full operational state during its whole service life and lower the level of isolated structure loads to the allowable values under the earthquake;
- during its service life the seismic isolation system shall function as the building foundation and ensure the absorption of all working loads thereby providing for the building position stability.

From the standpoint of mechanics it means the necessity to create the areas of increased stiffness in the mechanical system characteristic in the vicinity of the static equilibrium point. As this seismic isolation system is a multicomponent system, the area with increased stiffness is spatial and its dimensions are determined by the design level of loads, acting on the building while in service. Outside the area of increased stiffness the stiffness of mechanical system characteristic is to be minimized in order to ensure effective decrease of the loads, related to specific impacts (earthquake, airplane crash etc). The main minimization criteria under this conditions are the values of allowable design loads on the equipment and the limitations on the relative displacements.

Practical realization of this nonlinear approach for a multicomponent seismic isolation system involves serious difficulties which are to be overcome. Recently in the world practice of elaboration of seismic isolation systems for nuclear power facilities only a limited number of attempts to solve this problem are known.

As the base approach to the SIS problem solution in the given study the pneumatic-cinematic multicomponent low-frequency seismic isolation system of reactor building was accepted, this system has been developed in Russia. This seismic isolation system incorporates both supporting spherical rocking-type devices, which provide for the isolated object displacements in horizontal direction, and pneumatic dampers with rubber-cord diaphragm for seismic isolation in vertical direction. To decrease the relative displacements of the isolated object viscoelastic dampers are used in the system.

Damping device has been elaborated specially for the reactor building seismic isolation system with due regard for the experience in designing, investigation and operation of the HD-type hydrodampers designed in CKTI VIBROSEISM. Dynamic characteristics of all dimensions of dampers within the range of frequencies from 0 Hz to 60 Hz are received by experiment. HD-type hydrodamper structure ensures the necessary conditions of thermal and mechanical displacements compensation.T hus, the seismic isolation system is a composition of elastic-plastic dampers and damping devices. Selection of devices number and layout in each particular case is determined for the construction site conditions when solving the seismic protection problem.

Seismic isolation of a building both in vertical and horizontal directions involves a series of basic peculiarities into the structural and layout diagram of the construction. At the same time the seismic isolation system, being a mechanical system, has a certain sensitivity to various external and internal factors. These conditions cause the necessity to search for optimal seismic protection problem solving.

The main design and methodical features of the problem to be solved are as follows:

- functional purpose of seismic isolation system places a constraint on its design as regards dynamic efficiency and load capacity;
- necessity to provide for analysis of the influence of all possible operational modes of the building while under construction and operation on the seismic isolation system;
- as opposed to the non-seismic isolated version the pattern of load application to the building base slabs changes. This can give rise to ambiguity of these load values, that substantially complicates selection of the most adverse combination of loads when estimating the strength of plates;
- necessity to take into account the ultimate stiffness of the building construction, base slab and soil deformability while calculating the forces in the seismic isolation supports both under the operational condition and earthquake condition and under specific dynamic loads, which assumes the necessity to create large-size design models;
- rather rigid limitations on the placement of the system elements under the reactor building due to the conditions of their installation and servicing.

The peculiarities of seismic isolation system elaboration listed above presuppose the need to solve a set of correlated problems, the main of which is determination of the force characteristics of the system elements (elastic supports and dampers). These characteristics are to be optimal from the standpoint of dynamic efficiency.

In this case the following purpose-oriented functions are to be considered:

$$\begin{aligned} & k_0^j \longrightarrow \min, \text{for } u_n \in U; \\ & \Delta f < P \quad , \text{for } m \in M, \end{aligned} \tag{1}$$

where

Δf is the vector of changes of the total forces in seismic isolation system elements when the loads on it change in the prescribed limits;

m is any condition from the M set, related to the change of loads on the seismic isolation system, which is provided by technological or operational requirements or safety requirements (impact of the aircraft on the containment etc);

P is the minimal necessary value of force characteristic stiffening, realized in the system to provide for the stable position of the isolated structure under operation conditions;

k_0^j is the coefficient of dynamic loads decrease at the level j for any seismic input u_n of the typical set of design effects U (both in horizontal and vertical directions) or for the given design effect.

The coefficient stated above is usually defined as a relation of the peak values of floor spectra $X^j(\Delta\omega)$ and $X^{*j}(\Delta\omega)$ at the level j for seismic isolated and non-seismic isolated versions of the isolated structure respectively in the given frequency range (or ranges) $\Delta\omega$, i.e.

$$k_0^j = X^j(\Delta\omega)/X^{*j}(\Delta\omega)$$

Search of the optimal seismic isolator characteristics is regulated by a system of limitations, which are related to the necessity to meet the Norms and Standards requirements, as well as to the structural and layout diagram of the building, technical and economic requirements etc.When performing this work the following conditions were accepted as the criterion of dynamic SIS efficiency:

$$S_{Hor}(\Delta\omega) < \alpha \text{ for } \Delta\omega \in \{\omega_1^H, \omega_2^H\}$$
$$S_{Vert}(\Delta\omega) < \beta \text{ for } \Delta\omega \in \{\omega_1^V, \omega_2^V\},$$

where

α= const, β= const,

ω_1, ω_2 are the boundary frequencies,

$S_{Hor}(\Delta\omega)$,$S_{Vert}(\Delta\omega)$ are the values of response spectra for the vertical and horizontal components of the seismic response.

At elevation 24.6 m the following values of parameter were accepted:

$\alpha = 0.5g$, $\beta = 2.0g$, $\omega_1^H = 5Hz$, $\omega_2^H = 40$ Hz, $\omega_1^V = 10Hz$, $\omega_2^V = 40Hz$.

Taking into account the fact that the spectrum of the seismic input response (at the level of the base) has the values of dynamic coefficients higher than 1 within the frequency range $\Delta\omega${2Hz; 25Hz}, the seismic isolation stiffness characteristics should ensure that resonant effects are impossible. View of stiffness characteristic of the multicomponent low-frequency seismic isolation system which meets this requirement is shown in Fig. 13. Analysis of the data presented in Fig. 13 confirms the possibility of their realization in the pneumatic-cinematic seismic isolation system.

A quantity of seismic isolation supports was determined on the basis of their rated load capacity and dimensions and was accepted as 220. To reduce the time of the isolated building motion damping and its relative displacement decrease additional dampers are installed in the SIS, they ensure equivalent damping at the ~ 3–5% level.

2.6. Analytical study of the efficiency of seismic isolation system

All phases of seismic isolation system designing are followed by carrying out the design estimations. Under this condition depending on the goal of estimation the complexity of the design models under consideration and the necessary completeness of initial data can vary. Using the cantilever single-element model with equivalent lumped masses corresponds

to the initial phase of seismic isolation designing. When the initial phase is under performance the force characteristic parameters of the system which meet the initial requirements are specified, at the same time the possibility of structional characteristic realization in separate devices is under study. If there are alternate versions of seismic isolation system it is desirable to receive evaluation of their efficiency for each of them. Solving the problem of the isolator arrangement, determination of the base slab loads, installation procedure etc. is accomplished with the use of more complicated spatial finite-element models.At design estimation of the seismic isolation system efficiency the data on the design seismic input, required levels of protection at the specified building elevations and force characteristics of the system, chosen at the preliminary analysis stage, are used. To evaluate the efficiency of a dynamic seismic isolation we performed calculation of the parameters of motion of the model isolated part relative to the foundation at the prescribed seismic input and response spectra (floor spectra) in the points of discrete masses location which correspond the floor levels. Under this condition the system dynamics calculation is carried out separately for horizontal and vertical directions of motion. During design evaluation of efficiency two system versions were considered. In the Version-1 seismic isolation system the supports with pneumatic dampers are used, and in the Version-2 system the supports without pneumatic dampers are used. Efficiency of the isolation was evaluated due to the degree of load decrease on the isolated part relative to the version of building installation directly on the ground. Under this condition the maximum displacement value of the isolated part relative to the foundation was under control.

Force characteristics of seismic isolation system used in calculations are presented in 2.3. The main peculiarity of the system operation is repeated changing of deformation direction under the preset seismic input. In this circumstances it was found that the predominant influence on the isolated part response is of the stiffening value of the force characteristic initial part. It is evident, that reduction of the stiffening level of force characteristic and the stiffness of initial part will favorably effect the system efficiency. The seismic isolation system proposed has the following parameters of force characteristic:

- for horizontal direction the stiffening level of force characteristic corresponds 0.0025, and initial part stiffness is equal to 6 Hz frequency for both system versions;
- for vertical direction the stiffening level of force characteristic corresponds 0.005 for the Version-1, and for the Version-2 there is no stiffening at all; stiffness of the force characteristic initial part is equivalent to the frequencies: 15 Hz — for the Version-1 and 20 Hz — for the Version-2.

Different stiffness values of the force characteristic initial part of the system can involve the change of natural frequencies values of the model vibration for the model which incorporates seismic isolation system. Definition of the natural frequency of the model vibration is reduced to the solution of the following partial eigenvalues problem :

$$[K] \cdot \varphi = \lambda \cdot [M] \cdot \varphi \qquad (2)$$

where

[K] and [M] -are stiffness and mass matrices of a non-damped oscillatory system respectively.

The solution of this problem is a number of lowest eigenvalues λ_1 of non-damped system and corresponding forms of vibrations φ_1. To solve the equation (1) a subspace iteration method is used. Calculation data on natural vibration frequencies for two Versions of seismic isolation system are presented in Tables 6 and 7 for horizontal and vertical directions respective Analysis of natural vibration frequencies and response spectrum of the design effect had shown that occurrence of resonant vibrations in horizontal direction within the 5–8 Hz frequencies range is possible. Values of the dynamic coefficients in this frequency range

are 6–10. In this case, due to controlling the damping parameters in a seismic isolation system we can receive the solution which satisfies the initial requirements.

In vertical direction the seismic isolation system vibration frequencies are close to the vibration frequencies of a superstructure (more than 10 Hz). However, within the range of high vibration frequencies the dissipative properties of structural materials are displayed markedly, that gives no way for resonant vibrations of superstructures to be developed.

TABLE 6. EIGENVALUES FOR HORIZONTAL DIRECTION

N	Vertical direction		Horizontal direction	
	Natural frequency f(Hz)	Natural period T(s)	Natural frequency f(Hz)	Natural period T(s)
1	6.9	0.1449	4.4	0.2273
2	20.7	0.0484	7.4	0.1353
3	31.4	0.0319	11.4	0.088
4	37.6	0.0266	15.0	0.0664
5	51.5	0.0194	19.0	0.0526
6	62.2	0.0161	21.98	0.0455
7	84.0	0.0119	25.9	0.0386
8	91.1	0.0104	29.0	0.0344
9	120.5	0.0083	34.8	0.0288
10	133.9	0.0075	36.1	0.0277

TABLE 7. EIGENVALUES FOR VERTICAL DIRECTION

N	Vertical direction		Horizontal direction	
	Natural frequency f(Hz)	Natural period T(s)	Natural frequency f(Hz)	Natural period T(s)
1	10.1	0.0991	4.4	0.2273
2	21.0	0.0477	7.4	0.1353
3	31.5	0.0318	11.4	0.088
4	50.5	0.0198	15.0	0.0664
5	59.8	0.0167	19.0	0.0526
6	79.0	0.0127	21.98	0.0455
7	91.0	0.011	25.9	0.0386
8	99.2	0.0101	29.0	0.0344
9	121.5	0.0082	34.8	0.0288
10	134.5	0.0074	36.1	0.0277

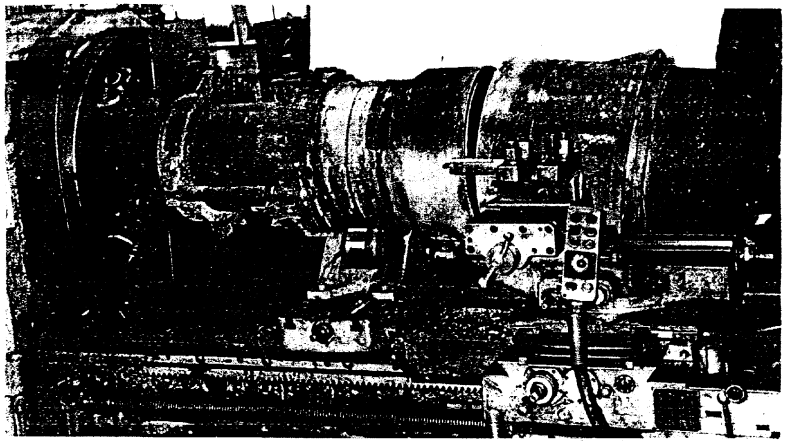

Fig. 12 Machine cutting

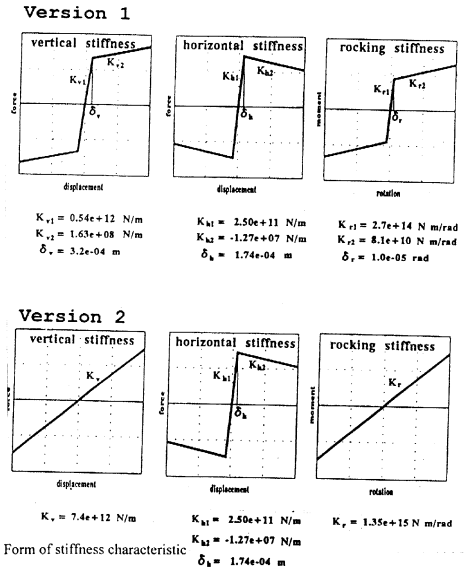

Fig. 13 Form of stiffness characteristic

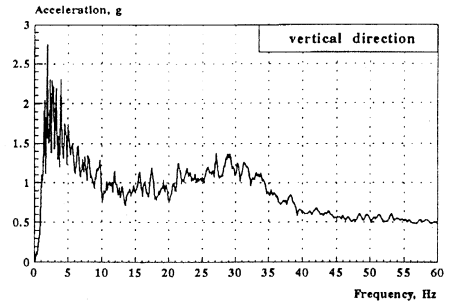

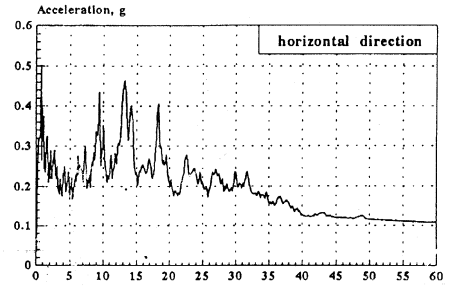

Fig. 14 Calculation results (version 1)

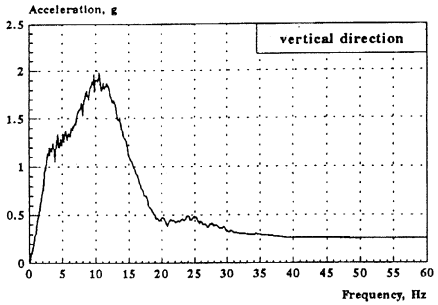

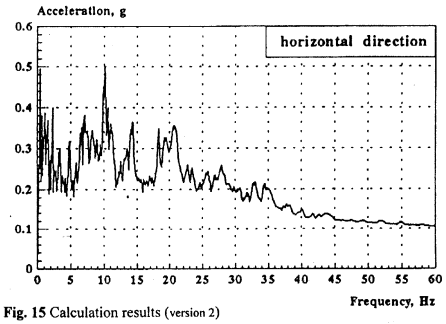

Fig. 15 Calculation results (version 2)

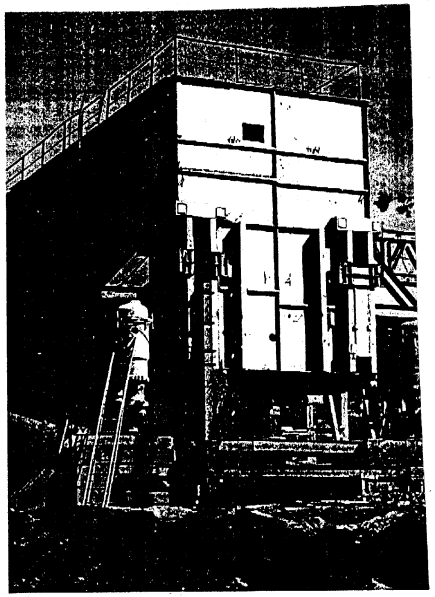

Fig. 16 General view of the testing construction

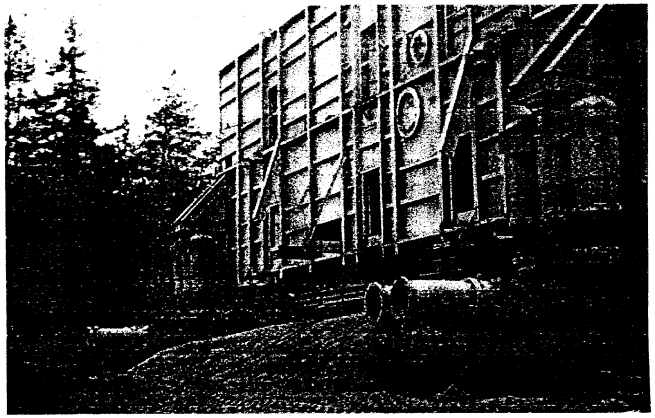

Fig. 17 General view of pneumatic damper

For calculation of dynamic loads of linear elastic structures with non-linear discrete relations, imposed in separate units, the finite element method algorithm (in displacements) is used.The basis of dynamic load design is the solution of differential matrix equations, which is recorded in the form of:

$$[M]\cdot\{u\}+[C]\{u\}+[K]\{u\}=\{P\}+\{R\} \qquad (3)$$

where

[M], [C], [K] -are, respectively, the mass, damping and structure stiffness matrices;

$\{u\},\{u\},\{u\}$ -are acceleration, speed and displacement vectors;

{P} — the vector of applied external loads.

{R}-the vector of the forces which simulate influence of discrete connections on the structure.

Vector {R} is determined by the relation:

$$\{R\} = [N]\ \{F\} \qquad (4)$$

where

[N] -is a topological matrix of integration of the external discrete connections with the structure of dimensions n × m (n — number of the structure degrees of freedom, m — total number of degrees of freedom of all connections);

{F} -is the vector of forces in the connections in the direction of degrees of freedom.

The components of vector {F}, in general case, are nonlinear functions of relative motion Δ and relative velocity Δ

$$F_1 = F_1(\Delta,\Delta), \qquad i=1,.....,m$$

Specific form of these functions is presented in 2.5.

The components of the damping matrix [C], which accounts for the mechanisms of structural and inner damping, are taken in the form, which is convenient for practical use (damping by Reilay):

$$[C] = \alpha[M] + \beta[K] \qquad (5)$$

where

α and β -are the constants, which are defined from two given values of the damping factor, which relate to two different vibration frequencies.

To solve the equation (3) the Newmark integration scheme and Newton-Rafson iterative method is used. Parameters of the integration scheme were taken as γ = 0.5 and δ = 0.25. Calculations of reactor building model dynamics had been performed for the prescribed seismic input for two Versions of the seismic isolation system, separately for vertical and horizontal directions. For the Version-1 seismic isolation system Table 8 presents the maximum values of displacements of the isolated part of building model relative to the base slab, as well as absolute value of acceleration of the model unit at elevation 24.65 m for vertical and horizontal directions of the input. The similar data, received for the Version-2 system, are listed in Table 9. Figs 14 and 15 show the floor response spectra received at elevation 24.65 m for the horizontal and vertical directions respectively.To perform comparative analysis the similar calculations had been conducted for the building model directly erected on the ground.

Comparison of structional versions of the building model (seismic isolated and non-seismic isolated) permits to make the following conclusions:

- seismic isolation system ensures the required level of decrease of the loads on building constructions and equipment in the frequency range higher than 5 Hz in horizontal direction and higher than 10 Hz in vertical direction with the use of any system versions (1 or 2);

TABLE 8. DYNAMICS CALCULATION RESULTS

(VERSION-1)

Item	Vertical direction	Horizontal direction
Maximum acceleration, m/s^2	2.6	0.93
Maximum displacement of isolation object, m	0.033	0.38

- on the basis of the calculations performed there were determined the damping values in seismic isolation system, that ensure meeting the initial requirements, which were:
    - for the Version-1–2% of the critical value in horizontal direction and 5% — in vertical direction;
    - for the Version-2–2% of the critical value in horizontal direction and 3% — vertical direction;
- for both seismic isolation system Versions the return of the building model into initial position after termination of the effect is ensured.

Dynamic loads reduction factors at elevation 24.65 m of the building model were:

- in horizontal direction (frequency range higher than 5 Hz):
    - for the Version-1 — 6-15;
    - for the Version-2 — 4–12;
- in vertical direction (frequency range higher than 10 Hz):
    - for the Version-1 — 4–10;
    - for the Version-2 — 5–12.

3.DESCRIPTION OF COMPUTER AND ANALYTICAL METHODS

3.1 Method of choosing the solution of the seismic isolation system

Dynamic, technical and economic indices of seismic isolation are formed in accordance with the specifications and the purposes of their use: for comparative analysis of the SIS versions at the feasibility report phase or for evaluation of the engineering solution level. These indices characterize the structional SIS design from the viewpoint of its conformity with the following groups of requirements [6], [7]:

- requirements on the seismic isolation system as it is, which are imposed upon the dynamic properties of the system and its technical and economic characteristics;
- requirements on the SIS elements and units;
- requirements on fulfilling its protective functions by the seismic isolation system.

The first group of the requirements corresponds with the following indices.

- Seismic isolation system reduction index of the load, transferred to the protected structures and components

$\Pi_1 = K_o^j/\alpha^j$,

where

$K_o^j = x_c^j(\omega_i)/x_H^j(\omega_i)$ -are the load reduction factor,

TABLE 9. DYNAMICS CALCULATION RESULTS
(VERSION-2)

Item	Vertical direction	Horizontal direction
Maximum acceleration, m/s^2	2.6	0.94
Maximum displacement of isolation object, m	0.000058	0.38

TABLE 10. CALCULATION RESULTS OF ALTERNATING BUILDING DISPLACEMENTS

Effects of soil	x 10^{-2} m	y 10^{-2} m	z 10^{-2} m	f 10^{-3} m	j 10^{-3} rad	q 10^{-3} rad	.. x g	.. y g	.. z g
OBE SG	2.8 -2.7	2.0 -2.4	0.6 -0.5	1.5 -1.3	1.3 -1,2	0.4 -0.3	0.16 - 0.16	0.16 - 0.17	0.12 - 0.11
SSE SG	5.5 -5.4	4.2 -4.7	1.3 -1.1	2.7 -2.3	2.4 -2.4	0.5 -0.4	0.17 - 0.18	0.19 - 0.19	0.15 - 0.13
QBE RG	2.3 -2.1	2.1 -2.3	0.7 -0.6	1.1 -1.0	1.1 -1.0	0.02 - 0.01	0.15 - 0.15	0.16 - 0.15	0.13 - 0.12
SSE RG	5.1 -5.0	4.7 -5.4	1.6 -1.4	2.2 -2.0	2.1 -2.1	4.6 -4.2	0.21 - 0.20	0.21 - 0.22	0.17 - 0.16

TABLE 11. DYNAMIC LOADS REDUCTION FACTORS

Elevation, m	-4,5	0,0	4,5	10,5	16.0	23,5	28,0
Vertical	3-5	3-6	4-8	4-10	5-15	6-22	8-30
Horizontal	3-4	3-8	5-10	5-15	6-20	8-30	10-40

where

$x_c^j(\omega_i)$ and $x_H^j(\omega_i)$ -are the peak values of floor spectra on the jth elevation level for the seismic isolated and non-seismic isolated versions of the protected object, respectively.

As a value of integrated reduction factor we can use the averaged over the preset frequency band $\Delta\omega$ value $K_{o,}\ \alpha^j$, — reduction factor, corresponding to the extreme level of possible dynamic loads from the seismic input (in each ith direction), transferred to the building constructions and components.

- Index of stability of the protected object setting position relatively the base slab (fencing structure) during the term of its operation taking into account possible change in inertial properties of the object

$$\Pi_2 = \varphi(t)/\varphi_0,$$

where

$\varphi(t)$ is the protected object tilting,

φ_0 is the allowable value of tilting with regard to standard tolerance,

t is the time of operation, on the moment of which the value of tilting is determined for all SIS versions under comparison.

The limiting value t is equal to the object operating time.

- Index of adaptability to external exposure in accordance with actual inertial and stiffness specifications of the system:

$$f(X, \Delta X, P) \quad f, \Delta X \{a \le \Delta X \le b\},$$
$$M_n$$

where

X is the vector of design parameters,

a, b is the design value of lower and upper boundaries of design parameter deviations ΔX,

P is the parameter of SIS actual state, enabling to compensate the deviations of design parameters within the range of $\{a_p , b_p \}$, $\Delta X \{a_p \le \Delta X \le b_p \}$, f,

f are total specifications of the system, respectively, realized and design ones,

M_n is the set of realized effects.

When comparing the versions of structional SIS designs the best one will be the version, which makes it possible to compensate the deviations of design parameters in more wide range, i.e. $(b_p–a_p) > (b–a)$ and under this condition $a_p < a$, $b_p\ 0 > b$.

- Index of adaptability Π_3 can be determined as relation of the realized range to the required one

$$\Pi_3 = (b_p–a_p)/(b–a),\ a_p < a,\ b_p > b.$$

- Index of the system sensitivity to the protected object changes of mass and displacement of the center of mass takes into account the cases, provided by technological and operational requirements, when slope of the object stays within the allowable limits.

In consequence of the object change of mass and displacement of center of mass a violation of insensitivity condition can be

$$\Delta f > 0 \text{ for } \forall m \in M,$$

where

Δf is the vector of total power characteristic of SIS,

m is any condition of a M-set.

Taking into account, that under this condition a part of SIS devices receives additional deformation in statics, the sensitivity index Π_4 can be determined as follows:

$$\Pi_4 = \Delta l_{max}/l_R \text{ for } \forall m \in M,$$

where

Δl_{max} is the peak value from the values of additional static deformation of the SIS devices,

l_R is the value of the working stroke in the additional deformation direction.

- Index of permanent deformations

$$\Pi_5 = \{\Delta X_0\}/\{\Delta X\},$$

where

$\{\Delta X_0\}$ and $\{\Delta X\}$ are the residual and permissible departures of the object center of mass position in absolute coordinate system.

$\{\Delta X_0\}$ includes the values of both linear and angular deviations.

- Index of invariance of SIS with the seismic input parameters changing

within certain limits

$$\Pi_6 = \max (K_j/a^j)_i \; \forall \; f_i(t) \in \{f_i\}, \; i \in [1, N],$$

where

$f_i(t)$ is the accelerogramm from the set (range) preset for the object design $\{f_i\}$, i = 1, 2... N.

- Technical and economic indices, for which the specific dimension-mass and value characteristic can be used:

$M = M_1/M_0$, $V = V_1/V_0$, $S = S_1/S_0$, $C = C_1/C_0$,

where

M_1 is the total mass of all SIS elements,

M_0 is the mass of the object to be protected,

V_1 is SIS space,

V_0 is the usable space of the object to be protected,

S_1 is the loss of room area for SIS arrangement and operation,

S_0 is the useful area of the object to be protected,

C_1 are the costs of SIS creation, including the costs for manufacturing technique development and erection works,

C_0 is the cost of measures for equipment modification and increasing the building construction strength.

The second group of requirements includes the following indices.

- Index of safety margin of the SIS elements

$$\Pi_7 = K_1/K,$$

where

K_1 is the reserve factor (design),

K is the assigned value of the reserve factor (minimum allowable).

- Index of relative deformations in the SIS (in vertical and horizontal

directions) with allowance for the assigned constraints:

$$\Pi_8 = \{KX\}/|X|,$$

where

|X| is the extreme deformation in the system, for example, working stroke of the seismic isolation devices,

X is the design deformation in the system,

K is the assigned deformation safety factor.

- Index of rationality of the SIS device arrangement

$$\Pi_9 = (S_1 + \max (S_2, S_3))/S_4,$$

where

S_2 is the total area, occupied by the seismic isolation devices,

S_3 is the additional area, required for servicing of all the SIS devices;

S_4 is the additional area, required for installation of all the SIS devices,

S_4 is the area of supporting elements, under which the SIS devices can be installed.

The indices which correspond to the third group of requirements reflect, mainly, the expenditures, related to the necessity of carrying out additional measures to provide for the SIS normal operation conditions and its protective functions realization. Circumstances and

reasons of these expenditures emergence for any of SIS versions under comparison can be different. However the total index of additional expenditures Π_{10}, can be roughly presented as follows:

$$\Pi_{10} = (C_1 + C_2 + C_3 + C_4)/C_5 ,$$

where

C_1 is the expenditure for realization of structional base slabs changes, related to the necessity to increase their bearing capacity in the seismic isolation devices installation places,

C_2 is the expenditure for the technological measures, related to the horizontality provision (in the preset limits) of the base slab embedded elements,

C_3 is the expenditure for the measures to provide for the necessary temperature-humidity conditions of the SIS operation,

C_4 is the expenditure for the measures to prevent the injurious effect of aggressive media on the SIS devices,

C_5 is the cost of measures for equipment modification and increasing the building constructions strength in the absence of the SIS.

Apart from the indices specified when designing the SIS versions the indices which reflect the expenditure on realization of some specific requirements, caused by peculiarities of building construction erection, SIS installation and other similar factors can be taken into account.

Evaluation of the SIS engineering solution level is carried out by comparison of values of integrated relative technical and economic indices with basic values of these indices.

The following indices can be proposed as the main basic technical and economic indices:

- specific mass of the seismic isolation device

$$\alpha_1 = G_1/G_2,$$

where

G_1 is the mass of the device,

G_2 is the load-carrying capacity of the device;

- unit costs of seismic isolation device

$$\alpha_2 = C_6/G_2,$$

where

C_6 is the expenditure on the SIS device production including the erection costs;

- metal consumption (or a material, assigned to metal in costs) for $1m_2$ ($1m_3$) of seismic isolated area (space) of the object

$$\alpha_3 = G_1/S_0 \text{ (or } \alpha_3 = G_1/V_0 \text{)},$$

where

S_0 is the seismic isolated area,

V_0 is the isolated facility;

- overloads on the isolated facility at the fundamental frequency of the seismic isolation system α_4, it.

3.2. Method of evaluation of dynamic seismic isolation system efficiency

Efficiency of application of a seismic isolation system is evaluated on the basis of intensity comparison of the loads, transmitted to the base slab and building constructions in cases with and without the seismic isolation (i.e. direct building construction on the soil). Under this condition the main criterion of dynamic SIS efficiency is performance of the following conditions.

Structural analysis of seismic isolated building with the help of two-dimensional model under the effect of natural seismicity with intensities 9~10 according to the MSK-64 scale has shown, that behaviour of a building with SIS is adequate to the behaviour of a rigid body with isolating suspension. It provides a way for solving the problem of evaluation of the 3d SSI efficiency with a simplified structural model.As a consequence a design model of the seismic isolation system acquired the rigid body-type form with imposed elastic-dissipative ties, which simulated dynamic characteristics of damping devices.

When calculating the dynamics of a NPP reactor building with seismic isolated foundation we accepted the following assumptions:

- effects of seismic input time delay and damping, related to the extent of the building construction base were not taken into account;
- in case of the rocks the seismic input was considered as applied in the attachment points of isolated facility bracings to the base slab;
- non-rock ground base was simulated by a system of elastic-dissipative discrete ties, characteristics of which were determined depending on the soil properties.

Procedure for determination of the floor response spectrum of seismic isolated reactor building included the following phases:

- calculation of the response spectrum for every seismic input in the nodal points, specified for each of the building levels;
- averaging the results of the response spectrum calculation for each of the specified nodal points over the entire set of seismic inputs;
- construction of the enveloping curve of the averaged response spectra over the entire set of nodal points of the given mark

As the result of the performance of all phases of the above procedure the floor respons spectra of seismic isolated NPP reactor building to the preset With the use of computer complex "STRUCTURE" the calculation of reactor building dynamics over the entire set of seismic input for two types of ground conditions had been conducted.

Table 10 presents the values of alternating building displacements relatively the base slab and angles of rotation averaged over a set of effects, as well as the absolute value of building center of mass acceleration over the entire set of the effects under consideration which correspond to the operating basis earthquake (OBE) level with magnitude 8 and to the safe-shutdown earthquake (SSE) with magnitude 9. The following symbols are used in the table :

x, y, z are the displacements of reactor building center of mass;
f, j, q are the absolute angles of reactor building turn;
x, y, z is the absolute acceleration of reactor building center of mass.
SG is the soft soil
RG is the rock soil

For the purpose of comparative analysis the similar calculations of reactor building with direct installation on the soil had been conducted.

Comparison of versions of structional design of building (with and without seismic isolation) permits to make the following conclusions:

- SSI introduction ensures the required level of decrease of loads on the building constructions and components in the frequency range from 2 Hz up to 40 Hz with reserve of about 50–100%;
- SSI ensures the building return to initial position upon completion of the effect.

Within the range up to 2 Hz some excess of the level of seismic isolated building spectrum relative to the non-seismic isolated building can be realized, this is related to the SIS frequency responses (0,5–1,0 Hz). However, this increase leaves unaffected the level of loads,

which are excited in the building constructions since characteristic vibration frequency bands are in the other part of the spectrum (5,0–10,0 Hz). Dynamic loads reduction factors for frequency ranges higher than 2,0 Hz on the characteristic building levels are listed in Table 11. Analysis of the calculation data for seismic isolated building dynamics indicates that in addition to a considerable decrease of peak acceleration amplitudes on various building elevations the floor response spectra are substantially transformed. Application of three-dimensional reactor building seismic isolation determines a set of basic peculiarities of the construction layout and structural configuration. The main of them are as follows:

- in the structure apart from the nuclear reactor building base slab which transfer the load from seismic isolators to the building construction there is an additional base slab, on which the seismic isolation system is located.
- deformability which is caused by this plate dimensions has a pronounced effect on the seismic isolators reaction depending on their layout and degree of ground base stiffness.

Construction of the seismic isolation system as a building foundation element assumes defining a set of additional requirements.

3.3. Requirements to seismic isolated building structional design

It is evident, that for a seismic isolation system an ideal condition would be absolute base slab non-deformability. However the selection of rational seismic isolators arrangement under the building to be protected shall take into account the strength and deformability constraints of these plates. The main constraints are as follows:

- constraint on maximum stress $\delta(x, t)$, acting in the base slab sections at static and dynamic loads

$$\max \delta^i (x, t) < [\delta],$$

where

i=1 is for building base slab;

i=2 is for construction base slab as a whole;

$[\delta]$ are the allowable stresses for reinforced concrete of corresponding grade, working at elastic stage;

- constraints on maximum conceivable slope of the embedded pieces in the seismic isolation bearings at base slab deformation under all loading conditions:

$$\max | H_i – H_i^0 | < \delta, \; i \in (1, N),$$

where

H_i^0 is the eccentric distance of embedded pieces of ith bearing, which are located on the base slabs;

H_I is the distance between the points, located on the embedded pieces contour of the bearing;

N is the number of bearings in the seismic isolation system;

δ is the allowable value of nonhorizontality of the embedded elements surfaces;

- constraint on the overall dimensions of seismic isolation bearings on the provision of sufficient load-carrying capacity:

$$\min r > \max (\min r_{i1}, \min r_2), \; i \; (l, l)$$

on the provision $NxQ > G$,

where

r is the minimum distance between the seismic isolation bearings (or between the bearings and lateral base slab walls);

r_1 is the minimum distance between the bearings, necessary for servicing and repairing the i-type bearings, given by the specifications;

r_2 is the minimum distance between the bearings, specified in accordance with the technological requirements on the system installation;

l is the number of the bearing types, used in the system;

Q is the load-carrying capacity of one device; G is the maximum total weight of the object to be protected; N is the total number of the seismic isolation bearings;

- constraint on the spread of forces value in the bearings ΔP relative to the average level P:

$$\Delta P \rightarrow \min,$$

where

$\Delta P = P_i - P$, i (1, N)

P_i is the force in the bearing.

Introducing the last constraint into consideration is related to the fact that when constructing a reactor building technological bearings (erection supports) are to be used, which after completion of the construction are replaced with seismic isolators. Removal of the erection supports is possible only in the event if the building weight load has been removed. In the proposed seismic isolation system version the erection supports removal is produced by filling all the pneumatic dissipators and does not involve additional devices.

It would appear reasonable to assume that when object designing the preference will be given to such a version of seismic isolation system, effective operation of which is related to fulfilling the maximum stress constraint. In view of this fact when designing advanced SIS the principle of system adaptability to the real object conditions had been used as the basic one in the new concept. Adaptive SIS design assumes incorporating the control (or self-control) elements. A perspective way of the above problem solution is incorporating the control units in the seismic isolator structure. This permits, first, to make "adjustment" of every bearing in accordance with its actual loads and deformations of the base slabs in installation place, second, to develop basic SIS components, suitable for any conditions of object fitting, third, to reduce substantially the requirements to base slabs stiffness.

As a result of calculations for various fitting conditions we had shown that verification of the range of the changing control parameters of bearing construction blocks and development of a special technology of SIS conversion from the mounting state to the operational one, permit to eliminate additional requirements for the building constructions. Disassembling of the technological bearings provides for their off-loading, for which purpose only pneumatic elements with monotonous characteristic are used, such elements form a part of every SIS bearing. This is equal to producing a low stiffness air layer between the base slabs, which assume a certain form of static equilibrium depending on the construction fitting conditions and distribution of the protected object mass. On the next stage we perform adjustment in the units (change of mounting dimension) which transfer the load, thus the system ensures the interference fit in the vertical direction (elements are in this moment unloaded), depending on the distance between the base slabs in the bearing arrangement positions. The pressure in the operational pneumatic elements decreases to a value, which was received from the results of determination of the protected object actual
mass and its distribution verification.

3.4. Mathematical model of adaptive pneumatic seismic isolator

Now let's consider the influence of lack of parallelizm and axiality of the embedded elements on the power characteristic of a bearing. Description of support structure is presented

in 2.3.1. It is apparent, that the factors specified mainly influence the values of bearing response in horizontal direction.

When designing a mathematical model the following assumptions had been made:

- support consists of two unyielding parts (upper and lower), dimensions of which correspond the actual hinge-connected structures;
- in view of support and loading pattern symmetry a 2D model is under consideration;
- ribs of curvilinear trapezoid are approximately replaced with constant radius circles;
- rolling of supports takes place without slipping;
- under the vertical load P_v and horizontal displacement the support comes to equilibrium position on the rectilinear site or lateral curvilinear surface; the value of horizontal force P_G, necessary for holding a support in the deflected position, is equal to the horizontal response value of the support;
- only static loading on the support is considered.

From the equations of support static equilibrium the expression for horizontal force determination will be as follows:

$$P_G = P_v (X_A – X_B) + P_0 (X_A – X_B)/(Y_A – Y_B)$$

here

P_0 is the weight of support, applied in the center of gravity;

x_A, y_A and x_B, y_B are the contact point coordinates of the support lower and upper sections with embedded elements, respectively.

To determine the influence of embedded elements location on the value of support response at its displacement within the working stroke in horizontal direction three states of support had been considered:

- support with parallel and coaxial embedded elements;
- support with non-parallel and coaxial embedded elements;
- support with non-parallel and non-coaxial embedded elements.

A support center of gravity being displacing to a value Δx, it is rotated through the angle á, value of which is determined from the formula:

$$\alpha = \arcsin (|x_1 – x_0|/R_{04}),$$

where

x_1, x_0 are the coordinates of center of horizontal site and the point of its integration with curvilinear surface, respectively;

R_{04} is the radius of curvilinear surface circle.

Coordinates of the rigid body points are combined from their X-axis displacement and displacement due to rotation around the center of curvilinear surface circle. In this case the current coordinates of the support points (x_i^* , y_i^*) at its displacement in horizontal direction are calculated from the formulae:

$$x_i^* = \Delta x – R_{4i} \sin (\varphi_{4i} + \alpha) y_{4i}$$

$$y_i^* = R_{4i} \cos (\varphi_{4i} + \alpha),$$

where

R_{4i} is the distance from the center of curvilinear surface circle to the point i;

φ_{4i} is the angle between the negative direction of OY-axis and the radius-vector, drawn from the point 4 (see Fig. 16) to the point i.

After substitution of the values P_B and P_O it is possible to determine the force of support transfer from the horizontal part to curvilinear surface. Table 12 presents the values P_G for different support displacements.

Let's consider rolling of the support with non-parallel embedded elements. It is assumed that upper embedded piece remains horizontal and lower one is rotated through

angle ß relative to the axis, passing through the center of the site. Such assumption is true, for the supports, as a rule, are located under the building walls. When the embedded piece slopes the support lower part is rotated together with it in such a way that the contact between the support and the embedded piece along the flat site is preserved. Formulae for calculation of the coordinates of contact points A and B change and acquire the following form:

$$x_i^* = \Delta x \sin(\beta) - R_{4i} \sin(\varphi_{4i} + \alpha)$$

$$y_i^* = R_{4i} \cos(\varphi_{4i} + \alpha) - \Delta x \cos(\beta),$$

If nonaxiality of embedded elements is taken into account additionally it was agreed that fracture along the internal hinge (see Fig. 16) occurs in the support. Under this condition we assumed, that the lower embedded piece has been rotated in the opposite direction through the same angle in such a way that the contact between the support and the embedded piece along the flat site is preserved. Formulae to calculate the coordinates of the contact points A and B will be similar in the shapes. Table 13 presents the calculation results of the response value P_G for both cases at the time of the support transfer from the horizontal section to the curvilinear one and at its maximum displacement.As a result of the calculations performed it was determined that:

- internal hinges in the support permit to realize its self-control conditions relative to the embedded piece with a certain slope As this takes place, for example, it is sufficient to provide for a gap of 10–12 mm between separate support components if the slope angle of the embedded piece is 0.02 rad;
- equilibrium position of the support if there is a "fracture" along the hinge is preserved throughout all design displacement range (taking into account the vertical displacements), i.e. the moment sign relative to the hinge does not change;
- embedded elements nonaxiality results in occurrence of non-symmetry of "interference fitting" in the support power characteristic.

Furthermore, adaptation is expedient for the systems with other types of seismic isolators, for example with steel rubber bearings. Evaluation of its realization due to the support rubber material properties in this case involves continual models. Analysis methods of dynamic and static characteristics of the support structures have been developed on the basis of comparison with known data, among the other things for natural rubber bearings (NRB).

4. THE RESULTS OF VERIFICATION OF THE CODES DUE TO THE CRP

Full-scale experimental investigations of a full-scale fragment of WWER-640 reactor building low-frequency seismic isolation system had been performed. General view of a seismic isolation system fragment, installed on the shake table, is shown in Fig. 16. The testing fragment consists of 2-story metal construction. The dimensions of this construction are about 22.0 × 6.0 × 7.0m.Elastic and inertial construction parameters has been chosen similar to the real building characteristics. Full-scale seismic isolators with 30% filling of the cassette assembly (2 devices from 6) had been used in the system. Principal view of the seismic isolation devices on the shake table is shown in Fig. 17. For prediction calculations of the behaviour of seismic isolation system under the input which simulates seismic ground motions, a simplified design model of the isolated facility has been used. The object itself was simulated with elastic beam, supported on the nonlinear isolation devices. Force characteristics of the isolators are shown in Fig. 7.

The data on geometrical, inertial and stiffness characteristics of the isolated facility are presented in Fig. 18. Figs 19–22 present the test results of a full-scale fragment of the seismic

isolation system under various conditions. Figs 19–20 correspond to the first test conditions (test1) and show the accelerogramms of the seismic stand and the isolated facility motion as well as the response spectra which correspond with them under natural oscillations of the system in horizontal direction due to nonzero entry conditions for the position. Figs 21–22 correspond to the second test conditions (test2) and present the similar results of seismic

TABLE 12. CALCULATION RESULTS FOR SUPPORT DISPLACEMENTS

Displacement of support, mm	0.0	30.0	60.0	120.0	150.0
Support angle of rotatation, rad	0.0	0.019	0.038	0.075	0.094
Reaction value P_G, t/f	89.23	89.04	88.83	88.31	88.01

TABLE 13. RESPONSE VALUE OF P_G

State of a support	of angles	P_G (values of support transition from the horizontal part to the curvilinear one)	P_G (maximum displacement in the horizontal direction)
Embedded pc	0.02	89.11	87.99
slope angle	-0.02	89.32	87.99
Support angle of fracture along the	0.02	78.52	77.34
internal hinge, β, rad	-0.02	99.95	98.33

TABLE 14. ELASTIC CONSTANTS

	C10.mPa	C01.mPa	C11.mPa	C20.mPa	C02.mPa	C30.mPa	G.mPa
1	0.4329	-0.05416	0.01039	0.00693	-0.001531	-	0.76
2	0.4856	-0.04484	0.004457	-0.008389	-	0.001052	0.88
3	0.4463	-0.01076	-	-0.003075	-	0.001018	0,87
4	0.4099	-0.03338	-	0.01559	0.000291	-	0.75
5	0.1566	0.0434	-0.07328	0.0869	0,0122	-	0.4
6	0.8284	-0.6284	-0.006014	0.0424	-	-0.000675	0.4
7	1.058	-0.858	-	0.03639	-	-0.000679	0.4
8	0,8627	-0.6627	-	0.2678	-0.000751	-	0.4
9	0.2261	0.1415	-0.022	-	-	0,00445	0.7352
10	0,3415	0.1196	-0.005142	-0.07412	-	0,007558	0.9222
11	0.1567	0,09905	-0.00675	-	-	0.000597	0,515

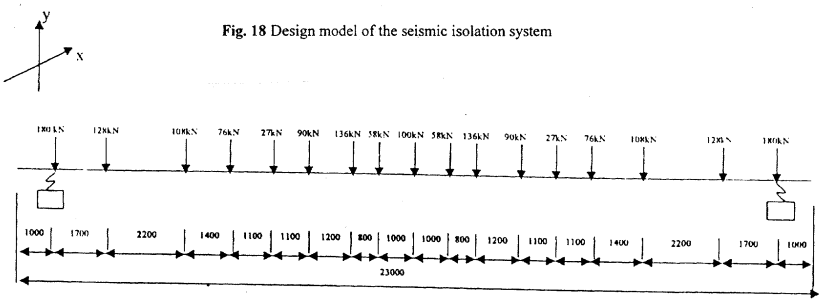

Fig. 18 Design model of the seismic isolation system

$I_x = 11.83\ m^4$, $I_y = 1.459 m^4$, along mass - 5800 kg/m

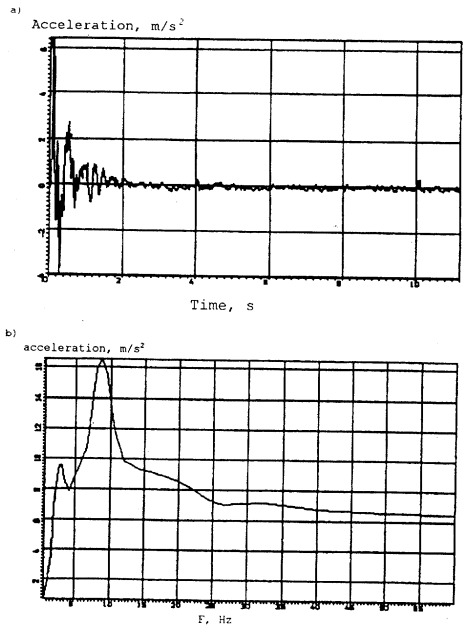

Fig. 19 Test 1
a) seismic acceleration (Gor)
b) response spectra

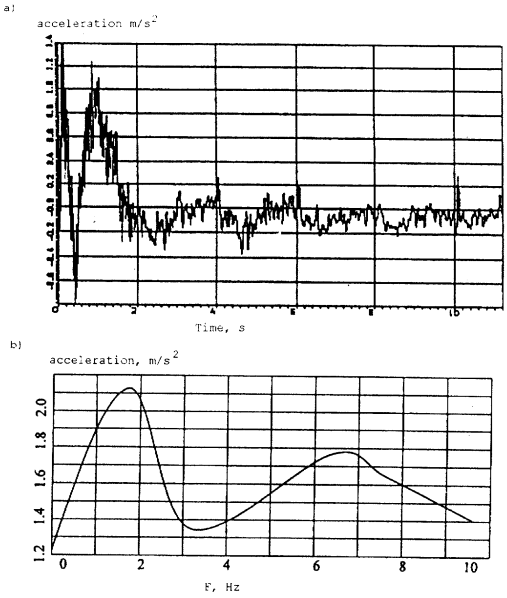

Fig. 20 Test 1
a) acceleration of seismic isolation building
b) response spectra

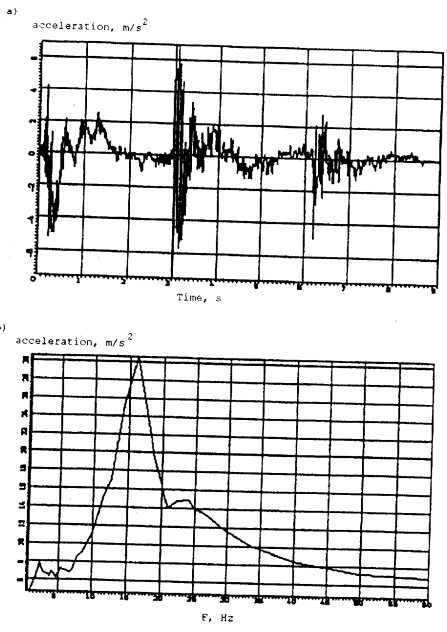

Fig. 21 Test 2
a) seismic acceleration
b) response spectra

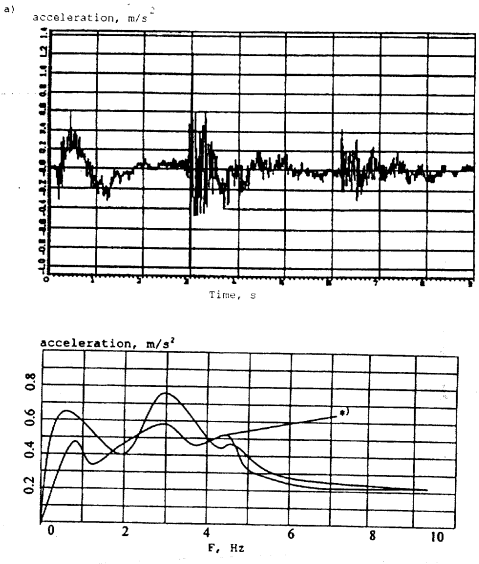

Fig. 22 Test 2
a) acceleration of seismic isolation building
b) response spectra

isolation system tests under excitation of vertical system motion due to explosive methods. Figure 22 (curve *)) presents calculation results of response spectra under the conditions of the test 2. Comparison of calculation and testing results has shown a small difference of reaction spectra in the large amplitude domain. We plan to carry out further seismic isolation system tests under various loading conditions and take into account variations of dissipative and elastic characteristics of the system.

5. COMPARISON OF THE TECHNICAL SOLUTIONS AND CALCULATIONS RESULTS

5.1. Main theoretical preconditions of the calculation

The problem of determination of the stressed-deformed state of bearing rubber layers has been solved under the conditions of the following method. At first a form of transformation $\bar{R}\left(\bar{r}\left(q_1,q_2,q_3\right)\right)$ of the undistorted reference configuration into the actual one with an accuracy of the TBD natural coordinate functions is specified. Further on the basis of this transformation a deformation measure expression, stress tensor and equilibrium equations are set up. After solving the equations for the unknown functions the fields of displacements, deformations and stresses are determined.

For the natural coordinates the cylindrical coordinates r,φ,ξ are accepted. Radius-vector of the reference configuration in this coordinate system assumes the form

$$\bar{r} = r\bar{e}_r + \xi\bar{k},$$

$$r \in \left[R_0, R_1\right], \quad \xi \in [0,h],$$

where

$\bar{e}_r$, $\bar{k}$ – are the unit vectors of coordinate axes.

Radius-vector of a deformed state is given as follows

$$\bar{R} = \left(a + ra_1\right)r\cos\varphi\,\bar{i}_1 + \left(b + rb_1\right)r\sin\varphi\,\bar{i}_2 + \alpha\,\bar{i}_1 + \lambda\,\bar{k}, \qquad (6)$$

where

$a, a_1, b, b_1, \alpha, \lambda$ – are the TBD functions of the natural coordinate ξ and time t,;

$\bar{i}_1, \bar{i}_2, \bar{k}$ – are the unit vectors of the Cartesian coordinate system (the horizontal load is applied in the direction of the unit vector $\bar{i}_1$).

Radius-vector $\bar{R}$ answers the following assumptions of the displacement field:

- section $\xi = const$ which was flat prior to deformation remains flat under the deformed state;

- circle of r radius (in the $\xi = const$ section) during the deformation process will be transformed into an ellipse with semi-axes $a + ra_1$, $b + rb_1$.

Dependence of the expressions for semi-axes on the coordinate r allows for "pressing-out" the material during the deformation process on both the external and internal boundary cylindrical surfaces $r = R_0$ and $r = R_1$, respectively.

It is accepted, that coupling of steel and rubber layers in a damper is “rigid” and there is no deformation on the contact surfaces. Then

$$\begin{aligned} &a(0) = a(h) = 1, \quad b(0) = b(h) = 1, \\ &a_1(0) = a_1(h) = 0, \quad b_1(0) = b_1(h) = 0. \end{aligned} \qquad (7)$$

In this relations parameters $\alpha_0, \alpha_h, \lambda_0, \lambda_h$ are defined as corresponding displacements of the steel plates adjacent to the rubber layer. These parameters are determined from the conditions of compatibility of strain components.

For the model of material (nonlinear elastic spring & viscous element) a viscoelastic model with a rheologic scheme in the form of parallel coupling of elastic and viscous elements is used. In addition it is assumed that damping properties are governed solely by rate-of-strain deviator and are independent of the given tensor ball part. The expression for stress tensor in this case will be as follows:

$$T = T_e + 2\eta\, dev(d), \tag{8}$$

where

$T_e = 2\sqrt{\frac{g}{G}}\left(\psi_0 E + \psi_1 F + \psi_2 F^2\right)$ – is the stress tensor of elastic element in the Cauchy form,

$$d = \frac{1}{2}\left(D + D^T\right), \quad D = \nabla \bar{v} - \frac{1}{3}\bar{v}\cdot E, \quad \bar{v} = \frac{\partial \bar{R}}{\partial t}, \tag{9}$$

E – is the unit tensor,

η – is the viscous factor

F - is the Finger deformation measure.

Equilibrium equations for the rubber layer in terms of the expression for $\bar{R}$ and relations (6) will have the following form

$$\iint_o \left\{ -\left[\sqrt{\frac{G}{g}}\left(\frac{\partial W}{\partial I_k}\frac{\partial I_k}{\partial u_i'} + \bar{r}_s\, \bar{R}^s \cdot d \cdot\cdot \frac{\partial \bar{R}_k}{\partial u_i'}\bar{r}^k \right) \right]' + \left[\sqrt{\frac{G}{g}}\left(\frac{\partial W}{\partial I_k}\frac{\partial I_k}{\partial u_i} + \bar{r}_s \bar{R}^s \cdot d \cdot\cdot \frac{\partial \bar{R}_k}{\partial u_i}\bar{r}^k \right)\right] \right\} r\,\partial\varphi\,\partial r = 0, \tag{10}$$

$$i = 1, \ldots, N$$

where

$W = W(I_1, I_2, I_3)$ – is the specific potential energy,

I_1, I_2, I_3 – are the invariants of Cauchy measure of deformation,

$\bar{r}_s, \bar{r}^s, \bar{R}_s, \bar{R}^s$ – are the vectors of main and mutual bases in the reference and actual configurations;

G, g – are the determinants of covariant components of unit tensors in the reference and actual configurations, respectively.

Hereinafter the rule of sum over the repeating ("dummy") indices is used, and the sign "'" means differentiation with respect to ξ.

Integration in equations (10) is carried out for the undistorted surface.

Complementing this formula with the relations:

$$\alpha(0) = \alpha_0, \quad \alpha(h) = \alpha_h, \quad \lambda(0) = \lambda_0, \quad \lambda(h) = \lambda_h,$$

we shall receive boundary conditions for the equations.

Dependence of potential energy on the invariants of the Cauchy measure of deformation is specified as follows

- for incompressible material:

$$W = \sum_{i+j=1}^{N} C_{ij}(I_1 - 3)^i (I_2 - 3)^j + p(I_3 - 1), \tag{11}$$

where

p – is the Lagrangian multiplier;

- for compressible material:

$$W = \sum_{i+j=1}^{N} C_{ij} \left(I_1 - 3\right)^i \left(I_2 - 3\right)^j + \sum_{i=1}^{N} K_i \left(\sqrt{I_3} - 1\right)^{2i}, \quad (12)$$

where

$I_1 = I_3^{-1/3} I_1, \quad I_2 = I_3^{-2/3} I_2.$

In case of incompressible material the multiplier $p = p(\xi, t)$ is among unknown functions.

Relations for the model (nonlinear elastic spring & elastic plastic element) are determined by axioms of sequential and parallel connections and physical dependencies which describe simple (classical) materials

$$d = d_\alpha = d_\beta + d_\gamma; \quad s = s_\alpha + s_\beta; \quad s_\beta = s_\gamma.$$

where

d – are the tensors of form deformation speed;

s – are the deviators of stress tensors.

Index α relates to values of elastic link of the model; indices β, γ - to elastic and plastic elements of elastic plastic link; the values of rheologic model as a whole are designated without indices.

Stress deviators of elastic elements are determined by the formula:

$$s = 2 I_3^{-0.5}(F) dev(\psi_1^+ F^+ + \psi_2^+ F^+),$$

where

$F^+ = I_3^{-1/3} F,$

$$\psi_1^+ = \frac{\partial W_2}{\partial I_1(F^+)} + I_1(F^+) \frac{\partial W_2}{\partial I_2(F^+)}; \quad \psi_2^+ = -\frac{\partial W_2}{\partial I_2(F^+)},$$

$$W = W_1(I_3^{1/2}) + W_2(I_1(F^+), I_2(F^+))$$

For plastic element the stress deviator is determined by the relation

$$\begin{cases} d_\gamma = 0, \ N(s_\gamma) < \tau_s \\ d_\gamma \neq 0, \ s_\gamma = \dfrac{\tau_s}{N(f)} f(d_\gamma), \end{cases}$$

where

f is the tensor function from the form deformation tensor d_γ, N is the norm in the space of stress deviators, τ_s is the material yield limit.

When calculating it was accepted that $f(d) = d$, and the norm N was chosen in the von Mises form

$$N(s) = \sqrt{I_2(s)} = \sqrt{\frac{1}{2} s \cdot\cdot s} \quad (13)$$

5.2. Method of solution

Equilibrium equations (10) take rather complicated form even when expressions for radius-vector (6) and specific potential energy (11), (12) are relatively simple; their notation in the form which is convenient for programming as well as the process of programming itself are stubborn problems. Therefore for solving the similar problems a method of continual

transformations has been developed. The procedure is as follows. On the preliminary stage the classes (in terms of object-oriented programming languages) of differential, tensor and vector transformations are realized by way of programming. Functions-methods of these classes over the expressions preset (strings or string arrays) perform the corresponding transformations (operations of differentiation, scalar and vector multiplication, convolution of tensors etc.) and return the results in the form of strings or string arrays. Further solving the problem follows the scheme below. The input data for the "A" program are the preset expressions (strings) of dependencies of specific potential energy on the invariants of Cauchy measure of deformation, dependencies of radius-vector components on the natural coordinates and unknown functions. On this basis the following parameters are determined sequentially (in the form of strings): basic vectors, tensor of Cauchy measure of deformation, its invariants, stress tensor, integrated force reactions (forces and moments required) as well as coefficients of equilibrium equations, brought into the form

$$\left(\iint\limits_{o} a_{ij}\left(u, u', u, u'\right) r\, \partial\varphi\, \partial r \right) u_j'' + \left(\iint\limits_{o} d_{ij}\left(u, u', u, u'\right) r\, \partial\varphi\, \partial r \right) u_j'' + \left(\iint\limits_{o} b_i\left(u, u', u, u'\right) r\, \partial\varphi\, \partial r \right) = 0, \quad i, j = 1, \ldots, N$$

where

$u -$ is the "vector" of unknown functions.

The result of the "A" program execution is creation of the source texts of subprograms in the form of separate files for computing the coefficients a_{ij}, d_{ij}, b_i and the required integrated force reactions (for example, forces and moments on the upper plate of the bearing). Then these files are compiled together with the “B” program which realizes dicsretization and integration of the equations. Integration of the equations has been carried out by net-point method and method of transforming the boundary-value problem into initial Cauchy problem.

5.3. Determination of material constants

To describe deformation properties of rubber we used various rheologic material models depending on requirements imposed on the material. In this case it is required to take into consideration nonlinear nature of dependence of stress on the deformation, material compressibility in stringent conditions, as well as material damping behavior under dynamic loads. The constants which enter the description of material model are determined on the basis of uniform deformation. For such deformations it is possible to construct an analytical solution and to receive experimental data from their practical realization. In general, material deformations can be divided into two components: form deformations and volumetric deformations. Thus, potential of elasticity can be presented as a sum of two components: the first one is responsible for form deformations and the second one — for volumetric deformations. To find a coefficient of compressibility experimental data on the compressibility are used. At compressibility the component which answers the form deformation may be neglected due to its small value as compared with the volumetric component. In turn, when finding the form deformation constants experimental data on uniform deformations are used, in which volumetric deformation may be neglected. Thus, coefficients of form deformation and compressibility can be determined independently from each other. When determining the potential coefficients answering for the form deformation we can might consider the material as incompressible and J=1. Let’s consider incompressible material.

For description of stressed-deformed state of the filled-up rubber as an incompressible material numerical models of elastic, viscoelastic and elastic plastic materials are under consideration.

To find the constants for each of material models under consideration experimental data, received for uniform deformation of elastomers are used. Thus the following uniform deformations had been considered: axial tension, biaxial symmetric tension, pure shear, and for the last two models the same uniform deformations with a cycle. Analysis of experimental data on the uniform deformation with a cycle and without it permits to generalize that superimposing the unloading-loading cycle on the uniform deformation does not prove any substantial influence at further load input. Therefore it is expedient to consider as a first approximation the elastic model of material and to determine coefficients of elasticity potential. Using the data received and adding elastic plastic or viscoelastic elements it is possible to find the constants answering for material damping behavior and to specify the constants in elastic part.

a)Elastic material

For description of the stressed-deformed state of incompressible material a potential of elasticity (6) is used. For uniform deformations we have:

axial tension

$$\lambda_1 = \lambda; \lambda_2 = \lambda_3 = \lambda^{-1/2}$$

$$\sigma = 2(\lambda - \lambda^{-2})\left[\frac{\partial W}{\partial I_1} + \lambda^{-1}\frac{\partial W}{\partial I_2}\right] \tag{14}$$

biaxial and symmetric tension

$$\lambda_3 = \lambda^{-2}; \lambda_2 = \lambda_1 = \lambda$$

$$\sigma = 2(\lambda^4 - \lambda^{-2})\left[\frac{\partial W}{\partial I_1} + \lambda^{2}\frac{\partial W}{\partial I_2}\right] \tag{15}$$

pure shear

$$\lambda_1 = \lambda; \lambda_2 = 1; \lambda_3 = \lambda^{-1}$$

$$\sigma = 2(\lambda - \lambda^{-3})\left[\frac{\partial W}{\partial I_1} + \frac{\partial W}{\partial I_2}\right] \tag{16}.$$

Using the expressions (14), (15), (16) and the results of corresponding tests on rubber specimens, the least-squares method has been applied to determine the values of constants C_{ij}. Under small deformation, the law of elasticity $\sigma_i = \lambda_i \frac{\partial W}{\partial \lambda_i}$ goes over into the Hook law, as this takes place the following condition is to be performed,

$$2(C_{10} + C_{01}) = G \tag{17}$$

where

G is the initial shear modulus of the material.

Thus, expression (17), if G is known, is an additional condition for determination of the constants C_{ij} from the experimental data. Further two options were considered:

- shear modulus is considered unknown and condition (10) is the expression for determination of G, from the C_{ij} found;

- shear modulus is considered preset and expression (10) is an additional condition when determining the constants C_{ij}.

b)Viscoelastic material

A viscoelastic material is considered, rheologic model of which is a parallel connection of a Hook element and Maxwell material. Dependence of potential energy on the invariants of Cauchy deformation measure for the Hook element (γ) is specified in the form

$$W_{\gamma} = \sum_{i,j} C_{ij} (I - 3)^{i} (II - 3)^{j} \tag{18}$$

and for the elastic element (α) in Maxwell material it is accepted in the form

$$W_{\alpha} = C(I_1^{\alpha} - 3) \tag{19}.$$

For a viscous element the stress deviator connection with the tensor of form deformation speeds has the form

$$dev(T_{\beta}) = 2\eta \, dev(d_{\beta}) \tag{20}.$$

To find the constants which enter the expressions for potential energies W_{γ} W_{α} and viscous factor η , the experimental data which had been received for uniform cyclic deformation are used. The following uniform deformation are considered:

axial tension

$$\lambda_1 = \lambda; \lambda_2 = \lambda_3 = \lambda^{-0.5}$$
$$\sigma = C\left(l^2 - l^{-1}\right) + \frac{\partial W_{\gamma}}{\partial I^{\gamma}}\left(\lambda^2 - \lambda^{-1}\right) + \frac{\partial W_{\gamma}}{\partial II^{\gamma}}\left(\lambda - \lambda^{-2}\right) \tag{21},$$

where variable l is determined from the equation

$$\frac{l}{l} = \frac{\lambda}{\lambda} - \frac{1}{3\eta}\left(l^2 - l^{-1}\right)C \tag{22}.$$

biaxial symmetric tension

$$\lambda_3 = \lambda^{-2}; \lambda_2 = \lambda_1 = \lambda$$
$$\sigma = 2C\left(l^2 - l^{-4}\right) + 2\left(\lambda^2 - \lambda^{-4}\right)\left(\frac{\partial W_{\gamma}}{\partial I^{\gamma}} + \frac{\partial W_{\gamma}}{\partial II^{\gamma}}\lambda^2\right) \tag{23},$$

where variable l is determined from the equation

$$\frac{l}{l} = \frac{\lambda}{\lambda} - \frac{1}{3\eta}\left(l^2 - l^{-4}\right)C \tag{24}.$$

pure shear

$$\lambda_3 = \lambda^{-1}; \lambda_2 = 1; \lambda_1 = \lambda$$
$$\tau = 2C\left(l_1^2 - (l_1 l_2)^{-2}\right) + 2\left(\lambda^2 - \lambda^{-2}\right)\left(\frac{\partial W_{\gamma}}{\partial I^{\gamma}} + \frac{\partial W_{\gamma}}{\partial II^{\gamma}}\right) \tag{25},$$

where variables l_1, l_2 are determined from the system of equations

$$\frac{l_1}{l_1} = \frac{\lambda}{\lambda} - \frac{1}{3\eta}\left(2l_1^2 - l_2^2 - (l_1 l_2)^{-2}\right)C$$
$$\frac{l_2}{l_2} = -\frac{1}{3\eta}\left(2l_2^2 - l_1^2 - (l_1 l_2)^{-2}\right)C \tag{26}.$$

On the basis of experimental data the constants of the viscous-elastic material model described are determined.

c) Elastic plastic material

Elastic plastic material is considered, rheologic model of this material is a parallel connection of a Hook element and Prandtle material. Dependence of potential energy on the

invariants of Cauchy deformation measure for a Hook element (γ) is specified in the form (18) and for a elastic element in Prandtle material — in the form (19). For a plastic element the connection of stress deviator with tensor of form deformation speeds is as follows

$$dev\left(T_\beta\right) = \delta\ dev\left(d_\beta\right) \tag{27},$$

where

$$\delta = 0, \quad \text{åñëè} \quad N\left(dev\left(T_\beta\right)\right) < \tau_S;$$

$$\delta \geq 0, \quad \text{åñëè} \quad N\left(dev\left(T_\beta\right)\right) = \tau_S; \tag{28};$$

$$N(S) = \sqrt{\frac{1}{2} S \bullet\bullet S}$$

τ_S is the yield limit.

To find the constants which enter expression for potential energies W_γ, W_α and yield limit τ_S the experimental data received for the uniform cyclic deformation are used. The following uniform deformation are considered:

axial tension

$$\lambda_1 = \lambda; \lambda_2 = \lambda_3 = \lambda^{-0.5}$$
$$\sigma = C\left(l^2 - l^{-1}\right) + \frac{\partial W_\gamma}{\partial I^\gamma}\left(\lambda^2 - \lambda^{-1}\right) + \frac{\partial W_\gamma}{\partial II^\gamma}\left(\lambda - \lambda^{-2}\right) \tag{29},$$

where variable l is determined from the equation

$$\frac{l}{l} = \begin{cases} \frac{\lambda}{\lambda}, \tau < \tau_S \\ 0, \tau = \tau_S \end{cases} \tag{30}.$$

biaxial symmetric tension

$$\lambda_3 = \lambda^{-2}; \lambda_2 = \lambda_1 = \lambda$$
$$\sigma = 2C\left(l^2 - l^{-4}\right) + 2\left(\lambda^2 - \lambda^{-4}\right)\left(\frac{\partial W_\gamma}{\partial I^\gamma} + \frac{\partial W_\gamma}{\partial II^\gamma}\lambda^2\right) \tag{31},$$

where variable l is determined from the equation

$$\frac{l}{l} = \begin{cases} \frac{\lambda}{\lambda}, \tau < \tau_S \\ 0, \tau = \tau_S \end{cases} \tag{32}.$$

pure shear

$$\lambda_3 = \lambda^{-1}; \lambda_2 = 1; \lambda_1 = \lambda$$
$$\tau = 2C\left(l_1^2 - (l_1 l_2)^{-2}\right) + 2\left(\lambda^2 - \lambda^{-2}\right)\left(\frac{\partial W_\gamma}{\partial I^\gamma} + \frac{\partial W_\gamma}{\partial II^\gamma}\right) \tag{33},$$

where variables l_1, l_2 are determined from the system of equations

$$\frac{l_1}{l_1} = \begin{cases} \frac{\lambda}{\lambda} - \frac{4}{3\delta}\left(2l_1^2 - l_2^2 - (l_1 l_2)^{-2}\right)C, \tau < \tau_S \\ 0, \quad \tau = \tau_S \end{cases} \tag{34}.$$

$$\frac{l_2}{l_2} = \begin{cases} -\frac{4}{3\delta}\left(2l_2^2 - l_1^2 - (l_1 l_2)^{-2}\right)C, \tau < \tau_S \\ 0, \quad \tau = \tau_S \end{cases}$$

On the basis of experimental data the constants of the elastic — plastic model described are determined.

When calculating steel rubber dampers it is required to take into account compressibility of thin rubber layers. To describe the stressed-deformed state of compressible elastomers a potential of elasticity of the form (12) is used, in which one part is responsible for the shear deformation, and the other — for the volumetric one. Here the constants C_{ij} have the values, found for potential (11) from the experimental data at uniform deformations, for which material compressibility may be neglected. Analytical solution of the problem on the compressibility of a specimen from elastic material is as follows:

$$\lambda_1 = J;\ \lambda_2 = \lambda_3 = 1.$$

$$\sigma = \frac{4}{3}\lambda^{-\frac{5}{3}}\left(\lambda^2 - 1\right)\left(\frac{\partial W}{\partial I_1} + \lambda^{-\frac{2}{3}}\frac{\partial W}{\partial I_2}\right) + \frac{\partial \varphi}{\partial J}, \qquad (35)$$

where

$$\varphi(J) = \sum_{i=1}^{N} K_i (J-1)^{2i},\ J = \sqrt{I_3}.$$

For other material models we have the following expression 36:

$$\sigma = \frac{4}{3}\left(C\left(l^2 - l^{-1}\right) + \frac{\partial W_\gamma}{\partial I^\gamma}\left(\beta^2 - \beta^{-1}\right) + \frac{\partial W_\gamma}{\partial II^\gamma}\left(\beta - \beta^{-2}\right)\right) + \frac{\partial \varphi}{\partial J},$$

$$\beta = \lambda^{2/3},$$

where variable l is determined from the following equations:
for the viscoelastic model

$$\frac{l}{l} = \frac{\beta}{\beta} - \frac{1}{3\eta}\left(l^2 - l^{-1}\right)C$$

for the elastic plastic model

$$\frac{l}{l} = \begin{cases} \frac{\beta}{\beta} & ,\tau < \tau_S \\ 0 & ,\tau = \tau_S \end{cases}$$

Using expression (36) and corresponding experimental data, the method of least squares determines the value of compressibility modulus.

5.4. Results of Experimental Data Processing

5.4.1. ENEA Damper

Values of constants C_{ij} in potential of elasticity (11) were determined from the experimental data for each type of uniform deformation for the preset and unknown shear module respectively. The stresses, calculated due to the formulae (14)–(16) for the coefficients received, fit corresponding experimental data well, but the values of coefficients in all cases are different. Table 14 for ENEA damper presents the values of constants, which has been found by simultaneous processing of experimental data due to various types of uniform deformations.

In this case fixing initial shear modulus G=0.4 MPa gives us no way to find a set of constants Cij, which would give a good coincidence of design and test values of stresses for all uniform deformations considered. However, the set of constants Cij determined without

fixing shear modulus permits to describe all the deformation types under consideration quite well (see Fig. 25–27), in this condition the shear modulus is 0.88 MPa. Figures 23–25 show comparison of the design curves with corresponding experimental curves. Points a), b), c) indicate the results due to axial tension, biaxial symmetric tension and pure shear, respectively. Fig. 23 demonstrates opportunities of the set of five constants $C_{10},C_{01},C_{11},C_{20},C_{02}$, Fig. 24 — $C_{10},C_{01},C_{11},C_{20},C_{30}$.

At last, Fig. 25 shows the curves due to four constants C_{10},C_{01}, C_{20},C_{30}. The values of these constants are listed in Table 14. The Figures show that at calculations it is necessary to give preference to the last two sets of constants. Using only four constants gives approximation which is close enough.

It is to be noted that coincidence on sections with large repetition factor of lengthening is good and some notconformity takes place at small repetition factor. As can be seen from the Figures presented, distinction of initial shear module at large lengthening repetition factor is compensated by the constants at maximum degrees of the first and the second invariant of strain tensor. At the same time the initial section is described more accurately by the curves with a shear modulus which differs from the preset 0.4 MPa value.

For determination of the damping constants in viscoelastic and elastic plastic models of material the data on cyclic load input of damper under shear effect were used. These data were treated as operation of some material at pure shear. After finding the elastic constants of this material: C_{10}=–0.2332, C_{01}=0.329, C_{11}=0.027, C_{02}=–0.01566 the damping constants were determined. For viscoelastic material model the damping constants C=1.7, η=0.12 are received. For elastic plastic material model the damping constants C=0.7, τ=0.5 are received.

On the basis of the expression (36) and corresponding experimental data the method of least squares determines the value of compressibility modulus. Figure 26 shows experimental data and design curves for the material of ENEA damper (N=1,2). When N=2, as can be seen in the Figure, the coincidence with the experimental results is good. It is to be noted, that change in elastic constants Cij does not prove substantial influence on the value of compressibility modulus. Therefore any set of constants Cij, found for potential (12), can be added with the received values of coefficients K_1 and K_2.

Taking into account the stressed state of thin rubber layer and its large area, neglecting the boundary conditions on its lateral surface the uniaxial compression of damper can be treated as rubber compressibility. Therefore the data on uniaxial compression of ENEA damper were used for compressibility modulus determination. The results received are shown in Fig.27. As can be seen, two coefficients in the function which characterize compressibility give good coincidence of design and experimental curves.

5.4.2. KAERI Damper

For the material of KAERI damper the constant Cij were determined from the experimental data for uniform deformation. Table 15 for this damper presents the values of constants, found by simultaneous processing of experimental data from the various types of uniform deformation. Potentials of elasticity with various numbers of constants are considered. In this condition the shear modulus is determined simultaneously with the constants. Its value practically coincides with the value specified in the given materials G=1.2 MPa. Figures 28–31 present design and experimental curves for one of the sets of the constants received.

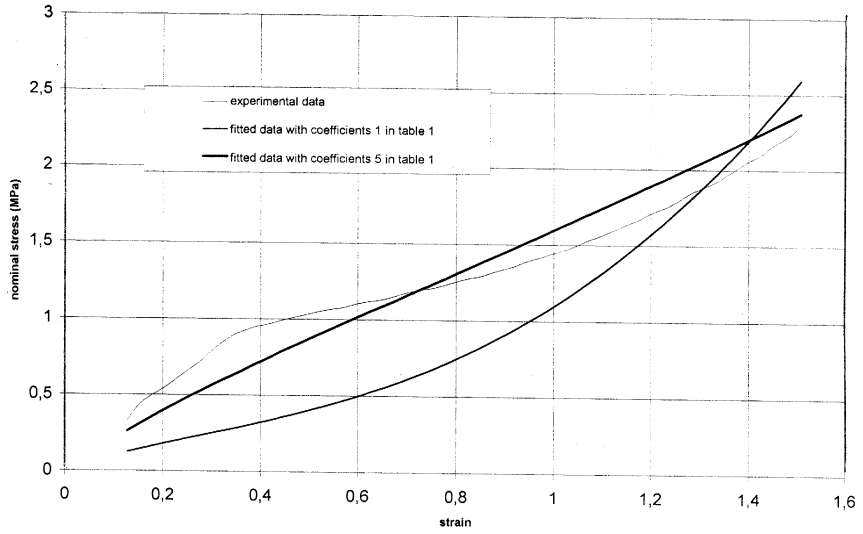

tsu1

Fig.23a Uniaxial tensile test.

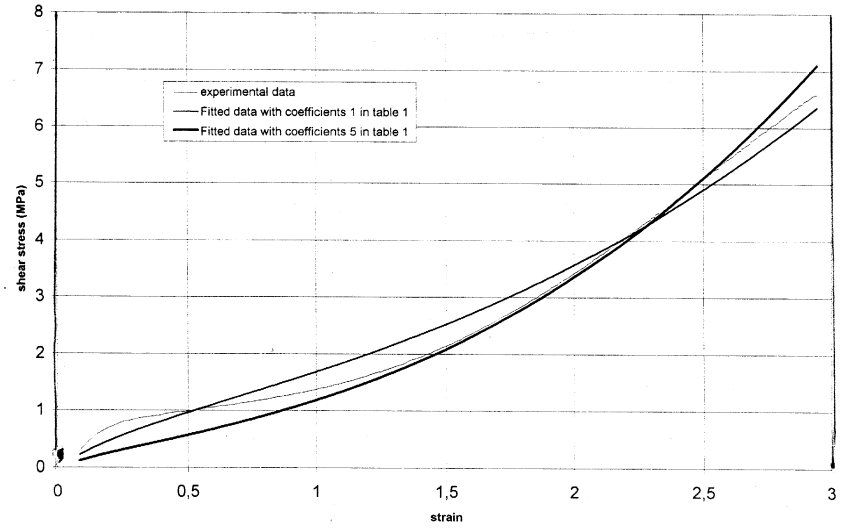

idvsu1

Fig. 23c Planar (pure shear) test

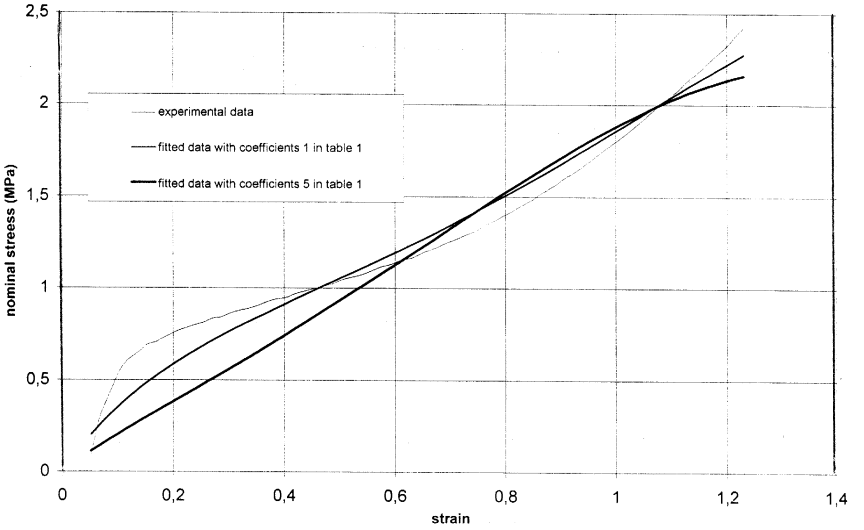

bexsu1

Fig. 23b Equibiaxial tensile test

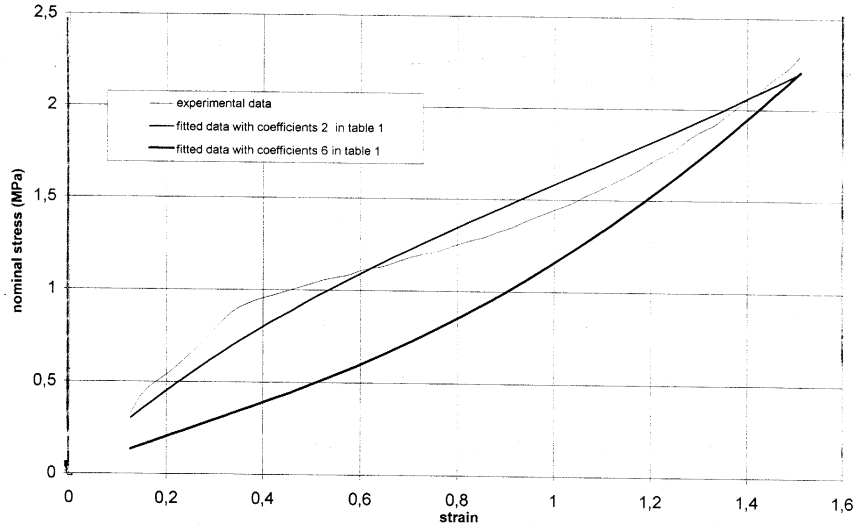

tss2

Fig. 24a Uniaxial tensile test

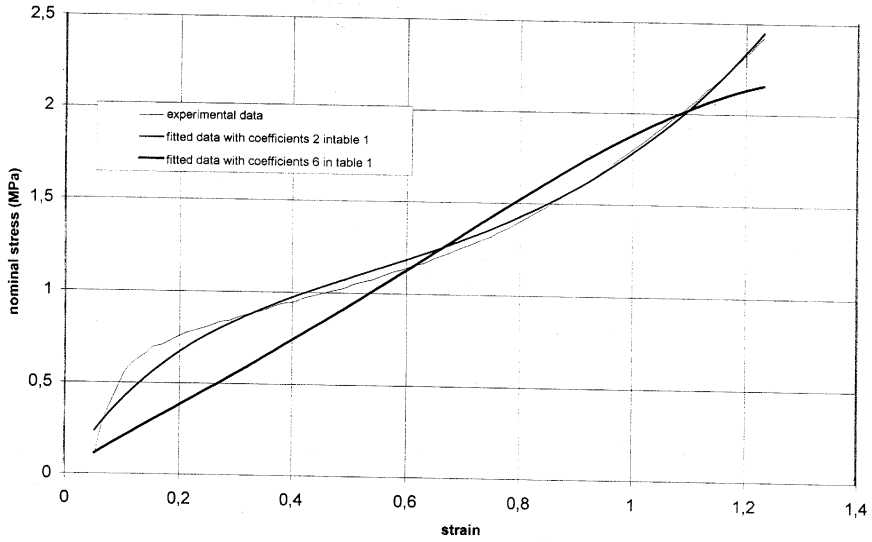

Fig. 24b Equibiaxile tensile test

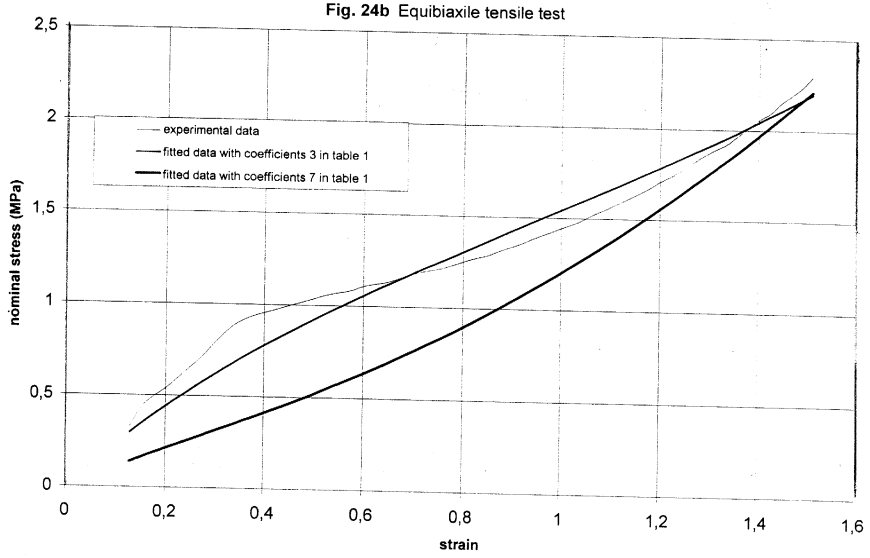

ras1su3

Fig. 25a Uniaxial tensile test

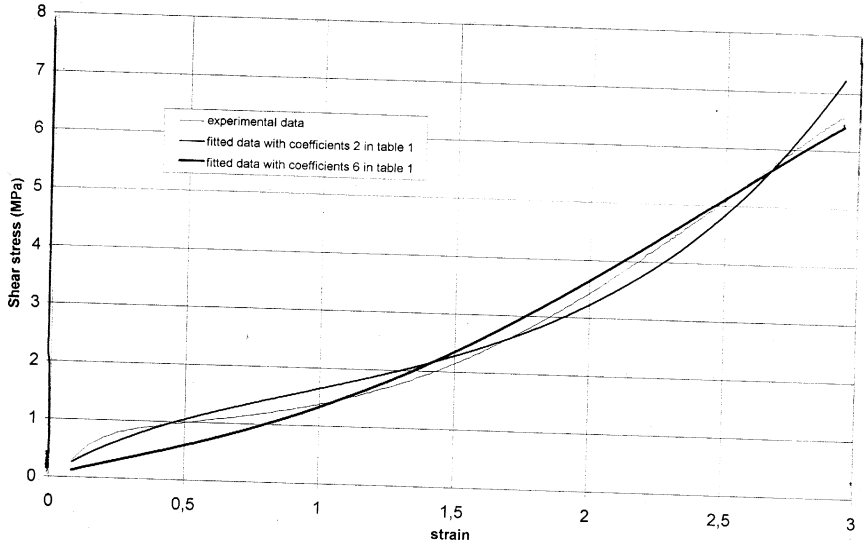

Fig. 24c Planar (pure shear) test

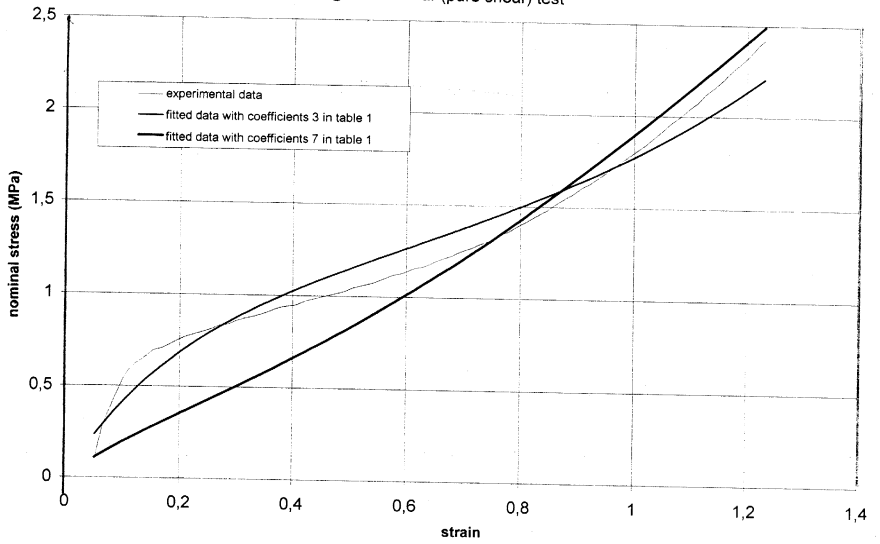

beaxsu3

Fig. 25b Equibiaxial tensile test

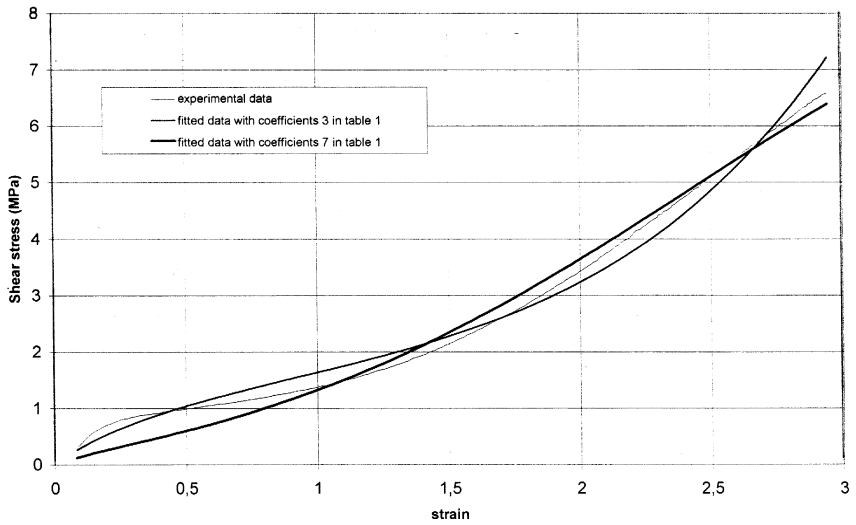

Fig. 25c Planar (pure shear) test.

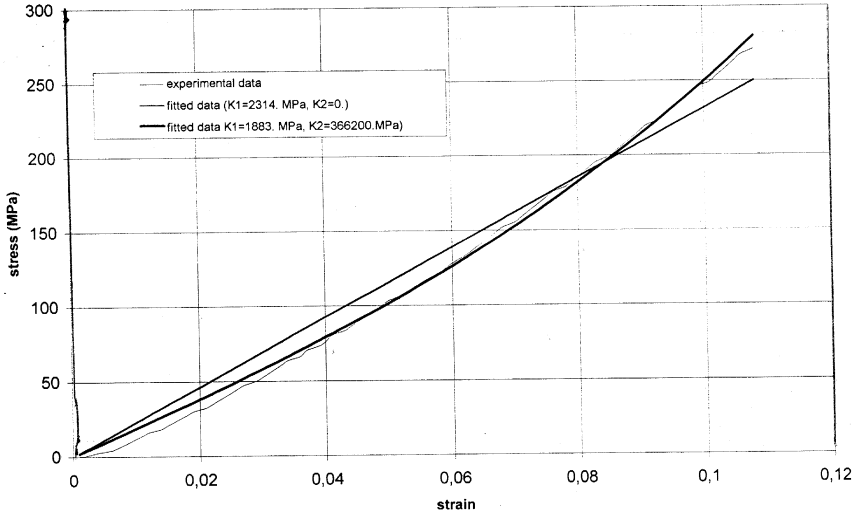

Fig. 26 Compression (volumetric) test

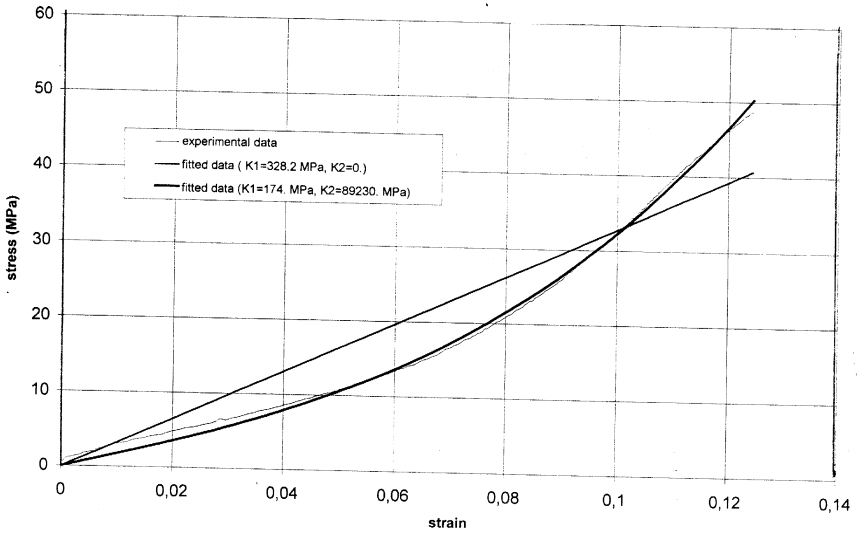

olsu8

Fig. 27 Compression HDRB

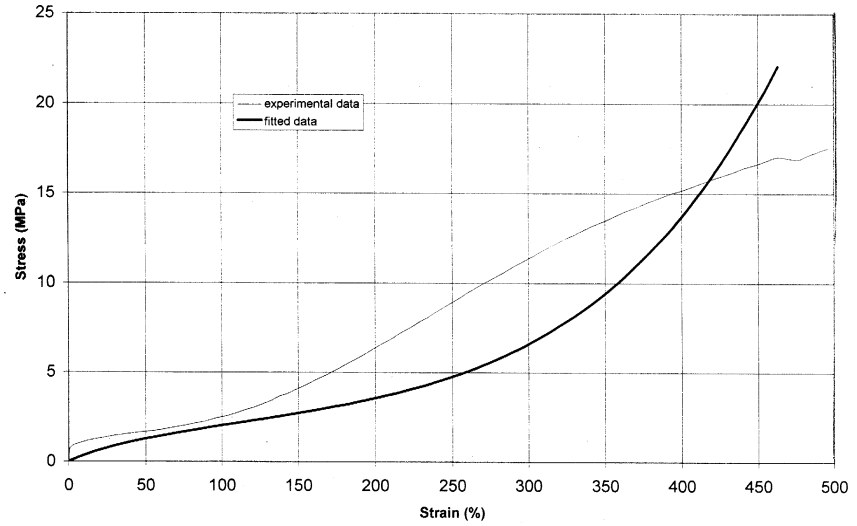

ktra_un

Fig. 28 Uniaxial tensile test.

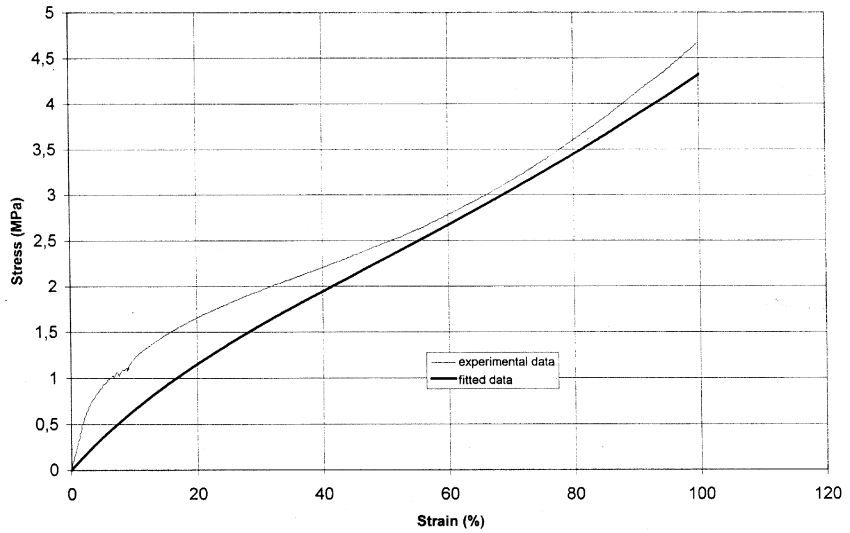

Fig. 29 Equibiaxial tensile test

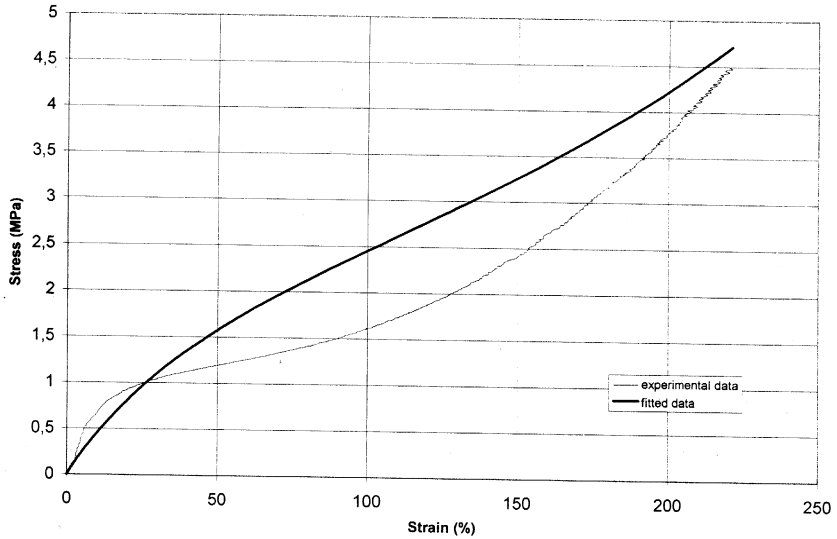

Fig. 30 Planar (pure shear) test.

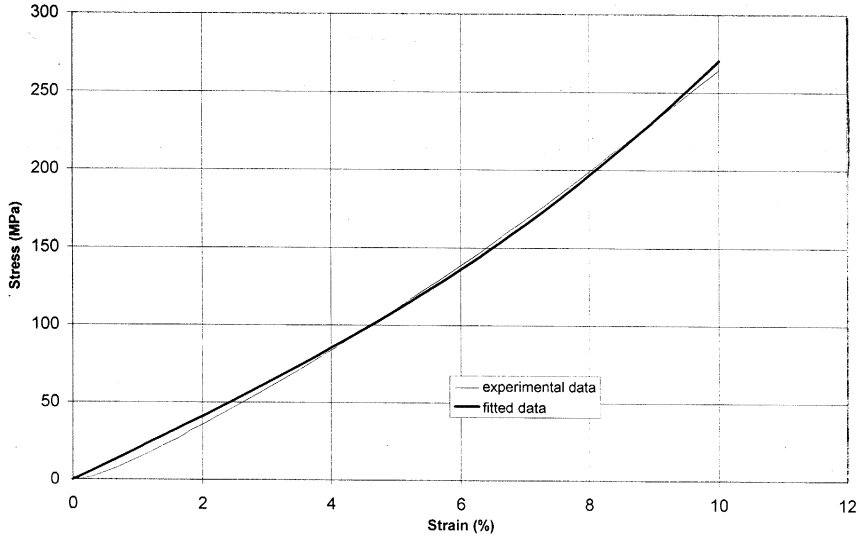

kcomco~1

Fig. 31 Confinated compression (volumetric) test.

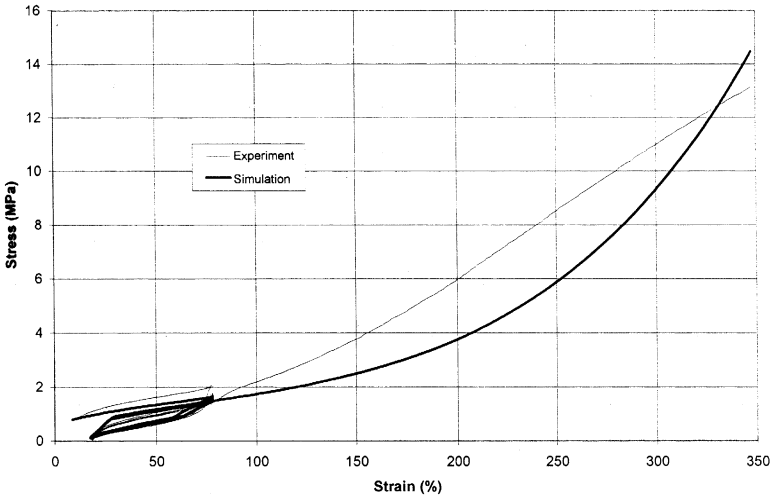

r1p22.xls

Fig. 32 Uniaxial tensile test.

TABLE 15. ELASTIC CONSTANTS

	C10,MPa	C01,MPa	C11,MPa	C20,MPa	C02,MPa	C30,MPa	G,MPa
1	0.2814	0.3426	-0.0539	0.045	0.0085	-	1.24
2	0.576	0.0927	-0.0416	0.0307	0.014	-	1.32
3	0.2993	0.3121	-0.0193	0.0126	0.00104	0.000755	1.22
4	0.4904	0.0818	-	0.0181	-	-	1.14
5	0.4327	0.2093	-	-0.0099	-	0.0011	1.26
6	0.279	0.464	-0.0987	0.0109	0.0171	0.0067	1.46
7	0.2907	0.2644	-	0.0062	-	-	1.1
8	0.281	0.2277	-	0.0138	-	-	1.00
9	0.4554	0.2471	-	-0.0467	-	0.0045	1.38
10	0.49	0.167	-0.051	0.035	0.0136	-	1.3
11	0.27	0.237	-	0.011	-	0.00097	1.00

For evaluation of damping behavior of KAERI damper material the experimental data on uniform deformation with cyclic load are used. For viscoelastic model uniform deformations are described by expressions (21)-(24). Using these expressions, values of elastic constants and experimental data the damping constants had been found. When determining the damping constants for particular type of uniform deformation it is possible to receive good coincidence of calculations and experiments, but the constants have various values. Figures 32–33 present experimental and design curves for viscoelastic model of material, received by simultaneous data processing due to axial and biaxial tension and pure shear.

Uniform deformations for elastic plastic material model are described by expressions (29)-(32). Using these expressions, values of elastic constants and experimental data the damping constants had been found. Let's consider some results of this investigation. For example, from the values of elastic constants from the Table 15 the damping constants for axial tension C=10.0 and τ=0.5, biaxial tension C=1.0 and τ=0.25, pure shear C=2.0 and τ=0.25, uniaxial compression C=0.5 and τ=0.1 had been found. As one can see, they differ substantially. Hence, at simultaneous processing of various types of deformation one and the same set of constants can't be equally good to describe all experimental curves. It is necessary to give the preference to the most significant types of deformation. For the same set of elasticity constants, when considering axial tension, biaxial tension and pure shear simultaneously, the constants of damping C=1.5 and τ=0.25 had been received. Design curves for elastic plastic model of material with these constants and experimental curves for corresponding uniform deformations are presented in Figures 34–36. For all types of deformation the design curves were plotted with the same set of constants of elasticity and damping.

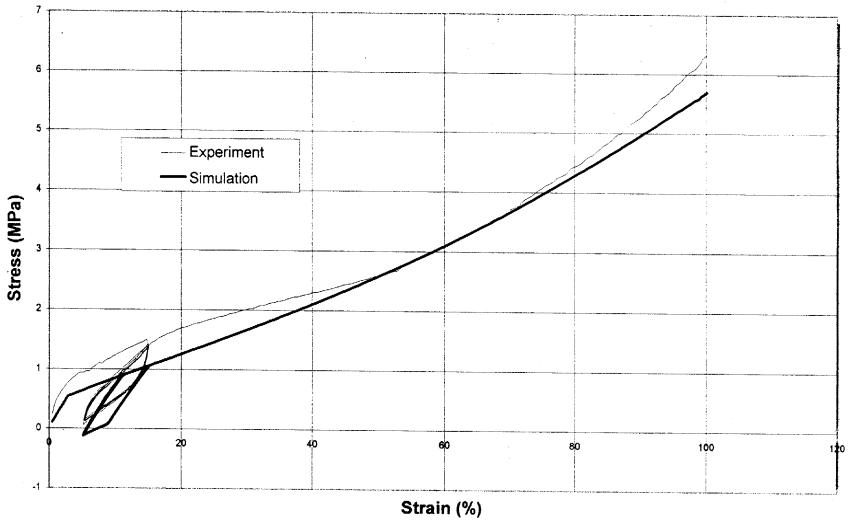

r2p2.txt

Fig. 33 Equibiaxial tensile test.

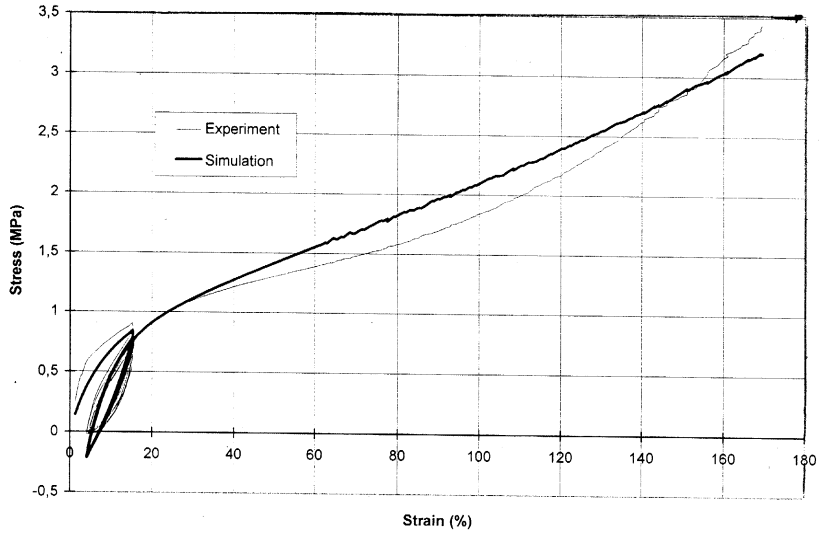

r3k5.exl

Fig. 35 Planar (pure shear) test.

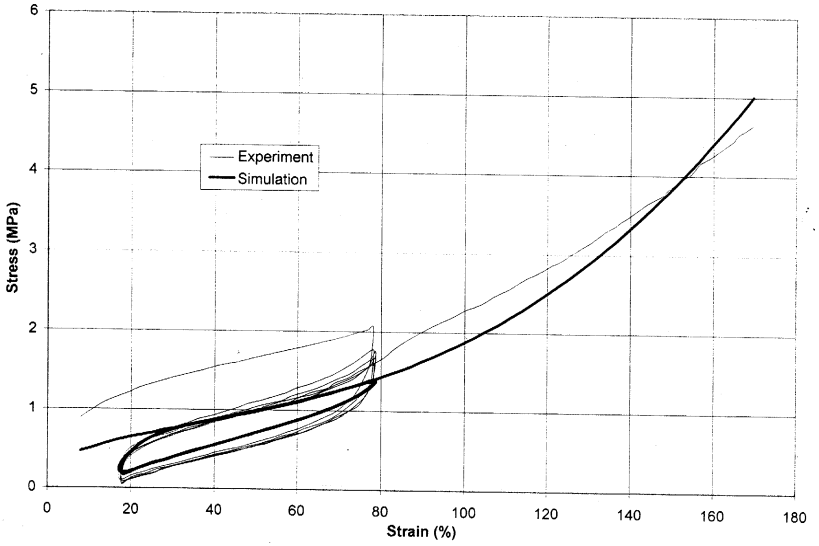

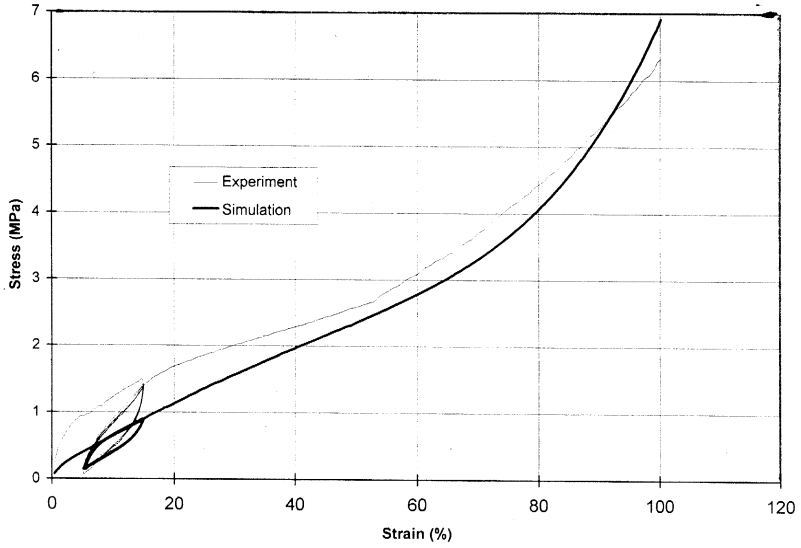

r2p3k5.exl

Fig. 36 Equibiaxial tensile test

On the basis of the expression (36) and corresponding experimental data, method of least squares determines the value of compressibility modulus. Fig. 37 shows experimental data and design curves for KAERI damper material (N=1,2). At N=2, as exemplified by the Figure, we have good coincidence with the results of experiment. It is to be noted, that changing the elastic constants Cij does not prove substantial influence on the value of compressibility modulus. Therefore any set of constants Cij, found for potential (6), can be added with the values of coefficients K_1 and K_2 received.

5.5. Results of calculations

5.5.1. ENEA high damping rubber bearing with soft compound

Compression test was performed with different values of target vertical loads up to 1100% of the design value (50 kN).Combined compression & shear test was performed for evaluation of horizontal stiffness at 50%–400% under vertical load equal to 50 kN, 100 kN.Calculations of force characteristics of ENEA damper model had been conducted for two material models

- nonlinear elastic spring & viscous element (E+V);
- nonlinear elastic spring & elastic plastic element (E+EP).

In course of the calculations due to the first model the material constants listed in the Table 14 were used. For a group of sets of constants of material (# 1–8, Table 14), which have been determined from the data on the specimen experiments, a substantial distinction of design and experimental data is observed. Maximum error reaches 200%. Calculation results with the constants (# 9,10) which were determined with partial use of experimental data on the damper model (compression test) also are in rather poor agreement with experiment (error is up to 100%).Figures 38–40 show characteristic curves for the material, constants for which were determined form the experimental data (#11) only. Satisfactory coincidence of experimental and design data had been received. For the elastic plastic model (E + EP) the similar results had been received, i.e. if we use the constants received from the test data with rubber specimens the correlation between experimental and design data is insufficient. Selection of constants directly from the experimental data permits to receive satisfactory coincidence with the experiment. Figures 41–43 present design and experimental curves as an illustration.

5.5.2 KAERI high damping rubber bearing

Combined compression & shear test was performed for evaluation of horizontal stiffness at 50%, 100%, 150% under design axial stress equal to 2.55MPa.

Comparison of design and experimental data had indicated that with the use of the constants, received from the results of processing the tests with specimens of materials, the design data are in poor agreement with the experiment. When selecting the constants from the experimental data a good coincidence of design and experimental data has been received. Figures 44–45 present design and experimental data at combined load input of damper for viscoelastic and elastic plastic models, respectively.

5.5.3 Model of isolated steel structure (miss)

MISS is a five-storied steel structure composed by 6 vertical columns (HEB-100) 4.5 m high, bolted on a base frame which was manufactured using HEM-140 beams. Four horizontal frames (HEB-100) can be bolted to the columns with an interstory distance of

0.9 m. The total weight of the steel frame is 37 kN. Each horizontal frame, which is 3.3 m × 2.1 m, can support up to 8 reinforced concrete masses, each weighting 12.8 kN (a total number of 20 masses is available).MISS was tested under both fixed and base isolated conditions. In the latter case 6 HDRBs by ENEA were used.In present report a comparison of experimental and design data has been carried out for the C3 configuration: 16 masses (4 for each floor), isolated base.Calculations has been conducted for two load input versions:

- test #135 Time-history — Tolmezzo NS, Direction — Y, Excitation level — 0 dB(1.);
- test #167 Time-history — Tolmezzo, Direction — XYZ, Excitation level — 0 dB(1.)

Measurement positions and excitation axis are shown in Fig. 46 of the initial data, presented by KAERI.When elaborating the design MISS model the matrices of stiffness, inertia and steel structure damping were determined within the finite element method. As a material model of rubber damper layers elastic plastic model (E + EP) was used.Comparison of experimental and design data was carried out from the response spectra in three points: at the base, in the middle, at the top for 1% and 5% damping. The results are presented in Fig. 47,48 (Tolmezzo NS) and in Fig. 49,50 (Tolmezzo 3D).

5.5.4 Isolated rigid mass (IRM)

A lumped mass-beam model for the mock-up is shown in Fig.51 . Weight of rigid mass is 17.9 ton, height of center of gravity of rigid mass — 1.5 m, moment of inertia — 39.19 $tonf \bullet m^2$
Cinematic load input on the IRM was performed under two conditions:

- design earthquake motion;
- beyond design earthquake motion.

As a material model of rubber layers of dampers elastic plastic model (E + EP) was used.A lead plug provided a Young modulus E=1.75E5 kg / cm^2, $\nu = 0.44$ and yield stress equal to 20 kg / cm^2. The following relationship (Hirata, 1996) was used to model post yielding behavior $\sigma_t = 4.*(1.+0.096 \cdot \log_{10} e_t)* e_t^{0.31}$, where σ_t and e_t are actual tensile stress and actual strain, respectively, and e_t is actual strain rate of lead.
Comparison of experimental and design data was carried out from the response spectra in three points at the bottom of rigid mass and at the top of rigid mass for 1% and 5% damping. Results are presented in Fig. 52,53 (design earthquake motion) and Fig. 54,55 (beyond design earthquake motion).

6. CONCLUSIONS AND RECOMMENDATIONS

The main technical complexity when implementing a multicomponent seismic isolation is the necessity to combine the observance of two contradictory requirements:

- seismic isolation system shall constantly remain in the full operational state during the whole service life and it shall lower the level of isolated structure loads to the allowable values under the earthquake;
- during its service life the seismic isolation system shall function as the building foundation and ensure the absorption of all working loads thereby providing for the building position stability.

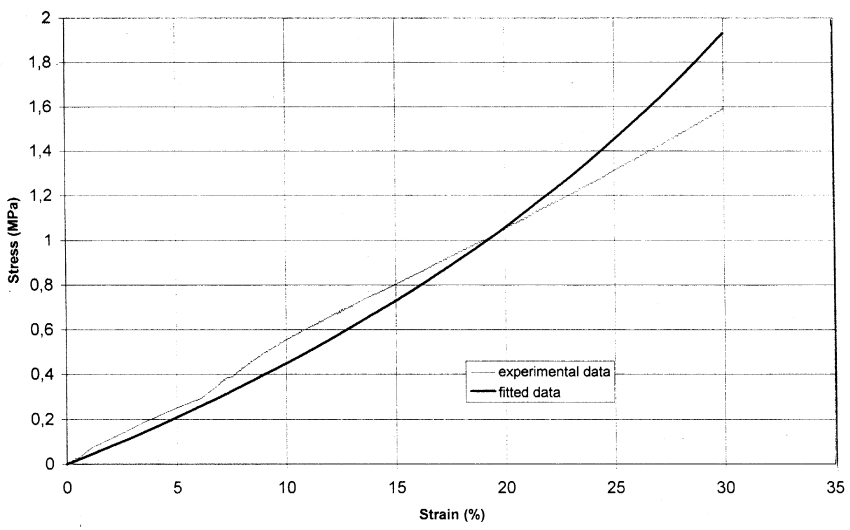

Fig. 37 Uniaxial compression test

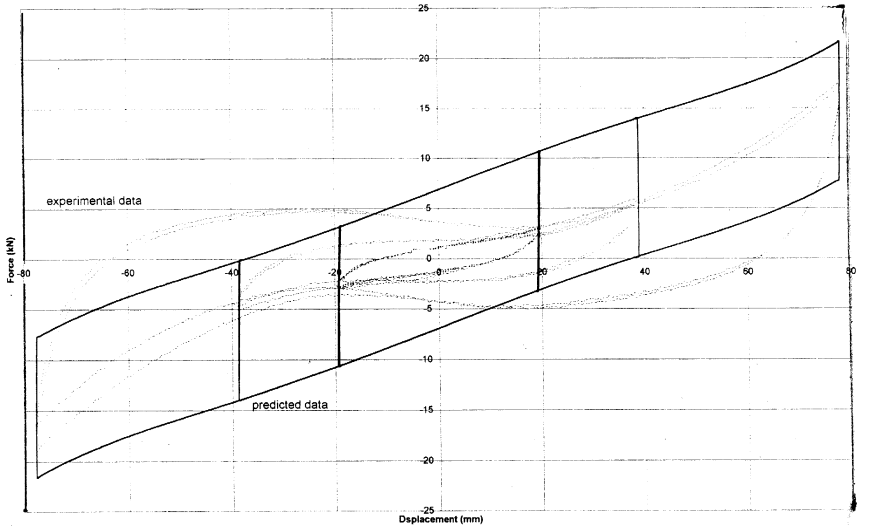

Fig. 40 Combined compression (100kN) shear load

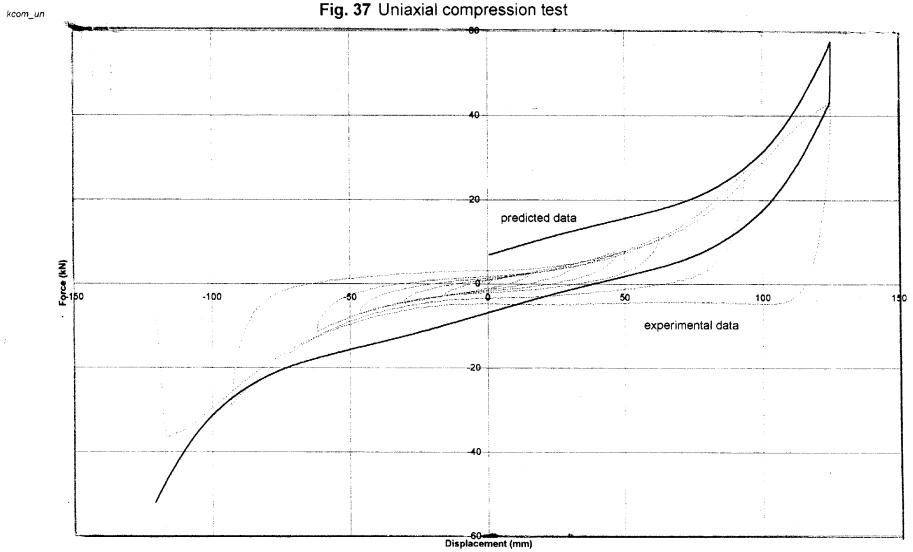

Fig.39 Combined compression (50kN) shear loads

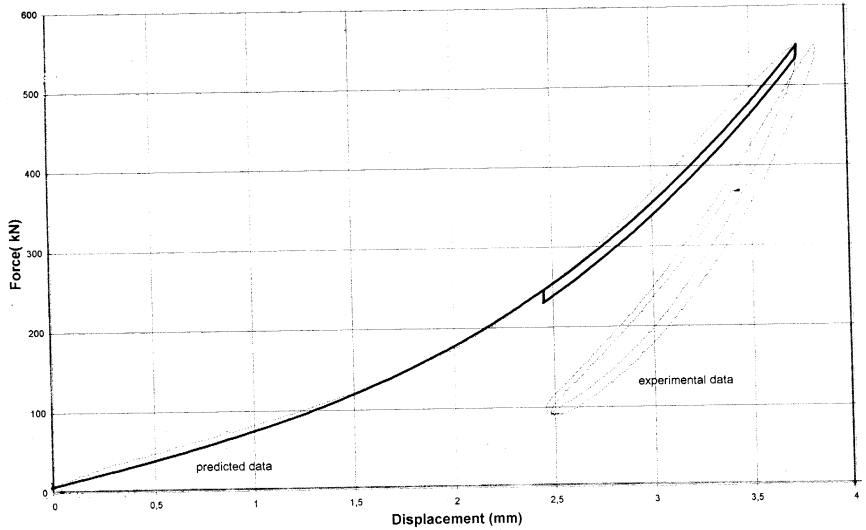

Fig.38 Compression at 1100% design vertical load

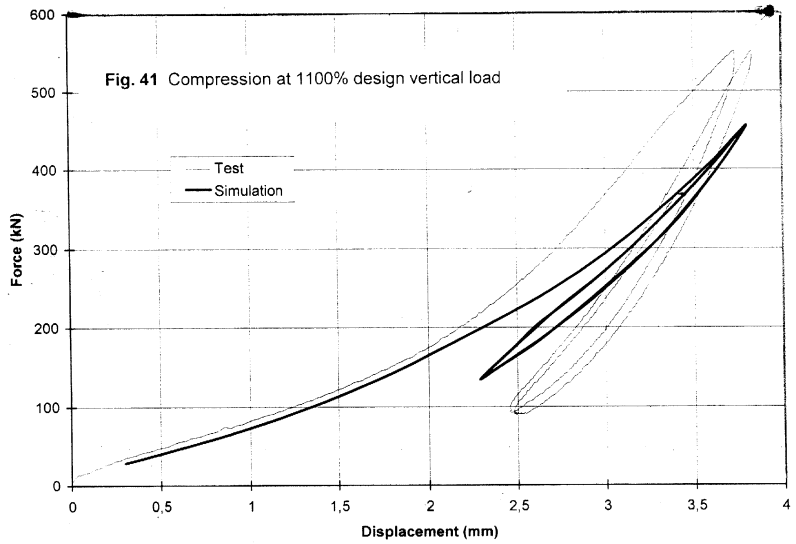

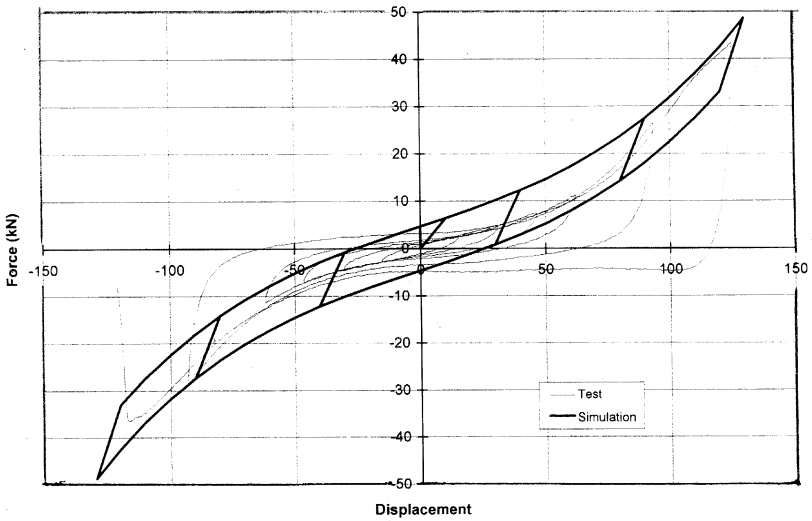

Fig. 42 Combined compression (50kN) shear loads

u_50_bq.xls

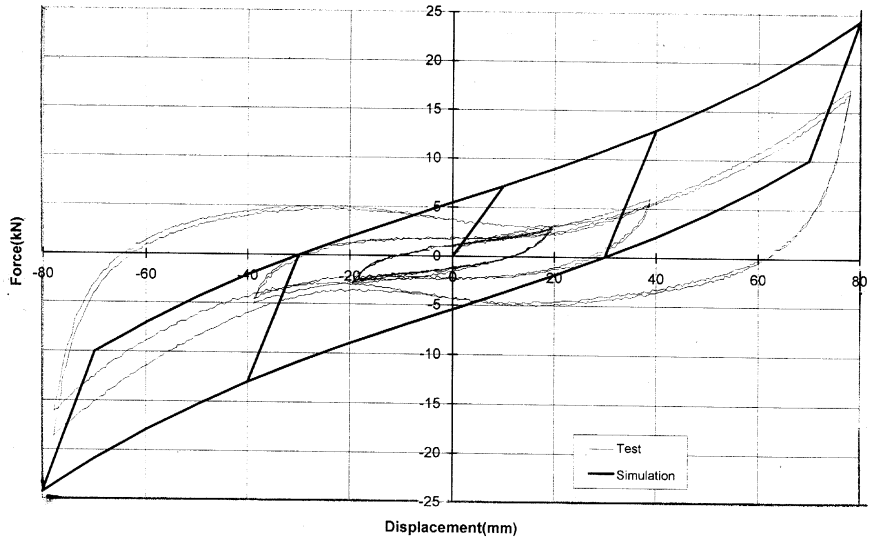

u_100_bq.xls

Fig. 43 Combined compression (100kN) shear loads

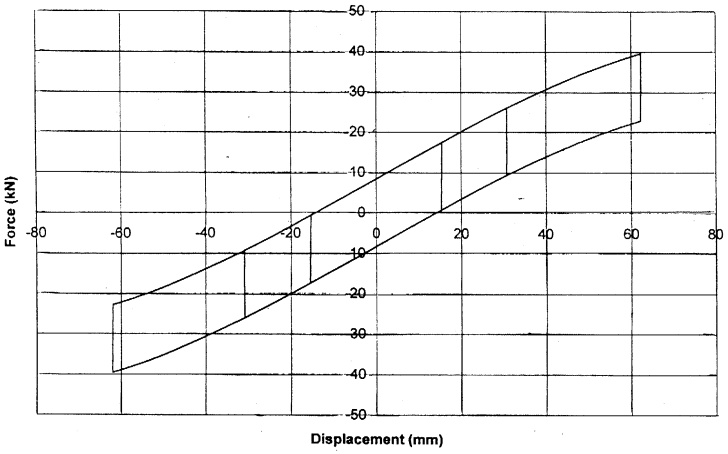

Fig. 44 Combined compression (40kN) shear loads

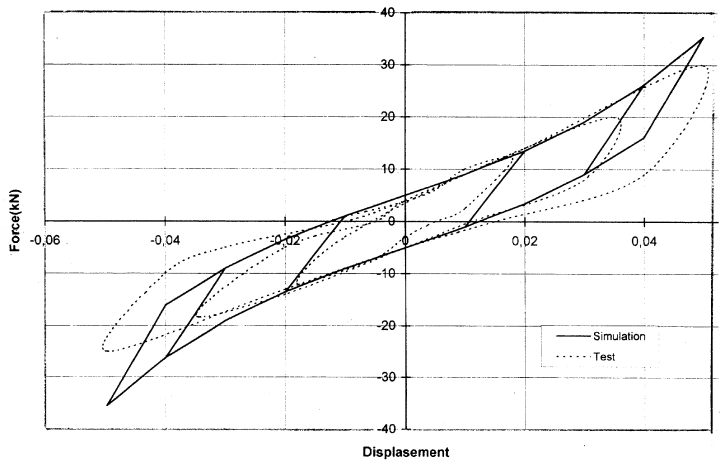

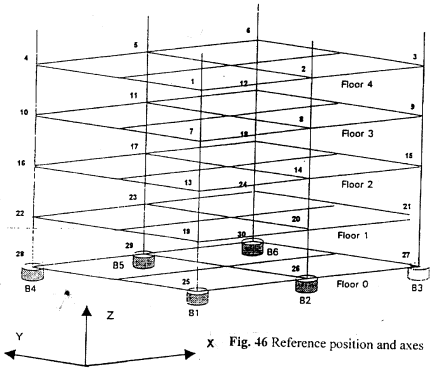

Fig. 46 Reference position and axes

u-10.xls

Fig. 45 Combined compression (axial stress =2.55MPa) shear loads.

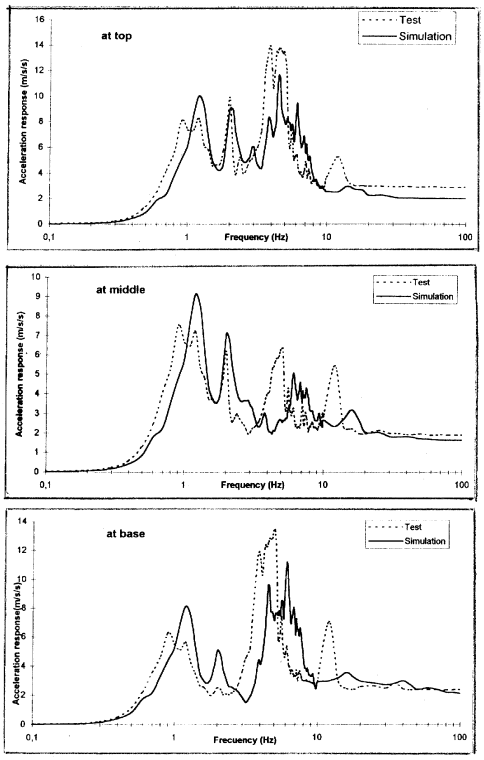

Fig. 47 Acceleration response spectra(1% damping) test end simulation (Tolmezzo NS).

_1%

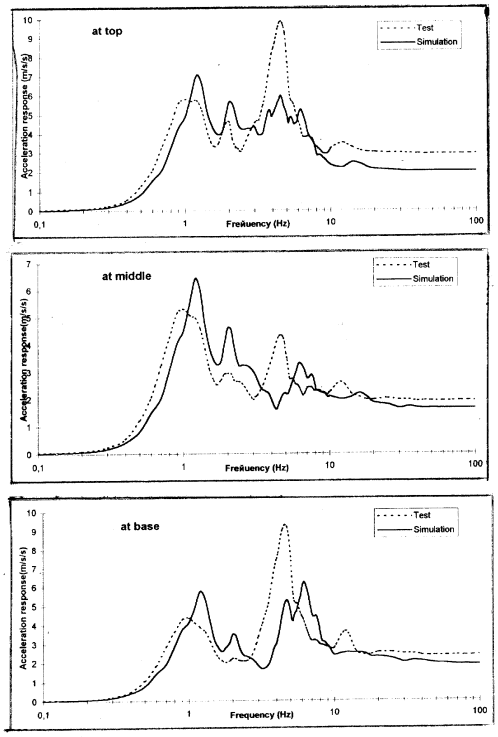

Fig. 48 Acceleration response spectra (5% damping) test and simulation (Tolmezzo NS).

s_5%

Practical realization of this nonlinear approach for a multicomponent seismic isolation system involves serious difficulties which are to be overcome. Recently in the world practice of elaboration of seismic isolation systems for nuclear power facilities only a limited number of attempts to solve this problem are known.

In the present study to solve the SIS problem a pneumatic-cinematic multicomponent low-frequency seismic isolation system of reactor building was accepted, this system has been developed in Russia. This seismic isolation system incorporates both supporting spherical rocking-type devices, which provide for the isolated object displacements in the horizontal

direction, and pneumatic dampers with rubber-cord diaphragm for seismic isolation in the vertical direction. To decrease the relative displacements of the isolated object the system uses viscoelastic dampers. This damping device has been elaborated specially for the reactor building seismic isolation system with due regard for the experience in designing, investigation and operation of the HD-type hydrodampers.

Full-scale experimental investigation of a full-scale fragment of WWER-640 reactor building low-frequency seismic isolation system had been performed due to explosive methods. The testing fragment consists of 2-story metal construction. Elastic and inertial construction parameters has been chosen similar to real building characteristics. Full-scale seismic isolators with 30% filling of the cassette assembly (2 devices from 6) had been used in the system.

As the seismic isolated part of nuclear power object building we can consider a building as a whole (common SIS), one or several rooms, as well as groups of equipment, located on one and the same floor (group SIS), separate unit of equipment (local SIS). In case of common SIS a joint action of ground base, base slab and building superstructure has substantial influence on its static and dynamic responses, in the long run, on seismic isolation efficiency. Therefore, on the one hand, the stressed-deformed state and the form of base slabs equilibrium are determined by distribution of SIS supports and values of active forces. On the other hand, the forces in supports depend on peculiarities of base slabs deformation under SIS-external loads.The procedure developed has been used for intercomparison of the testing data on model isolated steel structure (MISS) and isolated rigid mass (IRM), installed on isolators ENEA and KAERI. Furthermore, it has been used for intercomparison of the Russian-technique calculation results on the base of mathematical models of isolators and isolated structures.Calculated evaluation of force characteristic of HDRB model has been conducted by a special method of nonlinear elastic theory using the continual transformations method. A satisfactory agreement of the calculation and experimental data has been received[7].Results of the investigations performed had shown that the main problem of calculation of dynamic response of real steel rubber dampers consists not so much in development of their mathematical model (in selection of rheologic model of rubber, type of elasticity potential, cinematic assumptions etc.) and realization of design methods, but in accurate determination of material (rubber)constants.

The data presented in the tests with rubber specimens do not reflect real properties of rubber layers in damper structure. Using the constants received from these tests gives large discrepancy of design and experimental results. It is evident that it relates to the fact that during manufacturing of damper under the action of elevated temperature and pressure a substantial change of molecular structure of rubber layers takes place and, as a consequence, its physical properties vary.

Therefore to determine the constants experimental data on model testings of damper were used, which were treated (with some degree of approximation) as characteristics of simple types of stressed-deformed states.Such approach, first, permits to determine constants rather approximately since the type of experimental characteristics is influenced both by damping and real conditions of integration of steel and rubber layers, and, secondly, the results received in such a manner could not be generalized on calculations of a full-scale damper. It seems expedient for receiving rubber material constants to carry out not the model tests (which are vectorially similar to real ones), but the tests on fragments of a damper. In this condition the fragment during its manufacturing should pass the same technological processes which are identical to the processes at manufacturing of full-scale specimen. As such a fragment, as we see it, a cylindrical fragment without central opening with full-scale thickness of rubber and steel layers can be used. Therefore the number of layers should not necessarily coincide with their number in a full-scale damper.

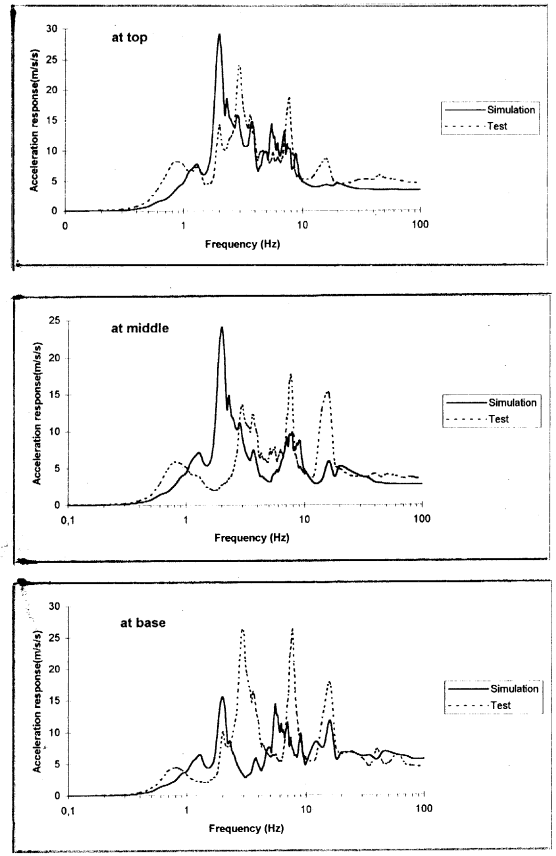

Fig.49 Acceleration response spectra (5% damping) test and simulation (Tolmezo 3D, direction X)

3dx1%

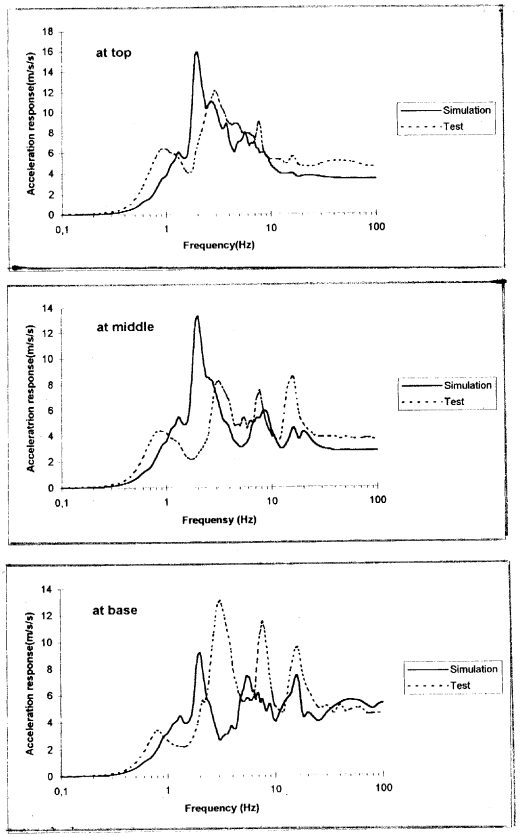

Fig.50 Acceleration response spectra (5% damping) test and simulation (Tolmezo 3D, direction X)

T3dx5%

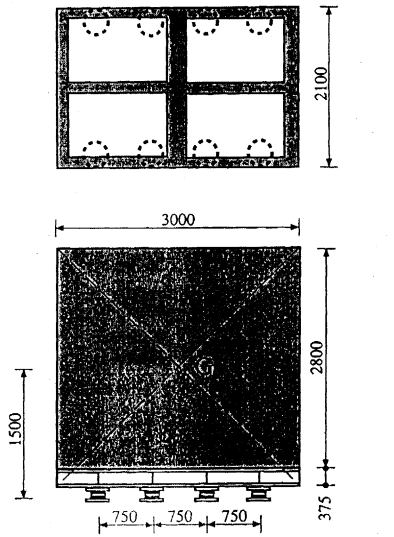

weight of rigit mass : 17.9ton
height of center of gravity of rigit mass: 1.5m
moment of inertia: 30.19tonf•m^2

Fig. 51 Mass-beam model

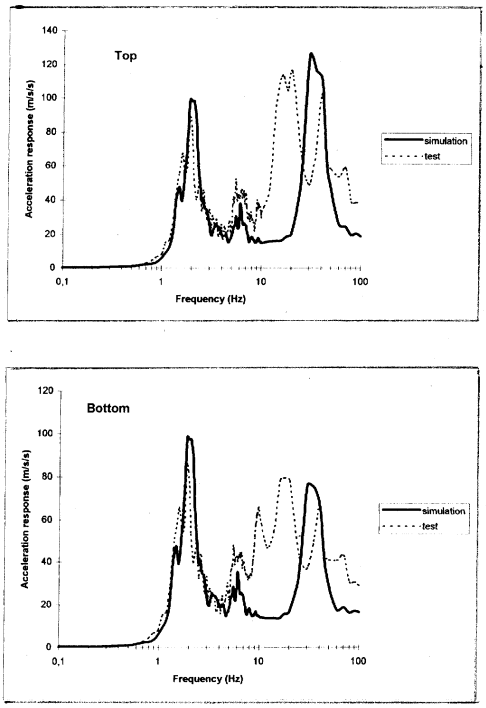

Fig. 54 Acceleration Response Spectrum (1% damping) (beyond design earthquake motion)

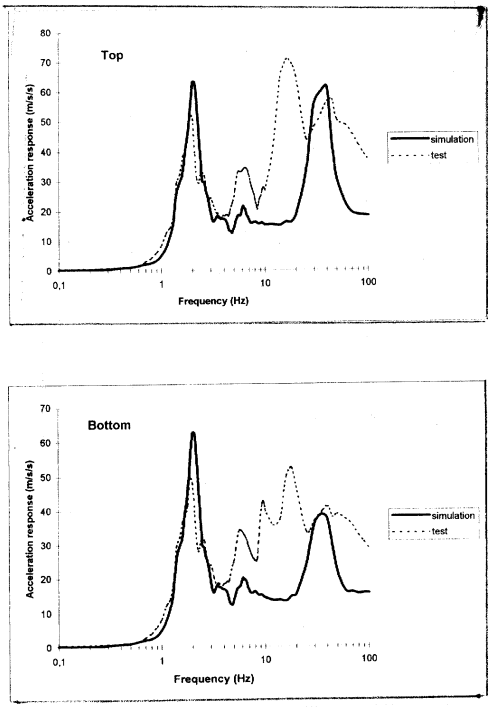

Fig. 55 Acceleration Response Spectrum (5% damping) (beyond design earthquake motion)

Brig_5%

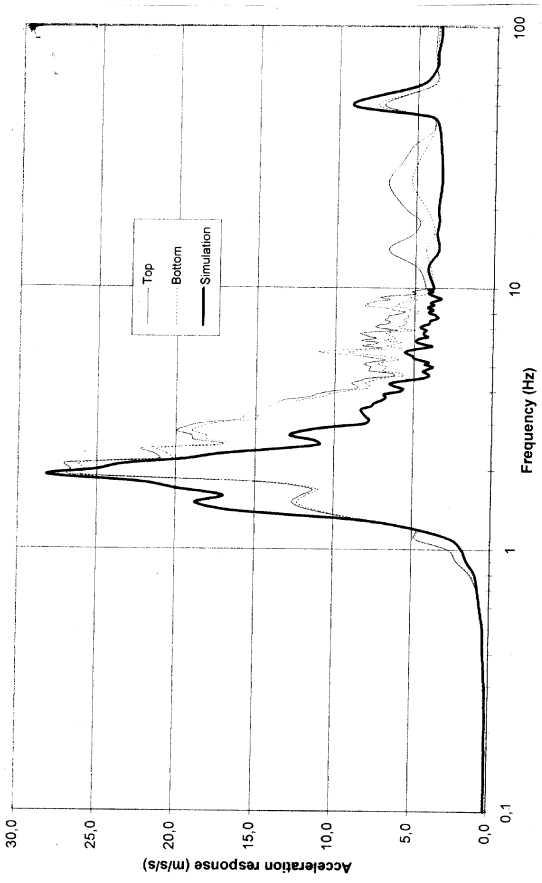

Fig. 52 Acceleration Response Spectrum (1% damping) (desing earthquake motion)

rites-1.xls

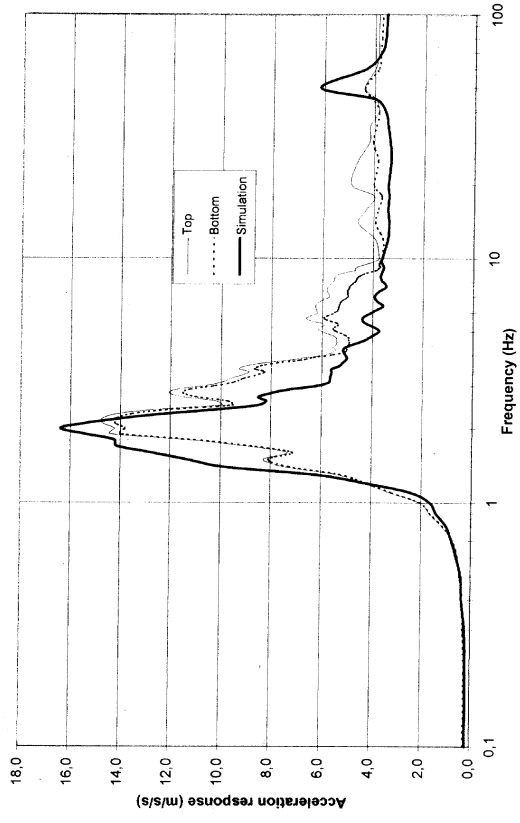

Fig. 53 Acceleration Respons Spectrum (5% damping) (desing earthquake motion)

% .xls

Test load inputs of fragment must exclude wherever possible the influence of boundary conditions on contact surface of rubber and steel layers. The most suitable loads are such load inputs as torsion and total compression. In smaller degree shear load input will be suitable. Tension-compression tests are to be conducted only for testing the material models received. For independent determination of elastic and dissipative constants it is necessary to carry out dynamic (cyclic), static and relaxation tests.

Participation of Russian specialists in the IAEA Coordinated Research Programme "Intercomparison Of Analysis Methods For Seismically Isolated Nuclear Structures" has promoted substantial progress in development of design and experimental methods of analysis of seismic isolation systems of nuclear objects. This work made a major contribution to harmonization of these methods under conditions of international cooperation. On the basis of the results, received in the course of this work, Norms and Standards had been prepared which ensure introduction of seismic isolation systems in the advanced NPP designs. At present such designs are under development in Russia. In our opinion our researches in the framework of CRP has created a base for preparing IAEA recommendations on application of seismic isolation systems of various types in constructions of nuclear power engineering.

REFERENCES

[1] STANDACHER K. Protection for Structures in Extreme Earthquake Full Base Isolation (3-D) by the Swiss Seismofloat System. Nuclear Eng. and Design, 1985, v. 84.

[2] HUFFMAN G. Helical Springs in Base Isolation Systems. (Proc. of the Int. Conference on Soil Dynamics and Earthquake Engineering), Karlsruhe, Germany, 1991.

[3] TAJIRIAN F.F., KELLY J.M., AIKEN I.D. Seismic Isolation for Advanced Nuclear Power Stations. Earthquake Spectra, Vol. 6, N 2, 1990.

[4] TOKUDA N., KASHIWASAKI A., OMATA I., OHNAKA T. Three-dimensional Base Isolation System for Assumed FBR Reactor Building. (Trans. of the 13 SMiRT, Porto Alegre, Brasil, 1995, vol. 3)

[5] BELIAEV V.S., VINOGRADOV V.V., GUSKOV V.D. et al. Pneumatic Seismic Isolation of Nuclear and Non-nuclear Structures. (Proc. of the Int. Post- SMiRT Conference Seminar, Capri (Napoli)), Italy, 1993.

[6] BELIAEV V.S, VINOGRADOV V.V., Optimization of Power Characteristics of Multicomponent Low-Frequency System of Seismic Protection of Building with Reactor Plant of WWER-640, (Trans. of the 13th SMiRT Int. Conf., Porto Alegre, Brasil), 1995, Vol.3, pp. 519–522.

[7] BELIAEV V.S, VINOGRADOV V.V., GUSKOV V.D., Most Recent Development of the Studies for Seismic Isolation of Nuclear Structures in Russia (Proc. Int. Post-SMiRT Conf. Seminar on Isolation, Energy Dissipation and Control of Vibration of Structures, Santiago, Chile, 1995), Vol.6, pp. 1–10.

[8] BELIAEV V.S VINOGRADOV.V.,KUZMITCVEV V.,PRIVALOV S., Analysis Method of Nuclear Structures with 3-D SIS and their intercomparison for Various Isolators Types. Proceedings of the International Post-SMiRT Conference Seminar, Taormina,Italy,25–27 August,1997,pp 535–558.

[9] BELIAEV V.S VINOGRADOV.V.,KUZMITCVEV V.,PRIVALOV S.,3-D Pneumatic SI of NPPs. Proceedings of the International Post-SMiRT Conference Seminar,Cheju, ROK, 23–25 August,1999,pp.913–930.

EXPERIMENTAL TESTING OF REDUCED SCALE SEISMIC ISOLATION BEARINGS FOR THE ADVANCED LIQUID METAL REACTOR

D. AIKEN, P.W. CLARK, J.M. KELLY
Earthquake Engineering Research Center, University of California at Berkeley,
Berkeley, California, United States of America

Abstract

A series of tests of reduced-scale seismic isolation bearings undertaken in support of the development of a seismic isolation concept for the Advanced Liquid Metal Reactor (ALMR) is described. A procurement specification applicable to both full-size and reduced-scale bearings was developed by the program participants and used to purchase bearings of four different designs from two manufacturers. The high-damping rubber isolators were subjected to horizontal, vertical, and failure tests designed to quantify their mechanical properties both within the range of design loads and displacements as well as to establish their margins before failure. The test results show that bearings from both manufacturers provide stable and repeatable behavior with minor variations in stiffness and damping as a function of loading frequency and load history. None of the bearings showed substantial variation in properties due to changes in axial load. All of the bearings exhibited exceptional behavior when loaded beyond the design level, with displacement margins greater than 3 and force margins greater than 4. This test program provides a thorough data-set for further analytical and experimental validations of the seismic isolation concept

1. INTRODUCTION

The current design of the reactor platform of the Advanced Liquid Metal Reactor (ALMR) calls for it to be supported on a seismic isolation system composed of 66 high-damping elastomeric bearings. This design is intended to limit the lateral shear transferred to the reactor and associated equipment under severe earthquake ground motions by shifting the fundamental period of the structure away from the most damaging portion of the input spectrum. As part of the design validation of this seismic isolation concept, a procurement specification was developed, reduced-scale isolation bearings were purchased from two different manufacturers, and an extensive series of tests were performed on these bearings at the Earthquake Engineering Research Center (EERC) of the University of California at Berkeley.

To date seismic isolation has been used in the construction of several nuclear power plants [Jolivet, 1977], many types of equipment [Tajirian, 1993], and a number of buildings and bridges [Kelly, 1993]. However, while the technology is at a relatively advanced stage, there remain applications which demand cutting-edge technology in terms of device performance and capacity. The ALMR installation is one such application because it calls for an elastomer compound with a relatively high shear modulus and isolators which can undergo shear strains in excess of 300 per cent without failure. These two factors make the bearings used for this project unique and led to the development of the design verification program described here.

The work described in this report is one portion of a multi-phase project related to the development of seismic isolation for the ALMR. It has required the cooperation of many participants including the General Electric Company, Bechtel National, Inc., and the Westinghouse Hanford Corporation. The project scope includes specification, purchase, and testing of reduced-scale isolation bearings, earthquake simulator testing of a system model, analytical studies of the performance of the isolated system under a wide range of input

ground motions, and finally, testing of full-sized isolators. The design of the earthquake simulator test model is now complete, and it is hoped that construction will start in the near future.

The objective of the reduced-scale bearing test program was to generate sufficient data to validate the current bearing design for the ALMR platform and establish bearing mechanical properties and failure characteristics that can be used for later experimental and analytical evaluation of the ALMR seismic isolation concept. In particular, emphasis was placed on determining

the variation in observed bearing properties in shear as a function of shear strain amplitude, loading frequency, applied axial load, and load history. Vertical tests of the isolators were also performed, both with zero horizontal displacement and in combination with initial horizontal displacement offsets. These tests were intended to quantify the vertical stiffness of the isolators as a function of horizontal displacement. Finally, shear failure tests were performed to establish margins for use in analyses of beyond-design level earthquakes. Four different bearing designs (including two different scale factors and various rubber layer thicknesses) were tested to examine the feasibility of manufacturing isolators with very small layer thicknesses as would be required for earthquake simulator tests of a reduced-scale model. An additional goal of this test program was to provide sufficient data for implementing mathematical models of isolator response for future analytical studies of the ALMR platform.

This report begins with a description of the bearing designs and the procurement specification that was developed specifically for this project. The specification is intended to be used in the purchase of both reduced-scale and full-size bearings. The experimental facilities at EERC and the test program are then outlined. Finally, the test results and conclusions are presented.

2. BEARING DESIGNS

The reference seismic isolation bearing design for the ALMR platform has been developed over the past several years by Bechtel National, Inc., and is shown in Figure 1. The design assumes the use of a high modulus, high damping rubber compound to attain the target effective stiffness and the target equivalent viscous damping ratio. Neglecting the top and bottom connecting flange plates, the outer bearing diameter is 48 in., and the total height is 18.625 in. There are 29 elastomer layers of 0.375 in. thickness and 28 steel shims of 0.1345 in. thickness. The rubber cover layer is 0.5 in. thick, and 1.25 in. steel endplates are incorporated to allow a bolted connection to the superstructure and foundation.

One of the goals of the design validation program was to quantify the force-displacement behavior of the bearings at loading rates similar to those expected in the final installation. Unfortunately, it is beyond the capacity of most existing facilities to test a full-size ALMR bearing to the design displacement at realistic rates of loading. Therefore, reduced-scale bearing designs were developed that would permit relatively high-frequency testing, and two different scale factors were selected that would also allow comparisons to be made based on scale so that the results could be extrapolated to the full-size isolator.

Scale factors of 1/4 and 1/8 were chosen considering the force, displacement, and frequency capacities of both the earthquake simulator and the single-bearing test machine at EERC, and similitude relationships were used to develop exact 1/4-scale and a 1/8-scale designs. (Because these bearings are precisely scaled, they are referred to here as true-scale (TS) bearings.) However, the individual rubber layers in the 1/8-scale bearing are only 0.047 in. thick, and there was some concern regarding the ability of potential suppliers to bond such

thin layers without substantially altering the properties of the cured elastomer. Two alternate 1/8-scale designs were therefore developed that had fewer rubber layers of increased thickness so that the total height of rubber was kept constant. These are referred to as pseudo-scale (PS) designs. The first PS design has 22 rubber layers of 0.0618 in., and the second has only 15 rubber layers of 0.0906 in.

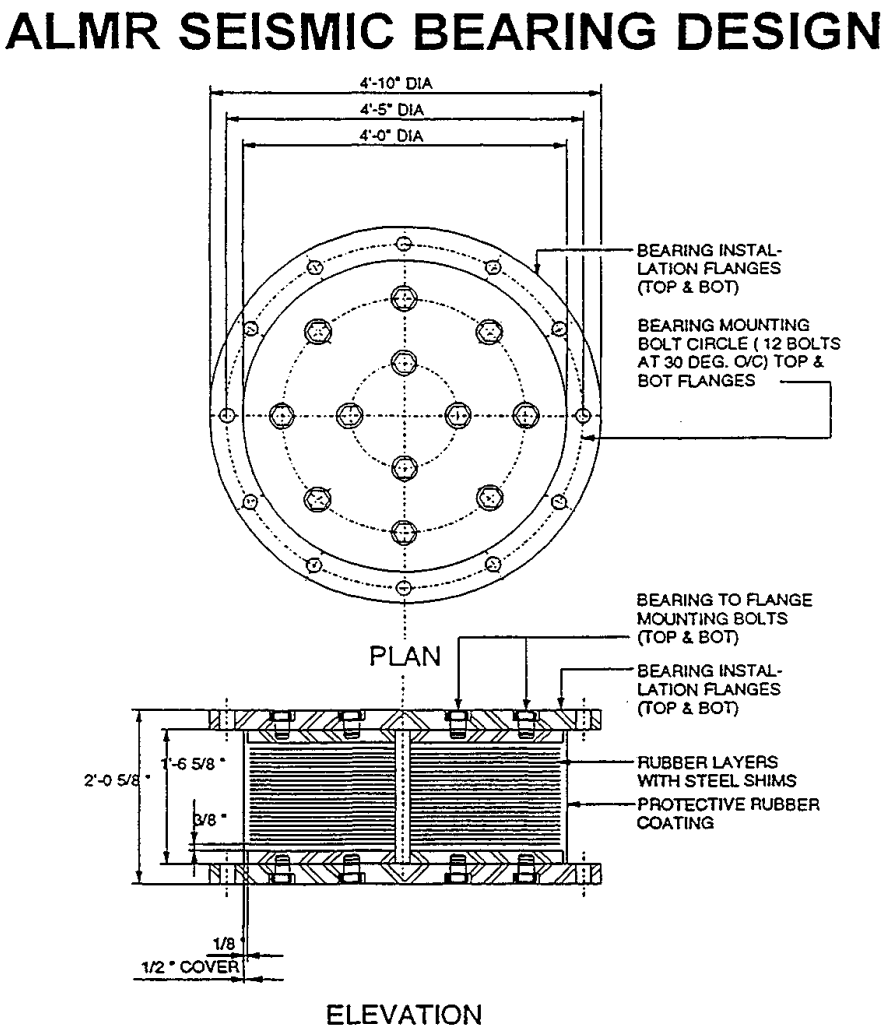

Figure 1: ALMR Full-Size Bearing Design Details.

The bearing dimensions and the nomenclature used for the various designs throughout this report (e.g. TS0250, PS0125/1) are provided in Figure 2. The numbers of bearings listed in this figure correspond to those outlined in the original specification and not to the actual number of bearings tested in this program. It should be noted that in some cases the steel shim thicknesses in the bearings procured for the test program were slightly different than those in the specification. This was due to the availability of steel shims in discrete sizes only and the desire to keep the final bearing costs reasonable by not requiring additional machining of the shims. It is not expected that the variations in shim thickness will lead to significant variations in the final bearing properties.

A total of 28 bearings were tested. Although the specification called for every bearing to be tested by the manufacturer before shipment to EERC, agreements were negotiated with the

manufacturers specifying that a certain number of bearings of each type would be delivered untested. The intent of this arrangement was to allow the virgin (unscragged) characteristics of the bearings to be determined in the same test machine that was used for the remainder of tests, thereby providing a baseline so that long-term testing of these same bearings could always be referred back to the original tests of the virgin bearings. ALGA S.p.A. of Milan, Italy, supplied eight PS0125/2 bearings, three of which were virgin. These used a compound called SISMI-75. The remainder were supplied by Bridgestone of Yokohama, Japan as follows: six TS0250 bearings (three virgin), eight TS0125 bearings (three virgin), three PS0125/1 bearings, and three PS0125/2 bearings. These bearings used a compound known as KL501.

Bearing ID	No of Bearings	H_2 in.	D_3 in.	D_4 in.	D_s in.	D_c in.	n	t_r in.	t_s in.	t_s Ga.	t_m in.	t_c in.
TS0250	10	7.73035	12.0	11.875	11.6875	1.50	29	0.09375	0.0897	13	1.25	0.15625
TS0125	18	5.24378	6.0	5.875	5.75	0.75	29	0.04688	0.0673	15	1.0	0.125
PS0125/1	3	4.92830	6.0	5.875	5.75	0.75	22	0.0618	0.0747	14	1.0	0.125
PS0125/2	3	4.40480	6.0	5.875	5.75	0.75	15	0.0906	0.0747	14	1.0	0.125

Notes:
n = number of rubber layers
t_s = thickness of steel shims
t_r = thickness of rubber layer
t_c = thickness of cover

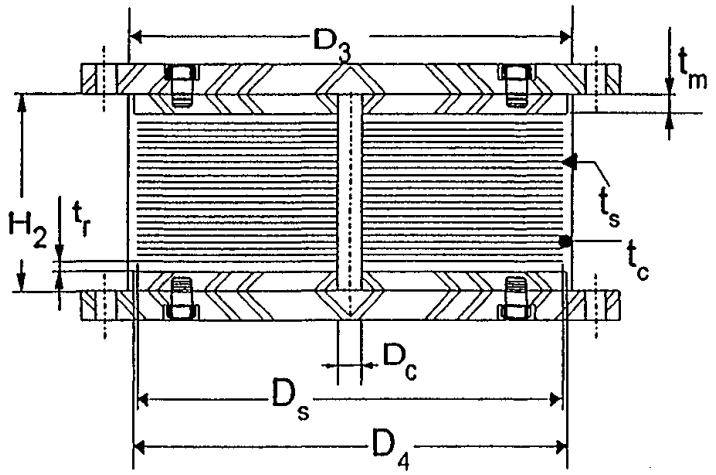

Figure 2: ALMR Reduced-Scale Bearing Design Details.

3. PROCUREMENT SPECIFICATION

The first phase of the test program was devoted to the development of a bearing procurement specification that would ensure high quality, high damping elastomeric isolators while providing a level basis for potential manufacturers to bid. Several members of the project team had previous experience in developing specifications for elastomeric isolation systems, and interaction with experienced suppliers during the preparation of the document resulted in a consensus specification that was appropriate for the procurement of both reduced-scale and full-size isolators. In fact, one of the primary goals of the program of purchasing and testing the reduced-scale isolators was to evaluate the adequacy of the specification for future applications of the ALMR. This section describes the most important requirements of the specification including material properties, manufacturing requirements, and testing procedures. The original specification is reproduced in its entirety as an Appendix to this report.

The first portion of the specification outlines a number of codes and standards by which the material properties and final manufactured bearing should be evaluated. The structural steel used in the bearing shim plates and endplates is required to meet the American Institute of Steel Construction (AISC) standard specification as well as the appropriate grade standard defined by the American Society of Testing and Materials (ASTM). The steel grade must be A36, A570, or better. Rigid requirements are placed on the elastomer including ASTM tests for compression, tension, and shear modulus, hardness, peel-off or bond quality, deterioration due to elevated temperatures and ozone exposure, and compression set under low temperatures. Finally, several of the prescribed tests on the completed bearing are based on the "Earthquake Regulations for Seismic-Isolated Structures" in the 1991 *Uniform Building Code* [International Conference of Building Officials, 1991].

The specified designs of both the reduced-scale and the full-size bearings are outlined in Section 2 and are not repeated here. The design bearing pressure under the ALMR platform is 370 psi, the target horizontal frequency is 0.7 Hz, and the target vertical frequency is 21 Hz. The specification requires that the full-size bearing be able to undergo a shear strain of 300 per cent or a lateral displacement of 33 inches, whichever is greater. The original requirement was for one supplier to manufacture a total of 34 reduced-scale bearings plus four prototypes as follows: 12 TS0250 bearings (ten plus two prototypes), 20 TS0125 bearings (18 plus two prototypes), three PS0125/1 bearings, and three PS0125/2 bearings. However, as described above, two suppliers were eventually chosen, each of whom supplied fewer bearings than originally outlined in the specification.

Probably the most unique requirement of the specification relates to the very high modulus of the elastomer. Typical high damping rubbers show moduli of between 70 and 125 psi at moderate shear strains. The required modulus of the elastomer in the ALMR bearing design is 200 psi at a shear strain of 100 per cent and a rate of loading of 0.5 Hz. High modulus elastomers typically have more damping than equivalent low-modulus compounds. The specification calls for the elastomer to have an equivalent viscous damping of 12 per cent of critical at a shear strain of 100 per cent and a rate of loading of 0.5 Hz, and it is believed that this is readily achievable in practice. The acceptance criteria for the elastomer is that the effective modulus measured in the fourth cycle of a five-cycle test must be within +/-10% of the target stiffness, and the equivalent viscous damping in this cycle must be greater than the specified 12 per cent.

Once the elastomer has been approved, the manufacturer is required to fabricate two 1/4-scale and two 1/8-scale prototype isolators to be subjected to an extensive test series. In the specification, the prototype test program is given as that outlined in Section 2381 of the 1991 Uniform Building Code. However, because the reduced-scale bearings were to be tested extensively at EERC, the manufacturers' prototype test program was substantially reduced. (This would not be the case during the manufacture of full-size isolators.) The first two prototype tests were cyclic tests at 0.5 Hz to 100 and 200 per cent shear strain, and the effective modulus and equivalent viscous damping at 100 per cent were required to satisfy the specification in the same way as required for the elastomer compound itself. The final prototype test required the manufacturer to monoton-ically load the bearing in shear to a strain of greater than 300 per cent without producing any damage in the bearing.

The tests performed on the reduced-scale production bearings for this project are the same as those outlined in the specification, namely combined compression and shear tests through three fully-reversed cycles of displacement at a shear strain of 200 per cent. The measured stiffness of each bearing is required to be within +/-10 per cent of the mean stiffness of all

bearings, and the force-deflection curve cannot show any sign of distress. A visual inspection is also required. The manufacturers are required to submit all prototype and production bearing test data for evaluation.

4. MANUFACTURERS' TEST RESULTS

One requirement placed on the manufacturers selected to supply reduced-scale seismic isolation bearings was that they produce and test prototype isolators to confirm that they could achieve the target stiffness and damping at 100 per cent shear strain. These prototype isolators were also required to be tested to beyond 300 per cent shear strain without exhibiting any sign of failure (either visually or in the force-displacement curve) to confirm that they had the appropriate displacement margin as outlined in the specification. Once these requirements were met, the manufacturers could proceed with the production bearings, additional quality control tests were required of each production bearing as outlined above.

Both manufacturers submitted the required test data showing conformance of their prototype and production bearings to the specification, and these submittals are reproduced as Appendices to this report. It should be noted, however, that both the limited budget for this project (and subsequent price concessions from the manufacturers) as well as time constraints led to some inconsistencies between the submittal requirements and the information received from the vendors. In general, the manufacturers' reports were not as detailed as required, and in some cases improper tests were performed or rubber coupon properties were outside of the range allowed by the specification. It is the opinion of the authors that these minor deviations from the specification donot substantially affect the conformance of their delivered products to the objectives of the specification.

5. EXPERIMENTAL FACILITIES

All of the tests of the reduced-scale seismic isolation bearings were carried out in the single-bearing test machine at the Earthquake Engineering Research Center of the University of California at Berkeley. This machine has been used extensively in the past to characterize all types of seismic isolation bearings, including many types of high-damping rubber isolators. A schematic diagram of the test machine is provided in Figure 3, showing the mechanism by which vertical load can be applied to an individual isolator and maintained while the isolator is sheared. A single, high-performance hydraulic actuator provides the horizontal shearing force. This actuator has a displacement capacity of +/-6 inches and a force capacity of approximately 75 kips. The maximum attainable velocity of the actuator is 25 inches/second. The vertical actuators are capable of delivering a combined axial load of 240 kips. The machine is typically run with the vertical actuators under load control and the horizontal actuator under displacement control. Although the majority of tests described here are cyclic, the machine may be reconfigured to have a peak horizontal displacement of 12 inches in one direction by inserting a spacer between the clevis of the actuator and the upper loading beam. This configuration permits monotonic failure tests to be performed.

The test machine is controlled and data acquired via the ATS system, developed by SHRP Equipment Corporation of Walnut Creek, California. This is a PC-based control and acquisition program which was customized specifically for use on the single-bearing test machine at EERC. It allows command signals to be generated either internally or from

imported data files. Data is typically scanned at a constant rate for a specified length of time and is stored as ASCII files on disk. Up to 16 channels of data (plus time) can be sampled in the current version of the program. An on-screen monitor provides continuously-updated readings from all of the channels, and *x-y* plots of specimen response can be displayed in real-time.

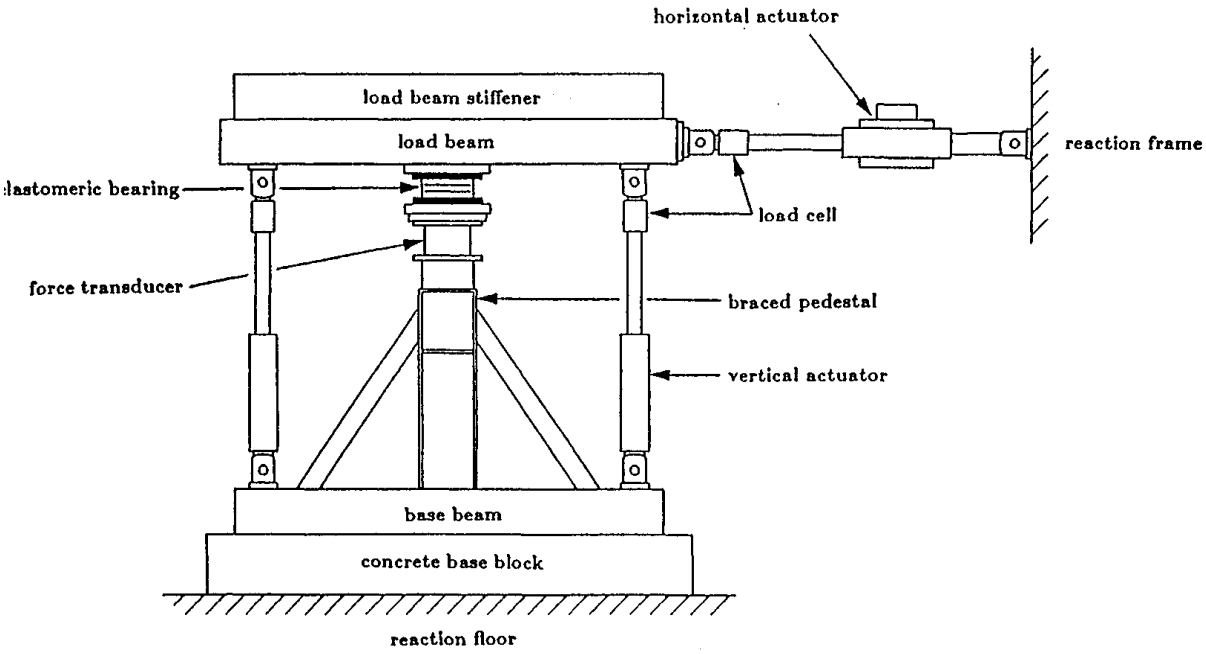

Figure 3: Schematic of EERC Single-Bearing Test Machine.

Loads in the actuators are measured via in-line loadcells while multi-component loadcells installed under the isolator simultaneously measure shear and axial load. In almost all of the tests of the ALGA PSO125/2 bearings there were two loadcells underneath the isolator. This arrangement was reconfigured to four loadcells for the tests of the larger Bridgestone TS0250 isolators to provide a greater force capacity. The four-loadcell configuration was in place for all of the tests of the Bridgestone isolators. The loadcells used under the bearings were custom-manufactured for use at EERC.

Displacement transducers are installed in-line with the actuators as well as vertically from the base of the test machine to the upper loading plate. These allow measurement of vertical displacements during horizontal shear tests. During vertical tests, a separate set of four displacement transducers is placed around the perimeter of the bearing which have a higher resolution appropriate for the very small displacements observed in the vertical tests. The vertical actuators use wire potentiometers while the horizontal actuator employs a linear variable differential transformer (LVDT). The vertical displacement transducers are direct current displacement transducers (DCDTs).

A complete channel listing and copies of the calibration files used in the Bridgestone tests are given in Figures 4 and 5 (horizontal and vertical, respectively). The calibration files used in the ALGA tests are not available. Loadcell calibration data is kept on file at EERC.

IN-PLANE BEARING TEST SET UP FOR THE BRIDGESTONE BEARINGS
1 INCH VERT. DCDT SET UP

12-14-94 WDN

CHAN #	CHANNEL I.D.	PACIFIC	GAIN	SWITCH CONFIG.	SENSITIVITY	P	D	SV	EXCVDC	PLUS CAL FINE TUNED	PACIFIC FILTER	INSTUMENT SERIAL #	CORE SERIAL #
0	Disp. Horiz.	85	1		0.00549239	1.5	0.25	1	6.00		1K		
1	Load H.(dP)	55	1000		-0.0513304	1	1	0	6.00		1K		
2	Load V1	118	500		0.0734605	1	1	2	6.00	26.96 KIPS	1K		
3	Load V2	111	500		0.0762228	1	1	3	6.00	28.05 KIPS	1K		
4	Disp. V1	97	2	1,5	0.0127524	1	1		6.00		1K		
5	Disp. V2	103	2	1,5	0.0125205	1	1		6.00		1K		
6	L.C. 7S2	50	1000		0.0150092	1	1		6.00	16.35 KIPS	1K		
7	L.C. 8S2	78	1000		0.0139796	1	1		6.00	15.06 KIPS	1K		
8	L.C. 4S2	79	1000		0.0151711	1	1		6.00	16.4 KIPS	1K		
9	L.C. 6S2	54	1000		-0.0143306	1	1		6.00	15.55 KIPS	1K		
10	VPM6&8	17	1		0.29403	1	1		6.00		1K		
11	VPM4&7	18	1		0.293253	1	1		6.00				
12	NE 1"V.DCDT	16	2	2,4,6	0.000532198	1	1		6.00				
13	NW 1"V.DCDT	20	2	2,4,6	0.000537634	1	1		6.00				
14	SE 1"V.DCDT	85	2	2,4,6	0.000577367	1	1		6.00				
15	SW 1"V.DCDT	19	2	2,4,6	0.000574053	1	1		6.00				

The following four vpm axial channels are being summed on a Moog summing amp which is installed in the ATS cart number one. The summed channels are then being read into the ATS data stream via channels 10 and 11.

external	L.C. 7A	73	1000		0.150025	1	1		5.00	270.34 KIPS	1K		
external	L.C. 8A	68	1000		0.156883	1	1		5.00	282.86 KIPS	1K		
external	L.C. 4A	51	1000		0.153384	1	1		5.00	275.17 KIPS	1K		
external	L.C. 6A	90	1000		0.14926	1	1		5.00	270.46 KIPS	1K		

Figure 4: Calibration File for Horizontal Test Setup

IN-PLANE BEARING TEST SET UP FOR THE BRIDGESTONE BEARINGS
.1" VERT DCDT SET UP

12-19-94 WDN

CHAN #	CHANNEL I.D.	PACIFIC	GAIN	SWITCH CONFIG.	SENSITIVITY	P	D	SV	EXCVDC	PLUS CAL FINE TUNED	PACIFIC FILTER	INSTRUMENT SERIAL #	CORE SERIAL #
0	Disp. Horiz.	85	1		0.00549239	1.5	0.25	1	6.00		1K		
1	Load H.(dP)	55	1000		-0.0513304	1	1	0	6.00		1K		
2	Load V1	118	500		0.0734605	1	1	2	6.00	26.96 KIPS	1K		
3	Load V2	111	500		0.0762228	1	1	3	6.00	28.05 KIPS	1K		
4	Disp. V1	97	2	1,5	0.0127524	1	1		6.00		1K		
5	Disp. V2	103	2	1,5	0.0125205	1	1		6.00		1K		
6	L.C. 7S2	50	1000		0.0150092	1	1		6.00	16.35 KIPS	1K		
7	L.C. 8S2	78	1000		0.0139796	1	1		6.00	15.06 KIPS	1K		
8	L.C. 4S2	79	1000		0.0151711	1	1		6.00	16.4 KIPS	1K		
9	L.C. 6S2	54	1000		-0.0143306	1	1		6.00	15.55 KIPS	1K		
10	VPM6&8	17	1		0.29403	1	1		6.00		1K		
11	VPM4&7	18	1		0.293253	1	1		6.00				
12	NE .1"V.DCDT	16	5	2,4,6	6.29787E-05	1	1		6.00				
13	NW .1"V.DCDT	20	2	2,4,6	6.96251E-05	1	1		7.91				
14	SE .1"V.DCDT	85	2	2,4,6	6.35401E-05	1	1		6.00				
15	SW .1"V.DCDT	19	2	2,4,6	6.31399E-05	1	1		5.63				

The following four vpm axial channels are being summed on a Moog summing amp which is installed in the ATS cart number one. The summed channels are then being read into the ATS data stream via channels 10 and 11.

external	L.C. 7A	73	1000		0.150025	1	1		5.00	270.34 KIPS	1K		
external	L.C. 8A	68	1000		0.156883	1	1		5.00	282.86 KIPS	1K		
external	L.C. 4A	51	1000		0.153384	1	1		5.00	275.17 KIPS	1K		
external	L.C. 6A	90	1000		0.14926	1	1		5.00	270.46 KIPS	1K		

Figure 5: Calibration File for Vertical Test Setup

Tests were performed with specific objectives. This section outlines the general groups into which the various tests fall. A sample of the test plan first developed for the ALGA bearings is provided in Figure 6. It should be noted, however, that as the test program progressed and different characteristics of the bearing response were understood, the initially-proposed program was altered on several occasions to focus in on the bearing properties which appeared to have the most influence on the response. For this reason, tests from one set of bearings to another are not always completely consistent. While this is unfortunate, this approach has given valuable insight into several aspects of these high-modulus bearings which have not been well-understood before, for example the effects of load history. The complete test program of the ALGA bearings is given in Table 1, and that for the Bridgestone bearings is given in Table 2.

The *characteristic* tests were intended to be performed on every bearing to provide a means of judging the consistency in manfacturing a given design. There were typically two horizontal tests and two vertical tests (sometimes combined into a single, longer vertical test) which made up the characteristic test series. The horizontal tests involved five cycles of fully-reversed displacement at strains of 10, 25, 50, 75, 100,125, and 150 per cent. These were run at 0.7 Hz — the full-scale frequency — and at a frequency corresponding to the scale factor of the isolator being tested (1.4 Hz for the 1/4-scale bearings and 2.0 Hz for the 1/8-scale bearings). The axial pressure in these tests was 370 psi. The vertical characteristic tests involved five cycles of pressure around the design pressure at a frequency of 0.1 Hz. The first pressure range was 370 +/- 185 psi, and the second was 370 +/- 370 psi. This was run as two separate tests for the ALGA bearings, while for the Bridgestone bearings it was combined into a single test.

A different kind of characteristic test sequence, intended to capture load-history effects in the bearings, involved a three separate tests of five cycles each, at strains of 10, 200, and again 10 per cent. The axial pressure in these tests was 370 psi. This group of tests was repeated on individual bearings at various times throughout the test program and after delays ranging from minutes to weeks. The objective of this group of tests was to examine the change in the effective modulus at 200 per cent due to repeated cycling and recovery. It is appropriate to perform these tests at 200 per cent (instead of the design shear strain of 100 per cent) because the production bearings were initially tested by the manufacturer to 200 per cent. Several long-term tests were also performed to a strain of only 100 per cent to evaluate the likely long-term stiffness of bearings in a final installation.

Additional tests to capture load-history effects were performed on previously tested bearings as well as the virgin bearings received from the manufacturers. In some cases the loading sequence was varied to evaluated the extent to which a particular test led to scragging in the bearing. For instance, one sequence was a 200 per cent shear strain test followed by a vertical compression test to three times the design pressure followed by a 200 per cent shear strain test. This could then be compared with a test sequence of vertical compression-200 per cent shear-vertical compression to assess the relative effects of compression versus shear in scragging the bearing. Similar sequences — referred to as strain-buildup tests — were performed via loading to shear strains of 10, 50, 10, 50,100,10, 50,100,150,10, 50, 100,150 to assess the change in modulus at lower shear strains due to cycling at higher shear strains. If these effects are great, then there can be significant implication on analytical models for bearing response, particularly for analyses of response to long-duration earthquakes where repeated cycling at a wide range of strains could occur.

Text cont. on page 331.

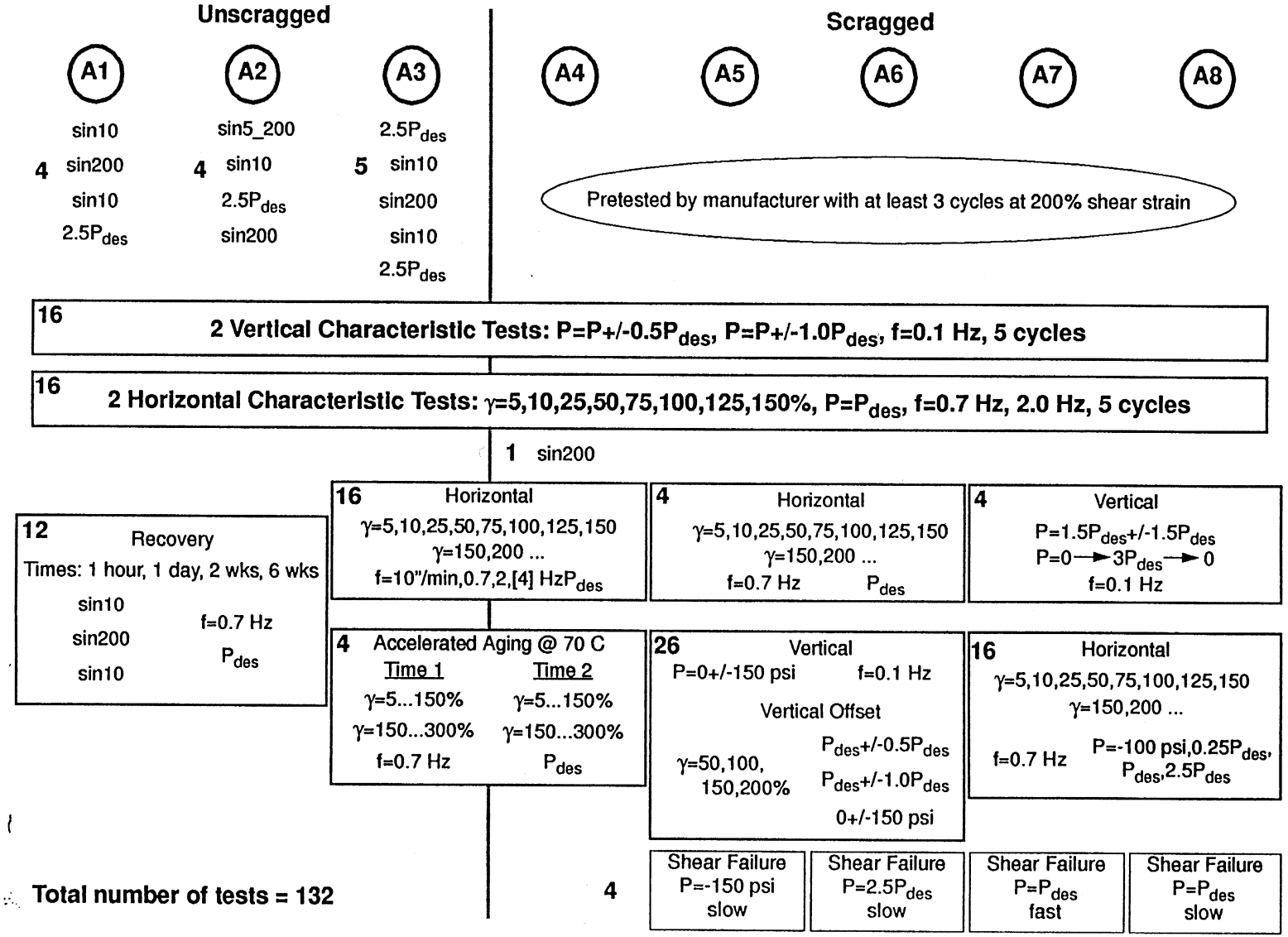

Figure 6: ALGA Bearing Test Program

TABLE 1: ALGA TEST SERIES

Filename	Brg Num	Test Type	Signal	Axial Load (kips)	Freq./ Peak Velocity* (Hz/in/s)	Peak Strain/ Pressure Change* (%/psi)	Comments
940912.02	4	Vert	vcyc2	9.61	0.1	370*	
940912.03	4	Horiz	hc07	9.61	0.7	150	First test to this strain since manufacture
940912.04	4	Horiz	hc2	9.61	2	150	
940912.05	4	Vert	v150	0	0.1	150*	This test not analyzed
940912.06	4	Vert	v150	0	0.1	150*	Repeat
940912.07	4	Vert	vcycl	9.61	0.1	185*	Offset test — 50 per cent shear strain
940912.08	4	Vert	vcyc2	9.61	0.1	370*	Offset test — 50 per cent shear strain
940912.09	4	Vert	v150	0	0.1	150*	Offset test — 50 per cent shear strain
940912.10	4	Vert	vcycl	9.61	0.1	185*	Offset test — 100 per cent shear strain
940912.11	4	Vert	vcyc2	9.61	0.1	370*	Offset test — 100 per cent shear strain
940912.12	4	Vert	v150	0	0.1	150*	Offset test — 1 00 per cent shear strain
• Changed signal conditioners on channels 5 and 14 because of apparent drift problems							
940912.13	4	Vert	vcycl	9.61	0.1	185*	Offset test — 150 per cent shear strain
940912.14	4	Vert	vcyc2	9.61	0.1	370*	Offset test — 1 50 per cent shear strain
940912.15	4	Vert	v150	0	0.1	150*	Offset test — 1 50 per cent shear strain

940912.16	4	Horiz	hc07	9.61	0.7	150	Checking for damage after vertical offset tests at 150% strain
940912.17	4	Horiz	sin200	9.61	0.7	200	First test to this strain level since manufacture
940912.18	4	Vert	vcycl	9.61	0.1	185*	Offset test • 200 per cent shear strain
940912.19	4	Vert	vcyc2	9.61	0.1	370*	Offset test — 200 per cent shear strain
940912.20	4	Vert	v150	0	0.1	150*	Offset test — 200 per cent shear strain
• NE and NW DCDT gains were 5 instead of 2 in the following five tests							
940912.21	4	Horiz	hc07	9.61	0.7	150	Checking for damage after vertical offset tests at 200% strain
940912.22	4	Fail	sfail	9.61	0.1359*	400	The bottom plates slipped approximately 0.35" during this test; this corresponds to about 25% shear strain in the bearing
940913.01	8	Horiz	sinIO	9.61	0.7	10	First test of this bearing ever
940913.02	8	Horiz	sin200	9.61	0.7	200	First test to this strain ever
940913.03	8	Horiz	sinIO	9.61	0.7	10	Extra smoothing of the data in this test
940913.04	8	Vert	vcyc2	12.01	0.1	463*	Signal scaled by 1.25

Filename	Brg Num	Test Type	Signal	Axial Load (kips)	Freq./ Peak Velocity* (Hz/in/s)	Peak Strain/ Pressure Change* (%/psi)	Comments
940908.01	3	Vert	vcyd	9.61	0.1	185*	File was erased because it contained no data
940908.02	3	Vert	vcyc2	9.61	0.1	370*	File was erased because it contained no data
940909.01	3	Horiz	hc07	9.61	0.7	150	This file contains no data
940909.02	3	Horiz	hc2	9.61	2	150	This test not analyzed
940909.03	3	Vert	vcyd	9.61	0.1	185*	One vertical DCDT was bad — results unreliable
940909.04	3	Vert	vcyc2	9.61	0.1	370*	
940909.05	3	Horiz	hc07	9.61	0.7	150	Bearing had been tested to this strain twice in the last 24 hours
940909.06	3	Horiz	hc2	9.61	2	150	
940909.07	3	Horiz	sin200	9.61	0.7	200	First test to this strain since manufacture
940909.08	3	Horiz	slowlO	9.61	0.167*	10	
940909.09	3	Horiz	slow25	9.61	0.167*	25	
940909.10	3	Horiz	slowSO	9.61	0.167*	50	Hysteresis is strange — reran this as 940909.12
940909.11	3	Horiz	slow75	9.61	0.167*	75	Hysteresis looks strange — reran this as 940909.13
• Substantial slip between the bearing and the connecting plates was observed during the two previous tests. The bearing was removed and the bolts retightened.							
940909.12	3	Horiz	slowSO	9.61	0.167*	50	Retest
940909.13	3	Horiz	slow75	9.61	0.167*	75	Retest

940909.14	3	Horiz	slowlOO	9.61	0.167*	100	
940909.15	3	Horiz	slow125	9.61	0.167*	125	
940909.16	3	Horiz	slow150	9.61	0.167*	150	
940909.17	3	Horiz	sslowlOO	9.61	0.0444*	100	
940909.18	3	Horiz	hc07	9.61	0.7	150	
940909.19	3	Horiz	hc2	9.61	2	150	
940909.20	3	Horiz	slow200	9.61	0.167*	200	
940909.21	3	Horiz	slow250	9.61	0.167*	250	Hysteresis looks peculiar — bearing may have been damaged during this test
940909.22	3	Horiz	slow300	9.61	0.167*	300	Bearing failed during the first reversed cycle of this test
940912.01	4	Vert	vcyd	9.61	0.1	185*	

Filename	Brg Num	Test Type	Signal	Axial Load (kips)	Freq./ Peak Velocity* (Hz/in/s)	Peak Strain/ Pressure Change* (%/psi)	Comments
940914.05	5	Vert	vcyc2	9.61	0.1	370*	
940914.06	5	Horiz	hc07	9.61	0.7	150	First test to this strain since manufacture
940914.07	5	Horiz	hc2	9.61	2	150	
940914.08	5	Vert	v150	0	0.1	150*	
940914.09	5	Vert	vcyd	9.61	0.1	185*	Vertical offset test — 50% initial strain
940914.10	5	Vert	vcyc2	9.61	0.1	370*	Vertical offset test • 50% initial strain
940914.11	5	Vert	v150	0	0.1	150*	Vertical offset test — 50% initial strain
940914.12	5	Vert	vcyd	9.61	0.1	185*	Vertical offset test — 100% initial strain
940914.13	5	Vert	vcyc2	9.61	0.1	370*	Vertical offset test — 100% initial strain
940914.14	5	Vert	v150	0	0.1	150*	Vertical offset test — 100% initial strain
940914.15	5	Vert	vcyd	9.61	0.1	185*	Vertical offset test — 1 50% initial strain
940914.16	5	Vert	vcyc2	9.61	0.1	370*	Vertical offset test — 150% initial strain
940914.17	5	Vert	v150	0	0.1	150*	Vertical offset test — 150% initial strain
• Vertical DCDTs not funct oning for following two tests							
940914.18	5	Horiz	hc07	9.61	0.7	150	Test to check damage caused by vertical offset tests
940914.19	5	Horiz	sin200	9.61	0.7	200	First test to this strain since manufacture

940914.20	5	Vert	vcyd	9.61	0.1	185*	Vertical offset test — 200% initial strain
940914.21	5	Vert	vcyc2	9.61	0.1	370*	Vertical offset test — 200% initial strain
940914.22	5	Vert	v150	0	0.1	150*	Vertical offset test — 200% initial strain
940914.23	5	Horiz	hc07	9.61	0.7	150	Test to evaluate damage due to vertical offset tests
940915.01	5	Fail	fastfail	24	10*	500	Failure test at high speed; shear load in one loadcell clipped
940915.02	10	Vert	vcyc2	12.02	0.1	463*	First test of this bearing; signal scaled by 1.25
940915.03	10	Horiz	sinIO	9.61	0.7	10	First shear test of this bearing
940915.04	10	Horiz	sin200	9.61	0.7	200	First test to this"strain ever
940915.05	10	Horiz	sinIO	9.61	0.7	10	Extra smoothing of the data in this test
940915.06	10	Vert	vcyc2	12.02	0.1	463*	Signal scaled by 1.25
940915.07	10	Vert	vcyd	9.61	0.1	185*	
940915.08	10	Vert	vcyc2	9.61	0.1	370*	
940915.09	10	Horiz	hc07	9.61	0.7	150	

Filename	Brg Num	Test Type	Signal	Axial Load (kips)	Freq./ Peak Velocity* (Hz/in/s)	Peak Strain/ Pressure Change* (%/psi)	Comments
940913.05	8	Vert	vcyd	9.61	0.1	185*	
940913.06	8	Vert	vcyc2	9.61	0.1	370*	
940913.07	8	Horiz	hc07	9.61	0.7	150	Some plate slip observed during this test
940913.08	8	Horiz	hc2	9.61	2	150	Likely more plate slip in this test
940913.09	8	Horiz	sinIO	9.61	0.7	10	Extra smoothing of the data in this test; first test in 1 hour and 11 minutes
940913.10	8	Horiz	sin200	9.61	0.7	200	More than 2 hour delay since last test to this strain
940913.11	8	Horiz	sinIO	9.61	0.7	10	
940913.12	8	Horiz	sinIO	9.61	0.7	10	
940913.13	8	Horiz	sin200	9.61	0.7	200	9 minute delay since last test to this strain
940913.14	8	Horiz	sinIO	9.61	0.7	10	
940913.15	9	Horiz	hc07	9.61	0.7	150	First test of this bearing ever
940913.16	9	Horiz	sinIO	9.61	0.7	10	
940913.17	9	Vert	vcyc2	12.01	0.1	433*	Signal scaled by 1.25
940913.18	9	Horiz	sin200	9.61	0.7	200	First test to this strain ever
940913.19	9	Vert	vcyd	9.61	0.1	185*	
940913.20	9	Vert	vcyc2	9.61	0.1	370*	

940913.21	9	Horiz	hc07	9.61	0.7	150	
940913.22	9	Horiz	hc2	9.61	2	150	
940913.23	9	Horiz	sinIO	9.61	0.7	10	
940913.24	9	Horiz	sin200	9.61	0.7	200	
940913.25	9	Horiz	sinIO	9.61	0.7	10	
940913.26	9	Horiz	sinIO	9.61	0.7	10	
940913.27	9	Horiz	sin200	9.61	0.7	200	9 minute delay since last test to this strain
940913.28	9	Horiz	sinIO	9.61	0.7	10	
940914.01	9	Horiz	sinIO	9.61	0.7	10	First test after about 1 7 hours
940914.02	9	Horiz	8in200	9.61	0.7	200	1 7 hour delay since last test to this strain
940914.03	9	Horiz	8in10	9.61	0.7	10	
940914.04	5	Vert	vcyd	9.61	0.1	185*	

Filename	Brg Num	Test Type	Signal	Axial Load (kips)	Freq./ Peak Velocity* (Hz/in/s)	Peak Strain/ Pressure Change* (%/psi)	Comments
940919.13	6	Horiz	hc07	9.61	0.7	150	
940919.14	6	Horiz	sin200	9.61	0.7	200	First test to this strain since manufacture
940919.15	6	Horiz	sin200	0.961	0.7	200	
940919.16	6	Horiz	sin200	24	0.7	200	
940919.17	6	Horiz	sin200	-2.6	0.7	200	Tension load test
940919.18	6	Horiz	sin200	9.61	0.7	200	
940919.19	6	Fail	sfail	24	0.1359*	400	Some evidence of plate slip apparent
940920.01	7	Horiz	hc07	9.61	0.7	150	First test of this bearing since manufacture
940920.02	7	Horiz	hc2	9.61	0.7	150	
940920.03	7	Vert	vcyd	9.61	0.1	185*	
940920.04	7	Vert	vcyc2	9.61	0.1	370*	
940920.05	7	Vert	vcyc2	14.41	0.1	555*	Signal scaled by 1.5
940920.06	7	Vert	vmonS	0	0.1	1110*	
940920.07	7	Horiz	hc07	9.61	0.7	150	
940920.08	7	Horiz	hc07	0.96	0.7	150	
940920.09	7	Horiz	hc07	-2.6	0.7	150	

940920.11	7	Horiz	hc07	9.61	0.7	150	
940920.12	7	Horiz	sin200	9.61	0.7	200	First test to this strain level
940920.13	7	Horiz	sin200	0.96	0.7	200	
940920.14	7	Horiz	sin200	24	0.7	200	
940920.15	7	Horiz	sin200	-2.6	0.7	200	
940920.16	7	Horiz	8in200	9.61	0.7	200	
940920.17	7	Horiz	hi 00.30	9.61	0.1	100	30cydesat0.1 Hz
940921.01	7	Horiz	sin200	9.61	0.7	100	First test in 22 hours; signal scaled by 0.5 (to 100 per cent)
940921.02	7	Horiz	hc2	9.61	0.7	150	
940921.03	7	Fail	sfail	-2.6	0.1359*	400	Bearing in tension; measured plate slip of about 0.19" in this test
940921.04	9	Horiz	sinIO	9.61	0.7	10	First test in one week
940921.05	9	Horiz	sin200	9.61	0.7	200	First test to this strain in one week
940921.06	9	Horiz	sinIO	9.61	0.7	10	

Filename	Brg Num	Test Type	Signal	Axial Load (kips)	Freq./ Peak Velocity* (Hz/in/s)	Peak Strain/ Pressure Change* (%/psi)	Comments
940915.10	10	Horiz	hc2	9.61	2	150	
940915.11	10	Horiz	sinIO	9.61	0.7	10	Extra smoothing of the data in this test
940915.12	10	Horiz	sin200	9.61	0.7	200	
940915.13	10	Horiz	sinIO	9.61	0.7	10	Extra smoothing of the data in this test
940915.14	10	Horiz	sinIO	9.61	0.7	10	First test in one hour; extra smoothing of the data in this test
940915.15	10	Horiz	sin200	9.61	0.7	200	First test in one hour
940915.16	10	Horiz	sinIO	9.61	0.7	10	Extra smoothing of the data in this test
940916.01	10	Horiz	sinIO	9.61	0.7	10	First test in 24 hours; extra smoothing of the data in this test
940916.02	10	Horiz	sin200	9.61	0.7	200	First test in about 24 hours
940916.03	10	Horiz	sinIO	9.61	0.7	10	Extra smoothing of the data in this test
940916.04	10	Horiz	sinIO	9.61	0.7	10	Data file truncated — test data complete, however
940916.05	10	Horiz	sinIO	9.61	0.7	10	Extra smoothing of the data in this test
940916.06	10	Horiz	sin200	9.61	0.7	200	
940916.07	10	Horiz	sinIO	9.61	0.7	10	Extra smoothing of the data in this test
• Axial loadcells were reading about 3.5 kips larger than the proper axial load during the following two tests because of drift — re-zeroed after these tests							
940919.01	6	Horiz	hc07	13	0.7	150	First test to this strain level since manufacture

940919.02	6	Horiz	hc2	13	2	150	
940919.03	6	Horiz	hc07	9.61	0.7	150	Retest at proper axial load
940919.04	6	Horiz	hc2	9.61	2	150	Retest at proper axial load
• DCDTs for vertical tests were moved from the external steel plates to very close to the bearing perimeter — vertical tests after this point should show better results							
940919.05	6	Vert	vcyd	9.61	0.1	185*	First vertical stiffness test with dcdts right next to bearing
940919.06	6	Vert	vcyc2	9.61	0.1	370*	
940919.07	6	Vert	vcyc2	14.41	0.1	555*	Signal scaled by 1.5
940919.08	6	Vert	vmonS	0	0.1	1110*	
940919.09	6	Horiz	hc07	9.61	0.7	150	
940919.10	6	Horiz	hc07	0.96	0.7	150	
940919.11	6	Horiz	hc07	24	0.7	150	
940919.12	6	Horiz	hc07	-2.6	0.7	150	

Filename	Brg Num	Test Type	Signal	Axial Load (kips)	Freq./ Peak Velocity* (Hz/in/s)	Peak Strain/ Pressure Change* (%/psi)	Comments
940923.01	10	Horiz	sinIO	9.61	0.7	10	First test in 1 week
940923.02	10	Horiz	sin200	9.61	0.7	200	First test to this strain in one week
940923.03	10	Horiz	sinIO	9.61	0.7	10	
940923.04	10	Horiz	hc2	0	2	150	
940923.05	10	Horiz	hc07	0	0.7	150	
940923.06	10	Horiz	slowlO	0	0.167*	10	
940923.07	10	Horiz	slow25	0	0.167*	25	
940923.08	10	Horiz	slowSO	0	0.167*	50	
940923.09	10	Horiz	slow75	0	0.167*	75	
940923.10	10	Horiz	slowl 00	0	0.167*	100	
940923.11	10	Horiz	slow125	0	0.167*	125	
940923.12	10	Horiz	slow 150	0	0.167*	150	
940923.13	10	Horiz	sslowlOO	0	0.0417*	100	
• The number of loadcells under the bearing was changed from 2 to 4 before the tests listed below. A new calibration file was also created.							
941103.01	9	Horiz	sinIO	9.61	' 0.7	10	First test in about 6 weeks
941103.02	9	Horiz	sin200	9.61	0.7	200	First test to this strain in about 6 weeks

941103.03	9	Horiz	sinIO	9.61	0.7	10	
941216.08	9	Horiz	sinIO	9.61	0.7	10	
• All of the following signals except sinIO were from the Bridgestone 1/4-scale tests and were scaled by 0.5 for these tests							
941216.09	9	Horiz	sin50_07	9.61	0.7	50	
941216.10	9	Horiz	s125_07	9.61	0.7	125	
941216.11	9	Horiz	s200_07	9.61	0.7	200	
941216.12	9	Horiz	sinIO	9.61	0.7	10	Used (3,3) smoothing for this test
941216.13	9	Horiz	sin50_07	9.61	0.7	50	
941216.14	9	Horiz	s125_07	9.61	0.7	125	
941216.15	9	Horiz	s200_07	9.61	0.7	200	

TABLE 2: BRIDGESTONE TEST SERIES

Filename	Brg Num	Test Type	Signal	Axial Load (kips)	Freq./ Peak Velocity* (Hz/in/s)	Peak Strain/ Pressure Change* (%/psi)	Comments
941109.01	TS0250-3	Horiz	sinIO	39.05	0.7	10	First test since manufacture
941109.02	TS0250-3	Horiz	sin200	39.05	0.7	200	First test to this strain since manufacture; bottom 30" sq. plate slipped by about +/-0.2" during this test.
941109.03	TS0250-3	Horiz	sinIO	39.05	0.7	10	Bearing removed and reinstalled, other work done after this test
941109.04	TS0250-3	Vert	vsig25	0	0.1	925*	
941109.05	TS0250-3	Horiz	sin 10	39.05	0.7	10	
941109.06	TS0250-3	Horiz	sin200	39.05	0.7	200	
941109.07	TS0250-3	Horiz	sinIO	39.05	0.7	10	
941109.08	TS0250-3	Vert	vchar	0	0.1	740*	
941109.09	TS0250-3	Horiz	hc07	39.05	0.7	150	
941109.10	TS0250-3	Horiz	hc14	39.05	1.4	150	Horizontal jack did not track the displacement signal at high strains
941110.01	TS0250-3	Horiz	sslowlO	39.05	0.083*	10	
941110.02	TS0250-3	Horiz	bslowlO	39.05	0.167*	10	
941110.03	TS0250-3	Horiz	sin10_01	39.05	0.1	10	
941110.04	TS0250-3	Horiz	sin10__07	39.05	0.7	10	

941110.05	TS0250-3	Horiz	sin10_14	39.05	1.4	10	
941110.06	TS0250-3	Horiz	bslow25	39.05	0.167*	25	
941110.07	TS0250-3	Horiz	sin25_01	39.05	0.1	25	
941110.08	TS0250-3	Horiz	sin25_07	39.05	0.7	25	
941110.09	TS0250-3	Horiz	sin25_14	39.05	1.4	25	
941110.10	TS0250-3	Horiz	sslowSO	39.05	0.083*	50	
941110.11	TS0250-3	Horiz	bslow50	39.05	0.167*	50	
941110.12	TS0250-3	Horiz	sin50_01	39.05	0.1	50	
941110.13	TS0250-3	Horiz	sin50__07	39.05	0.7	50	
941110.14	TS0250-3	Horiz	8in50_14	39.05	1.4	50	

Filename	Brg Num	Test Type	Signal	Axial Load (kips)	Freq./ Peak Velocity* (Hz/in/s)	Peak Strain/ Pressure Change* (%/psi)	Comments
941114.10	TS0250-3	Horiz	sin10_07	39.05	0.7	10	
941114.11	TS0250-3	Horiz	sin50_07	39.05	0.7	50	
941114.12	TS0250-3	Horiz	s100_07	39.05	0.7	100	
941114.13	TS0250-3	Horiz	s150_07	39.05	0.7	150	
941114.14	TS0250-3	Horiz	s200_07	39.05	0.7	200	
941114.15	TS0250-3	Horiz	sin10_07	39.05	0.7	10	
941114.16	TS0250-3	Horiz	sin50_07	39.05	0.7	50	
941114.17	TS0250-3	Horiz	s100_07	39.05	0.7	100	
941114.18	TS0250-3	Horiz	s150_07	39.05	0.7	150	
941114.19	TS0250-2	Horiz	sin10_07	39.05	0.7	10	First test of this bearing since manufacture?
941114.20	TS0250-2	Horiz	sin50_07	39.05	0.7	50	
941114.21	TS0250-2	Horiz	sin10_07	39.05	0.7	10	
941114.22	TS0250-2	Horiz	sin50_07	39.05	0.7	10	
941114.23	TS0250-2	Horiz	s100_07	39.05	0.7	100	
941114.24	TS0250-2	Horiz	sin10_07	39.05	0.7	10	
941114.25	TS0250-2	Horiz	sin50_07	39.05	0.7	50	

941114.26	TS0250-2	Horiz	s100_07	39.05	0.7	100	
941114.27	TS0252-2	Horiz	s150_07	39.05	0.7	150	
941114.28	TS0250-2	Horiz	sin10_07	39.05	0.7	10	
941114.29	TS0250-2	Horiz	sin50_07	39.05	0.7	50	
941114.30	TS0250-2	Horiz	s100_07	39.05	0.7	100	
941114.31	TS0250-2	Horiz	8150_07	39.05	0.7	150	
941114.32	TS0250-2	Horiz	8200_07	39.05	0.7	200	
941114.33	TS0250-2	Horiz	sin10_07	39.05	0.7	10	
941114.34	TS0250-2	Horiz	8in50_07	39.05	0.7	50	
941114.35	TS0250-2	Horiz	8100_07	39.05	0.7	100	
941114.36	TS0250-2	Horiz	S150_07	39.05	0.7	150	

Filename	Brg Num	Test Type	Signal	Axial Load (kips)	Freq./ Peak Velocity* (Hz/in/s)	Peak Strain/ Pressure Change* (%/psi)	Comments
941110.15	TS0250-3	Horiz	bslow75	39.05	0.167*	75	
941110.16	TS0250-3	Horiz	sin75_01	39.05	0.1	75	
941110.17	TS0250-3	Horiz	Sin75_07	39.05	0.7	75	
941110.18	TS0250-3	Horiz	sin75_14	39.05	1.4	75	
941110.19	TS0250-3	Horiz	sslowlOO	39.05	0.083*	100	
941110.20	TS0250-3	Horiz	bslowlOO	39.05	0.167*	100	
941110.21	TS0250-3	Horiz	s100_01	39.05	0.1	100	
941110.22	TS0250-3	Horiz	s100_07	39.05	0.7	100	
941110.23	TS0250-3	Horiz	8100_14	39.05	1.4	100	
941110.24	TS0250-3	Horiz	bslowl 25	39.05	0.167*	125	
941110.25	TS0250-3	Horiz	s125_01	39.05	0.1	125	
941110.26	TS0250-3	Horiz	s125_07	39.05	0.7	125	
941110.27	TS0250-3	Horiz	sslowl 50	39.05	0.083*	150	
941110.28	TS0250-3	Horiz	bslowl 50	39.05	0.167*	150	
941110.29	TS0250-3	Horiz	8150_01	39.05	0.1	150	
941110.30	TS0250-3	Horiz	s150_07	39.05	0.7	150	

941110.31	TS0250-3	Horiz	sslow200	39.05	0.083*	200	
941110.32	TS0250-3	Horiz	bslow200	39.05	0.167*	200	
941110.33	TS0250-3	Horiz	8200_01	39.05	0.1	200	
941110.34	TS0250-3	Horiz	s200_07	39.05	0.7	200	
941114.01	TS0250-3	Horiz	sin10_07	39.05	0.7	10	First test of this bearing in 3 days
941114.02	TS0250-3	Horiz	sin50_07	39.05	0.7	50	
941114.03	TS0250-3	Horiz	sin10_07	39.05	0.7	10	
941114.04	TS0250-3	Horiz	8in50_07	39.05	0.7	50	
941114.05	TS0250-3	Horiz	s100_07	39.05	0.7	100	
941114.06	TS0250-3	Horiz	8in10_07	39.05	0.7	10	
941114.07	TS0250-3	Horiz	sin50_07	39.05	0.7	50	
941114.08	TS0250-3	Horiz	8100_07	39.05	0.7	100	
941114.09	TS0250-3	Horiz	s150_07	39.05	0.7	150	

Filename	Brg Num	Test Type	Signal	Axial Load (kips)	Freq./ Peak Velocity* (Hz/in/s)	Peak Strain/ Pressure Change* (%/psi)	Comments
941117.19	TS0250-5	Horiz	sin25_07	39.05	0.7	25	
941117.20	TS0250-5	Horiz	sin50_07	39.05	0.7	50	
941117.21	TS0250-5	Horiz	sin75_07	39.05	0.7	75	
941117.22	TS0250-5	Horiz	s100_07	39.05	0.7	100	
941117.23	TS0250-5	Horiz	s125_07	39.05	0.7	125	
941117.24	TS0250-5	Horiz	s150_07	39.05	0.7	150	
941117.25	TS0250-5	Horiz	s200_07	39.05	0.7	200	Bearing was warm to the touch after this test
941117.27	TS0250-5	Horiz	sin10_07	39.05	0.7	10	
941117.28	TS0250-5	Horiz	s200_07	39.05	0.7	200	
941117.29	TS0250-5	Horiz	sin10_07	39.05	0.7	10	
• There was a slight horizontal offset in the bearing during the following two tests. It was corrected before 941118.03.							
941118.01	TS0250-5	Vert	vchar	0	0.1	740*	Test not analyzed
941118.02	TS0250-5	Vert	v150	0	0.1	150*	Test not analyzed
941118.03	TS0250-5	Vert	vchar	0	0.1	740*	
941118.04	TS0250-5	Vert	v150	0	0.1	150*	
941118.05	TS0250-5	Vert	vchar	0	0.1	740*	50 per cent horizontal offset

941118.06	TS0250-5	Vert	v150	0	0.1	150*	50 per cent horizontal offset
941118.07	TS0250-5	Vert	vchar	0	0.1	740*	1 00 per cent horizontal offset
941118.08	TS0250-5	Vert	v150	0	0.1	150*	100 per cent horizontal offset (DCDTs a little strange)
941118.09	TS0250-5	Vert	vchar	0	0.1	740*	150 per cent horizontal offset
941118.10	TS0250-5	Vert	v150	0	0.1	150*	150 per cent horizontal offset
941118.11	TS0250-5	Vert	vchar	0	0.1	740*	200 per cent horizontal offset
941118.12	TS0250-5	Vert	v150	0	0.1	150*	200 per cent horizontal offset (DCDTs a little strange)
941118.13	TS0250-5	Horiz	sin10_07	39.05	0.7	10	First horizontal test in 18 hours
941118.14	TS0250-5	Horiz	s200_07	39.05	0.7	200	First test to this strain in 18 hours
941118.15	TS0250-5	Horiz	sin10_07	39.05	0.7	10	
941118.16	TS0250-6	Vert	vchar	0	0.1	925*	Signal scaled by 1.25
941118.17	TS0250-6	Horiz	sin10_07	39.05	0.7	10	First horizontal test of this bearing since manufacture
941118.18	TS0250-6	Horiz	s200_07	39.05	0.7	200	First test to this strain since manufacture

Filename	Brg Num	Test Type	Signal	Axial Load (kips)	Freq./ Peak Velocity* (Hz/in/s)	Peak Strain/ Pressure Change* (%/psi)	Comments
• Before the following test the 4 shear loadcell channels were recalibrated to increase their maximum load capacity. This recalibration was done only on the horizontal channel setup, not on the vertical channel setup. Therefore, from 941115.XX to halfway through 941 214.XX any tests performed using the vertical channel setup will show shear loads of 1/2 of the true value. This should not have any affect on the results because the shear loading is not usually measured during the vertical tests.							
941115.01	TS0250-2	Fail	sfail	39.05	0.272*	500	Bearing didn't fail due to force limitations of the test machine; peak strain was approximately 307 per cent.
• No vertical DCDTs were in place for the following three tests							
941116.01	TS0250-1	Horiz	sin10_07	39.05	0.7	10	Bearing previously tested by manufacturer to 320% strain
941116.02	TS0250-1	Horiz	s200_07	39.05	0.7	200	Bearing previously tested by manufacturer to 320% strain
941116.03	TS0250-1	Horiz	sin10_07	39.05	0.7	10	
• NE DCDT may have been hitting the test frame during the following three tests							
941117.01	TS0250-4	Horiz	sin10_07	39.05	0.7	10	First test of this bearing ever
941117.02	TS0250-4	Horiz	s200_07	39.05	0.7	200	First test to this strain ever
941117.03	TS0250-4	Horiz	sin10_07	39.05	0.7	10	
941117.04	TS0250-4	Vert	vchar	0	0.1	925*	Signal scaled by 1.25
941117.05	TS0250-4	Vert	vchar	0	0.1	740*	
941117.06	TS0250-4	Horiz	hc07	39.05	0.7	150	
941117.07	TS0250-4	Horiz	sin10_07	39.05	0.7	10	

941117.08	TS0250-4	Horiz	s200_07	39.05	0.7	200	
941117.09	TS0250-4	Horiz	sin10_07	39.05	0.7	10	
941117.10	TS0250-5	Horiz	sin10_07	39.05	0.7	10	First test of this bearing since manufacture
941117.11	TS0250-5	Horiz	sin25_07	39.05	0.7	25	
941117.12	TS0250-5	Horiz	sin50_07	39.05	0.7	50	
941117.13	TS0250-5	Horiz	8in75_07	39.05	0.7	75	
941117.14	TS0250-5	Horiz	s100_07	39.05	0.7	100	
941117.15	TS0250-5	Horiz	S125_07	39.05	0.7	125	
941117.16	TS0250-5	Horiz	s150_07	39.05	0.7	150	
941117.17	TS0250-5	Horiz	s200_07	39.05	0.7	200	
941117.18	TS0250-5	Horiz	sin10_07	39.05	0.7	10	

Filename	Brg Num	Test Type	Signal	Axial Load (kips)	Freq./ Peak Velocity* (Hz/in/s)	Peak Strain/ Pressure Change* (%/psi)	Comments
941207.01	TS0250-2	Horiz	sin10_07	39.05	0.7	10	First test since manufacture
941207.02	TS0250-2	Horiz	s200_07	39.05	0.7	200	First test to this strain since manufacture
941207.03	TS0250-2	Horiz	sin10_07	39.05	0.7	10	
941207.04	TS0250-2	Horiz	sin10_07	39.05	0.7	10	Bearing was rotated 90 degrees
941207.05	TS0250-2	Horiz	s200_07	39.05	0.7	200	
941207.06	TS0250-2	Horiz	sin10_07	39.05	0.7	10	
941207.07	TS0250-2	Horiz	hc07	39.05	0.7	150	
• NW and SW DCDTs were recalibrated by altering the excitation voltage because there was a problem with recalibrating in ATS. The NW excitation voltage was changed from 6.00 VDC to 7.91 VDC, and the SW was changed from 6.00 VDC to 5.63 VDC. The NW gain was also changed from 5 to 2. These changes were needed becase the cores in these two instruments were damaged and had to be replaced.							
941207.08	TS0250-2	Vert	vchar	0	0.1	740*	
941207.09	TS0250-2	Vert	vchar	0	0.1	1110*	Signal scaled by 1.5
941207.10	TS0250-2	Vert	vmonS	0	0.1	1110*	
941207.11	TS0250-2	Horiz	hc07	3.905	0.7	150	
941207.12	TS0250-2	Horiz	hc07	39.05	0.7	150	
941207.13	TS0250-2	Horiz	hc07	97.6	0.7	150	
941207.14	TS0250-2	Horiz	hc07	-10.56	0.7	150	

941207.15	TS0250-2	Horiz	s200_07	3.905	0.7	200	
941207.16	TS0250-2	Horiz	s200_07	39.05	0.7	200	
941207.17	TS0250-2	Horiz	s200_07	97.6	0.7	200	
941207.18	TS0250-2	Horiz	S200_07	-10.56	0.7	200	
941207.19	TS0250-2	Horiz	sin10_07	39.05	0.7	10	
941207.20	TS0250-2	Horiz	S200_07	39.05	0.7	200	
941207.21	TS0250-2	Horiz	sin10_07	39.05	0.7	10	
941208.01	PS01 25/2-1	Horiz	sinIO	9.61	0.7	10	First test to this strain since manufacture
941208.02	PS01 25/2-1	Horiz	sin200	9.61	0.7	200	First test to this strain since manufacture
941208.03	PS01 25/2-1	Horiz	sinIO	9.61	0.7	10	
941208.04	PS01 25/2-1	Vert	vchar	0	0.1	925*	DCDTs look great
941208.05	PS01 25/2-1	Horiz	hc07	9.61	0.7	150	

Filename	Brg Num	Test Type	Signal	Axial Load (kips)	Freq./ Peak Velocity* (Hz/in/s)	Peak Strain/ Pressure Change* (%/psi)	Comments
941118.19	TS0250-6	Horiz	sin10_07	39.05	0.7	10	
• NE and NW DCDTs should be scaled by 2.5 in the following two tests — the gain was set at 2 instead of 5							
941118.20	TS0250-6	Vert	vchar	0	0.1	925	Signal scaled by 1.25
941118.21	TS0250-6	Vert	vchar	0	0.1	740	
941118.22	TS0250-6	Horiz	hc07	39.05	0.7	150	
941118.23	TS0250-6	Horiz	sin10_01	0	0.1	10	
941118.24	TS0250-6	Horiz	sin10_07	0	0.7	10	
941118.25	TS0250-6	Horiz	sin25_01	0	0.1	25	
941118.26	TS0250-6	Horiz	sin25_07	0	0.7	25	
941118.27	TS0250-6	Horiz	sin50_01	0	0.1	50	
941118.28	TS0250-6	Horiz	sin50_07	0	0.7	50	
941118.29	TS0250-6	Horiz	sin75_01	0	0.1	75	
941118.30	TS0250-6	Horiz	sin75_07	0	0.7	75	Ran out of disk space after 2-1/8 loops; not analyzed
941129.01	TS0250-6	Horiz	sin75_01	0	0.1	75	First test in 11 days
941129.02	TS0250-6	Horiz	sin75_07	0	0.7	75	
941129.03	TS0250-6	Horiz	s100_01	0	0.1	100	

941129.04	TS0250-6	Horiz	s100_07	0	0.7	100	
941129.05	TS0250-6	Horiz	S125_01	0	0.1	125	
941129.06	TS0250-6	Horiz	8125.07	0	0.7	125	
941129.07	TS0250-6	Horiz	s150_01	0	0.1	150	
941129.08	TS0250-6	Horiz	s150_07	0	0.7	150	
941129.09	TS0250-6	Horiz	s200_01	0	0.1	200	
941129.10	TS0250-6	Horiz	s200_07	0	0.7	200	
941129.11	TS0250-6	Horiz	sin10_07	39.05	0.7	10	
941129.12	TS0250-6	Horiz	s200_07	39.05	0.7	200	
941129.13	TS0250-6	Horiz	sin10_07	39.05	0.7	10	
941206.01	TS0250-6	Horiz	sin10_07	39.05	0.7	10	First test in one week
941206.02	TS0250-6	Horiz	s200_07	39.05	0.7	200	First test to this strain in one week
941206.03	TS0250-6	Horiz	sin10_07	39.05	0.7	10	

Filename	Brg Num	Test Type	Signal	Axial Load (kips)	Freq./ Peak Velocity* (Hz/in/s)	Peak Strain/ Pressure Change* (%/psi)	Comments
941209.23	PS01 25/2-2	Horiz	sinIO	9.61	0.7	10	
941209.24	PS01 25/2-2	Horiz	sin200	9.61	0.7	200	
941209.25	PS01 25/2-2	Horiz	sinIO	9.61	0.7	10	
941209.26	PS01 25/2-2	Fail	fastfail	9.61	10*	500	
941212.01	PS01 25/2-3	Vert	vchar	0	0.1	925*	Signal scaled by 1.25; DCDT readings are very unpredict-able
• Gain on summed axial load channel VPM4+7 was set at 2 instead of 1 , therefore the vertical loads in. all of the horizontal tests through 941 214.07 varied such that in extension of the horizontal actuator the vertical load was too high and during retraction it was too low. Vertical tests are OK.							
941212.02	PS01 25/2-3	Horiz	sinIO	9.61	0.7	10	First shear test since manufacture
941212.03	PS01 25/2-3	Horiz	sin200	9.61	0.7	200	
941212.04	PS01 25/2-3	Horiz	sinIO	9.61	0.7	10	
941212.05	PS01 25/2-3	Vert	vchar	0	0.1	925*	Signal scaled by 1.25
941212.06	PS01 25/2-3	Vert	vchar	0	0.1	740*	DCDTs a bit peculiar
941212.07	PS01 25/2-3	Horiz	hc07	9.61	0.7	150	
941212.08	PS01 25/2-3	Horiz	hc2	9.61	2	150	
941212.09	PS01 25/2-3	Vert	vmon	0	0.1	1110*	
941212.10	PS01 25/2-3	Vert	v150	0	0.1	150*	DCDTs 1 and 2 seemed to drift a lot

941212.11	PS01 25/2-3	Vert	vchar	0	0.1	740*	50 per cent horizontal offset — DCDTs strange again
941212.12	PS01 25/2-3	Vert	vmon	0	0.1	1110*	50 per cent horizontal offset — wrong signal run, should have been v150
941212.13	PS01 25/2-3	Vert	vchar	0	0.1	740*	100 per cent horizontal offset
941212.14	PS01 25/2-3	Vert	v150	0	0.1	150*	100 per cent horizontal offset — DCDTs a bit strange
941212.15	PS01 25/2-3	Vert	vchar	0	0.1	740*	150 per cent horizontal offset — DCDTs look OK
941212.16	PS01 25/2-3	Vert	v150	0	0.1	150*	150 per cent horizontal offset — no damping in hysteresis loop
941212.17	PS01 25/2-3	Vert	vchar	0	0.1	740*	200 per cent horizontal offset
941212.18	PS01 25/2-3	Vert	v150	0	0.1	150*	200 per cent horizontal offset — DCDTs 1 and 2 deleted
941212.19	PS01 25/2-3	Horiz	sinIO	9.61	0.7	10	
941212.20	PS01 25/2-3	Horiz	sin200	9.61	0.7	200	
941212.21	PS01 25/2-3	Horiz	sinIO	9.61	0.7	10	

Filename	Brg Num	Test Type	Signal	Axial Load (kips)	Freq./ Peak Velocity* (Hz/in/s)	Peak Strain/ Pressure Change* (%/psi)	Comments
941208.06	PS01 25/2-1	Horiz	hc2	9.61	2	150	
941208.07	PS01 25/2-1	Vert	vchar	0	0.1	740*	
941208.08	PS01 25/2-1	Horiz	sslowlO	9.61	0.083*	10	
941208.09	PS01 25/2-1	Horiz	bslowlO	9.61	0.167*	10	
941208.10	PS01 25/2-1	Horiz	sin10_01	9.61	0.1	10	
941208.11	PS01 25/2-1	Horiz	sin10_07	9.61	0.7	10	
941208.12	PS01 25/2-1	Horiz	bslow25	9.61	0.167*	25	
941208.13	PS01 25/2-1	Horiz	sin25_01	9.61	0.1	25	
941208.14	PS01 25/2-1	Horiz	sin25_07	9.61	0.7	25	
941208.15	PS01 25/2-1	Horiz	sslowSO	9.61	0.083*	50	
941208.16	PS01 25/2-1	Horiz	bslowSO	9.61	0.167*	50	
941208.17	PS01 25/2-1	Horiz	sin50_01	9.61	0.1	50	
941208.18	PS01 25/2-1	Horiz	sin50_07	9.61	0.7	50	
941208.19	PS01 25/2-1	Horiz	bslow75	9.61	0.167*	75	
941208.20	PS01 25/2-1	Horiz	sin75_01	9.61	0.1	75	
941208.21	PS01 25/2-1	Horiz	sin75_07	9.61	0.7	75	

941208.22	PS01 25/2-1	Horiz	sslowl 00	9.61	0.083*	100	
941208.23	PS01 25/2-1	Horiz	bslowl 00	9.61	0.167*	100	
941208.24	PS01 25/2-1	Horiz	s100_01	9.61	0.1	100	
941208.25	PS01 25/2-1	Horiz	s100_07	9.61	0.7	100	
941208.26	PS01 25/2-1	Horiz	bslowl 25	9.61	0.167*	125	
941208.27	PS01 25/2-1	Horiz	s125_01	9.61	0.1	125	
941208.28	PS01 25/2-1	Horiz	s125_07	9.61	0.7	125	
941208.29	PS01 25/2-1	Horiz	8slow150	9.61	0.083*	150	
941208.30	PS01 25/2-1	Horiz	bslowl 50	9.61	0.167*	150	
941208.31	PS01 25/2-1	Horiz	s150_01	9.61	0.1	150	
941208.32	PS01 25/2-1	Horiz	8150_07	9.61	0.7	150	
941208.33	PS01 25/2-1	Horiz	sslow200	9.61	0.083*	200	
941208.34	PS01 25/2-1	Horiz	bs!ow200	9.61	0.167*	200	

Filename	Brg Num	Test Type	Signal	Axial Load (kips)	Freq./ Peak Velocity* (Hz/in/s)	Peak Strain/ Pressure Change* (%/psi)	Comments
941213.01	PS01 25/2-3	Horiz	sinIO	9.61	0.7	10	First test in 1 5.5 hours
941213.02	PS01 25/2-3	Horiz	sin200	9.61	0.7	200	First test to this strain in 15.5 hours
941213.03	PS01 25/2-3	Horiz	sinIO	9.61	0.7	10	
941213.04	PS01 25/1-1	Horiz	sinIO	9.61	0.7	10	First test of this bearing since manufacture;extra data smoothing performed
941213.05	PS01 25/1-1	Horiz	sin200	9.61	0.7	200	First test to this strain since manufacture
941213.06	PS01 25/1-1	Horiz	sinIO	9.61	0.7	10	
941213.07	PS01 25/1-1	Vert	vchar	0	0.1	925*	Signal scaled by 1.25; not analyzed
941213.08	PS01 25/1-1	Horiz	hc07	9.61	0.7	150	
941213.09	PS01 25/1-1	Horiz	hc2	9.61	2	150	
941213.10	PS01 25/1-1	Vert	vchar	0	0.1	740*	Not analyzed
941213.11	PS01 25/1-1	Horiz	sslowlO	9.61	0.083*	10	
941213.12	PS01 25/1-1	Horiz	bslowlO	9.61	0.167*	10	
941213.13	PS01 25/1-1	Horiz	sin10_01	9.61	0.1	10	
941213.14	PS01 25/1-1	Horiz	sin10_07	9.61	0.7	10	
941213.15	PS01 25/1-1	Horiz	bslow25	9.61	0.167*	25	
941213.16	PS01 25/1-1	Horiz	sin25_01	9.61	0.1	25	

941213.17	PS01 25/1-1	Horiz	sin25_07	9.61	0.7	25	
941213.18	PS01 25/1-1	Horiz	sslowSO	9.61	0.083*	50	
941213.19	PS01 25/1-1	Horiz	bslowSO	9.61	0.167*	50	
941213.20	PS0125/1-1	Horiz	sin50_01	9.61	0.1	50	
941213.21	PS01 25/1-1	Horiz	sin50_07	9.61	0.7	50	
941213.22	PS01 25/1-1	Horiz	bslow75	9.61	0.167*	75	
941213.23	PS01 25/1-1	Horiz	sin75_01	9.61	0.1	75	
941213.24	PS01 25/1-1	Horiz	sin75_07	9.61	0.7	75	
941213.25	PS01 25/1-1	Horiz	sslowlOO	9.61	0.083*	100	
941213.26	PS01 25/1-1	Horiz	bslowlOO	9.61	0.167*	100	
941213.27	PS01 25/1-1	Horiz	s100_01	9.61	0.1	100	
941213.28	PS01 25/1-1	Horiz	s100_07	9.61	0.7	100	

Filename	Brg Num	Test Type	Signal	Axial Load (kips)	Freq./ Peak Velocity* (Hz/in/s)	Peak Strain/ Pressure Change* (%/psi)	Comments
941208.35	PS01 25/2-1	Horiz	S200_01	9.61	0.1	200	
941208.36	PS01 25/2-1	Horiz	S200_07	9.61	0.7	200	
941208.37	PS01 25/2-1	Horiz	hc07	9.61	0.7	150	
941208.38	PS01 25/2-1	Horiz	hc2	9.61	2	150	
941208.39	PS01 25/2-1	Horiz	Sin10	9.61	0.7	10	
941208.40	PS01 25/2-1	Horiz	sin200	9.61	0.7	200	
941208.41	PS01 25/2-1	Horiz	sinIO	9.61	0.7	10	
941209.01	PS01 25/2-1	Horiz	sinIO	9.61	0.7	10	First test in 1 6 hours
941209.02	PS01 25/2-1	Horiz	sin200	9.61	0.7	200	First test to this strain in 16 hours
941209.03	PS01 25/2-1	Horiz	sinIO	9.61	0.7	10	
941209.04	PS01 25/2-1	Fail	sfail	9.61	0.1359*	500	
941209.05	PS01 25/2-2	Horiz	hc07	9.61	0.7	150	First test since manufacture
941209.06	PS01 25/2-2	Horiz	sin200	9.61	0.7	200	First test to this strain since manufacture
941209.07	PS01 25/2-2	Horiz	sinIO	9.61	0.7	10	
941209.08	PS01 25/2-2	Vert	vchar	0	0.1	925*	Signal scaled by 1.25
• Following three tests run with vertical channel setup — vertical DCDTs not functional, and shear loads had to be scaled by 2.0 (see earlier note)							

941209.09	PS01 25/2-2	Horiz	sin200	9.61	0.7	200	Shear loads scaled by 2.0 to correct for wrong gains
941209.10	PS01 25/2-2	Horiz	hc07	9.61	0.7	150	Shear loads scaled by 2.0 to correct for wrong gains
941209.11	PS01 25/2-2	Horiz	hc2	9.61	2	150	Shear loads scaled by 2.0 to correct for wrong gains
941209.12	PS01 25/2-2	Vert	vchar	0	0.1	740*	
941209.13	PS01 25/2-2	Horiz	hc07	0.96	0.7	150	
941209.14	PS01 25/2-2	Horiz	hc07	9.61	0.7	150	
941209.15	PS01 25/2-2	Horiz	hc07	24	0.7	150	
941209.16	PS01 25/2-2	Horiz	hc07	-2.6	0.7	150	
941209.17	PS01 25/2-2	Horiz	sin200	-2.6	0.7	200	
941209.18	PS01 25/2-2	Horiz	sin200	0.96	0.7	200	
941209.19	PS01 25/2-2	Horiz	sin200	9.61	0.7	200	
941209.20	PS01 25/2-2	Horiz	sin200	24	0.7	200	
941209.22	PS01 25/2-2	Horiz	sin200	-2.6	0.7	200	

Filename	Brg Num	Test Type	Signal	Axial Load (kips)	Freq./ Peak Velocity* (Hz/in/s)	Peak Strain/ Pressure Change* (%/psi)	Comments
941214.11	PS0125/1-2	Vert	vchar	0	0.1	925*	Signal scaled by 1.25; DCDTs look a little strange
941214.12	PS0125/1-2	Horiz	sin200	9.61	0.7	200	
941214.13	PS0125/1-2	Horiz	hc07	9.61	0.7	150	
941214.14	PS0125/1-2	Horiz	hc2	9.61	2	150	
941214.15	PS0125/1-2	Vert	vchar	0	0.1	740*	DCDTs a little strange again
941214.16	PS0125/1-2	Horiz	hc07	0.96	0.7	150	
941214.17	PS0125/1-2	Horiz	hc07	9.61	0.7	150	
941214.18	PS0125/1-2	Horiz	hc07	24	0.7	150	
941214.19	PS0125/1-2	Horiz	hc07	-2.6	0.7	150	
941214.20	PS0125/1-2	Horiz	sin200	0.96	0.7	200	
941214.21	PS0125/1-2	Horiz	sin200	9.61	0.7	200	
941214.22	PS0125/1-2	Horiz	sin200	24	0.7	200	
941214.23	PS0125/1-2	Horiz	sin200	-2.6	0.7	200	
941214.24	PS0125/1-2	Horiz	sinIO	9.61	0.7	10	
941214.25	PS0125/1-2	Horiz	sin200	9.61	0.7	200	
941214.26	PS0125/1-2	Horiz	sinIO	9.61	0.7	10	

941215.01	PS0125/1-2	Horiz	sinIO	9.61	0.7	10	
941215.02	PS0125/1-2	Horiz	sin200	9.61	0.7	200	
941215.03	PS0125/1-2	Horiz	sinIO	9.61	0.7	10	
941215.04	PS0125/1-3	Vert	vchar	0	0.1	925*	A couple DCDTs look a little strange, but hysteresis is worse without them
941215.05	PS0125/1-3	Horiz	sinIO	9.61	0.7	10	
941215.06	PS0125/1-3	Horiz	sin200	9.61	0.7	200	
941215.07	PS0125/1-3	Horiz	sinIO	9.61	0.7	10	
941215.08	PS0125/1-3	Vert	vchar	0	0.1	925*	Signal scaled by 1.25
941215.09	PS0125/1-3	Vert	vchar	0	0.1	740*	
941215.10	PS0125/1-3	Horiz	hc07	9.61	0.7	150	
941215.11	PS0125/1-3	Horiz	hc2	9.61	2	150	Disk full — only 3-1/2 cycles of the 1 25 per cent strain data was saved; not analyzed

Filename	Brg Num	Test Type	Signal	Axial Load (kips)	Freq./ Peak Velocity* (Hz/in/s)	Peak Strain/ Pressure Change* (%/psi)	Comments
941213.29	PS01 25/1-1	Horiz	bslowl 25	9.61	0.167*	125	
941213.30	PS01 25/1-1	Horiz	s125_01	9.61	0.1	125	
941213.31	PS01 25/1-1	Horiz	s125_07	9.61	0.7	125	
941213.32	PS01 25/1-1	Horiz	sslow150	9.61	0.083*	150	
941213.33	PS01 25/1-1	Horiz	bslowl 50	9.61	0.167*	150	
941213.34	PS01 25/1-1	Horiz	s150_01	9.61	0.1	150	
941213.35	PS01 25/1-1	Horiz	s150_07	9.61	0.7	150	
941213.36	PS01 25/1-1	Horiz	sslow200	9.61	0.083*	200	
941213.37	PS01 25/1-1	Horiz	bslow200	9.61	0.167*	200	
941213.38	PS01 25/1-1	Horiz	s200_01	9.61	0.1	200	
941213.39	PS01 25/1-1	Horiz	S200_07	9.61	0.7	200	
941213.40	PS01 25/1-1	Horiz	hc07	9.61	0.7	150	
941213.41	PS01 25/1-1	Horiz	hc2	9.61	2	150	
941213.42	PS01 25/1-1	Horiz	sinIO	9.61	0.7	10	
941213.43	PS01 25/1-1	Horiz	sin200	9.61	0.7	200	
941213.44	PS01 25/1-1	Horiz	sinIO	9.61	0.7	10	

941214.01	PS01 25/1-1	Horiz	sinIO	9.61	0.7	10	
941214.02	PS01 25/1-1	Horiz	sin200	9.61	0.7	200	
941214.03	PS01 25/1-1	Horiz	sin 10	9.61	0.7	10	
941214.04	PS01 25/1-1	Fail	sfail	9.61	0.1359*	500	
941214.05	PS0125/1-2	Horiz	hc07	9.61	0.7	150	Not analyzed — bad vertical loads
941214.06	PS0125/1-2	Horiz	sin200	9.61	0.7	200	Not analyzed — bad vertical loads
941214.07	PS0125/1-2	Horiz	sinIO	9.61	0.7	10	Not analyzed — bad vertical loads
• At this time the improperly calibrated shear channels in the vertical channel setup (see 94111 5.01) and the gain on the axial 4+7 load channel were properly set. Also, the sensitivity of the 4 shear loadcells was increased from 500 to 1000 in the horizontal channel setup to match the changed sensitivities in the vertical channel setup file.							
941214.08	PS0125/1-2	Horiz	hc07	9.61	0.7	150	
941214.09	PS0125/1-2	Horiz	sin200	9.61	0.7 __j	200	
941214.10	PS0125/1-2	Horiz	sinIO	9.61	0.7	10	

Filename	Brg Num	Test Type	Signal	Axial Load (kips)	Freq./ Peak Velocity* (Hz/in/s)	Peak Strain/ Pressure Change* (%/psi)	Comments
941216.26	TS0125-2	Vert	vchar	0	0.1	740*	200 per cent horizontal offset
941216.27	TS0125-2	Vert	v150	0	0.1	150*	200 per cent horizontal offset
941216.28	TS0125-2	Horiz	sinIO	9.61	0.7	10	
941216.29	TS0125-2	Horiz	sin75_07	9.61	0.7	75	
941216.30	TS0125-2	Horiz	s150_07	9.61	0.7	150	
941216.31	TS0125-2	Horiz	s200_07	9.61	0.7	200	
941219.01	TS0125-2	Horiz	sinIO	9.61	0.7	10	First test in three days
941219.02	TS0125-2	Horiz	sin200	9.61	0.7	200	First test to this strain in three days
941219.03	TS0125-2	Horiz	sinIO	9.61	0.7	10	
941219.04	TS0125-2	Fail	sfail	9.61	0.136*	500	Some plate slip in this test
941219.05	TS0125-3	Horiz	s100_07	9.61	0.7	100	First test since manufacture
941219.06	TS0125-3	Horiz	hc07	9.61	0.7	150	
941219.07	TS0125-3	Horiz	hc2	9.61	2	150	
941219.08	TS0125-3	Vert	vchar	0	0.1	740*	
941219.09	TS0125-3	Vert	v150	0	0.1	150*	
941219.10	TS0125-3	Vert	vchar	0	0.1	740*	50 per cent horizontal offset

941219.11	TS0125-3	Vert	v150	0	0.1	150*	50 per cent horizontal offset
941219.12	TS0125-3	Vert	vchar	0	0.1	740*	1 00 per cent horizontal offset
941219.13	TS0125-3	Vert	v150	0	0.1	150*	100 per cent horizontal offset
941219.14	TS0125-3	Vert	vchar	0	0.1	740*	150 per cent horizontal offset
941219.15	TS0125-3	Vert	v150	0	0.1	150*	1 50 per cent horizontal offset
941219.16	TS0125-3	Vert	vchar	0	0.1	740*	200 per cent horizontal offset
941219.17	TS0125-3	Vert	v150	0	0.1	150*	200 per cent horizontal offset
941219.18	TS0125-3	Horiz	sinIO	9.61	0.7	10	
941219.19	TS0125-3	Horiz	sin75_07	9.61	0.7	75	
941219.20	TS0125-3	Horiz	s150_07	9.61	0.7	150	
941219.21	TS0125-3	Horiz	sinIO	9.61	0.7	10	
941219.22	TS0125-3	Fail	fastfail	9.61	10*	500	Some plate slip was apparent in this test
941219.23	TS0125-4	Horiz	s100_07	9.61	0.7	100	First test since manufacture

Filename	Brg Num	Test Type	Signal	Axial Load (kips)	Freq./ Peak Velocity* (Hz/in/s)	Peak Strain/ Pressure Change* (%/psi)	Comments
941215.12	PS0125/1-3	Vert	vmon	0	0.1	1110*	
941215.13	PS0125/1-3	Vert	v150	0	0.1	150*	DCDTs 1 and 2 looked a little strange
941215.14	PS0125/1-3	Vert	vchar	0	0.1	740*	50 per cent horizontal offset — DCDTs a little strange
941215.15	PS0125/1-3	Vert	v150	0	0.1	150*	50 per cent horizontal offset
941215.16	PS0125/1-3	Vert	vchar	0	0.1	740*	100 per cent horizontal offset — DCDTs peculiar
941215.17	PS0125/1-3	Vert	v150	0	0.1	150*	100 per cent horizontal offset
941215.18	PS0125/1-3	Vert	vchar	0	0.1	740*	150 per cent horizontal offset
941215.19	PS0125/1-3	Vert	v150	0	0.1	150*	1 50 per cent horizontal offset
941215.20	PS0125/1-3	Vert	vchar	0	0.1	740*	200 per cent horizontal offset
941215.21	PS0125/1-3	Vert	v150	0	0.1	150*	200 per cent horizontal offset
941215.22	PS0125/1-3	Horiz	sinIO	9.61	0.7	10	
941215.23	PS0125/1-3	Horiz	sin200	9.61	0.7	200	
941215.24	PS0125/1-3	Horiz	sinIO	9.61	0.7	10	
941216.01	TS0125-2	Horiz	sinIO	9.61	0.7	10	First test of this bearing since manufacture
941216.02	TS0125-2	Horiz	8in75_07	9.61	0.7	75	First test to this strain since manufacture
941216.03	TS0125-2	Horiz	8150_07	9.61	0.7	150	First test to this strain since manufacture

941216.04	TS0125-2	Horiz	sinIO	9.61	0.7	10	
941216.05	TS0125-2	Horiz	sin75_07	9.61	0.7	75	
941216.06	TS0125-2	Horiz	8150_07	9.61	0.7	150	
941216.16	TS0125-2	Horiz	hc07	9.61	0.7	150	
941216.17	TS0125-2	Horiz	hc2	9.61	2	150	
941216.18	TS0125-2	Vert	vmon	0	0.1	1110*	
941216.19	TS0125-2	Vert	vchar	0	0.1	740*	50 per cent horizontal offset
941216.20	TS0125-2	Vert	v150	0	0.1	150*	50 per cent horizontal offset
941216.21	TS0125-2	Vert	vchar	0	0.1	740*	1 00 per cent horizontal offset
941216.22	TS0125-2	Vert	vchar	99	0.1	150*	Not certain initial vertical load was 0 — repeat
941216.23	TS0125-2	Vert	v150	0	0.1	150*	100 per cent horizontal offset
941216.24	TS0125-2	Vert	vchar	0	0.1	740*	1 50 per cent horizontal offset
941216.25	TS0125-2	Vert	v150	0	0.1	150*	150 per cent horizontal offset

Filename	Brg Num	Test Type	Signal	Axial Load (kips)	Freq./ Peak Velocity* (Hz/in/s)	Peak Strain/ Pressure Change* (%/psi)	Comments
941221.13	TS0125-4	Horiz	sin75_07	9.61	0.7	75	
941221.14	TS0125-4	Horiz	sin75_07	0.96	0.7	75	
941221.15	TS0125-4	Horiz	sin75_07	24	0.7	75	
941221.16	TS0125-4	Horiz	sin75_07	-2.6	0.7	75	
941221.17	TS0125-4	Horiz	s100_07	9.61	0.7	100	
941221.18	TS0125-4	Horiz	s100_07	0.96	0.7	100	
941221.19	TS0125-4	Horiz	8100_07	24	0.7	100	
941221.20	TS0125-4	Horiz	s100_07	-2.6	0.7	100	
941221.21	TS0125-4	Horiz	8125_07	9.61	0.7	125	
941221.22	TS0125-4	Horiz	8125_07	0.96	0.7	125	
941221.23	TS0125-4	Horiz	8125_07	24	0.7	125	
941221.24	TS0125-4	Horiz	8125_07	-2.6	0.7	125	
941221.25	TS0125-4	Horiz	8150_07	9.61	0.7	150	Disk full before test complete — 4 full loops captured; not analyzed, but may be useful for first-cycle effects
941221.26	TS0125-4	Horiz	8150_07	9.61	0.7	150	
941221.27	TS0125-4	Horiz	s150_07	0.96	0.7	150	
941221.28	TS0125-4	Horiz	8150_07	24	0.7	150	

941221.29	TS0125-4	Horiz	8150_07	-2.6	0.7	150	
941221.30	TS0125-4	Horiz	s200_07	9.61	0.7	200	
941221.31	TS0125-4	Horiz	S200_07	0.96	0.7	200	
941221.32	TS0125-4	Horiz	S200_07	24	0.7	200	
941221.33	TS0125-4	Horiz	s200_07	-2.6	0.7	200	
941 221.34	TS0125-4	Horiz	hc07	9.61	0.7	150	
941 221.35	TS0125-5	Horiz	sin10_07	9.61	0.7	10	First test of this bearing since manufacture
941221.36	TS0125-5	Horiz	8in50_07	9.61	0.7	50	
941221.37	TS0125-5	Horiz	sin10_07	9.61	0.7	10	
941221.38	TS0125-5	Horiz	sin50_07	9.61	0.7	50	
941221.39	TS0125-5	Horiz	s100_07	9.61	0.7	100	
941221.40	IS0 125-5	Horiz	sin10_07	9.61	0.7	10	

Filename	Brg Num	Test Type	Signal	Axial Load (kips)	Freq./ Peak Velocity* (Hz/in/s)	Peak Strain/ Pressure Change* (%/psi)	Comments
941219.24	TS0125-4	Horiz	hc07	9.61	0.7	150	
941219.25	TS0125-4	Horiz	hc2	9.61	2	150	
941219.26	IS0 125-4	Vert	vchar	0	0.1	740*	
941219.27	IS0 125-4	Vert	vchar	0	0.1	740*	Not clear why this test was repeated
941219.28	TS0125-4	Vert	vmonS	0	0.1	1110	
941219.29	TS0125-4	Horiz	hc07	0.96	0.7	150	
941219.30	TS0125-4	Horiz	hc07	9.61	0.7	150	
941219.31	IS0 125-4	Horiz	hc07	24	0.7	150	
941219.32	IS0 125-4	Horiz	hc07	-2.6	0.7	150	
941219.33	TS0125-4	Horiz	s100_07	9.61	0.7	100	
941220.01	TS01 25-4	Horiz	sinIO	9.61	0.7	10	First test in 1 5 hours
941220.02	IS0 125-4	Horiz	sin200	9.61	0.7	200	First test to this strain since manufacture
941220.03	TS01 25-4	Horiz	sinIO	9.61	0.7	10	
941220.04	TS0125-4	Horiz	sin200	0.96	0.7	200	
941220.05	IS0 125-4	Horiz	sin200	24	0.7	200	
941220.06	TS0125-4	Horiz	sin200	-2.6	0.7	200	

941220.07	TS0125-4	Horiz	s100_07	9.61	0.7	100	
941221.01	TS0125-4	Horiz	sin10_07	9.61	0.7	10	
941221.02	TS0125-4	Horiz	8in10_07	0.96	0.7	10	
941221.03	TS0125-4	Horiz	sin10_07	24	0.7	10	
941221.04	TS0125-4	Horiz	sin10_07	-2.6	0.7	10	
941221.05	TS0125-4	Horiz	sin25_07	9.61	0.7	25	
941221.06	TS0125-4	Horiz	sin25_07	0.96	0.7	25	
941221.07	TS0125-4	Horiz	sin25_07	24	0.7	25	
941221.08	TS0125-4	Horiz	sin25_07	-2.6	0.7	25	
941221.09	TS0125-4	Horiz	sin50_07	9.61	0.7	50	
941221.10	TS0125-4	Horiz	sin50_07	0.96	0.7	50	
941221.11	TS0125-4	Horiz	sin50_07	24	0.7	50	
941221.12	TS0125-4	Horiz	sin50_07	-2.6	0.7	50	

Filename	Brg Num	Test Type	Signal	Axial Load (kips)	Freq./ Peak Velocity* (Hz/in/s)	Peak Strain/ Pressure Change* (%/psi)	Comments
941221.70	TS0125-5	Horiz	s125_07	0	0.7	125	
941221.71	TS01 25-5	Horiz	s150_01	0	0.1	150	
941221.72	TS0125-5	Horiz	s150_07	0	0.7	150	
941221.73	TS01 25-5	Horiz	S200_01	0	0.1	200	
941221.74	TS0125-5	Horiz	S200_07	0	0.7	200	
941222.01	TS0125-5	Horiz	sinIO	9.61	0.7	10	
941222.02	TS0125-5	Horiz	sinIO	9.61	0.7	10	
941222.03	TS0125-5	Horiz	sin200	9.61	0.7	200	
941222.04	TS0125-5	Horiz	sinIO	9.61	0.7	10	
941222.05	TS0125-5	Fail	sfail	-2.6	0.136*	550	Failure test with bearing in tension
941222.06	TS0125-6	Horiz	sinIO	9.61	0.7	10	First test since manufacture
941222.07	TS0125-6	Horiz	sin200	9.61	0.7	200	First test to this strain since manufacture
941222.08	TS0125-6	Horiz	sinIO	9.61	0.7	10	
941222.09	TS01 25-6	Vert	vchar	0	0.1	925*	Signal scaled by 1.25
941222.10	TS0125-6	Vert	vchar	0	0.1	740*	DCDTs look a bit peculiar
941222.11	TS01 25-6	Horiz	hc07	9.61	0.7	150	

941222.12	TS01 25-6	Horiz	hc2	9.61	2	150	
941222.13	TS01 25-6	Horiz	sinIO	9.61	0.7	10	
941222.14	TS0125-6	Horiz	sin200	9.61	0.7	200	
941222.15	TS0125-6	Horiz	sinIO	9.61	0.7	10	
941222.16	TS0125-6	Horiz	s100_07	9.61	0.7	100	
941222.17	TS0125-7	Horiz	hc07	9.61	0.7	150	First test of this bearing ever
941222.18	TS0125-7	Horiz	sin200	9.61	0.7	200	First test to this strain level ever
941222.19	TS0125-7	Horiz	sinIO	9.61	0.7	10	
941222.20	TS0125-7	Vert	vchar	0	0.1	925*	Signal scaled by 1.25
941222.21	TS0125-7	Horiz	sin200	9.61	0.7	200	
941222.22	TS01 25-7	Vert	vchar	0	0.1	740*	
941222.23	TS01 25-7	Horiz	hc07	9.61	0.7	150	
941222.24	TS0125-7	Horiz	hc2	9.61	2	150	Disk full — no data obtained

Filename	Brg Num	Test Type	Signal	Axial Load (kips)	Freq./ Peak Velocity* (Hz/in/s)	Peak Strain/ Pressure Change* (%/psi)	Comments
941221.41	TS0125-5	Horiz	sin50_07	9.61	0.7	50	
941221.42	TS0125-5	Horiz	s100_07	9.61	0.7	100	
941221.43	TS0125-5	Horiz	s150_07	9.61	0.7	150	
941221.44	TS0125-5	Horiz	sin10_07	9.61	0.7	10	
941221.45	TS0125-5	Horiz	sin50_07	9.61	0.7	50	
941221.46	TS0125-5	Horiz	s100_07	9.61	0.7	100	
941221.47	TS0125-5	Horiz	s150_07	9.61	0.7	150	
941221.48	TS0125-5	Horiz	s200_07	9.61	0.7	200	
941221.49	TS0125-5	Horiz	sin10_07	9.61	0.7	10	
941221.50	TS0125-5	Horiz	sin50_07	9.61	0.7	50	
941221.51	TS0125-5	Horiz	s100_07	9.61	0.7	100	
941221.52	TS0125-5	Horiz	s150_07	9.61	0.7	150	
941221.53	TS0125-5	Horiz	S200_07	9.61	0.7	200	
941221.54	TS0125-5	Vert	vchar	0	0.1	740*	DCDTs look strange — poor results
941221.55	TS0125-5	Horiz	hc07	0	0.7	150	
941221.56	TS0125-5	Horiz	hc2	0	2	150	

941221.57	TS0125-5	Horiz	s200_07	0	0.7	200	
941221.58	TS0125-5	Horiz	sin10_07	0	0.7	10	
941221.59	TS0125-5	Horiz	sin10_01	0	0.1	10	
941221.60	TS0125-5	Horiz	sin10_07	0	0.7	10	
941221.61	TS0125-5	Horiz	sin25_01	0	0.1	25	
941221.62	TS0125-5	Horiz	sin25_07	0	0.7	25	
941221.63	TS0125-5	Horiz	sin50_01	0	0.1	50	
941221.64	TS0125-5	Horiz	sin50_07	0	0.7	50	
941221.65	TS0125-5	Horiz	sin75_01	0	0.1	75	
941221.66	TS0125-5	Horiz	sin75_07	0	0.7	75	
941221.67	TS0125-5	Horiz	s100_01	0	0.1	100	
941221.68	TS0125-5	Horiz	s100_07	0	0.7	100	
941221.69	TS0125-5	Horiz	s125_01	0	0.1	125	

Filename	Brg Num	Test Type	Signal	Axial Load (kips)	Freq./ Peak Velocity* (Hz/in/s)	Peak Strain/ Pressure Change* (%/psi)	Comments
941223.29	TS0125-9	Horiz	bslowlOO	9.61	0.167*	100	
941223.30	TS0125-9	Horiz	s100_01	9.61	0.1	100	
941223.31	TS0125-9	Horiz	s100_07	9.61	0.7	100	
941223.32	TS01 25-9	Horiz	bslowl 25	9.61	0.167*	125	
941223.33	TS0125-9	Horiz	s125_01	9.61	0.1	125	
941223.34	TS0125-9	Horiz	S125_07	9.61	0.7	125	
941223.35	TS0125-9	Horiz	sslow150	9.61	0.083*	150	
941223.36	TS0125-9	Horiz	bslowl 50	9.61	0.167*	150	
941223.37	TS0125-9	Horiz	S150_01	9.61	0.1	150	
941223.38	TS0125-9	Horiz	s150_07	9.61	0.7	150	
941223.39	TS0125-9	Horiz	6s(ow200	9.61	0.083*	200	
941223.40	TS0125-9	Horiz	bslow200	9.61	0.167*	200	
941223.41	TS0125-9	Horiz	s200_01	9.61	0.1	200	
941223.42	TS0125-9	Horiz	s200_07	9.61	0.7	200	
941223.43	TS0125-9	Horiz	sinIO	9.61	0.7	10	
941223.44	TS0125-9	Horiz	sin200	9.61	0.7	200	

941223.45	TS0125-9	Horiz	sinIO	9.61	0.7	10	
950106.01	TS0125-9	Horiz	sin10_07	9.61	0.7	10	First test of this bearing in 1 5 days
950106.02	TS0125-9	Horiz	sin50_07	9.61	0.7	50	
950106.03	TS0125-9	Horiz	sin10_07	9.61	0.7	10	
950106.04	TS0125-9	Horiz	sin50_07	9.61	0.7	50	
950106.05	TS0125-9	Horiz	s100_07	9.61	0.7	100	
950106.06	TS0125-9	Horiz	sin10_07	9.61	0.7	10	
950106.07	TS0125-9	Horiz	sin50_07	9.61	0.7	50	
950106.08	TS0125-9	Horiz	8100_07	9.61	0.7	100	
950106.09	TS0125-9	Horiz	8150_07	9.61	0.7	150	
950106.10	TS0125-9	Horiz	8in10_07	9.61	0.7	10	
950106.11	TS0125-9	Horiz	sin50_07	9.61	0.7	50	
950106.12	TS01 25-9	Horiz	s100_07	9.61	0.7	100	

Filename	Brg Num	Test Type	Signal	Axial Load (kips)	Freq./ Peak Velocity* (Hz/in/s)	Peak Strain/ Pressure Change* (%/psi)	Comments
941222.25	TS0125-7	Horiz	hc2	9.61	2	150	
941223.01	TS0125-7	Horiz	sinIO	9.61	0.7	10	First test in 1 5 hours
941223.02	TS0125-7	Horiz	s100_07	9.61	0.7	100	First test to this strain in 1 5 hours
941223.03	TS0125-7	Horiz	sinIO	9.61	0.7	10	
941223.04	TS0125-7	Horiz	sin200	9.61	0.7	200	
941223.05	TS0125-7	Horiz	sinIO	9.61	0.7	10	
941223.06	TS0125-9	Vert	vchar	0	0.1	925*	Signal scaled by 1.25
941223.07	TS0125-9	Horiz	sinIO	9.61	0.7	10	Loop looks strange
941223.08	TS0125-9	Horiz	sin200	9.61	0.7	200	First test of this bearing to this strain
941223.09	TS0125-9	Horiz	sinIO	9.61	0.7	10	
941223.10	TS0125-9	Vert	vchar	0	0.1	925*	Signal scaled by 1.25
941223.11	TS0125-9	Vert	vchar	0	0.1	740*	
941223.12	TS0125-9	Horiz	hc07	9.61	0.7	150	
941223.13	TS0125-9	Horiz	hc2	9.61	2	150	
941223.14	TS0125-9	Horiz	sslowlO	9.61	0.083*	10	
941223.15	TS0125-9	Horiz	bslowlO	9.61	0.167*	10	

941223.16	TS0125-9	Horiz	sin10_01	9.61	0.1	10	
941223.17	TS0125-9	Horiz	sin10_07	9.61	0.7	10	
941223.18	TS0125-9	Horiz	bslow25	9.61	0.167*	25	
941223.19	TS0125-9	Horiz	sin25_01	9.61	0.1	25	
941223.20	TS0125-9	Horiz	sin25_07	9.61	0.7	25	
941223.21	TS0125-9	Horiz	sslowSO	9.61	0.083*	50	
941223.22	TS0125-9	Horiz	bslowSO	9.61	0.167*	50	
941223.23	TS0125-9	Horiz	sin50_01	9.61	0.1	50	
941223.24	TS0125-9	Horiz	sin50_07	9.61	0.7	50	
941223.25	TS0125-9	Horiz	bslow75	9.61	0.167*	75	
941223.26	TS0125-9	Horiz	sin75_01	9.61	0.1	75	
941223.27	TS0125-9	Horiz	sin75_07	9.61	0.7	75	
941223.28	TS0125-9	Horiz	sslowlOO	9.61	0.083*	100	

Filename	Brg Num	Test Type	Signal	Axial Load (kips)	Freq./ Peak Velocity* (Hz/in/s)	Peak Strain/ Pressure Change* (%/psi)	Comments
950106.42	TS0125-9	Horiz	8125_01	9.61	0.1	125	
950106.43	TS0125-9	Horiz	s150_01	9.61	0.1	150	
950106.44	TS0125-9	Horiz	s200_01	9.61	0.1	200	
950106.45	TS0125-9	Horiz	hc07	9.61	0.7	150	
950106.46	TS0125-9	Horiz	s200_07	9.61	0.7	200	
950106.47	TS0125-9	Horiz	hc2	9.61	2	150	
950109.01	TS0125-8	Horiz	sin10_07	9.61	0.7	10	First test of this bearing ever
950109.02	TS0125-8	Horiz	sin50_07	9.61	0.7	50	First test of this bearing to this strain
950109.03	TS0125-8	Horiz	sin10_07	9.61	0.7	10	
950109.04	TS0125-8	Horiz	sin50_07	9.61	0.7	50	
950109.05	TS0125-8	Horiz	6100_07	9.61	0.7	100	First test to this strain ever
950109.06	TS0125-8	Horiz	sin10_07	9.61	0.7	10	
950109.07	TS0125-8	Horiz	sin50_07	9.61	0.7	50	
950109.08	TS0125-8	Horiz	8100_07	9.61	0.7	100	
950109.09	TS0125-8	Vert	vchar	0	0.1	740*	Some strange behavior in vertical DCDTS
950109.10	TS0125-8	Horiz	sslowlO	9.61	0.083*	10	

950109.11	TS0125-8	Horiz	bslowlO	9.61	0.167*	10	
950109.12	TS0125-8	Horiz	sin10_01	9.61	0.1	10	
950109.13	TS0125-8	Horiz	sin10_07	9.61	0.7	10	
950109.14	TS0125-8	Horiz	bslow25	9.61	0.167*	25	
950109.15	TS0125-8	Horiz	sin25_01	9.61	0.1	25	
950109.16	TS0125-8	Horiz	sin25_07	9.61	0.7	25	
950109.17	TS0125-8	Horiz	sslow50	9.61	0.083*	50	
950109.18	TS0125-8	Horiz	bslowSO	9.61	0.167*	50	
950109.19	TS0125-8	Horiz	sin50_01	9.61	0.1	50	
950109.20	TS0125-8	Horiz	sin50_07	9.61	0.7	50	
950109.21	TS0125-8	Horiz	bslow75	9.61	0.167*	75	
950109.22	TS0125-8	Horiz	sin75_01	9.61	0.1	75	
950109.23	TS0125-8	Horiz	sin75_07	9.61	0.7	75	

Filename	Brg Num	Test Type	Signal	Axial Load (kips)	Freq./ Peak Velocity* (Hz/in/s)	Peak Strain/ Pressure Change* (%/psi)	Comments
950106.13	TS0125-9	Horiz	8150_07	9.61	0.7	150	
950106.14	TS0125-9	Horiz	B200_07	9.61	0.7	200	
950106.15	TS0125-9	Horiz	sin10_07	9.61	0.7	10	
950106.16	TS0125-9	Horiz	sin50_07	9.61	0.7	50	
950106.17	TS0125-9	Horiz	8100_07	9.61	0.7	100	
950106.18	TS0125-9	Horiz	S150_07	9.61	0.7	150	
950106.19	TS0125-9	Horiz	S200_07	9.61	0.7	200	
950106.20	TS0125-9	Horiz	bslowlO	9.61	0.167*	10	
950106.21	TS0125-9	Horiz	bslow25	9.61	0.167*	25	
950106.22	TS0125-9	Horiz	bslowSO	9.61	0.167*	50	
950106.23	TS0125-9	Horiz	bslow75	9.61	0.167*	75	
950106.24	TS0125-9	Horiz	bslowlOO	9.61	0.167*	100	
950106.25	TS0125-9	Horiz	bslow125	9.61	0.167*	125	
950106.26	TS0125-9	Horiz	bslowl 50	9.61	0.167*	150	
950106.27	TS0125-9	Horiz	bslow200	9.61	0.167*	200	This file is missing.
950106.28	TS0125-9	Horiz	8in10_07	9.61	0.7	10	

950106.29	TS0125-9	Horiz	sin25_07	9.61	0.7	25	
950106.30	TS0125-9	Horiz	sin50_07	9.61	0.7	50	
950106.31	TS0125-9	Horiz	8in75_07	9.61	0.7	75	
950106.32	TS0125-9	Horiz	s100_07	9.61	0.7	100	
950106.33	TS0125-9	Horiz	8125_07	9.61	0.7	125	
950106.34	TS0125-9	Horiz	S150_07	9.61	0.7	150	
950106.35	TS0125-9	Horiz	S200_07	9.61	0.7	200	
950106.36	TS0125-9	Horiz	hc07	9.61	0.7	150	
950106.37	TS0125-9	Horiz	sin10_01	9.61	0.1	10	
950106.38	TS0125-9	Horiz	sin25_01	9.61	0.1	25	
950106.39	TS0125-9	Horiz	sin50_01	9.61	0.1	50	
950106.40	IS0 125-9	Horiz	sin75_01	9.61	0.1	75	
950106.41	TS0125-9	Horiz	s100_01	9.61	0.1	100	

Filename	Brg Num	Test Type	Signal	Axial Load (kips)	Freq./ Peak Velocity* (Hz/in/s)	Peak Strain/ Pressure Change* (%/psi)	Comments
950109.53	TS0125-8	Horiz	s100_07	9.61	0.7	100	
950109.54	TS0125-8	Horiz	8125_07	9.61	0.7	125	
950109.55	TS0125-8	Horiz	s150_07	9.61	0.7	150	
950109.56	TS0125-8	Horiz	s200_07	9.61	0.7	200	
950109.57	TS0125-8	Vert	vchar	0	0.1	740*	DCDT #4 looked a little strange
950109.58	TS0125-8	Horiz	hc07	9.61	0.7	150	
950109.59	TS0125-8	Horiz	hc2	9.61	2	150	
950109.60	TS0125-8	Horiz	sin10_07	9.61	0.7	10	
950109.61	TS0125-8	Horiz	sin50_07	9.61	0.7	50	
950109.62	TS0125-8	Horiz	8100_07	9.61	0.7	100	
950110.01	PS0125/1-3	Horiz	sinIO	9.61	0.7	10	First test of this bearing in about 25 days
950110.02	PS0125/1-3	Horiz	sin200	9.61	0.7	200	First test to this strain in about 25 days
950110.03	PS0125/1-3	Horiz	sinIO	9.61	0.7	10	
950110.04	PS0125/1-3	Vert	vchar	0	0.1	925*	Signal scaled by 1.25
950110.05	PS0125/1-3	Horiz	sslowlO	9.61	0.083*	10	
950110.06	PS0125/1-3	Horiz	bslowlO	9.61	0.167*	10	

950110.07	PS0125/1-3	Horiz	sin10_07	9.61	0.7	10	
950110.08	PS0125/1-3	Horiz	sin10_07	9.61	0.7	10	
950110.09	PS0125/1-3	Horiz	bs!ow25	9.61	0.167*	25	
950110.10	PS0125/1-3	Horiz	sin25_01	9.61	0.1	25	
950110.11	PS0125/1-3	Horiz	sin25_07	9.61	0.7	25	
950110.12	PS0125/1-3	Horiz	sslowSO	9.61	0.083*	50	
950110.13	PS0125/1-3	Horiz	bslowSO	9.61	0.167*	50	
950110.15	PS0125/1-3	Horiz	sin50_07	9.61	0.7	50	
950110.16	PS0125/1-3	Horiz	bslow75	9.61	0.167*	75	
950110.17	PS0125/1-3	Horiz	8in75_01	9.61	0.1	75	
950110.18	PS0125/1-3	Horiz	8in75_07	9.61	0.7	75	
950110.19	PS0125/1-3	Horiz	sslowlOO	9.61	0.083*	100	
950110.20	PS0125/1-3	Horiz	bslowlOO	9.61	0.167*	100	

Filename	Brg Num	Test Type	Signal	Axial Load (kips)	Freq./ Peak Velocity* (Hz/in/s)	Peak Strain/ Pressure Change* (%/psi)	Comments
950109.24	TS0125-8	Horiz	sslowl 00	9.61	0.083*	100	
950109.25	TS0125-8	Horiz	bslowl 00	9.61	0.167*	100	
950109.26	TS0125-8	Horiz	s100_01	9.61	0.1	100	
950109.27	TS0125-8	Horiz	s100_07	9.61	0.7	100	
950109.28	TS0125-8	Horiz	sin10_01	0	0.1	10	
950109.29	TS0125-8	Horiz	sin10_07	0	0.7	10	
950109.30	TS0125-8	Horiz	sin25_01	0	0.1	25	
950109.31	TS0125-8	Horiz	sin25_07	0	0.7	25	
950109.32	TS0125-8	Horiz	sin50_01	0	0.1	50	
950109.33	TS0125-8	Horiz	sin50_07	0	0.7	50	
950109.34	TS0125-8	Horiz	sin75_01	0	0.1	75	
950109.35	TS0125-8	Horiz	sin75_07	0	0.7	75	
950109.36	TS0125-8	Horiz	s100_01	0	0.1	100	
950109.37	TS0125-8	Horiz	s100_07	0	0.7	100	
950109.38	TS0125-8	Horiz	sin10_07	24	0.7	10	
950109.39	TS0125-8	Horiz	sin25_07	24	0.7	25	

950109.40	TS0125-8	Horiz	sin50_07	24	0.7	50	
950109.41	TS0125-8	Horiz	sin75_07	24	0.7	75	
950109.42	TS0125-8	Horiz	8100_07	24	0.7	100	
950109.43	TS0125-8	Horiz	sin10_07	-2.6	0.7	10	
950109.44	TS0125-8	Horiz	sin25_07	-2.6	0.7	25	
950109.45	TS0125-8	Horiz	sin50_07	-2.6	0.7	50	
950109.46	TS0125-8	Horiz	sin75_07	-2.6	0.7	75	
950109.47	TS0125-8	Horiz	s100_07	-2.6	0.7	100	
950109.48	TS0125-8	Horiz	s200_07	9.61	0.7	200	First test to this strain
950109.49	IS0 125-8	Horiz	sin10_07	9.61	0.7	10	
950109.50	TS0125-8	Horiz	sin25_07	9.61	0.7	25	
950109.51	TS0125-8	Horiz	sin50_07	9.61	0.7	50	
950109.52	TS0125-8	Horiz	sin75_07	9.61	0.7	75	

Filename	Brg Num	Test Type	Signal	Axial Load (kips)	Freq./ Peak Velocity* (Hz/in/s)	Peak Strain/ Pressure Change* (%/psi)	Comments
950113.01	PS0 125/2-3	Horiz	8100 07	9.61	0.7	100	First test in three days
950113.02	PS0 125/2-3	Horiz	s200_07	9.61	0.7	200	
950113.03	PS0 125/2-3	Horiz	s100_07	9.61	0.7	100	
950113.04	PS01 25/2-3	Vert	vchar	0	0.1	740*	DCDT #3 looked a bit strange
950113.05	PS01 25/2-3	Vert	v150	0	0.1	150*	
950113.06	PS01 25/2-3	Vert	vchar	0	0.1	740*	50 per cent horizontal offset; DCDT #3 looked strange
950113.07	PS01 25/2-3	Vert	v150	0	0.1	150*	50 per cent horizontal offset
950113.08	PS01 25/2-3	Vert	vchar	0	0.1	740*	100 per cent horizontal offset
950113.09	PS01 25/2-3	Vert	v150	0	0.1	150*	100 per cent horizontal offset
950113.10	PS01 25/2-3	Vert	vchar	0	0.1	740*	1 50 per cent horizontal offset
950113.11	PS01 25/2-3	Vert	v150	0	0.1	150*	150 per cent horizontal offset
950113.12	PS01 25/2-3	Vert	vchar	0	0.1	740*	200 per cent horizontal offset
950113.13	PS01 25/2-3	Vert	v150	0	0.1	150*	200 per cent horizontal offset
950113.14	PS01 25/2-3	Horiz	bslowlO	9.61	0.167*	10	
950113.15	PS01 25/2-3	Horiz	bslowlO	0	0.167*	10	
950113.16	PS01 25/2-3	Horiz	sin10_07	0	0.7	10	

950113.17	PS01 25/2-3	Horiz	bslow25	0	0.167*	25	
950113.18	PS01 25/2-3	Horiz	sin25_07	0	0.7	25	
950113.19	PS01 25/2-3	Horiz	bslowSO	0	0.167*	50	
950113.20	PS01 25/2-3	Horiz	sin50_07	0	0.7	50	
950113.21	PS01 25/2-3	Horiz	bslow75	0	0.167*	75	
950113.22	PS01 25/2-3	Horiz	sin75_07	0	0.7	75	
950113.23	PS01 25/2-3	Horiz	bslowlOO	0	0.167*	100	
950113.24	PS01 25/2-3	Horiz	s100_07	0	0.7	100	
950113.25	PS01 25/2-3	Horiz	bslowl 25	0	0.167*	125	
950113.26	PS01 25/2-3	Horiz	s125_07	0	0.7	125	
950113.27	PS01 25/2-3	Horiz	bslowl 50	0	0.167*	150	
950113.28	PS01 25/2-3	Horiz	s150_07	0	0.7	150	
950113.29	PS0 125/2-3	Horiz	bslow200	0	0.167*	200	

Filename	Brg Num	Test Type	Signal	Axial Load (kips)	Freq./ Peak Velocity* (Hz/in/s)	Peak Strain/ Pressure Change* (%/psi)	Comments
950110.21	PS0125/1-3	Horiz	s100_01	9.61	0.1	100	
950110.22	PS0125/1-3	Horiz	8100_07	9.61	0.7	100	
950110.23	PS0125/1-3	Horiz	bslow125	9.61	0.167*	125	
950110.24	PS0125/1-3	Horiz	s125_01	9.61	0.1	125	
950110.25	PS0125/1-3	Horiz	8125_07	9.61	0.7	125	
950110.26	PS0125/1-3	Horiz	sslowl 50	9.61	0.083*	L 150	
950110.27	PS0125/1-3	Horiz	bslowl 50	9.61	0.167*	150	
950110.28	PS0125/1-3	Horiz	s150_01	9.61	0.1	150	
950110.30	PS0125/1-3	Horiz	sslow200	9.61	0.083*	200	
950110.31	PS0125/1-3	Horiz	bslow200	9.61	0.167*	200	
950110.32	PS0125/1-3	Horiz	s200_01	9.61	0.1	200	
950110.33	PS0125/1-3	Horiz	s200_07	9.61	0.7	200	
950110.34	PS0125/1-3	Horiz	hc07	0.96	0.7	150	
950110.35	PS0125/1-3	Horiz	hc07	9.61	0.7	150	
950110.36	PS0125/1-3	Horiz	hc07	24	0.7	150	
950110.37	PS0125/1-3	Horiz	hc07	-2.6	0.7	150	

950110.38	PS01 25/2-3	Horiz	sin10_07	9.61	0.7	10	First test of this bearing in 28 days
950110.39	PS01 25/2-3	Horiz	sin50_07	9.61	0.7	50	
950110.40	PS01 25/2-3	Horiz	8in10_07	9.61	0.7	10	
950110.41	PS01 25/2-3	Horiz	sin50_07	9.61	0.7	50	
950110.42	PS01 25/2-3	Horiz	8100_07	9.61	0.7	100	
950110.43	PS01 25/2-3	Horiz	sin10_07	9.61	0.7	10	
950110.44	PS01 25/2-3	Horiz	sin50_07	9.61	0.7	50	
950110.45	PS01 25/2-3	Horiz	8100_07	9.61	0.7	100	
950110.46	PS01 25/2-3	Horiz	s200_07	9.61	0.7	200	
950110.47	PS01 25/2-3	Horiz	sin10_07	9.61	0.7	10	
950110.48	PS01 25/2-3	Horiz	sin50_07	9.61	0.7	50	
950110.49	PS01 25/2-3	Horiz	s100_07	9.61	0.7	100	
950110.50	PS01 25/2-3	Horiz	8200_07	9.61	0.7	200	

Filename	Brg Num	Test Type	Signal	Axial Load (kips)	Freq./ Peak Velocity* (Hz/in/s)	Peak Strain/ Pressure Change* (%/psi)	Comments
950113.30	PS01 25/2-3	Horiz	s200_07	0	0.7	200	
• Decreased the gain in the shear loadcell channels from 1000 to 500 — simultaneously increased the calibration factor by 2 (to test the bigger bearings)							
950117.01	TS0250-6	Horiz	Sbild	39.05	0.7	200	First test in 6 weeks
• Changed all of the setting back to their original values							
950117.02	TS0250-6	Vert	vchar	0	0.1	740	
950117.03	TS0250-6	Vert	v150	0	0.1	-150	
950117.04	TS0250-6	Vert	vchar	0	0.1	740	50 per cent horizontal offset
950117.05	TS0250-6	Vert	v150	0	0.1	-150	50 per cent horizontal offset
950117.06	TS0250-6	Vert	vchar	0	0.1	740	1 00 per cent horizontal offset
950117.07	TS0250-6	Vert	v150	0	0.1	-150	100 per cent horizontal offset
950117.08	TS0250-6	Vert	vchar	0	0.1	740	1 50 per cent horizontal offset
950117.09	TS0250-6	Vert	v150	0	0.1	-150	1 50 per cent horizontal offset
950117.10	TS0250-6	Vert	vchar	0	0.1	740	200 per cent horizontal offset
950117.11	TS0250-6	Vert	v150	0	0.1	-150	200 per cent horizontal offset
950118.01	TS0250-6	Horiz	s100_07	39.05	0.7	100	

Other tests were intended to evaluate the effects of loading frequency or applied axial load on the observed bearing mechanical properties. However, even these showed some effects of load-history if the test sequence was not consistent. Therefore, two types of these tests were defined. For example, to evaluate the effect of loading frequency, the *VF1* and *VF2* sequences are outlined as follows. In the VF1 sequence, a single test signal consisting of five cycles at strain amplitudes of 10 to 150 per cent was first run on a bearing at a given frequency. Therefore, this bearing has now been strained to 150 per cent. The next test is another signal running from strain amplitudes of 10 to 150 per cent, but at a different frequency. This is then continued over the frequency range of 0.1 Hz to 1.4 Hz (1/4-scale) or 2.0 Hz (1/8-scale). Constant-velocity (sawtooth) tests at velocities of 5 in/min and 10 in/min are also run in this VF1 sequence.

In contrast, a VF2 sequence was performed by first running tests over the range of frequencies at only 10 per cent strain, then running the range of frequencies at 25 per cent strain, then at 50 per cent strain, and so on. In this way, the influence of previous cycles to larger strains does not contaminate the results observed at lower cycles. The axial pressure in all of the VF1 and VF2 tests was 370 psi.

A similar approach was taken to investigate the effect of axial loads. The *VA1* series consisted of a continuous test from 10 to 150 per cent strain which was run repeatedly at a range of axial pressures — 370 psi, 37 psi, 925 psi, and 100 psi tension. The *VA2* sequence, in contrast, consisted of repeated tests at 10 per cent shear strain at axial pressures of 370, 37, 925, and -100 psi, followed by repeated tests at 25 per cent strain and the same range of pressures, etc. The loading frequency in all of the VA1 and VA2 tests was 0.7 Hz.

There were essentially two types of vertical tests undertaken in addition to the vertical characteristic tests. In the first, a bearing was held at 0 psi and subjected to pressures of +/-150 psi (including tension), or a bearing was cycled over a pressure range from 0 to 1110 psi (three times the design pressure). The second consisted of so-called vertical offset tests in which the bearing was first strained horizontally and then held at that prestrain while the vertical pressure was varied. These tests were performed at axial pressures of 370 psi +/-185 psi, 370 psi +/- 370 psi, and 0 psi +/- 150 psi.

The final tests performed were failure tests, and the majority of these involved imposing a monotonic lateral displacement on the bearing at a constant shear strain rate of 10 per cent/second. The applied axial pressure was changed for each of these tests to determine the influence of pressure on ultimate strain and the failure mechanism, if any. One additional type of failure test was performed in which a bearing was subjected to a half-cycle of strain at an amplitude of 25 per cent and then strained at 10 inches/second in the opposite direction until failure. These tests were designed to show the difference between failure tests at slow rates and those at higher rates.

7. TEST RESULTS

Introduction

A total of 984 tests performed on the ALGA and Bridgestone bearings. Obviously it is not possible to provide a detailed evaluation of each test, however, individual summaries of each test are provided in Parts 2-6 of the report. The standard processing of each horizontal and failure test generates at least two pages of output, as shown in Figure 7. The first page provides a summary of the type of bearing being tested, the test signal and axial load, any comments on the test (added at the time of analysis) and the relevant results for each cycle of

the test. The second page and subsequent pages provide the hysteretic behavior and any strain-modulus or strain-damping relationship that can be inferred from the single test. Vertical tests are associated with only a single page; as described below it is difficult to get very accurate, detailed results from the vertical tests, and therefore only the measured hysteresis is plotted.

ALMR/Bridgestone Bearing Tests

Filename: 941219.24
Bearing Number: TS0125-4
Compound: KL501

Signal: hc07
Frequency: 0.7 Hz
Initial Axial Load: 9.61 kips
Initial Axial Pressure: 370 psi
Target Peak Strain: 150%
Comments:

Summary of Results

Cycle Number	γ (%)	k_{eff} (k/in)	G_{eff} (psi)	EDC (kip-in)	ξ_{eq} (%)
1	9.2	8.77	462.5	0.16	21.55
2	9.3	8.63	455.2	0.15	16.87
3	9.2	8.59	453.4	0.14	16.56
4	9.2	8.65	456.5	0.14	16.34
5	9.2	8.5	448.3	0.14	16.13
1	23.9	6.44	339.7	0.69	15.83
2	24	6.23	328.5	0.65	15.42
3	24	6.13	323.7	0.63	15.25
4	23.9	6.14	324.2	0.62	15.03
5	23.9	6.08	321	0.62	15
1	48.6	4.85	255.7	2.06	15.26
2	48.5	4.63	244.5	1.93	15.01
3	48.7	4.55	240.2	1.91	15.02
4	48.6	4.53	239.2	1.89	14.93
5	48.6	4.51	238.2	1.86	14.76
1	73.4	4.02	212	3.76	14.73
2	73.4	3.87	204.4	3.65	14.81
3	73.3	3.83	202.2	3.55	14.62
4	73.4	3.79	199.7	3.49	14.52
5	73.4	3.77	199	3.49	14.55
1	98.1	3.78	199.7	5.88	13.7
2	98.3	3.64	192.1	5.68	13.69
3	98.3	3.59	189.1	5.57	13.63
4	98.1	3.54	186.5	5.52	13.77
5	98.3	3.52	185.7	5.47	13.64
1	123.1	3.79	199.7	8.6	12.71
2	123	3.54	187	8.14	12.88
3	123.2	3.46	182.3	7.96	12.88
4	122.9	3.4	179.5	7.87	12.99
5	123	3.38	178.3	7.77	12.88
1	147.8	3.8	200.3	11.59	11.85
2	147.8	3.52	185.9	10.96	12.08
3	147.8	3.43	180.7	10.73	12.15
4	147.7	3.37	177.7	10.54	12.16
5	147.8	3.34	176	10.36	12.07

Figure 7: Sample Output from Data Reduction Program.

In the results from horizontal tests, the bearing mechanical properties are typically expressed in terms of the effective shear modulus, G^, and the equivalent viscous damping, §. These two quantities are found from the following relationships:

$$G_{eff} = \frac{K_{eff} t_r}{A_{shim}} \quad \text{and} \quad \xi_{eq} = \frac{EDC}{2\pi K_{eff} \Delta_{max}^2}$$

where K_e^ is the peak-to-peak stiffness of the hysteresis loop,
t is the total rubber thickness,

A shim k ^e cross-sectional area of the internal steel shims,

EDC is the energy dissipated in a single cycle, and

tfnax *s ^e sQuare of the peak displacement.

In the majority of the figures that follow, G_{eff} and £ are plotted as a function of shear strain under various loading conditions.

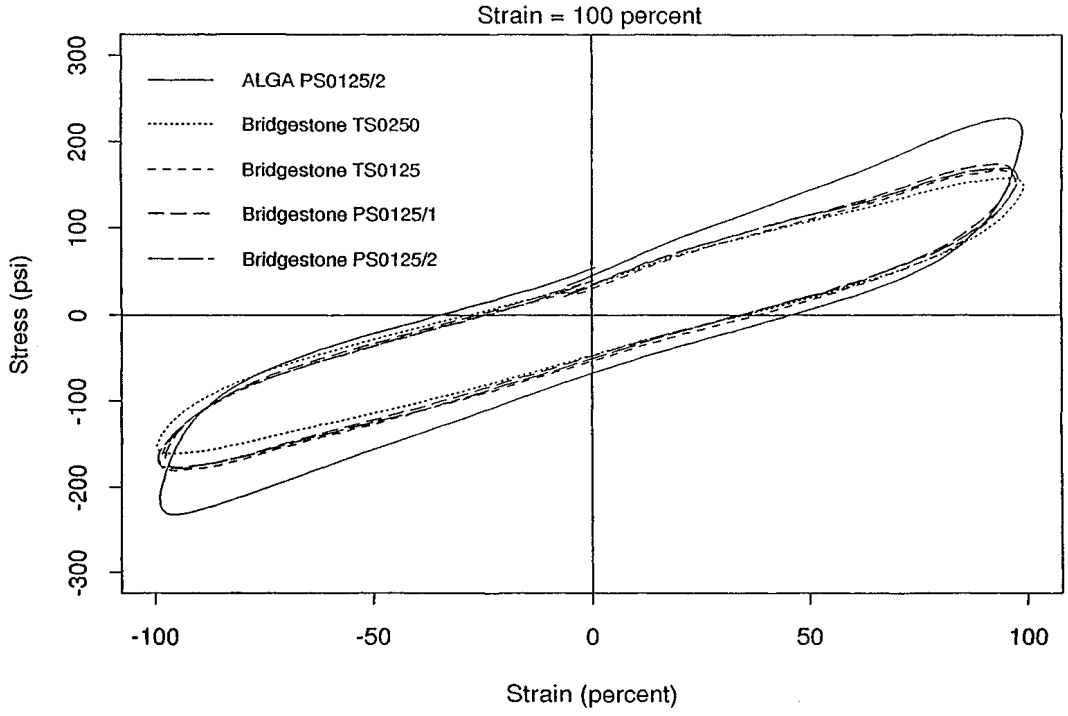

Figure 8: Comparison of Bearing Hysteretic Behavior.

A representative comparison of the response of each type of bearing, normalized in terms of stress and strain, is given in Figure 8. This shows the hysteretic behavior from the first cycle at 100 per cent shear strain in a horizontal characteristic test at 0.7 Hz, and several typical aspects of the response of the various bearings that are seen throughout the test program are evident. First, in general the ALGA compound is stiffer than the Bridgestone compound, and exhibits slightly more energy dissipation per cycle. In this figure it is clear that the peak stress in the ALGA bearing is well above 200 psi (the target effective modulus at 100 per cent shear strain), while each of the Bridgestone bearings exhibits a stress somewhat below 200 psi. Also of interest here is the almost insignificant difference between the various 1/8-scale Bridgestone bearings. Even though the three different bearing designs have different shape

factors, their force-displacement response is nearly identical. This may be due to the relatively low applied axial pressure during this test (370 psi). Also, the stiffness of the 1/4-scale Bridgestone bearing is not substantially different from that of the 1/8-scale bearings, a trend which is seen throughout the test program.

Alga — General Results

Results from all of the horizontal characteristic tests at 370 psi and 0.7 Hz are shown for the ALGA bearings in Figure 9. The scatter in the data at 10 per cent shear strain is likely not meaningful because the displacement corresponding to 10 per cent strain is only 0.136 in. At higher strains the scatter reduces somewhat, although there is still a substantial variation in measured stiffness, particularly first-cycle stiffness. It also appears from the plot of the damping values at 125 and 150 per cent shear strain that there is one bearing which has substantially less damping than the others. It is not clear whether this is a result of the load history imposed on this bearing before the characteristic test or some other factor, although in the course of identifying the appropriate tests for inclusion in these characteristic test comparisons, consideration was given to prior load history.

Bridgestone — General Results

Similar plots are shown for each of the Bridgestone designs in Figures 10 through 13. These show the difference between the first-cycle stiffness and the third-cycle stiffness over the range of strains, and, as expected, the third-cycle stiffness is lower. However, an interesting result which is seen for all of the bearing designs (including the ALGA bearings) is that the mean of the third-cycle damping is less than that of the first-cycle damping at low strains, but above about 75 per cent shear strain it becomes larger than the first-cycle mean. Because the effective stiffness (or equivalently, the effective modulus) enters into the denominator in the damping calculation, if a constant amount of energy is dissipated in the first and third cycles, the third-cycle damping will be larger than the first. The data imply that the energy dissipated per cycle actually decreases substantially with repeated cycling at strains less than 75 per cent, but remains approximately constant at higher strains.

The degree of scatter in the damping results for the TS0250 bearings appears to be anomalous when compared with that observed in the other bearing designs. However, the variation in effective modulus in these bearings seems to be smaller than that in the other bearings, particularly at higher shear strains. Unfortunately, because there were only three bearings of types PS0125/1 and PS0125/2, there is insufficient data to draw further conclusions from these observations.

Comparisions

When the mean values of stiffness and damping from characteristic tests of all bearing types are plotted against one another, similar trends emerge. Figures 14 and 15 compare the first-cycle and third-cycle results, respectively, and again the ALGA bearings show substantially greater stiffness and damping than the Bridgestone bearings. The third-cycle damping at the design shear strain of 100 per cent is well in excess of the specified 12 per cent for all bearings, however both bearing types miss the target modulus of 200 psi at 100 per cent shear strain by more than the 10 per cent allowed by the specification. The mean modulus of the ALGA bearings is greater than 230 psi while those of the different designs of Bridgestone bearings are less than 175 psi. Because these are mean values, it is unlikely that the results are influenced significantly by load history. It therefore appears that either the compounds must be adjusted or the bearing designs refined to bring the isolators within the specification.

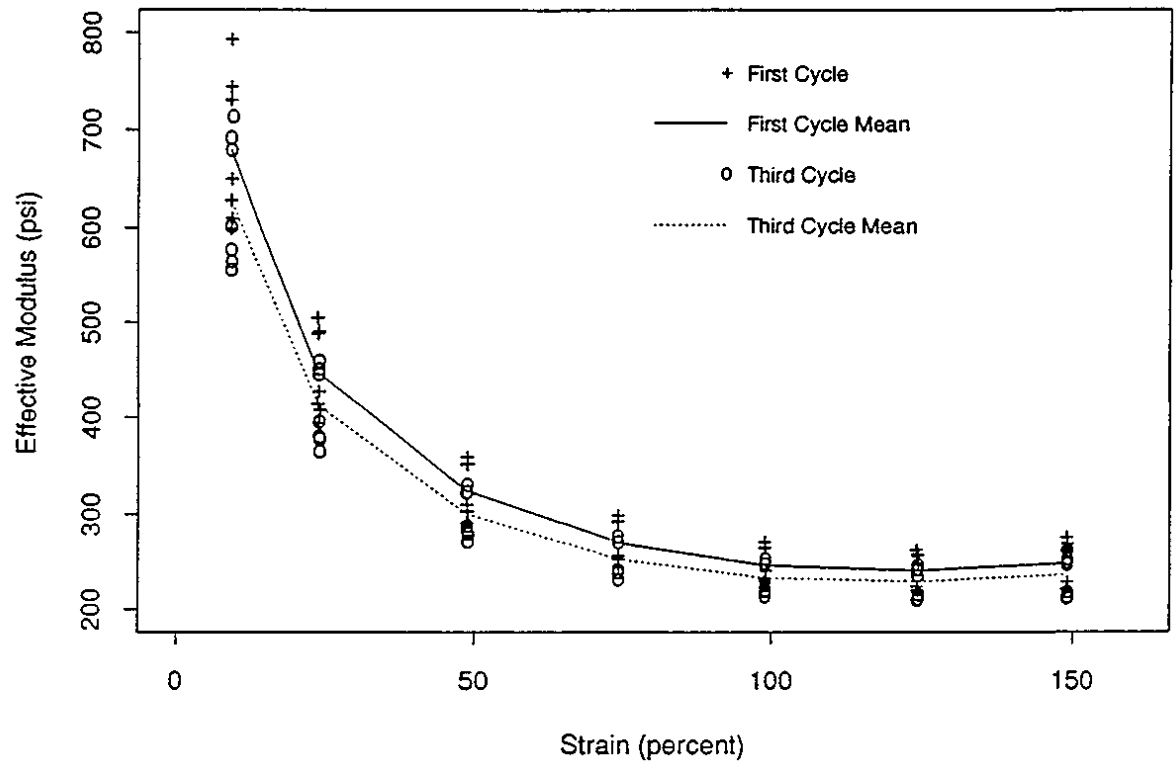

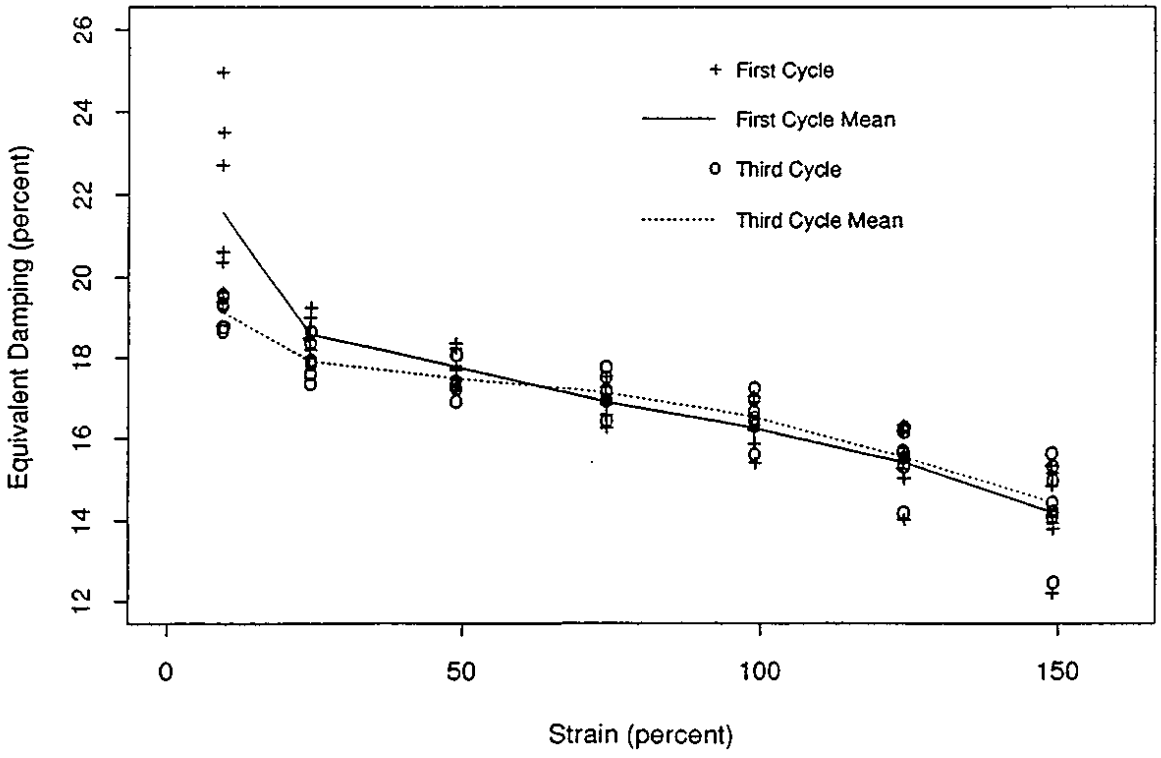

Figure 9: Results from Characteristic Tests of ALGA PS0125/2 Bearings.

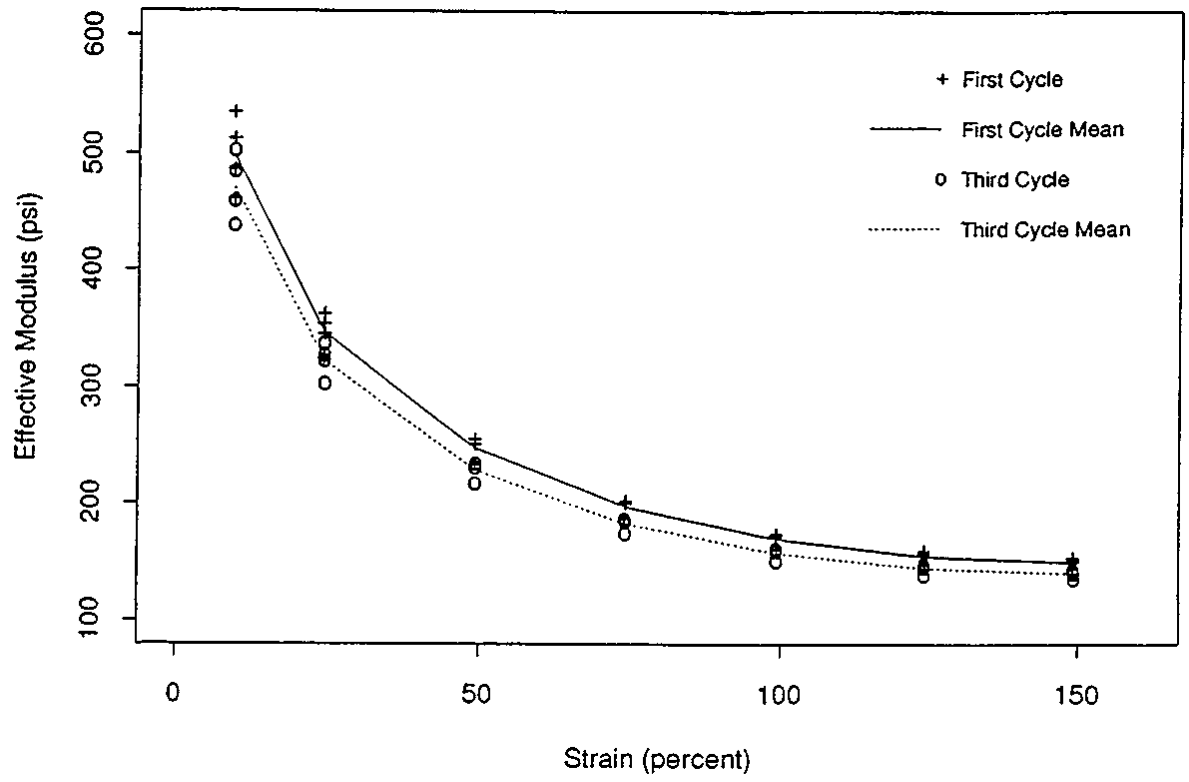

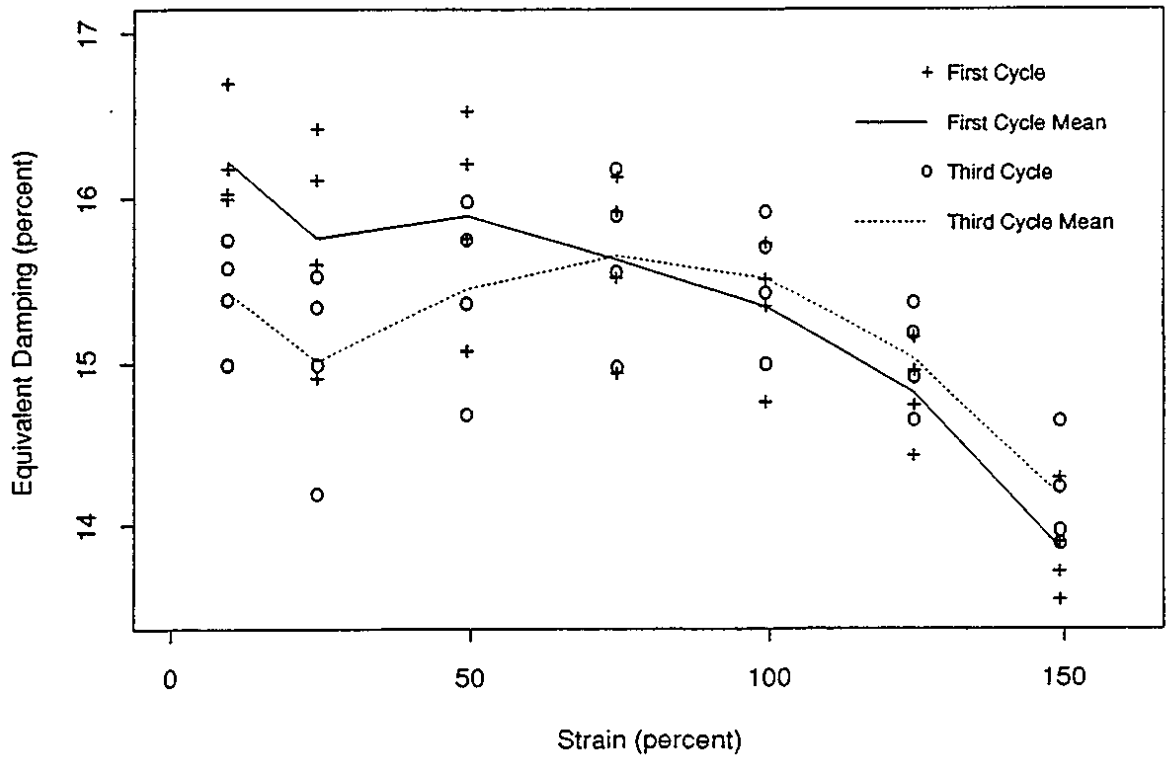

Figure 10: Results from Characteristic Tests of Bridgestone TS0250 Bearings.

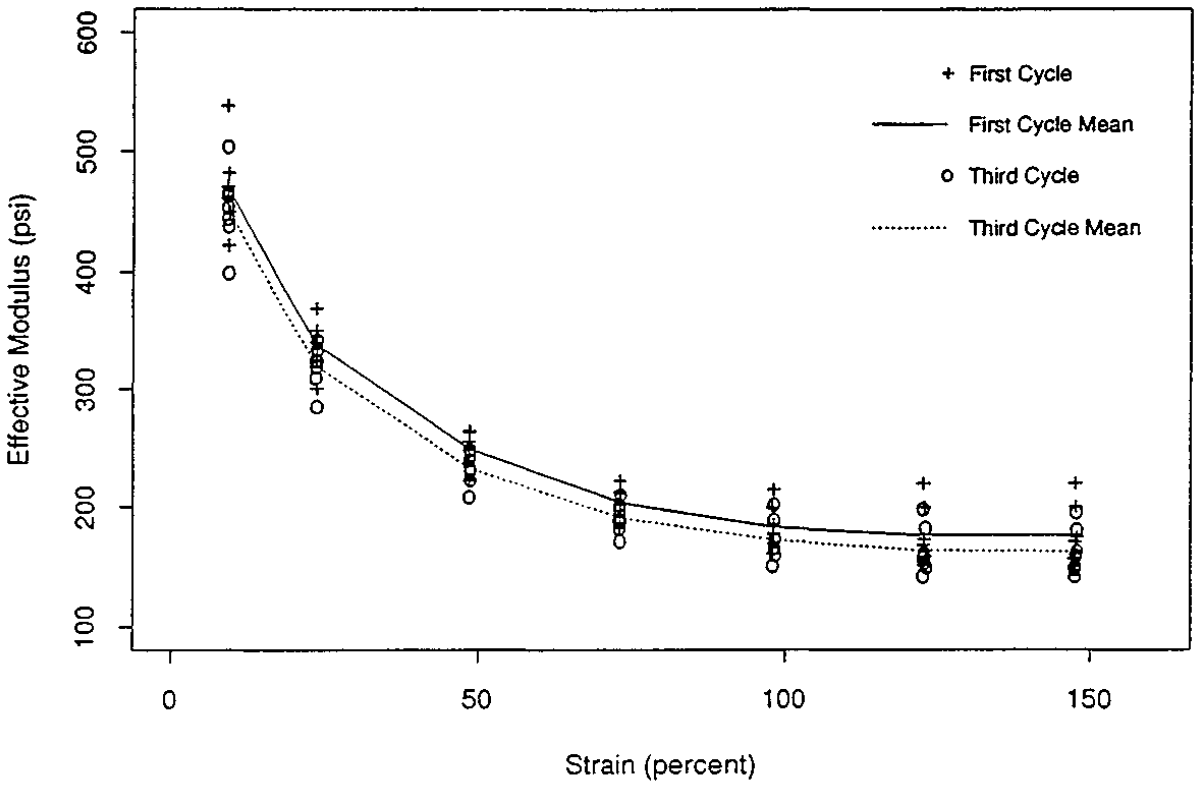

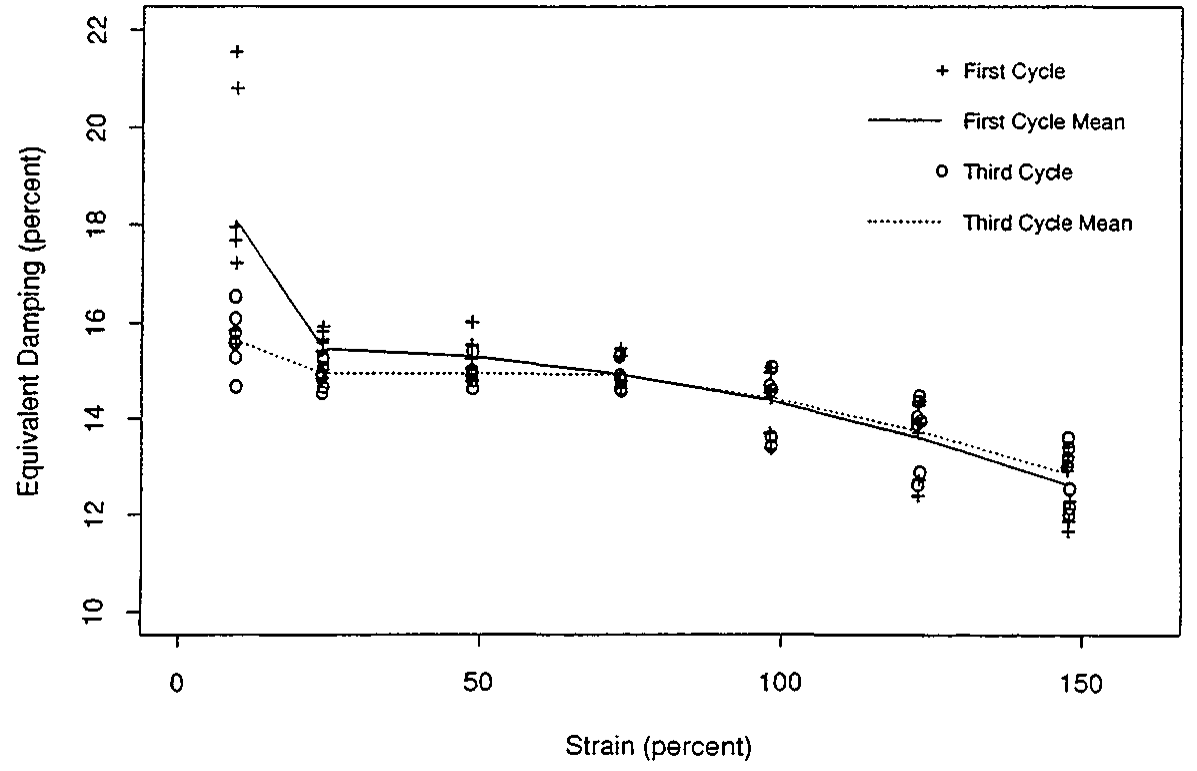

Figure 11: Results from Characteristic Tests of Bridgestone TS0125 Bearings.

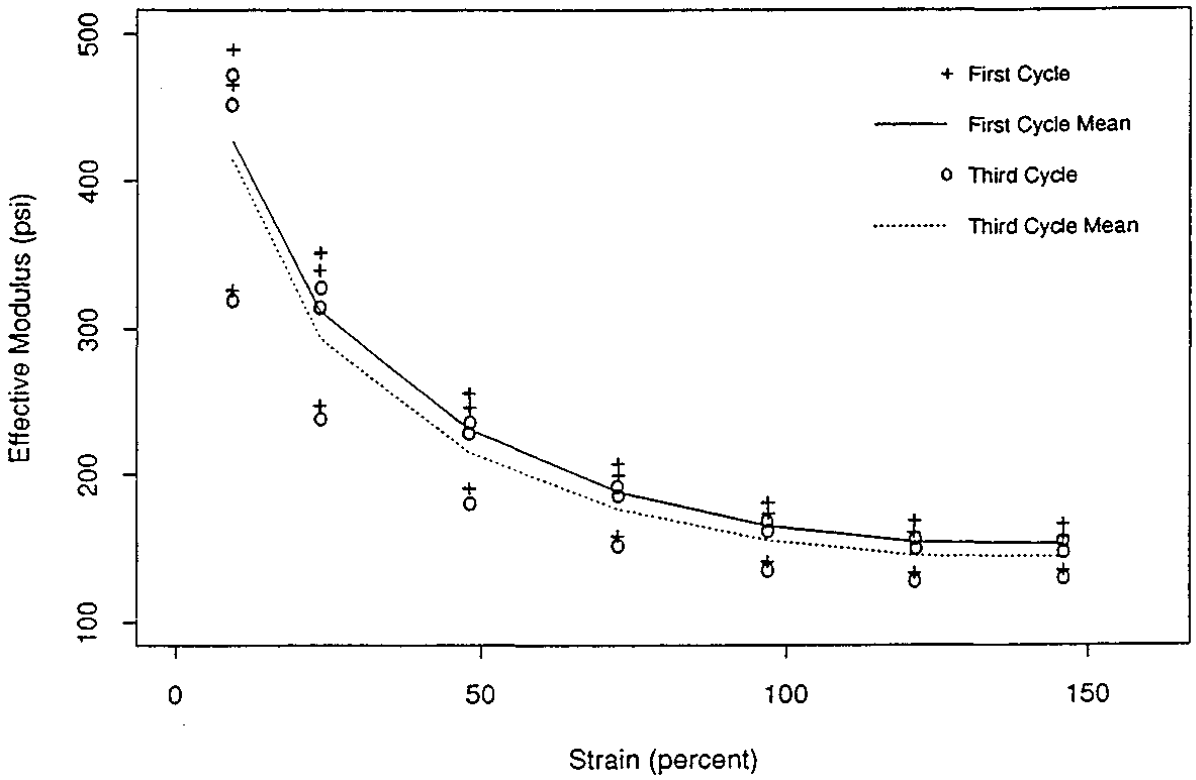

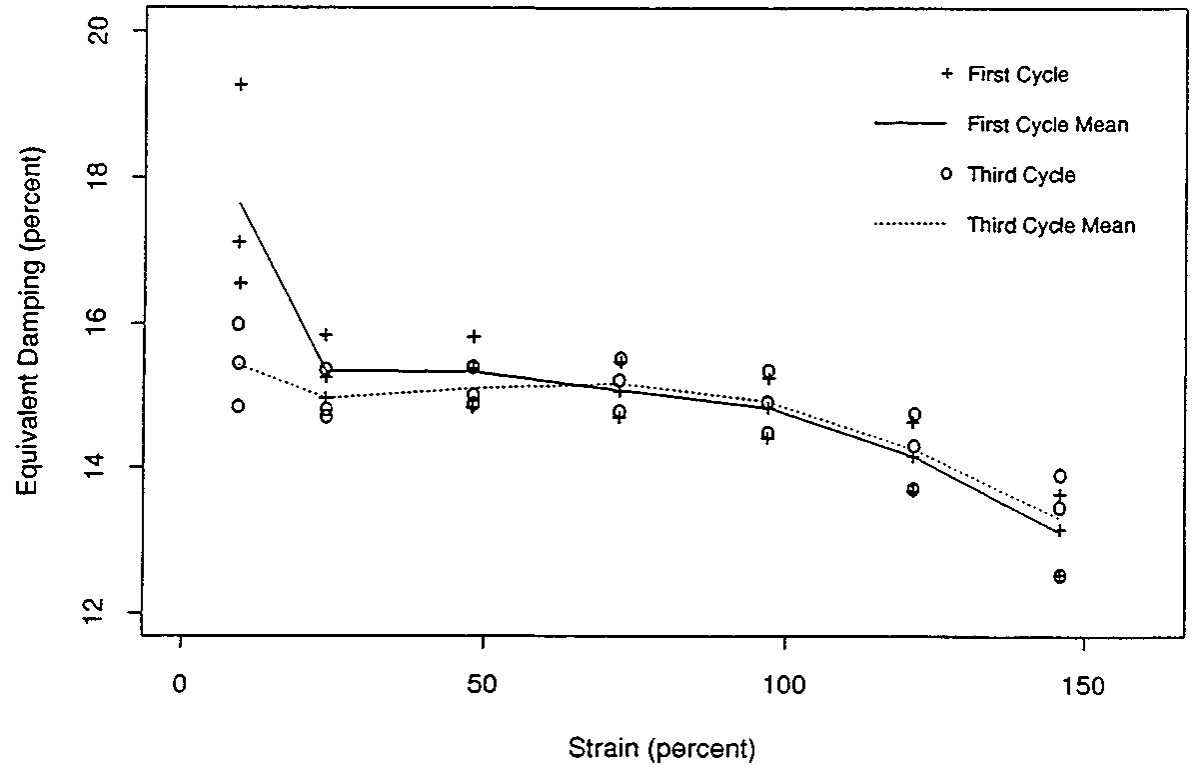

Figure 12: Results from Characteristic Tests of Bridgestone PS0125/1 Bearings.

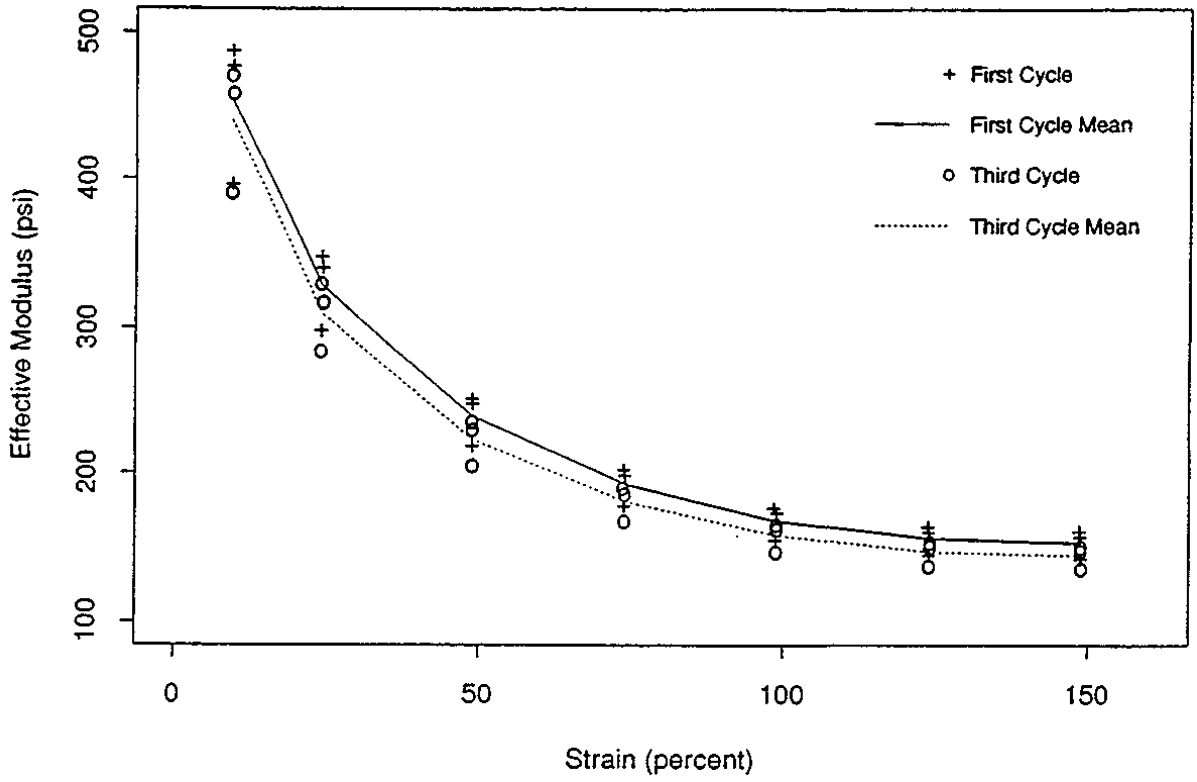

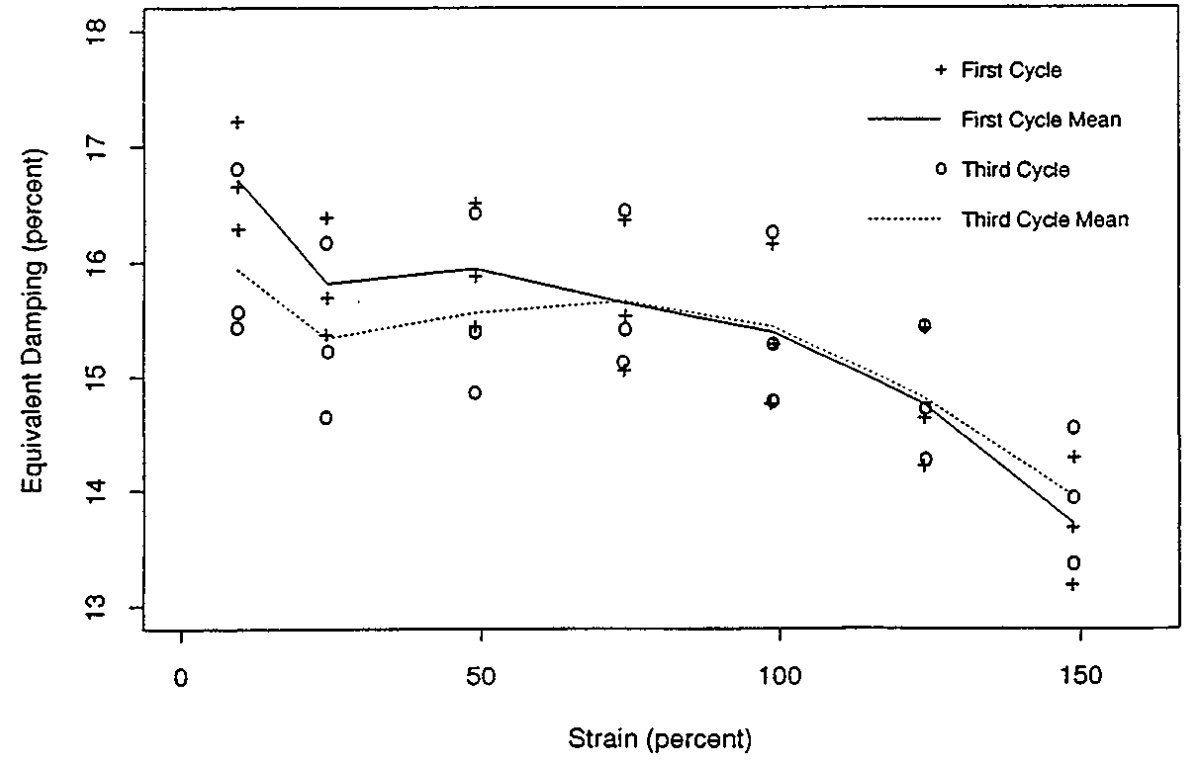

Figure 13: Results from Characteristic Tests of Bridgestone PS0125/2 Bearings.

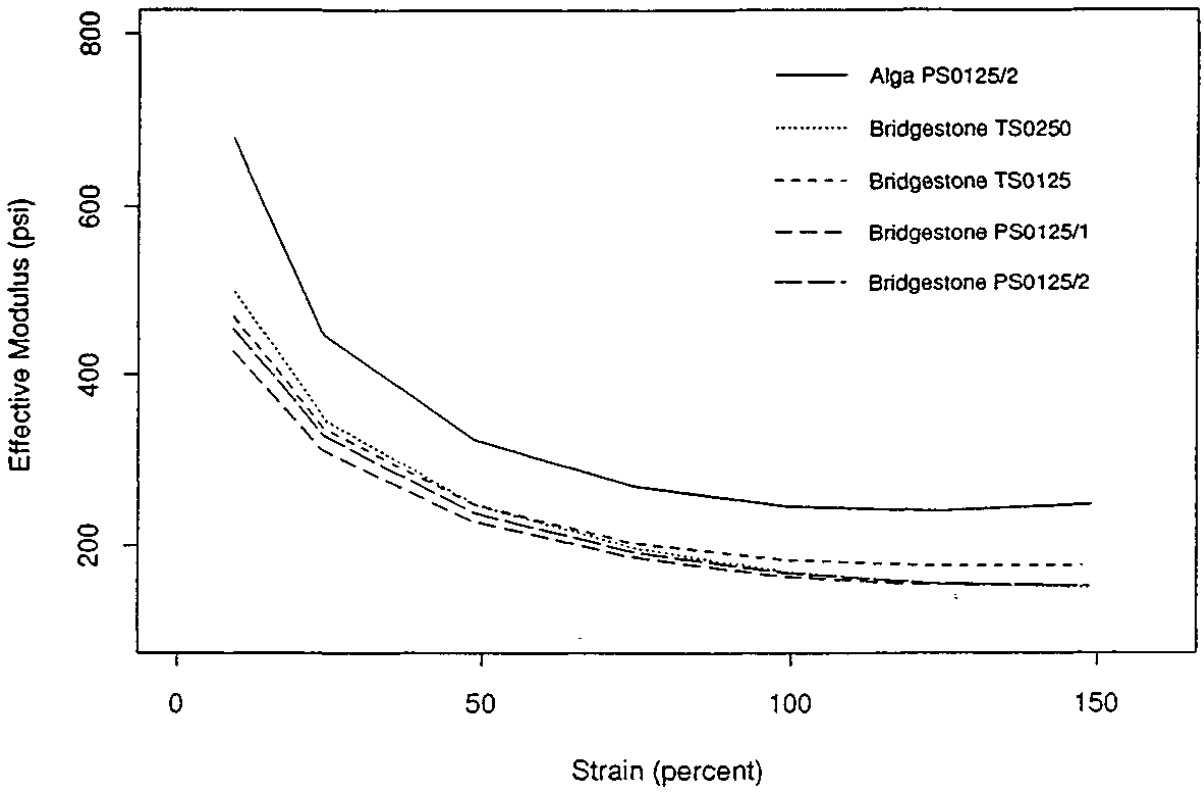

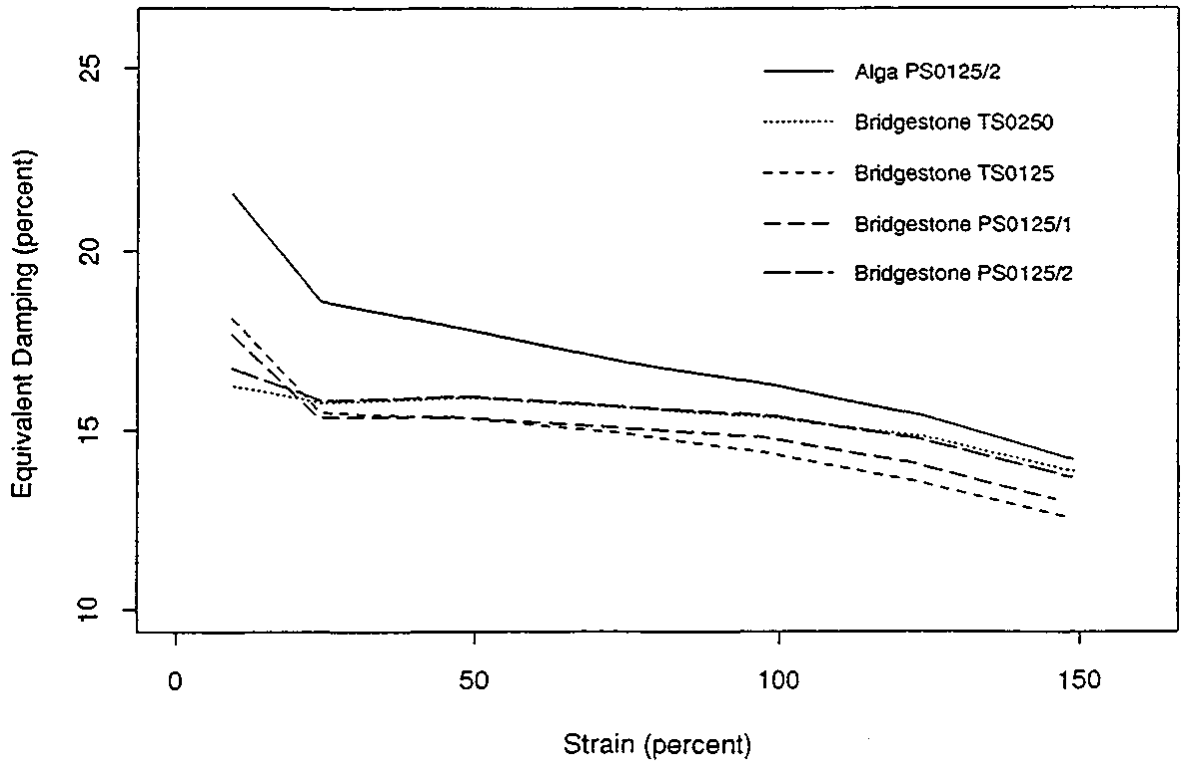

Figure 14: Comparison of First-Cycle Stiffness and Damping — All Bearing Types.

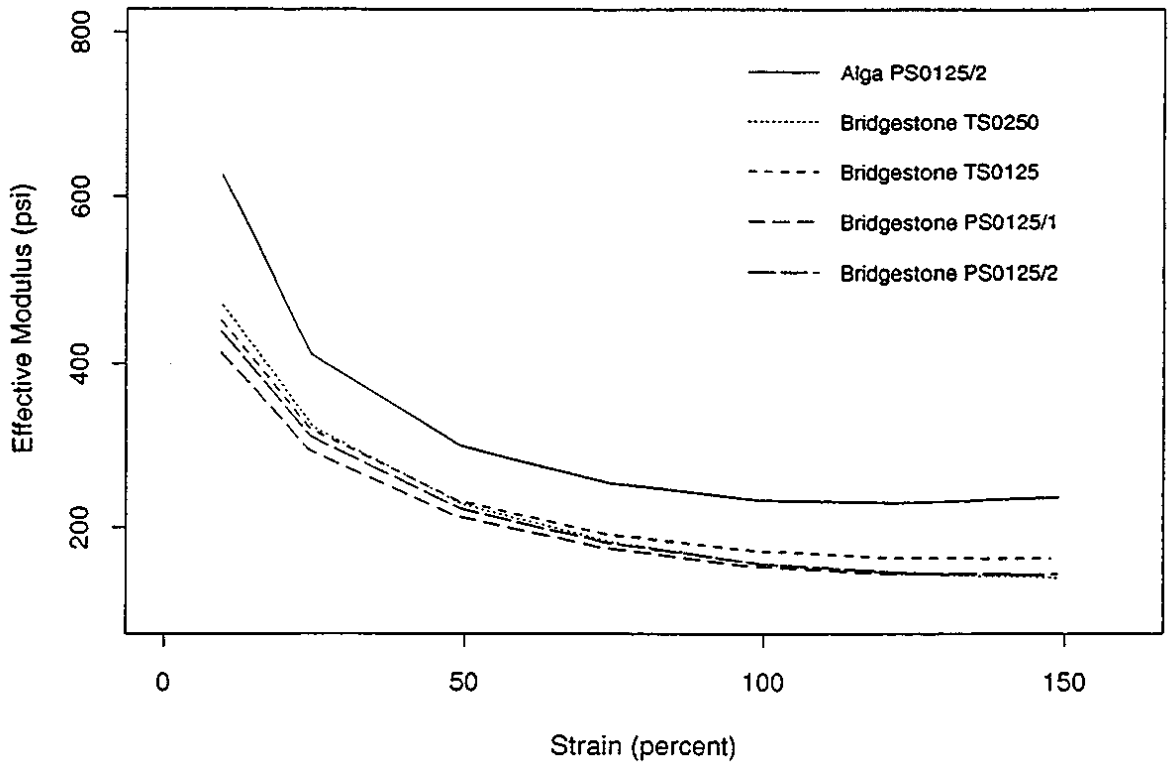

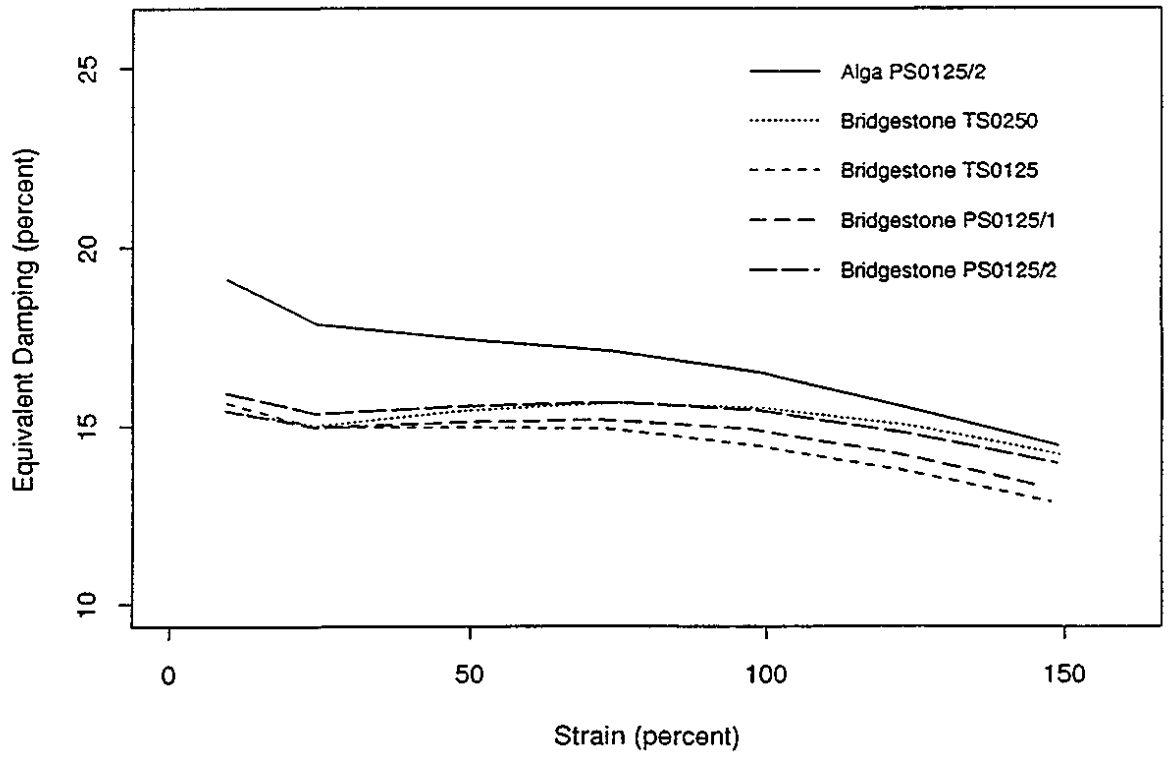

Figure 15: Comparison of Third-Cycle Stiffness and Damping — All Bearing Types.

A direct comparison of the stress-strain behavior of the two compounds is provided in Figures 16 and 17. These plots show the first and third cycles from characteristic tests of PSO125/2 bearings at 0.7 Hz and an axial pressure of 370 psi, and these particular characteristic tests were the first time the bearings had been tested at EERC after having been tested to 200 per cent shear strain by the manufacturers. Because filled rubber compounds which have been previously scragged can regain stiffness if they are undisturbed over a period of time, the first cycle of these tests should be somewhat stiffer than subsequent cycles. However, while this is true for the Bridgestone bearing, there is very little difference between the first-cycle and third-cycle behavior of the ALGA bearing. This implies that the ALGA compound is more stable over time and may not substantially increase in stiffness if left undisturbed. Future tests are planned on these bearings to more clearly establish this preliminary observation.

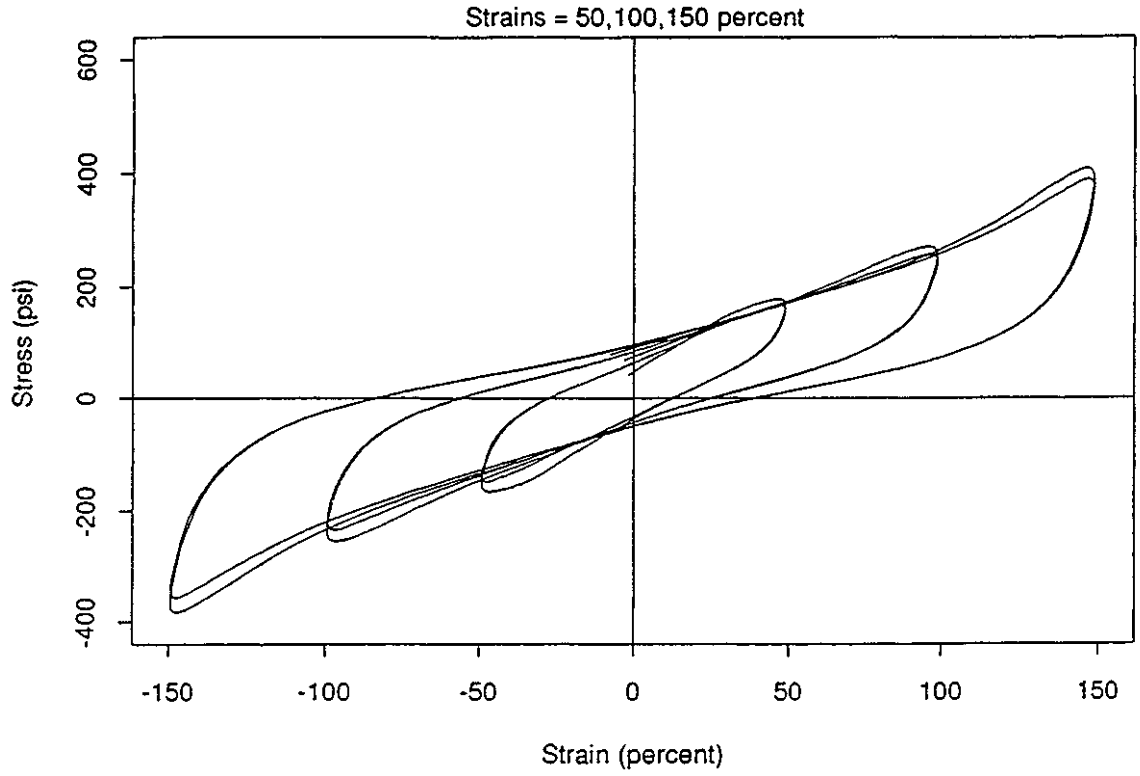

Figure 16: Characteristic Hysteretic Behavior of ALGA PS0125/2 Bearinq.

Virgin Loading

Figure 18 shows the first test of one bearing of each compound to a shear strain of 200 per cent. Each of these tests was preceded by only one test to 10 per cent shear strain, so this essentially represents the virgin force-displacement behavior of these bearings. As expected, both isolators exhibit a significant drop in shear force at maximum displacement from the first cycle to the third, and the ALGA bearing again shows a higher stiffness. However, it is interesting to note that the Bridgestone bearing actually has a higher stiffness than the ALGA bearing along the initial loading curve (but not the reversed loading curve) before a strain of about 150 per cent. While this data is not directly applicable in the context of the design requirements and specification for the ALMR bearings, it is useful to have as a baseline for future tests of these bearings in which their long-term stiffness characteristics are evaluated.

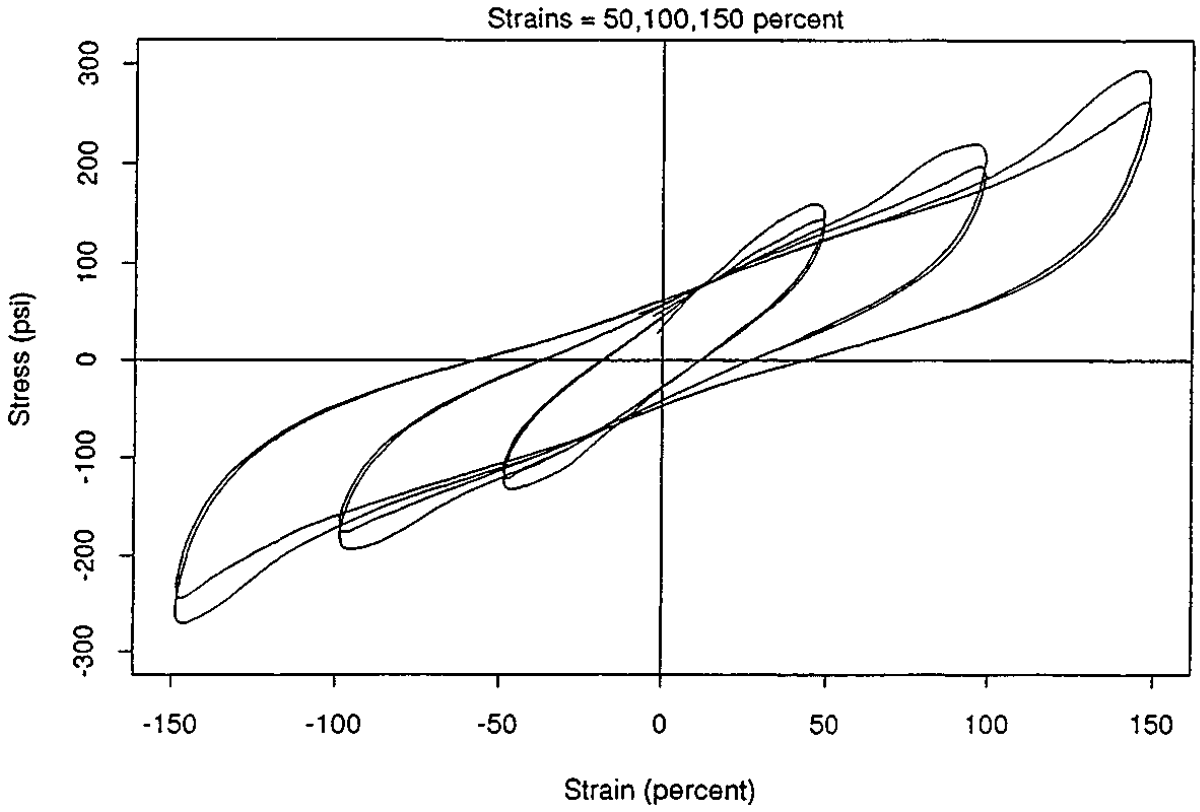

Figure 17: Characteristic Hysteretic Behavior of Bridgestone PS0125/2 Bearing.

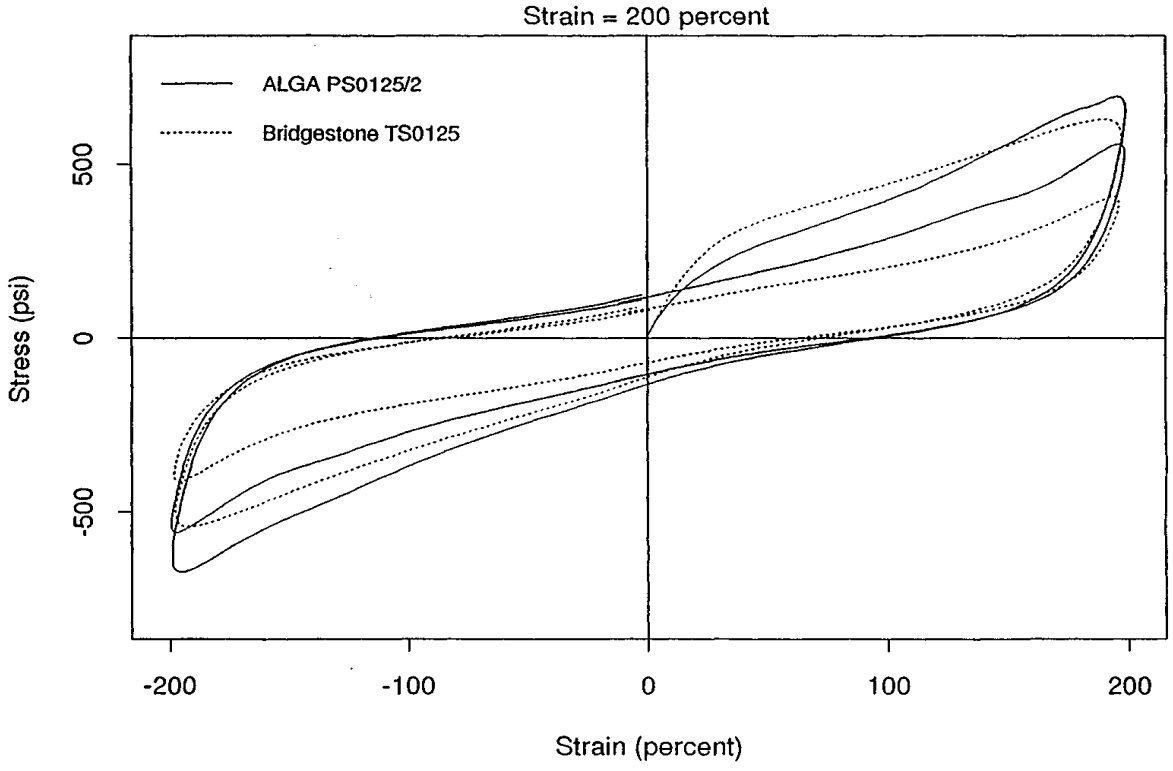

Figure 18: Comparison of Virgin Behavior.

Rate Effects

Because high damping rubber exhibits some viscous behavior, it is to be expected that both the stiffness and damping of the bearings evaluated here will show some dependence on loading frequency. In general an increase in the rate of loading will lead to an increase in both the effective modulus and the equivalent viscous damping. Figure 19 illustrates these effects on the third-cycle properties of an ALGA bearing, while Figure 20 shows these effects for a Bridgestone TS0250 bearing. Note that the 5 in./min. and 10 in./min. tests are constant velocity (sawtooth) tests while the other tests are sinusoidal. The modulus of the ALGA bearing increases slightly with frequency, but the damping is significantly affected. However, it still remains well above 12 per cent at 100 per cent shear strain and a loading rate of 10 in./min. In contrast, the modulus of the Bridgestone bearing shows somewhat more variation due to change in loading frequency, but even more significant is the reduction in damping in the 5 in./min. and 10 in./min.; the damping drops below the specified value of 12 per cent, implying that the Bridgestone bearing would not meet the specification if it was subjected to a slow, constant velocity test.

Axial Load/Load History Effects

While Figures 21 and 22 are intended to illustrate the influence of axial pressure on the third-cycle properties of a Bridgestone TS0125 bearing, the conclusion which can be drawn from them is related more to load history than to axial pressure. Figure 21 shows the results from a VA1 sequence whereby a single sweep over shear strains from 10 to 150 per cent is made and then repeated for a range of axial loads. These results appear to imply that the modulus is greatest under a pressure of 37 psi and least under a pressure of -100 psi (tension), a result which is clearly counter-intuitive. The result for the damping is more in line with what would be anticipated — an increase as the pressure is increased. When these results are compared with those shown in Figure 22 from a VA2 sequence (cycling over a range of axial pressures at a single shear strain, and then incrementally increasing the strain and repeating the axial pressure sweep) the modulus is nearly constant with pressure. In fact, while it appears that there is a reduction in modulus as the pressure goes from 370 to 37 to 925 to -100 psi, this is due to repeated cycling at a constant strain — the sequence of applied pressures at each strain was 370, 37,925, -100. These results have significant implications for the interpretation of tests and the need for consideration of load history in developing test programs.

Vertical Tests

Hysteresis loops derived from vertical tests of each of the bearing types are presented in Part 6 of this report. There was substantial difficulty in obtaining reliable measurements of the vertical response of the reduced-scale bearings, and the results are not analyzed in detail here. This was because the very high modulus of the compound used in these bearings leads to very small displacements, on the order of the resolution of the instruments being used to measure the vertical bearing displacements. Also, because the displacements are small, any warping of the connecting plates in the test machine will contaminate the recordings, and in many cases it was difficult to determine if the displacement traces recorded by the vertical DCDTs were real or an artifact of the elastic deformation of the testing machine. Finally, adding to this problem is the fact that the reduced-scale isolators naturally deflect less, magnifying the resolution difficulties. It is hoped that in the future additional resources can be devoted to a more detailed analysis of the vertical tests to extract the necessary response data, but in this initial evaluation it is difficult to accurately determine the bearing behavior in the vertical tests.

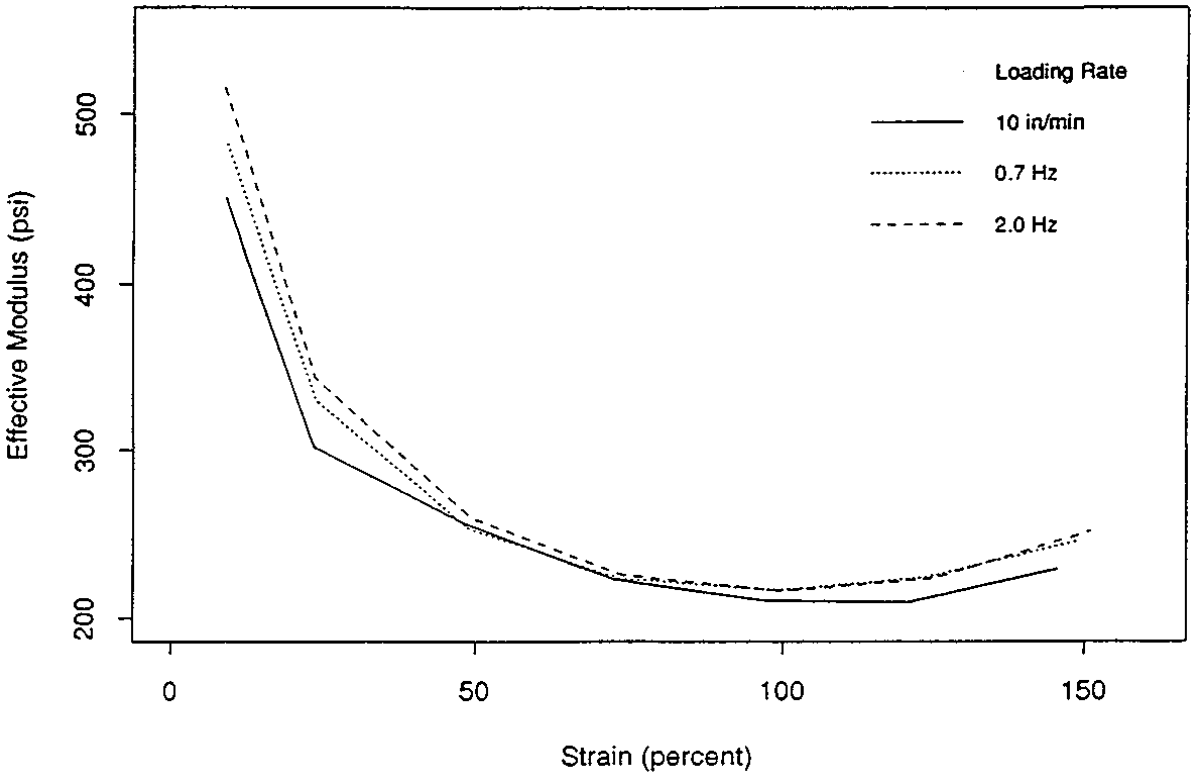

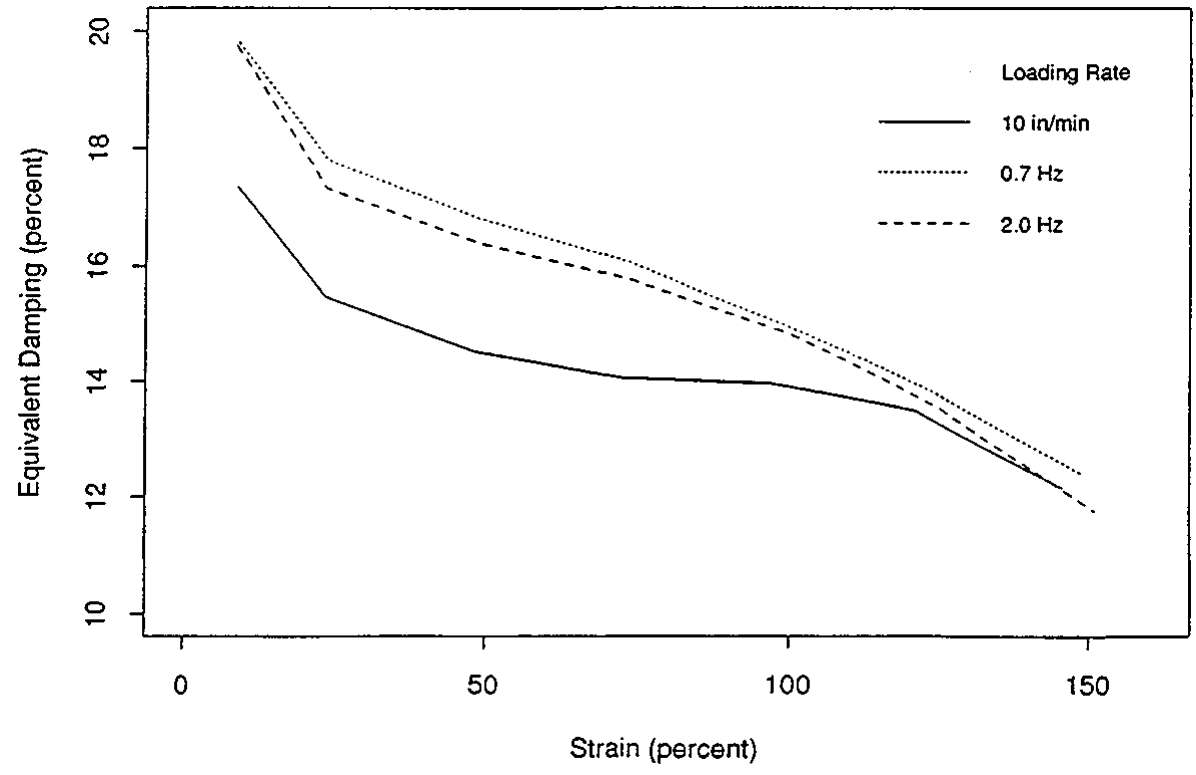

Figure 19: Change in Stiffness and Damping Due to Loading Rate — ALGA.

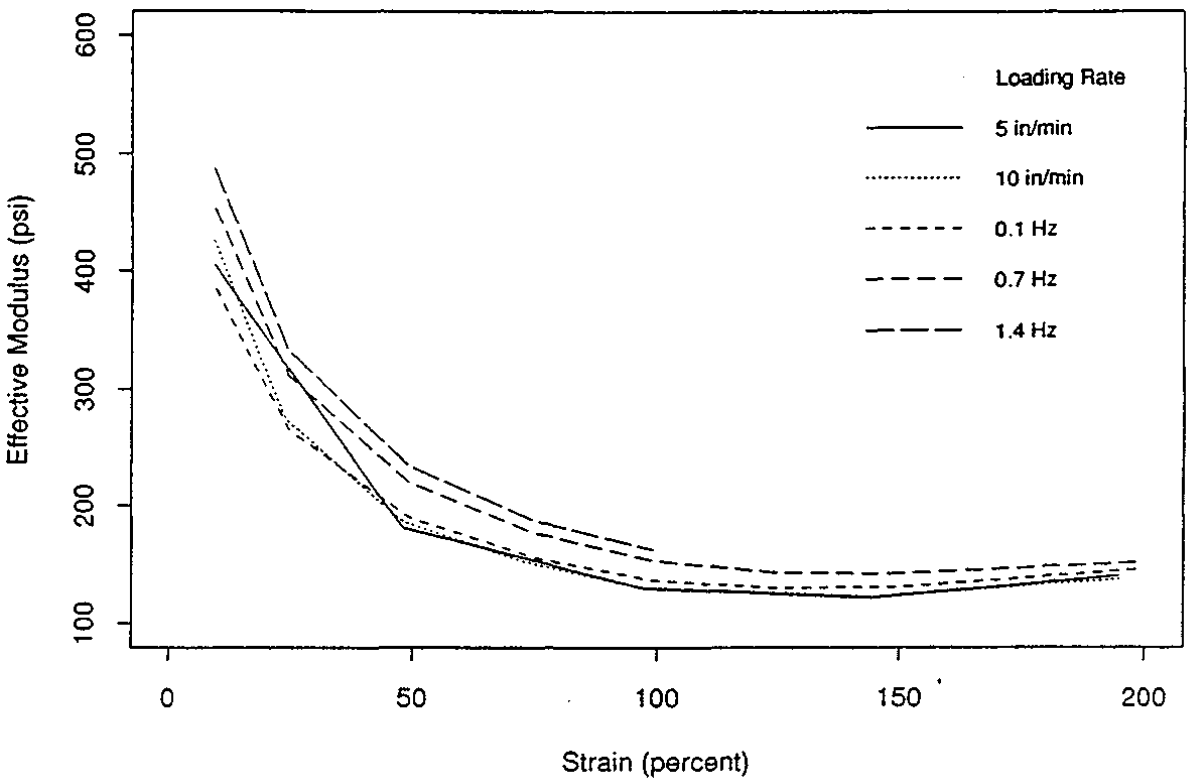

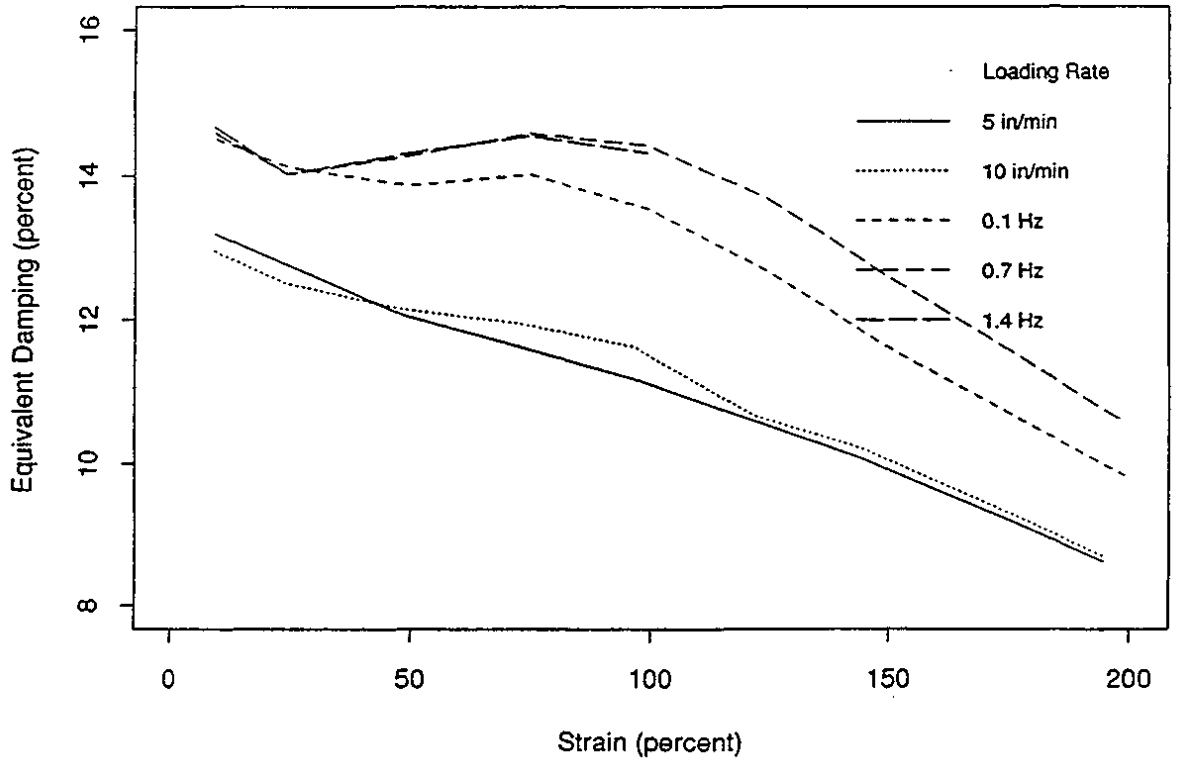

Figure 20: Change In Stiffness and Damping Due to Loading Rate — Bridgestone.

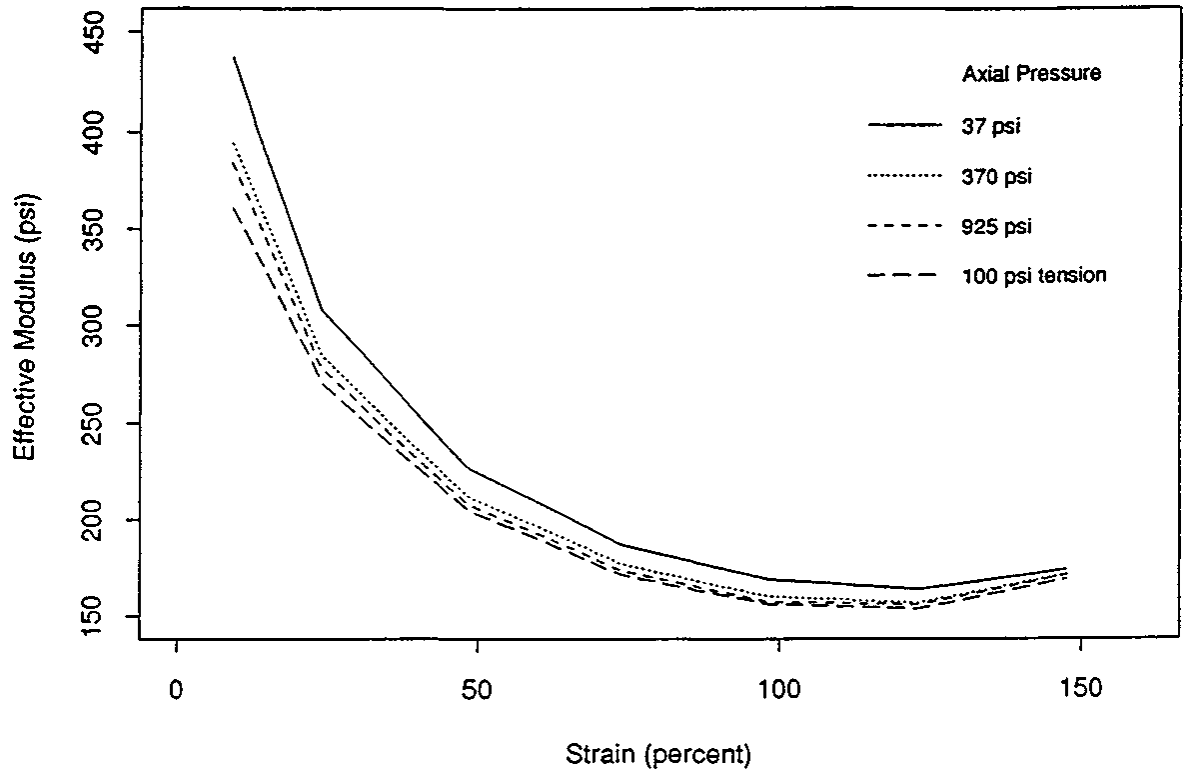

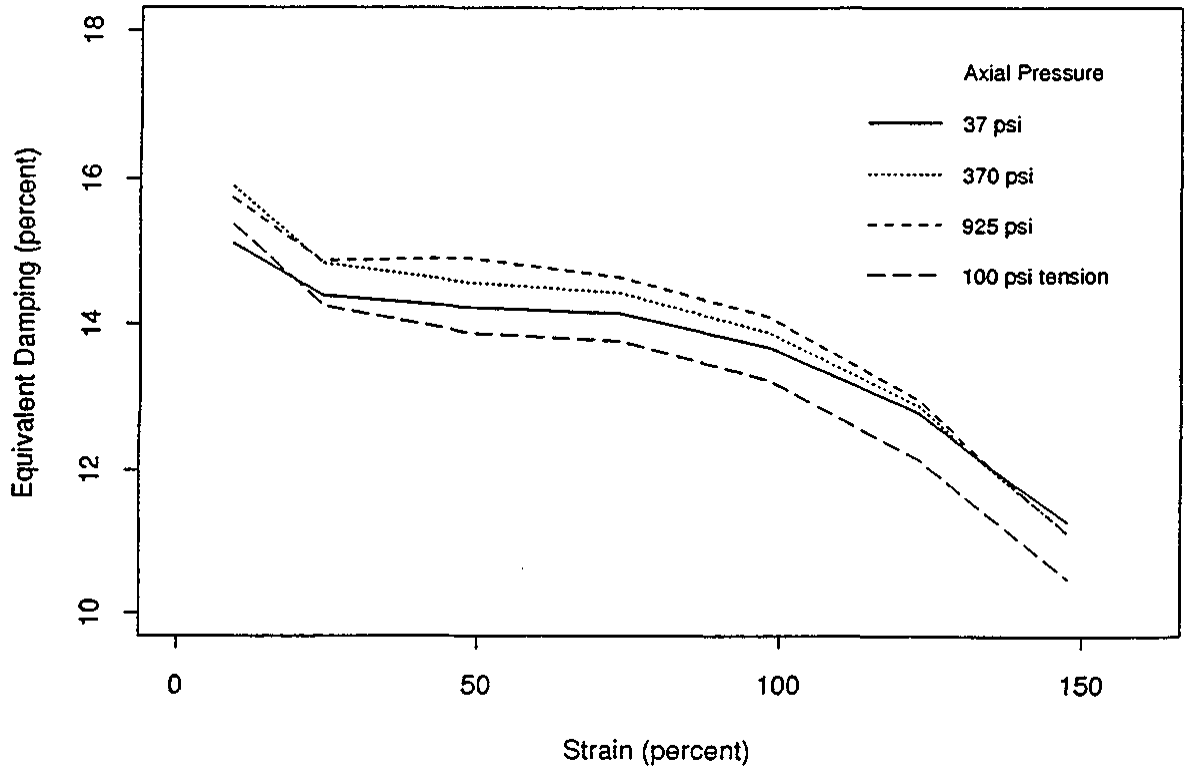

Figure 21: Dependence on Axial Pressure, VA1 Sequence — Bridgestone.

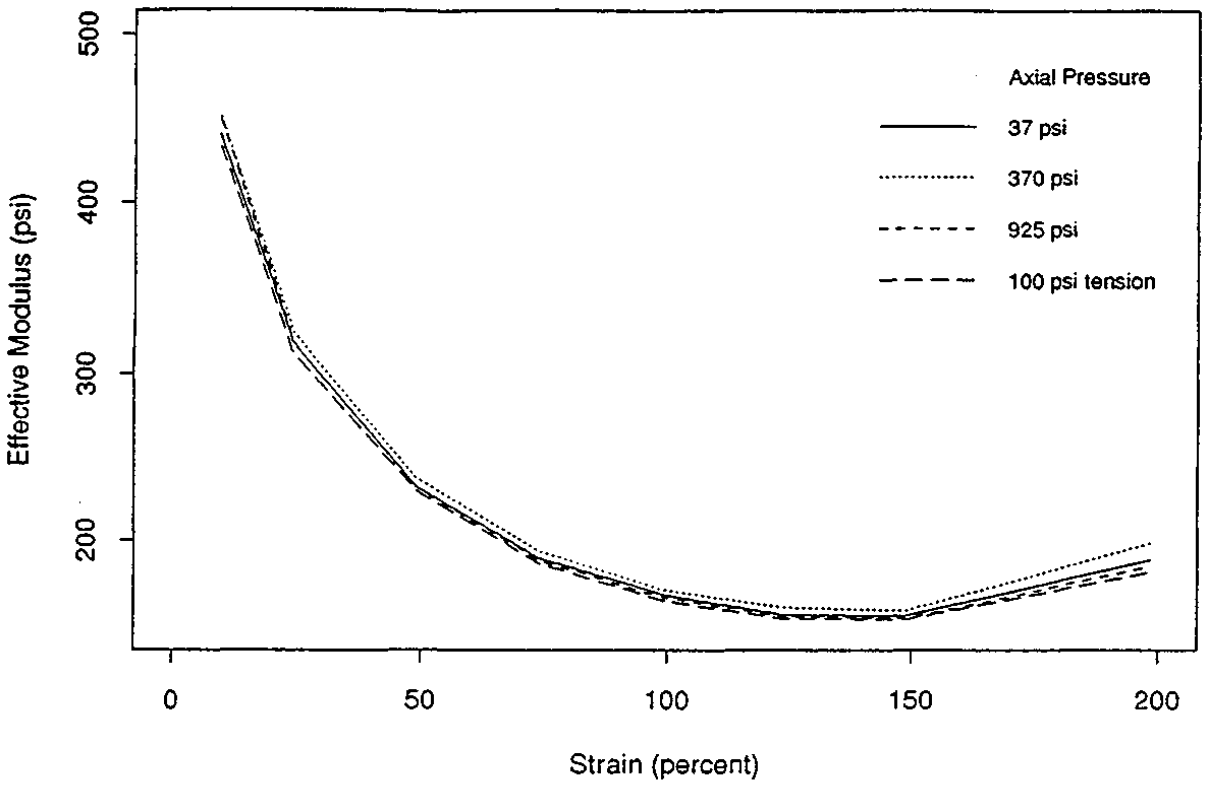

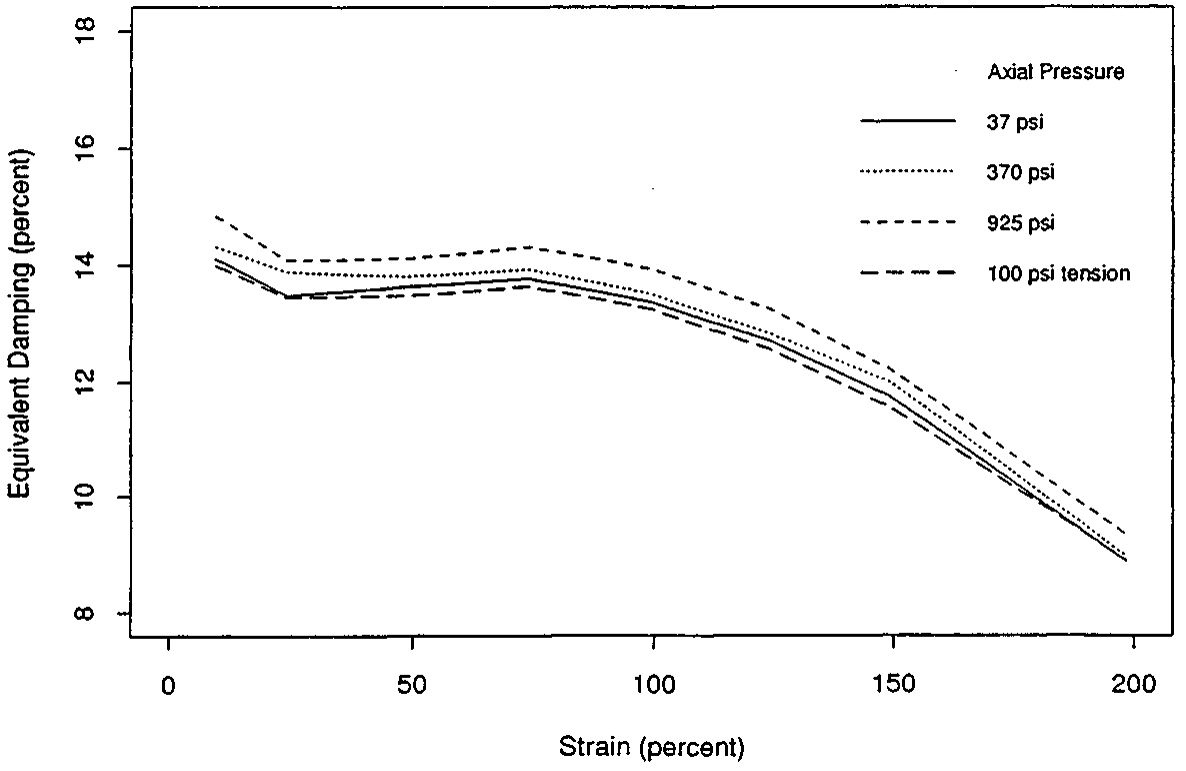

Figure 22: Dependence on Axial Pressure, VA2 Sequence — Bridgestone.

TABLE 3: CHARACTERISTICS OF FAILURE TESTS

Filename	Bearing	Number	Signal	Axial Load (kips)	Peak Strain (%)	Peak Stress (psi)	Comments
940912.22	ALGA	4	sfail	9.61	352	1296	The bottom plates slipped approximately 0.35" corresponding to 25% shear strain in the bearing
940915.01	ALGA	5	fastfail	24	328	1391	Failure test at high speed
940919.19	ALGA	6	sfail	24	305	1358	Some evidence of plate slip apparent
940921.03	ALGA	7	sfail	-2.6	317	1405	Measured plate slip of about 0.19" in this test
941115.01	Bridgestone	TS0250-2	sfail	39.05	285	650	Bearing didn't fail due to force limitations of the test machine
941209.04	Bridgestone	PS01 25/2-1	sfail	9.61	402	1106	
941209.26	Bridgestone	PS0125/2-2	fastfail	9.61	366	1003	
941214.04	Bridgestone	PS01 25/1-1	sfail	9.61	374	1009	
941219.04	Bridgestone	TS0125-2	sfail	9.61	343	849	Some plate slip in this test
941219.22	Bridgestone	TS0125-3	fastfail	9.61	344	1002	Some plate slip was apparent in this test
941222.05	Bridgestone	TS0125-5	sfail	-2.6	323	774	

Failure Tests

The results of numerous failure tests are provided in Parts 2-5 of this report, so detailed evaluations are not included here. Table 3 provides a summary of the observed failure data indicating that all of the bearings endured shear strains in excess of the specified 300 per cent before failing. There was no discernable trend based on applied axial load, but the limited dataset makes such evaluations difficult. In general the ALGA bearings exhibited substantially higher shear stresses at failure than did the Bridgestone bearings, although the Bridgestone bearings endured larger shear strains. These tests indicate that reduced-scale bearings from either of these manufacturers have sufficient margin above the design shear strain as required in the specification.

8. SUMMARY AND CONCLUSIONS

This report has summarized a series of tests of reduced-scale seismic isolation bearings undertaken in support of the development of a seismic isolation concept for the Advanced Liquid Metal Reactor (ALMR). A procurement specification applicable to both full-size and reduced-scale bearings was developed by the program participants and then used to purchase bearings of four different designs from two manufacturers. The high-damping rubber isolators were subjected to horizontal, vertical, and failure tests designed to quantify their mechanical properties both within the range of design loads and displacements as well as to establish their margins before failure. The test results showed that bearings from both manufacturers provided relatively stable and repeatable behavior with minor variations in stiffness and damping as a function of loading frequency and load history. In fact, much of the variation in observed behavior can be attributed to load history. None of the bearings showed substantial variation in properties due to changes in applied axial load. Both types of bearings exhibited damping characteristics significantly in excess of that required by the specification. However, the mean values of the effective moduli of the two bearing types, independent of bearing design, were outside of the specification — the ALGA bearings were slightly too stiff while the Bridges tone bearings were slightly too soft. It is likely that with minor changes to the compounds these results could be brought into specification. All of the bearings exhibited exceptional behavior under beyond-design level loading with displacement margins of greater than 3 and force margins greater than 4. This test program provides a thorough data-set for further analytical and experimental validations of the seismic isolation concept for the ALMR.

ACKNOWLEDGEMENTS

The work described in this report was performed with funding from the United States Department of Energy and administered by the Westinghouse Hanford Corporation (WHC), Han-ford, Washington. Dr. Peter Shen and Dr. Ronald Baker of WHC are gratefully acknowledged for this support. Additional technical and financial assistance was provided by Dr. Emil Gluekler of the General Electric Corporation, San Jose, California. This ongoing support and encouragement is appreciated. The authors would also like to express their thanks to the laboratory staff at the Earthquake Engineering Research Center, particularly Mr. Wesley Neighbor, for their assistance in carrying out the test program.

REFERENCES

Jolivet, J., and Richli, M.H., "Aseismic Foundation System for Nuclear Power Stations," in *Proceedings ofSMiRT-4,* Paper K-9/2, San Francisco, California, 1977.

Tajirian, F.F., "Seismic Isolation of Critical Components and Tanks," in *Proceedings ofATC-17-1, Seminar on Seismic Isolation, Energy Dissipation, and Active Control,* Applied Technology Council, Applied Technology Council, San Francisco, California, March 11-12, 1993.

Kelly, J.M., "State-of-the-Art and State-of-the-Practice in Base Isolation," in *Proceedings ofATC-17-1, Seminar on Seismic Isolation, Energy Dissipation, and Active Control,* Applied Technology Council, Applied Technology Council, San Francisco, California, March 11-12, 1993.

International Conference of Building Officials, *Uniform Building Code,* Whittier, California, 1991.

CONTRIBUTION OF THE JRC ISPRA TO THE INTERCOMPARISON OF ANALYSIS METHODS FOR SEISMICALLY ISOLATED NUCLEAR STRUCTURES

G. MAGONETTE, V. RENDA
European Commission Joint Research Centre Elsa Laboratory,
Ispra, Italy

Abstract

Aim of the work done at JRC has been essentially to investigate the potentiality of the Pseudo-Dynamic (PsD) method to test structures incorporating anti-seismic protection devices based on materials with a strain-rate dependent behaviour. This is of relevant importance due to the interest to perform tests on large-scale mock-ups to assess the behaviour of realistic structure of civil engineering interest. Two specific typologies of protection have been analysed and tested at the European Laboratory for Structural Assessment (ELSA) of JRC Ispra. The first dealing with base isolation and the second with energy dissipation devices. In both cases the protection devices were based on high damping rubber material which is characterised by a moderate dependence from the strain rate of the application of the displacements. To validate a standard procedure to test base isolated structures by the PsD method, a collaboration was set up with the Italian Working Group on Seismic Isolation which includes the national research centre ENEA, the national electricity board ENEL, the industrial research centre ISMES and a manufacturer of isolators ALGA. In the framework of this collaboration it was decided to test at the ELSA laboratory a scaled 5-storey frame structure (provided by ENEL), isolated by means of high damping rubber bearings (HDRBs), which had been tested on the shaking table of ISMES. This experimental activity aimed to compare the results which can be obtained by means of the PsD testing technique with those which can be obtained by means of a truly-dynamic test on a shaking table. To validate a standard procedure to test structures incorporating energy dissipation devices, an international collaboration has been set up with Industries, Research Centres and Universities in the framework of a project partially funded by the European Commission through the General Directorate for Science and Technology. The obtained results show once more that the PsD method, when properly applied, may reliably be used to test structures protected by devices based on high damping rubber. This has been shown effective both in the case of base isolation and energy dissipation devices by using a specific procedure for the improvement of the PsD method.

1 INTRODUCTION

The European Laboratory for Structural Assessment (ELSA) of the Joint Research Centre (JRC) is specially fitted out with up-to-date means for carrying out Pseudo-dynamic (PsD) tests to reproduce the behaviour of large scale structures subjected to earthquake loading.

The ELSA laboratory is at present engaged in international consortia to develop, optimise and test innovative anti-seismic devices based on passive vibration control. To this end, a collaboration was set up with the Italian Working Group on Seismic Isolation (Gruppo di Lavoro sull'Isolamento Sismico GLIS) which contributed to the present work [1, 2]. In the framework of this collaboration it was decided to test at the ELSA laboratory a scaled 5-storey frame structure (provided by ENEL), isolated by means of high damping rubber bearings (HDRBs), which had been tested on the shaking table of ISMES.

PsD testing is, by virtue of the expanded time scale of the tests with respect to real seismic events, normally restricted to materials assumed to behave in a rate-independent

manner. As regards to seismic isolation by rubber bearings, although the strain rate effect cannot be taken into account at the experimental stage, it can be taken into account in the numerical part of the method. A standard procedure for the PsD testing of large-scale models of base-isolated structures has been developed and validated at the ELSA laboratory.

The experimental activity described in this paper aims to compare the results which can be obtained by means of the PsD testing technique with those which can be obtained by means of a truly-dynamic test on a shaking table.

The PsD test procedure includes the following steps:

- Characterisation of the isolators for different frequencies to evaluate the stiffening effect due to the strain rate and the corresponding correction that must be applied to the shear force.
- Comparison between a dynamic snap-back and a PsD snap-back.
- PsD tests for seismic inputs and comparison with shaking table results.

2 PRINCIPLES OF SEISMIC ISOLATION

In the last years an important effort has been done to introduce new seismic protection techniques, some of which are now included in design standards for seismic areas.

Traditional earthquake design methodologies use high strength or high ductility concepts to mitigate damage from seismic effects. An alternative approach consists in isolating the structure base from the ground by means of flexible devices, called isolators, placed between the superstructure and its foundation [3]. A base-isolated system is characterised by a very low frequency, such that during a strong earthquake, the superstructure moves like a rigid body over its isolation system. Deformations and energy dissipation are mostly concentrated in the isolators. A seismic isolator must be rigid in the vertical direction (to support the dead load of the superstructure), flexible in the horizontal plane (to allow for large relative displacements between the superstructure and the ground) and possibly, it must be able to dissipate a significant amount of energy.

From the various devices proposed for seismic isolators, the laminated elastomeric bearing is emerging as the preferred device for large buildings/structures, such as nuclear reactors plants. A great number of experimental and numerical studies have already been performed for all kinds of rubber bearings and several applications to bridges, buildings and industrial plants already exist in many countries. HDRBs are formed by two end plates and several relatively thin inner steel plates embedded in a high damping rubber matrix, to which they are connected through bonding. These isolators can sustain large vertical loads with small deformations due to confining effect of the inner steel plate and are characterised by a low horizontal stiffness when subjected to horizontal loads, which allows for large transverse deformations in severe earthquakes. In these bearings, high damping is obtained by mixing the rubber with suitable additives (carbon, oils and resins); this allows combining in a single element both the frequency filtering and energy dissipation capacities necessary to achieve an effective isolation action. The HDRBs behaviour is mostly characterised by the rubber mechanical properties, which are highly non-linear, both in terms of stiffness and damping. As a matter of fact, the ‘width’ of the experimental hysteresis loop, that determines the amount of damping, increases with the shear strain. The horizontal force-displacement envelope is described by an initially high stiffness that decreases to a nearly constant stiffness in the range

between 50% and 150% shear strain; finally, the stiffness increases up to isolator severe damage, which can occur even over 400% shear strain [4].

3 ISOLATION DEVICES

3.1 Specimen Rubber Bearings

The HDRBs used in this test campaign were fabricated with a soft compound (G = 0.4 MPa), attached to the structure with bolts and a dowel system, and provided an isolation frequency (about 1 Hz) in the range of interest for seismic isolation. These isolators have a diameter of 125 mm and are made of 12 rubber layers with a thickness of 2.5 mm (30 mm of total rubber height and a shape factor S equal to 12), and 11 steel layers of 1 mm alternating between the rubber layers. A 10 mm thick steel plate is used at each end of the bearing for mounting to flange plates of 15 mm which, in turn, are attached to the base and the superstructure [5]. Consequently, the total height of each isolator was 91 mm. They were designed for a working shear strain of 100% (30 mm of horizontal displacement) and a nominal load of 50 kN. Six of these isolators were made available to ELSA for this test campaign.

3.2 Characterisation tests and Strain Rate Effect Compensation

For elastomeric bearings, a decrease in the testing speed of two or three orders of magnitude, as is usual for PsD tests [7], may introduce considerable changes in the stress-strain behaviour, especially for filled rubber bearings [8]. As reported before, these changes may be described as a proportional force reduction.

Because high damping rubber exhibits some viscous behaviour, it is to be expected that both the stiffness and damping of the bearings evaluated here will show some dependence on loading frequency. In general an increase in the rate of loading will lead to an increase in both the effective modulus and the equivalent viscous damping. In order to analyse the variations in stiffness and damping as a function of the loading frequency, a campaign of characterisation tests was undertaken. Before installing the test structure over the isolator bearings, preliminary tests were performed by using a specific set-up which was able to supply a constant vertical load while simultaneously imposing a specified horizontal displacement history to four rubber bearings. Using a vertical load of 40 kN per isolator, sinusoidal displacement histories with amplitudes decreasing from 200% shear strain (i.e. to a horizontal displacement equal to two time the total rubber height) were imposed at different speeds (Fig. 1).

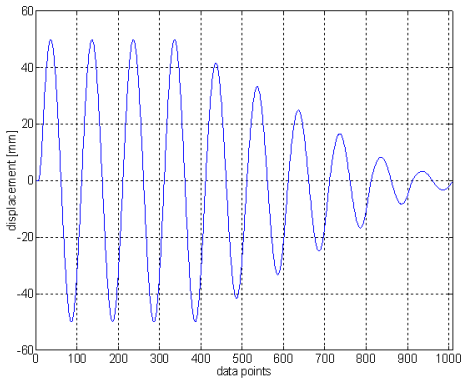

Figure 1: Decreasing amplitude characterization signal.

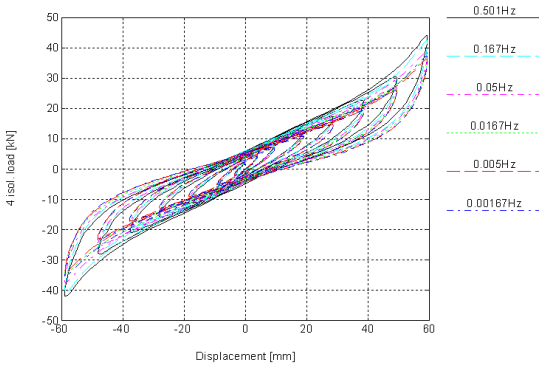

Figure 2: Hysteretic behavior of the HCRBs at different strain rates.

The highest speed corresponded to the application of a sinusoidal displacement with a frequency of 0.5 Hz. In the successive tests this speed was reduced by a factor of 3, 10, 30, 100, and 300 respectively, while practically identical displacements were attained for all the tests thanks to the quality of the digital control system [6]. After disregarding the initial 3 large amplitude cycles, the relationship between the shear force and the shear strain of the four isolators set is represented for different speeds in (Fig. 2.) From this figure, it was found that the shear stiffness tends to increase as the frequency of the cycle increases, while the rubber damping is hysteretic, i.e. practically independent of velocity. It was estimated that for the fast test the required horizontal force was 19% greater than for the slowest test.

(Fig. 3) shows in detail the results of two strain rate tests performed with a speed ratio of 300. The multiplication of the shear force of the lowest speed test by a correction factor of 1.19 has generated corrected force-displacement hysteresis loops which are very close to the loop produced by the fastest test.

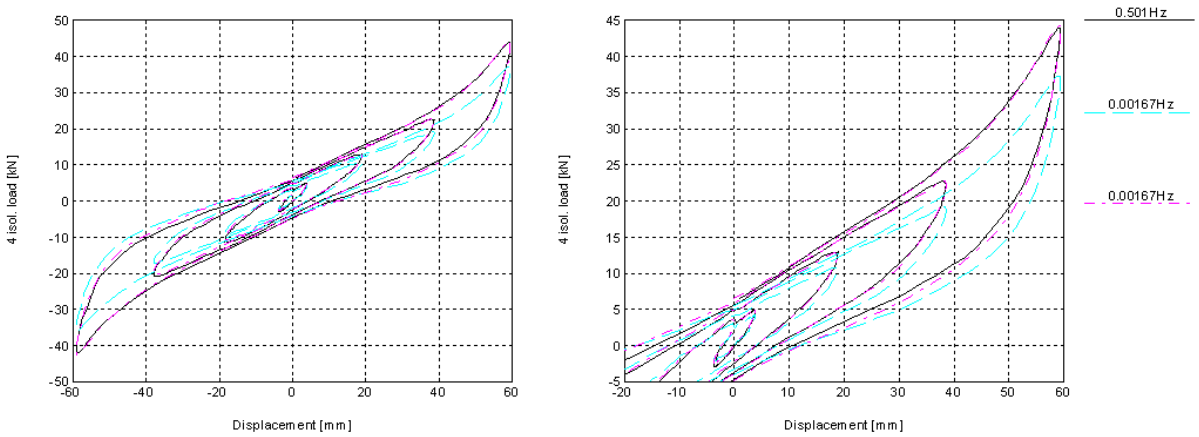

Figure 3: Hysteric behaviour of the isolators: Fast test, slow test and slow corrected test (corr. fact. 1.19).

The hysteretic behaviour showed also that the bearings provided relatively stable and repeatable behaviour with minor variations in damping in function of the loading frequency and loading history, and that the HDRBs can sustain several cycles at very large strains without appreciable change in their dynamic properties (in general, the first load-displacement cycle of a bearing shows higher damping values than the succeeding cycles, and conditions close to steady state are reached after 2 or 3 cycles).

These considerations opened the possibility of using a compensation technique within the PsD tests. In the proposed tests a correction function has been inserted into the PsD algorithm to allow for strain-rate effects in the isolators. That is to say, at every integration step, the measured force should be corrected so as to account for an increase of a specified percentage on the force in the isolators. More details on this compensation technique may be found in [9, 10 and 15].

3.3 Description of the Structure

The mock-up MISS (Model of Isolated Steel Structure) was realised in the framework of a co-operation among European partners, aimed at the optimisation of seismic isolators

[11, 12]. The MISS was subjected to a wide-range experimental campaign of shaking table tests consisting in the application of sinusoidal excitations and natural artificial earthquakes (1D, 2D and 3D) for both the isolated and fixed-base configurations.

The MISS structure is described in detail in the ISMES Test Report [13]. The characteristics of the model that are relevant to the present work are described in the following.

MISS is made of HEM and HEB steel sections of 275 MPa strength. The structure is a four storey, six column tri-dimensional frame, composed of two 2-bay frames in the x direction and of three 1-bay frames in y direction. The centre to centre corner column dimensions in plan are 3.30 m in the x direction and 2.1 m in the y direction; interstorey heights are set at 0.9 m. This structure can support up to 20 concrete masses, each weighting 1300 kg (Fig. 5).

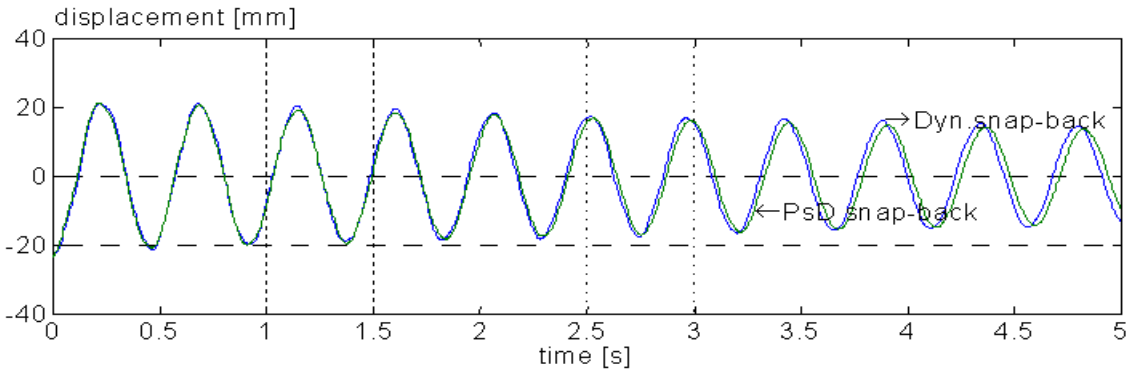

Figure 4: Non –isolated structure: Comparison of displacement time history at 4th floor for the dynamic and PsD snap-back tests.

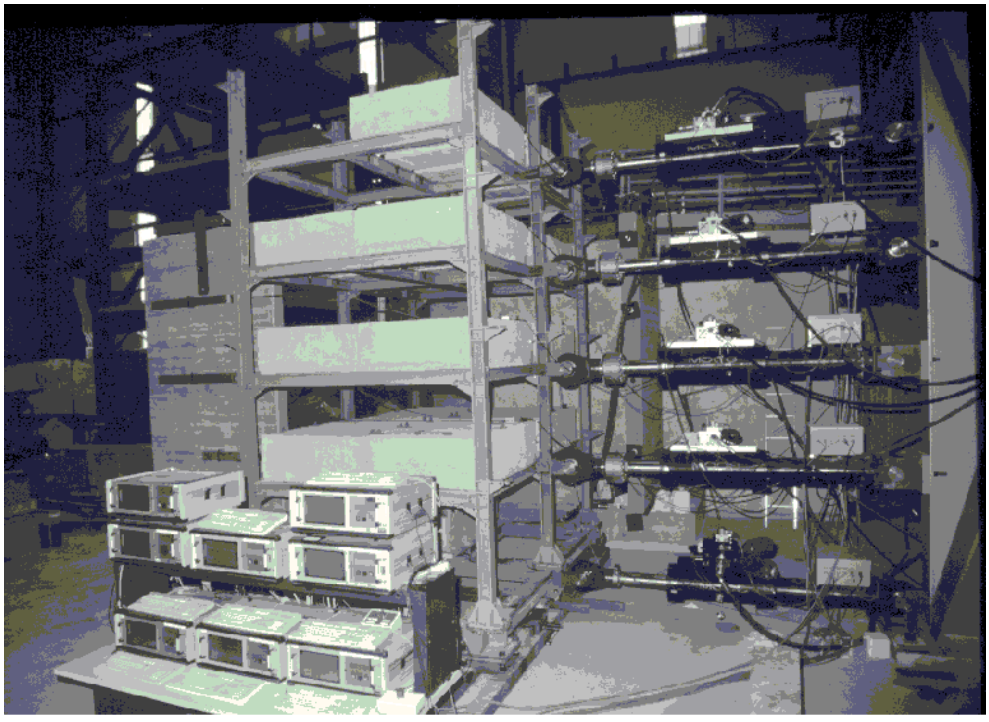

Figure 5: MISS mock-up and PsD apparatus.

The frequencies of the structure can be chosen to vary in quite a large range, depending on the interstorey distance and the number of masses used and their disposition (which can also be asymmetric). The actual isolation system is formed by 6 HDRBs (Fig. 6) described in the previous paragraph, and provides an isolation frequency in the range of interest for seismic isolation (below 1 Hz). Following specifications provided by ISMES, the maximum bending strain allowable at the base of the steel frame resulted to be (800 με); after this limit undesired plastic deformations are expected.

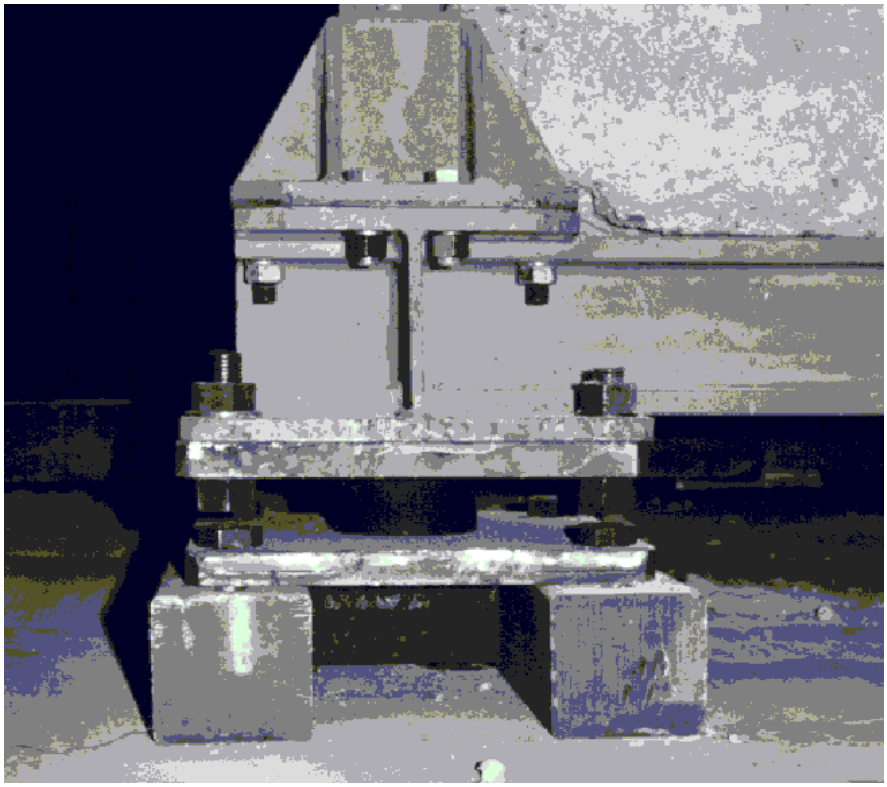

Figure 6: MISS mock-up: rubber bearing detail.

The structure was analysed in two of the four configurations tested at ISMES [13]:

- B9 configuration: non isolated, four masses placed on each one of storeys 1 to 4;
- B19 configuration: base isolated, four masses placed on each one of storeys 1 to 4.

4 CONTINUOUS PsD TECHNIQUE

The conventional PsD test procedure requires a considerable time to complete a test run, because pauses in driving the test machines must be set to adjust the actuators at right positions and to acquire the instrument readings [6]. Moreover, the pauses in driving prevent the smooth movement of the structure. The quality of the PsD tests described in this paper has been improved by applying a technique called continuous PsD testing, which can considerably reduce the test duration and opens the way to more accurate testing of the earthquake response of structures with velocity-dependant devices.

In the conventional PsD test procedure, the actuator motion is stopped when the test specimen reaches the target displacement (hold period) so that the reaction force can be measured and the next target displacement computed. Instead of stopping the actuator, in

continuous PsD testing, the actuators move continuously and the reaction force is measured when the specimen passes the target displacement. Recognising this reaction force as the restoring force at the target displacement, the equations of motion are integrated 'on the fly' (without hold period), the next target displacement is determined and the motion proceeds without any interruption. This has been achieved by incorporating the central difference algorithm (to solve the equation of motion) into the digital controller of the electro-hydraulic system, in place of the displacement target generator.

One significant departure from the conventional PsD system is that in the continuous PsD technique, for each of the **m** g^m discrete values of the ground acceleration read from the acceleration file, a sequence of **n** acceleration values g_n^m is computed by interpolation between g^m and $g^{m\ 1}$ (i.e. $g_0^m(\quad g^m), g_1^m, \ldots g_n^m, \ldots g_{\mathbf{n}\ 1}^m$).

After completion of computation of these **n** intermediate acceleration values, the PsD procedure is computed **n** times at the sampling rate of the controller performing **n** sub-steps in one conventional PsD step.

The basic sequence used in the continuous PsD test system remains the same as that used in the conventional PsD test. That is, at sub-step n of step m, this sequence proceeds as followed:

g_n^m is read and the external load is computed

the restoring force r_n^m is measured.

the equation of motion is solved by direct integration; the displacement is computed and used as target displacement by the control algorithm. The actuators leads the test structure to the target position; wait the end of the controller sampling time (2 ms), and then go to 1).

In the tests considered here, we had typically N=1000, Δt =2 ms, ΔT =5 ms giving λ=500, which means that 1 second of the earthquake takes 500 seconds in the test.

In the PsD sequence described here, the reaction force is measured at the sampling rate of the controller (typically 500 or 1000 Hz). This procedure not only generates a smooth displacement of the structure, but also performs a noise filtering of the load measurements with respect to a classical PsD test in which much less measurements enter in the algorithm. The conjunction of these two improvements has made possible to run tests on the 5 degree of freedom (DoF) structure considered here without having to insert numerical dissipative mechanism in the algorithm. These numerical damping techniques are usually required when using the classical PsD method on structures with many degrees of freedom [7].

Moreover, the results of exploratory tests performed on a large-scale 3-Dof steel structure which is described in [9], have shown that this procedure enabled test speed to be improved by a factor ranging between 10 and 20. Further investigations are currently in progress. This increase of the loading rate will improve the quality of PsD tests especially those conducted on structures with load rate sensitive material.

In the present work, even though the continuous technique was used, the PsD tests were driven at relatively low speed, due to the incompatibility between the size of the actuators (500 kN) and the maximum load requested at each level (20 kN max.). For most of the time, the actuators and load cells were used within 1 or 2% of their actual range. In these conditions, it was not possible to increase the speed of the test without an explosion of the higher modes due to force-measurement errors that result in artificial energy input to those higher modes.

4.1.1 PsD Tests on the non isolated structure

Every seismic PsD campaign is usually preceded by a snap-back test that is performed both dynamically and pseudodynamically. The result of these tests gives valuable data for checking the quality of the whole PsD modelling system.

4.1.1.1 Real-Time Snap-Back Tests

The bottom of the MISS mock-up was fixed to the strong floor of the ELSA. For the snap-back test, the mock-up was pushed by means of a hydraulic jack acting at the centre of the fourth floor. After reaching the desired displacement, the structure was released using a mechanical uncoupling device. This test was repeated by acting on the first floor, to excite more the higher modes. The PsD model consisted of a 4-DoF structure and used the diagonal mass matrix: diag(5140, 5450, 5340, 5460) kg. The applied forces and the displacements were recorded at every floor during the tests.

4.1.1.2 PsD Snap-Back Tests

Four actuators were connected between a strong reaction frame and the centre of each floor of the structure. Each actuator was equipped with a load cell and the displacement was controlled by means of a digital optical displacement transducer fixed to an independent common reference structure [6]. The digital control loop of each actuator also included an additional feedback signal from an accelerometer to improve the stability margin of the control. The dynamic snap-back was repeated pseudodynamically by prescribing as external load the history of load measured during the dynamic test. The integration was made by the Explicit Newmark Method with a time increment of 0.005 s.

The results of the dynamic and PsD snap-back tests of the displacement of the fourth floor are plotted in (Fig. 4). They show a good agreement between the dynamic and the PsD responses as is typical for a linear structure. The small discrepancies are mainly due to the diagonal discrete mass matrix adopted in the PsD tests. The eigen frequencies tabulated in Table 1 confirm the good quality of the PsD snap-back test.

TABLE 1: COMPARISON OF EIGEN FREQUENCIES AND DAMPING RATIOS FOR DYNAMIC SNAP-BACK AND PSD TESTS ON THE NON-ISOLATED STRUCTURE

	Mode 1		Mode 2		Mode 3		Mode 4	
	Hz	Damp.	Hz	Damp.	Hz	Damp.	Hz	Damp.
Dyn. snap-back	2.19	0.7 %	8.38	0.5 %	17.0	1.8 %	23.3	5.4 %
PsD snap-back	2.17	0.8 %	8.00	1.3 %	16.7	1.5 %	23.8	0.9 %

4.2 PsD Seismic Tests

On the shaking table of ISMES, several synthetic and natural base acceleration time-histories had been applied to the MISS mock-up. The Tolmezzo NS –6dB record was selected because it was the only one for which mono-axial responses of the structure in the non-isolated and isolated configurations were available.

The input accelerogram used in the PsD tests is displayed in (Fig. 7). This signal is the registration of the acceleration response of the shaking table during the test of MISS submitted to the Tolmezzo NS –6dB earthquake. It was recorded in the y direction with a sampling time of 10 ms. Fig. 7 also shows the displacement response spectrum of this accelerogram for damping ratios of 1, 6 and 15%. The PsD experiments were performed for the first 12.5 s of the time history.

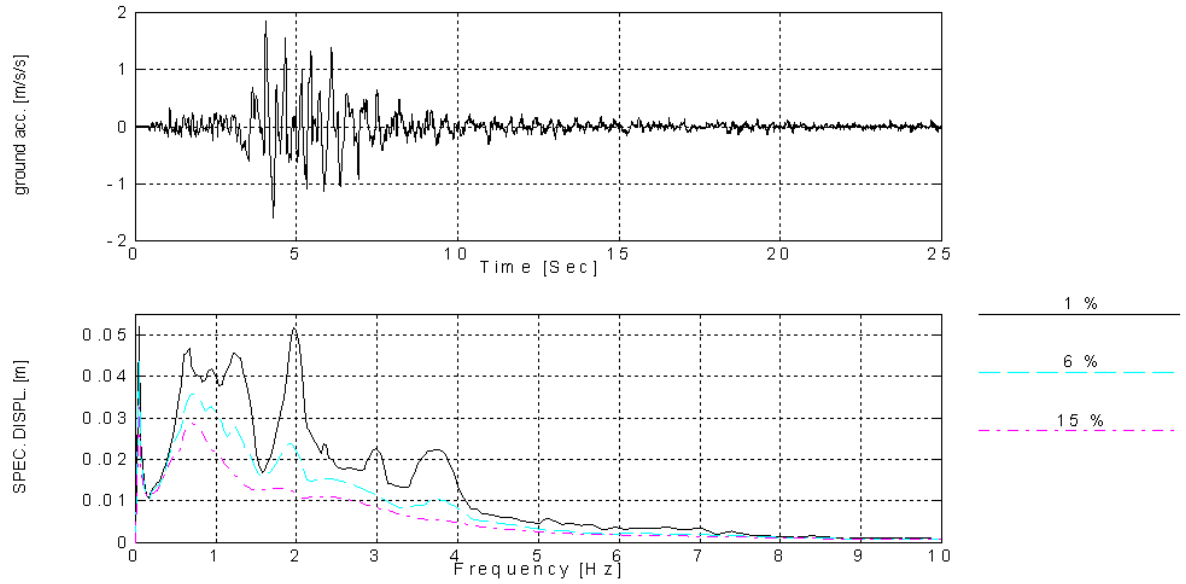

Figure 7: Ground acceleration and associated displacement responses spectrum (for damping ratios 1, 6 and 15%) recorded on the shaking table and corresponding to the Tolomezzo Earthquake – 6db.

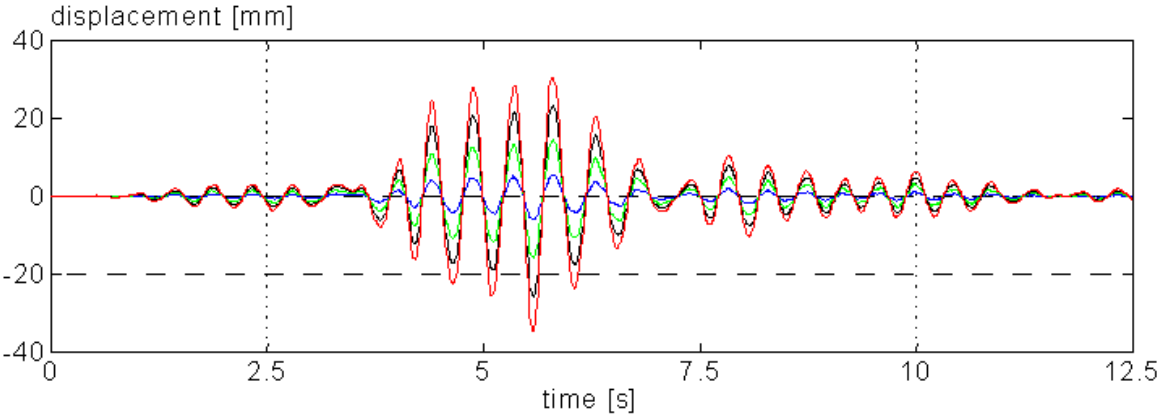

Figure 8: Non-isolated structure seismic PsD test: floor 1,2,3,4 displacements.

(Figs. 8 and 10) illustrate, respectively, the structural displacements of the four floors and the shear loads and inter-storey drifts. Usually, this type of result, which is very useful for the identification of damage or development of numerical models, cannot easily be measured during shaking table tests.

(Fig. 11) shows the comparison of the displacement at the second floor of the structure measured in the PsD and shaking table tests. To analyse the discrepancies of the PsD and shaking table results, a Finite Element Model (FEM) of MISS was elaborated using the program CASTEM [14]. The steel structure frame was represented using linear beam elements that consider bending, shear and axial deformations. The flexibility of the beam to

column connections was modelled with Timoshenko beam elements of infinitesimal length. The FEM was condensed to the transverse degrees of freedom of the four storeys of the structure. The mass matrix was further lumped at each storey to simulate the PsD testing. Rayleigh damping was set for the first eigenvalue and for a frequency of 25 Hz. Time history analysis was performed using the step-by-step centered Newmark algorithm.

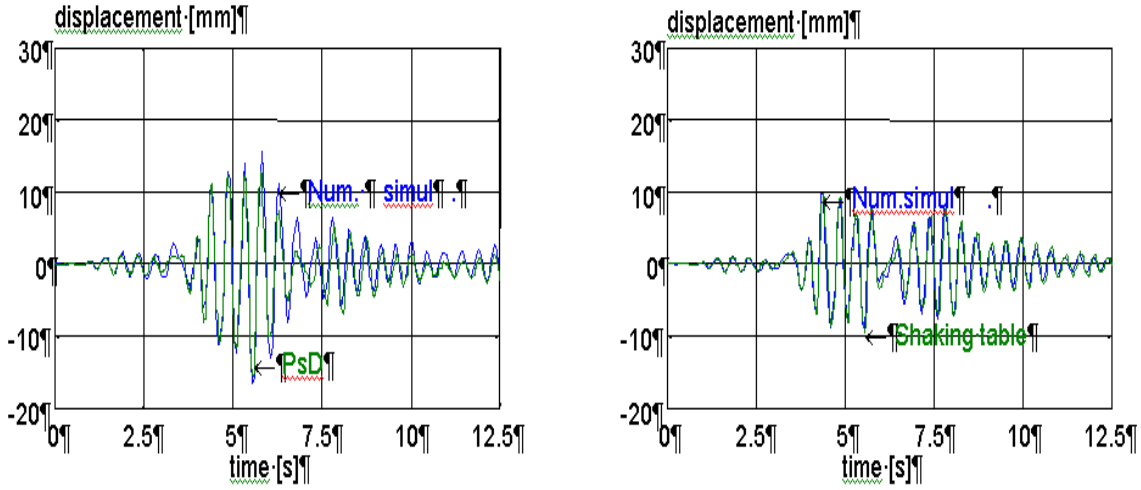

Figure 9: Non-isolated structure seismic tests: Second floor displ., PsD, Shaking tale and Num. comparison

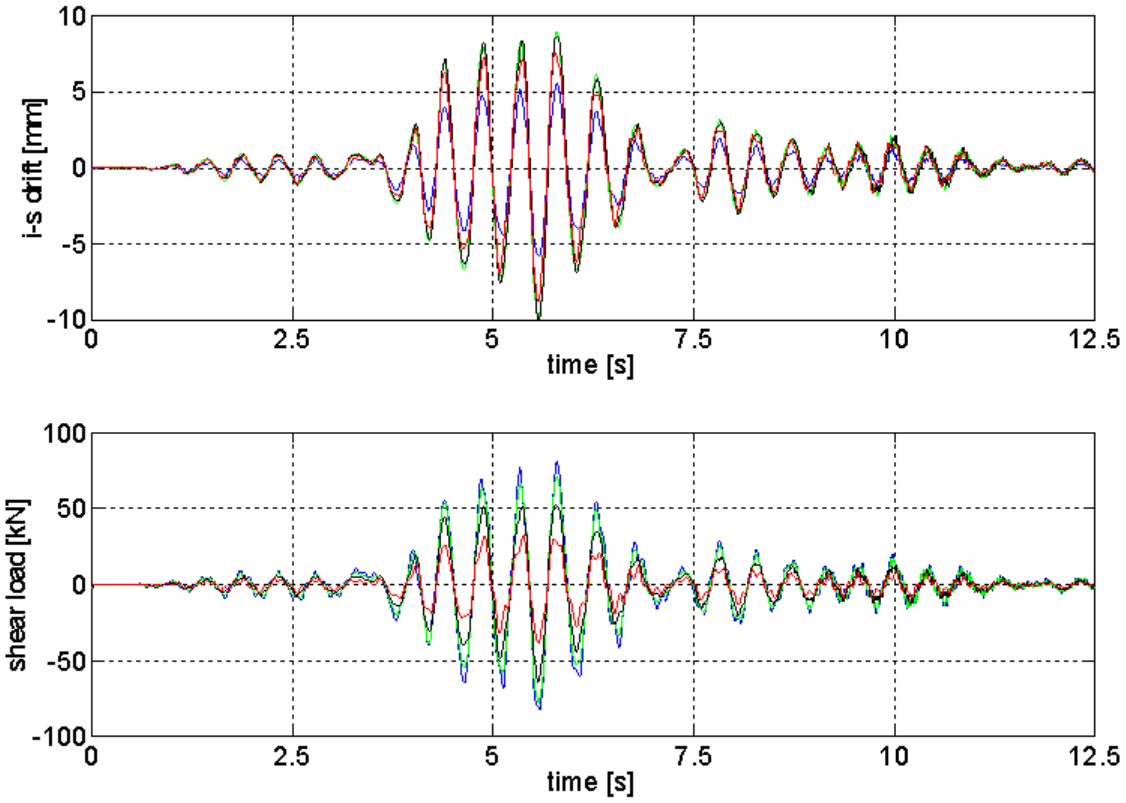

Figure 10: Non-isolated structure seismic PsD test: floor 1,2,3,4 inter-storey drift and shear load

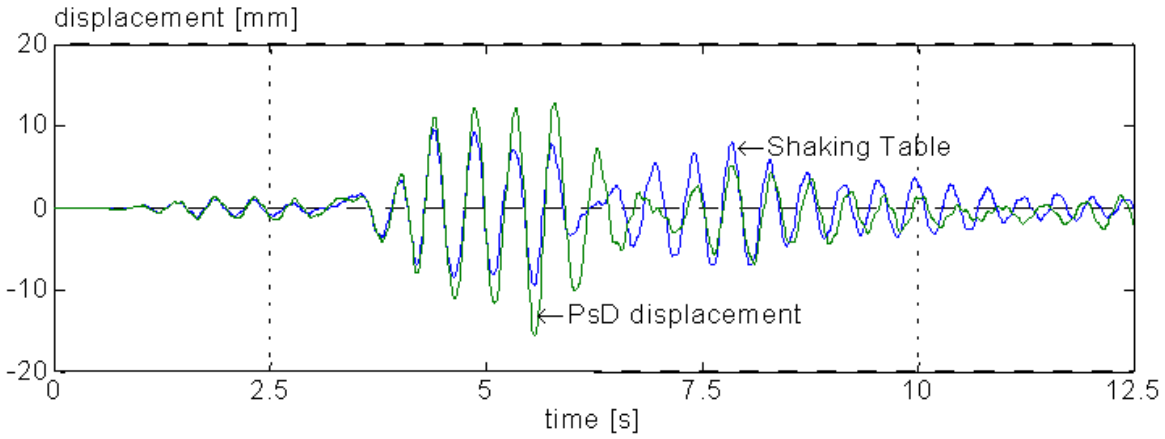

Figure 11: Non isolated structure.-6dB Tolomezzo Earthquake: second floor displacement shaking table and PsD test comparison.

On (Fig. 9), a comparison is made between the experimental results of the PsD and shaking table tests with the numerical model whose parameters were adjusted in order to obtain the best fitting of the respective tests. From that figure and from the data contained in Table 2, one can see how the experimental results are well matched by a linear model, which is reasonable for this type of structure within the range of attained deformations. However, the parameters of the best-fit model differ for both tests, mainly for the damping ratio of the first mode and lightly for the associated frequency. In the case of the PsD test, that damping ratio was found to be about 1% both for the dynamic and PsD snap-back tests as well as for the PsD seismic test. However, in the case of the shaking table test, the damping was found to be about 6%, which could be due to: differences in the coupling bolts stressing, attachment to the table, existence of residual pitching of the table, or some other facts which are still to be analysed in collaboration with ISMES. The response spectrum contained in Fig.7 may also justify why, for a frequency around 2.2Hz, a difference in damping from 1% to 6% may represent a decrement of a 30% in the response as was observed in the shaking table test with respect to the PsD test.

TABLE 2: COMPARISON OF SEISMIC TESTS EIGEN FREQUENCIES AND DAMPING RATIOS FOR SHAKING TABLE TEST, PSD TEST AND NUMERIC SIMULATION ON THE NON-ISOLATED STRUCTURE

	Mode 1		Mode 2		Mode 3		Mode 4	
	Hz	Damp.	Hz	Damp.	Hz	Damp.	Hz	Damp.
Shaking table	2.37		9.20		18.90		27.1	
PsD	2.17	0.8 %	8.00	1.3 %	16.70	1.5 %	23.8	0.9 %
Num. 6%	2.30	6.0 %	8.46		18.35		29.76	
Num. 1%	2.25	1.0 %	6.35		11.81		17.97	

5 PsD TESTS ON THE ISOLATED STRUCTURE

5.1 Real-Time Snap-Back Tests

The base of the mock-up was mounted on six HDRBs isolator devices. This new base floor will be called here floor 0. The real-time snap-back was executed as described before by

pushing at the centre of the isolated base (floor 0). The applied force was recorded during the entire loading phase. Two snap-back tests were performed at an initial displacement equal to 22.5 mm and 40 mm, which correspond to a 75% and 133% shear strain in the rubber bearings respectively. As expected, the curves (Fig. 12) indicate a free damped response, with a significantly high value of damping. The figure shows a decrease of the time interval between two subsequent peaks during the oscillation; this is due to the non-linear behaviour of the isolators, which display an increasing horizontal stiffness with decreasing displacement.

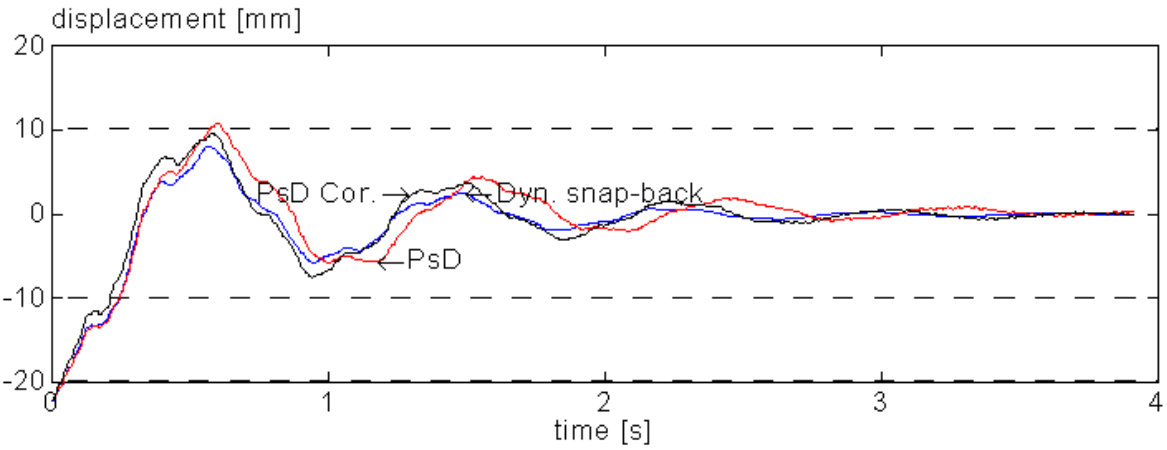

Figure 12: Dynamic snap-back tests on the isolated structure (initial displacement: 22.5 mm), non corrected PsD and corrected (23%) PsD.

5.2 PsD Snap-Back Tests

The base of the mock-up was guided in a rail system fixed on the strong floor to assure a motion in the transversal direction only while avoiding any torsional displacements. Five actuators were attached to the structure and the snap-back tests were repeated pseudodynamically by prescribing as external load the history measured during the dynamic test. This time, the PsD model consisted of 5-DoF (one per floor including the base) and the following mass matrix was used: diag(1840, 5140, 5450, 5340, 5460) kg. Firstly, a PsD test without strain rate compensation was performed. In order to assess the validity of the strain rate compensation, the PsD test was repeated adding a 23% correction to the shear load measured at the isolators. Such value was selected after some trial and error in order to optimise the frequency and amplitude in comparison with the dynamic snap-back test. Note that this correction of a 23% is larger than the one of the characterisation tests (19%, see Fig.3). This is due to the larger time scale used in this tests ($\lambda = 500$, instead of 300). Fig. 12 shows the free vibration displacement history of floor 0 recorded during the 22.5 mm snap-back test and the comparison of the results of this test with the non-corrected and corrected PsD tests. Table 3 gives the natural frequencies and the equivalent damping ratios of every mode. From Fig. 12 and Table 3, it is clear that the strain rate effect slows down the frequency of the first mode (rigid body oscillation of the isolated frame) in the non-corrected PsD test, while this effect is compensated in the corrected PsD test.

From the data of this table, it appears that the applied technique of force correction on the isolators was able to compensate the strain rate effect by adjusting the frequency of the first mode, while it showed no significant influence on any of the damping ratios or any of the higher frequencies.

TABLE 3: COMPARISON OF EIGEN FREQUENCIES AND DAMPING RATIOS FOR DYNAMIC, NON-CORRECTED PSD AND CORRECTED PSD (23%) SNAP-BACK TESTS ON THE ISOLATED STRUCTURE

	Mode 0		Mode 1		Mode 2		Mode 3		Mode 4	
	Hz	Damp.	Hz	Damp.	Hz	Damp.	Hz	Damp.	Hz	Damp.
Dyn.	1.20	15.5 %	4.5	4.4 %	11.9	1.3 %	21.6	1 .0 %	27.9	7.8 %
P 0%	1.05	14.6 %	4.32	3.8 %	11	1.3 %	20.3	0.6 %	29.7	3.0 %
P 23%	1.15	14.9 %	4.4	3.9 %	11	1.4 %	20.2	0.5 %	29.3	1.9 %

5.3 PsD Seismic Tests

The above described PsD tests have shown the possibility to correct in a suitable way the response of the isolators to account for the sensitivity of the material to strain rate effect. Since the time-scale factor of the seismic PsD test with respect to real-time always remained approximately of the same order of magnitude as for the snap-back test ($\lambda = 500$), the 23% of shear load correction was maintained for seismic tests.

(Fig. 13) shows the comparison of the displacements at the base floor and at the second floor of the structure for the PsD and shaking table tests. Both PsD and dynamic approaches have produced results very close to each other. Some small discrepancies in the comparisons are fully justified by the experimental errors and by minor variations of the HDRBs stiffness and damping as a function of the manufacturing series, loading frequency and load history. In fact, much of the variation in the observed behaviour can be attributed to the loading history on the isolators.

(Fig. 14) shows the inter-storey drift and shear load measured at each floor of the isolated MISS, in the PsD tests. As expected, respectively to Fig.10, a relevant reduction both in drift and shear due to isolation is observed.

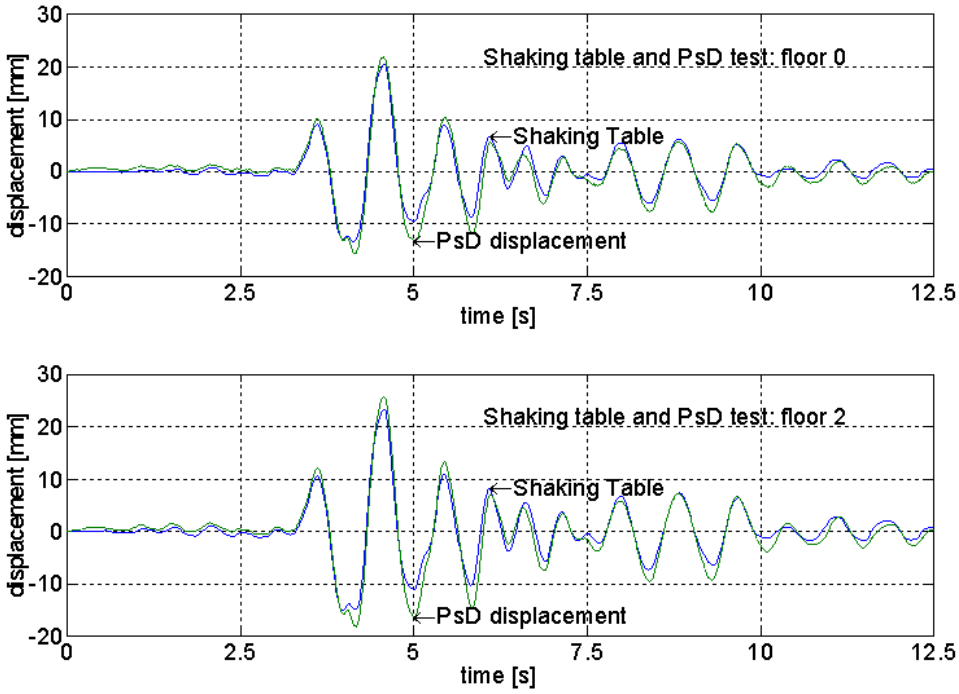

Figure 13: Isolated structure.-6dB Tolmezzo Earthquake: floor 0 and 2 displacements Shaking table and PsD tests comparison.

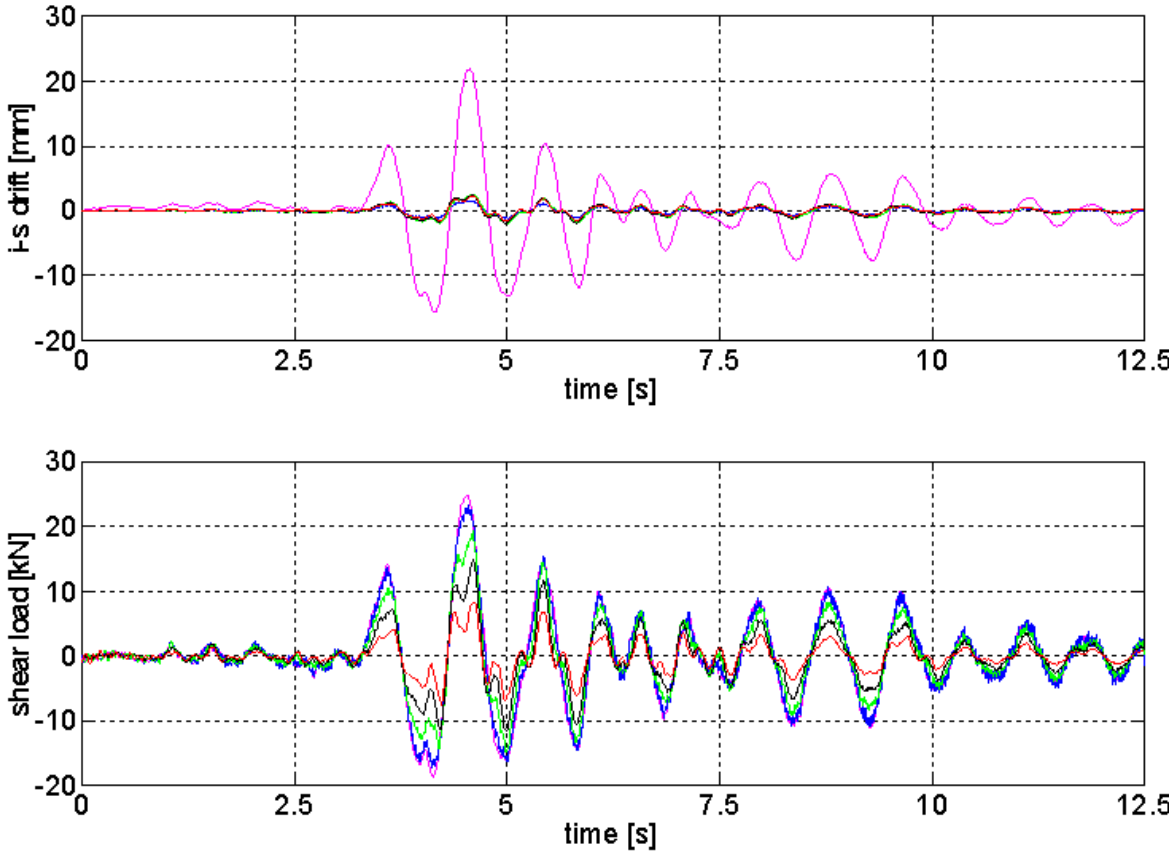

Figure 14: Isolated structure: -6dB Tolmezzo Earthquake: inter-storey drift and shear load.

6 PSEUDO-DYNAMIC SEISMIC TESTING OF LARGE SCALEMODELS OF CIVIL BUILDING WITH DISSIPATION DEVICES

The problem of the correction of the coefficients of the PsD method must be applied also in the case of testing of mock-up protected with dissipation devices based on materials with a strain rate dependent behaviour. As well known, this is the case of rubber and in the previous paragraphs it has been shown how to overcome the difficulties correlated with the PsD method.

A very similar procedure of correction applies also to the case of energy dissipation devices based on high damping rubber. This has been investigated and validated at JRC ELSA laboratory by testing a large-scale civil building incorporating such type of devices.

7 CHARACTERIZATION OF THE MODEL

A project, named "REEDS", was funded by the EC through the Brite-EuRam programme. It has been set up to focus the efforts of manufacturers, developers and end-users of anti-seismic devices towards identifying methods to augment the options currently available and therefore greatly increase the possibility that economic seismic protection can be provided to any particular structure, plant or equipment.

ELSA took part in the research by testing a large-scale model of reinforced concrete building protected with energy dissipation devices. These are made with high dumping natural rubber interposed between steel plates subjected to differential displacements through cross bracing. The main point to be investigated were the characterization of the model and the performance for imposed earthquake signals defined according the Eurocode-8.

A major point was the comparison of the behavior of the building with and without the protection system.

7.1 Description of the Mock-up

A two-storey mock-up of a reinforced concrete office building was designed for pseudo-dynamic (PsD) testing to be performed at JRC [16]. To make the mock-up compatible with the experimental equipment and with the available space in the laboratory, it was necessary to agree about its dimensions and about the characteristics of the attachment of the electro-hydraulic actuators. The mock-up (10m long, 4m wide and 5.2m high) represents a portion of the building scaled by 2/3 in dimension and consists of two bays of 5m in the direction of testing and of one bay across its width (Fig. 15). Eight energy dissipation devices were placed in each bay along the longitudinal facades and were supported by steel K-bracings (Fig. 16). The RC frame was constructed at the ELSA laboratory following the design specifications provided by Bouygues.

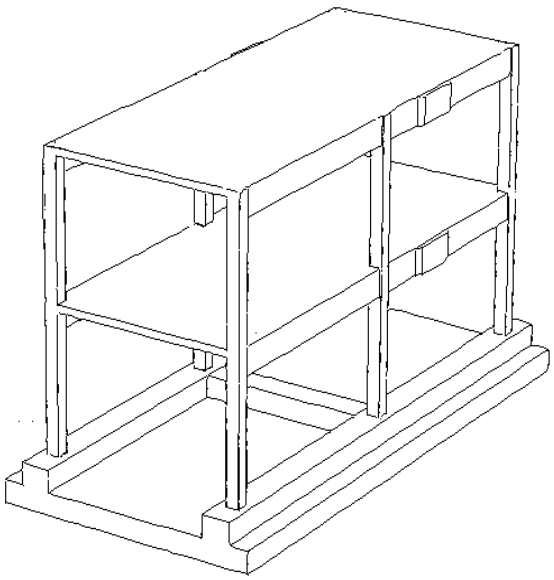

Figure 15: Isometric view of the mock-up.

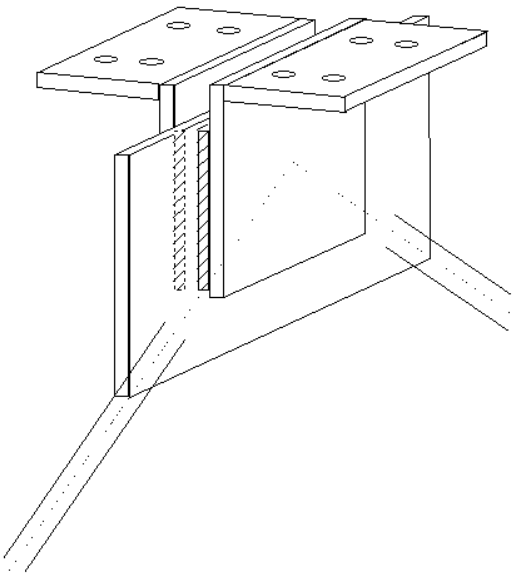

Figure 16: Details of the attachment of the VE devices to the mock-up structure.

The civil building has been moved into the laboratory and fixed to the strong floor. The steel wedges for the application of the force from the actuators were mounted against the floor slabs by means of post-tensioning rods. The bracing was installed in the bare frame and a specific interface has been designed and mounted to connect the visco-elastic device provided by TARRC. The connections of the steel bracing with the reinforced concrete frame have been made by means of anchor bolts to simulate a real retrofitting situation. The masses to be placed on the floor slabs have been installed. JRC in co-operation with Bouygues carried out

material characterization of the concrete and reinforced steel used in the construction of the mock-up.

A particular attention has been devoted to the instrumentation of the mock-up, to measure the relative rotation between beam and column at the joints, and to measure the deformation of the antiseismic devices. The JRC has designed and instrumented the steel bracing in order to measure the shear force developed by the TARRC devices. This measurement was necessary to compensate the strain rate effect induced by the PsD method.

7.2 Characterization of the system

The identification of seismically vulnerable structures and equipment leaded to the adoption of a reinforced concrete frame civil structure. The choices practiced until now to meet seismic criteria for this type of structure are mainly based on strengthening of the design. The introduction of Viscoelastic Energy-Dissipative (VED) devices brings a "soft" alternative to the well known strengthening method or more recent seismic isolation technology. Seismic regulations are relatively recent and consequently many buildings have no or very little protection. The fact that the life of most buildings is around 100 years has lead to the realization that seismic retrofitting is potentially a big market, and VED devices may well be the most economic solution in many cases. The tests performed at the ELSA laboratory have been lasted to verify and quantify the effectiveness of such a system. To this end a large-scale two-floor and two-bay building was built outdoor of the laboratory and brought indoors in front of the reaction wall to be tested with the Pseudo-Dynamic (PsD) method (Fig. 17).

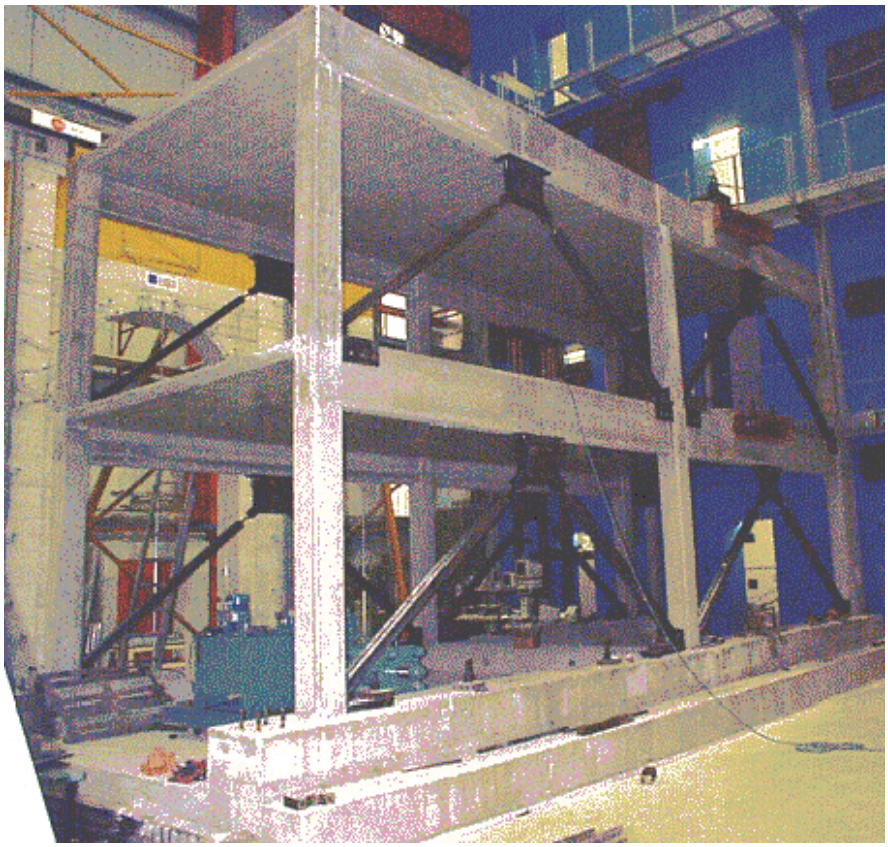

Figure 17: Large-scale model of the civil building with anti-seismic protection for earthquake simulation tests at ELSA.

The model of building has been equipped with damping devices made with natural rubber and the tests were performed with and without the damping devices for the same earthquake signal used as input. Being the rubber behavior of the devices sensitive to strain-rate, the execution of the PsD tests needs a specific characterization of the devices in order to take into account the strain rate effects as a numerical correction to be applied to the forces measured on the devices themselves. This procedure is made possible tanks to the flexibility of the PsD intrinsic characteristics. It is in fact a hybrid numerical-experimental method coupling the equation of the motion (used to evaluate the displacements induced by the earthquake) with the restoring forces of the structure measured on line on the model during the ongoing of the testing. This procedure bypass the problem of the theoretical assessment of the restoring forces and allows the precise calibration of the PsD method also for materials moderately sensitive to strain rate by introducing correction factors to account the real expected forces produced by the strain-rate dependent devices.

The results of the characterization tests for various strain-rates and the effectiveness of the correction by comparison of dynamic and PsD tests including a correction factor are shown in (Fig. 18).

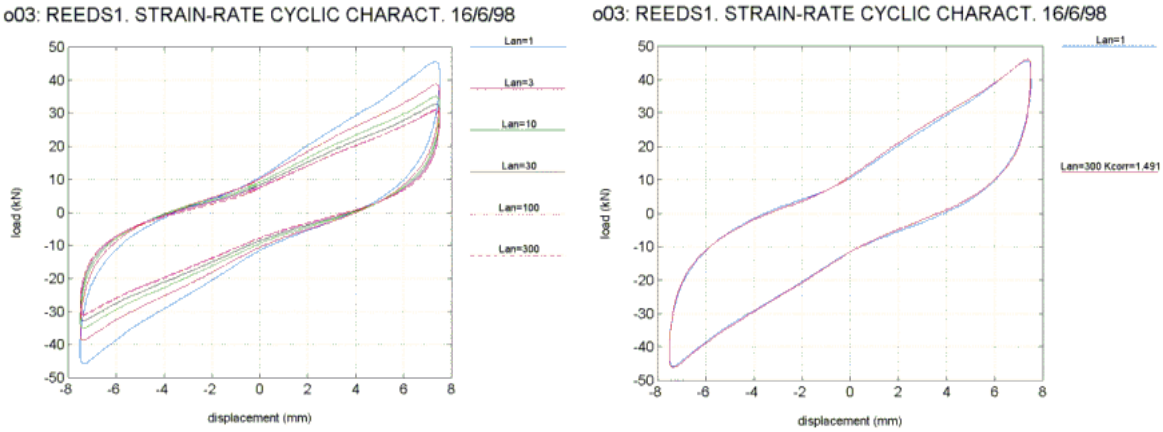

Figure 18: Results of the characterisation tests on the devices and comparison of a high strain rate test with a corrected PsD test.

8 PSEUDODYNAMIC TESTING OF THE SYSTEM

8.1 The pseudodynamic method

The Pseudo-Dynamic (PsD) test method is a hybrid numerical-experimental technique based mainly on the knowledge of the mathematical equation of the motion of the structure. When strong non-linear behavior occurs, the Restoring Force of the structure is no more computable so that the numerical integration becomes impossible. To overcome this difficulty the PsD method consists in running in parallel the integration of the numerical equation of the motion of the structure, imposing the assessed displacements generated by the earthquake and measuring the Restoring Force.

The experimental measure of the Restoring Force allows the integration of the equation of the motion until the end of the signal also for structures with strong non-linear behavior. The process doesn't need the generation of the inertia forces, computed from the equation, so that the time-scale of the operation is strongly expanded. This allows the direct visual diagnosis of the state of the structure and decisions about the limit to reach during the test.

The PsD method is fully complementary to the dynamic analysis based on Shaking Table. The main advantages of the PsD approach is the possibility to test full/large scale model of structure being the pumping power used to impose displacements and not for generating inertia forces. A second relevant advantage is the possibility of substructuring the model limiting the test to the part of structure with non-linear behavior while the linear one is computed in parallel with the numerical part of the PsD equation. The two substructures are coupled at the points of contact. With this technique it is possible to assess bridges only testing the piers, computing the deck and coupling the numerical part of the two structures.

The PsD method cannot be applied in case of materials whose behavior is strongly sensitive to strain rate or of structure with fully distributed mass. For this class of models it is mandatory to use the Shaking Table to perform meaningful tests.

8.2 Main results and achievements from the tests

The tests performed at JRC-Ispra showed a relevant reduction of displacements and highlighted the effectiveness of the devices for earthquake engineering applications.

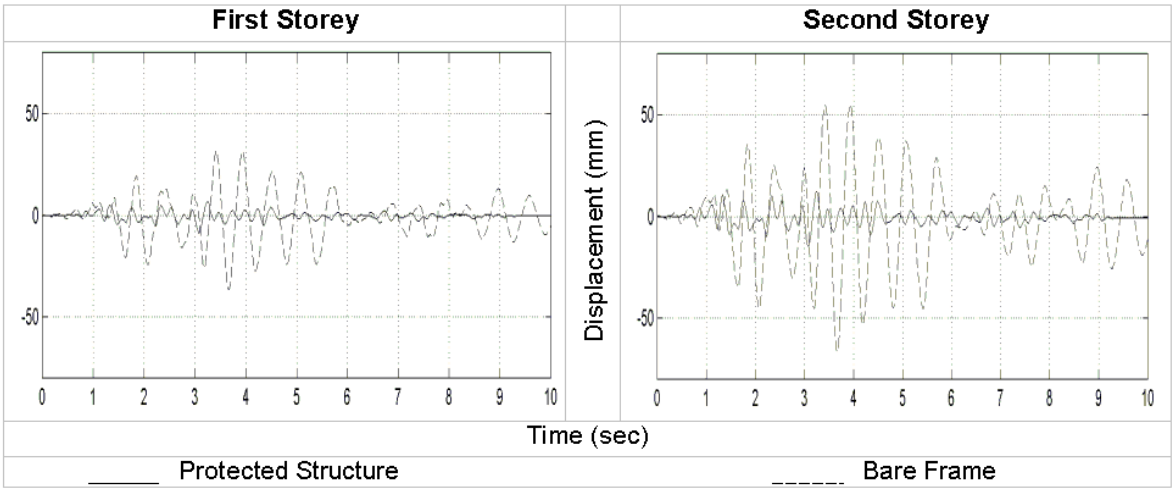

Figure 19: Dispalcement comparison between PsD tests ofthe protected structure an bare frame.

The VED devices need to experience a minimum amount of displacement during an earthquake to operate efficiently. Therefore their total stiffness per floor must be of the order of the floor stiffness of the building. Consequently, the use of these devices could be difficult for very stiff concrete structures, especially those containing shear walls. Nevertheless, with frame structures, which are quite common in seismic areas of Europe, the technical study has proved that reinforced concrete frame buildings designed initially for non-seismic areas may be up-graded, by incorporating viscoelastic dampers to respond elastically to earthquakes specified in European Seismic Code - EuroCode 8.

The devices can indeed provide an alternative protection strategy for such buildings. The dampers raise the stiffness between floors, the increase itself contributing to the reduction in the response. However, the inherent damping of the devices reduces the response much further. The PsD tests carried out at ELSA on the large-scale civil building have shown that when the structure is installed with the devices it responds elastically to earthquakes twice the magnitude of that for the bare structure.

The first and second storey displacements of the PsD tests on the protected and bare frame are shown in (Fig. 19). The efficiency of the energy dissipation devices is demonstrated by a reduction of the displacements of the frame by more than a factor of four, keeping thus the ductility demands on the RC members below unity, as shown by the hysteresis loops of the RC frame.

The efficiency of the energy dissipation devices can also be demonstrated by examining the energy absorbed during the PsD test of the protected frame, as shown in (Fig. 21), where the energy dissipation devices absorb 75% of the total energy that goes into the system

Although the forces in the RC frame are not sensibly reduced in the protected frame test, only a fraction of the force goes into the RC frame, the remaining of the force is absorbed by the energy dissipation devices. The introduction of stiffness of comparable value to the intrinsic interstorey one and of dissipation capability of the devices allowed a strong reduction in the hysteretic loops. This is shown in (Fig. 20) where the forces, for the protected case, are referred only to the structure (the horizontal component of the K-bracings is not accounted).

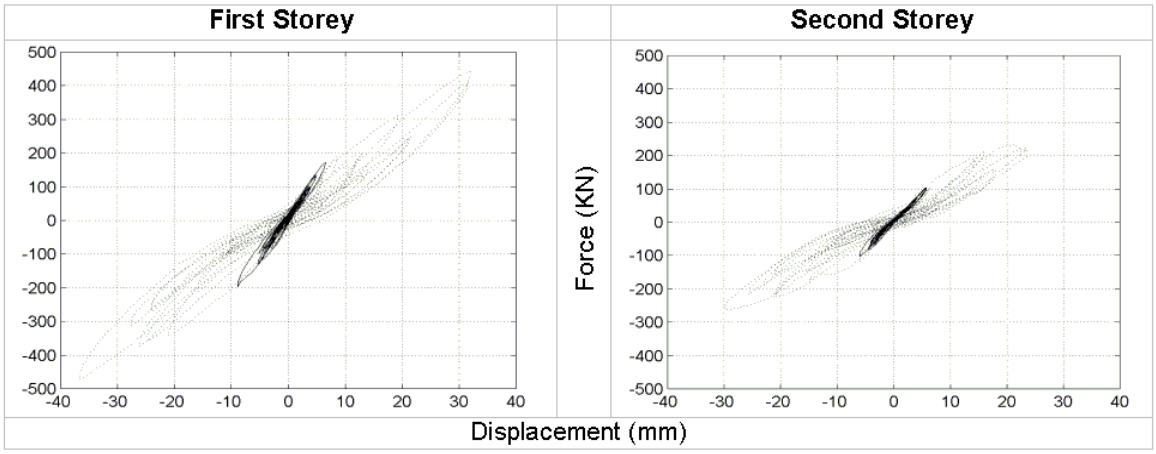

Figure 20: Comparison of energy dissipation in bare and protected frame.

.

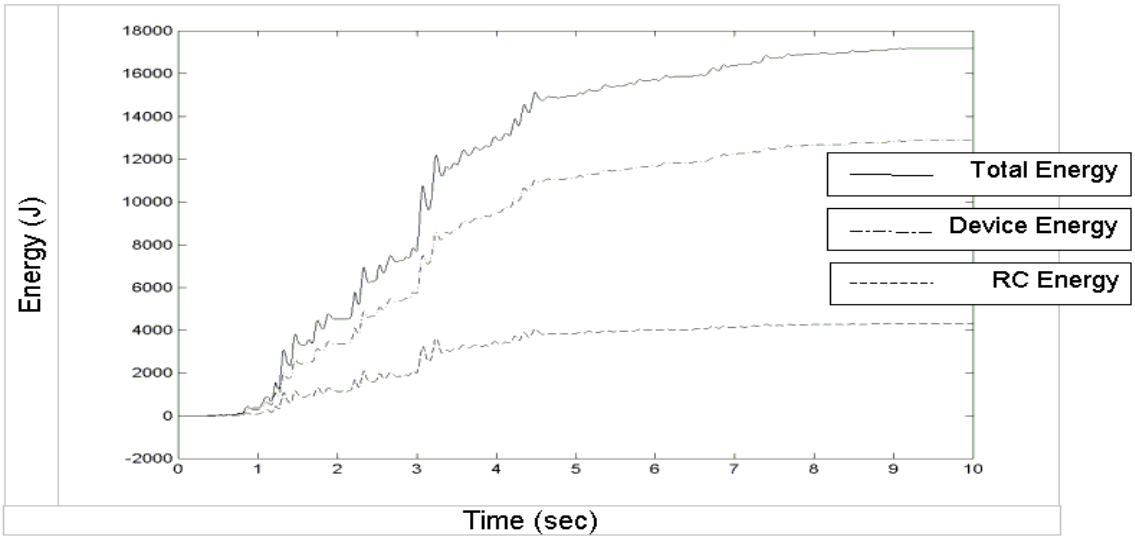

Figure 21: Energy absorbed during the PsD test of the protected structure.

9 CONCLUSION

The work performed and presented was finalised to the improvement and validation of the PsD testing method for structures protected against earthquake by devices based on materials strain rate dependent as it is the case of high damping rubber.

The investigation was done both for cases of base isolated mock-ups and for a model of civil building protected by energy dissipation devices.

As regards base isolation the work done at JRC, in collaboration with the Italian Working Group on Seismic Isolation, was finalised to compare the results obtained from PsD and shaking table tests performed on the isolated MISS mock-up. PsD seismic excitation tests performed on the isolated and non isolated structure have confirmed that HDRBs allow a very effective reduction of the earthquake response of the structure.

As regards energy dissipation devices the work was done in collaboration with an international consortium in the framework of a project partially financed by the European Commission. The mock-up was a large scale model of civil building not designed for seismic zones and seismically upgraded by using energy dissipation devices.

In both cases the test results showed that, thanks to specific strain-rate compensation procedure, the PsD method is able to reproduce with good accuracy the response of a large-scale model of structures protected by strain rate dependent devices. This was observed during the dynamic snap-back tests or the seismic tests performed on shaking table.

REFERENCES

[1] RENDA, V., et al, (1995a), Research activities and programmes on Seismic Isolation at the Joint Research Centre of the European Commission, 13-th Post SMIRT specialized conference, 21-23 AUG., Chile.

[2] RENDA, V., et al, (1995b), A European collaboration Research Programme to study and test Large Scale Base Isolated Structures, 13-th SMIRT, 13-18 AUG., Porto Alegre, Brazil.

[3] BETTINALI, F., et al., Status of Italian Test Data on Isolated Structures and Comparison with Computer Predictions. IAEA Research Co-ordination Meeting (RCM) on “Intercomparison of Analysis Methods for Seismically Isolated Nuclear Structures”, Saint Petersburg, Russian Federation, 27-31 May (1996).

[4] DUSI, A., et. al., Behaviour of seismic isolators at very large shear strain, Proc. ABAQUS Users’ Conference, Newport, RI, USA (1996).

[5] FORNI, M., et al, Development and Validation of Finite Element Models of Rubber Bearings. Proceedings of the First European Conference on Structural Control. Barcelona (1996). 266-273. World ScientificPublishing Co.

[6] MAGONETTE, G., (1991) – Digital Control of Pseudodynamic Tests. Experimental and Numerical Methods in Earthquake Engineering, p63-99, Editors J. Donea and P.M. Jones, Kluwer Academic Publishers, Dordrech, The Netherlands.

[7] DONEA, J., Magonette G., Negro P., Pegon P., Pinto A., and Verzeletti G. - February (19960 - Pseudodynamic Capabilities of the ELSA Laboratory for Earthquake Testing of Large Structures. Earthquake Spectra, Volume 12, No 1.

[8] KELLY, J.M., (1993), Earthquake-Resistant Design with Rubber. Springer-Verlag. London.

[9] MOLINA, F.J., et al, (1996), Tests on the 3-Storey Steel Frame with and without Base Isolation. JRC-Ispra, ELSA Laboratory, Technical Note No. I.96.69.
[10] MOLINA, F.J., et al, (1996), Pseudo-dynamic simulation of base isolation on a reinforced concrete building by means of substructuring. Proceedings of the First European Conference on Structural Control. Barcelona, May 29-31.
[11] DUSI, A., et al., Numerical and Experimental Evaluation of Benefits of Seismic Isolation on the Structural Behaviour. Proceedings of the First European Conference on Structural Control. Barcelona (1996). 239-248. World ScientificPublishing Co.
[12] ENEL S.pA., DSR/CRIS, ALGA, DYWIDAG, ENEA, MRPRA, SHW and STIN, Optimization of design and performance of High Damping Rubber Bearings for seismic and vibration isolation. EC Contract BRE2-CT93-0524, Prolect BE7010, Bruxelles, Belgium (1993).
[13] ENEL S.pA. DSR/CRIS, (1996), BRITE EURAM II Project BE 1070, Task n.6, Seismic tests on MOCK-UP MISS (Model of Isolated Steel Structure) Test report, Proj. STR-7940; Doc. RAT-STR-1734/96.
[14] TAUCER, F., Numerical Simulations of Shaking Table and Pseudodynamic Tests performed on a 4-storey Base Isolated Steel Frame. Technical Note (in publication), JRC-Ispra, (1997).
[15] MOLINA, F.J., et al, Pseudo-dynamic Tests of a Base-isolated steel frame. Proceeding of the Eleventh World Conference on Earthquake Engineering, Acapulco, Mexico, 23-28 June (1996).
[16] TAUCER, F., MAGONETTE, G., MARAZZI, F., MOLINA, J., VERZELETTI, G., RENDA, V., (1999) "PsD tests on the seismic retrofit of a large scale RC civil building with energy dissipation devices "Proceedings of the ASSISI-99 International Workshop on Seismic Performance of Built Heritage in Small Historic Centres, April 22-24, (1999), Assisi, Italy.

LIST OF PARTICIPANTS

Ahmadi, H.	Tun Abdul Razak Research Centre, United Kingdom
Aiken, I.D.	Earthquake Engineering Research Centre, United States of America
Beliaev, V.S.	Research Centre of Fundamental Engineering, Russian Federation
Bergamo, G.	ENEL-HYDRO-ISMES. Engineering and Testing Centre, Italy
Bertola, S.	ENEL-HYDRO. Hydraulic and Structure Centre, Italy
Bettinali, F.	ENEL-HYDRO. Hydraulic and Structure Centre, Italy
Bhoje, S.B.	Indira Gandhi Centre for Atomic Research, India
Bonacina, G.	ENEL-HYDRO-ISMES. Engineering and Testing Centre, Italy
Chellapandi, P.	Indira Gandhi Centre for Atomic Research, India
Chetal, S.	Indira Gandhi Centre for Atomic Research, India
Clark, P.W.	Earthquake Engineering Research Centre, United States of America
Dolgaya, A.A.	CEEND, Russian Federation
Dusi, A.	ENEL-HYDRO. Hydraulic and Structure Centre, Italy
Forni, M.	National Agency for New Technology, Italy
Fuller, K.N.G.	Tun Abdul Razak Research Centre, United Kingdom
Gough, J.	Tun Abdul Razak Research Centre, United Kingdom
Hirata, K.	Central Research Institute of Electric Power Industry, Japan
Koo, Gyeng-Hoi	Korea Atomic Energy Research Institute, Republic of Korea
Kelly, J.M.	Earthquake Engineering Research Centre, United States of America
Kostarev, V.V.	CKTI — Vibroseism, Russian Federation
Krylova, I.N.	Research Centre of Fundamental Engineering, Russian Federation
Kupitz, J.	International Atomic Energy Agency
Kuzmitchev, V.P.	Research Centre of Fundamental Engineering, Russian Federation
La Grotteria, M.	National Agency for New Technology, Italy
Lee, Jae-Han	Korea Atomic Energy Research Institute, Republic of Korea
Magonette, G.	Joint Research Centre of the EC
Martelli, A.	National Agency for New Technology, Italy
Matsuda, A.	Central Research Institute of Electric Power Industry, Japan
Muralikrishna, R.	Indira Gandhi Centre for Atomic Research, India
Privalov, S.A.	Research Centre of Fundamental Engineering, Russian Federation
Renda, V.	Joint Research Centre of the EC
Rineiskii, A.	International Atomic Energy Agency
Salvaraj, T.	Indira Gandhi Centre for Atomic Research, India
Siro, V.A.	Research Centre of Fundamental Engineering, Russian Federation

Stanculescu, A.	International Atomic Energy Agency
Uzdin, A.M.	CEEND, Russian Federation
Vasiliev, A.V.	CKTI-Vibroseism, Russian Federation
Vinogradov, V.V.	Research Centre of Fundamental Engineering, Russian Federation
Yabana, S.	Central Research Institute of Electric Power Industry, Japan
Yoo, Bong	Korea Atomic Energy Research Institute, Republic of Korea